



ON THE RELIABILITY OF TRIANGULAR FINITE ELEMENTS FOR SHELLS

Iria Paris

► To cite this version:

Iria Paris. ON THE RELIABILITY OF TRIANGULAR FINITE ELEMENTS FOR SHELLS. Mathematics [math]. Université Pierre et Marie Curie - Paris VI, 2006. English. NNT : . tel-00169852v2

HAL Id: tel-00169852

<https://theses.hal.science/tel-00169852v2>

Submitted on 5 Sep 2007

HAL is a multi-disciplinary open access archive for the deposit and dissemination of scientific research documents, whether they are published or not. The documents may come from teaching and research institutions in France or abroad, or from public or private research centers.

L'archive ouverte pluridisciplinaire **HAL**, est destinée au dépôt et à la diffusion de documents scientifiques de niveau recherche, publiés ou non, émanant des établissements d'enseignement et de recherche français ou étrangers, des laboratoires publics ou privés.

THÈSE

présentée à

L'UNIVERSITÉ PIERRE ET MARIE CURIE (PARIS VI)

pour obtenir le titre de

DOCTEUR DE L'UNIVERSITÉ PARIS VI

Spécialité

Mathématiques Appliquées

Présentée par

Iria PARIS SUAREZ

Titre

ROBUSTESSE DES ÉLÉMENTS FINIS TRIANGULAIRES DE COQUE

Directeur: **Dominique CHAPELLE**

Soutenue le 28 Novembre 2006 devant le jury composé de:

Dominique CHAPELLE	Directeur
Hervé LE DRET	Président
Patrick LE TALLEC	Examineur
Gunar LORENZ	Examineur
Annie RAOULT	Rapporteur
Jean-Marie THOMAS	Rapporteur

Thèse réalisée au sein du projet MACS à l'INRIA Rocquencourt

Remerciements

Je tiens à remercier tout d'abord Dominique Chapelle, mon directeur de thèse, qui m'a fait l'honneur de partager sa passion pour la Recherche, ses connaissances et ses idées, et qui m'a guidé dans mes travaux. Je lui suis très reconnaissante pour sa rigueur dans le travail, ainsi que la confiance qu'il m'a accordée au long de ces trois années.

J'ai été très honorée que Mme Annie Raoult et M. Jean-Marie Thomas aient accepté d'être les rapporteurs de cette thèse. J'exprime aussi toute ma gratitude à M. Hervé Le Dret, M. Patrick Le Tallec et M. Gunar Lorenz qui m'ont fait l'honneur de participer au jury.

Une pensée très reconnaissante est adressée à Marina Vidrascu. Merci du fond du cœur pour le soutien que tu m'as apporté dans les moments difficiles en m'aidant à les remonter et pour m'avoir appris que la vie n'est qu'un problème de minimisation avec des contraintes ...

Merci à tous les membres du project Macs qui m'ont accueillie pendant ces trois années et qui m'ont permis de partager leur richesse professionnelle et personnelle. Je tiens aussi à remercier les chercheurs du bâtiment 16 qui m'ont chaleureusement accueillie par leurs petits mots en espagnol lesquels m'ont toujours fait plaisir...

Je voudrais aussi remercier Juan Manuel Viaño, Marisa Seoane et Regina Castro pour m'avoir initiée dans la Recherche, ainsi que pour leur gentillesse et bon savoir faire.

J'ai été très honorée que la "Fundación Caixa Galicia - Claudio San Martin" m'ait assigné une bourse d'études pour financer ma première année de thèse.

J'adresse une pensée à Lourenço Beirão da Veiga avec qui j'ai eu le bonheur de travailler à la fin de ma thèse et de partager des discussions très enrichissantes.

J'arrive enfin à mes collègues et amis de l'INRIA. Je vous remercie très profondément pour vos conseils, vos histoires et votre joie au long de ces années de thèse. Merci à Miguel, Fred (qui apporte tous les jours un rayon de soleil du Sud), Adrien ("Lolo"), Mathieu, Loïc, Nuno, Pierre-Lin, Boris, Azzeddine, Antoine... aussi Claire, Astrid, Cécile, Emmanuel, Paola, Michel... Etant donné qu'une belle amitié peut naître d'une autre, j'adresse une pensée spéciale à Sylvianne, Stéphanie, Marie-Sylvie et Marie-Élyse. Merci, les amis!

J'adresse aussi une pensée à Hyam, Tomas, Jean-Baptiste et Mirna qui m'ont donné leur amitié depuis mon arrivée en France et qui ont toujours été à mes côtés quand j'en ai eu besoin. Un grand merci...

Je remercie très profondément à Claire Soma, Benoît, Fina et René qui m'ont accueillie comme un membre de leur famille. Vous aurez toujours une place dans mon cœur.

Je dois énormément à mes amis espagnols qui malgré la distance ont été proches de moi et m'ont prouvé leur amitié. Merci à Judit, Cris et Carlos, Sandra et Yuman, Bego, Nati, Luís et "la bande de la fac". *Gracias por vuestros mails, vuestras palabras de ánimo y aliento en los momentos difíciles, y por la alegría*

que acompaña vuestras visitas, los reencuentros y las charlas sin fin. Gracias de corazón, mil gracias.

Et rien ne vaut le soutien de ma famille et ma nouvelle famille. Gracias a mis padres pour haber estado siempre a mi lado y darme su amor y apoyo día tras día sin condición. Gracias a Patricia, mi hermana, simplemente por serlo, y a David por su cariño y apoyo. No podría pasar sin agradecer a Loli, Sesé y los chicos, a Plácido, Inés y las peques, asique a Lisardo y Cristina, Luís, Marija, Marcelino e Isabel su cariño y apoyo constante. También quiero agradecer desde lo más hondo de mi corazón a mis suegros, Julia y Luís, que me han hecho sentir como una más de la familia desde el primer día brindándome un gran cariño.

Et finalement, je remercie celui que j'aime le plus ... Hernán. La vie avec toi est le rêve devenu réalité. Merci pour ta patience et pour m'avoir soutenue au long de cette période. Tu m'as aidé à croire en moi même. Sans toi je ne serais jamais arrivée jusque là...

C'est l'inspiration qui fait bouger le monde

À Hernán et Patricia

Introduction

Une *coque* est une structure tridimensionnelle caractérisée par une épaisseur très petite par rapport aux autres dimension caractéristiques. Ce type de structure apparaît fréquemment dans des constructions courantes (ponts, toits de bâtiments,...), dans la conception industrielle (turbines, pièces de mécanique, carrosserie de voiture,...), et même dans le monde du vivant (artères, bronches,...). De fait, celles-ci sont des structures légères qui répondent de façon efficace aux efforts subis, principalement grâce à la courbure de leur surface. Dans le milieu industriel, l'objectif principal est d'obtenir une structure la plus mince et robuste possible pour utiliser un minimum de matériau dans sa construction, tandis que par exemple, en biomécanique la modélisation et simulation numérique du couplage fluide/structure mince peut apporter de l'information pour le traitement de diverses pathologies, comme les anévrismes.

Afin de simuler numériquement le comportement des structures minces, il est important de formuler des méthodes d'éléments finis de coques qui soient robustes vis-à-vis du *verrouillage numérique*, mais aussi *consistantes*. On trouve fréquemment des structures minces de géométrie complexe qui nécessitent l'utilisation de maillages surfaciques non-structurés qui incluent *forcément des éléments finis triangulaires*, ce qui constitue la motivation majeure de cette thèse.

L'obtention des modèles de plaques et coques a été un sujet de recherche primordial en mécanique (voir Calladine 1983 [28], Flügge 1973 [38], Naghdi 1963 [50], Reissner 1952 [57], Timoshenko & Woinowsky-Krieger 1959 [63], Valid 1995 [64], Wunderlich 1980 [65]). L'idée de base dans la théorie de ces modèles est d'utiliser des hypothèses et simplifications physiquement justifiables à travers l'épaisseur pour obtenir la déformation d'une structure mince tridimensionnelle à partir d'un problème formulé sur sa surface moyenne. Par exemple, on néglige l'influence de la composante normale des contraintes, les effets des déformations à travers l'épaisseur, ou on utilise souvent des hypothèses cinématiques du type Reissner-Mindlin qui supposent que les composantes tangentielles du déplacement $3D$ sont linéaires dans la variable transverse, tandis que la composante transversale est constante (voir Koiter 1965 [44], Mindlin 1951 [49], Novozhilov 1970 [51], Reissner 1945 [56] et leurs références). Mais on peut aussi penser à des hypothèses cinématiques d'ordre plus élevé, voir en particulier Chapelle, Ferent & Bathe 2004 [32].

L'énergie de déformation d'une coque peut être décomposée en trois termes

principaux: flexion, membrane et cisaillement (voir Chapelle & Bathe 2003 [31]). Lorsqu'on fait tendre l'épaisseur vers zéro, l'énergie de cisaillement devient négligeable et la déformation subie par la coque appartient à l'une des trois catégories asymptotiques suivantes en fonction de la géométrie, des conditions aux limites et des forces appliquées:

1. flexion-dominante
2. membrane-dominante
3. mixte

Dans les premier et deuxième cas, c'est la partie correspondante de l'énergie de déformation qui est dominante, tandis que dans les situations mixtes aucune partie n'est négligeable par rapport à l'autre. En considérant la même force, matériau et conditions aux limites, une coque peut exhiber des comportements asymptotiques complètement différents en fonction de la nature géométrique de la surface moyenne (voir en particulier Bathe, Chapelle & Lee 2003 [11], Pitkäranta, Leino, Ovaskainen & Piila 1995 [54], Sanchez-Hubert & Sanchez-Palencia 2001 [59], Baiocchi & Lovadina 2002 [5] et leurs références).

L'espace continu des déplacements inextensionnels – avec énergies de membrane et cisaillement nulles et nommé \mathcal{V}_0 – joue un rôle fondamental dans le classement évoqué ci-dessus: dans le cas flexion-dominante, le problème limite est formulé dans cet espace qui doit être différent de zéro, tandis que dans le cas membrane-dominante, cet espace est réduit au champ nul (pour une analyse asymptotique détaillée voir Chapelle & Bathe 2003 [31] et ses références).

Notre démarche se concentre dans la formulation d'éléments finis de coque qui puissent montrer une convergence optimale – en fonction de l'ordre d'approximation des éléments choisis – et uniforme de la solution approchée par rapport à l'épaisseur et dans toutes les catégories asymptotiques. Il est bien connu que les techniques d'éléments finis standard marchent bien dans des situations à membrane dominante, mais en général celles-ci donnent des solutions approchées trop rigides pour les problèmes à flexion dominante, principalement lorsque l'épaisseur est très petite, phénomène connu sous le nom de *verrouillage numérique* (voir Bathe & Chapelle 2003 [31]). De fait, la convergence de la méthode des éléments finis est influencée par le contenu de l'espace de déplacements inextensionnels discrets qui peut être réduit à zéro, tandis que l'espace continu correspondant ne l'est pas (voir Chapitre 3).

Le *verrouillage numérique* est l'une des difficultés majeures dans la formulation d'éléments finis robustes pour l'analyse numérique des structures minces, mais ce phénomène concerne aussi les formulations incompressibles de la mécanique des milieux continus en particulier (voir Bathe 1996 [6], Brezzi & Fortin 1991 [23], Batoz & Dhatt 1990 [16], Hughes 1987 [41]). Des nombreux travaux ont été réalisés dans la recherche de remèdes contre cette pathologie. Les *méthodes mixtes* – dont les fondements théoriques ont été établis par Babuška 1973 [4]

et Brezzi 1974 [21] – constituent un outil efficace pour la conception et l’analyse rigoureuse des méthodes numériques qui échappent au verrouillage, en particulier dans la mécanique des fluides incompressibles et les modèles de plaques (voir Brezzi & Fortin 1991 [23], Chinosi & Lovadina 1995 [34], Roberts-Thomas 1991 [58]). Il faut souligner que d’autres méthodes –comme la technique des *enhanced elements*– ont été aussi employées avec succès dans certains cas (voir Armero 2000 [2], Lovadina & al. 2005 [3], Lovadina & Auricchio 2003 [27], Simo & Rafai 1990 [42], Simo & Reddi 1995 [17],). Cette méthode est basée sur une forme de discrétisation du sous-espace contraint, mais une formulation générale pour les coques est difficile à obtenir car une discrétisation du sous-espace de déplacements de flexion pure n’est pas évidente pour des géométries générales (voir Havu & Pitkäranta 2002 [39]).

Les problèmes de robustesse des méthodes d’éléments finis pour les coques, et notamment le phénomène de verrouillage numérique – de cisaillement et de membrane – qui intervient lorsque la structure considérée est mince, sont désormais bien compris, voir en particulier Chapelle & Bathe 2003 [31] et ses références. Même si l’on ne connaît pas, pour l’instant, d’élément dont on ait pu démontrer qu’il serait *parfaitement robuste*, on dispose de méthodologies détaillées et rigoureuses pour évaluer la robustesse des éléments de coques au moyen de cas-tests (voir Bathe, Iosilevich & Chapelle 2000 [14], Chapelle & Bathe 2003 [31]). De fait, certains éléments existants comme l’élément quadrangulaire MITC4 (Bathe 1996 [6]) montrent un très bon comportement à travers ces tests. Cependant, aucun élément *triangulaire* ne semblait présenter un degré de robustesse réellement satisfaisant à l’heure de début de cette thèse, malgré de nombreux travaux sur la question. Ce problème est de grande importance pour les applications industrielles, car de nombreuses structures de géométrie complexe nécessitent l’utilisation de maillages surfaciques non-structurés qui incluent forcément des éléments finis triangulaires.

Les “*general shell elements*” sont formulés à partir d’hypothèses cinématiques du type Reissner-Mindlin (voir Chapitre 4.1). Les déformations de la coque sont donc décrites à partir de deux inconnues: le déplacement de la surface moyenne \vec{u} (3 composantes scalaires), et la rotation de la normale θ (2 composantes scalaires), c’est à dire

$$\vec{U} = \vec{u} + \xi^3 \vec{\theta}$$

avec $\vec{\theta} \cdot \vec{a}_3 = 0$ aux noeuds, où \vec{a}_3 est la normale unitaire et ξ^3 représente la coordonnée transverse (voir Bathe 1996 [6] et Chapitre 4.1). Le modèle mathématique correspondant est déduit du modèle d’élasticité 3D en considérant que la composante normale des contraintes est nulle, et l’étude mathématique en a été faite dans Chapelle & Bathe 2000 [30]. Cette démarche s’applique bien pour les cas des petites déformations et de nombreux éléments de ce type ont été formulés (voir Bathe 1996 [6], Bernadou 1996 [18] et leurs références). Leur développement avait été initié par Ahmad et al. [1] dans les années soixante-dix, tandis que des techniques formulées pour éviter le verrouillage ont été proposées dans Bathe & Dvorkin 1986 [13], Brezzi, Bathe & Fortin 1989 [22], Brezzi, Fortin & Stenberg

1991 [24], Bucalem & Bathe 1993 [26] et Dvorkin & Bathe 1984 [37], en particulier.

Les éléments finis MITC de coque appartiennent à la famille des “general shell elements” mentionnée ci-dessus. La technique MITC¹ a été formulée au départ comme un outil pour éviter le verrouillage numérique pour des éléments à 4 et 8 noeuds par Dvorkin & Bathe 1984 [37] et Bathe et Dvorkin 1986 [13]. Cela a été ensuite étendue à des éléments à 9 et 16 noeuds par Bucalem et Bathe 1993 [26], et aussi proposée pour des éléments triangulaires pour les plaques (voir en particulier Bathe, Brezzi & Cho 1989 [9] and Brezzi, Fortin & Stenberg 1991 [24]).

Il faut souligner que la formulation d’éléments MITC de coque est nettement différente de celle des éléments finis MITC pour les plaques (voir Bathe 1996 [6] et Bathe & Dvorkin 1985 [12]), ceux-ci étant formulés à partir d’une formulation 2D et fondamentalement basés sur une analogie existante entre la contrainte de déformation de cisaillement nul et l’incompressibilité pour des problèmes d’élasticité (voir Bathe & Brezzi 1985 [7], Bathe & Brezzi 1987 [8], Brezzi, Bathe & Fortin 1989 [22], Bathe, Bucalem & Brezzi 1990 [10]).

Pour la formulation des éléments finis MITC de coque on interpole séparément les déplacements et le tenseur de déformations (au lieu de le déduire directement des déplacements), et on relie les deux interpolations à des points spécifiques nommés *tying points* (voir Chapitre 4). L’objectif est d’éviter le phénomène de verrouillage numérique lié aux problèmes à flexion-dominante en remplaçant le tenseur de déformation d’origine par des composantes réduites, mais le risque est d’introduire des *modes parasites de membrane* qui pourraient considérablement détériorer la solution discrète dans des situations à membrane dominante comme nous l’avons observé dans le Chapitre 7.

Il est à noter que pour l’obtention d’éléments finis MITC robustes, la formulation discrète associée doit satisfaire quelques propriétés (voir Chapitre 4):

- *coercivité*
- *consistence*
- *condition inf-sup*

La condition inf-sup est particulièrement délicate. De fait, à l’heure actuelle on ne connaît l’existence d’aucune méthode d’éléments finis de coques minces dont on ait pu démontrer qu’elle vérifie la condition *inf-sup* en dehors de géométries particulières (par exemple voir Pitkäranta 1992 [53]), ce qui garantirait qu’elle est insensible au verrouillage. Néanmoins, un test *inf-sup* a été proposé par Bathe, Iosilevich et Chapelle [15], et l’idée d’une forme relaxée a été introduite par Bramble et Sun dans [20]. Par ailleurs, le seul résultat de convergence uniforme en flexion dominante est dû à Chapelle & Stenberg 1998 [33] et concerne une méthode mixte *stabilisée*.

¹MITC provient de “Mixed Interpolation of Tensorial Components”

Lorsque qu'on formule des éléments finis triangulaires, une quatrième condition qui garanti que la matrice de rigidité ne dépend pas de la numérotation des noeuds (ou de façon équivalente, de l'orientation des éléments) doit être aussi satisfaite: on parle d'"isotropie" des éléments.

Organisation du mémoire

Les trois premiers chapitres de cette thèse résument les concepts théoriques fondamentaux à retenir pour l'analyse théorique des coques. Dans le quatrième chapitre nous descrivons la formulation des "general shell elements", et en particulier des éléments MITC.

Dans une première phase on a passé en revue les travaux antérieurs, en particulier les résultats de la thèse de Phill-Seung Lee [45] achevée au MIT sous la direction de K.J. Bathe. Ensuite, nous avons formulé un test numérique qui nous aide à détecter le phénomène de verrouillage numérique membranaire pour les éléments finis MITC et on a testé différents choix de *tying points* pour des éléments finis triangulaires à six noeuds (ceux-ci sont l'objectif principal de notre travail). Ce test numérique que nous avons développé nous permet ainsi de savoir, *à priori*, si des modes parasites de membrane risquent d'apparaître.

Ensuite, on a formulé des éléments finis MITC triangulaires à six noeuds à partir des conclusions obtenues en utilisant ce test. Nous avons réalisé une analyse approfondie des résultats de convergence –en utilisant des normes adéquates– des différents éléments considérés pour des géométries variées et les catégories asymptotiques à flexion et membrane dominante, qui s'obtiennent en modifiant les conditions aux limites pour une même géométrie et force appliquée. Nous avons aussi fait une analyse énergétique détaillée et précise pour chaque cas, ce qui nous a permis de déduire qu'aucun des éléments présentés n'est assez robuste étant donné que (voir Chapitre 6)

- ou bien un fort verrouillage numérique se manifeste pour des problèmes à flexion dominante;
- ou sinon il y a des modes parasites de membrane qui apparaissent dans des situations à membrane dominante.

Il est à noter que les couches limites ont été soigneusement traitées pour chaque cas-test en particulier (voir Annexe E).

L'élément MITC6a qui avait déjà été introduit par Bathe & Lee 2004 [47] semble être le meilleur candidat triangulaire à six noeuds qu'on puisse trouver, mais il exhibe des modes parasites de membrane qui peuvent considérablement détériorer la solution dicrète pour des problèmes à membrane dominante (voir Chapitres 6 et 7). On a donc cherché une façon de filtrer ces modes sans remettre en cause la performance du MITC6a pour des problèmes à flexion dominante. On a alors défini un problème à membrane dominante spécialement conçu pour faire apparaître ces modes et qui nous permet ainsi de savoir comment ceux-ci se comportent

(voir Chapitre 7.2). On a déduit un moyen de filtrage en ajoutant des termes de stabilisation de cisaillement non réduit, et un nouvel élément nommé MITC6rs a aussi été formulé, lequel utilise la même réduction que le MITC6a pour la membrane, mais une interpolation un peu plus riche pour le cisaillement (voir Chapitre 7). Après une analyse détaillée, nous avons observé que les techniques de stabilisation présentées améliorent nettement les résultats obtenus pour des problèmes à membrane dominante, tandis que la performance de la technique MITC n'est pas trop altérée par cette ce traitement (voir Chapitre 7).

Pour compléter l'étude, on a considéré un problème mal posé bien connu en mécanique (Chapitre 8): le toit de Scordelis-Lo soumis à une force verticale. On sait bien que l'analyse asymptotique de ce problème peut être ramenée à une couche limite proche de la frontière libre, où la solution connaît des fortes variations (voir en particulier Chapelle & Bathe 2003 [31], Baiocchi & Lovadina 2002 [5], Sanchez-Hubert & Sanchez-Palencia 2001 [60]). On a écrit la formulation détaillée du problème mis à l'échelle dans la couche limite, ce qui correspond à une formulation pénalisée qui typiquement induira un verrouillage numérique, bien que différent de celui qui apparaît dans les cas à flexion dominante, et nous avons ensuite défini une norme adéquate pour étudier la convergence des déplacements. Ce cas-test nous a permis de vérifier que la performance de la technique MITC n'est pas endommagée par les méthodes de stabilisation formulées pour le filtrage des modes parasites de membrane.

Logiciels

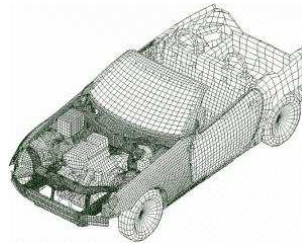
Les éléments finis que nous avons considérés ont été implémentés dans OpenFEM, un logiciel libre d'éléments finis – pour MATLAB et SCILAB – développé conjointement par le projet MACS et la société SDTools (<http://www-rocq.inria.fr/OpenFEM/>). Nous avons aussi développé des outils de calcul en FORTRAN qui sont exécutables depuis MATLAB (MEX-files). Les maillages ont été construits avec MODULEF (<http://www-rocq.inria.fr/modulef/>).

Financement

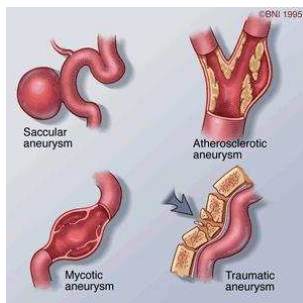
- “Fundación Caixa Galicia Claudio San Martin”
- Researching Training Network : "New Materials, Adaptive Systems and their Nonlinearities: Modelling, Control and Numerical Simulation" (HPRN-CT-2002-00284), European Commission's 5th Framework Programme



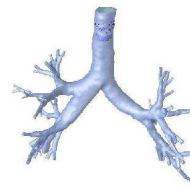
(a) Viaduc de Millau



(b) Carrosserie de voiture



(c) Anévrismes



(d) Bronches

Exemples coques

Contents

1	Shell preliminaries	11
1.1	Differential geometry	12
1.2	Kinematics	14
1.3	Shell mathematical models	16
1.3.1	The basic shell model	16
1.3.2	The s-m-b model	17
1.3.3	The m-b model	18
1.3.4	Plate models	19
2	Asymptotic analysis of shells	21
2.1	Geometrical influence	22
2.2	Loading influence	23
2.2.1	Non-inhibited shells	23
2.2.2	Inhibited shells	24
2.3	Influence of boundary conditions	24
3	Numerical locking	27
3.1	Example: Timoshenko beam model	28
3.1.1	Locking treatment	30
3.1.2	Numerical results	32
4	MITC triangular shell elements	35
4.1	Formulation of general shell elements	35
4.2	MITC shell finite elements	39
4.3	Element specifications	40
4.3.1	Ellipticity	41
4.3.2	Consistency	41
4.3.3	Inf-Sup condition	42
4.3.4	Spatial isotropy	43
5	Detecting membrane locking	47
5.1	Preliminaries	47
5.2	Membrane test	50
5.3	Conclusions	57

6	Assessing MITC triangular shell elements	61
6.1	Error measures	63
6.2	MITC elements	65
6.3	Benchmarks and numerical results	70
6.3.1	Clamped plate problem	70
6.3.2	Cylindrical shell problems	78
6.3.3	Axisymmetric hyperboloid shell problems	115
6.4	Concluding remarks on the assessment results	152
7	Improving the MITC6a shell finite element	155
7.1	MITC membrane spurious modes	156
7.2	The trace benchmark	158
7.2.1	MITC6a membrane spurious modes	159
7.2.2	P_2 and MITC6a solutions	161
7.3	Improving the MITC6a element	173
7.3.1	Weighted shear stabilization	173
7.3.2	Free boundary shear stabilization	175
7.3.3	A richer shear interpolation: the MITC6rs	176
7.4	The trace benchmark: improvements	178
7.5	Axisymmetric hyperboloid	202
7.5.1	Fully clamped hyperboloid shell problem	203
7.5.2	Bottom clamped hyperboloid shell problem	206
7.5.3	Free hyperboloid shell problem	209
7.6	Concluding remarks	260
8	The “Scordelis-Lo Roof”: a mixed behavior	263
8.1	The “Scordelis-Lo Roof” shell problem	264
8.2	The layer problem	266
8.3	Norms for the Scordelis-Lo Roof shell problem	275
8.4	Numerical computations and conclusions	277
A	The MITC4 element	295
B	MITC7 static condensation	297
C	Projection into shell meshes	299
D	The s-norm	305
E	Analysis of boundary layers	309
F	Other strategies	323
F.1	Projection into $\mathcal{V}_{0,h}$	326
F.2	Projection into $[\gamma(\mathcal{V}_{0,h})]^\perp$	327
F.3	Enhanced shell finite elements	328

Chapter 1

Shell preliminaries

A shell is a solid medium geometrically defined by a *midsurface* \mathcal{S} immersed in the physical space \mathcal{E} and a parameter t representing the thickness of the medium around this surface. The midsurface is normally described by a collection of charts from domains in \mathbb{R}^2 into \mathcal{E} . Since in complex configurations the analysis can be decomposed according to each chart and reference domain¹, we will focus on shells represented using a single chart. Henceforth, we will consider a shell with a midsurface \mathcal{S} defined by a 2D chart denoted by $\vec{\phi}$, i.e. an injective mapping from the closure of a bounded open subset $\omega \in \mathbb{R}^2$ into \mathcal{E} .

We use Greek indices for the components of surface tensors (in $\{1, 2\}$) and latin indices for components of 3D tensors (in $\{1, 2, 3\}$). The *Einstein summation convention on repeated indices* is assumed from now on.

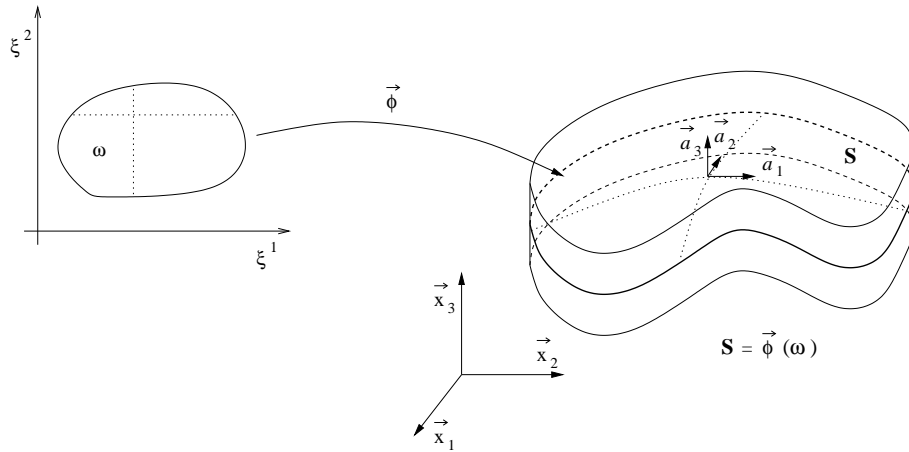


Figure 1.1: Shell geometry description

¹The global energy is the sum of energies on all subparts.

We assume that the $2D$ chart $\vec{\phi}$ is such that the vectors

$$\vec{a}_\alpha = \frac{\partial \vec{\phi}}{\partial \xi^\alpha} \quad (1.1)$$

are linearly independent at each point of the midsurface, and we introduce the unit normal vector

$$\vec{a}_3 = \frac{\vec{a}_1 \wedge \vec{a}_2}{\|\vec{a}_1 \wedge \vec{a}_2\|} \quad (1.2)$$

The $3D$ medium corresponding to the shell can be defined using a *curvilinear coordinate system* which consists of a reference domain

$$\Omega = \left\{ (\xi^1, \xi^2, \xi^3) \in \mathbb{R}^3 / (\xi^1, \xi^2) \in \omega, \xi^3 \in \left[-\frac{t(\xi^1, \xi^2)}{2}, \frac{t(\xi^1, \xi^2)}{2} \right] \right\} \quad (1.3)$$

and the $3D$ chart

$$\vec{\Phi}(\xi^1, \xi^2, \xi^3) = \vec{\phi}(\xi^1, \xi^2) + \xi^3 \vec{a}_3(\xi^1, \xi^2), \quad (\xi^1, \xi^2, \xi^3) \in \Omega \quad (1.4)$$

We recall that $t(\xi^1, \xi^2)$ is the thickness at the point of coordinates (ξ^1, ξ^2) .

We denote by $\mathcal{B} = \vec{\Phi}(\Omega)$ the region of the Euclidean space occupied by the shell body. Any point M in \mathcal{B} is uniquely defined by its coordinates in this curvilinear coordinate system, namely the three real numbers (ξ^1, ξ^2, ξ^3) such that

$$OM = \vec{\Phi}(\xi^1, \xi^2, \xi^3) \quad (1.5)$$

where O denotes the origin in \mathcal{E} .

The $3D$ chart $\vec{\Phi}$ together with the reference domain Ω give a natural parametrization of the shell body.

1.1 Differential geometry

For the ordinary derivatives of a generic tensor T , we adopt the classical notation

$$T_{,m} = \frac{\partial T}{\partial \xi^m}, \quad m = 1, 2, 3$$

At each point of the midsurface, we define the covariant basis of the tangent plane as the basis constituted by the vectors $\{\vec{a}_1, \vec{a}_2\}$ that we have defined in (1.1). We also introduce the contravariant basis $\{\vec{a}^1, \vec{a}^2\}$ given by

$$\vec{a}_\alpha \cdot \vec{a}^\beta = \delta_\alpha^\beta \quad (1.6)$$

where δ denotes the Kronecker symbol².

² $\delta_i^i = 1$ and $\delta_i^j = 0$ for $i \neq j$.

Using the definition of the 3D chart (1.4), at any point in \mathcal{B} of coordinates (ξ^1, ξ^2, ξ^3) we can consider the vectors \vec{g}_m defined by

$$\vec{g}_\alpha = \frac{\partial \vec{\Phi}}{\partial \xi^\alpha} = \vec{a}_\alpha + \xi^3 \vec{a}_{3,\alpha}, \quad \vec{g}_3 = \frac{\partial \vec{\Phi}}{\partial \xi^3} = \vec{a}_3 \quad (1.7)$$

We call $\{\vec{g}_1, \vec{g}_2, \vec{g}_3\}$ the local covariant basis at (ξ^1, ξ^2, ξ^3) and we recall that these vectors are tangent to the three coordinate curves passing through (ξ^1, ξ^2, ξ^3) . The associated local contravariant basis $\{\vec{g}^1, \vec{g}^2, \vec{g}^3\}$ is defined by

$$\vec{g}_m \cdot \vec{g}^n = \delta_m^n \quad (1.8)$$

as usual.

We introduce now some essential symmetric tensors for the analysis of shells:

- *The first fundamental form* of the surface \underline{a} is a crucial surface tensor whose covariant-covariant components are given by:

$$a_{\alpha\beta} = \vec{a}_\alpha \cdot \vec{a}_\beta \quad (1.9)$$

and the contravariant-contravariant components are:

$$a^{\alpha\beta} = \vec{a}^\alpha \cdot \vec{a}^\beta \quad (1.10)$$

The infinitesimal area corresponding to the differentials $(d\xi^1, d\xi^2)$ of the coordinates can be expressed as

$$dS = \sqrt{a} d\xi^1 d\xi^2 \quad (1.11)$$

with

$$a = a_{11}a_{22} - (a_{12})^2 \quad (1.12)$$

- *The second fundamental form* \underline{b} is also called the *curvature tensor* because it contains all the information about the curvature of the surface. Its covariant-covariant components are given by:

$$b_{\alpha\beta} = \vec{a}_3 \cdot \vec{a}_{\alpha,\beta} = -\vec{a}_{3,\beta} \cdot \vec{a}_\alpha \quad (1.13)$$

whereas the covariant-contravariant components are defined as:

$$b_\alpha^\beta = a^{\beta\lambda} b_{\lambda\alpha} \quad (1.14)$$

The mean and Gaussian curvatures of the surface can be respectively obtained by

$$H = \frac{1}{2} \text{tr}(\underline{b}) \quad (1.15)$$

and

$$K = \det(\underline{b}) \quad (1.16)$$

- The third fundamental form \underline{c} is obtained by a combination of the first and second forms, namely:

$$c_{\alpha\beta} = b_{\alpha\gamma} a^{\gamma\lambda} b_{\lambda\beta} \quad (1.17)$$

- The 3D metric tensor in covariant-covariant components is derived from (1.7):

$$\begin{aligned} g_{\alpha\beta} &= \vec{g}_\alpha \cdot \vec{g}_\beta = a_{\alpha\beta} - 2\xi^3 b_{\alpha\beta} + (\xi^3)^2 c_{\alpha\beta} \\ g_{\alpha 3} &= \vec{g}_\alpha \cdot \vec{g}_3 = 0 \\ g_{33} &= \vec{g}_3 \cdot \vec{g}_3 = 1 \end{aligned} \quad (1.18)$$

In the same way, the twice-contravariant components of this metric tensor are defined by

$$g^{mn} = \vec{g}^m \cdot \vec{g}^n \quad (1.19)$$

The infinitesimal volume corresponding to the coordinate differentials $(d\xi^1, d\xi^2, d\xi^3)$ can be expressed as:

$$dV = \sqrt{g} d\xi^1 d\xi^2 d\xi^3 \quad (1.20)$$

where g denotes the Jacobian corresponding to (ξ^1, ξ^2, ξ^3) that is given by the determinant of the matrix of coefficients $(g_{mn})_{m,n=1,2,3}$, and we have

$$\sqrt{g} = |\vec{g}_1 \cdot (\vec{g}_2 \wedge \vec{g}_3)| = \sqrt{a} (1 - 2H\xi^3 + K(\xi^3)^2) \quad (1.21)$$

Hence, the integral of a function h in curvilinear coordinates takes the form:

$$\int_{\Omega} h dV = \int_{\xi^1, \xi^2, \xi^3} h(\xi^1, \xi^2, \xi^3) \sqrt{g} d\xi^1 d\xi^2 d\xi^3 \quad (1.22)$$

Given a surface vector \underline{u} , we denote by $u_{\alpha|\beta}$ the *surface covariant derivative* of u_α defined as

$$u_{\alpha|\beta} = u_{\alpha,\beta} - \Gamma_{\alpha\beta}^\lambda u_\lambda \quad (1.23)$$

where $\Gamma_{\alpha\beta}^\lambda$ denote the surface Christoffel symbols

$$\Gamma_{\alpha\beta}^\lambda = \vec{a}_{\alpha,\beta} \cdot \vec{a}^\lambda \quad (1.24)$$

1.2 Kinematics

Mathematical shell models are usually based on kinematical assumptions. It is commonly assumed that *any material line orthogonal to the midsurface in the undeformed configuration remains straight and unstretched* during deformations.

This hypothesis is known as the *Reissner-Mindlin kinematical assumption* and displacements obtained when considering this assumption can be expressed by the following equation:

$$\vec{U}(\xi^1, \xi^2, \xi^3) = \vec{u}(\xi^1, \xi^2) + \xi^3 \theta_\lambda(\xi^1, \xi^2) \vec{a}^\lambda(\xi^1, \xi^2) \quad (1.25)$$

where $\vec{u}(\xi^1, \xi^2)$ typically represents the global displacement of a line in the direction of $\vec{a}_3(\xi^1, \xi^2)$ at the point of coordinates (ξ^1, ξ^2) in the undeformed configuration with all particles displacing by the same amount, and $\theta_\lambda(\xi^1, \xi^2) \vec{a}^\lambda(\xi^1, \xi^2)$ an infinitesimal rotation vector normal to that line (see Fig. 1.2).

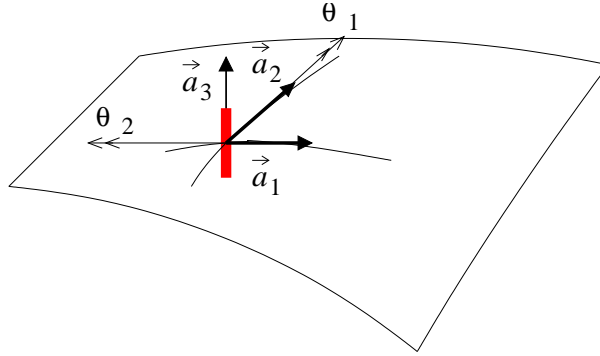


Figure 1.2: Infinitesimal rotations

From now on, the *Reissner-Mindlin kinematical assumption* is assumed for displacements in our analysis.

Given a general displacement $\vec{U}(\xi^1, \xi^2, \xi^3)$, the covariant-covariant components of the linearized 3D Green-Lagrange strain tensor are defined as:

$$e_{ij}(\vec{U}) = \frac{1}{2}(\vec{g}_i \cdot \vec{U}_{,j} + \vec{g}_j \cdot \vec{U}_{,i}) \quad i, j = 1, 2, 3 \quad (1.26)$$

When considering displacements that verify the *Reissner-Mindlin kinematical assumption*, this linearized strain tensor can be expressed as a function of the midsurface displacement \vec{u} and the surface rotation field $\underline{\theta} = \theta_\lambda \vec{a}^\lambda$. Therefore, using the definition of covariant differentiation (1.23) for surface tensors, we can evaluate (1.26) to obtain:

$$\begin{aligned} e_{\alpha\beta} &= \gamma_{\alpha\beta}(\vec{u}) + \xi^3 \chi_{\alpha\beta}(\vec{u}, \underline{\theta}) - (\xi^3)^2 \kappa_{\alpha\beta}(\underline{\theta}) \\ e_{\alpha 3} &= \zeta_\alpha(\vec{u}, \underline{\theta}) \\ e_{33} &= 0 \end{aligned} \quad (1.27)$$

with

$$\begin{aligned}
\gamma_{\alpha\beta}(\vec{u}) &= \frac{1}{2}(u_{\alpha|\beta} + u_{\beta|\alpha}) - b_{\alpha\beta}u_3 \\
\chi_{\alpha\beta}(\vec{u}, \underline{\theta}) &= \frac{1}{2}(\theta_{\alpha|\beta} + \theta_{\beta|\alpha} - b_{\beta}^{\lambda}u_{\lambda|\alpha} - b_{\alpha}^{\lambda}u_{\lambda|\beta}) + c_{\alpha\beta}u_3 \\
\kappa_{\alpha\beta}(\underline{\theta}) &= \frac{1}{2}(b_{\beta}^{\lambda}\theta_{\lambda|\alpha} + b_{\alpha}^{\lambda}\theta_{\lambda|\beta}) \\
\zeta_{\alpha}(\vec{u}, \underline{\theta}) &= \frac{1}{2}(\theta_{\alpha} + u_{3,\alpha} + b_{\alpha}^{\lambda}u_{\lambda})
\end{aligned} \tag{1.28}$$

The tensors $\underline{\underline{\gamma}}$, $\underline{\underline{\chi}}$ and $\underline{\underline{\zeta}}$ are respectively called the membrane, bending and shear strain tensors.

1.3 Shell mathematical models

Let us consider an isotropic linear elastic material. In a general curvilinear coordinate system, Hooke's law defines the contravariant-contravariant stress tensor components as

$$\sigma^{ij} = H^{ijkl}e_{kl} \tag{1.29}$$

with

$$H^{ijkl} = L_1 g^{ij}g^{kl} + L_2(g^{ik}g^{jl} + g^{il}g^{jk}) \tag{1.30}$$

where L_1 and L_2 represent the Lamé constants

$$L_1 = E \frac{\nu}{(1+\nu)(1-2\nu)}, \quad L_2 = \frac{E}{2(1+\nu)}$$

and E denotes Young's modulus and ν Poisson's ratio for the material in consideration.

1.3.1 The basic shell model

This model is mathematically crucial for understanding the essential characteristics of most classical shell models. It is based on the assumption that *the state of the stresses in the shell corresponds to plane stress tangent to the midsurface of the shell, at least approximately*, namely

$$\sigma^{33} = 0 \tag{1.31}$$

Taking into account the assumption of zero normal stress, we can write the equivalent modified constitutive equations:

$$\begin{aligned}
\sigma^{\alpha\beta} &= C^{\alpha\beta\lambda\mu}e_{\lambda\mu} \\
\sigma^{\alpha 3} &= \frac{1}{2}D^{\alpha\lambda}e_{\lambda 3}
\end{aligned} \tag{1.32}$$

with

$$\begin{aligned} C^{\alpha\beta\lambda\mu} &= \frac{E}{2(1+\nu)}(g^{\alpha\lambda}g^{\beta\mu} + g^{\alpha\mu}g^{\beta\lambda} + \frac{2\nu}{1-\nu}g^{\alpha\beta}g^{\lambda\mu}) \\ D^{\alpha\lambda} &= \frac{2E}{1+\nu}g^{\alpha\lambda} \end{aligned} \quad (1.33)$$

and the variational formulation directly derived from continuum mechanics reads

$$\int_{\Omega} \left[C^{\alpha\beta\lambda\mu} e_{\alpha\beta}(\vec{U}) e_{\lambda\mu}(\vec{V}) + D^{\alpha\lambda} e_{\alpha 3}(\vec{U}) e_{\lambda 3}(\vec{V}) \right] dV = \int_{\Omega} \vec{F} \cdot \vec{V} dV \quad (1.34)$$

where \vec{U} represents the unknown that satisfies the Reissner-Mindlin kinematical assumption and boundary conditions, and \vec{V} denotes an arbitrary test function

$$\vec{V}(\xi^1, \xi^2, \xi^3) = \vec{v}(\xi^1, \xi^2) + \xi^3 \eta_{\lambda}(\xi^1, \xi^2) \vec{a}^{\lambda}(\xi^1, \xi^2) \quad (1.35)$$

satisfying the same kinematical assumption and the appropriate boundary conditions (i.e. zero displacement wherever the displacement \vec{U} is described). The quantity \vec{F} denotes the external 3D loading applied to the shell structure.

The *basic shell model* is defined as the model represented by the variational formulation (1.34). It is the model considered in our shell analysis.

1.3.2 The s-m-b model

The shear-membrane-bending (s-m-b) model is directly obtained from the basic shell model by truncating the expressions to the lowest-order terms with respect to the coordinate ξ^3 and considering that the loading is constant through the thickness. We substitute:

- $\gamma_{\alpha\beta} + \xi^3 \chi_{\alpha\beta}$ for $e_{\alpha\beta}$ (see (1.27))
- \sqrt{a} for \sqrt{g}
- ${}^0C^{\alpha\beta\lambda\mu}$ and ${}^0D^{\alpha\lambda}$ respectively for $C^{\alpha\beta\lambda\mu}$ and $D^{\alpha\lambda}$, where

$$\begin{aligned} {}^0C^{\alpha\beta\lambda\mu} &= \frac{E}{2(1+\nu)}(a^{\alpha\lambda}a^{\beta\mu} + a^{\alpha\mu}a^{\beta\lambda} + \frac{2\nu}{1-\nu}a^{\alpha\beta}a^{\lambda\mu}) \\ {}^0D^{\alpha\lambda} &= \frac{2E}{1+\nu}a^{\alpha\lambda} \end{aligned} \quad (1.36)$$

In such a case, the following variational problem is obtained:

$$\begin{aligned} \int_{\omega} {}^0C^{\alpha\beta\lambda\mu} \left[t\gamma_{\alpha\beta}(\vec{u})\gamma_{\lambda\mu}(\vec{v}) + \frac{t^3}{12}\chi_{\alpha\beta}(\vec{u}, \underline{\theta})\chi_{\lambda\mu}(\vec{v}, \underline{\eta}) \right] dS + \\ \int_{\omega} t {}^0D^{\alpha\lambda} \zeta_{\alpha}(\vec{u}, \underline{\theta}) \zeta_{\lambda}(\vec{v}, \underline{\eta}) dS = \int_{\omega} t \vec{F} \cdot \vec{v} dS \end{aligned} \quad (1.37)$$

for arbitrary test functions $(\vec{v}, \underline{\eta})$, and it is the variational formulation that defines the shear-membrane-bending model.

There is another formulation frequently used in engineering analysis that introduces a coefficient k smaller than one, *the shear correction factor*, which accounts for the fact that the transverse shear strain is not constant through the thickness of the shell and must vanish on the outside surfaces³:

$$\int_{\omega} {}^0C^{\alpha\beta\lambda\mu} \left[t\gamma_{\alpha\beta}(\vec{u})\gamma_{\lambda\mu}(\vec{v}) + \frac{t^3}{12}\chi_{\alpha\beta}(\vec{u}, \underline{\theta})\chi_{\lambda\mu}(\vec{v}, \underline{\eta}) \right] dS + \quad (1.38)$$

$$k \int_{\omega} t {}^0D^{\alpha\lambda}\zeta_{\alpha}(\vec{u}, \underline{\theta})\zeta_{\lambda}(\vec{v}, \underline{\eta}) dS = \int_{\omega} t\vec{F} \cdot \vec{v} dS$$

1.3.3 The m-b model

The membrane-bending (m-b) model includes a stronger assumption: the *Kirchhoff-Love kinematical assumption*. This hypothesis states that any material line originally orthogonal to the midsurface in the undeformed configuration remains straight and unstretched (Reissner-Mindlin kinematical assumption) and *always orthogonal to the midsurface* during the deformations. So, a new constraint is introduced:

Proposition 1 *A general displacement field $\vec{U}(\xi^1, \xi^2, \xi^3)$ satisfies the Kirchhoff-Love kinematical assumption if and only if the displacement field \vec{U} can be expressed under the form*

$$\vec{U}(\xi^1, \xi^2, \xi^3) = \vec{u}(\xi^1, \xi^2) + \xi^3\theta_{\lambda}(\xi^1, \xi^2)\vec{a}^{\lambda}(\xi^1, \xi^2) \quad (1.39)$$

with

$$\theta_{\lambda} = -u_{3,\lambda} - b_{\lambda}^{\mu}u_{\mu}, \quad \lambda = 1, 2 \quad (1.40)$$

Namely

$$\zeta(\vec{u}, \underline{\theta}) = \underline{0} \quad (1.41)$$

(See [31] for the proof).

For a Kirchhoff-Love displacement, the expression of $\underline{\theta}$ given by (1.40) allows us to represent the bending strain tensor $\underline{\chi}$ by:

$$\chi_{\alpha\beta}(\vec{u}, \underline{\theta}) = -\bar{\rho}_{\alpha\beta}(\vec{u}) \quad (1.42)$$

where

$$\bar{\rho}_{\alpha\beta}(\vec{u}) = u_{3|\alpha\beta} + b_{\alpha|\beta}^{\mu}u_{\mu} + b_{\alpha}^{\mu}u_{\mu|\beta} + b_{\beta}^{\mu}u_{\mu|\alpha} - c_{\alpha\beta}u_3 \quad (1.43)$$

It can be shown that for a smooth displacement field \vec{u} , the tensor $\bar{\rho}(\vec{u})$ is the tensor of linearized change of curvature of the midsurface (see [31]).

If we consider in (1.37) the unknown and arbitrary test functions as displacements that satisfy the Kirchhoff-Love kinematical assumption, we obtain the variational form associated with the membrane-bending model:

$$\int_{\omega} {}^0C^{\alpha\beta\lambda\mu} \left[t\gamma_{\alpha\beta}(\vec{u})\gamma_{\lambda\mu}(\vec{v}) + \frac{t^3}{12}\bar{\rho}_{\alpha\beta}(\vec{u})\bar{\rho}_{\lambda\mu}(\vec{v}) \right] dS = \int_{\omega} t\vec{F} \cdot \vec{v} dS \quad (1.44)$$

³For any model deriving from the present one, the same coefficient k can be introduced.

1.3.4 Plate models

Plate models can be obtained from shell models by considering planar midsurfaces. In such a case, the curvature tensor is zero and the normal vector \vec{a}_3 is constant. Consequently, from (1.18), (1.33) and (1.36) we obtain

$$\begin{aligned} g_{\alpha\beta} &= a_{\alpha\beta} \\ g &= a \end{aligned} \tag{1.45}$$

and

$$\begin{aligned} {}^0C^{\alpha\beta\lambda\mu} &= C^{\alpha\beta\lambda\mu} \\ {}^0D^{\alpha\lambda} &= D^{\alpha\lambda} \end{aligned} \tag{1.46}$$

The strain measures take also a simpler form and the unknowns $\underline{u} \equiv (u_1, u_2)$ can be independently treated from $(u_3, \underline{\theta})$.

Two decoupled variational problems describe the s-m-b model for plates:

- *The membrane problem:*

$$\int_{\omega} tC^{\alpha\beta\lambda\mu} \gamma_{\alpha\beta}(\underline{u}) \gamma_{\lambda\mu}(\underline{v}) dS = \int_{\omega} t\underline{F} \cdot \underline{v} dS \tag{1.47}$$

where

$$\underline{F} \cdot \underline{v} = F^1 v_1 + F^2 v_2 \tag{1.48}$$

for any test function $\underline{v} \equiv (v_1, v_2)$.

- *The Reissner-Mindlin plate model:*

$$\int_{\omega} \frac{t^3}{12} C^{\alpha\beta\lambda\mu} \chi_{\alpha\beta}(\underline{\theta}) \chi_{\lambda\mu}(\underline{\eta}) dS + \int_{\omega} tD^{\alpha\lambda} \zeta_{\alpha}(u_3, \underline{\theta}) \zeta_{\lambda}(v_3, \underline{\eta}) dS = \int_{\omega} tF_3 v_3 dS \tag{1.49}$$

for any test function $(v_3, \underline{\eta})$.

For the m-b model for plates, the *membrane problem* remains the same, whereas the second problem differs and it is given by:

$$\int_{\omega} \frac{t^3}{12} C^{\alpha\beta\lambda\mu} \bar{\rho}_{\alpha\beta}(u_3) \bar{\rho}_{\lambda\mu}(v_3) dS = \int_{\omega} tF_3 v_3 dS \tag{1.50}$$

for any test function v_3 . This variational problem is known as the *Kirchhoff-Love plate model*.

Chapter 2

Asymptotic analysis of shells

A shell is known to be a *thin* structure, which means that one dimension –the thickness– is smaller by several orders of magnitude as compared to the other two dimensions of the structure.

Let us denote by L an overall characteristic dimension of the shell. We define the relative thickness

$$\varepsilon = \frac{t_{min}}{L} \quad (2.1)$$

where t_{min} denotes the minimum thickness over the surface. We also introduce the *thickness profile*

$$l = \frac{t}{\varepsilon} \quad (2.2)$$

A family of shell structures with the same midsurface and thickness profile can be obtained by simply making $\varepsilon \rightarrow 0$ and keeping l fixed. The overall thickness becomes smaller, which allows us to study the asymptotic behavior of the shell.

In the previous chapter we have introduced some classical shell models. We see that the thickness t appears with different powers in the bilinear forms associated with the s-m-b and m-b shell models, respectively described by (1.37) and (1.44). It is interesting to determine how the properties of these models are affected when this parameter vanishes, i.e. it is important to know if the model converges towards a limit model when t tends to zero, which will allow us to use a “simpler” formulation instead of the original one on the one hand, and know the asymptotic behavior of the thin structure, on the other hand.

We observe that we can introduce a general variational formulation for both models referred above as follows:

Find $U^\varepsilon \in \mathcal{V}$ such that

$$\varepsilon^3 A_b(U^\varepsilon, V) + \varepsilon A_m(U^\varepsilon, V) = F^\varepsilon(V), \quad \forall V \in \mathcal{V} \quad (2.3)$$

where

U^ε denotes the unknown solution;

\mathcal{V} is the Sobolev space containing the solution;

V denotes an arbitrary test function;

A_b is a scaled representation of the bending energy;

A_m is a scaled representation of the membrane energy for the m-b model and of the membrane and shear energy for the s-m-b model;

F^ε represents the external virtual work.

We emphasize that the bilinear forms A_b and A_m are independent of the thickness parameter ε . We assume that essential boundary conditions are prescribed in such a way that *no rigid motion is allowed*.

The asymptotic behavior of a shell depends on the geometrical nature of the midsurface, boundary conditions and applied load, as we describe below (see Fig. 2.1).

2.1 Geometrical influence

We introduce a proper closed subspace of \mathcal{V} that plays a special role in the asymptotic analysis of shells:

$$\mathcal{V}_0 = \{V \in \mathcal{V} | A_m(V, V) = 0\} \quad (2.4)$$

This subspace \mathcal{V}_0 is called the *subspace of pure-bending displacements* because it corresponds to zero membrane¹ and shear energies. The elements $V \equiv (\vec{v}, \underline{\eta})$ of this space are characterized by:

$$\underline{\zeta}(\vec{v}, \underline{\eta}) = \underline{0} \quad (2.5)$$

and

$$\underline{\underline{\gamma}}(\vec{v}) = \underline{\underline{0}} \quad (2.6)$$

Equation (2.5) gives

$$\underline{\eta} = -(\underline{\nabla} v_3 + \underline{\underline{b}} \cdot \underline{v}) \quad (2.7)$$

and then the system of partial differential equations (2.6) completely characterizes the subspace of inextensional displacements (whether or not pure bending is inhibited). Its nature – elliptic, parabolic or hyperbolic – is the same as the geometric nature of the midsurface at the point in consideration (see [59]). In addition, in the parabolic and hyperbolic case, the characteristics of the system are also the asymptotic lines of the surface.

Depending on the content of \mathcal{V}_0 , the shell is said to have:

- “non-inhibited pure bending”, when $\mathcal{V}_0 \neq \{0\}$,
- “inhibited pure bending”, if $\mathcal{V}_0 = \{0\}$.

¹For this reason, elements of \mathcal{V}_0 are also called *inextensional displacements*

2.2 Loading influence

In order to study the asymptotic behavior as ε tends to zero, we will scale the right-hand side in the form:

$$F^\varepsilon(V) = \varepsilon^\rho G(V) \quad (2.8)$$

where $G \in \mathcal{V}'$ must be independent of ε and $\rho \in \mathbb{R}$. As it is well known, there exists at most one exponent ρ that provides an admissible asymptotic behavior (see [31]), which is equivalent to have a finite non-zero limit for the equivalent scaled strain energy:

$$\varepsilon^{3-\rho} A_b(U^\varepsilon, U^\varepsilon) + \varepsilon^{1-\rho} A_m(U^\varepsilon, U^\varepsilon) \quad (2.9)$$

In such case it can be shown that

$$1 \leq \rho \leq 3 \quad (2.10)$$

We refer the reader to [31] for a detailed proof, see also [19], [5].

2.2.1 Non-inhibited shells

This situation usually results in the bending-dominated state.

- If the loading activates the pure bending displacements, namely if

$$\exists V \in \mathcal{V}_0 / G(V) \neq 0 \quad (2.11)$$

it can be shown that a proper loading scaling is

$$\rho = 3 \quad (2.12)$$

(see [61], [53]). The limit problem is given by:

Find $U^0 \in \mathcal{V}_0$ such that

$$A_b(U^0, V) = G(V), \quad \forall V \in \mathcal{V}_0 \quad (2.13)$$

and the following proposition holds (see [31]):

Proposition 2 *Assume that $\mathcal{V}_0 \neq \{0\}$.*

Then, setting $\rho = 3$, U^ε converges strongly into \mathcal{V} to U^0 , the solution of (2.13). Moreover, we have:

$$\lim_{\varepsilon \rightarrow 0} \frac{1}{\varepsilon^2} A_m(U^\varepsilon, U^\varepsilon) = 0 \quad (2.14)$$

- When the loading does not activate \mathcal{V}_0 , we have an unstable “membrane-dominated” situation (see [31] and the references therein).

2.2.2 Inhibited shells

In this case we introduce the subspace \mathcal{V}_m , which is the completion of the space \mathcal{V} with respect to the *membrane norm* $\|\cdot\|_m$ defined by the bilinear form A_m :

$$\|V\|_m = \sqrt{A_m(V, V)}, \quad V \in \mathcal{V} \quad (2.15)$$

- If $G \in \mathcal{V}'_m$ (i.e. G is an admissible membrane loading²), the adequate load-scaling factor corresponds to

$$\rho = 1 \quad (2.16)$$

and the membrane-dominated limit problem reads:

Find $U^m \in \mathcal{V}_m$ such that

$$A_m(U^m, V) = G(V), \quad \forall V \in \mathcal{V}_m \quad (2.17)$$

Furthermore, the following proposition holds (see [62], [52], [31]):

Proposition 3 *Assume that pure bending is not inhibited and also that $G \in \mathcal{V}'_m$. Then, setting $\rho = 1$, U^ε converges strongly in \mathcal{V}_m to U^m the solution of (2.17). Moreover, we have:*

$$\lim_{\varepsilon \rightarrow 0} \varepsilon^2 A_b(U^\varepsilon, U^\varepsilon) = 0 \quad (2.18)$$

- If G is a non-admissible membrane loading, the membrane problem is ill-posed, but other admissible asymptotic behaviors may exist with $1 < \rho < 3$ (see [31] and the references therein).

2.3 Influence of boundary conditions

Even if the geometric nature of the midsurface plays a crucial role in the asymptotic behavior, it also depends on the boundary conditions that together with the system of differential equations (2.6) define a Cauchy problem (see [31] and the references therein).

For example, when considering elliptic surfaces, imposing zero displacements on the whole boundary is sufficient to inhibit pure bending displacements and the membrane problem set in \mathcal{V}_m is well-posed. But if the displacements are fixed only on a limited part of the boundary, we fall in an ill-posed membrane problem (see [59], [36], [48]).

² $G \in \mathcal{V}'_m$ is equivalent to $|G(V)| \leq C(A_m(V, V))^{1/2} \quad \forall V \in \mathcal{V}$ with C constant, and this condition ensures that the loading can be resisted by membrane stresses only.

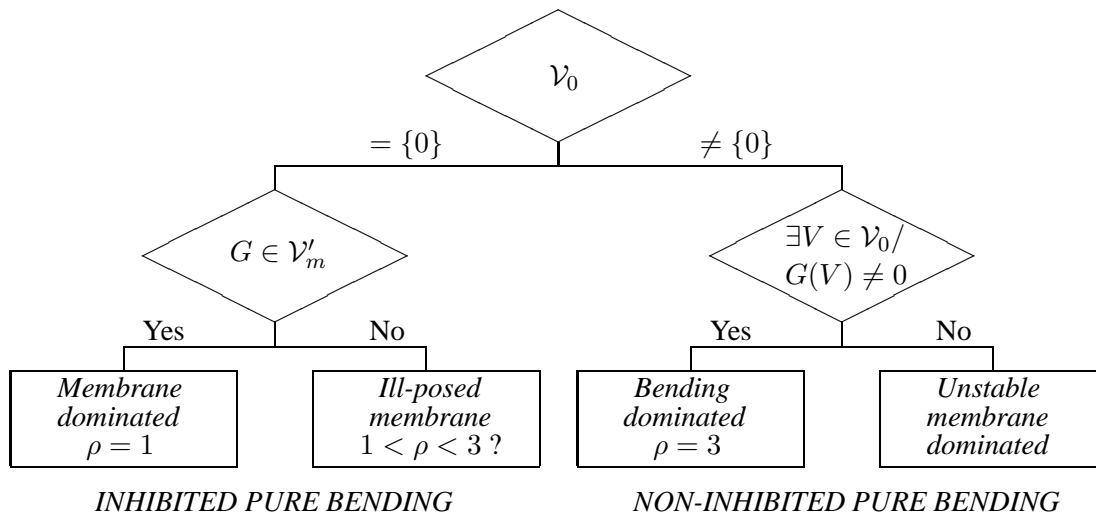


Figure 2.1: Asymptotic behavior of shells.

Chapter 3

Numerical locking

The *numerical locking phenomena* have been deeply analyzed for years and new strategies different from standard shell finite elements have been designed (we refer the reader to [29], [23], [6] and the references therein).

As we have seen in the previous chapter, shell structures can show different behaviors with decreasing thickness depending on the shell geometry, boundary conditions and applied loading. Shell mathematical models and finite elements incorporate kinematical assumptions pertaining to the displacement distribution across the thickness of the structure, which avoids discretizing the problem across the transverse direction, and only the midsurface –or equivalently the $2D$ domain that corresponds to the in-plane coordinates– needs to be meshed. Uniform convergence of the finite element solution with respect to the thickness parameter is sought as *the accuracy of the finite element solution as compared to the exact solution of the shell model must not depend on the thickness value*. Furthermore, the convergence rate should be optimal (with respect to the shape functions used).

In general, standard finite element techniques –such as displacement-based shell finite elements– are known to give finite element approximations in bending-dominated –or otherwise penalized– situations that tend to deteriorate when the thickness of the structure gets small. Namely, the phenomena of *numerical locking* occurs, giving an exceedingly stiff behavior of the thin structure. In a bending-dominated framework, the finite element method convergence is influenced by the content of

$$\mathcal{V}_h \cap \mathcal{V}_0 \quad (3.1)$$

In the worst case, we can have

$$\mathcal{V}_h \cap \mathcal{V}_0 = \{0\} \quad (3.2)$$

and total loss of convergence would result since

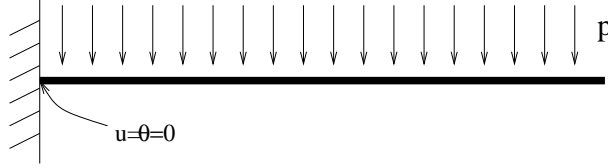
$$\lim_{\varepsilon \rightarrow 0} U_h^\varepsilon = 0 \neq \lim_{\varepsilon \rightarrow 0} U^\varepsilon = U^0 \quad (3.3)$$

In order to quickly illustrate this difficulty, we consider a particular Timoshenko beam problem that asymptotically shows a bending-dominated behavior

and two possible cures to the locking phenomena appearing in this framework are proposed.

3.1 Example: Timoshenko beam model

Let us consider a straight beam in plane stress conditions, of length L , constant rectangular cross-section S and constant thickness t , clamped at $x = 0$ and loaded by its own weight.



The variational formulation for this problem can be derived from the Reissner-Mindlin plate model by using the assumption that the displacement and rotation quantities do not change in the direction orthogonal to the plane of the beam, and that the rotation causing displacements in this orthogonal direction is zero. It reads:

Find $(u, \theta) \in \mathcal{V}$ such that

$$EI \int_0^L \theta' \eta' ds + GS k \int_0^L (u' - \theta)(v' - \eta) ds = - \int_0^L \rho g S v ds, \forall (v, \eta) \in \mathcal{V} \quad (3.4)$$

with

$$\mathcal{V} = \{(v, \eta) \in (H^1(]0, L[))^2; v(0) = \eta(0) = 0\} \quad (3.5)$$

and where g represents the gravity acceleration for this particular problem, u denotes the transverse displacement and θ the rotation of a cross-section, and the test functions (v, η) are defined in a similar way; ρ represents the density of the material, E Young's modulus, ν Poisson's ratio, G the shear modulus, I the inertia moment for the section given by

$$I = \frac{St^2}{12} \quad (3.6)$$

and k a shear correction factor (in general, $k = 5/6$).

The subspace of pure bending displacements

$$\mathcal{V}_0 = \{(v, \eta) \in \mathcal{V}; v' - \eta = 0\} \quad (3.7)$$

is never reduced to zero and the asymptotic behavior corresponds to a bending dominated situation. As a consequence, using the parameters:

$$\varepsilon = \frac{1}{L} \sqrt{\frac{EI}{GS k}}, \quad \tilde{p} = \frac{\rho g S L^2}{EI} \quad (3.8)$$

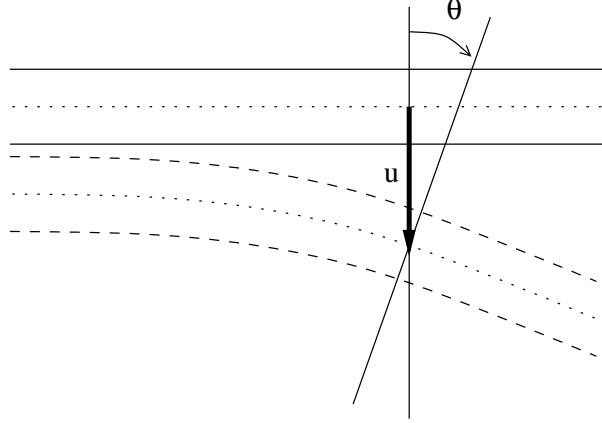


Figure 3.1: Original beam - Deformed beam

the loading can be scaled by ε^3 and we obtain an equivalent formulation to (3.4) that corresponds to our general framework in a bending-dominated situation¹:

Find $(u^\varepsilon, \theta^\varepsilon) \in \mathcal{V}$ such that

$$L^2 \int_0^L \theta^{\varepsilon'} \eta' ds + \frac{1}{\varepsilon^2} \int_0^L (u^{\varepsilon'} - \theta^\varepsilon)(v' - \eta) ds = - \int_0^L \tilde{p} v ds, \forall (v, \eta) \in \mathcal{V} \quad (3.9)$$

We know that the sequence $\{(u^\varepsilon, \theta^\varepsilon)\}_\varepsilon$ converges for the H^1 -norm –namely the norm of \mathcal{V} – to the solution of the limit problem:

Find $(u^0, \theta^0) \in \mathcal{V}_0$ such that

$$L^2 \int_0^L \theta^{0'} \eta' ds = - \int_0^L \tilde{p} v ds, \forall (v, \eta) \in \mathcal{V}_0 \quad (3.10)$$

which is the formulation of the Bernoulli beam problem in plane strain conditions².

This shell problem can be discretized using P_1 -Lagrange finite elements. The discretized variational formulation reads:

Find $(u_h^\varepsilon, \theta_h^\varepsilon) \in \mathcal{V}_h$ that satisfies

$$L^2 \int_0^L \theta_h^{\varepsilon'} \eta' ds + \frac{1}{\varepsilon^2} \int_0^L (u_h^{\varepsilon'} - \theta_h^\varepsilon)(v' - \eta) ds = - \int_0^L \tilde{p} v ds, \forall (v, \eta) \in \mathcal{V}_h \quad (3.11)$$

where \mathcal{V}_h denotes the finite element space for displacements. Keeping h fixed, the discrete solutions $(u_h^\varepsilon, \theta_h^\varepsilon)$ must converge in the H^1 -norm to the solution of the limit problem:

¹Notice that ε is proportional to t , even if a different definition has been set up in order to obtain a simpler formulation.

²This formulation corresponds to the Kirchhoff-Love kinematical assumption (1.41).

Find $(u_h^0, \theta_h^0) \in \mathcal{V}_h \cap \mathcal{V}_0$ that satisfies

$$L^2 \int_0^L \theta_h^{0t} \eta' ds = - \int_0^L \tilde{p} v ds, \forall (v, \eta) \in \mathcal{V}_h \cap \mathcal{V}_0 \quad (3.12)$$

However, *numerical locking* occurs. In fact, $\mathcal{V}_h \cap \mathcal{V}_0$ is exactly reduced to the zero displacement in this case, which does not correspond at all with the exact solution of the problem that can be analytically calculated. In practice, the thickness never becomes zero, but the beam, as seen through the finite element analysis, behaves increasingly stiffly as the thickness gets smaller. Consequently, uniform convergence is not achieved at all.

3.1.1 Locking treatment

In order to avoid numerical locking in the framework described above, the following solutions can be undertaken:

P_3 -Hermite finite elements

We can directly solve the limit problem (3.10) using P_3 -Hermite finite elements. In this case, the continuum problem to be solved is called the *Bernoulli beam problem in plane stress conditions*, and it is defined by the following variational formulation:

Find $u \in \mathcal{W}$ that satisfies

$$L^2 \int_0^L u'' v'' ds = - \int_0^L \tilde{p} v ds \quad \forall v \in \mathcal{W} \quad (3.13)$$

where:

$$\mathcal{W} = \{v \in H^2([0, L]); v(0) = v'(0) = 0\} \quad (3.14)$$

Mixed formulations

Given ε , an auxiliary unknown is introduced:

$$\gamma^\varepsilon = \frac{1}{\varepsilon^2} (u^{\varepsilon t} - \theta^\varepsilon) \in \mathcal{T} = L^2([0, L]) \quad (3.15)$$

and the following mixed variational formulation is equivalent to (3.9):

Find $((u^\varepsilon, \theta^\varepsilon), \gamma^\varepsilon) \in \mathcal{V} \times \mathcal{T}$ that satisfies

$$\begin{cases} L^2 \int_0^L \theta^{\varepsilon t} \eta' ds + \int_0^L \gamma^\varepsilon (v' - \eta) ds = f(v) & \forall (v, \eta) \in \mathcal{V} \\ \int_0^L (u^{\varepsilon t} - \theta^\varepsilon) r ds - \varepsilon^2 \int_0^L \gamma^\varepsilon r ds = 0 & \forall r \in \mathcal{T} \end{cases} \quad (3.16)$$

where

$$f(v) = - \int_0^L \tilde{p} v ds \quad (3.17)$$

It is important to notice that the parameter ε appears with a positive exponent in (3.16), and the candidate limit problem reads

Find $((u^0, \theta^0), \gamma^0) \in \mathcal{V} \times \mathcal{T}$ that satisfies

$$\begin{cases} L^2 \int_0^L \theta^{0r} \eta' ds + \int_0^L \gamma^0 (v' - \eta) ds = f(v) & \forall (v, \eta) \in \mathcal{V} \\ \int_0^L (u^{0r} - \theta^0) r ds = 0 & \forall r \in \mathcal{T} \end{cases} \quad (3.18)$$

The subspace \mathcal{V}_0 defined by (3.7) is equivalent to:

$$\mathcal{V}_0 = \left\{ (v, \eta) \in \mathcal{V}; \quad \int_0^L (v' - \eta) r ds = 0, \quad \forall r \in \mathcal{T} \right\} \quad (3.19)$$

and problems (3.16) and (3.18) are well-posed (see [31] and references therein).

Polynomial P_p continuous shape functions can be used for the discretization of u and θ , and P_{p-1} discontinuous shape functions for the scaled shear force γ , with $p \geq 1$, which respectively define the discrete subspaces \mathcal{V}_h and \mathcal{T}_h . The associated discretized problems are

Find $((u_h^\varepsilon, \theta_h^\varepsilon), \gamma_h^\varepsilon) \in \mathcal{V}_h \times \mathcal{T}_h$ that satisfies

$$\begin{cases} L^2 \int_0^L \theta_h^{\varepsilon r} \eta' ds + \int_0^L \gamma_h^\varepsilon (v' - \eta) ds = f(v) & \forall (v, \eta) \in \mathcal{V}_h \\ \int_0^L (u_h^{\varepsilon r} - \theta_h^\varepsilon) r ds - \varepsilon^2 \int_0^L \gamma_h^\varepsilon r ds = 0 & \forall r \in \mathcal{T}_h \end{cases} \quad (3.20)$$

and the limit formulation reads

Find $((u_h^0, \theta_h^0), \gamma_h^0) \in \mathcal{V}_h \times \mathcal{T}_h$ that satisfies

$$\begin{cases} L^2 \int_0^L \theta_h^{0r} \eta' ds + \int_0^L \gamma_h^0 (v' - \eta) ds = f(v) & \forall (v, \eta) \in \mathcal{V}_h \\ \int_0^L (u_h^{0r} - \theta_h^0) r ds = 0 & \forall r \in \mathcal{T}_h \end{cases} \quad (3.21)$$

Once more, the analysis of problem (3.21) involves the subspace:

$$\mathcal{V}_{0h} = \left\{ (v, \eta) \in \mathcal{V}_h; \quad \int_0^L (v' - \eta) r ds = 0 \quad \forall r \in \mathcal{T}_h \right\} \quad (3.22)$$

Its elements must verify the constraint:

$$\Pi_h(v' - \eta) = v' - \Pi_h(\eta) = 0 \quad (3.23)$$

where Π_h denotes the L^2 -projection onto the subspace \mathcal{T}_h . Notice that v' already lies in the subspace of discontinuous piecewise P_{p-1} polynomials (namely, in \mathcal{T}_h).

It can be shown that the discretized mixed-formulations (3.20) and (3.21) respectively have a unique solution that converges to the exact ones in h (see [31]). Notice that the second equation in (3.20) can be rewritten as:

$$\gamma_h^\varepsilon = \varepsilon^{-2} \Pi_h(u_h^{\varepsilon r} - \theta_h^\varepsilon) \quad (3.24)$$

and, as a consequence, the problem to be considered reads:

Find $(u_h^\varepsilon, \theta_h^\varepsilon) \in \mathcal{V}_h$ such that

$$L^2 \int_0^L \theta_h^{\varepsilon'} \eta' ds + \frac{1}{\varepsilon^2} \int_0^L \Pi_h(u_h^{\varepsilon'} - \theta_h^\varepsilon)(v' - \eta) ds = - \int_0^L \tilde{p} v ds, \forall (v, \eta) \in \mathcal{V}_h \quad (3.25)$$

Given $\varphi \in L^2(]0, L[)$, $\Pi_h(\varphi) \in \mathcal{T}_h$ is defined as:

$$\int_0^L \Pi_h(\varphi) r ds = \int_0^L \varphi r ds \quad \forall r \in \mathcal{T}_h \quad (3.26)$$

We clearly see that for $\varphi = u_h^{\varepsilon'} - \theta_h^\varepsilon$ and $r = v' - \eta$ we have:

$$\int_0^L \Pi_h(u_h^{\varepsilon'} - \theta_h^\varepsilon)(v' - \eta) ds = \int_0^L \Pi_h(u_h^{\varepsilon'} - \theta_h^\varepsilon) \Pi_h(v' - \eta) ds \quad (3.27)$$

So, the first part of equation (3.25) *corresponds to a symmetric bilinear form*.

Then, we have seen that by introducing a mixed formulation originally equivalent to the original displacement-based problem given by (3.9), we can finally deduce a modified finite element problem in the displacement and rotation variables to be solved, even if the continuous mixed formulation introduces one additional unknown field (the scaled shear force).

We can conclude that the modified finite element problem obtained converges uniformly in ε , thus it is proven to be *locking-free*³.

3.1.2 Numerical results

A mesh of 20 finite elements has been used for the discretization of a beam of length $L = 5$ m, width $l = 0.5$ m and thickness $t = 0.5$ m, Young's modulus $E = 30000$ MPa, Poisson's ratio $\nu = 0.3$ and density $\rho = 3.1 \text{ tm}^{-3}$. The shear modulus is given by

$$G = E/2(1 + \nu) \quad (3.28)$$

and a shear correction factor $k = 5/6$ has been introduced into the variational formulations.

Even if this problem is fairly simple and only one thickness value is considered, the numerical results show that the bending nature of the problem is not captured when using standard finite elements. The analytical solution can be easily calculated, and when comparing the discretized solution obtained using P_1 -Lagrange finite elements to the analytical values, we clearly see that the beam behaves too stiffly: shear locking occurs, although not so striking because t is considerably big (refer to Fig. 3.2). But the results obtained when using either P_3 -Hermite finite elements (*Bernoulli beam*) or the operator Π_h —which corresponds to the L^2 -projection onto constants in this case—are substantially improved and closer to exact values (see Figs. 3.3 and 3.4).

³For the results of convergence see [31] and references therein.

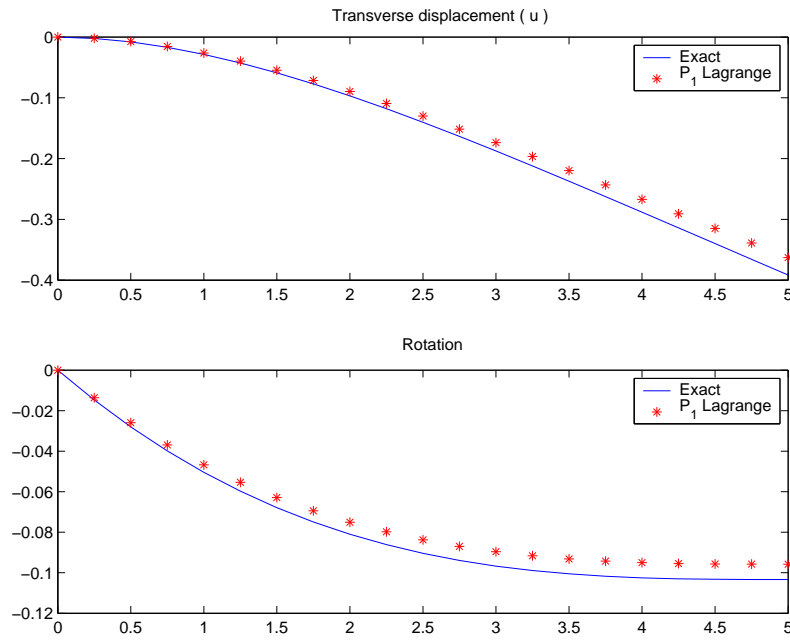
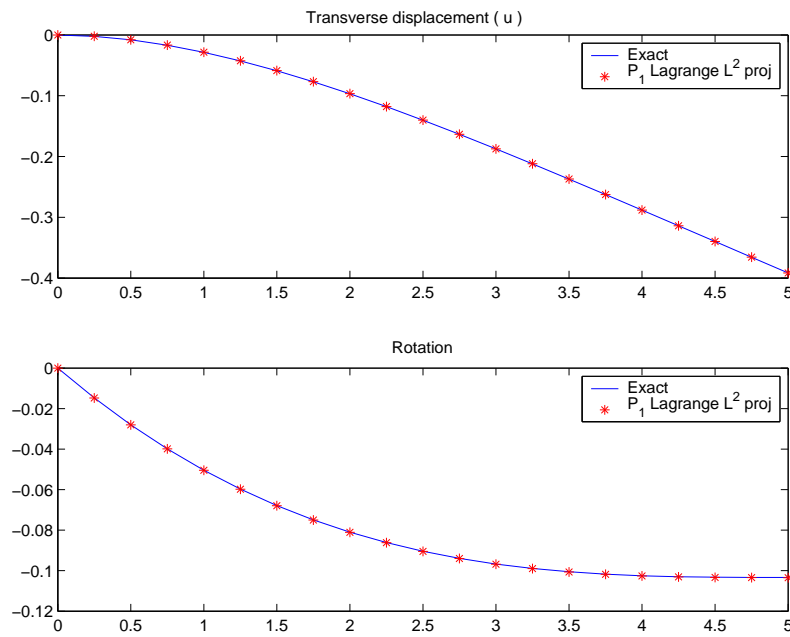


Figure 3.2: Timoshenko Beam

Figure 3.3: Timoshenko Beam - L^2 -projection

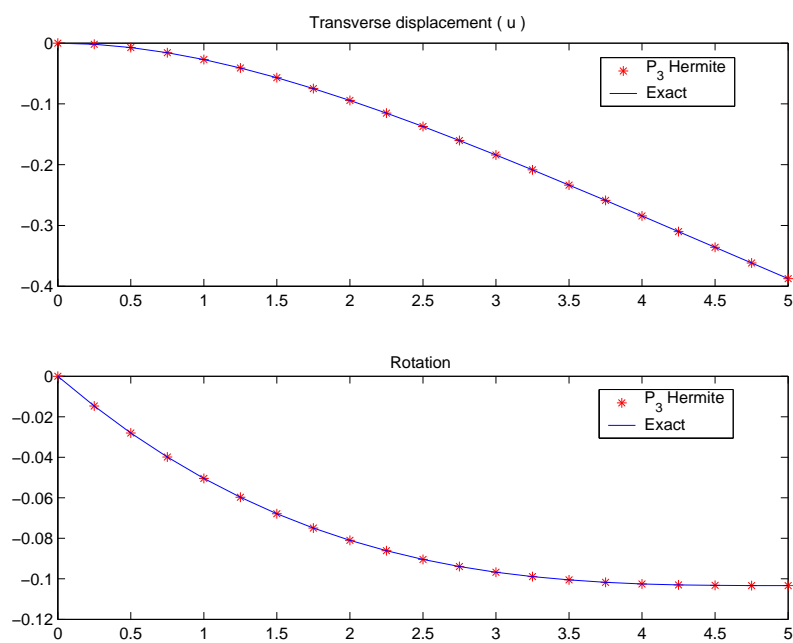


Figure 3.4: Bernoulli Beam

Chapter 4

MITC triangular shell elements

The terminology for the MITC general shell elements stands for “*Mixed Interpolation of Tensorial Components*”. They are formulated in order to avoid numerical locking by using a specific interpolation strategy for each component of the strain tensor within each element instead of deriving them directly from the displacements. The associated interpolation points for strains are called *tying points* (see [6], [13]).

Efficient shell elements must avoid locking in bending dominated –or equivalently penalized– shell problems, whereas consistency must not be lost in membrane dominated situations. When a non-inhibited –or otherwise penalized– shell problem is posed, the phenomena of “numerical locking” may occur, which strongly affects the convergence for standard shell element procedures. As is well known, displacement-based finite elements suffer from this phenomena regardless of the displacement interpolation order, and new strategies must be designed. The MITC approach has been developed as a useful locking reduction tool for quadrilateral plate/shell finite elements (see [12], [9], [14]).

4.1 Formulation of general shell elements

General shell elements constitute a category of finite elements widely used in engineering practice. They are based on the idea of degenerating a 3D general formulation from continuum mechanics into a modified variational problem by considering a plane stress assumption, a special mesh for \mathcal{B} and displacement functions that verify the Reissner-Mindlin kinematical assumption at nodes (voir [31]). Exact normal vectors are not exactly known except at nodal positions.

The domain \mathcal{B} is meshed by nodes located on the midsurface \mathcal{S} . The curvilinear variables (ξ^1, ξ^2, ξ^3) are related to the *local coordinates*

$$(r, s, z) \in \hat{K} = \hat{T} \times [-1, 1] \quad (4.1)$$

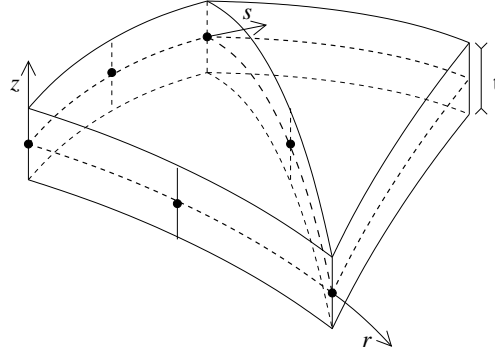


Figure 4.1: 6-node general shell element

by the following one-to-one relations inside each element:

$$\begin{pmatrix} \xi^1 \\ \xi^2 \end{pmatrix} = \sum_{i=1}^k \lambda_i(r, s) \begin{pmatrix} \xi_{(i)}^1 \\ \xi_{(i)}^2 \end{pmatrix} \quad (4.2)$$

$$\xi^3 = z \frac{t}{2} \quad (4.3)$$

where $(\xi_{(i)}^1, \xi_{(i)}^2)$ denote the nodal coordinates in ω , the set $\{\lambda_i\}_{i=1}^k$ represents the 2D shape functions of the standard k -node isoparametric procedure and \hat{T} is a domain to be specified for each type of element¹ (see Fig. 4.1).

The position vector \vec{x} inside an element is defined as:

$$\vec{x}(r, s, z) = \sum_{i=1}^k \lambda_i(r, s) \left(\vec{x}^{(i)} + z \frac{t^{(i)}}{2} \vec{a}_3^{(i)} \right) \quad (4.4)$$

where $\vec{x}^{(i)}$, $t^{(i)}$ and $\vec{a}_3^{(i)}$ respectively denote the position vector in the global Cartesian coordinate system, thickness and unit normal vector at node i .

The standard isoparametric approach (4.4) is related to the *approximate chart*

$$\vec{\Phi}_h(\xi^1, \xi^2, \xi^3) = \mathcal{I}(\vec{\phi})(\xi^1, \xi^2) + \xi^3 \frac{\mathcal{I}(t\vec{a}_3)(\xi^1, \xi^2)}{t} \quad (4.5)$$

where \mathcal{I} is the interpolation operator defined for a smooth function ψ as

$$\mathcal{I}(\psi)(\xi^1, \xi^2) = \sum_{i=1}^k \lambda_i(r, s) \psi(\xi_{(i)}^1, \xi_{(i)}^2) \quad (4.6)$$

¹For example, for quadrangular shell elements, $\hat{T} = [-1, 1]^2$, so we consider $(r, s, z) \in [-1, 1]^3$. For triangular shell elements, $\hat{T} = \{(r, s); 0 \leq r \leq 1, 0 \leq s \leq 1 - r\}$.

The subspace of discretized displacements is as usual denoted by \mathcal{V}_h , and it consists of displacements \vec{V} obtained by varying the nodal positions and normal vectors, namely:

$$\vec{V}(r, s, z) = \sum_{i=1}^k \lambda_i(r, s) \vec{v}^{(i)} + z \sum_{i=1}^k \lambda_i(r, s) \frac{t^{(i)}}{2} \left(\alpha_1^{(i)} \vec{V}_1^{(i)} + \alpha_2^{(i)} \vec{V}_2^{(i)} \right) \quad (4.7)$$

where

- $\vec{v}^{(i)}$ denotes the nodal displacement;
- $\vec{V}_1^{(i)}$ and $\vec{V}_2^{(i)}$ are unit vectors orthogonal to $\vec{a}_3^{(i)}$ and to each other defined so that $\{\vec{V}_1^{(i)}, \vec{V}_2^{(i)}, \vec{a}_3^{(i)}\}$ is a direct orthonormal base at each node i ;
- $\alpha_1^{(i)}$ and $\alpha_2^{(i)}$ respectively denote the rotation of $\vec{a}_3^{(i)}$ along $\vec{V}_1^{(i)}$ and $\vec{V}_2^{(i)}$.

In practice, \vec{V}_1 and \vec{V}_2 are often defined by

$$\vec{V}_1 = \frac{\vec{a}_3 \wedge \vec{e}}{\|\vec{a}_3 \wedge \vec{e}\|}, \quad \vec{V}_2 = \vec{a}_3 \wedge \vec{V}_1 \quad (4.8)$$

where \vec{e} is taken as one of the Cartesian base vectors. Notice that the Reissner-Mindlin kinematical assumption is satisfied at all nodes of the mesh as

$$\vec{\eta}^{(i)} \cdot \vec{a}_3^{(i)} = 0 \quad \forall i \quad (4.9)$$

for

$$\vec{\eta}^{(i)} = \alpha_1^{(i)} \vec{V}_1^{(i)} + \alpha_2^{(i)} \vec{V}_2^{(i)} \quad (4.10)$$

the rotation at node i .

In the case of an isotropic elastic material, substituting the exact chart $\vec{\Phi}$ by (4.5) in the left hand side of equation (1.34), the discretized internal work is given by:

$$A(\vec{U}_h, \vec{V}) = \int_{\Omega} \left[\bar{C}^{\alpha\beta\lambda\mu} \bar{e}_{\alpha\beta}(\vec{U}_h) \bar{e}_{\lambda\mu}(\vec{V}) + \bar{D}^{\alpha\lambda} \bar{e}_{\alpha 3}(\vec{U}_h) \bar{e}_{\lambda 3}(\vec{V}) \right] \sqrt{g} d\xi^1 d\xi^2 d\xi^3 \quad (4.11)$$

where the bar-symbol means that the quantity is affected by the geometric approximation, i.e. we have

$$\bar{e}_{ij}(\vec{V}) = \frac{1}{2} \left(\frac{\partial \vec{V}}{\partial \xi^i} \cdot \vec{g}_j + \frac{\partial \vec{V}}{\partial \xi^j} \cdot \vec{g}_i \right) \quad (4.12)$$

with

$$\vec{g}_i = \frac{\partial \vec{\Phi}_h}{\partial \xi^i} \quad (4.13)$$

and

$$\sqrt{g} = |\vec{g}_1 \cdot (\vec{g}_2 \wedge \vec{g}_3)| \quad (4.14)$$

The local (r, s, z) coordinate system inside each finite element will be used instead of (ξ^1, ξ^2, ξ^3) . Considering the change of variables (4.2) and (4.3) at the element level, we can give an equivalent expression for the discretized internal work in (4.11) that reads:

$$\begin{aligned} A(\vec{U}_h, \vec{V}) = & \sum_K \int_K \left[\bar{C}^{\alpha\beta\lambda\mu} \bar{e}_{\alpha\beta}(\vec{U}_h) \bar{e}_{\lambda\mu}(\vec{V}) + \right. \\ & \left. \frac{4}{t^2} \bar{D}^{\alpha\lambda} \bar{e}_{\alpha z}(\vec{U}_h) \bar{e}_{\lambda z}(\vec{V}) \right] \sqrt{g} dr ds dz \end{aligned} \quad (4.15)$$

where the Greek dummy indices are associated with (r, s) and \sqrt{g} denotes the Jacobian corresponding to (r, s, z) . Furthermore, each covariant-covariant strain component

$$\bar{e}_{ij}(\vec{V}) = \frac{1}{2} \left(\frac{\partial \vec{V}}{\partial r_j} \cdot \frac{\partial \vec{x}}{\partial r_i} + \frac{\partial \vec{V}}{\partial r_i} \cdot \frac{\partial \vec{x}}{\partial r_j} \right) \quad (4.16)$$

for $r_1 = r$, $r_2 = s$ and $r_3 = z$ can be expressed in terms of the elemental nodal displacement/rotation vector \mathbf{V} associated with the displacement \vec{V} , namely

$$\bar{e}_{ij}(r, s, z) = [B_{ij}(r, s, z)] \mathbf{V} \quad (4.17)$$

In addition, the discretized membrane, bending and shear strain tensors can be separately calculated, and we have:

$$\begin{aligned} \bar{e}_{\alpha\beta}(\vec{V}) &= \bar{\gamma}_{\alpha\beta}(\vec{v}) + z \frac{t}{2} \bar{\chi}_{\alpha\beta}(\vec{v}, \vec{\eta}) + z^2 \frac{t^2}{4} \bar{\kappa}_{\alpha\beta}(\vec{\eta}) \\ \bar{e}_{\alpha z}(\vec{V}) &= \frac{t}{2} [\bar{\zeta}_{\alpha}(\vec{v}, \vec{\eta}) + z \frac{t}{2} \bar{\delta}_{\alpha}(\vec{\eta})] \end{aligned} \quad (4.18)$$

with

$$\bar{\gamma}_{\alpha\beta}(\vec{v}) = \frac{1}{2} (\vec{v}_{,\alpha} \cdot \vec{a}_{\beta} + \vec{v}_{,\beta} \cdot \vec{a}_{\alpha}) \quad (4.19)$$

$$\bar{\chi}_{\alpha\beta}(\vec{v}, \vec{\eta}) = \frac{1}{2} (\vec{\eta}_{,\alpha} \cdot \vec{a}_{\beta} + \vec{\eta}_{,\beta} \cdot \vec{a}_{\alpha} + \vec{v}_{,\alpha} \cdot \vec{a}_{3,\beta} + \vec{v}_{,\beta} \cdot \vec{a}_{3,\alpha}) \quad (4.20)$$

$$\bar{\kappa}_{\alpha\beta}(\vec{\eta}) = \frac{1}{2} (\vec{\eta}_{,\alpha} \cdot \vec{a}_{3,\beta} + \vec{\eta}_{,\beta} \cdot \vec{a}_{3,\alpha}) \quad (4.21)$$

$$\bar{\zeta}_{\alpha}(\vec{v}, \vec{\eta}) = \frac{1}{2} (\vec{v}_{,\alpha} \cdot \vec{a}_3 + \vec{\eta} \cdot \vec{a}_{\alpha}) \quad (4.22)$$

for

$$\vec{v} = \sum_{i=1}^k \lambda_i(r, s) \vec{v}^{(i)}, \quad \vec{\eta} = \sum_{i=1}^k \lambda_i(r, s) \vec{\eta}^{(i)} \quad (4.23)$$

and

$$\vec{a}_{\alpha} = \sum_{i=1}^k \lambda_{i,\alpha}(r, s) \vec{x}^{(i)}, \quad \vec{a}_3 = \sum_{i=1}^k \lambda_i(r, s) \vec{a}_3^{(i)} \quad (4.24)$$

where $\cdot_{,\alpha}$ denotes the ordinary derivative $\frac{\partial \cdot}{\partial r_\alpha}$. The additional term

$$\bar{o}_\alpha(\vec{\eta}) = \frac{1}{2} (\vec{\eta} \cdot \vec{a}_3)_{,\alpha} \quad (4.25)$$

is known to verify

$$\|\vec{\eta} \cdot \vec{a}_3\|_{H^1(\omega)} \leq Ch \|\vec{\eta}\|_{H^1(\omega)} \quad (4.26)$$

and consequently it can be *neglected* in numerical calculations (see [31] and the references therein).

From (4.17) we infer that (4.18) can be rewritten in a matrix form as:

$$\bar{e}_{\alpha\beta}(r, s, z) = [B_{\alpha\beta}(r, s) + zB_{\alpha\beta}^z(r, s) + z^2B_{\alpha\beta}^{zz}(r, s)] \mathbf{V} \quad (4.27)$$

$$\bar{e}_{\alpha z}(r, s, z) = [B_{\alpha z}(r, s)] \mathbf{V} \quad (4.28)$$

where $B_{\alpha\beta}$, $B_{\alpha\beta}^z$ and $B_{\alpha z}$ respectively denote the elemental matrices associated with the discretized membrane, bending and shear strains.

4.2 MITC shell finite elements

MITC shell finite elements are formulated from the continuum mechanics based shell finite elements described in the previous section (see [6]). The essence of the MITC approach is to use a mixed formulation to separately interpolate strains (referred as *assumed strains*) and displacements, and connect both interpolations at specific *tying points*.

For each covariant strain component e_{ij} we define a set of *tying points* on the shell midsurface of coordinates (r_{ij}^l, s_{ij}^l) , for $l = 1, \dots, n_{ij}$ and the set $\{\lambda_{ij}^l\}_{l=1}^{n_{ij}}$ of polynomial functions satisfying:

$$\lambda_{ij}^l(r_{ij}^m, s_{ij}^m) = \delta_l^m, \quad m = 1, \dots, n_{ij} \quad (4.29)$$

The *assumed covariant strain components* e_{ij}^h are then defined as

$$e_{ij}^h(r, s, z) = \sum_{l=1}^{n_{ij}} \lambda_{ij}^l(r, s) \bar{e}_{ij}(r_{ij}^l, s_{ij}^l, z) \quad (4.30)$$

and from (4.17) we have that

$$e_{ij}^h(r, s, z) = \left[\sum_{l=1}^{n_{ij}} \lambda_{ij}^l(r, s) B_{ij}(r_{ij}^l, s_{ij}^l, z) \right] \mathbf{V} = [B_{ij}^h(r, s, z)] \mathbf{V} \quad (4.31)$$

Recalling (4.18) it follows that

$$\begin{aligned} e_{\alpha\beta}^h(\vec{V}) &= \gamma_{\alpha\beta}^h(\vec{v}) + z \frac{t}{2} \chi_{\alpha\beta}^h(\vec{v}, \vec{\eta}) + z^2 \frac{t^2}{4} \kappa_{\alpha\beta}^h(\vec{\eta}) \\ \bar{e}_{\alpha z}^h(\vec{V}) &= \frac{t}{2} [\zeta_\alpha^h(\vec{v}, \vec{\eta}) + z \frac{t}{2} o_\alpha^h(\vec{\eta})] \end{aligned} \quad (4.32)$$

where $\underline{\gamma}^h$, $\underline{\chi}^h$ and $\underline{\zeta}^h$ respectively denote the *assumed* membrane, bending and shear strain tensors. Furthermore, from (4.27) and (4.28) we obtain

$$\begin{aligned}
e_{\alpha\beta}^h(r, s, z) &= \sum_{l=1}^{n_{\alpha\beta}} \lambda_{\alpha\beta}^l(r, s) \left\{ B_{\alpha\beta}(r_{\alpha\beta}^l, s_{\alpha\beta}^l) + z B_{\alpha\beta}^z(r_{\alpha\beta}^l, s_{\alpha\beta}^l) + \right. \\
&\quad \left. z^2 B_{\alpha\beta}^{zz}(r_{\alpha\beta}^l, s_{\alpha\beta}^l) \right\} \mathbf{V} \\
&= \left[B_{\alpha\beta}^h(r, s) + z B_{\alpha\beta}^{z,h}(r, s) + z^2 B_{\alpha\beta}^{zz,h}(r, s) \right] \mathbf{V}
\end{aligned} \tag{4.33}$$

and

$$\begin{aligned}
e_{\alpha z}^h(r, s, z) &= \sum_{l=1}^{n_{\alpha z}} \lambda_{\alpha z}^l(r, s) B_{\alpha z}(r_{\alpha z}^l, s_{\alpha z}^l) \mathbf{V} \\
&= [B_{\alpha z}^h(r, s)] \mathbf{V}
\end{aligned} \tag{4.34}$$

and then $B_{\alpha\beta}^h$, $B_{\alpha\beta}^{z,h}$ and $B_{\alpha z}^h$ respectively refer to the elemental matrices for *assumed* membrane, bending and shear strains.

Since this tying procedure is developed at the elemental level and for each individual element, the elemental stiffness matrix is constructed in the same manner as for the standard isoparametric shell elements, but the proper matrix B_{ij}^h must be used. Namely, the discretized internal work to be considered when using the MITC approach reads:

$$\begin{aligned}
A^h(\vec{U}_h, \vec{V}) &= \sum_K \int_K \left[\bar{C}^{\alpha\beta\lambda\mu} e_{\alpha\beta}^h(\vec{U}_h) e_{\lambda\mu}^h(\vec{V}) + \right. \\
&\quad \left. \frac{4}{t^2} \bar{D}^{\alpha\lambda} e_{\alpha z}^h(\vec{U}_h) e_{\lambda z}^h(\vec{V}) \right] \sqrt{g} dr ds dz
\end{aligned} \tag{4.35}$$

4.3 Element specifications

Efficient MITC triangular shell finite elements must satisfy ellipticity, consistency, inf-sup condition and spatial isotropy.

A shell elasticity problem can be written in a general form as:

Find $\vec{U}^\varepsilon \in \mathcal{V}$ such that

$$A^\varepsilon(\vec{U}^\varepsilon, \vec{V}) = F^\varepsilon(\vec{V}) \quad \forall \vec{V} \in \mathcal{V} \tag{4.36}$$

where \vec{U}^ε denotes the exact displacement solution of the mathematical model and \vec{V} is an arbitrary function in \mathcal{V} , the space where the solution lies for ε fixed. $A^\varepsilon(\cdot, \cdot)$ denotes the bilinear form of the mathematical model associated with ε , and $F^\varepsilon(\cdot)$ the corresponding external virtual work.

The discretized formulation based on geometric approximations and obtained when using the MITC approach reads:

Find $\vec{U}_h^\varepsilon \in \mathcal{V}_h$ such that

$$A^{\varepsilon,h}(\vec{U}_h^\varepsilon, \vec{V}) = F^\varepsilon(\vec{V}) \quad \forall \vec{V} \in \mathcal{V}_h \tag{4.37}$$

where \vec{U}_h denotes the finite element solution, \vec{V} is an arbitrary test function in the space \mathcal{V}_h where the finite element solution lies and $A^{\varepsilon,h}(\cdot, \cdot)$ denotes the discretized formulation incorporating the MITC rules of strain interpolation described above.

In order to illustrate the main difficulties when developing effective shell finite elements, let us consider a shell of constant thickness. We can substitute (4.32) into (4.35), replace $\bar{C}^{\alpha\beta\lambda\mu}$ and $\bar{D}^{\alpha\lambda}$ by the respective (approximate) midsurface values ${}^0\bar{C}^{\alpha\beta\lambda\mu}$ and ${}^0\bar{D}^{\alpha\lambda}$, and perform the integration through the thickness to obtain

$$A^{\varepsilon,h}(\vec{V}, \vec{W}) = \varepsilon^3 A_b^h(\vec{V}, \vec{W}) + \varepsilon^3 A_m^h(\vec{V}, \vec{W}) \quad (4.38)$$

for $\vec{V}, \vec{W} \in \mathcal{V}_h$, where

$$\begin{aligned} A_b^h(\vec{V}, \vec{W}) &= \sum_K \frac{L^3}{12} \int_{\hat{K}} \left[{}^0\bar{C}^{\alpha\beta\lambda\mu} \chi_{\alpha\beta}^h(\vec{v}, \vec{\eta}) \chi_{\lambda\mu}^h(\vec{w}, \vec{\tau}) \right. \\ &\quad \left. + {}^0\bar{D}^{\alpha\lambda} o_\alpha^h(\vec{\eta}) o_\lambda^h(\vec{\tau}) \right] \sqrt{a} \, dr \, ds \\ A_m^h(\vec{V}, \vec{W}) &= \sum_K L \int_{\hat{K}} \left[{}^0\bar{C}^{\alpha\beta\lambda\mu} \gamma_{\alpha\beta}^h(\vec{v}) \gamma_{\lambda\mu}^h(\vec{w}) \right. \\ &\quad \left. + {}^0\bar{D}^{\alpha\lambda} \zeta_\alpha^h(\vec{v}, \vec{\eta}) \zeta_\lambda^h(\vec{w}, \vec{\tau}) \right] \sqrt{a} \, dr \, ds \end{aligned} \quad (4.39)$$

These expressions can be compared to the terms appearing in the s-m-b model formulation (1.37).

4.3.1 Ellipticity

This condition, also called *coercivity*, states if the problem is solvable. The finite element problem is said to be elliptic if:

$$\exists \alpha > 0 \quad / \quad \forall \vec{V} \in \mathcal{V}_h, \quad A^{\varepsilon,h}(\vec{V}, \vec{V}) \geq \alpha \|\vec{V}\|_1^2 \quad (4.40)$$

It can be easily verified by counting the number of zero eigenvalues of the stiffness matrix of one unsupported shell finite element, which must be exactly *six* (corresponding to the physical rigid body modes).

4.3.2 Consistency

The MITC procedure incorporates two possible sources of consistency errors:

- *Substitution of A_b^h for A_b* : the geometric approximation in itself is known to be well-controlled as we can see in [31], but the impact of the MITC procedure is more difficult to analyze mathematically. However, it can be numerically assessed by comparing MITC elements defined like (4.32) to particular formulations obtained by only interpolating those terms that induce locking (i.e. the membrane and shear strains) without affecting the approximate bending strains, namely setting

$$\tilde{e}_{\alpha\beta}^h(\vec{V}) = \gamma_{\alpha\beta}^h(\vec{v}) + z \frac{t}{2} \bar{\chi}_{\alpha\beta}(\vec{v}, \vec{\eta}) + z^2 \frac{t^2}{4} \bar{\kappa}_{\alpha\beta}(\vec{\eta}) \quad (4.41)$$

- *Consistency of A_m^h with respect to A_m* : this consistency must hold in the norm that prevails in membrane dominated situations, namely the membrane energy norm. For example, it would be sufficient to obtain an estimate of the kind needed in the Strang Lemma (see [35]), namely

$$|A_m(\vec{V}, \vec{W}) - A_m^h(\vec{V}, \vec{W})| \leq Ch^p A_m(\vec{V}, \vec{V})^{1/2} A_m(\vec{W}, \vec{W})^{1/2} \quad (4.42)$$

for all $\vec{V}, \vec{W} \in \mathcal{V}_h$. But this type of consistency estimate is difficult to establish given that the consistency errors arising from the geometric approximation can be bounded in the H^1 -norm, not in the membrane norm, and the analysis of consistency errors arising from the MITC approach in Sobolev norms is still an open issue (see [31] and references therein).

4.3.3 Inf-Sup condition

Ideally, all mixed finite element discretizations must satisfy the inf-sup condition, which guarantees that the shell finite element is free from shear and membrane locking in bending-dominated situations of any thickness.

In a bending-dominated situation and when considering the s-m-b or m-b shell models, the problem to be solved can be written as:

Find $\vec{U}^\varepsilon = (\vec{u}^\varepsilon, \underline{\theta}^\varepsilon) \in \mathcal{V}$ such that

$$A_b(\vec{U}^\varepsilon, \vec{V}) + \frac{1}{\varepsilon^2} A_m(\vec{U}^\varepsilon, \vec{V}) = G(\vec{V}) \quad \forall \vec{V} = (\vec{v}, \underline{\eta}) \in \mathcal{V} \quad (4.43)$$

When ε tends to zero, vanishing membrane and shear strains must be satisfied, namely:

$$\underline{\underline{\gamma}}(\vec{v}) = \underline{\underline{0}} \quad (4.44)$$

and

$$\underline{\underline{\zeta}}(\vec{v}, \underline{\eta}) = \underline{\underline{0}} \quad (4.45)$$

One possible choice to circumvent locking is to introduce the membrane and shear strains as auxiliary unknowns by using mixed formulations. Such formulations can be written in a general form as follows:

$$\begin{cases} A_b(\vec{U}^\varepsilon, \vec{V}) + B(\vec{V}, \Sigma^\varepsilon) = G(\vec{V}) & \forall \vec{V} \in \mathcal{V} \\ B(\vec{U}^\varepsilon, \Xi) - \varepsilon^2 D(\Sigma^\varepsilon, \Xi) = 0 & \forall \Xi \in \mathcal{T}^+ \end{cases} \quad (4.46)$$

where \mathcal{T}^+ corresponds to L^2 for all components of the stress. Using a finite element procedure, we can obtain the corresponding discretized formulation:

$$\begin{cases} A_b(\vec{U}_h^\varepsilon, \vec{V}) + B(\vec{V}, \Sigma_h^\varepsilon) = G(\vec{V}) & \forall \vec{V} \in \mathcal{V}_h \\ B(\vec{U}_h^\varepsilon, \Xi) - \varepsilon^2 D(\Sigma_h^\varepsilon, \Xi) = 0 & \forall \Xi \in \mathcal{T}_h \end{cases} \quad (4.47)$$

where a geometric approximation is used. The last equation in (4.47) defines a projection into \mathcal{T}_h , namely

$$\Sigma_h^\varepsilon = \Pi_h(\underline{\gamma}(\vec{u}_h^\varepsilon), \underline{\zeta}(\vec{u}_h^\varepsilon, \underline{\theta}_h^\varepsilon)) \quad (4.48)$$

and then, after performing an elimination of the stress unknowns, the finite element formulation can be written as

Find $\vec{U}_h^\varepsilon \in \mathcal{V}_h$ such that

$$A_b(\vec{U}_h^\varepsilon, \vec{V}) + \frac{1}{\varepsilon^2} A_m^h(\vec{U}_h^\varepsilon, \vec{V}) = G(\vec{V}) \quad \forall \vec{V} \in \mathcal{V}_h \quad (4.49)$$

where A_m^h is a reduced form of A_m .

The inf-sup condition that guarantees an error estimate uniform in ε for the finite element approximation of the mixed problem reads

$$\sup_{V \in \mathcal{V}_h, V \neq 0} \frac{B(\vec{V}, \Xi)}{\|\vec{V}\|_{\mathcal{V}}} \geq \varrho \sup_{V \in \mathcal{V}, V \neq 0} \frac{B(\vec{V}, \Xi)}{\|\vec{V}\|_{\mathcal{V}}}, \quad \forall \Xi \in \mathcal{T}_h \quad (4.50)$$

Note that the norm of \mathcal{T} is not used explicitly in this form of the inf-sup condition. In fact, the problem of characterizing this space and the associated norm for general shell geometries and boundary conditions still remains to be solved (see [31] and the references therein).

A formal proof of the inf-sup condition has not been achieved for any general shell finite element procedure so far, although a relaxed formulation under particular conditions has been proposed in [20] and numerical inf-sup tests are of general value to assess mixed formulations (see in particular [15]).

4.3.4 Spatial isotropy

Spatial isotropy is another requirement for effective *triangular* shell finite elements, which guarantees that the numerical results do not depend on the element orientation, namely on the nodal numbering. This property is not difficult to achieve in the definition of the tying points and the interpolation space considered for each covariant strain component.

From the local coordinate system (r, s) inside a triangular element as the one displayed in Fig. 4.1, we can introduce the coordinates (\bar{r}, \bar{s}) given by:

$$(\bar{r}, \bar{s}) = (r, 1 - r - s) \quad (4.51)$$

which define a new orientation for the triangular finite element as shown in Figure 4.2. From (4.51) we have

$$\begin{aligned} \frac{\partial r}{\partial \bar{r}} &= 1, & \frac{\partial s}{\partial \bar{r}} &= -1 \\ \frac{\partial r}{\partial \bar{s}} &= 0, & \frac{\partial s}{\partial \bar{s}} &= -1 \end{aligned} \quad (4.52)$$

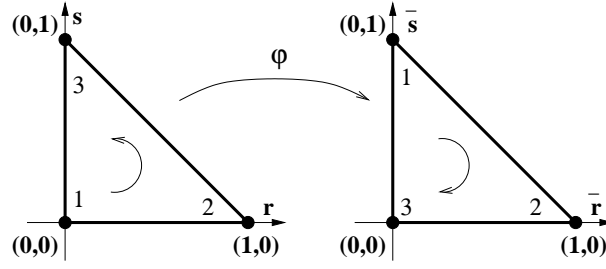


Figure 4.2: Change of element orientation

and consequently

$$\begin{aligned}\frac{\partial}{\partial \bar{r}} &= \frac{\partial r}{\partial \bar{r}} \frac{\partial}{\partial r} + \frac{\partial s}{\partial \bar{r}} \frac{\partial}{\partial s} = \frac{\partial}{\partial r} - \frac{\partial}{\partial s} \\ \frac{\partial}{\partial \bar{s}} &= \frac{\partial r}{\partial \bar{s}} \frac{\partial}{\partial r} + \frac{\partial s}{\partial \bar{s}} \frac{\partial}{\partial s} = -\frac{\partial}{\partial s}\end{aligned}\quad (4.53)$$

Using these expressions, we can express the covariant components of the linearized strain tensor in the new coordinates (\bar{r}, \bar{s}) as a function of those in (r, s) , namely:

$$\begin{aligned}e_{\bar{r}\bar{r}} &= e_{rr} + e_{ss} - 2e_{rs} \\ e_{\bar{s}\bar{s}} &= e_{ss} \\ e_{\bar{r}\bar{s}} &= e_{ss} - e_{rs} \\ e_{\bar{r}z} &= e_{rz} - e_{sz} \\ e_{\bar{s}z} &= -e_{sz}\end{aligned}\quad (4.54)$$

Denoting

$$q = -\sqrt{2}\bar{r} \quad (4.55)$$

we can define the transverse shear strain corresponding to the hypotenuse of the right-angled triangle in the natural coordinate system as:

$$e_{qz} = -\frac{1}{\sqrt{2}}e_{\bar{r}z} = \frac{1}{\sqrt{2}}(e_{sz} - e_{rz}) \quad (4.56)$$

This covariant strain component must be incorporated to the shell analysis in order to achieve MITC isotropic triangular shell elements.

Furthermore, the covariant in-plane strains –i.e. the normal strains e_{rr} , e_{ss} and the in-plane shear strain e_{rs} – cannot be treated separately. One more normal in-plane strain in the hypotenuse direction or the right-angled triangle in the local coordinate system must be considered, and it is related to the other ones by the following expression:

$$e_{qq} = \frac{1}{2}e_{\bar{r}\bar{r}} = \frac{e_{rr} + e_{ss}}{2} - e_{rs} \quad (4.57)$$

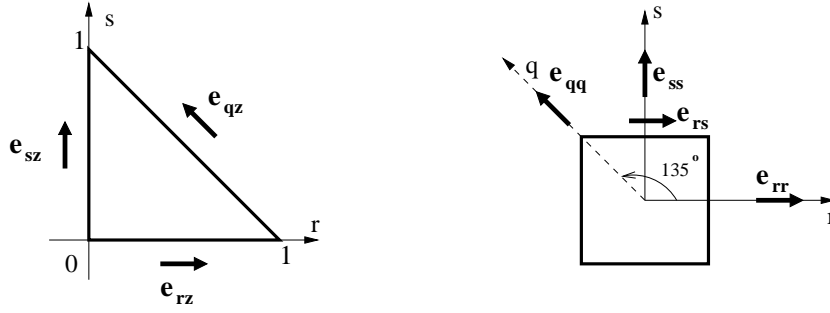


Figure 4.3: Strain fields

(see Fig. 4.3). Hence, instead of interpolating the in-plane strain components e_{rr} , e_{ss} and e_{rs} , we will be interested in interpolating e_{rr} , e_{ss} and e_{qq} and then we obtain e_{rs} from (4.57).

When developing MITC isotropic triangular general shell elements, a certain starting polynomial space is selected for the interpolation of the in-plane strains, namely

$$\begin{aligned} e_{rr}^h &= a_1 + b_1 r + c_1 s + \dots \\ e_{ss}^h &= a_2 + b_2 r + c_2 s + \dots \\ e_{qq}^h &= a_3 + b_3 r + c_3 s + \dots \end{aligned} \quad (4.58)$$

The corresponding tying positions and conditions must be properly set in order to determine those coefficients.

In the same way, the starting polynomials associated with the assumed transverse shear strains e_{rz}^h and e_{sz}^h may be formulated as:

$$\begin{aligned} e_{rz}^h &= a_4 + b_4 r + c_4 s \dots \\ e_{sz}^h &= a_5 + b_5 r + c_5 s \dots \end{aligned} \quad (4.59)$$

and then from (4.56) we have:

$$e_{qz}^h = \frac{1}{\sqrt{2}} [(a_4 + b_4 r + c_4 s \dots) - (a_5 + b_5 r + c_5 s \dots)] \quad (4.60)$$

The unknown coefficients $a_4, a_5, b_4, b_5, \dots$ are calculated by suitably choosing the tying points and conditions associated with each shear strain component.

Hence, in order to guarantee that a MITC triangular general shell element is *isotropic*, it is necessary to verify that:

- the *tying points* are “symmetrically” chosen, which means that no particular choice is made for any specific component: all the tying positions must be chosen in the same manner for the three edges of the triangular element in consideration;

- changing (r, s) into (\bar{r}, \bar{s}) , the same polynomial spaces are found for the interpolation of strains.

Chapter 5

Detecting membrane locking

Dominique Chapelle, Iria París

Abstract

We present a simple numerical test aimed at detecting membrane locking, which is the main obstacle when developing effective general shell finite elements. The presence of parasitic membrane modes is also revealed. These modes are related to the MITC approach and may considerably deteriorate the solution of membrane dominated shell problems.

Several 6-node MITC tying schemes have been assessed using this test problem based on a midsurface of the same geometric nature as the parabolic hyperboloid, and the results that we have obtained are summarized here. The MITC6a triangular shell finite element formulated by Lee and Bathe ([47]) has also been considered in this assessment.

5.1 Preliminaries

When considering shell models based on the *Reissner-Mindlin kinematical assumption*, it is assumed that any material line in the direction of $\vec{a}_3(\xi^1, \xi^2)$ and orthogonal to the midsurface at the point of coordinates (ξ^1, ξ^2) in the undeformed configuration remains straight and unstretched during deformations. Displacements under this assumption can be expressed by equation (1.25). As we have seen in Section 2, the asymptotic behavior that a shell structure may undergo depends on the contents of the subspace of inextensional displacements \mathcal{V}_0 , which

is characterized by *vanishing membrane* and *shear strains*. The condition of zero shear strains gives an explicit expression of $\underline{\theta}$ as a function of \vec{u} (recall (1.40)) and consequently we can focus on the condition of zero membrane strain, namely on the system of partial differential equations given by:

$$\underline{\underline{\gamma}}(\vec{u}) = \underline{\underline{0}} \quad (5.1)$$

for

$$\gamma_{\alpha\beta}(\vec{u}) = \frac{1}{2} (u_{\alpha|\beta} + u_{\beta|\alpha}) - b_{\alpha\beta}u_3 \quad \alpha, \beta = 1, 2 \quad (5.2)$$

and

$$u_{\alpha|\beta} = u_{\alpha,\beta} - \Gamma_{\alpha\beta}^{\lambda} u_{\lambda} \quad (5.3)$$

$$\Gamma_{\alpha\beta}^{\lambda} = \vec{a}_{\alpha,\beta} \cdot \vec{a}^{\lambda} \quad (5.4)$$

$$b_{\alpha\beta} = \vec{a}_3 \cdot \vec{a}_{\alpha,\beta} \quad (5.5)$$

It is known that the differential nature of System (5.1) is the same as the geometric nature of the midsurface at the point in consideration (see [59] and references therein). Furthermore, the characteristics of the system are also the asymptotic lines of the surface in the parabolic and hyperbolic cases.

Therefore, System (5.1) is of hyperbolic nature for a hyperbolic surface. Boundary conditions together with (5.1) define a Cauchy problem. We can use the coordinate system (y^1, y^2) defined by the asymptotic lines of the surface –such that $b_{11} = b_{22} = 0$, but $b_{12} \neq 0$ – and then system (5.1) becomes:

$$\gamma_{11} = u_{1|1} = 0 \quad (5.6)$$

$$\gamma_{22} = u_{2|2} = 0 \quad (5.7)$$

$$\gamma_{12} = \frac{1}{2} (u_{1|2} + u_{2|1}) - b_{12}u_3 = 0 \quad (5.8)$$

Figure 5.1 displays the reference domain for a hyperbolic surface in this particular choice of coordinates. If the fields u_1 and u_2 are set to zero along AB , the Cauchy problem is well-posed in the ABC area, and therefore u_1 and u_2 are known zero on the whole subdomain ABC , and in particular along BC and AC , respectively. Setting u_1 and u_2 arbitrarily outside of these segment and along these same lines (see Fig. 5.1), the solution can be obtained over the whole domain¹.

If a bending dominated problem is discretized using a displacement-based finite element formulation, *numerical locking* occurs owing to the constraint of vanishing membrane strains. In order to avoid such phenomena, *mixed formulations* – which introduce the membrane and shear strains as auxiliary unknowns– are used, but existing triangular shell finite elements are known to be insufficiently reliable. During our research, we designed a simple numerical test aimed at detecting membrane locking.

¹Equation (5.8) allows us to calculate u_3 as a function of u_1 and u_2 .

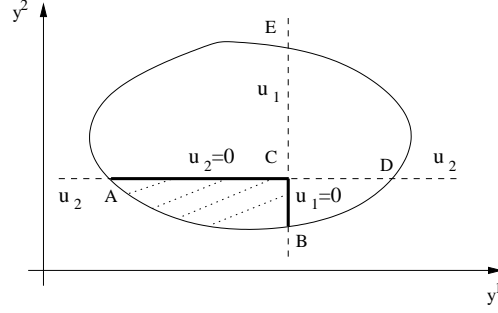


Figure 5.1: Reference domain of a hyperbolic surface in the asymptotic coordinates.

Let us consider a shell with a regular hyperbolic midsurface fixed on some part of its boundary. Suppose that the problem is discretized using triangular shell finite elements and focus on an arbitrary element of the mesh with \vec{u} set to zero on any of its edges. Three situations are possible:

- The element is completely covered by the asymptotic lines originating from this edge (Fig. 5.2 left).
- The element is only partially covered (Fig. 5.2 right).
- The element edge is part of an asymptotic line.

For the first possibility, \vec{u} must be zero over the whole element due to the hyperbolic nature of System (5.1); in the second case we still have $\vec{u} = \vec{0}$ on a part of non-zero area but the discretized solution should not be zero over the whole element in order to avoid membrane locking.

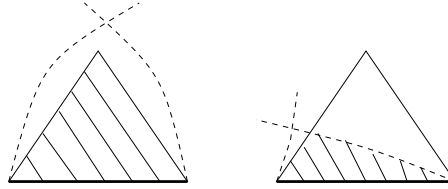


Figure 5.2: Asymptotic lines from fixed edge and inhibited region.

The formulation of MITC shell finite elements was described in Section 4.2. We recall that the *assumed covariant-covariant membrane strain components* can be expressed in matrix form and in terms of the element nodal displacement/rotation vector components \mathbf{V} at any point of local coordinates (r, s) inside an element, namely

$$\gamma_{\alpha\beta}^h(r, s) = \left[B_{\alpha\beta}^h(r, s) \right] \mathbf{V} \quad (5.9)$$

with

$$B_{\alpha\beta}^h(r, s) = \sum_{l=1}^{n_{\alpha\beta}} \lambda_{\alpha\beta}^l(r, s) B_{\alpha\beta}(r_{\alpha\beta}^l, s_{\alpha\beta}^l) \quad (5.10)$$

where $B_{\alpha\beta}$ denotes the elemental matrix associated with the non-reduced membrane strain component.

As we have discussed in Section 4.3, the covariant in-plane strains (namely the components e_{rr} , e_{ss} and the in-plane shear strain e_{rs}) cannot be treated independently if we want to obtain isotropic elements (refer to [47]). One more in-plane strain in the hypotenuse direction of the right-angled triangle in the natural coordinate system must be considered as displayed in Figure 4.3, which is related to the other ones by the following expression:

$$e_{qq} = \frac{e_{rr} + e_{ss}}{2} - e_{rs} \quad (5.11)$$

Instead of interpolating the in-plane components e_{rr} , e_{ss} and e_{rs} , we will be interested in interpolating e_{rr} , e_{ss} and e_{qq} and we obtain e_{rs} from (5.11), and the same consideration holds for the membrane strain components.

Hence, from equations (5.9)-(5.10) we have that the assumed membrane strain vanishes over the whole element only if each non-reduced component is zero at all associated tying points. This condition can be expressed in a matrix form that corresponds to the discretized formulation of vanishing membrane strains given by (5.1):

$$\begin{bmatrix} B_{rr}(r_{rr}^1, s_{rr}^1) \\ \vdots \\ B_{rr}(r_{rr}^{n_{rr}}, s_{rr}^{n_{rr}}) \\ \\ B_{ss}(r_{ss}^1, s_{ss}^1) \\ \vdots \\ B_{ss}(r_{ss}^{n_{ss}}, s_{ss}^{n_{ss}}) \\ \\ B_{qq}(r_{qq}^1, s_{qq}^1) \\ \vdots \\ B_{qq}(r_{qq}^{n_{qq}}, s_{qq}^{n_{qq}}) \end{bmatrix} \mathbf{V} = \mathbf{0} \quad (5.12)$$

5.2 Membrane test

The main obstacle when developing effective shell finite elements is the membrane locking phenomenon arising in bending dominated shell problems (see [31]), since the discretized solution asymptotically belongs to the subspace $\mathcal{V}_h \cap \mathcal{V}_0$ and locking is critical when it is exactly reduced to $\{0\}$ as we have seen in Section 3.

When considering a single MITC shell finite element, *the existence of discretized inextensional displacements different from zero will be determined by the*

rank of the matrix associated with (5.12), and when assembling refined meshes, it will be determined by the *number of zero membrane energy modes*.

The test that we present here is based on the above considerations. We focus on three elements of same geometric nature as the parabolic hyperboloid (see Figure 5.3):

1. an element completely covered by asymptotic lines originating from fixed edge,
2. a partially covered element,
3. an element whose fixed edge is part of an asymptotic line of the hyperbolic midsurface.

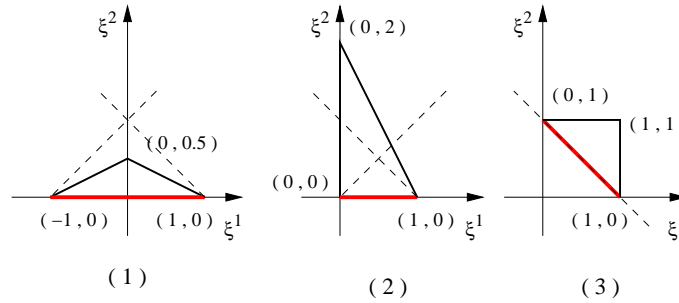


Figure 5.3: Reference domains considered (dashed lines represent asymptotic lines originating from fixed edge).

The midsurface geometry is defined by the chart:

$$\vec{\phi}(\xi^1, \xi^2) = \begin{pmatrix} \xi^1 \\ \xi^2 \\ \frac{(\xi^1)^2 - (\xi^2)^2}{2} \end{pmatrix} \quad (5.13)$$

and the normal vector at each point of global Cartesian coordinates (x, y, z) is given by:

$$\vec{a}_3(x, y, z) = (-x, y, 1)^T \quad (5.14)$$

An orthonormal basis can be easily obtained at each point in consideration as

$$\vec{V}_1 = \frac{\vec{a}_3 \times \vec{e}_x}{\|\vec{a}_3 \times \vec{e}_x\|}, \quad \vec{V}_2 = \vec{a}_3 \times \vec{V}_1 \quad (5.15)$$

for $\vec{e}_x = (1, 0, 0)^T$.

For a single 6-node triangular shell finite element, system (5.12) involves $6 \times 3 = 18$ unknowns, but $3 \times 3 = 9$ boundary conditions are set along the fixed edge. Therefore, the optimal rank will be 9 for the first situation and 7 for the third case. The membrane locking phenomenon might be circumvented if rank 9 is not obtained for the partially covered situation.

There exist many alternatives for the choice of tying positions. We have analyzed some of them, mainly based on the tying points used for quadrilateral MITC elements (see [47]), but also points with particular properties like the barycenter, Gauss integration points or points on the edges. The results that we obtained are summarized in Tables 5.1-5.4.

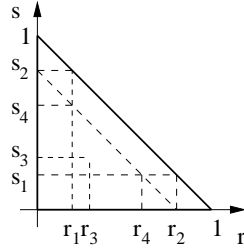


Figure 5.4: $r_1 = s_1 = \frac{1}{2} - \frac{1}{2\sqrt{3}}, r_2 = s_2 = \frac{1}{2} + \frac{1}{2\sqrt{3}}, r_3 = s_3 = \frac{1}{3}, r_4 = s_4 = \frac{1}{\sqrt{3}}$

TYING POINTS	COMPLETELY COVERED	PARTIALLY COVERED	ASYMPTOTIC LINE
	7	7	7
	9	9	8

Table 5.1:
MITC6 triangular shell finite elements: tying schemes and associated ranks.

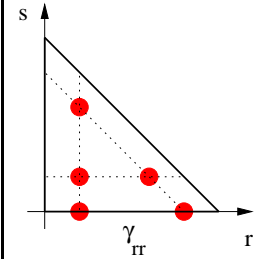
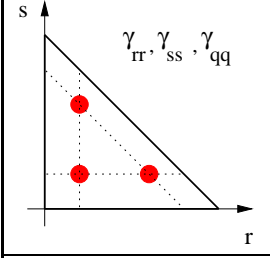
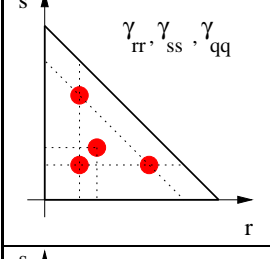
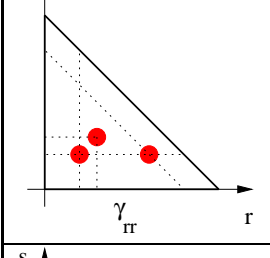
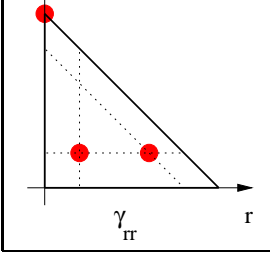
TYING POINTS	COMPLETELY COVERED	PARTIALLY COVERED	ASYMPTOTIC LINE
	9	9	7
	8	8	7
	9	9	8
	8	8	7
	8	8	7

Table 5.2:
MITC6 triangular shell finite elements: tying schemes and associated ranks.

TYING POINTS	COMPLETELY COVERED	PARTIALLY COVERED	ASYMPTOTIC LINE
	9	9	8
	7	7	7
	7	7	7
	9	9	8
	7	7	7

Table 5.3:
MITC6 triangular shell finite elements: tying schemes and associated ranks.

TYING POINTS	COMPLETELY COVERED	PARTIALLY COVERED	ASYMPTOTIC LINE
	8	8	7
	7	7	7
	7	7	7
	9	9	7
	8	8	7

Table 5.4:
MITC6 triangular shell finite elements: tying schemes and associated ranks.

Tables 5.1-5.4 show that for several tying schemes, whereas satisfactory ranks are obtained when the element is partially covered by asymptotic lines originating from the fixed edge or it is part of an asymptotic line of the hyperbolic midsurface, desirable $rank = 9$ is not achieved for the completely covered situation. It means that *membrane spurious modes* may arise². We have analyzed in more depth different tying selections.

MITC6a:

This MITC6 shell finite element was firstly formulated by Lee and Bathe in [47]. The tying points for the assumed membrane strains are displayed in Figure 5.5.

Although this element does not suffer from severe numerical locking since $rank = 7$ is obtained for the partially covered case, desirable $rank = 9$ is not obtained for the completely covered situation (refer to Table 5.1 first line) and membrane spurious modes may arise. In fact, there exist two modes of zero membrane energy – corresponding to $rank = 7$ – for a single finite element. When assembling refined meshes, such modes remain present (see Table 5.5) and the multiplicity of the zero eigenvalue associated with the membrane stiffness matrix is increased as the mesh is refined.

The same behavior is observed when considering the tying positions represented in Figure 5.6 and Figure 5.7.

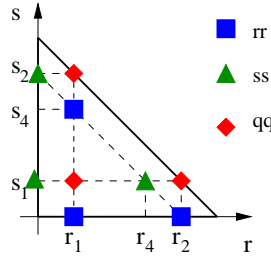


Figure 5.5: MITC6a tying points associated with each membrane strain component ($r_1 = s_1 = \frac{1}{2} - \frac{1}{2\sqrt{3}}$, $r_2 = s_2 = \frac{1}{2} + \frac{1}{2\sqrt{3}}$, $r_4 = s_4 = \frac{1}{\sqrt{3}}$).

Other schemes:

Other choices of tying positions that have been analyzed are displayed in Figure 5.8 and Figure 5.9. Tables 5.2-5.4 show that for these tying schemes $rank = 8$ is obtained when $rank = 9$ is expected, and one zero membrane energy mode exists for a single finite element, which continues to be present when assembling refined

²The number of membrane spurious modes corresponds to the multiplicity of the zero eigenvalue of the membrane – shear terms not included – stiffness matrix.

Number of elements	Number of nodes	Number of active DOF	Multiplicity zero eigenvalue
1	6	9	2
4	15	30	4
16	45	108	8
64	153	408	16

Table 5.5:
Meshes properties and multiplicity of zero for the MITC6a element.

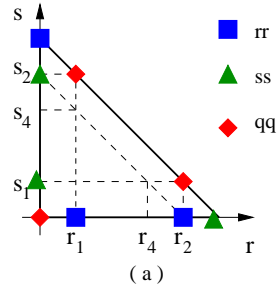


Figure 5.6: Tying points associated with each membrane strain component ($r_1 = s_1 = \frac{1}{2} - \frac{1}{2\sqrt{3}}$, $r_2 = s_2 = \frac{1}{2} + \frac{1}{2\sqrt{3}}$).

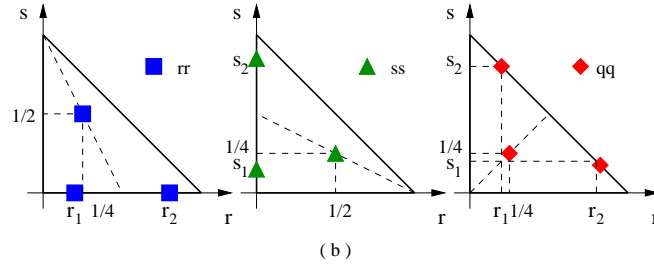


Figure 5.7: Tying points associated with each membrane strain component ($r_1 = s_1 = \frac{1}{2} - \frac{1}{2\sqrt{3}}$, $r_2 = s_2 = \frac{1}{2} + \frac{1}{2\sqrt{3}}$).

meshes. Nevertheless, no additional zero membrane energy modes arise as the mesh is refined (refer to Table 5.6).

5.3 Conclusions

We have proposed here a simple numerical test aimed at detecting membrane locking on the one hand, and the existence of parasitic membrane modes related

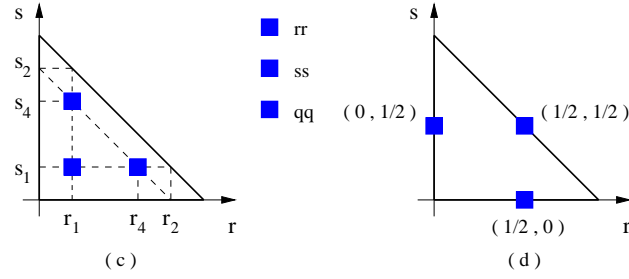


Figure 5.8: Tying points associated with all membrane strain components ($r_1 = s_1 = \frac{1}{2} - \frac{1}{2\sqrt{3}}$, $r_4 = s_4 = \frac{1}{\sqrt{3}}$).

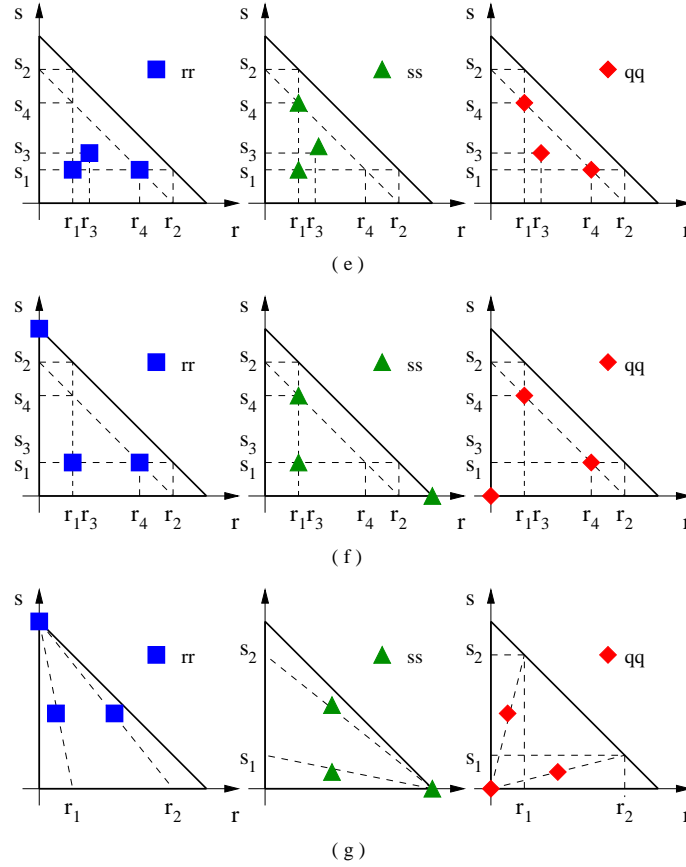


Figure 5.9: Tying points associated with each membrane strain component ($r_1 = s_1 = \frac{1}{2} - \frac{1}{2\sqrt{3}}$, $r_2 = s_2 = \frac{1}{2} + \frac{1}{2\sqrt{3}}$, $r_3 = s_3 = 1/3$, $r_4 = s_4 = \frac{1}{\sqrt{3}}$).

to the MITC procedure on the other hand. We have then analyzed several tying choices for 6-node MITC isotropic triangular shell finite elements, and we observe

Number of elements	Number of nodes	Number of active DOF	Multiplicity zero eigenvalue
1	6	9	1
4	15	30	1
16	45	108	1
64	153	408	1

Table 5.6:
Meshes properties and multiplicity of zero for the choices represented in
Figure 5.8 and Figure 5.9.

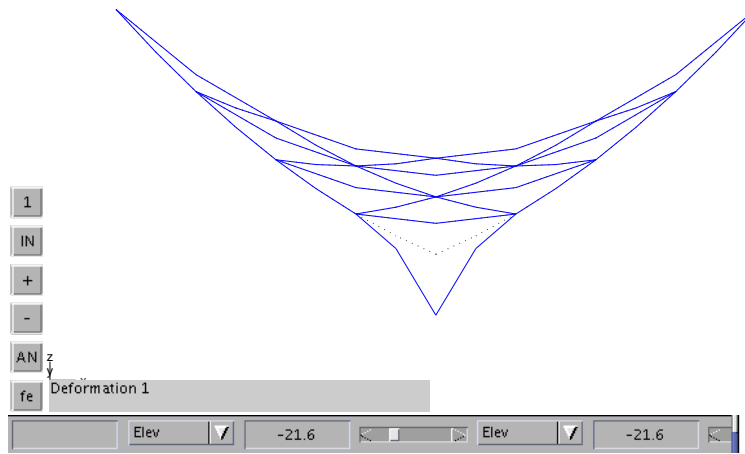


Figure 5.10: Zero membrane energy mode corresponding to the selection of tying points represented in Figure 5.9(f) when considering a mesh of 16 elements.

that some of them lock because $rank = 9$ is obtained for the partially covered case, which means that the solution will correspond to the zero displacement when it should not happen. For other tying schemes, desirable $rank = 9$ is not achieved for the completely covered situation – when zero displacements are expected – whereas satisfactory ranks are obtained in the other cases, and consequently modes of zero membrane energy may be propagated. The MITC6a triangular shell finite element lies inside this category, and difficulties may be induced in the case of membrane dominated shell problems.

This numerical test constitutes an useful tool to develop effective shell finite elements, even if it shows once more that uniformly optimal 6-node triangular shell finite elements are difficult to attain.

Chapter 6

Assessing MITC triangular shell elements

Dominique Chapelle, Iria Paris

Abstract

As is well known, in the finite element analysis of shells numerical locking occurs due to shear and membrane vanishing strains for bending dominated situations and general isoparametric shell finite elements show a good behavior for membrane dominated shell problems, but they clearly lock in a bending dominated framework independently of the degree of interpolation. Effective general shell finite elements are meant to well circumvent the locking problem without loss of consistency for membrane dominated shell problems (see [6], [31] and the references therein). An optimal triangular shell finite element remains to be found.

New strategies need to be designed, and one possible choice is the MITC technique (*Mixed Interpolation of Tensorial Components*) that has already been implemented as a useful locking removal tool for quadrangular plate/shell finite elements (MITC4, MITC9,...) and also for triangular plate/shell elements (MITC3, MITC7, MITC6a, ...) (see [6], [9],[12], [14], [47]). This strategy consists in making a reduction of strain components in order to prevent numerical locking and strains are connected to displacements at particular *tying points* (refer to Section 4.2). Recall that it corresponds to a mixed formulation and as a consequence parasitic membrane energy modes may appear.

We report upon the numerical results we have obtained for some particular choices of tying positions, which respectively define different 6-node MITC triangular shell finite elements. The MITC6a shell finite element firstly formulated

by Lee and Bathe in [47] has also been incorporated to our shell analysis, which complets [47] as:

- suitable norms are used to study the convergence of displacements: in [47] the convergence was analyzed by means of the *s-norm*, which is useful to analyze the convergence of strains, but it does not provide complete information regarding the displacements convergence as in particular it does not detect the presence of *membrane spurious modes*;
- reduced and unreduced energy values are summarized for each benchmark;
- proper boundary layer treatment is performed in each case (see Appendix E for more details).

The original MITC7 triangular finite element for plates ([9]) has also been investigated, being the in-plane strain components treated in the same manner as for the MITC6a shell finite element. We also present a MITC6b shell finite element that differs from the one appearing in [47].

Three different geometries and the bending and membrane dominated asymptotic behaviors are considered in our benchmarks: a clamped plate problem is analyzed in order to verify that the developed elements do not show shear locking for plates; afterwards, we focus on two cylindrical and two hyperboloid shell problems. *Quadratic convergence is expected*, but we observe that it is only approximately achieved for strains – as seen through the s-norm – although it is fairly reached for displacements when convergence holds (obviously seen through appropriate norms in each case). In all cases, convergence curves are displayed when only shear, shear and membrane and even bending tensors are treated in order to well understand what differs in each case and numerically assess the consistency of A_b^h with respect to A_b . Total and partial shear, membrane and bending energies are also computed for all the tying schemes and benchmarks analyzed. A comparison with the corresponding unreduced energies – with no interpolation for strains – is also made in order to determine how parasitic membrane energy modes can be revealed and compared to weak or strong numerical locking.

Although both sources of shell difficulties are well understood, all the attempts we have made until now tend to fail either because of membrane locking or spurious membrane modes. The results we have obtained show once more that uniformly optimal MITC6 isotropic triangular shell finite elements are difficult to attain.

The MITC6a shell finite element seems to be one of the best candidates that can be obtained, even if it is not optimal and needs to be improved.

6.1 Error measures

The concept of *shell* alludes to the idea of the thickness t being small as compared to the other dimensions of the structure. This property motivates the modeling of a 3D continuum medium as a shell in engineering analysis.

When defining shell models, kinematical assumptions through the thickness are incorporated in order to discretize the problem over the midsurface only (see Section 1.2). We expect uniform relative errors that could be bounded as follows:

$$\frac{\|U^\varepsilon - U_h^\varepsilon\|^2}{\|U^\varepsilon\|^2} \leq ch^{2p} \quad (6.1)$$

where $\varepsilon = t/L$ is the relative thickness, c denotes a positive bounding constant and p the order of convergence, both of them independent of the thickness value. The exact solution U^ε is hardly ever known, but in the practical use it can be replaced by a reference one, and h typically denotes the mesh size.

It is known that numerical locking occurs due to membrane and shear vanishing strains in bending dominated situations and displacement-based shell finite elements behave too stiffly (see Section 3). The MITC technique involves the interpolation of displacements on the one hand and the interpolation of strains on the other hand (sometimes referred to as *assumed strains*), and connects both interpolations at particular *tying points* (recall Section 4.2). This approach is done to prevent shear and membrane locking, but efficient MITC shell finite elements are supposed to preserve consistency for membrane dominated situations. As is well known, parasitic membrane energy modes may be introduced by mixed formulations and they *cannot be seen* through the corresponding reduced membrane energy. Nevertheless, we think that they should be detected through the displacement-based membrane and shear energies when no reduction of strains is done.

For the convergence studies that we present in this work the following appropriate norms have been considered:

- **The “s-norm”**: this norm is obtained by comparing the approximate and reference strains by means of the governing energy. Recall that it is useful to analyze the convergence of strains, but it does not provide complete information regarding the displacements convergence as in particular it does not detect the presence of *membrane spurious modes*.

For general shell element procedures and in the case of an isotropic material, we define:

$$\|U^\varepsilon - U_h^\varepsilon\|_s^2 = \int_{\Omega} \Delta\epsilon^T \Delta\sigma dV \quad (6.2)$$

where U^ε denotes the exact (or reference) solution and U_h^ε the solution of the finite element discretization. Here, $\Delta\epsilon$ and $\Delta\sigma$ denote the difference between the strain and stress component-vectors in the global Cartesian coordinate system:

$$\Delta\epsilon = \epsilon(\vec{x}) - \epsilon_h(\vec{x}_h) \quad (6.3)$$

$$\Delta\sigma = \sigma(\vec{x}) - \sigma_h(\vec{x}_h) = \mathbf{C}(\vec{x})\epsilon(\vec{x}) - \mathbf{C}_h(\vec{x}_h)\epsilon_h(\vec{x}_h) \quad (6.4)$$

where we have denoted:

$$\epsilon = [\epsilon_{xx}, \epsilon_{yy}, \epsilon_{zz}, 2\epsilon_{xy}, 2\epsilon_{yz}, 2\epsilon_{zx}]^T \quad (6.5)$$

$$\sigma = [\sigma_{xx}, \sigma_{yy}, \sigma_{zz}, \sigma_{xy}, \sigma_{yz}, \sigma_{zx}]^T \quad (6.6)$$

and \mathbf{C} denotes the material stress-strain matrix associated with the exact (or reference) geometry and \mathbf{C}_h denotes the discretized one. The position vectors \vec{x} and \vec{x}_h correspond to the continuum (or reference) and discretized (current) domain, respectively, and the relationship between them is given by a one-to-one mapping:

$$\vec{x} = \Pi(\vec{x}_h) \quad (6.7)$$

that is described in Appendix C. See also Appendix D for more details about the *s-norm* computation.

- **Asymptotic convergence norms:** these are the norms in which exact solutions are proven to converge to limit solutions. We will consider the membrane energy norm denoted by A_m for membrane dominated shell problems and the $A_b + A_m$ norm—which is equivalent to the norm of the displacement space, namely the H^1 norm—for bending dominated shell problems.

In order to compute the matrix associated with the membrane energy norm, a one point integration of the energy through the thickness is used in the displacement-based formulation. Sometimes large errors come from the approximation of rotations fields, and shear terms can be discarded from the A_m norm in order to determine if displacements *per se* are well predicted. In such a case, we will compute the A_m norm without shear terms.

The matrix associated with the $A_b + A_m$ norm corresponds to the displacement-based formulation energy when $\varepsilon = 1$.

When computing these norms, it is necessary to calculate the current displacement and rotation fields for nodes pertaining to the reference domain from current displacements and rotations. In order to localise the reference nodes in the current mesh we use the strategy described in Appendix C.

The relative error mentioned in the convergence curves summarized in this work is defined as:

$$relative\ error = \frac{\|U_{ref}^\varepsilon - U_h^\varepsilon\|^2}{\|U_{ref}^\varepsilon\|^2} \quad (6.8)$$

for a suitable norm $\|\cdot\|$.

It is important to notice that convergence curves are given in logarithmic scale, which implies that small variations between curves correspond to high differences between norm values.

6.2 MITC elements

The formulation of MITC shell finite elements was described in Section 4.2. Geometry and displacements are constructed by a standard 6-node isoparametric procedure (see Fig. 6.1), but strains are interpolated in a different way. The *tying procedure* connecting displacements and strains is carried out for each individual element (recall Section 4.2).

Isotropic elements are searched, which means that the element stiffness matrix must not depend on the node numbering that defines the element orientation and as discussed in Section 4.3, the normal in-plane and shear strain fields in the hypotenuse direction of the the right-angled triangle –namely, e_{qq} and e_{qz} – must be incorporated to our analysis.

We have investigated the MITC6a shell finite element firstly formulated by Lee and Bathe [47], and also other choices of tying positions that define elements of the MITC6 family (called MITC6b, MITC6c, MITC6d and MITC6e) which may not lock since they “pass” the membrane locking test presented in Section 5.2 for the partially covered element. We have also analyzed the MITC7 triangular shell finite element (originally formulated for plates [9]) which differs from the MITC6 family in the rotation interpolation: it involves the barycenter of the triangle for the interpolation of rotation fields, the corresponding degrees of freedom being treated by static condensation (refer to Appendix B for more details).

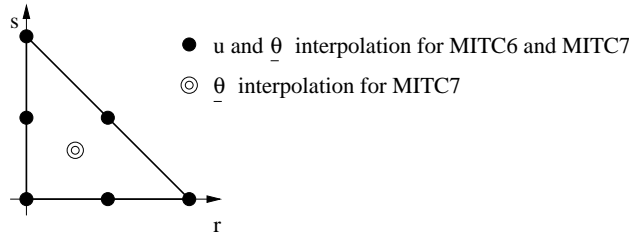


Figure 6.1: Displacement and rotation interpolation.

The different tying schemes that have been tested in this section are displayed in Fig. 6.2-6.6. The *assumed strains* are defined as follows:

Assumed in-plane covariant strains

In order to obtain isotropic elements and linear variations for in-plane strains along edges, two tying points are chosen at each edge in a same manner.

The tying schemes associated with the MITC6a, MITC6b and MITC7 shell finite elements are shown in Fig. 6.2 and Fig. 6.3. The corresponding assumed strains are given by the polynomials:

$$e_{rr}^h(r, s) = a_1 + b_1 r + c_1 s \quad (6.9)$$

$$e_{ss}^h(r, s) = a_2 + b_2 r + c_2 s \quad (6.10)$$

$$e_{qq}^h(r, s) = a_3 + b_3 r + c_3(1 - r - s) \quad (6.11)$$

In order to obtain the associated coefficients, we denote by:

$$m_{rr}^{(1)} = \frac{1}{2} (e_{rr}(r_1, 0) + e_{rr}(r_2, 0)) \quad l_{rr}^{(1)} = \frac{\sqrt{3}}{2} (e_{rr}(r_2, 0) - e_{rr}(r_1, 0)) \quad (6.12)$$

$$m_{ss}^{(2)} = \frac{1}{2} (e_{ss}(0, s_1) + e_{ss}(0, s_2)) \quad l_{ss}^{(2)} = \frac{\sqrt{3}}{2} (e_{ss}(0, s_2) - e_{ss}(0, s_1)) \quad (6.13)$$

$$m_{qq}^{(3)} = \frac{1}{2} (e_{qq}(r_1, s_2) + e_{qq}(r_2, s_1)) \quad l_{qq}^{(3)} = \frac{\sqrt{3}}{2} (e_{qq}(r_1, s_2) - e_{qq}(r_2, s_1)) \quad (6.14)$$

and the following conditions are set:

$$\begin{aligned} e_{rr}^h(0, 0) &= m_{rr}^{(1)} - l_{rr}^{(1)} & e_{rr}^h(1/2, 0) &= m_{rr}^{(1)} & e_{rr}^h(1, 0) &= m_{rr}^{(1)} + l_{rr}^{(1)} \\ e_{ss}^h(0, 0) &= m_{ss}^{(2)} - l_{ss}^{(2)} & e_{ss}^h(0, 1/2) &= m_{ss}^{(2)} & e_{ss}^h(0, 1) &= m_{ss}^{(2)} + l_{ss}^{(2)} \\ e_{qq}^h(1, 0) &= m_{qq}^{(3)} - l_{qq}^{(3)} & e_{qq}^h(1/2, 1/2) &= m_{qq}^{(3)} & e_{qq}^h(0, 1) &= m_{qq}^{(3)} + l_{qq}^{(3)} \\ e_{rr}^h(r_1, s_4) &= e_{rr}(r_1, s_4) & e_{ss}^h(r_4, s_1) &= e_{ss}(r_4, s_1) & e_{qq}^h(r_1, s_1) &= e_{qq}(r_1, s_1) \end{aligned} \quad (6.15)$$

The solution of these equations gives

$$\begin{aligned} a_1 &= m_{rr}^{(1)} - l_{rr}^{(1)}, & b_1 &= 2l_{rr}^{(1)}, \\ a_2 &= m_{ss}^{(2)} - l_{ss}^{(2)}, & c_2 &= 2l_{ss}^{(2)}, \\ a_3 &= m_{qq}^{(3)} + l_{qq}^{(3)}, & b_3 &= -2l_{qq}^{(3)}, \\ c_1 &= \sqrt{3} (e_{rr}(r_1, s_4) - a_1 - b_1 r_1), \\ b_2 &= \sqrt{3} (e_{ss}(r_4, s_1) - a_2 - c_2 s_1), \\ c_3 &= \sqrt{3} (e_{qq}(r_1, s_1) - a_3 - b_3 r_1) \end{aligned} \quad (6.16)$$

The tying schemes associated with the MITC6c, MITC6d and MITC6e shell finite elements are displayed in Fig. 6.4, 6.5 and 6.6. For each in-plane covariant component we consider three tying points and a set of functions $\{\lambda_{rr}^l\}_{l=1}^3$, $\{\lambda_{ss}^l\}_{l=1}^3$ and $\{\lambda_{qq}^l\}_{l=1}^3$ satisfying :

$$\lambda_{ii}^l(r_{ii}^m, s_{ii}^m) = \delta_{lm}, \quad l, m = 1, \dots, 3 \quad (6.17)$$

for $i = r, s, q$. We define the assumed in-plane covariant strain components as:

$$e_{ii}^h(r, s, z) = \sum_{l=1}^3 \lambda_{ii}^l(r, s) e_{ii}(r_{ii}^l, s_{ii}^l, z) \quad \text{for } i = r, s, q \quad (6.18)$$

Transverse shear strains

Linear transverse shear strains along edges are assumed and consequently two tying points are chosen at each edge in a symmetric way. Quadratic variations inside each element are desired, and the *assumed covariant transverse shear strains* that we consider are defined as:

$$e_{rz}^h(r, s) = a_4 + b_4 r + c_4 s + s(dr + es) \quad (6.19)$$

$$e_{sz}^h(r, s) = a_5 + b_5 r + c_5 s - r(dr + es) \quad (6.20)$$

We must also have in mind (4.56) to determine the polynomial coefficients. We denote by:

$$m_{rz}^{(1)} = \frac{1}{2} (e_{rz}(r_1, 0) + e_{rz}(r_2, 0)) \quad l_{rz}^{(1)} = \frac{\sqrt{3}}{2} (e_{rz}(r_2, 0) - e_{rz}(r_1, 0)) \quad (6.21)$$

$$m_{sz}^{(2)} = \frac{1}{2} (e_{sz}(0, s_1) + e_{sz}(0, s_2)) \quad l_{sz}^{(2)} = \frac{\sqrt{3}}{2} (e_{sz}(0, s_2) - e_{sz}(0, s_1)) \quad (6.22)$$

$$m_{qz}^{(3)} = \frac{1}{2} (e_{qz}(r_1, s_2) + e_{qz}(r_2, s_1)) \quad l_{qz}^{(3)} = \frac{\sqrt{3}}{2} (e_{qz}(r_1, s_2) - e_{qz}(r_2, s_1)) \quad (6.23)$$

and we the following conditions are set:

$$\begin{aligned} e_{rz}^h(0, 0) &= m_{rz}^{(1)} - l_{rz}^{(1)} & e_{rz}^h(1/2, 0) &= m_{rz}^{(1)} & e_{rz}^h(1, 0) &= m_{rz}^{(1)} + l_{rz}^{(1)} \\ e_{sz}^h(0, 0) &= m_{sz}^{(2)} - l_{sz}^{(2)} & e_{sz}^h(0, 1/2) &= m_{sz}^{(2)} & e_{sz}^h(0, 1) &= m_{sz}^{(2)} + l_{sz}^{(2)} \\ e_{qz}^h(1, 0) &= m_{qz}^{(3)} - l_{qz}^{(3)} & e_{qz}^h(1/2, 1/2) &= m_{qz}^{(3)} & e_{qz}^h(0, 1) &= m_{qz}^{(3)} + l_{qz}^{(3)} \\ e_{rz}^h(1/3, 1/3) &= e_{rz}^c & e_{sz}^h(1/3, 1/3) &= e_{sz}^c & e_{qz}^h(1/3, 1/3) &= e_{qz}^c \end{aligned} \quad (6.24)$$

We have

$$\begin{aligned}
 a_4 &= m_{rz}^{(1)} - l_{rz}^{(1)}, & b_4 &= 2l_{rz}^{(1)}, \\
 a_5 &= m_{sz}^{(2)} - l_{sz}^{(2)}, & c_5 &= 2l_{sz}^{(2)}, \\
 c_4 &= 6e_{rz}^c - 3e_{sz}^c + 2m_{sz}^{(3)} - 2m_{rz}^{(3)} - 4a_4 - b_4 + a_5, \\
 d &= -3e_{rz}^c + 6e_{sz}^c - 3m_{sz}^{(3)} + 3m_{rz}^{(3)} + l_{sz}^{(3)} - l_{rz}^{(3)} - b_4 - 3a_5 - c_5, \\
 b_5 &= -3e_{rz}^c + 6e_{sz}^c - 2m_{sz}^{(3)} + 2m_{rz}^{(3)} - 4a_5 + a_4 - c_5, \\
 e &= -6e_{rz}^c + 3e_{sz}^c - 3m_{sz}^{(3)} + 3m_{rz}^{(3)} - l_{sz}^{(3)} + l_{rz}^{(3)} + 3a_4 + b_4 + c_5
 \end{aligned} \tag{6.25}$$

For the MITC6a, MITC7, MITC6c, MITC6d and MITC6e shell finite elements we define:

$$e_{iz}^c = e_{iz}(1/3, 1/3) \quad \text{for } i = r, s, z$$

The element that slightly differs for the assumed transverse shear covariant strains interpolation is the MITC6b shell finite elements. In this case we consider:

$$e_{iz}^c = \frac{1}{3} [e_{iz}(r_1, s_1) + e_{iz}(r_4, s_1) + e_{iz}(r_1, s_4)]$$

for $i = r, s, q$.

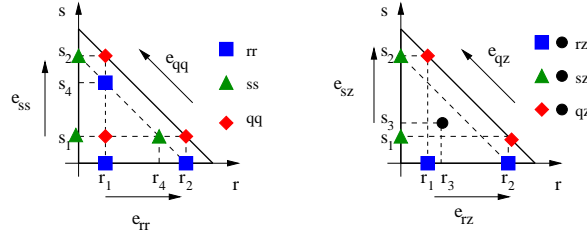


Figure 6.2: MITC6a and MITC7 tying positions for each strain component ($r_1 = s_1 = \frac{1}{2} - \frac{1}{2\sqrt{3}}$, $r_2 = s_2 = \frac{1}{2} + \frac{1}{2\sqrt{3}}$, $r_3 = s_3 = \frac{1}{3}$, $r_4 = s_4 = \frac{1}{\sqrt{3}}$).

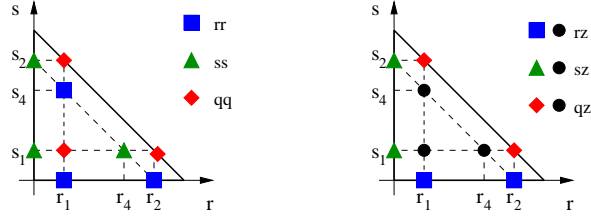


Figure 6.3: MITC6b tying positions for each strain component ($r_1 = s_1 = \frac{1}{2} - \frac{1}{2\sqrt{3}}$, $r_2 = s_2 = \frac{1}{2} + \frac{1}{2\sqrt{3}}$, $r_4 = s_4 = \frac{1}{\sqrt{3}}$).

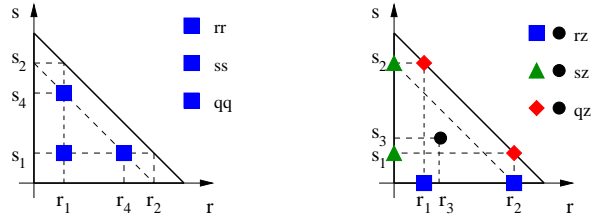


Figure 6.4: MITC6c tying positions for each strain component ($r_1 = s_1 = \frac{1}{2} - \frac{1}{2\sqrt{3}}$, $r_2 = s_2 = \frac{1}{2} + \frac{1}{2\sqrt{3}}$, $r_3 = s_3 = \frac{1}{3}$, $r_4 = s_4 = \frac{1}{\sqrt{3}}$).

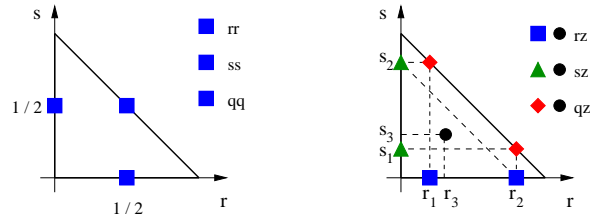


Figure 6.5: MITC6d tying positions for each strain component ($r_1 = s_1 = \frac{1}{2} - \frac{1}{2\sqrt{3}}$, $r_2 = s_2 = \frac{1}{2} + \frac{1}{2\sqrt{3}}$, $r_3 = s_3 = \frac{1}{3}$).

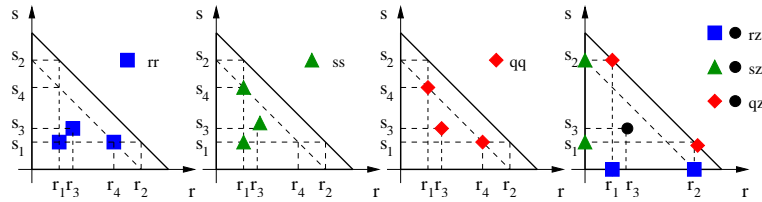


Figure 6.6: MITC6e tying positions for each strain component ($r_1 = s_1 = \frac{1}{2} - \frac{1}{2\sqrt{3}}$, $r_2 = s_2 = \frac{1}{2} + \frac{1}{2\sqrt{3}}$, $r_3 = s_3 = \frac{1}{3}$, $r_4 = s_4 = \frac{1}{\sqrt{3}}$).

6.3 Benchmarks and numerical results

We report upon some numerical tests that have been carried out for the MITC isotropic shell finite elements described in the previous section.

6.3.1 Clamped plate problem

For the first benchmark test we consider a plate bending problem given by a fully clamped square plate of dimension $2L \times 2L$ and uniform thickness t subjected to self-weight loading (see Fig. 6.7).

The normal vector corresponding to all nodal positions is given by:

$$\vec{a}_3 = (0, 0, 1)^T \quad (6.26)$$

As usual, we define \vec{V}_1 and \vec{V}_2 orthogonal to \vec{a}_3 and to each other:

$$\vec{V}_1 = \frac{\vec{a}_3 \times \vec{e}_x}{\|\vec{a}_3 \times \vec{e}_x\|}, \quad \vec{V}_2 = \vec{a}_3 \times \vec{V}_1 \quad (6.27)$$

for $\vec{e}_x = (1, 0, 0)^T$ and we obtain:

$$\vec{V}_1 = (0, 1, 0)^T \quad (6.28)$$

$$\vec{V}_2 = (-1, 0, 0)^T \quad (6.29)$$

Due to symmetry properties, only one quarter of the structure needs to be analyzed. The symmetry and boundary conditions are imposed as follows:

$$u_x = \alpha_2 = 0 \quad \text{along} \quad BC \quad (6.30)$$

$$u_y = \alpha_1 = 0 \quad \text{along} \quad DC \quad (6.31)$$

$$u_x = u_y = u_z = \alpha_1 = \alpha_2 = 0 \quad \text{along} \quad AB \quad \text{and} \quad AD \quad (6.32)$$

The reference solution is obtained using a mesh of 96×96 MITC4 shell finite elements.

Conclusions

For this particular framework, membrane strains vanish and consequently this test problem shows if the shear tensor is well predicted by the MITC interpolation.

Numerical locking clearly occurs for P_2 displacement-based shell finite elements (refer to Fig. 6.8), whereas displacements and strains are reasonably predicted for all choices of tying positions presented here (respectively seen by means of the $A_b + A_m$ norm and s -norm). Actually, convergence curves obtained when *only shear* or *shear and membrane*—even *bending*—tensors are treated do not really mismatch, except for the MITC7 finite element (see Fig. 6.9-6.20).

As expected, the MITC6- convergence curves do not differ except for the MITC6b shell finite element which incorporates a slightly different interpolation

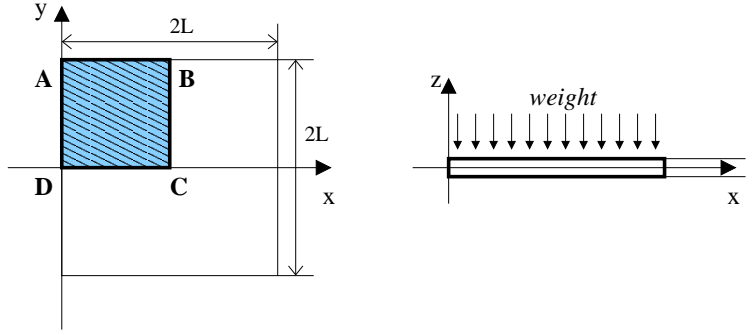


Figure 6.7: Clamped plate loaded by self-weight ($L = 1.0$, $E = 1.7472 \times 10^7$, $\nu = 0.3$ and $\rho = 3000$).

of transverse shear strains. On the other hand, the MITC7 rotations involve P_3 interpolation and consequently the displacement-based bending tensor verifies that $\underline{\chi} \in P_2$, whereas the corresponding bending treatment gives $\underline{\chi}^h \in P_1$. Hence, the MITC7 convergence curves rather differ when bending is treated.

Optimal convergence rate is fairly achieved, although s-norm convergence curves tend to slightly rise as ε and h decreases, but this fact may be due to the absence of boundary layer treatment.

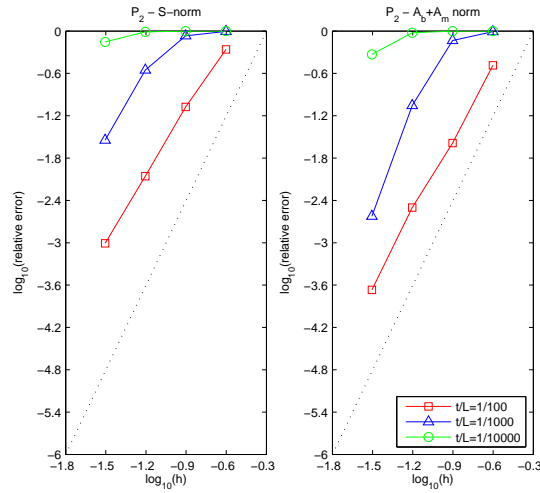


Figure 6.8: S-norm and $A_b + A_m$ -norm convergence curves associated with the clamped plate problem and P_2 displacement-based shell finite elements. The dotted line shows the optimal convergence rate which is 4.

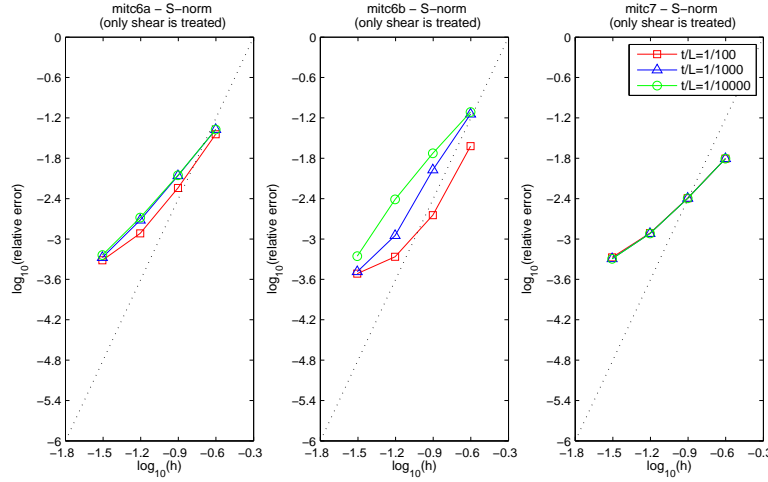


Figure 6.9: S-norm convergence curves associated with the clamped plate problem: MITC6a, MITC6b and MITC7 shell finite elements when *only shear* is treated. The dotted line shows the optimal convergence rate which is 4 for quadratic elements.

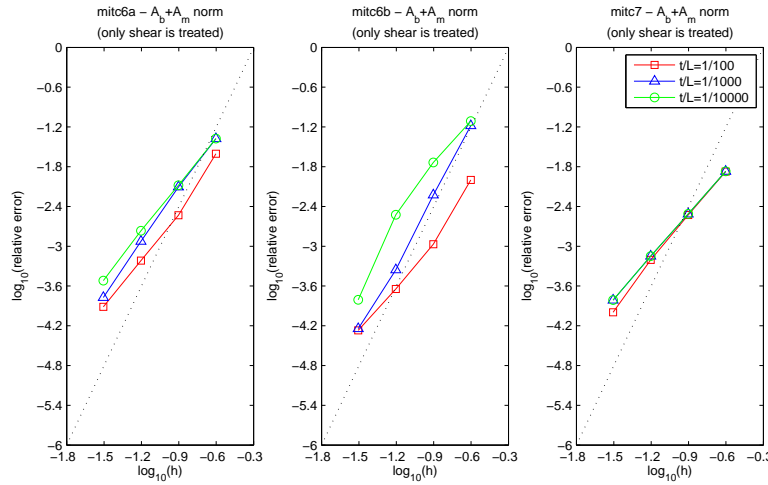


Figure 6.10: $A_b + A_m$ -norm convergence curves associated with the clamped plate problem: MITC6a, MITC6b and MITC7 shell finite elements when *only shear* is treated. The dotted line shows the optimal convergence rate which is 4 for quadratic elements.

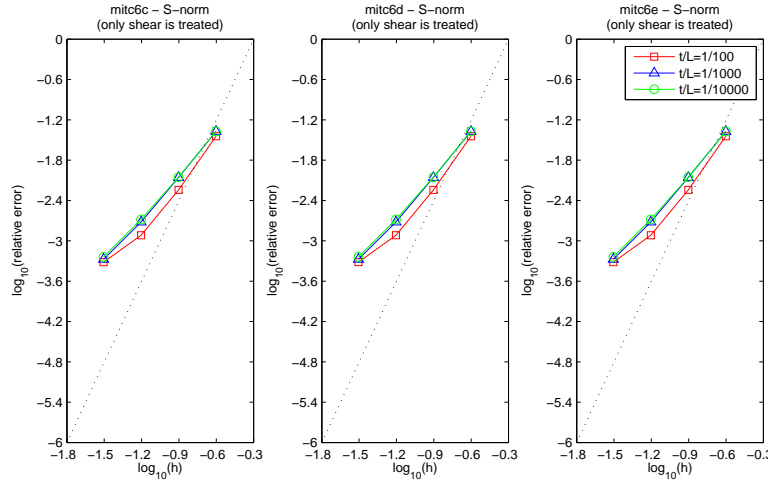


Figure 6.11: S-norm convergence curves associated with the clamped plate problem: MITC6c, MITC6d and MITC6e shell finite elements when *only shear* is treated. The dotted line shows the optimal convergence rate which is 4 for quadratic elements.

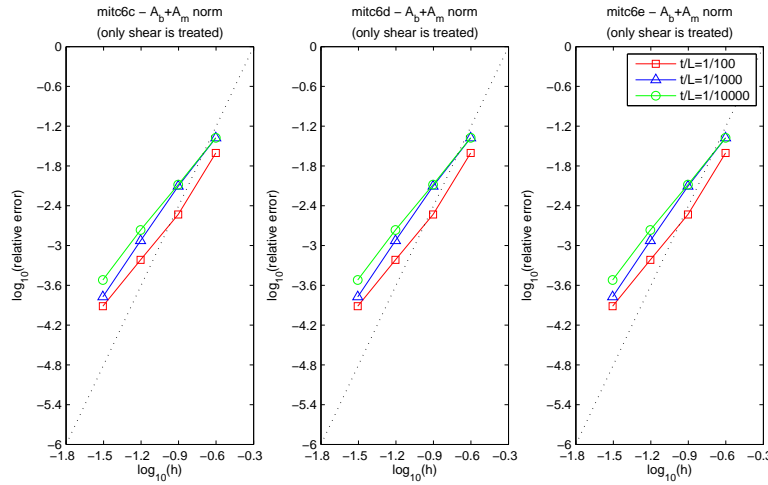


Figure 6.12: $A_b + A_m$ -norm convergence curves associated with the clamped plate problem: MITC6c, MITC6d and MITC6e shell finite elements when *only shear* is treated. The dotted line shows the optimal convergence rate which is 4 for quadratic elements.

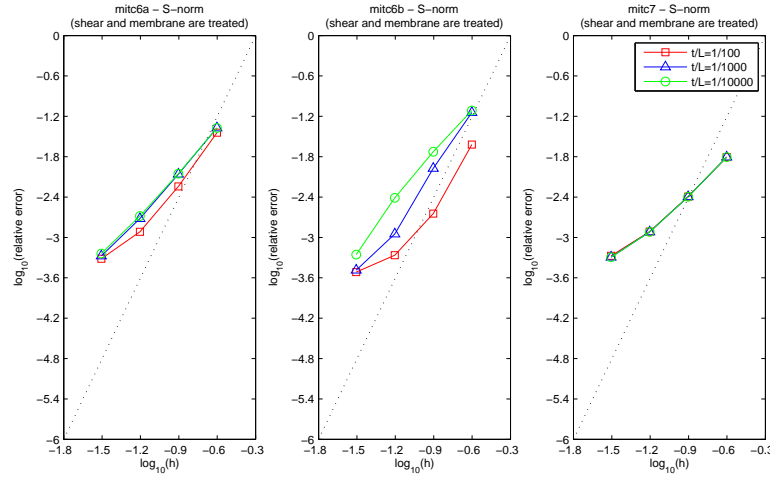


Figure 6.13: S-norm convergence curves associated with the clamped plate problem: MITC6a, MITC6b and MITC7 shell finite elements when *shear and membrane* are treated. The dotted line shows the optimal convergence rate which is 4 for quadratic elements.

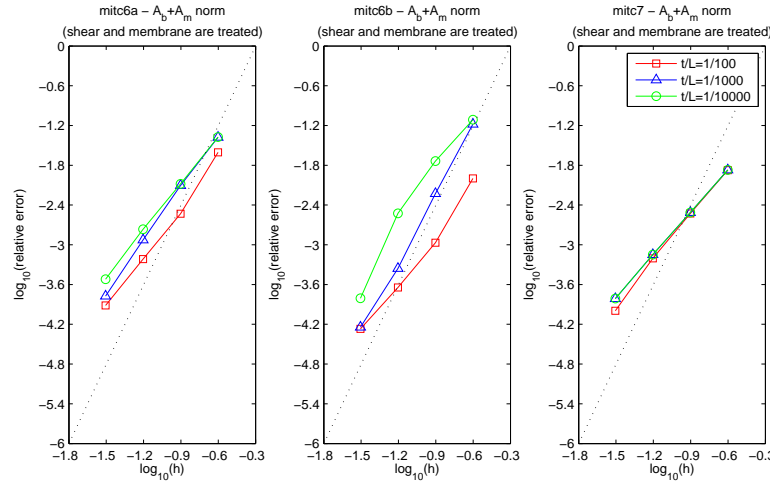


Figure 6.14: $A_b + A_m$ -norm convergence curves associated with the clamped plate problem: MITC6a, MITC6b and MITC7 shell finite elements when *shear and membrane* are treated. The dotted line shows the optimal convergence rate which is 4 for quadratic elements.

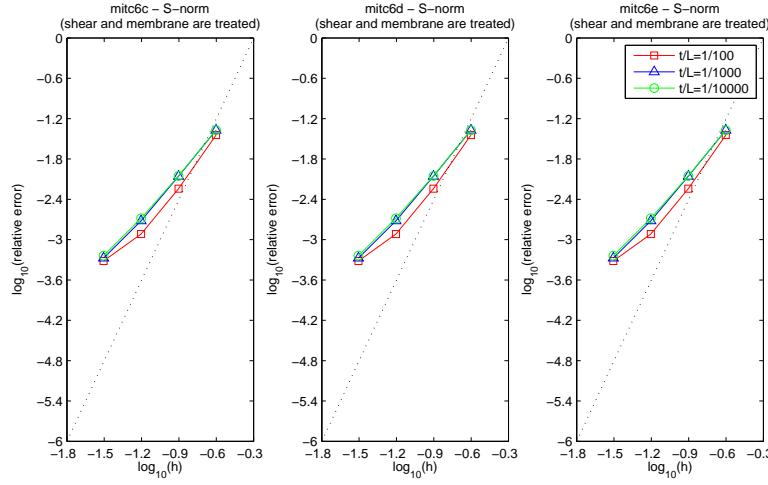


Figure 6.15: S-norm convergence curves associated with the clamped plate problem: MITC6c, MITC6d and MITC6e shell finite elements when *shear and membrane* are treated. The dotted line shows the optimal convergence rate which is 4 for quadratic elements.

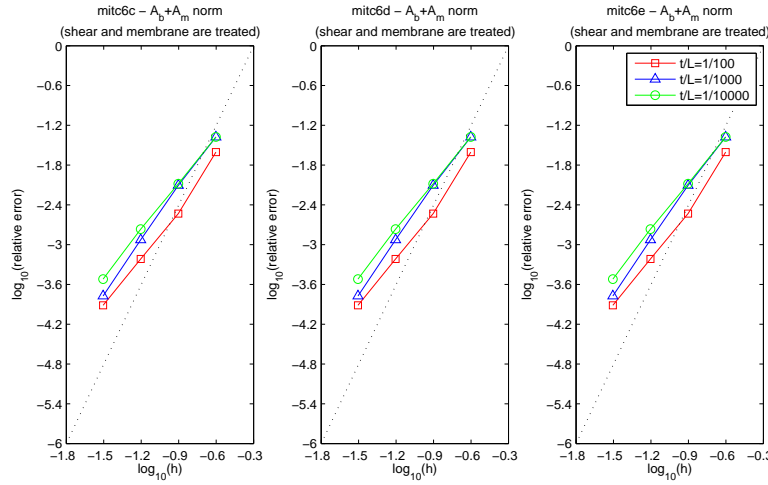


Figure 6.16: $A_b + A_m$ -norm convergence curves associated with the clamped plate problem: MITC6c, MITC6d and MITC6e shell finite elements when *shear and membrane* are treated. The dotted line shows the optimal convergence rate which is 4 for quadratic elements.

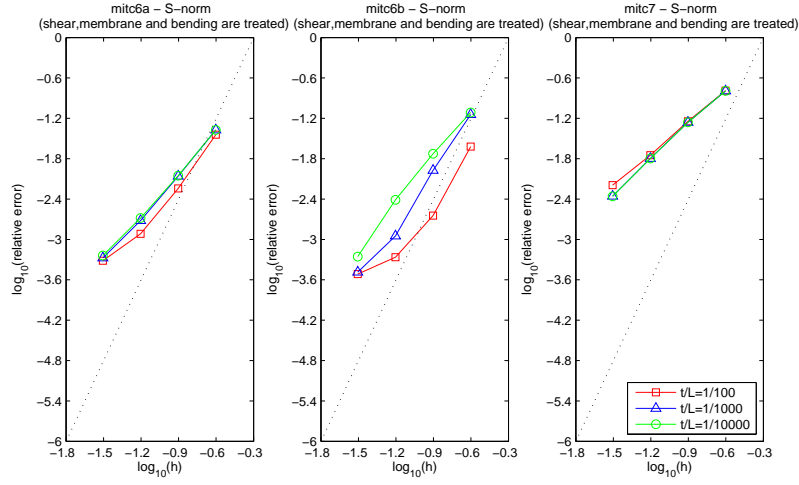


Figure 6.17: S-norm convergence curves associated with the clamped plate problem: MITC6a, MITC6b and MITC7 shell finite elements when *shear, membrane and bending* are treated. The dotted line shows the optimal convergence rate which is 4 for quadratic elements.

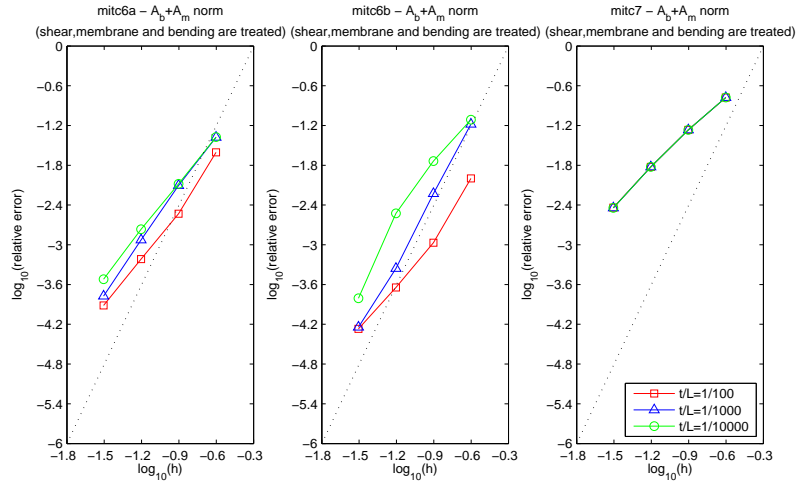


Figure 6.18: $A_b + A_m$ -norm convergence curves associated with the clamped plate problem: MITC6a, MITC6b and MITC7 shell finite elements when *shear, membrane and bending* are treated. The dotted line shows the optimal convergence rate which is 4 for quadratic elements.

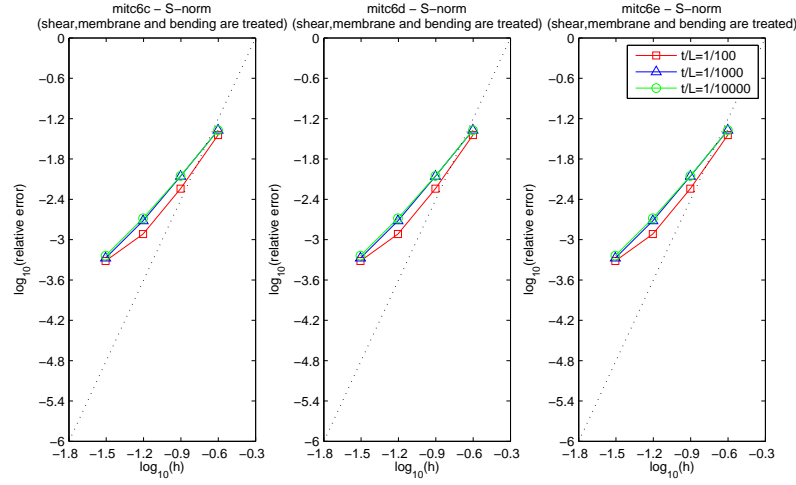


Figure 6.19: S-norm convergence curves associated with the clamped plate problem: MITC6c, MITC6d and MITC6e shell finite elements when *shear, membrane and bending* are treated. The dotted line shows the optimal convergence rate which is 4 for quadratic elements.

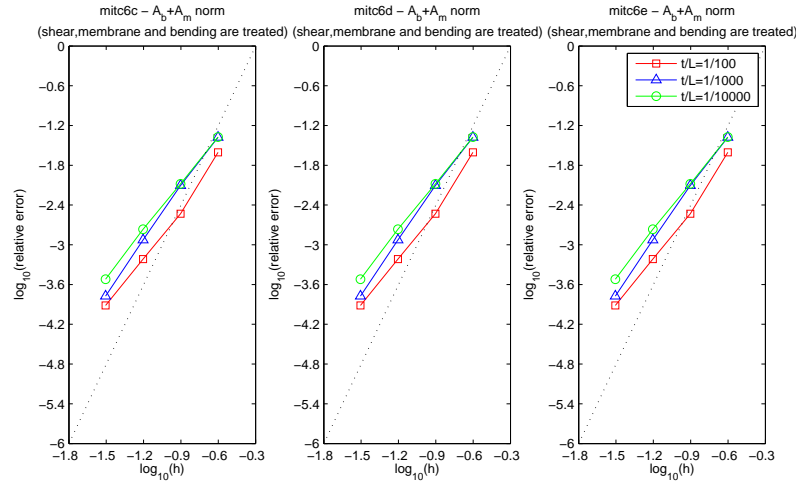


Figure 6.20: $A_b + A_m$ -norm convergence curves associated with the clamped plate problem: MITC6c, MITC6d and MITC6e shell finite elements when *shear, membrane and bending* are treated. The dotted line shows the optimal convergence rate which is 4 for quadratic elements.

6.3.2 Cylindrical shell problems

For these test problems we consider a cylindrical shell of uniform thickness t , length $2L$ and radius R loaded by the periodic pressure distribution normal to the shell midsurface defined as follows:

$$p(\varphi) = p_0 \cos(2\varphi) \quad (6.33)$$

The shell midsurface is described by:

$$x \in [-L, L], \quad y^2 + z^2 = R^2 \quad (6.34)$$

and the normal vector corresponding to a point of coordinates (x, y, z) in the global Cartesian coordinate system is given by:

$$\vec{a}_3(x, y, z) = \frac{1}{R}(0, y, z)^T \quad (6.35)$$

The vectors \vec{V}_1 and \vec{V}_2 —that together with \vec{a}_3 constitute a local orthonormal basis at each point of the midsurface—are defined as:

$$\vec{V}_1 = \frac{\vec{a}_3 \times \vec{e}_x}{\|\vec{a}_3 \times \vec{e}_x\|}, \quad \vec{V}_2 = \vec{a}_3 \times \vec{V}_1 \quad (6.36)$$

for $\vec{e}_x = (1, 0, 0)^T$. We obtain:

$$\vec{V}_1(x, y, z) = \frac{1}{R}(0, z, -y)^T, \quad \vec{V}_2(x, y, z) = (-1, 0, 0)^T \quad (6.37)$$

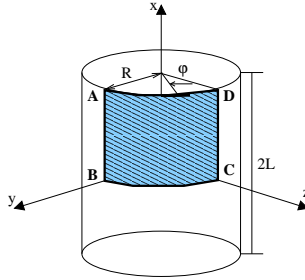


Figure 6.21: Cylindrical shell problem under pressure load ($L = R = 1.0$, $E = 2.0 \times 10^5$, $\nu = 1/3$ and $p_0 = 1.0$).

This cylindrical shell is sensitive to boundary conditions: it exhibits a *bending dominated behavior* when both ends are free and a *membrane dominated behavior* when the ends are clamped. The analysis of both situations can be restricted to

one eighth of the whole structure –the $ABCD$ region shown in Fig. 6.21– and the following symmetry conditions are set:

$$u_x = \alpha_2 = 0 \quad \text{along } BC \quad (6.38)$$

$$u_y = \alpha_1 = 0 \quad \text{along } CD \quad (6.39)$$

$$u_z = \alpha_1 = 0 \quad \text{along } AB \quad (6.40)$$

For the *clamped case* we must also impose the boundary conditions:

$$u_x = u_y = u_z = \alpha_1 = \alpha_2 = 0 \quad \text{along } AD \quad (6.41)$$

The numerical results presented below were obtained by properly meshing a boundary layer numerically identified to be of length $5\sqrt{\varepsilon}L$ for the clamped situation. The sequence of meshes was constructed accordingly: $N+1$ (axial direction) by $2N+1$ (circumferential direction) vertex outside of the boundary layer area and $N_{BL}(\varepsilon)+1$ (axial) by $2N+1$ (circumferential) vertex into the boundary layer area, where $N_{BL}(\varepsilon) \sim N\varepsilon^{-1/4}$ (see Table 6.1 and Fig. 6.22). The P_2 displacement-based shell finite element is taken as reference for the error computations in this case.

	N	$N_{BL}(10^{-2})$	$N_{BL}(10^{-3})$	$N_{BL}(10^{-4})$	h
<i>Target</i>	2	7	12	20	0.25
	4	14	24	40	0.125
	8	28	48	80	0.0625
<i>Reference</i>	22	77	132	220	

Table 6.1: ε -dependent sequence of reference and target meshes for the clamped cylindrical shell problem.

For the free cylindrical shell problem uniform meshes defined by $2N+1$ vertex in axial and circumferential directions are considered (taking $N = 2, 4, 8, 16$). The reference solutions consist of 96 (axial direction) by 96 (circumferential direction) MITC4¹ shell finite elements for all thickness values.

We refer the reader to Appendix E for more details on boundary layer treatment.

Structure with clamped ends

First of all, we focus on the membrane dominated situation. Displacement and strain errors are respectively seen by means of the displacement-based membrane energy norm –denoted by A_m – and s -norm.

As expected, P_2 displacement-based shell finite elements provide good numerical solutions (see Fig. 6.23), and uniform quadractic convergence is achieved for

¹Described in Appendix A.

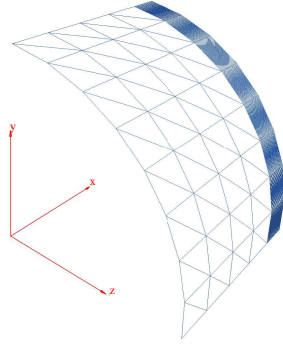


Figure 6.22: Example of mesh used for the clamped cylindrical shell problem ($N = 4$, $\varepsilon = 10^{-3}$ and $N_{BL} = 24$).

strains (seen through the s -norm) and displacements and rotations (through the A_m norm, with shear terms discarded and not).

Once shear is reduced, strains uniformly converge (see Fig. 6.25 and Fig. 6.27) but the convergence curves displayed on Fig. 6.37-6.38 show that displacements are not well predicted for coarse meshes and small thickness. In order to more precisely understand its origin, similar curves have been calculated when the shear terms are discarded from the A_m norm –only midsurface displacements are considered- and they show uniform convergence as thickness decreases and meshes are refined (refer to Fig. 6.26 and 6.28). Consequently, we conclude that large errors in the original A_m norm come from rotations.

Once the membrane is treated, some deterioration is observed in the strain fields as seen by means of the s -norm (see Fig. 6.29, 6.31, 6.33 and 6.35) independently of bending treatment. We also point out that displacements get worse as seen through the A_m norm –displacement-based membrane and shear- and errors are larger (see Fig. 6.39-6.42), even not admissible. On the other hand, similar curves have been calculated when the shear terms are discarded from the A_m norm, only displacements *per se* being computed, and convergence curves get better, although they are not uniform and they deteriorate for small thickness and coarse meshes for the MITC6a, MITC6b, MITC6c, MITC6e and particularly for the MITC7 shell finite element (refer to Fig. 6.30, 6.32, 6.34 and 6.36). On the contrary, the A_m norm without shear convergence curves associated with the MITC6d shell finite element show an optimal behavior.

It is important to notice that numerical results do not get worse because of bending treatment², except for the MITC7 shell finite element, for which convergence curves deteriorate due to P_3 interpolation of rotation fields.

Total and partial energy values associated with the P_2 reference and target so-

²Originally, only shear and membrane tensors should be treated.

lutions are displayed in Table 6.2. It confirms that the asymptotic behavior of the structure is membrane-dominated: shear and bending energies vanish as thickness decreases, whereas the membrane energy becomes dominant and it can be scaled by a factor of ε . Given a thickness value, total and partial energy values converge as the mesh is refined.

Tables 6.3-6.8 summarize a comparison between reduced and unreduced energy values for different meshes and all the MITC shell finite elements considered in this work as ε decreases once *shear*, *membrane* and *bending* tensors are reduced:

- for the MITC7 shell finite element only the membrane energy can be calculated separately because shear and bending tensors are mixed at the element level by the static condensation associated with the barycenter rotation fields;
- for all the MITC6 shell finite elements, reduced shear and bending energies vanish as thickness decreases, whereas the MITC membrane energy becomes dominant, close to P_2 reference values and it can be scaled by a factor of ε ; namely, these elements behave quite well from the energy point of view and the asymptotic nature of the problem is well detected by them;
- the MITC7 shell finite element also behaves correctly from the energy point of view: reduced membrane energy gets close to reduced total energy for all thickness as the mesh is refined and it can be scaled by a factor of ε ;
- we observe also that reduced and unreduced bending energy values remain quite close for all the MITC6 shell elements independently of the thickness and mesh refinement, although they are a little higher than the bending energies associated with the P_2 solutions for each ε and h ;
- in all cases, reduced and unreduced shear energies differ by several orders of magnitude, while such difference is weaker for reduced and unreduced membrane energies; furthermore, reduced shear energies remain higher than the shear energy values associated with the P_2 solution as the mesh is refined. This fact makes us think that *parasitic membrane energy modes may be present and they are revealed through the unreduced shear energy*, which would explain large errors when shear terms are not discarded from the A_m norm.

We invite the reader to focus on Fig. 6.43: midsurface deformed meshes are displayed for the different MITC elements considered and $\varepsilon = 0.0001$, using a scale factor equal to 0.5 for all figures. The expected behavior corresponds to the P_2 isoparametric shell element, which constitutes a good candidate for membrane-dominated shell problems. It is clearly observed that parasitic membrane modes seem to be propagated along MITC deformed meshes except for the MITC6d shell element.

Structure with free ends

As is well known, the P_2 displacement-based shell finite elements behave too stiffly in the case of bending-dominated shell problems as Fig. 6.24 shows: we observe that s -norm and $A_b + A_m$ convergence curves deteriorate as ε decreases, and for small thickness they don't seem to converge at all.

As is well known, shear treatment is not sufficient to prevent numerical locking (refer to Fig. 6.44-6.47), and membrane tensor components must be also reduced to get better numerical solutions.

For the MITC6c, MITC6d and MITC6e shell finite elements, strains (s -norm) and displacements ($A_b + A_m$ norm) show a behavior similar to the P_2 displacement-based element once the membrane –and bending– components are treated (see Fig. 6.50, 6.51, 6.54 and 6.55): strong numerical locking clearly occurs.

On the other hand, we observe that the MITC6a, MITC6b and MITC7 shell finite elements behave considerably better (see Fig. 6.48, 6.49, 6.52 and 6.53): the corresponding convergence curves show a good behavior once shear and membrane –even bending– components are treated, as displacements are seen through the $A_b + A_m$ norm and strains by means of the usual s -norm (refer to Fig. 6.48, 6.49, 6.52 and 6.53). Optimal convergence rate is nearly achieved for displacements seen through the $A_b + A_m$ norm, although s -norm convergence tends to slightly rise as ε decreases. Results get a little worse for the MITC7 shell finite element when bending tensor is also treated, because of higher rotation interpolation.

Partial and total energy values are summarized in Table 6.9 for the MITC4 shell finite element taken as reference. It shows that the bending nature of the problem is well captured by the MITC4 element as shear and membrane energies vanish for decreasing thickness, whereas the bending energy becomes dominant and it can be scaled by a factor of ε^3 .

The reduced and unreduced energy values associated with the MITC and P_2 displacement-based shell finite elements are displayed in Tables 6.10-6.16:

- for the MITC7 shell finite element only the membrane energy can be calculated separately because shear and bending tensors are mixed at the element level by the static condensation associated with the barycenter rotation fields;
- the table associated with the displacement-based P_2 finite element shows that it clearly locks as membrane energy remains dominant for small thickness and refined meshes (see Table 6.10);
- a similar behavior is observed for the MITC6c, MITC6d and MITC6e shell finite elements (see Tables 6.14-6.16); it is important to notice how energies behave for such shell finite elements: reduced and unreduced membrane and bending energies get of the same order of magnitude for all relative thickness values as meshes are refined, whereas reduced and unreduced shear energy values differ by several orders of magnitude independently of mesh refinement for small thickness values;

- the MITC6a and MITC6b shell finite elements seem to well capture the nature of the problem as reduced bending energy values can be scaled by ε^3 and they converge to the MITC4 reference values for all ε as the mesh is refined; we observe that reduced bending energy is always dominant (and close to reduced total energy), whereas reduced membrane and shear energies decrease as thickness decreases and the mesh is refined;
- in the case of the MITC7 shell finite element, total reduced energy also tends to the total MITC4 reference energy for all thickness values as the mesh is refined;
- unreduced membrane energy is higher –by several orders of magnitude– than reduced membrane energy for the MITC6a, MITC6b, MITC7 shell finite elements, in contrast with the MITC6c, MITC6d and MITC6e shell finite elements;
- in the case of the MITC6a and MITC6b shell finite elements we observe that reduced and unreduced shear energies also differ by several orders of magnitude, and unreduced membrane energy is always higher than unreduced shear energy.

In spite of the bending-dominated nature of the problem, numerical results do not get worse because of bending treatment, except for the MITC7 shell finite element, for which convergence curves rise.

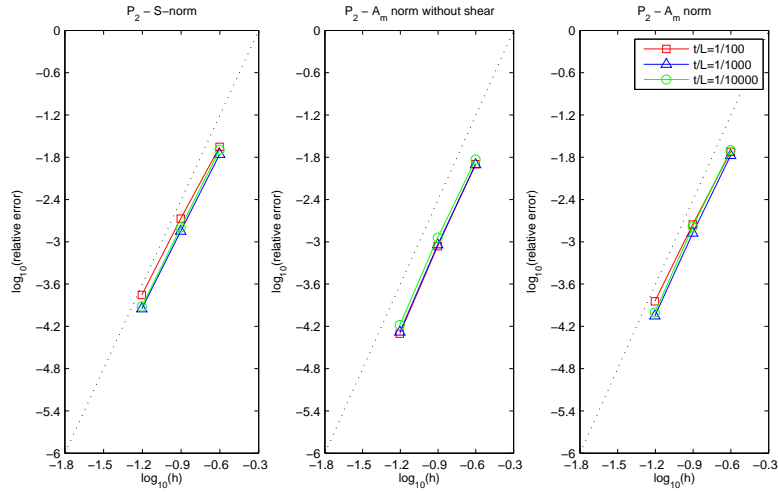


Figure 6.23: Convergence curves associated with the s-norm and membrane energy norm (with shear terms discarded or not) for the clamped cylindrical shell problem and P_2 displacement-based shell finite elements. The dotted line shows the optimal convergence rate which is 4.

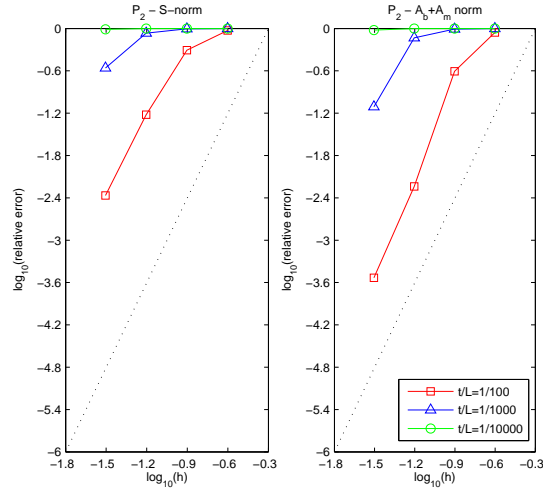


Figure 6.24: S-norm and $A_b + A_m$ -norm convergence curves associated with the free cylindrical shell problem and P_2 displacement-based shell finite elements. The dotted line shows the optimal convergence rate which is 4.

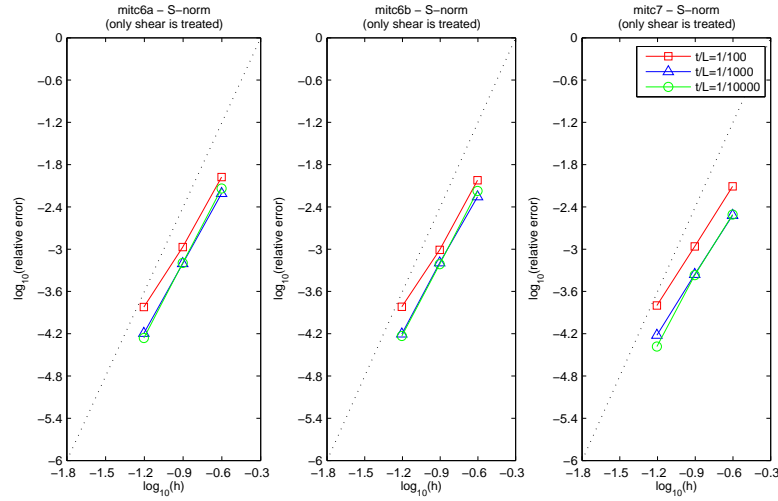


Figure 6.25: S-norm convergence curves associated with the clamped cylindrical shell problem: MITC6a, MITC6b and MITC7 shell finite elements when *only shear* is treated. The dotted line shows the optimal convergence rate which is 4 for quadratic elements.

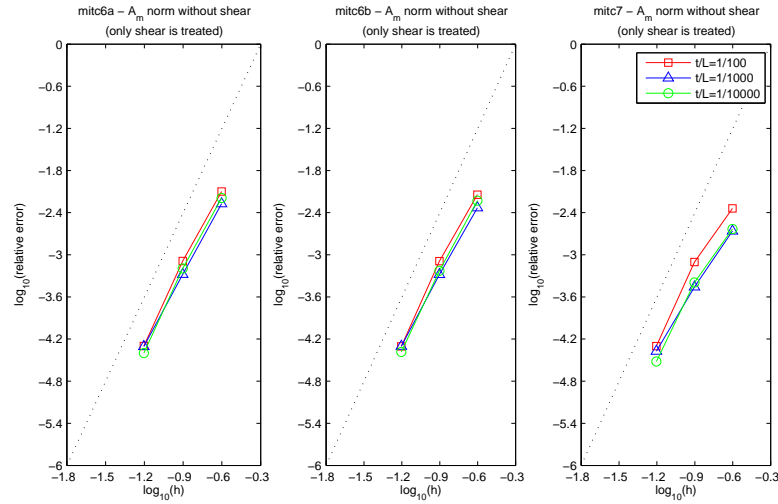


Figure 6.26: Convergence curves associated with the membrane energy norm without shear for the clamped cylindrical shell problem: MITC6a, MITC6b and MITC7 shell finite elements when *only shear* is treated. The dotted line shows the optimal convergence rate which is 4 for quadratic elements.

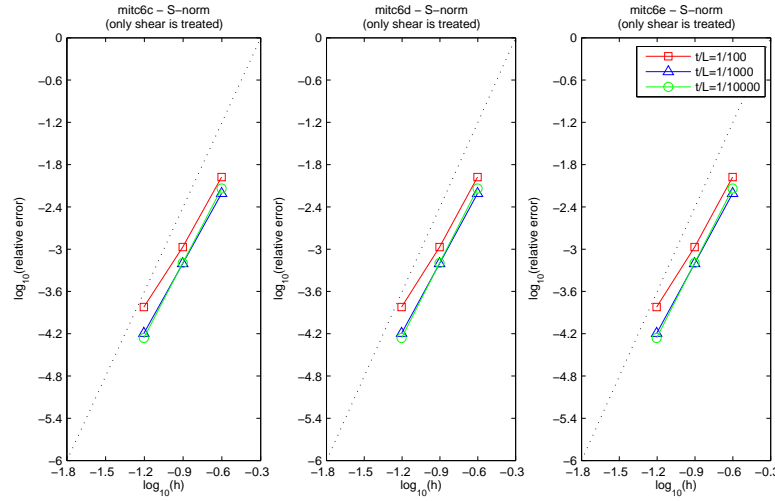


Figure 6.27: S-norm convergence curves associated with the clamped cylindrical shell problem: MITC6c, MITC6d and MITC6e shell finite elements when *only shear* is treated. The dotted line shows the optimal convergence rate which is 4 for quadratic elements.

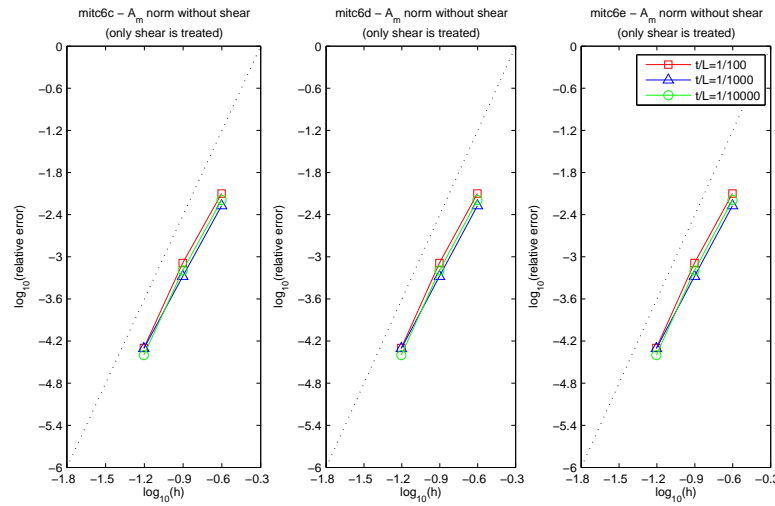


Figure 6.28: Convergence curves associated with the membrane energy norm without shear for the clamped cylindrical shell problem: MITC6c, MITC6d and MITC6e shell finite elements when *only shear* is treated. The dotted line shows the optimal convergence rate which is 4 for quadratic elements.

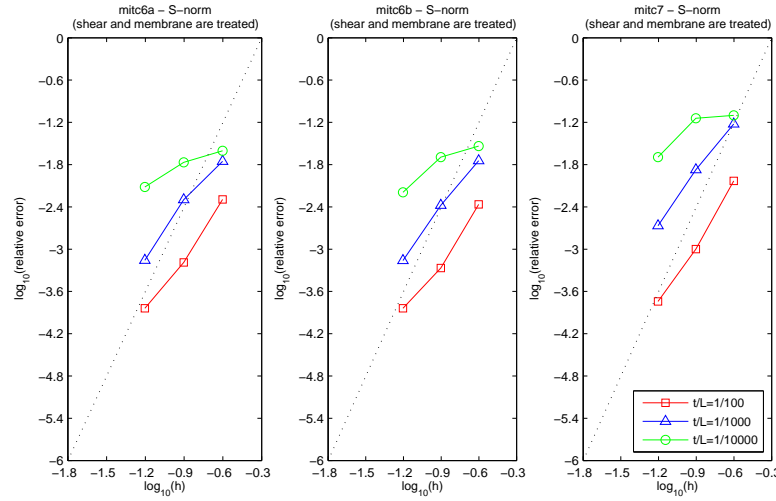


Figure 6.29: S-norm convergence curves associated with the clamped cylindrical shell problem: MITC6a, MITC6b and MITC7 shell finite elements when *shear and membrane* are treated. The dotted line shows the optimal convergence rate which is 4 for quadratic elements.

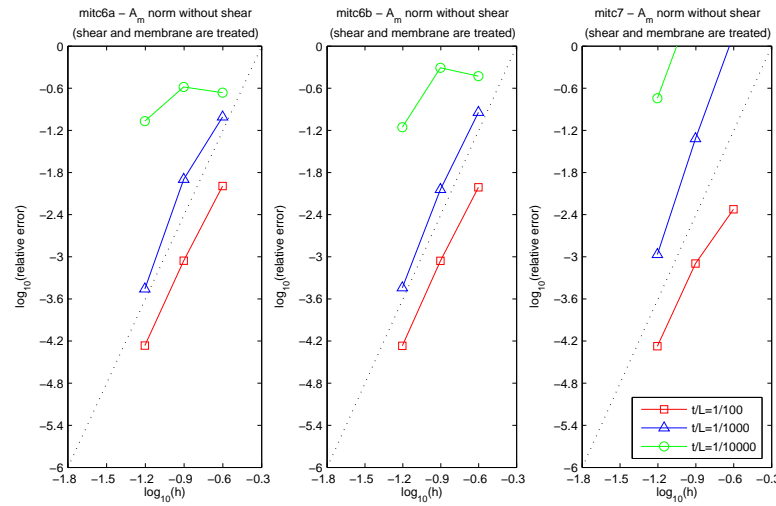


Figure 6.30: Convergence curves associated with the membrane energy norm without shear for the clamped cylindrical shell problem: MITC6a, MITC6b and MITC7 shell finite elements when *shear and membrane* are treated. The dotted line shows the optimal convergence rate which is 4 for quadratic elements.

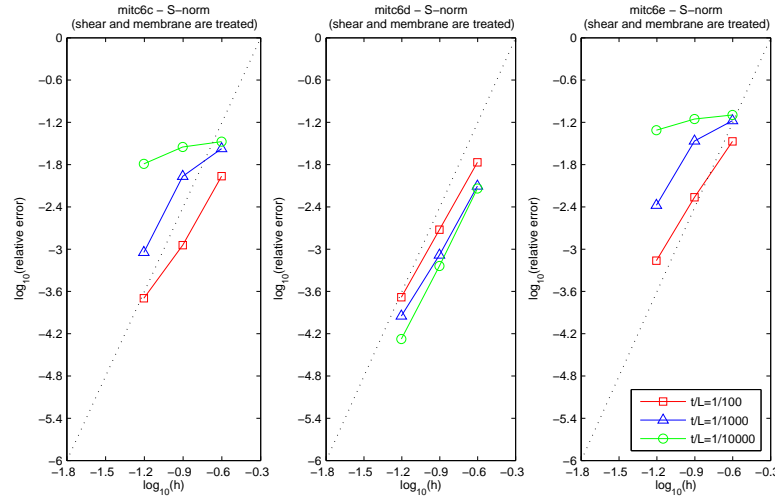


Figure 6.31: S-norm convergence curves associated with the clamped cylindrical shell problem: MITC6c, MITC6d and MITC6e shell finite elements when *shear and membrane* are treated. The dotted line shows the optimal convergence rate which is 4 for quadratic elements.

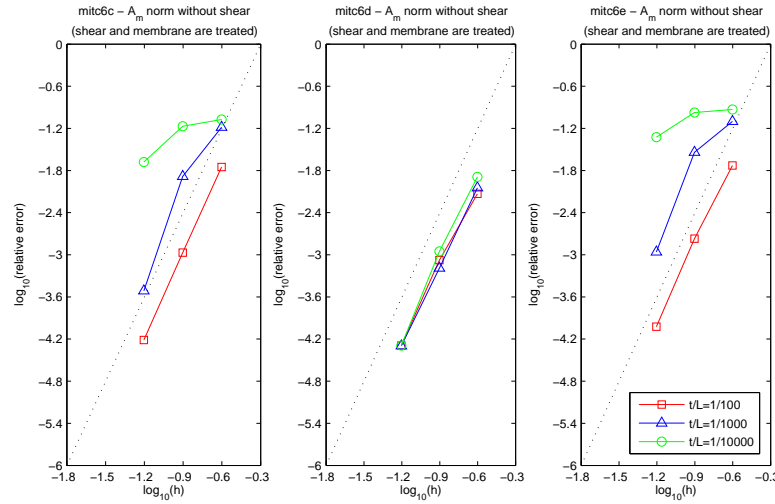


Figure 6.32: Convergence curves associated with the membrane energy norm without shear for the clamped cylindrical shell problem: MITC6c, MITC6d and MITC6e shell finite elements when *shear and membrane* are treated. The dotted line shows the optimal convergence rate which is 4 for quadratic elements.

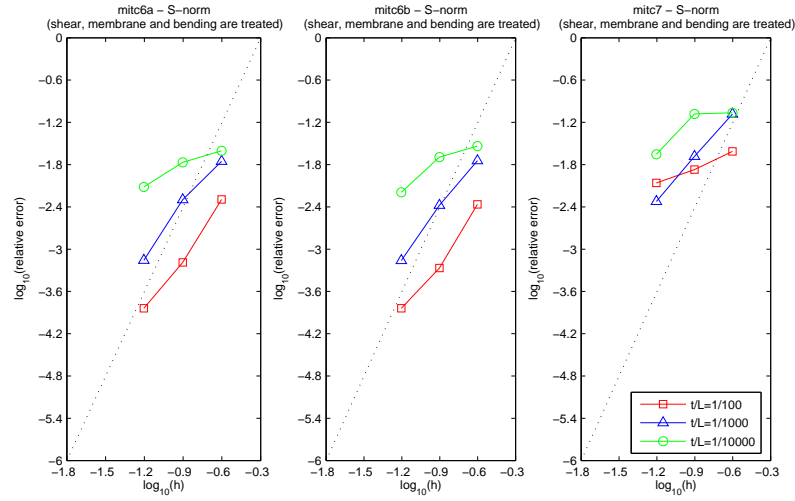


Figure 6.33: S-norm convergence curves associated with the clamped cylindrical shell problem: MITC6a, MITC6b and MITC7 shell finite elements when *shear, membrane and bending* are treated. The dotted line shows the optimal convergence rate which is 4 for quadratic elements.

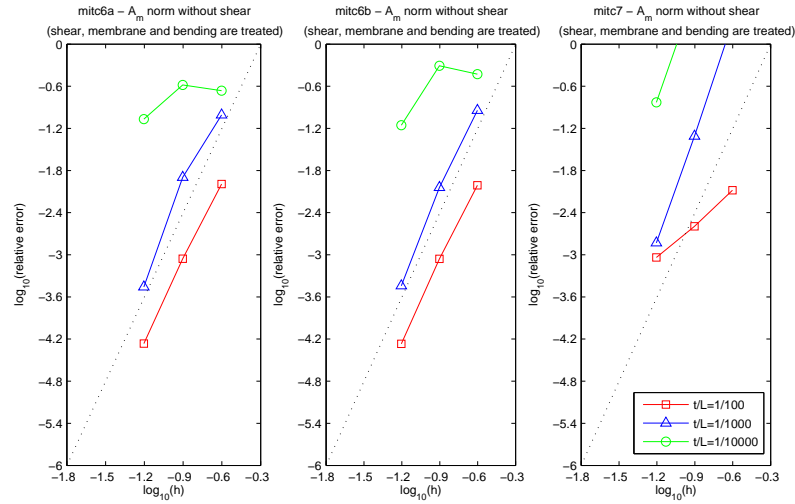


Figure 6.34: Convergence curves associated with the membrane energy norm without shear for the clamped cylindrical shell problem: MITC6a, MITC6b and MITC7 shell finite elements when *shear, membrane and bending* are treated. The dotted line shows the optimal convergence rate which is 4 for quadratic elements.

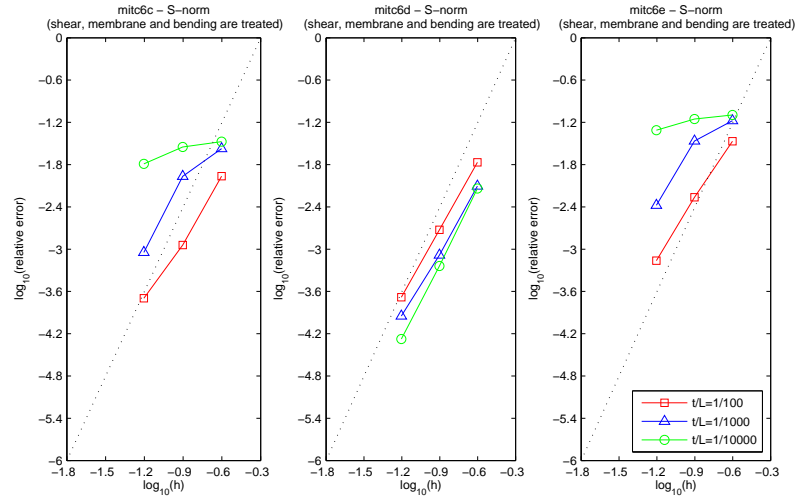


Figure 6.35: S-norm convergence curves associated with the clamped cylindrical shell problem: MITC6c, MITC6d and MITC6e shell finite elements when *shear*, *membrane* and *bending* are treated. The dotted line shows the optimal convergence rate which is 4 for quadratic elements.

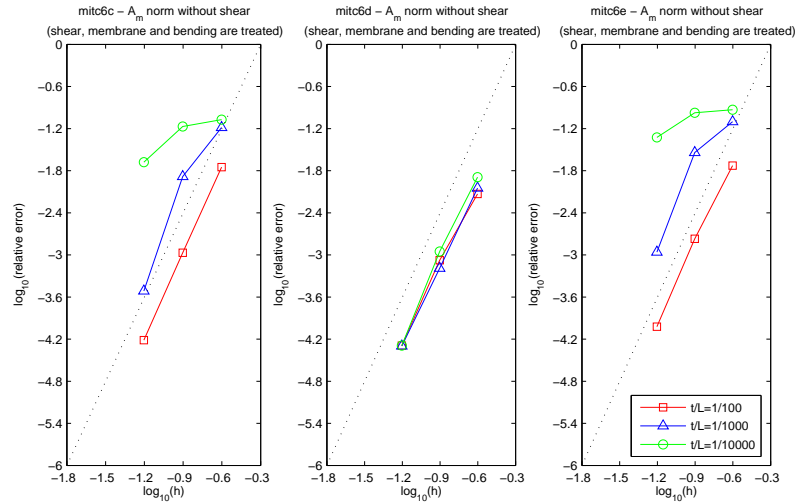


Figure 6.36: Convergence curves associated with the membrane energy norm without shear for the clamped cylindrical shell problem: MITC6c, MITC6d and MITC6e shell finite elements when *shear*, *membrane* and *bending* are treated. The dotted line shows the optimal convergence rate which is 4 for quadratic elements.

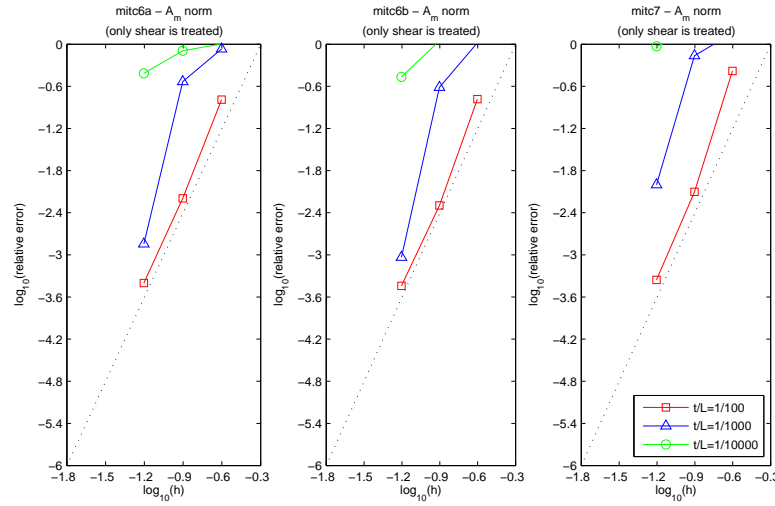


Figure 6.37: Convergence curves associated with the membrane and shear energy norm for the clamped cylindrical shell problem: MITC6a, MITC6b and MITC7 shell finite elements when *only shear* is treated. The dotted line shows the optimal convergence rate which is 4 for quadratic elements.

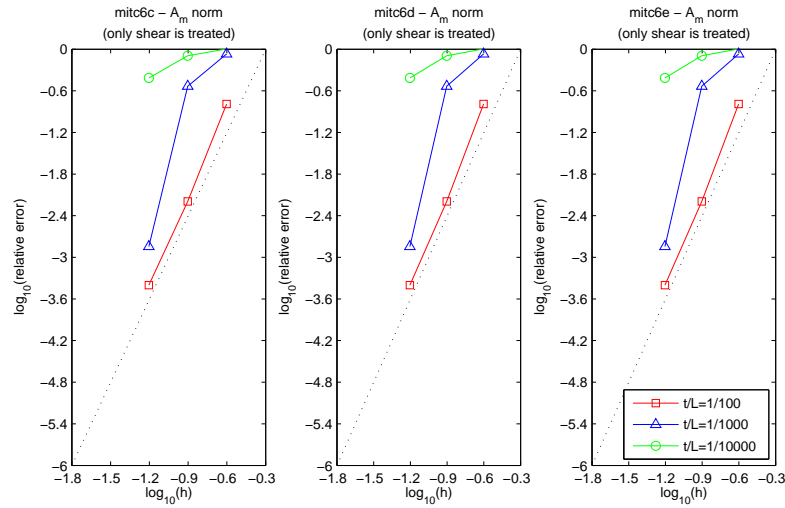


Figure 6.38: Convergence curves associated with the membrane and shear energy norm for the clamped cylindrical shell problem: MITC6c, MITC6d and MITC6e shell finite elements when *only shear* is treated. The dotted line shows the optimal convergence rate which is 4 for quadratic elements.

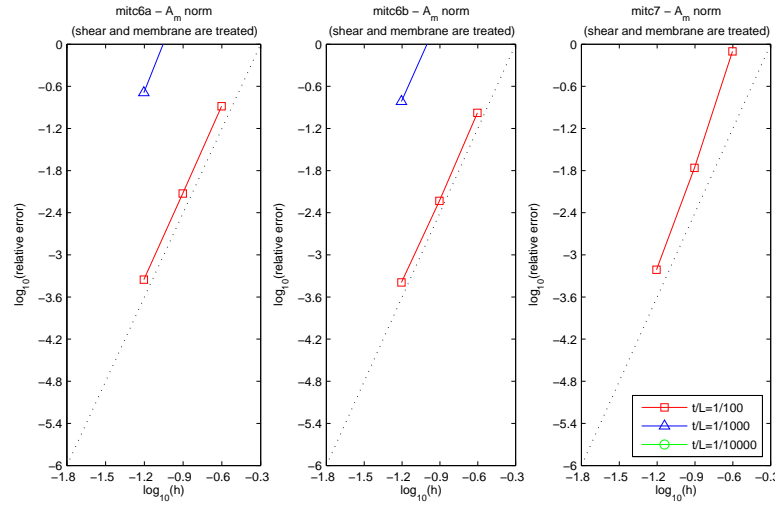


Figure 6.39: Convergence curves associated with the membrane and shear energy norm for the clamped cylindrical shell problem: MITC6a, MITC6b and MITC7 shell finite elements when *shear and membrane* are treated. The dotted line shows the optimal convergence rate which is 4 for quadratic elements.

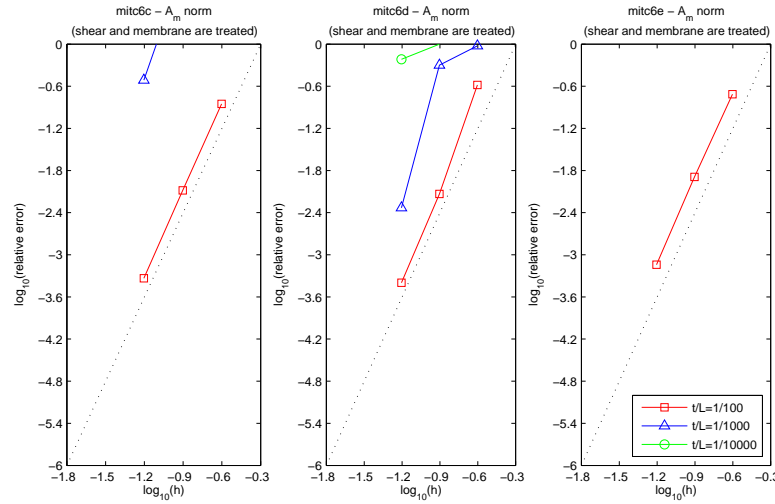


Figure 6.40: Convergence curves associated with the membrane and shear energy norm for the clamped cylindrical shell problem: MITC6c, MITC6d and MITC6e shell finite elements when *shear and membrane* are treated. The dotted line shows the optimal convergence rate which is 4 for quadratic elements.

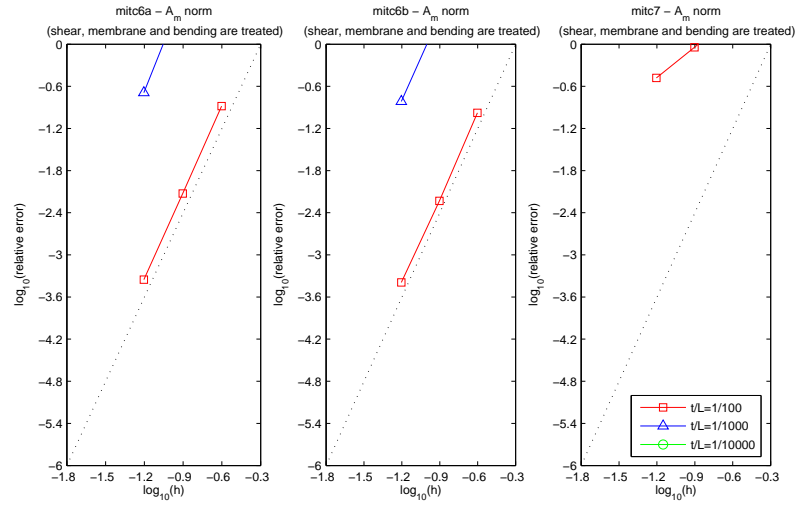


Figure 6.41: Convergence curves associated with the membrane and shear energy norm for the clamped cylindrical shell problem: MITC6a, MITC6b and MITC7 shell finite elements when *shear, membrane and bending* are treated. The dotted line shows the optimal convergence rate which is 4 for quadratic elements.

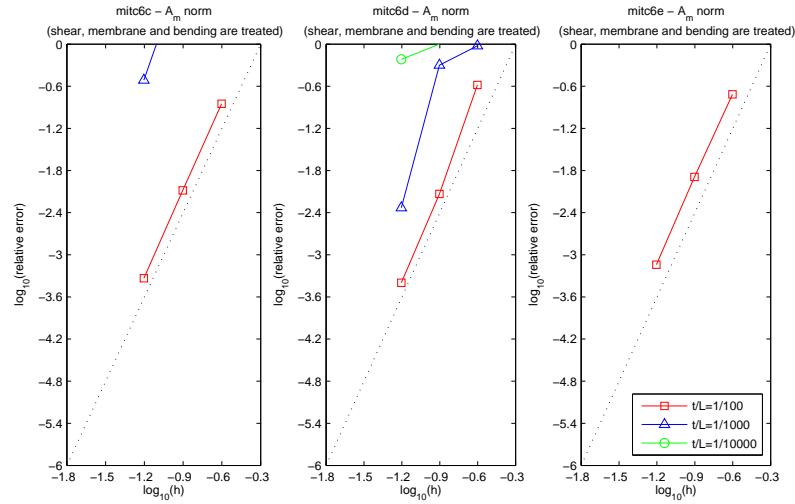


Figure 6.42: Convergence curves associated with the membrane and shear energy norm for the clamped cylindrical shell problem: MITC6c, MITC6d and MITC6e shell finite elements when *shear, membrane and bending* are treated. The dotted line shows the optimal convergence rate which is 4 for quadratic elements.

$\varepsilon = 10^{-2}$	$h = 0.25$	$h = 0.125$	$h = 0.0625$	<i>ref sol</i>
<i>Total</i>	8.750736673e-04	8.940823623e-04	8.958893825e-04	8.960383461e-04
<i>Bending</i>	1.442188465e-05	1.686244550e-05	1.736719640e-05	1.743665284e-05
<i>Membrane</i>	8.546304940e-04	8.761418507e-04	8.781478885e-04	8.783127187e-04
<i>Shear</i>	6.039995045e-06	1.097881720e-06	3.940671795e-07	3.087302932e-07
$\varepsilon = 10^{-3}$	$h = 0.25$	$h = 0.125$	$h = 0.0625$	<i>ref sol</i>
<i>Total</i>	9.148515561e-03	9.308248761e-03	9.320965878e-03	9.321962748e-03
<i>Bending</i>	2.149492629e-05	2.891151688e-05	2.989689587e-05	3.006104401e-05
<i>Membrane</i>	9.086458925e-03	9.275727952e-03	9.290629997e-03	9.291806864e-03
<i>Shear</i>	4.056758864e-05	3.616886355e-06	4.468307264e-07	1.027111669e-07
$\varepsilon = 10^{-4}$	$h = 0.25$	$h = 0.125$	$h = 0.0625$	<i>ref sol</i>
<i>Total</i>	9.195040339e-02	9.380235444e-02	9.394740630e-02	9.395820152e-02
<i>Bending</i>	2.911793446e-05	6.693056388e-05	7.525516070e-05	7.604454826e-05
<i>Membrane</i>	9.142581064e-02	9.369459244e-02	9.386862518e-02	9.388181145e-02
<i>Shear</i>	4.954761196e-04	4.083368519e-05	3.528849728e-06	3.482896252e-07

Table 6.2: Energy values associated with the clamped cylindrical shell problem and P_2 displacement-based shell finite elements for different values of ε and h , also the P_2 solution taken as reference.

$\varepsilon = 10^{-2}$		$h = 0.25$	$h = 0.125$	$h = 0.0625$
<i>Total</i>	<i>Reduced</i>	8.766438824e-04	8.914511104e-04	8.949478881e-04
	<i>Unreduced</i>	9.752220550e-04	8.935368743e-04	8.943224773e-04
<i>Bending</i>	<i>Reduced</i>	1.714815237e-05	1.729739495e-05	1.738671895e-05
	<i>Unreduced</i>	1.715092593e-05	1.729826104e-05	1.738693779e-05
<i>Membrane</i>	<i>Reduced</i>	8.583071458e-04	8.737143344e-04	8.772200625e-04
	<i>Unreduced</i>	8.476368965e-04	8.692418564e-04	8.759459212e-04
<i>Shear</i>	<i>Reduced</i>	1.204308922e-06	4.582573699e-07	3.606417499e-07
	<i>Unreduced</i>	1.104494441e-04	7.015794352e-06	1.009199370e-06
$\varepsilon = 10^{-3}$		$h = 0.25$	$h = 0.125$	$h = 0.0625$
<i>Total</i>	<i>Reduced</i>	9.208651795e-03	9.306438090e-03	9.313736837e-03
	<i>Unreduced</i>	1.310002288e-01	5.299303122e-02	1.130982310e-02
<i>Bending</i>	<i>Reduced</i>	4.396407135e-05	4.685360732e-05	3.369554887e-05
	<i>Unreduced</i>	4.396124480e-05	4.685795780e-05	3.369579232e-05
<i>Membrane</i>	<i>Reduced</i>	9.139665784e-03	9.257430734e-03	9.279444337e-03
	<i>Unreduced</i>	9.990780400e-03	9.371672506e-03	9.279053054e-03
<i>Shear</i>	<i>Reduced</i>	2.500264550e-05	2.154668657e-06	6.051453541e-07
	<i>Unreduced</i>	1.209654482e-01	4.357449793e-02	1.997082359e-03
$\varepsilon = 10^{-4}$		$h = 0.25$	$h = 0.125$	$h = 0.0625$
<i>Total</i>	<i>Reduced</i>	9.339213822e-02	9.491361842e-02	9.451899547e-02
	<i>Unreduced</i>	2.592171205e+00	1.773400561e+01	1.622949131e+01
<i>Bending</i>	<i>Reduced</i>	1.138622643e-04	1.429783952e-04	3.181134633e-04
	<i>Unreduced</i>	1.138615029e-04	1.429853359e-04	3.181300335e-04
<i>Membrane</i>	<i>Reduced</i>	9.287770845e-02	9.461156369e-02	9.419056939e-02
	<i>Unreduced</i>	1.132303644e-01	1.192743988e-01	1.053766878e-01
<i>Shear</i>	<i>Reduced</i>	4.005643204e-04	1.590456540e-04	1.029056413e-05
	<i>Unreduced</i>	2.478826972e+00	1.761458818e+01	1.612379645e+01

Table 6.3: *Reduced* and *unreduced* energy values associated with the clamped cylindrical shell problem and MITC6a triangular shell finite element for different values of ε and h (*shear*, *membrane* and *bending* are treated).

$\varepsilon = 10^{-2}$		$h = 0.25$	$h = 0.125$	$h = 0.0625$
<i>Total</i>	<i>Reduced</i>	8.751637303e-04	8.910520879e-04	8.948655709e-04
	<i>Unreduced</i>	9.491076189e-04	8.912857736e-04	8.941058623e-04
<i>Bending</i>	<i>Reduced</i>	1.710630196e-05	1.724649134e-05	1.736126156e-05
	<i>Unreduced</i>	1.710893288e-05	1.724734947e-05	1.736148170e-05
<i>Membrane</i>	<i>Reduced</i>	8.569433238e-04	8.733474069e-04	8.771448710e-04
	<i>Unreduced</i>	8.455390086e-04	8.688468296e-04	8.758691262e-04
<i>Shear</i>	<i>Reduced</i>	1.129803554e-06	4.772164893e-07	3.790301890e-07
	<i>Unreduced</i>	8.647442992e-05	5.210769172e-06	8.948903804e-07
$\varepsilon = 10^{-3}$		$h = 0.25$	$h = 0.125$	$h = 0.0625$
<i>Total</i>	<i>Reduced</i>	9.210552872e-03	9.298167439e-03	9.313598599e-03
	<i>Unreduced</i>	1.721551514e-01	3.117791208e-02	1.087549246e-02
<i>Bending</i>	<i>Reduced</i>	5.492606912e-05	4.216215109e-05	3.352745797e-05
	<i>Unreduced</i>	5.494180528e-05	4.216346359e-05	3.352756397e-05
<i>Membrane</i>	<i>Reduced</i>	9.129062736e-03	9.253249995e-03	9.279469275e-03
	<i>Unreduced</i>	1.014342806e-02	9.323945672e-03	9.278986749e-03
<i>Shear</i>	<i>Reduced</i>	2.656190240e-05	2.762545605e-06	6.101033581e-07
	<i>Unreduced</i>	1.619567404e-01	2.181180567e-02	1.562986310e-03
$\varepsilon = 10^{-4}$		$h = 0.25$	$h = 0.125$	$h = 0.0625$
<i>Total</i>	<i>Reduced</i>	9.377847071e-02	9.519614114e-02	9.440578092e-02
	<i>Unreduced</i>	4.828078376e+00	3.951732585e+01	8.970185154e+00
<i>Bending</i>	<i>Reduced</i>	1.060073697e-04	2.977573960e-04	2.705437313e-04
	<i>Unreduced</i>	1.060125398e-04	2.978117094e-04	2.705493367e-04
<i>Membrane</i>	<i>Reduced</i>	9.322117012e-02	9.472914467e-02	9.412463343e-02
	<i>Unreduced</i>	1.286480613e-01	1.403011408e-01	1.031235383e-01
<i>Shear</i>	<i>Reduced</i>	4.512929747e-04	1.692273964e-04	1.060429003e-05
	<i>Unreduced</i>	4.699324291e+00	3.937672680e+01	8.866791050e+00

Table 6.4: *Reduced* and *unreduced* energy values associated with the clamped cylindrical shell problem and MITC6b triangular shell finite element for different values of ε and h (*shear*, *membrane* and *bending* are treated).

$\varepsilon = 10^{-2}$		$h = 0.25$	$h = 0.125$	$h = 0.0625$
<i>Total</i>	<i>Reduced</i>	8.940036384e-04	9.023104432e-04	9.024873526e-04
	<i>Unreduced</i>	3.079509079e-03	1.712251182e-03	1.210180914e-03
<i>Membrane</i>	<i>Reduced</i>	8.749294091e-04	8.871642529e-04	8.857627414e-04
	<i>Unreduced</i>	8.718944120e-04	8.837389149e-04	8.847138656e-04
$\varepsilon = 10^{-3}$		$h = 0.25$	$h = 0.125$	$h = 0.0625$
<i>Total</i>	<i>Reduced</i>	9.913098089e-03	9.456965575e-03	9.351529720e-03
	<i>Unreduced</i>	3.309444174e+00	5.174232914e-01	5.043716799e-02
<i>Membrane</i>	<i>Reduced</i>	9.751805784e-03	9.349867458e-03	9.314086176e-03
	<i>Unreduced</i>	2.916427158e-02	9.982776554e-03	9.344178215e-03
$\varepsilon = 10^{-4}$		$h = 0.25$	$h = 0.125$	$h = 0.0625$
<i>Total</i>	<i>Reduced</i>	1.003824772e-01	1.013420569e-01	9.591141458e-02
	<i>Unreduced</i>	5.685022421e+01	6.919068634e+02	1.211756208e+02
<i>Membrane</i>	<i>Reduced</i>	1.003014049e-01	1.001811814e-01	9.512572083e-02
	<i>Unreduced</i>	4.397421218e-01	6.077576505e-01	1.133766034e-01

Table 6.5: *Reduced* and *unreduced* energy values associated with the clamped cylindrical shell problem and MITC7 triangular shell finite element for different values of ε and h (*shear*, *membrane* and *bending* are treated).

$\varepsilon = 10^{-2}$		$h = 0.25$	$h = 0.125$	$h = 0.0625$
<i>Total</i>	<i>Reduced</i>	8.972504531e-04	8.971892383e-04	8.964196485e-04
	<i>Unreduced</i>	1.025762359e-03	9.056804922e-04	8.972858991e-04
<i>Bending</i>	<i>Reduced</i>	1.815089686e-05	1.755673174e-05	1.743544518e-05
	<i>Unreduced</i>	1.817383059e-05	1.756156578e-05	1.743659196e-05
<i>Membrane</i>	<i>Reduced</i>	8.773537984e-04	8.790596784e-04	8.786084528e-04
	<i>Unreduced</i>	8.947027666e-04	8.806948679e-04	8.788481475e-04
<i>Shear</i>	<i>Reduced</i>	1.768060089e-06	5.930534061e-07	3.954541622e-07
	<i>Unreduced</i>	1.129206717e-04	7.447017960e-06	1.021513359e-06
$\varepsilon = 10^{-3}$		$h = 0.25$	$h = 0.125$	$h = 0.0625$
<i>Total</i>	<i>Reduced</i>	9.422439875e-03	9.408490401e-03	9.330749912e-03
	<i>Unreduced</i>	4.219421123e-02	1.130618009e-01	1.231195931e-02
<i>Bending</i>	<i>Reduced</i>	3.817828947e-05	6.889931342e-05	3.496781699e-05
	<i>Unreduced</i>	3.818658891e-05	6.890541515e-05	3.496818432e-05
<i>Membrane</i>	<i>Reduced</i>	9.364234901e-03	9.334299928e-03	9.294550273e-03
	<i>Unreduced</i>	1.010693679e-02	9.584161110e-03	9.312299153e-03
<i>Shear</i>	<i>Reduced</i>	2.003350162e-05	5.291571874e-06	1.240810022e-06
	<i>Unreduced</i>	3.204909705e-02	1.034087307e-01	2.964700938e-03
$\varepsilon = 10^{-4}$		$h = 0.25$	$h = 0.125$	$h = 0.0625$
<i>Total</i>	<i>Reduced</i>	9.528982184e-02	9.626516975e-02	9.545081340e-02
	<i>Unreduced</i>	5.567049704e-01	7.993246318e+00	3.707040289e+01
<i>Bending</i>	<i>Reduced</i>	1.346043310e-04	1.241772275e-04	5.930400281e-04
	<i>Unreduced</i>	1.346056049e-04	1.241805321e-04	5.930491056e-04
<i>Membrane</i>	<i>Reduced</i>	9.493198581e-02	9.605994731e-02	9.483878357e-02
	<i>Unreduced</i>	1.045565244e-01	1.047135795e-01	9.887969448e-02
<i>Shear</i>	<i>Reduced</i>	2.232339097e-04	8.103755995e-05	1.894051919e-05
	<i>Unreduced</i>	4.520138430e-01	7.888408547e+00	3.697093007e+01

Table 6.6: *Reduced* and *unreduced* energy values associated with the clamped cylindrical shell problem and MITC6c triangular shell finite element for different values of ε and h (*shear*, *membrane* and *bending* are treated).

$\varepsilon = 10^{-2}$		$h = 0.25$	$h = 0.125$	$h = 0.0625$
<i>Total</i>	<i>Reduced</i>	8.853765827e-04	8.955612495e-04	8.962142357e-04
	<i>Unreduced</i>	1.108769904e-03	9.016475096e-04	8.968058394e-04
<i>Bending</i>	<i>Reduced</i>	1.731868377e-05	1.726495519e-05	1.741320048e-05
	<i>Unreduced</i>	1.732222963e-05	1.726500298e-05	1.741320018e-05
<i>Membrane</i>	<i>Reduced</i>	8.657551991e-04	8.779300887e-04	8.784851494e-04
	<i>Unreduced</i>	8.634371963e-04	8.774207904e-04	8.784460386e-04
<i>Shear</i>	<i>Reduced</i>	2.308307017e-06	3.848410530e-07	3.354698183e-07
	<i>Unreduced</i>	2.280164205e-04	6.980271649e-06	9.661728298e-07
$\varepsilon = 10^{-3}$		$h = 0.25$	$h = 0.125$	$h = 0.0625$
<i>Total</i>	<i>Reduced</i>	9.270017178e-03	9.316319054e-03	9.321389891e-03
	<i>Unreduced</i>	1.803798659e-02	1.369268116e-02	9.364935593e-03
<i>Bending</i>	<i>Reduced</i>	2.326196335e-05	3.019534681e-05	3.003274762e-05
	<i>Unreduced</i>	2.326299033e-05	3.019528179e-05	3.003274362e-05
<i>Membrane</i>	<i>Reduced</i>	9.238235851e-03	9.285770803e-03	9.291270354e-03
	<i>Unreduced</i>	9.291472533e-03	9.287317212e-03	9.291025142e-03
<i>Shear</i>	<i>Reduced</i>	8.522862726e-06	3.589786048e-07	9.455409379e-08
	<i>Unreduced</i>	8.723254825e-03	4.375174622e-03	4.388546765e-05
$\varepsilon = 10^{-4}$		$h = 0.25$	$h = 0.125$	$h = 0.0625$
<i>Total</i>	<i>Reduced</i>	9.350578931e-02	9.391647091e-02	9.395532093e-02
	<i>Unreduced</i>	1.916738542e-01	1.821301747e-01	1.509813320e-01
<i>Bending</i>	<i>Reduced</i>	3.645123333e-05	6.552490417e-05	7.601871521e-05
	<i>Unreduced</i>	3.645126524e-05	6.552494424e-05	7.601869569e-05
<i>Membrane</i>	<i>Reduced</i>	9.338339585e-02	9.384798866e-02	9.387918416e-02
	<i>Unreduced</i>	9.437278427e-02	9.391413270e-02	9.388235716e-02
<i>Shear</i>	<i>Reduced</i>	8.594359614e-05	2.959635151e-06	1.204309563e-07
	<i>Unreduced</i>	9.726462018e-02	8.815051915e-02	5.702295883e-02

Table 6.7: *Reduced* and *unreduced* energy values associated with the clamped cylindrical shell problem and MITC6d triangular shell finite element for different values of ε and h (*shear*, *membrane* and *bending* are treated).

$\varepsilon = 10^{-2}$		$h = 0.25$	$h = 0.125$	$h = 0.0625$
<i>Total</i>	<i>Reduced</i>	8.692763819e-04	8.949948908e-04	8.964893454e-04
	<i>Unreduced</i>	1.017106467e-03	9.052433287e-04	8.976994049e-04
<i>Bending</i>	<i>Reduced</i>	1.876185421e-05	1.762755146e-05	1.745203891e-05
	<i>Unreduced</i>	1.877403712e-05	1.763759277e-05	1.745454550e-05
<i>Membrane</i>	<i>Reduced</i>	8.438842626e-04	8.762532641e-04	8.784793599e-04
	<i>Unreduced</i>	8.409533755e-04	8.769472004e-04	8.790161072e-04
<i>Shear</i>	<i>Reduced</i>	6.643021924e-06	1.133899197e-06	5.777076180e-07
	<i>Unreduced</i>	1.574034114e-04	1.068431372e-05	1.249985878e-06
$\varepsilon = 10^{-3}$		$h = 0.25$	$h = 0.125$	$h = 0.0625$
<i>Total</i>	<i>Reduced</i>	9.312905742e-03	9.535604260e-03	9.353002442e-03
	<i>Unreduced</i>	4.090475775e-02	1.834834170e-01	2.164140261e-02
<i>Bending</i>	<i>Reduced</i>	6.420658860e-05	1.060665050e-04	5.056718036e-05
	<i>Unreduced</i>	6.423285627e-05	1.061241646e-04	5.057036446e-05
<i>Membrane</i>	<i>Reduced</i>	9.154115053e-03	9.404344026e-03	9.296750031e-03
	<i>Unreduced</i>	1.002278495e-02	9.981583176e-03	9.365142412e-03
<i>Shear</i>	<i>Reduced</i>	9.458979674e-05	2.518784915e-05	5.695342000e-06
	<i>Unreduced</i>	3.081775117e-02	1.733957017e-01	1.222569973e-02
$\varepsilon = 10^{-4}$		$h = 0.25$	$h = 0.125$	$h = 0.0625$
<i>Total</i>	<i>Reduced</i>	9.550799797e-02	9.933485348e-02	9.835098326e-02
	<i>Unreduced</i>	6.765399858e-01	1.022832182e+01	6.567760112e+01
<i>Bending</i>	<i>Reduced</i>	3.944358019e-04	1.864359627e-04	1.120187320e-03
	<i>Unreduced</i>	3.944398964e-04	1.864795156e-04	1.120357429e-03
<i>Membrane</i>	<i>Reduced</i>	9.440864518e-02	9.892228199e-02	9.717017911e-02
	<i>Unreduced</i>	1.080834466e-01	1.143477868e-01	1.073130009e-01
<i>Shear</i>	<i>Reduced</i>	7.049186208e-04	2.261300218e-04	6.054527400e-05
	<i>Unreduced</i>	5.680621018e-01	1.011378754e+01	6.556916765e+01

Table 6.8: *Reduced* and *unreduced* energy values associated with the clamped cylindrical shell problem and MITC6e triangular shell finite element for different values of ε and h (*shear*, *membrane* and *bending* are treated).

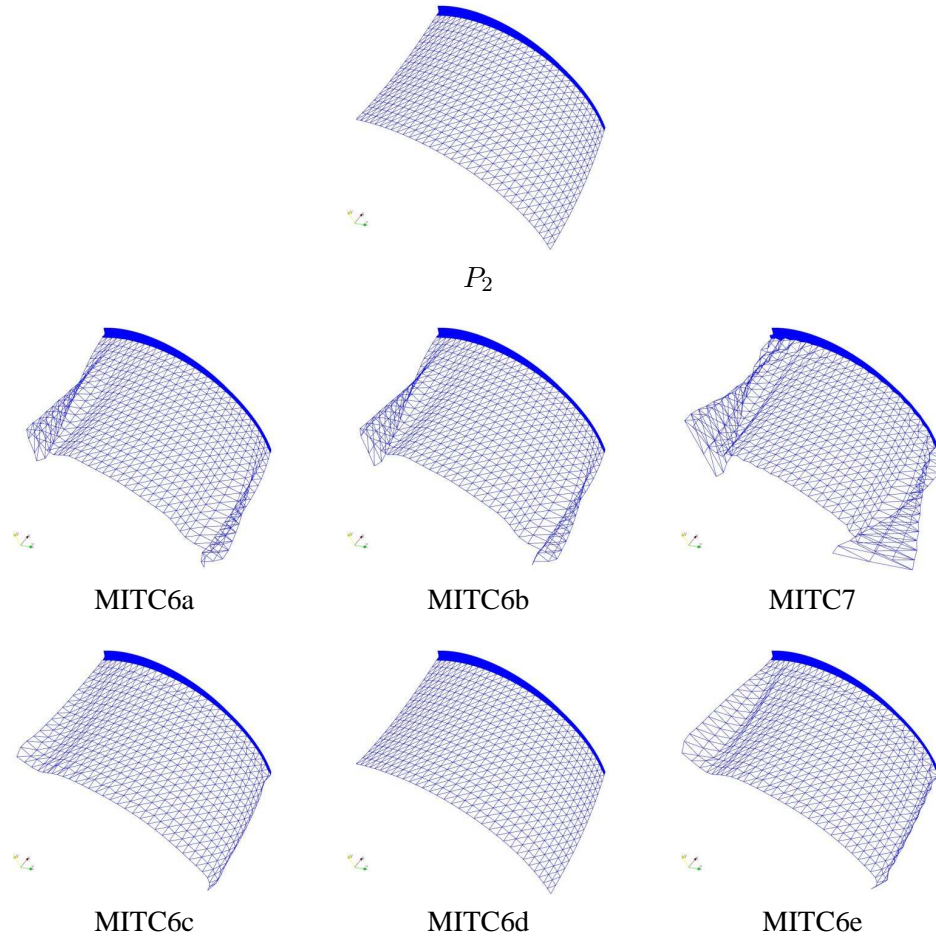


Figure 6.43: Midsurface deformed meshes associated with the clamped cylindrical shell problem (5841 nodes, 2816 elements, $L = 1$, $\varepsilon = 10^{-4}$, boundary layer of width $5\sqrt{\varepsilon}L$, $scale = 0.5$).

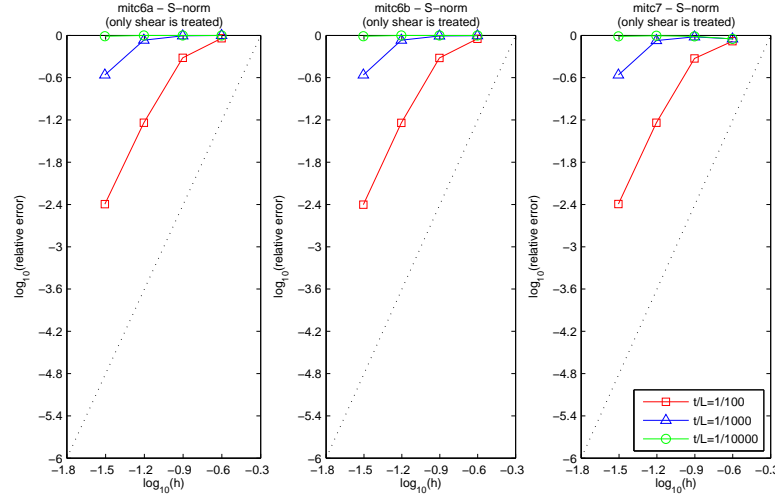


Figure 6.44: S-norm convergence curves associated with the free cylindrical shell problem: MITC6a, MITC6b and MITC7 shell finite elements when *only shear* is treated. The dotted line shows the optimal convergence rate which is 4 for quadratic elements.

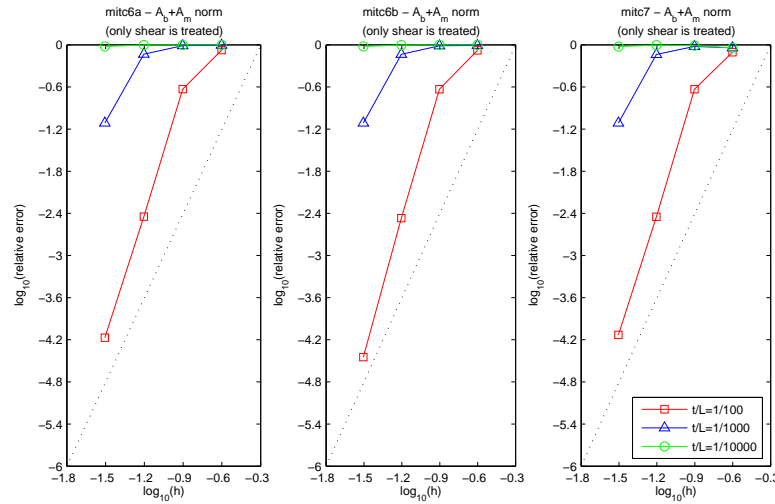


Figure 6.45: $A_b + A_m$ -norm convergence curves associated with the free cylindrical shell problem: MITC6a, MITC6b and MITC7 shell finite elements when *only shear* is treated. The dotted line shows the optimal convergence rate which is 4 for quadratic elements.

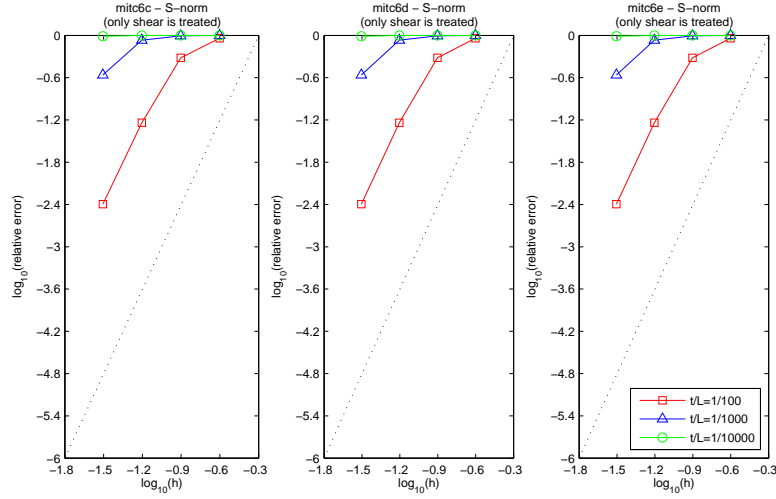


Figure 6.46: S-norm convergence curves associated with the free cylindrical shell problem: MITC6c, MITC6d and MITC6e shell finite elements when *only shear* is treated. The dotted line shows the optimal convergence rate which is 4 for quadratic elements.

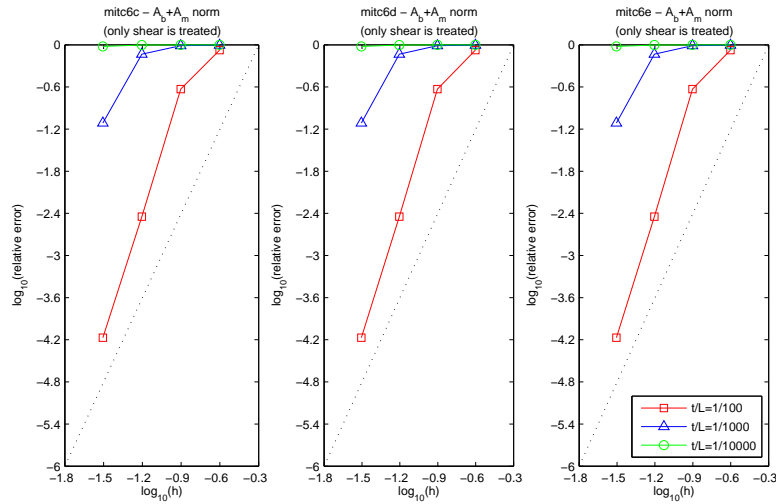


Figure 6.47: $A_b + A_m$ -norm convergence curves associated with the free cylindrical shell problem: MITC6c, MITC6d and MITC6e shell finite elements when *only shear* is treated. The dotted line shows the optimal convergence rate which is 4 for quadratic elements.

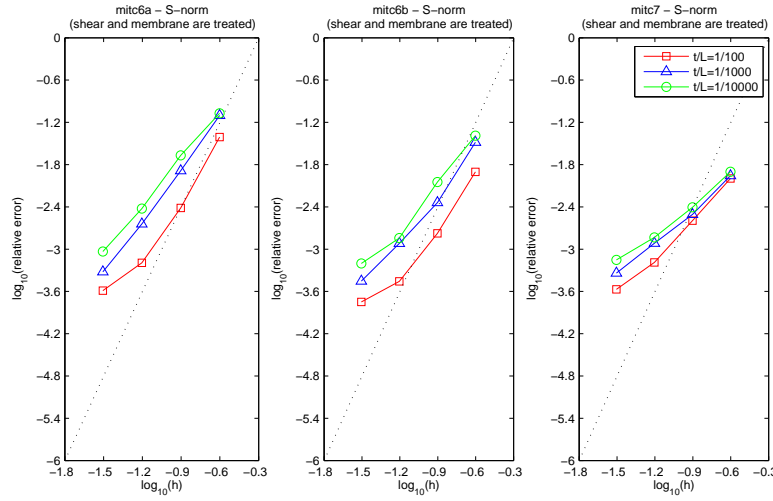


Figure 6.48: S-norm convergence curves associated with the free cylindrical shell problem: MITC6a, MITC6b and MITC7 shell finite elements when *shear and membrane* are treated. The dotted line shows the optimal convergence rate which is 4 for quadratic elements.

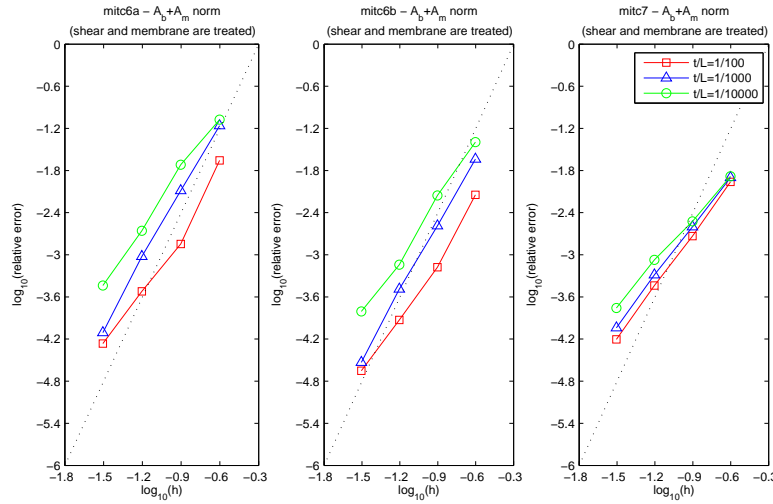


Figure 6.49: $A_b + A_m$ -norm convergence curves associated with the free cylindrical shell problem: MITC6a, MITC6b and MITC7 shell finite elements when *shear and membrane* are treated. The dotted line shows the optimal convergence rate which is 4 for quadratic elements.

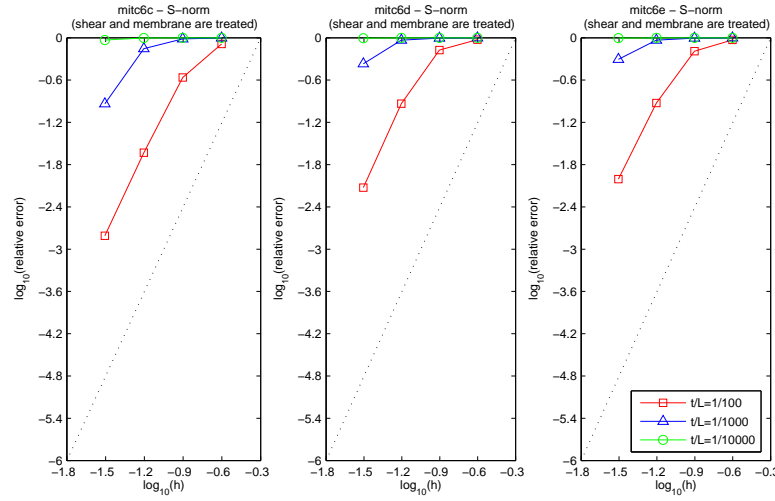


Figure 6.50: S-norm convergence curves associated with the free cylindrical shell problem: MITC6c, MITC6d and MITC6e shell finite elements when *shear and membrane* are treated. The dotted line shows the optimal convergence rate which is 4 for quadratic elements.

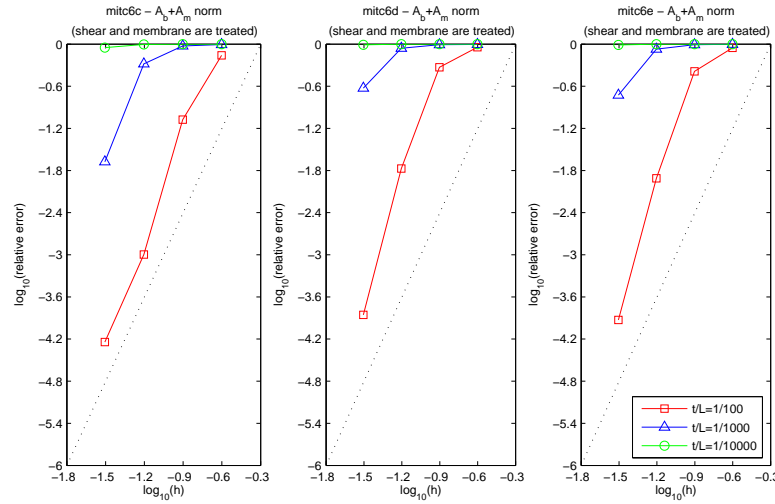


Figure 6.51: $A_b + A_m$ -norm convergence curves associated with the free cylindrical shell problem: MITC6c, MITC6d and MITC6e shell finite elements when *shear and membrane* are treated. The dotted line shows the optimal convergence rate which is 4 for quadratic elements.

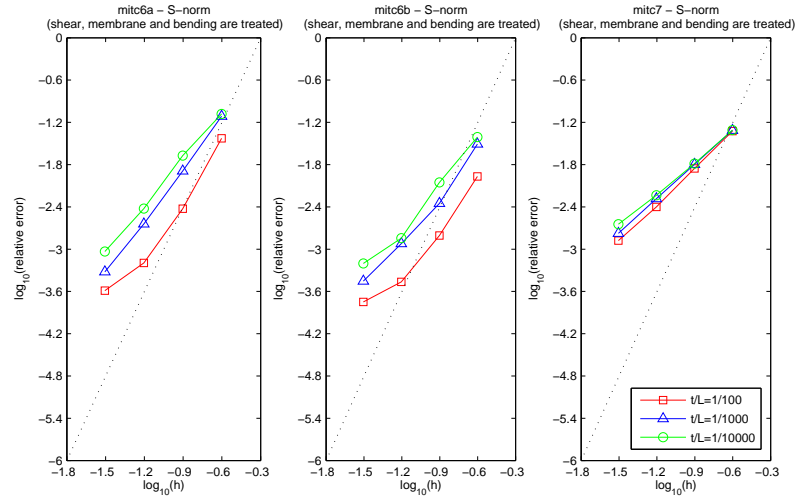


Figure 6.52: S-norm convergence curves associated with the free cylindrical shell problem: MITC6a, MITC6b and MITC7 shell finite elements when *shear, membrane and bending* are treated. The dotted line shows the optimal convergence rate which is 4 for quadratic elements.

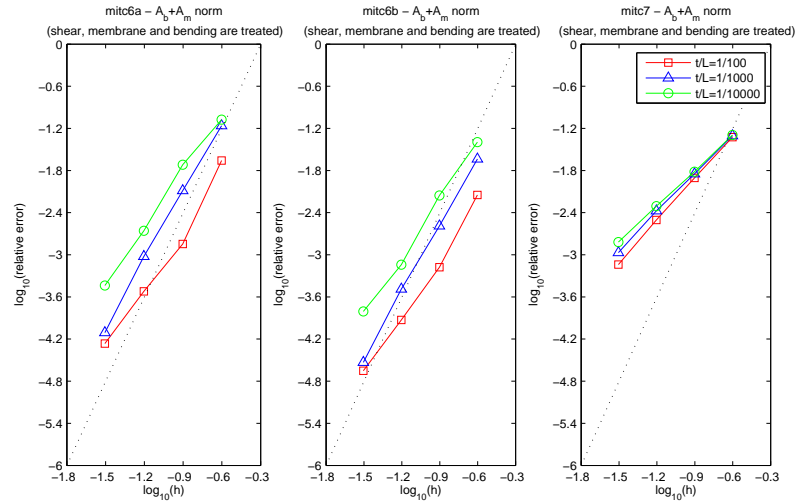


Figure 6.53: $A_b + A_m$ -norm convergence curves associated with the free cylindrical shell problem: MITC6a, MITC6b and MITC7 shell finite elements when *shear, membrane and bending* are treated. The dotted line shows the optimal convergence rate which is 4 for quadratic elements.

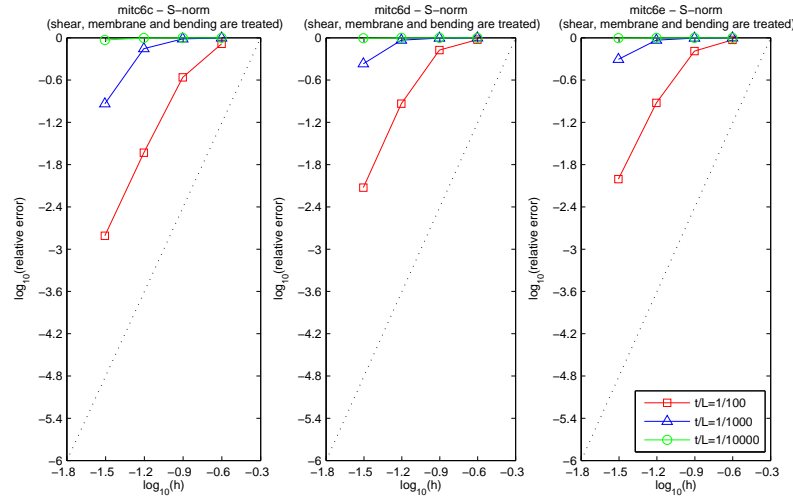


Figure 6.54: S-norm convergence curves associated with the free cylindrical shell problem: MITC6c, MITC6d and MITC6e shell finite elements when *shear, membrane and bending* are treated. The dotted line shows the optimal convergence rate which is 4 for quadratic elements.

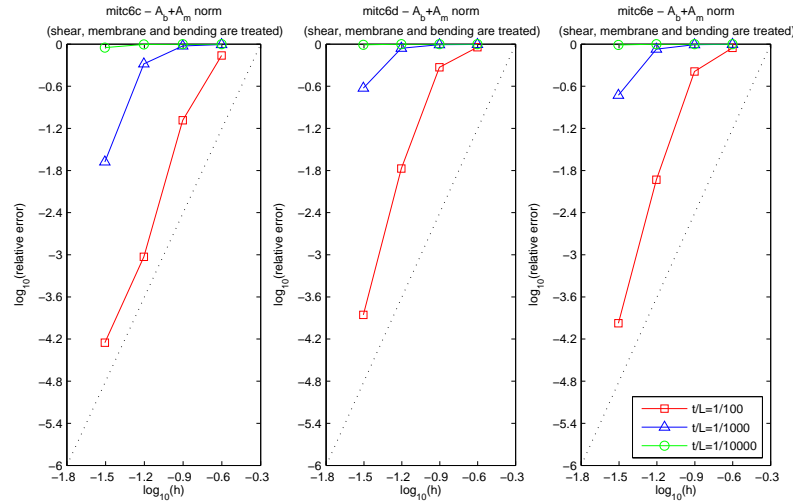


Figure 6.55: $A_b + A_m$ -norm convergence curves associated with the free cylindrical shell problem: MITC6c, MITC6d and MITC6e shell finite elements when *shear, membrane and bending* are treated. The dotted line shows the optimal convergence rate which is 4 for quadratic elements.

	$\varepsilon = 10^{-2}$	$\varepsilon = 10^{-3}$	$\varepsilon = 10^{-4}$
<i>Total</i>	2.346770803e+00	2.332387642e+03	2.327688500e+06
<i>Bending</i>	2.341470061e+00	2.330718017e+03	2.327144026e+06
<i>Membrane</i>	5.130316767e-03	1.666691197e+00	5.497055218e+02
<i>Shear</i>	2.851386909e-04	3.670433908e-03	1.382879987e+01

Table 6.9: Reference energy values associated with the free cylindrical shell problem and MITC4 shell finite element.

$\varepsilon = 10^{-2}$	$h = 0.25$	$h = 0.125$	$h = 0.0625$	$h = 0.03125$
<i>Total</i>	1.492689617e-01	1.187971116e+00	2.205901436e+00	2.337479034e+00
<i>Bending</i>	9.964504224e-03	6.069912735e-01	2.073055122e+00	2.322751997e+00
<i>Membrane</i>	1.326574332e-01	5.737869415e-01	1.312654476e-01	1.405785355e-02
<i>Shear</i>	6.645653491e-03	7.217723184e-03	1.682053481e-03	7.829356160e-04

$\varepsilon = 10^{-3}$	$h = 0.25$	$h = 0.125$	$h = 0.0625$	$h = 0.03125$
<i>Total</i>	1.598620617e+00	2.410978495e+01	3.284105327e+02	1.683965946e+03
<i>Bending</i>	1.148918859e-03	2.518917388e-01	4.634665620e+01	1.215460277e+03
<i>Membrane</i>	1.522183955e+00	2.360041011e+01	2.812416656e+02	4.680610850e+02
<i>Shear</i>	7.528752516e-02	2.574802406e-01	8.221947090e-01	4.449120182e-01

$\varepsilon = 10^{-4}$	$h = 0.25$	$h = 0.125$	$h = 0.0625$	$h = 0.03125$
<i>Total</i>	1.599759109e+01	2.436179175e+02	3.817709347e+03	5.909650683e+04
<i>Bending</i>	1.150626777e-04	2.572353760e-02	6.268779487e+00	1.499930092e+03
<i>Membrane</i>	1.524361071e+01	2.409651789e+02	3.800470636e+03	5.755115521e+04
<i>Shear</i>	7.538652924e-01	2.627014699e+00	1.096990636e+01	4.542351537e+01

Table 6.10: *Reduced* and *unreduced* energy values associated with the free cylindrical shell problem and P_2 displacement-based shell finite elements for different values of ε and h .

$\varepsilon = 10^{-2}$		$h = 0.25$	$h = 0.125$	$h = 0.0625$	$h = 0.03125$
<i>Total</i>	<i>Reduced</i>	2.289637465e+00	2.353177331e+00	2.350567969e+00	2.348545860e+00
	<i>Unreduced</i>	4.490663987e+01	5.826077029e+00	2.584373424e+00	2.364106778e+00
<i>Bending</i>	<i>Reduced</i>	2.252388554e+00	2.343601849e+00	2.345097484e+00	2.343223969e+00
	<i>Unreduced</i>	2.252339555e+00	2.343594753e+00	2.345097390e+00	2.343224016e+00
<i>Membrane</i>	<i>Reduced</i>	1.069575700e-02	5.833861731e-03	5.138370022e-03	5.093854469e-03
	<i>Unreduced</i>	3.292070820e+01	2.286951161e+00	1.504044681e-01	1.420575148e-02
<i>Shear</i>	<i>Reduced</i>	2.652735916e-02	3.834490301e-03	4.451678638e-04	3.426215497e-04
	<i>Unreduced</i>	9.734009831e+00	1.195632147e+00	8.898514200e-02	6.791701183e-03
$\varepsilon = 10^{-3}$		$h = 0.25$	$h = 0.125$	$h = 0.0625$	$h = 0.03125$
<i>Total</i>	<i>Reduced</i>	2.146526366e+03	2.310957561e+03	2.331924442e+03	2.333998776e+03
	<i>Unreduced</i>	3.277504538e+06	2.708803650e+05	2.305341800e+04	3.764434461e+03
<i>Bending</i>	<i>Reduced</i>	2.127563809e+03	2.302193895e+03	2.328824736e+03	2.332130262e+03
	<i>Unreduced</i>	2.127614466e+03	2.302198494e+03	2.328827148e+03	2.332130348e+03
<i>Membrane</i>	<i>Reduced</i>	1.361615841e+01	6.557423235e+00	2.095558426e+00	1.754525743e+00
	<i>Unreduced</i>	3.154124581e+06	2.233299967e+05	1.435801523e+04	9.049430559e+02
<i>Shear</i>	<i>Reduced</i>	5.341152946e+00	2.200669509e+00	1.004019399e+00	1.146421798e-01
	<i>Unreduced</i>	1.212529553e+05	4.524820428e+04	6.366578421e+03	5.273616327e+02
$\varepsilon = 10^{-4}$		$h = 0.25$	$h = 0.125$	$h = 0.0625$	$h = 0.03125$
<i>Total</i>	<i>Reduced</i>	2.115440768e+06	2.277755705e+06	2.321706597e+06	2.327931549e+06
	<i>Unreduced</i>	3.319102504e+11	2.279111758e+10	1.632568804e+09	1.323359133e+08
<i>Bending</i>	<i>Reduced</i>	2.114800131e+06	2.274345811e+06	2.319255133e+06	2.327301793e+06
	<i>Unreduced</i>	2.114921436e+06	2.274355414e+06	2.319255039e+06	2.327302131e+06
<i>Membrane</i>	<i>Reduced</i>	5.093475773e+02	2.972804460e+03	2.283288380e+03	5.656925089e+02
	<i>Unreduced</i>	3.137966882e+11	2.215796520e+10	1.429066728e+09	8.995585463e+07
<i>Shear</i>	<i>Reduced</i>	1.061479944e+02	4.384453794e+02	1.782801617e+02	7.201479204e+01
	<i>Unreduced</i>	1.811144786e+10	6.308780754e+08	2.011828189e+08	4.005275809e+07

Table 6.11: *Reduced* and *unreduced* energy values associated with the free cylindrical shell problem and MITC6a triangular shell finite element for different values of ε and h (*shear*, *membrane* and *bending* are treated).

$\varepsilon = 10^{-2}$		$h = 0.25$	$h = 0.125$	$h = 0.0625$	$h = 0.03125$
<i>Total</i>	<i>Reduced</i>	2.344113196e+00	2.352012203e+00	2.349366167e+00	2.348186870e+00
	<i>Unreduced</i>	4.993273868e+01	5.674725302e+00	2.563046505e+00	2.362010423e+00
<i>Bending</i>	<i>Reduced</i>	2.330546296e+00	2.345358254e+00	2.343999361e+00	2.342903806e+00
	<i>Unreduced</i>	2.330622763e+00	2.345362813e+00	2.343999501e+00	2.342903851e+00
<i>Membrane</i>	<i>Reduced</i>	6.018281542e-03	5.960648614e-03	5.173313488e-03	5.103170698e-03
	<i>Unreduced</i>	3.395312091e+01	2.291125113e+00	1.504552617e-01	1.421546271e-02
<i>Shear</i>	<i>Reduced</i>	7.599942994e-03	8.043326514e-04	3.080167853e-04	2.945961711e-04
	<i>Unreduced</i>	1.364922063e+01	1.038351618e+00	6.870632874e-02	5.005847563e-03
$\varepsilon = 10^{-3}$		$h = 0.25$	$h = 0.125$	$h = 0.0625$	$h = 0.03125$
<i>Total</i>	<i>Reduced</i>	2.267908296e+03	2.329970702e+03	2.333045876e+03	2.333756317e+03
	<i>Unreduced</i>	3.655058656e+06	3.021433097e+05	2.288402695e+04	3.665432199e+03
<i>Bending</i>	<i>Reduced</i>	2.248329139e+03	2.326733507e+03	2.330770244e+03	2.331973057e+03
	<i>Unreduced</i>	2.248260395e+03	2.326734937e+03	2.330772030e+03	2.331973127e+03
<i>Membrane</i>	<i>Reduced</i>	1.201393133e+01	2.205929290e+00	2.012164023e+00	1.763899296e+00
	<i>Unreduced</i>	3.373084700e+06	2.256948642e+05	1.437706145e+04	9.049896958e+02
<i>Shear</i>	<i>Reduced</i>	7.550219476e+00	1.028234895e+00	2.640709815e-01	1.998254949e-02
	<i>Unreduced</i>	2.797261307e+05	7.412172212e+04	6.176195500e+03	4.284699661e+02
$\varepsilon = 10^{-4}$		$h = 0.25$	$h = 0.125$	$h = 0.0625$	$h = 0.03125$
<i>Total</i>	<i>Reduced</i>	2.234269029e+06	2.310079980e+06	2.327339559e+06	2.328311890e+06
	<i>Unreduced</i>	3.436806568e+11	2.341476156e+10	1.847538181e+09	1.286678249e+08
<i>Bending</i>	<i>Reduced</i>	2.233645541e+06	2.306408807e+06	2.326536464e+06	2.327770447e+06
	<i>Unreduced</i>	2.233599323e+06	2.306405034e+06	2.326535896e+06	2.327770551e+06
<i>Membrane</i>	<i>Reduced</i>	3.935215895e+02	3.037440874e+03	6.857943918e+02	4.882257950e+02
	<i>Unreduced</i>	3.380160489e+11	2.256652281e+10	1.433414870e+09	9.000220402e+07
<i>Shear</i>	<i>Reduced</i>	2.282016624e+02	6.331012371e+02	1.253993861e+02	4.328541076e+01
	<i>Unreduced</i>	5.662374842e+09	8.459323789e+08	4.117967704e+08	3.633785377e+07

Table 6.12: *Reduced* and *unreduced* energy values associated with the free cylindrical shell problem and MITC6b triangular shell finite element for different values of ε and h (*shear*, *membrane* and *bending* are treated).

$\varepsilon = 10^{-2}$		$h = 0.25$	$h = 0.125$	$h = 0.0625$	$h = 0.03125$
<i>Total</i>	<i>Reduced</i>	2.443426502e+00	2.376503619e+00	2.356244828e+00	2.350390988e+00
	<i>Unreduced</i>	1.339762986e+02	1.238826853e+01	3.097342290e+00	2.414586395e+00
<i>Membrane</i>	<i>Reduced</i>	2.535120666e-03	4.283434908e-03	4.640977126e-03	4.911174273e-03
	<i>Unreduced</i>	3.829509539e+01	2.367585249e+00	1.511648578e-01	1.404518544e-02
$\varepsilon = 10^{-3}$		$h = 0.25$	$h = 0.125$	$h = 0.0625$	$h = 0.03125$
<i>Total</i>	<i>Reduced</i>	2.434571337e+03	2.367512110e+03	2.343400685e+03	2.336410154e+03
	<i>Unreduced</i>	1.291724666e+07	1.029970378e+06	8.595355234e+04	8.567656566e+03
<i>Membrane</i>	<i>Reduced</i>	1.046257574e+00	6.967803626e-01	8.367277831e-01	1.492976888e+00
	<i>Unreduced</i>	3.780363430e+06	2.349195548e+05	1.456874005e+04	9.077941938e+02
$\varepsilon = 10^{-4}$		$h = 0.25$	$h = 0.125$	$h = 0.0625$	$h = 0.03125$
<i>Total</i>	<i>Reduced</i>	2.433056585e+06	2.365518647e+06	2.341619410e+06	2.333301477e+06
	<i>Unreduced</i>	1.291855653e+12	1.024669428e+11	8.337643465e+09	7.624354811e+08
<i>Membrane</i>	<i>Reduced</i>	2.219995578e+01	2.061707303e+02	1.739934514e+02	1.924338557e+02
	<i>Unreduced</i>	3.771834362e+11	2.340890568e+10	1.453257510e+09	9.050544323e+07

Table 6.13: *Reduced* and *unreduced* energy values associated with the free cylindrical shell problem and MITC7 triangular shell finite element for different values of ε and h (*shear*, *membrane* and *bending* are treated).

$\varepsilon = 10^{-2}$		$h = 0.25$	$h = 0.125$	$h = 0.0625$	$h = 0.03125$
<i>Total</i>	<i>Reduced</i>	4.629818940e-01	1.695923606e+00	2.291437622e+00	2.344884359e+00
	<i>Unreduced</i>	1.243484744e+01	3.642592305e+00	2.473815103e+00	2.357773299e+00
<i>Bending</i>	<i>Reduced</i>	1.588864696e-01	1.218117170e+00	2.227325952e+00	2.335617469e+00
	<i>Unreduced</i>	1.603260167e-01	1.225187397e+00	2.230640456e+00	2.336489167e+00
<i>Membrane</i>	<i>Reduced</i>	2.911542265e-01	4.736608057e-01	6.372947893e-02	9.038053352e-03
	<i>Unreduced</i>	9.144135566e-01	1.262987243e+00	1.571841265e-01	1.519553725e-02
<i>Shear</i>	<i>Reduced</i>	1.270866774e-02	4.149610212e-03	4.857806291e-04	3.428264622e-04
	<i>Unreduced</i>	1.136076124e+01	1.159137527e+00	8.831203499e-02	6.786232880e-03
$\varepsilon = 10^{-3}$		$h = 0.25$	$h = 0.125$	$h = 0.0625$	$h = 0.03125$
<i>Total</i>	<i>Reduced</i>	2.437726087e+01	8.855590368e+01	6.511301058e+02	1.996993043e+03
	<i>Unreduced</i>	4.838202326e+04	6.896007766e+04	9.167167262e+03	2.963214750e+03
<i>Bending</i>	<i>Reduced</i>	5.649609015e+00	2.676575699e+01	1.881408615e+02	1.706996373e+03
	<i>Unreduced</i>	5.650169827e+00	2.677889992e+01	1.884052066e+02	1.707632144e+03
<i>Membrane</i>	<i>Reduced</i>	1.518729897e+01	6.072863566e+01	4.622213509e+02	2.898431907e+02
	<i>Unreduced</i>	4.614925547e+01	1.887593076e+02	1.202921179e+03	7.356919177e+02
<i>Shear</i>	<i>Reduced</i>	3.531340740e+00	1.048780897e+00	7.657967509e-01	1.537043049e-01
	<i>Unreduced</i>	4.833021358e+04	6.874453106e+04	7.776014593e+03	5.203150765e+02
$\varepsilon = 10^{-4}$		$h = 0.25$	$h = 0.125$	$h = 0.0625$	$h = 0.03125$
<i>Total</i>	<i>Reduced</i>	3.320952928e+02	3.589494826e+03	1.613331223e+04	1.336169652e+05
	<i>Unreduced</i>	1.118987724e+06	1.045102832e+08	3.484091860e+08	5.635730656e+07
<i>Bending</i>	<i>Reduced</i>	1.427252092e+00	5.333373442e+02	5.076431595e+03	1.067981776e+04
	<i>Unreduced</i>	1.427323780e+00	5.333405387e+02	5.076623510e+03	1.068259681e+04
<i>Membrane</i>	<i>Reduced</i>	2.674557492e+02	2.772440705e+03	1.095965771e+04	1.228735862e+05
	<i>Unreduced</i>	7.459123808e+02	7.180609822e+03	3.396346300e+04	3.165367145e+05
<i>Shear</i>	<i>Reduced</i>	6.321026008e+01	2.835237681e+02	9.655301736e+01	6.344333940e+01
	<i>Unreduced</i>	1.118240382e+06	1.045025691e+08	3.483701452e+08	5.603008895e+07

Table 6.14: *Reduced* and *unreduced* energy values associated with the free cylindrical shell problem and MITC6c triangular shell finite element for different values of ε and h (*shear*, *membrane* and *bending* are treated).

$\varepsilon = 10^{-2}$		$h = 0.25$	$h = 0.125$	$h = 0.0625$	$h = 0.03125$
<i>Total</i>	<i>Reduced</i>	1.777492936e-01	7.625815401e-01	2.048974143e+00	2.326464335e+00
	<i>Unreduced</i>	1.003808219e+01	1.549859582e+00	1.984707779e+00	2.320070217e+00
<i>Bending</i>	<i>Reduced</i>	8.956422868e-02	2.620719240e-01	1.781902917e+00	2.299337687e+00
	<i>Unreduced</i>	8.954439972e-02	2.620248390e-01	1.781889955e+00	2.299336810e+00
<i>Membrane</i>	<i>Reduced</i>	7.400067754e-02	4.888918443e-01	2.654623117e-01	2.687290067e-02
	<i>Unreduced</i>	6.272811605e-02	2.265471055e-01	1.156110690e-01	1.404279121e-02
<i>Shear</i>	<i>Reduced</i>	1.396171666e-02	1.158274103e-02	1.686390710e-03	3.655781737e-04
	<i>Unreduced</i>	9.885579213e+00	1.061217599e+00	8.727313294e-02	6.801673061e-03
$\varepsilon = 10^{-3}$		$h = 0.25$	$h = 0.125$	$h = 0.0625$	$h = 0.03125$
<i>Total</i>	<i>Reduced</i>	1.414176620e+01	3.548549369e+01	1.573424158e+02	1.200277433e+03
	<i>Unreduced</i>	2.030377904e+04	5.706591953e+04	6.235124840e+03	1.343288652e+03
<i>Bending</i>	<i>Reduced</i>	2.306131845e+00	2.070207546e+01	1.813523512e+01	6.174360649e+02
	<i>Unreduced</i>	2.304411128e+00	2.069991113e+01	1.813433147e+01	6.174352199e+02
<i>Membrane</i>	<i>Reduced</i>	8.856196124e+00	1.347874452e+01	1.381676295e+02	5.820029763e+02
	<i>Unreduced</i>	2.412066651e+01	1.738018107e+01	5.961677040e+01	2.406652844e+02
<i>Shear</i>	<i>Reduced</i>	2.975677978e+00	1.293339397e+00	1.038016464e+00	8.381448201e-01
	<i>Unreduced</i>	2.027735039e+04	5.702782677e+04	6.157371577e+03	4.851872795e+02
$\varepsilon = 10^{-4}$		$h = 0.25$	$h = 0.125$	$h = 0.0625$	$h = 0.03125$
<i>Total</i>	<i>Reduced</i>	1.709840302e+02	2.115109637e+03	7.445760055e+03	2.675781931e+04
	<i>Unreduced</i>	3.185110212e+05	4.432620541e+07	3.037091810e+08	4.022764687e+07
<i>Bending</i>	<i>Reduced</i>	3.895321690e-01	2.158983055e+02	4.316801410e+03	2.517073166e+03
	<i>Unreduced</i>	3.892521998e-01	2.158542079e+02	4.316660930e+03	2.517049882e+03
<i>Membrane</i>	<i>Reduced</i>	1.302467342e+02	1.664808390e+03	2.988632240e+03	2.418913049e+04
	<i>Unreduced</i>	3.502201667e+02	5.553879448e+03	7.818958766e+03	1.028020926e+04
<i>Shear</i>	<i>Reduced</i>	4.034719048e+01	2.343240272e+02	1.397208120e+02	5.153075464e+01
	<i>Unreduced</i>	3.181604112e+05	4.432043560e+07	3.036970447e+08	4.021484951e+07

Table 6.15: *Reduced* and *unreduced* energy values associated with the free cylindrical shell problem and MITC6d triangular shell finite element for different values of ε and h (*shear*, *membrane* and *bending* are treated).

$\varepsilon = 10^{-2}$		$h = 0.25$	$h = 0.125$	$h = 0.0625$	$h = 0.03125$
<i>Total</i>	<i>Reduced</i>	1.923637388e-01	8.693492920e-01	2.100049148e+00	2.331168780e+00
	<i>Unreduced</i>	9.189487034e+00	1.920766933e+00	2.147035143e+00	2.334439671e+00
<i>Bending</i>	<i>Reduced</i>	8.085770965e-02	3.358964749e-01	1.870565944e+00	2.308084132e+00
	<i>Unreduced</i>	8.099133113e-02	3.396316510e-01	1.876526415e+00	2.309938121e+00
<i>Membrane</i>	<i>Reduced</i>	8.976670214e-02	5.219749799e-01	2.282614355e-01	2.283930091e-02
	<i>Unreduced</i>	1.304876963e-01	4.729173395e-01	1.860128071e-01	1.905126071e-02
<i>Shear</i>	<i>Reduced</i>	2.163508353e-02	1.147296995e-02	1.303180354e-03	3.574995280e-04
	<i>Unreduced</i>	8.977975574e+00	1.110725095e+00	8.857099039e-02	6.804122202e-03

$\varepsilon = 10^{-3}$		$h = 0.25$	$h = 0.125$	$h = 0.0625$	$h = 0.03125$
<i>Total</i>	<i>Reduced</i>	1.135032754e+01	3.331147944e+01	1.898825132e+02	1.324851281e+03
	<i>Unreduced</i>	1.465004415e+04	4.064997274e+04	5.795508657e+03	1.698843104e+03
<i>Bending</i>	<i>Reduced</i>	1.647642042e+00	1.538513046e+01	2.253293649e+01	7.526284948e+02
	<i>Unreduced</i>	1.647720879e+00	1.538868611e+01	2.257763236e+01	7.532299652e+02
<i>Membrane</i>	<i>Reduced</i>	6.425679867e+00	1.631060018e+01	1.659458663e+02	5.715134088e+02
	<i>Unreduced</i>	8.722496944e+00	1.825955802e+01	1.394545004e+02	4.542300460e+02
<i>Shear</i>	<i>Reduced</i>	3.274473278e+00	1.609101711e+00	1.403655672e+00	7.096127215e-01
	<i>Unreduced</i>	1.463967076e+04	4.061631677e+04	5.633506106e+03	4.917847399e+02

$\varepsilon = 10^{-4}$		$h = 0.25$	$h = 0.125$	$h = 0.0625$	$h = 0.03125$
<i>Total</i>	<i>Reduced</i>	1.341192634e+02	1.466925371e+03	6.273953843e+03	3.249170591e+04
	<i>Unreduced</i>	2.250858738e+05	2.424836311e+07	1.870748538e+08	3.365837121e+07
<i>Bending</i>	<i>Reduced</i>	2.642693550e-01	1.193136771e+02	2.929828356e+03	2.368094588e+03
	<i>Unreduced</i>	2.642847672e-01	1.193157826e+02	2.929986879e+03	2.368455263e+03
<i>Membrane</i>	<i>Reduced</i>	8.951317339e+01	1.168131439e+03	3.233652386e+03	3.004544389e+04
	<i>Unreduced</i>	1.198251184e+02	1.313097718e+03	3.546416715e+03	2.453563451e+04
<i>Shear</i>	<i>Reduced</i>	4.434143595e+01	1.794376342e+02	1.101245696e+02	7.811732652e+01
	<i>Unreduced</i>	2.249657839e+05	2.424693065e+07	1.870683770e+08	3.363146726e+07

Table 6.16: *Reduced* and *unreduced* energy values associated with the free cylindrical shell problem and MITC6e triangular shell finite element for different values of ε and h (*shear*, *membrane* and *bending* are treated).

6.3.3 Axisymmetric hyperboloid shell problems

We consider the axisymmetric hyperboloid of uniform thickness t and length $2L$. This particular geometry was chosen given that two non-zero principal curvatures of opposite signs exist, no corner singularities are present –which means that no special grading other than boundary layers capturing is necessary– and the two fundamental asymptotic behaviors with well-posed limit problems can be reached by changing the boundary conditions.

The shell midsurface is described by the cartesian equation:

$$y^2 + z^2 = 1 + x^2, \quad x \in [-L, L] \quad (6.42)$$

and as a consequence the normal vector corresponding to a point of coordinates (x, y, z) in the global Cartesian coordinate system is given by:

$$\vec{a}_3(x, y, z) = \frac{1}{\sqrt{x^2 + y^2 + z^2}}(-x, y, z)^T \quad (6.43)$$

As usual, we define \vec{V}_1 and \vec{V}_2 orthogonal to \vec{a}_3 and to each other as:

$$\vec{V}_1 = \frac{\vec{a}_3 \times \vec{e}_x}{\|\vec{a}_3 \times \vec{e}_x\|}, \quad \vec{V}_2 = \vec{a}_3 \times \vec{V}_1 \quad (6.44)$$

for $\vec{e}_x = (1, 0, 0)^T$.

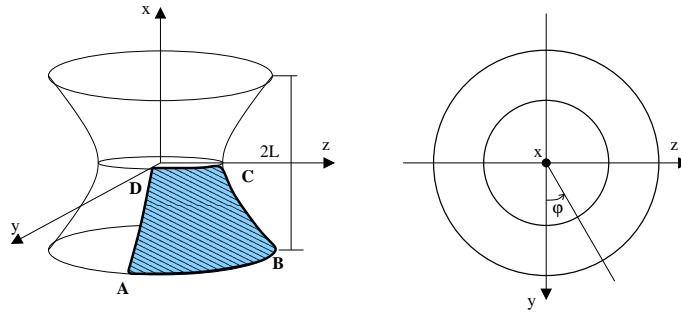


Figure 6.56: Axisymmetric hyperboloid shell problem loaded by smoothly varying periodic pressure normal to the surface ($L = 1.0$, $E = 2.0 \times 10^{11}$, $\nu = 1/3$ and $p_0 = 1.0$).

The loading imposed is the smoothly varying periodic pressure normal to the midsurface given by:

$$p(\varphi) = p_0 \cos(2\varphi) \quad (6.45)$$

Once more, two different asymptotic behaviors are observed depending on boundary conditions: a *bending dominated* problem is obtained when the ends are free and a *membrane dominated* problem is obtained when both ends are clamped.

Due to symmetry, the analysis can be restricted to the $ABCD$ domain shown in Fig. 6.56, which represents one eighth of the whole structure, the following conditions being imposed:

$$u_x = \alpha_2 = 0 \quad \text{along } CD \quad (6.46)$$

$$u_y = \alpha_1 = 0 \quad \text{along } BC \quad (6.47)$$

$$u_z = \alpha_1 = 0 \quad \text{along } AD \quad (6.48)$$

For the *clamped case* we must also set:

$$u_x = u_y = u_z = \alpha_1 = \alpha_2 = 0 \quad \text{along } AB \quad (6.49)$$

Boundary layers must be appropriately meshed in order to obtain accurate results. In both cases (free and clamped) it is known that boundary layers are present, and their width is of order $\sqrt{\varepsilon}L$.

When both ends are clamped the boundary layer was numerically identified to be of width $6\sqrt{\varepsilon}L$. The sequence of meshes was constructed as the clamped cylindrical shell problem: $N + 1$ (axial direction) by $2N + 1$ (circumferential direction) vertex outside of the boundary layer area and $N_{BL}(\varepsilon) + 1$ (axial) by $2N + 1$ (circumferential) vertex into the boundary layer area, where $N_{BL}(\varepsilon) \sim N\varepsilon^{-1/4}$ (refer to Table 6.17 and Fig. 6.57). Naturally, the P_2 displacement-based shell finite element is taken as reference for the error computations.

	N	$N_{BL}(10^{-2})$	$N_{BL}(10^{-3})$	$N_{BL}(10^{-4})$	h
<i>Target</i>	2	7	12	20	0.25
	4	14	24	40	0.125
	8	28	48	80	0.0625
<i>Reference</i>	16	56	96	160	

Table 6.17: ε -dependant sequence of reference and target meshes for the clamped hyperboloid shell problem.

When both ends are free, the boundary layer was estimated to be of width $0.5\sqrt{\varepsilon}L$ and the meshing strategy used is described as follows: $2N + 1$ (axial direction) by $2N + 1$ (circumferential direction) vertex for the area outside of the boundary layers and $N + 1$ (axial) by $2N + 1$ (circumferential) vertex for the boundary layer area (taking $N = 2, 4, 8, 16$). The reference meshes were constructed by the same strategy using the MITC4³ shell finite element –which does not seem to suffer from locking in this case– for $N = 32$.

We refer the reader to Appendix E for more details on boundary layer treatment.

³Described in Appendix A.

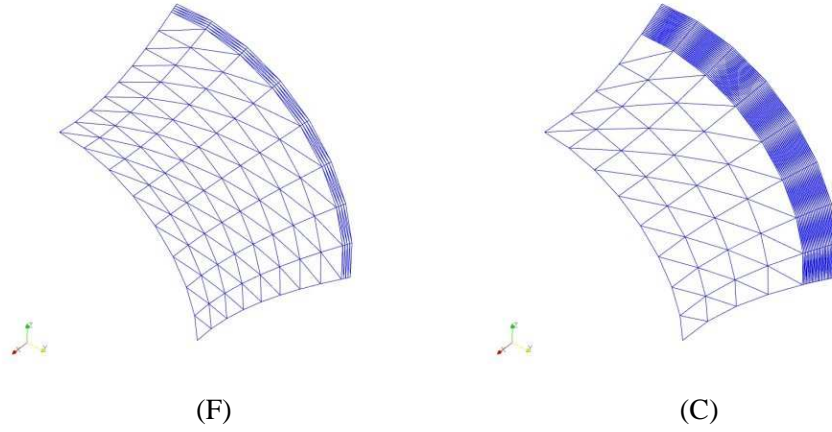


Figure 6.57: Examples of meshes used for the free hyperboloid shell problem – figure (F) on the left– for $N = 4$ and $\varepsilon = 10^{-2}$, and for the clamped hyperboloid shell problem –figure (C) on the right– taking $N = 4$, $\varepsilon = 10^{-3}$ and $N_{BL} = 24$.

Structure with clamped ends

This hyperbolic shell exhibits a membrane dominated behavior when both ends are clamped. Consequently, displacements and strains are well predicted by P_2 displacement-based shell finite elements as seen through the A_m norm –shear terms being discarded or not– and the s -norm (refer to Fig. 6.58). Uniform and optimal convergence rate is achieved for displacements and strains.

Total and partial energy values associated with the reference and P_2 target solutions are displayed in Table 6.18. It confirms that the asymptotic behavior of the structure is membrane-dominated: shear and bending energies vanish as thickness decreases, whereas the membrane energy becomes dominant and it can be scaled by a factor of ε . Given a thickness value, energy values converge as the mesh is refined.

Like for the clamped cylindrical shell problem, the s -norm convergence curves corresponding to the MITC triangular shell finite elements presented in this work show a quite good behavior when only shear, shear and membrane or even bending tensors are treated, except for the MITC7 shell finite element. For the MITC7, bending treatment makes convergence worsen due to P_3 rotation fields interpolation (see Fig. 6.60, 6.62, 6.64, 6.66, 6.68 and 6.70).

If only shear is reduced, strains uniformly converge (see Fig. 6.60 and Fig. 6.62) but the convergence curves displayed on Fig. 6.72-6.73 show that displacements and rotations deteriorate for coarse meshes and small thickness, especially for the MITC7 shell finite element, as seen through the original A_m norm. Similar curves have been calculated when the shear terms are discarded from the A_m norm –only midsurface displacement being considered– and we observe that midsurface displacements *per se* show optimal and uniform convergence as thick-

ness decreases and meshes are refined (refer to Fig. 6.61 and Fig. 6.63). In consequence, we conclude that large errors in the original A_m norm come from rotations.

Once the membrane components are treated we observe that strain fields are slightly deteriorated as seen by means of the s -norm independently of bending treatment (see Fig. 6.64, 6.66, 6.68 and 6.70) except for the MITC6d shell finite element which continues to show an optimal and uniform convergence rate for strains. In addition, the convergence curves related to the A_m norm when shear terms are not discarded are not good for all the MITC shell finite elements we analyzed: either relative errors are not admissible, or convergence worsen for small thickness in the case of the MITC6d shell finite element (see Fig. 6.74-6.77). In fact, displacements and rotations behave worse as seen through such norm once membrane strains are treated, whereas midsurface displacements *per se* remain well predicted as seen by the A_m norm without shear terms except for the MITC7 shell finite element that gives not admissible relative errors for small relative thickness and coarse meshes (refer to Fig. 6.65, 6.67, 6.69 and 6.71). Only the MITC6d shell finite element shows a nearly optimal and uniform convergence for midsurface displacements as seen through the A_m norm when shear terms are discarded. For the other MITC6 shell finite elements we have analyzed, A_m norm without shear convergence curves rise for small thickness values.

These observations make us suspect the presence of spurious membrane modes that may be introduced by the mixed formulation associated with the MITC approach, and we think that they should be detected through the unreduced energies as compared to the reduced ones for each MITC scheme.

Tables 6.19-6.24 summarize a comparison between reduced and unreduced energy values for different meshes and all the MITC triangular shell finite elements considered in this work as ε decreases once *shear*, *membrane* and *bending* tensors are reduced:

- for the MITC7 shell finite element only the membrane energy can be calculated separately because shear and bending tensors are mixed at the elemental level by the static condensation associated with the barycenter rotation fields;
- for all the MITC6 shell finite elements, reduced shear and bending energies vanish as thickness decreases, whereas the reduced membrane energy becomes dominant and it can be scaled by a factor of ε ; namely, these elements behave well from the energy point of view and the asymptotic nature of the problem is well detected by them;
- the MITC7 shell finite element also behaves correctly from the energy point of view: reduced membrane energy gets close to reduced total energy for all thickness values as the mesh is refined and it can be scaled by a factor of ε ;
- we see that for $\varepsilon \ll 1$ the MITC6 reduced shear energy values are slightly higher than the displacement-based reference ones, although they are lower than the corresponding reduced membrane energy values;

- we observe that reduced and unreduced bending energies remain quite close for all the MITC6 finite elements we have analyzed, and also a little higher than the corresponding P_2 energy values as the mesh is refined;
- for all the MITC6 shell finite elements we consider, reduced and unreduced shear energies differ by several orders of magnitude, whereas such difference is weaker for reduced and unreduced membrane energies; this fact explains large errors that appear when shear terms are not discarded from A_m norm computations and *parasitic membrane energy modes* seem to be present⁴ and blow up through unreduced shear energy.

Midsurface deformations are displayed in Fig. 6.78 for the different MITC elements considered in this work when $\varepsilon = 0.0001$. The expected behavior corresponds to the P_2 isoparametric shell element which constitutes a good candidate for membrane-dominated shell problems. It is clearly observed that parasitic membrane modes seem to be propagated along MITC deformed meshes except for the MITC6d shell element.

Structure with free ends

When both ends are free, the problem corresponds to a bending-dominated situation. In such a case we see that P_2 displacement-based shell finite elements clearly behave too stiffly: s -norm and $A_b + A_m$ convergence curves deteriorate as ε decreases, and for small thickness they don't seem to converge at all (refer to Fig. 6.59).

As is well known, shear treatment is not enough to prevent numerical locking (refer to Fig. 6.79-6.80), and membrane tensor components must be also reduced in order to get better numerical solutions.

Once the membrane tensor is treated, numerical results are improved. We observe that the finite elements that show the best behavior are the MITC6a, MITC6b and MITC7 shell finite elements, which slightly lock for small thickness values and coarse meshes, but *convergence is quickly improved as the mesh is refined* for strains –seen by means of the s -norm– and displacements and rotations –through the $A_b + A_m$ norm– (refer to Fig. 6.83, 6.84, 6.87 and 6.88). The MITC7 shell finite element shows a slightly worse behavior. The other tying schemes strongly lock like the P_2 isoparametric shell finite element (see Fig. 6.85, 6.86, 6.89 and 6.90).

Partial and total energy values are summarized in Table 6.25 for the MITC4 shell finite element taken as reference. It states that the bending nature of the problem is well captured by the MITC4 element as shear and membrane energies vanish for decreasing thickness, whereas the bending energy becomes dominant and it can be scaled by a factor of ε^3 .

Reduced and unreduced total, bending, membrane and shear energy values are summarized in Tables 6.27-6.32 for the MITC shell finite elements we focus on with *shear, membrane and bending* treatment:

⁴Such modes tend to vanish as $h \rightarrow 0$ when they appear

- for the MITC7 shell finite element only the membrane energy can be calculated separately because shear and bending tensors are mixed at the elemental level by the static condensation associated with the barycenter rotation fields;
- the table associated with the displacement-based P_2 finite element shows that it clearly suffers from severe shear and membrane locking, as shear and mainly membrane energies remain dominant for small thickness and refined meshes (see Table 6.26);
- reduced membrane energy remains particularly large as ε decreases as compared to total reduced energy especially for the MITC6c, MITC6d and MITC6e shell finite elements that clearly lock (see Tables 6.30-6.32); reduced membrane and shear energies associated with the MITC6a and MITC6b elements are large as compared to total reduced energy for small thickness and coarse meshes, although they decrease as the mesh is refined and reduced bending energy becomes dominant;
- MITC7 reduced membrane energy is also large as compared to total reduced energy for small thickness and coarse meshes, although it gets lower as the mesh is refined;
- for all the MITC6 shell finite elements we consider, reduced and unreduced bending energy values remain close for all thickness independently of the mesh refinement;
- we observe that reduced and unreduced shear energy values differ by several orders of magnitude independently of mesh refinement for small thickness values for all the MITC6 shell finite elements we analyzed;
- for the MITC6a and MITC6b shell finite elements reduced and unreduced membrane energy values also differ by several orders of magnitude, whereas such difference is weaker for the MITC6c, MITC6d and MITC6e shell finite elements that show strong numerical locking;
- actually, the MITC6a, MITC6b and also the MITC7 shell finite elements suffer from numerical locking only for small thickness and coarse meshes whereas a better behavior is quickly achieved as the mesh is refined, which does not happen to the MITC6c, MITC6d and MITC6e shell finite elements.

It is important to notice that numerical results do not get worse because of bending treatment, except for the MITC7 shell finite element, for which convergence curves loosen due to P_3 interpolation of rotation fields.

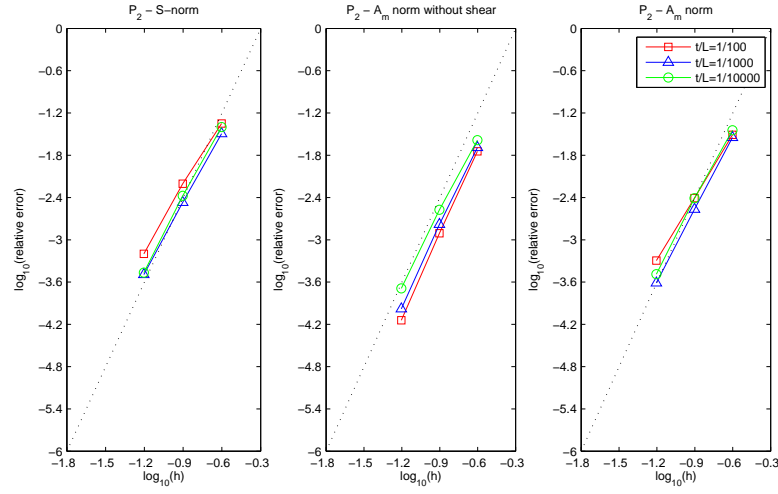


Figure 6.58: Convergence curves associated to the s-norm and membrane energy norm without shear for the clamped hyperboloid shell problem and P_2 displacement-based shell finite elements. The dotted line shows the optimal convergence rate which is 4.

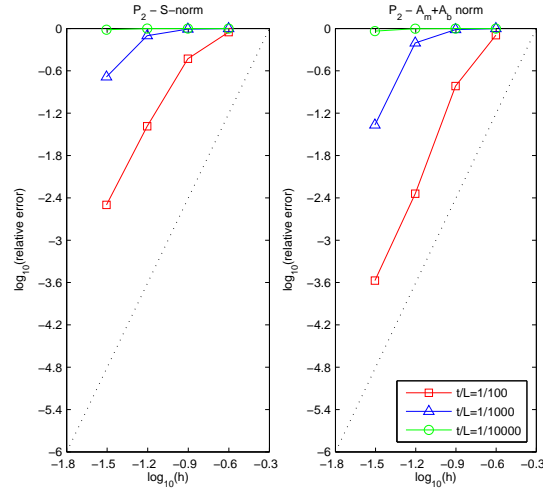


Figure 6.59: S-norm and $A_b + A_m$ -norm convergence curves associated to the free hyperboloid shell problem and P_2 displacement-based shell finite elements. The dotted line shows the optimal convergence rate which is 4.

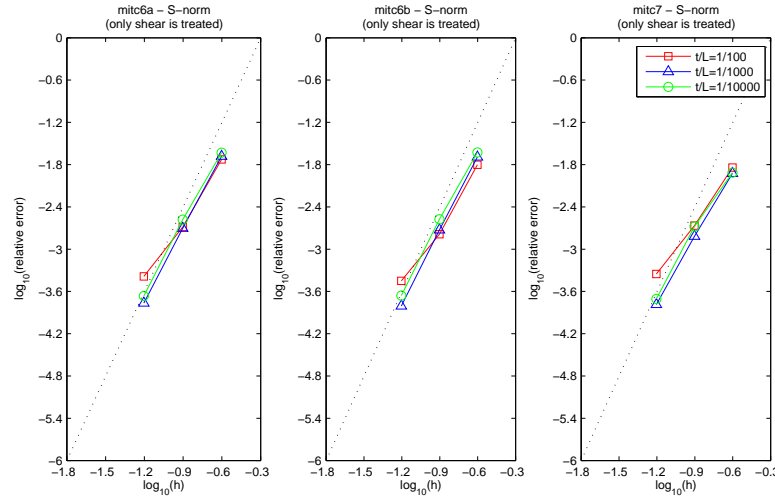


Figure 6.60: S-norm convergence curves associated with the clamped hyperboloid shell problem: MITC6a, MITC6b and MITC7 shell finite elements when *only shear* is treated. The dotted line shows the optimal convergence rate which is 4 for quadratic elements.

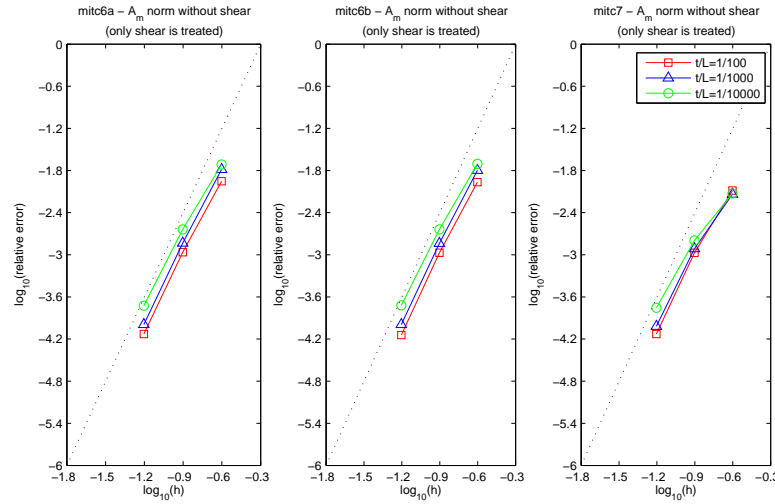


Figure 6.61: Convergence curves associated with the membrane energy norm without shear for the clamped hyperboloid shell problem: MITC6a, MITC6b and MITC7 shell finite elements when *only shear* is treated. The dotted line shows the optimal convergence rate which is 4 for quadratic elements.

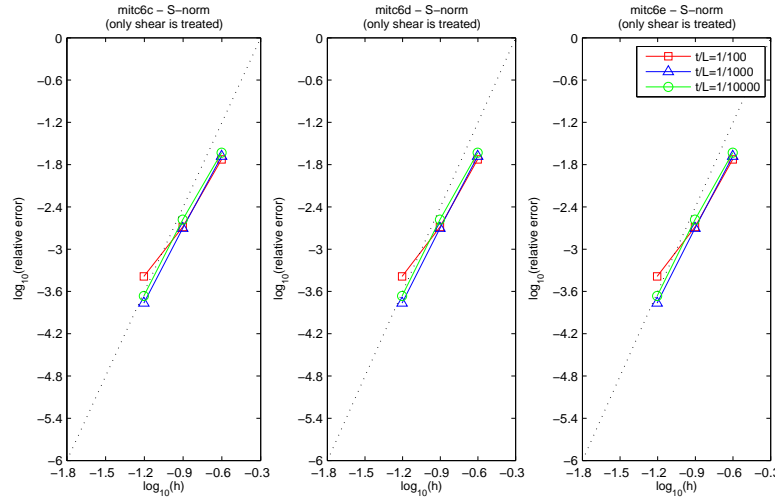


Figure 6.62: S-norm convergence curves associated with the clamped hyperboloid shell problem: MITC6c, MITC6d and MITC6e shell finite elements when *only shear* is treated. The dotted line shows the optimal convergence rate which is 4 for quadratic elements.

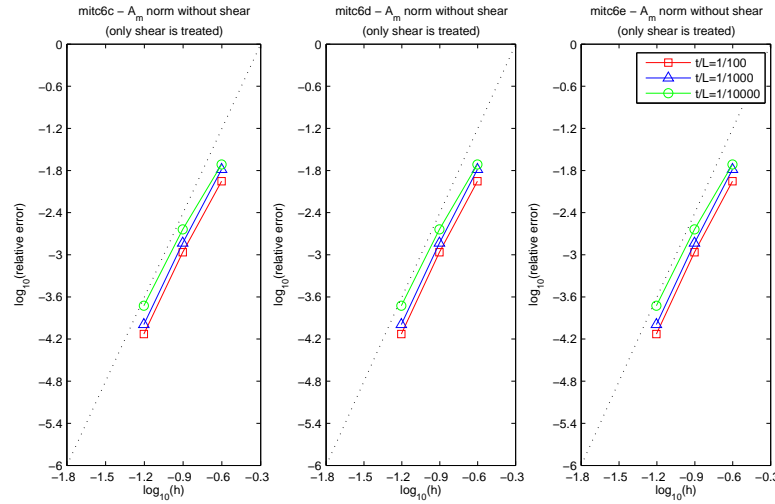


Figure 6.63: Convergence curves associated with the membrane energy norm without shear for the clamped hyperboloid shell problem: MITC6c, MITC6d and MITC6e shell finite elements when *only shear* is treated. The dotted line shows the optimal convergence rate which is 4 for quadratic elements.

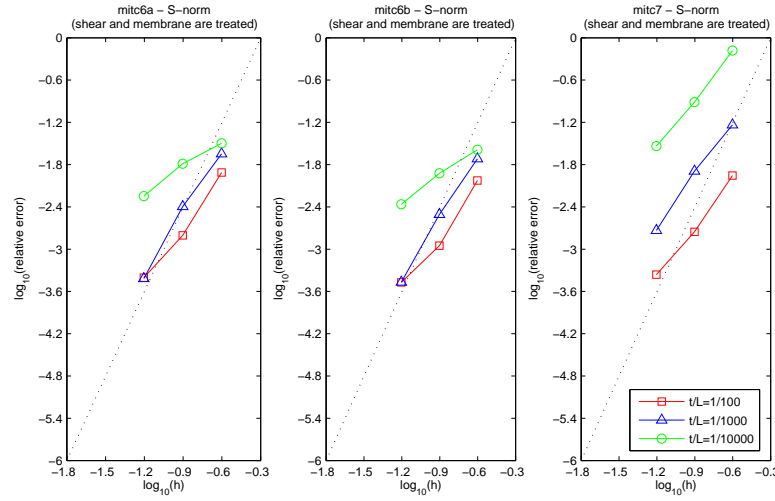


Figure 6.64: S-norm convergence curves associated with the clamped hyperboloid shell problem: MITC6a, MITC6b and MITC7 shell finite elements when *shear and membrane* are treated. The dotted line shows the optimal convergence rate which is 4 for quadratic elements.

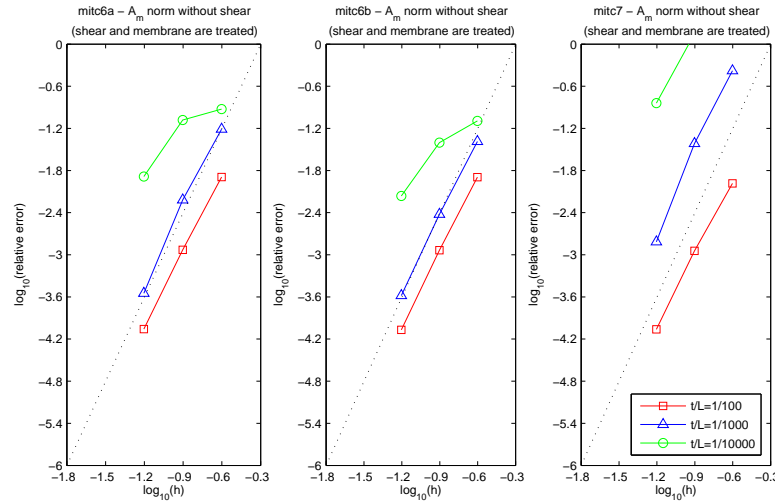


Figure 6.65: Convergence curves associated with the membrane energy norm without shear for the clamped hyperboloid shell problem: MITC6a, MITC6b and MITC7 shell finite elements when *shear and membrane* are treated. The dotted line shows the optimal convergence rate which is 4 for quadratic elements.

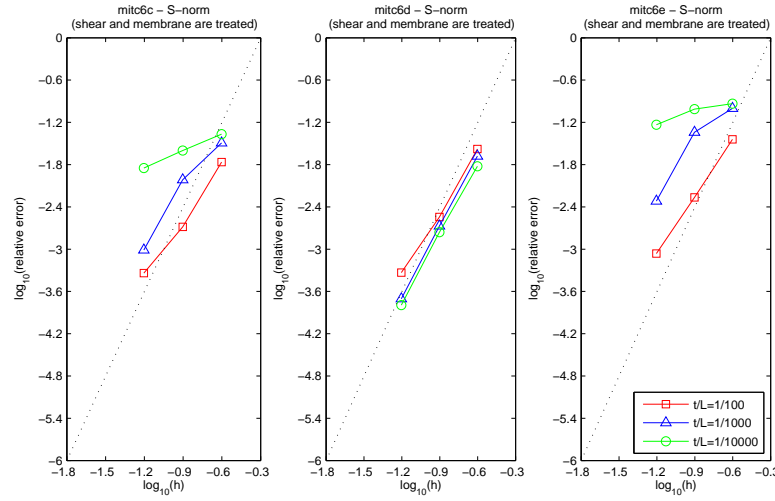


Figure 6.66: S-norm convergence curves associated with the clamped hyperboloid shell problem: MITC6c, MITC6d and MITC6e shell finite elements when *shear and membrane* are treated. The dotted line shows the optimal convergence rate which is 4 for quadratic elements.

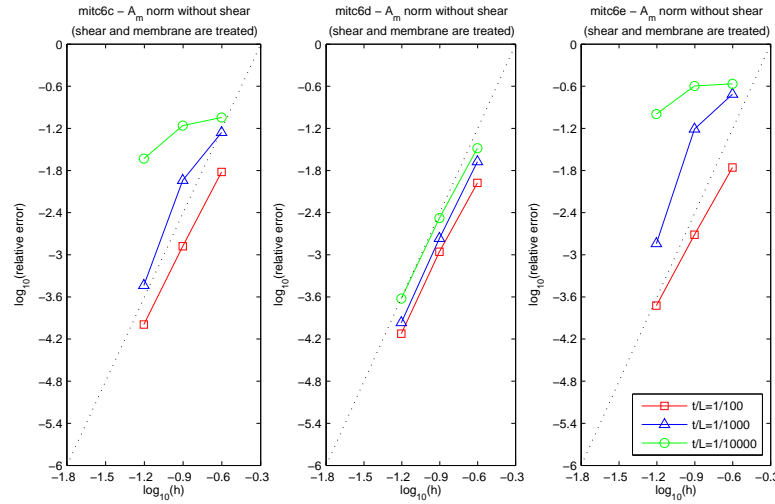


Figure 6.67: Convergence curves associated with the membrane energy norm without shear for the clamped hyperboloid shell problem: MITC6c, MITC6d and MITC6e shell finite elements when *shear and membrane* are treated. The dotted line shows the optimal convergence rate which is 4 for quadratic elements.

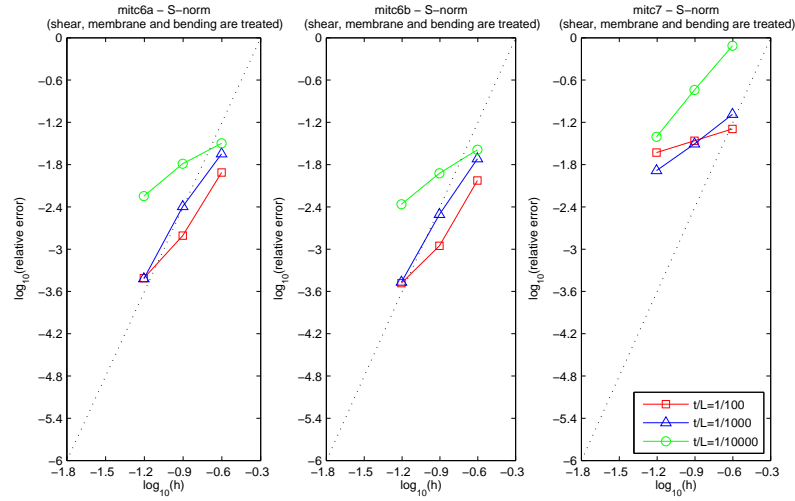


Figure 6.68: S-norm convergence curves associated with the clamped hyperboloid shell problem: MITC6a, MITC6b and MITC7 shell finite elements when *shear, membrane and bending* are treated. The dotted line shows the optimal convergence rate which is 4 for quadratic elements.

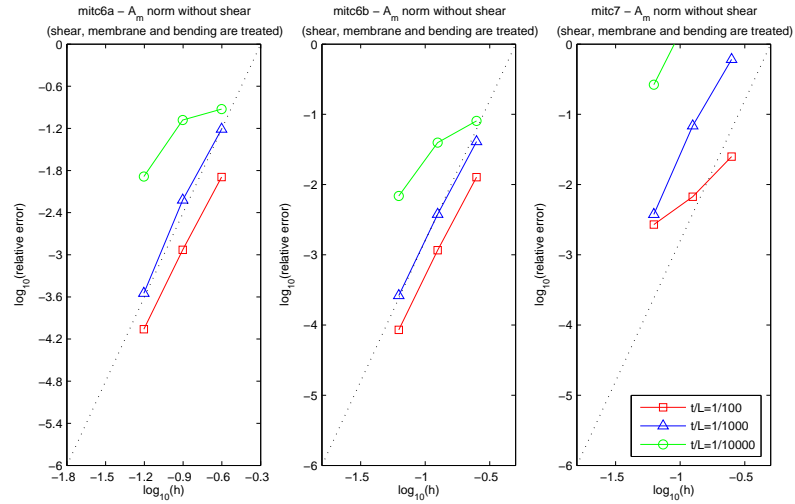


Figure 6.69: Convergence curves associated with the membrane energy norm without shear for the clamped hyperboloid shell problem: MITC6a, MITC6b and MITC7 shell finite elements when *shear, membrane and bending* are treated. The dotted line shows the optimal convergence rate which is 4 for quadratic elements.

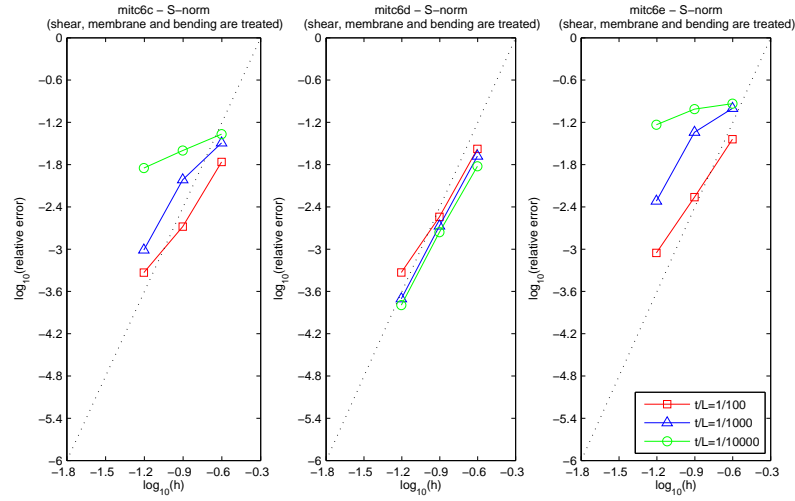


Figure 6.70: S-norm convergence curves associated with the clamped hyperboloid shell problem: MITC6c, MITC6d and MITC6e shell finite elements when *shear*, *membrane* and *bending* are treated. The dotted line shows the optimal convergence rate which is 4 for quadratic elements.

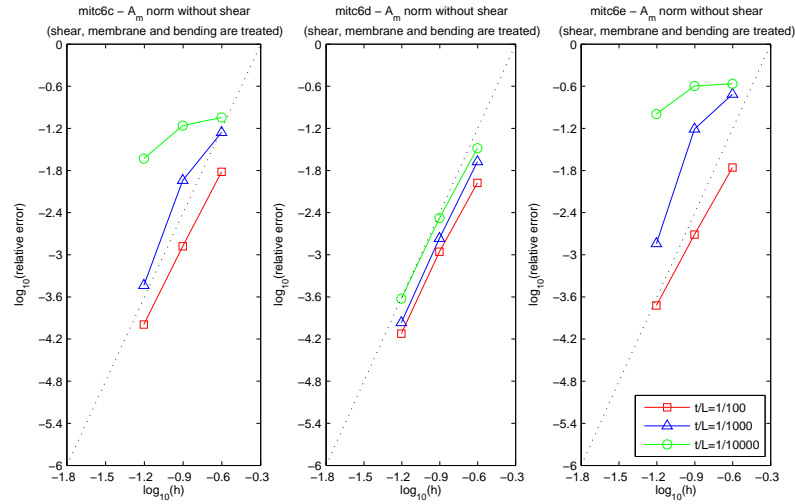


Figure 6.71: Convergence curves associated with the membrane energy norm without shear for the clamped hyperboloid shell problem: MITC6c, MITC6d and MITC6e shell finite elements when *shear*, *membrane* and *bending* are treated. The dotted line shows the optimal convergence rate which is 4 for quadratic elements.

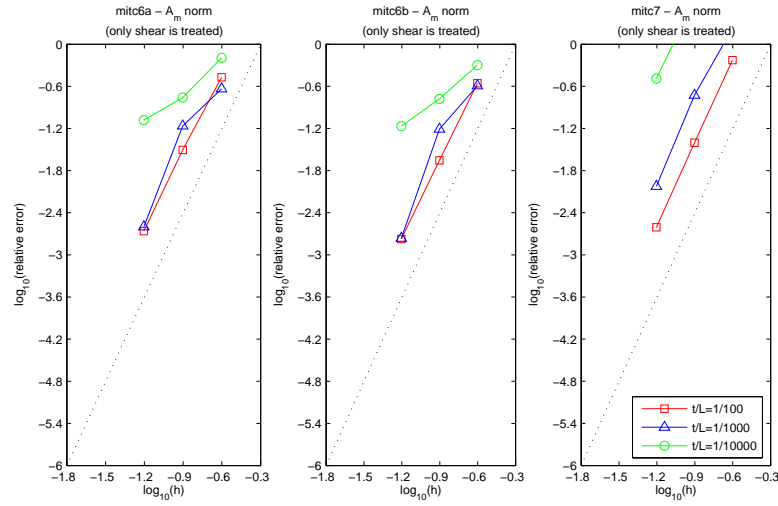


Figure 6.72: Convergence curves associated with the membrane and shear energy norm for the clamped hyperboloid shell problem: MITC6a, MITC6b and MITC7 shell finite elements when *only shear* is treated. The dotted line shows the optimal convergence rate which is 4 for quadratic elements.

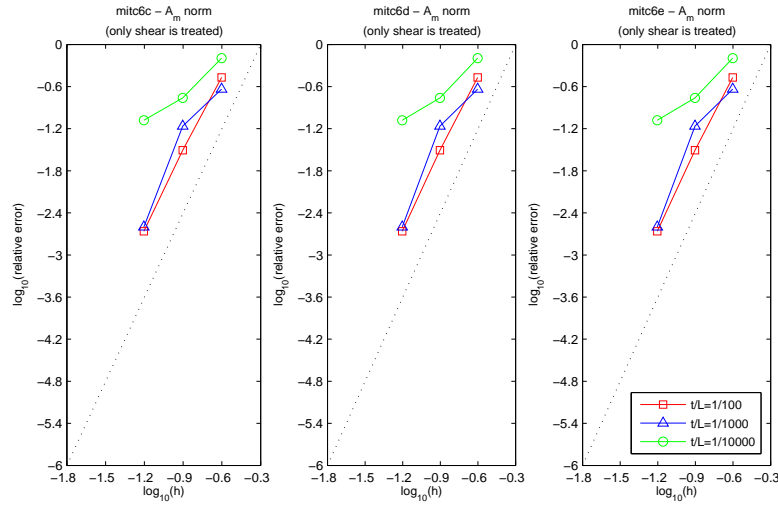


Figure 6.73: Convergence curves associated with the membrane and shear energy norm for the clamped hyperboloid shell problem: MITC6c, MITC6d and MITC6e shell finite elements when *only shear* is treated. The dotted line shows the optimal convergence rate which is 4 for quadratic elements.

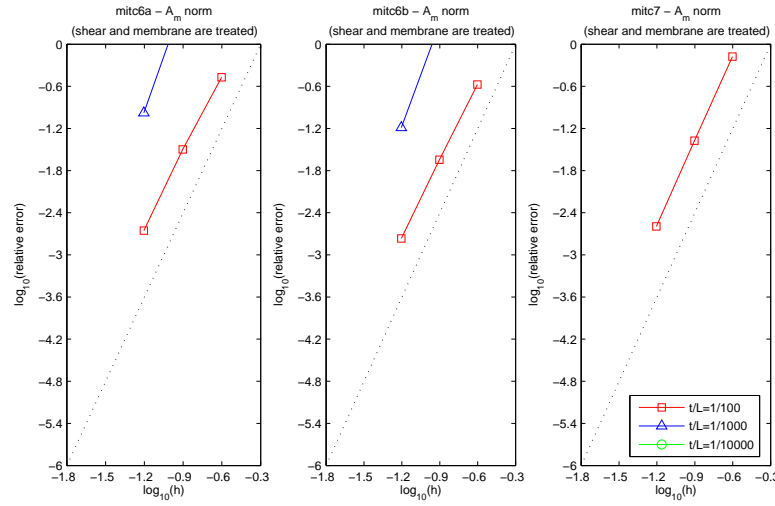


Figure 6.74: Convergence curves associated with the membrane and shear energy norm for the clamped hyperboloid shell problem: MITC6a, MITC6b and MITC7 shell finite elements when *shear and membrane* are treated. The dotted line shows the optimal convergence rate which is 4 for quadratic elements.

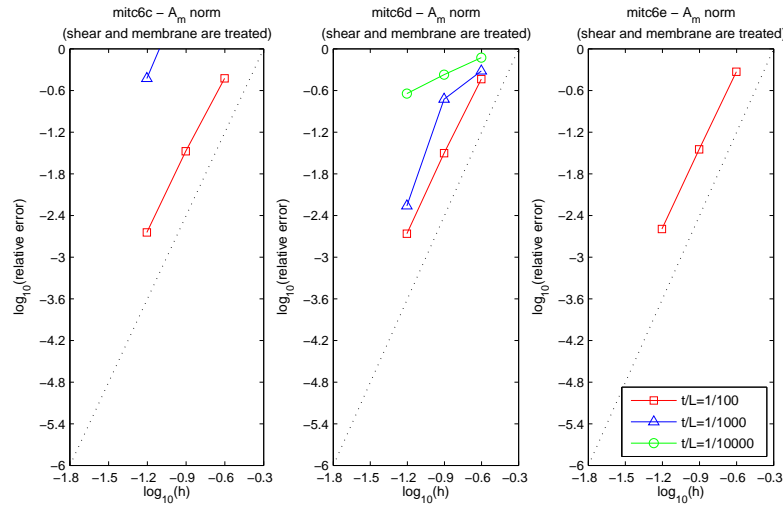


Figure 6.75: Convergence curves associated with the membrane and shear energy norm for the clamped hyperboloid shell problem: MITC6c, MITC6d and MITC6e shell finite elements when *shear and membrane* are treated. The dotted line shows the optimal convergence rate which is 4 for quadratic elements.

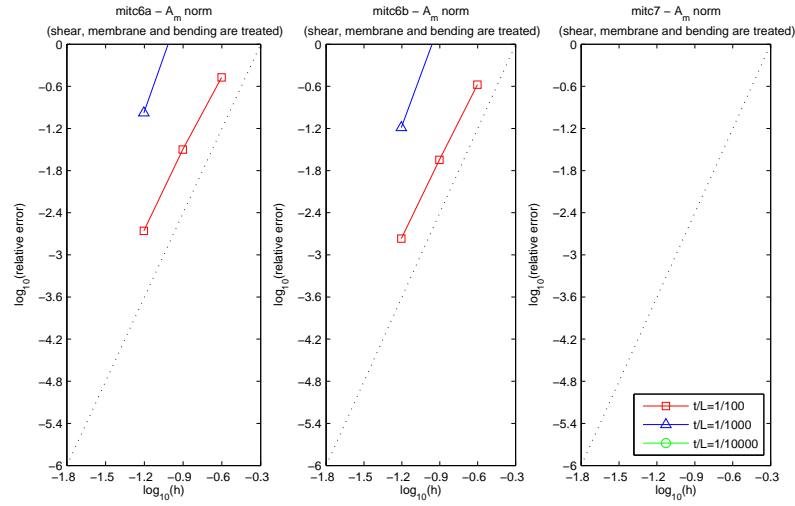


Figure 6.76: Convergence curves associated with the membrane and shear energy norm for the clamped hyperboloid shell problem: MITC6a, MITC6b and MITC7 shell finite elements when *shear, membrane and bending* are treated. The dotted line shows the optimal convergence rate which is 4 for quadratic elements.

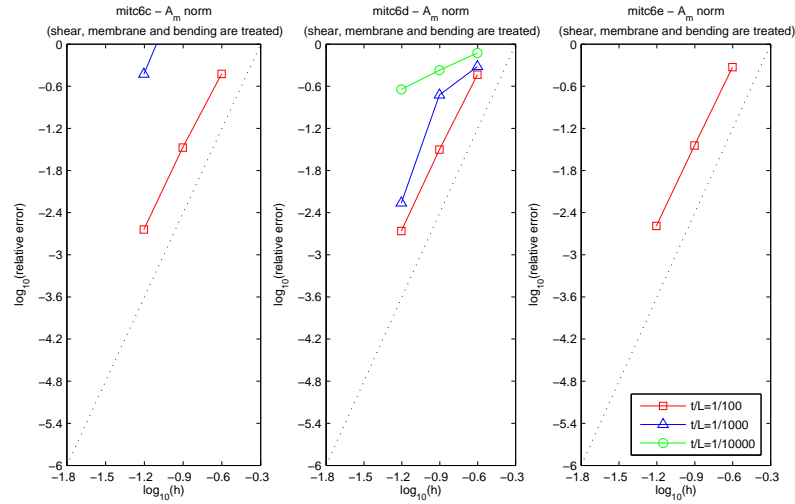


Figure 6.77: Convergence curves associated with the membrane and shear energy norm for the clamped hyperboloid shell problem: MITC6c, MITC6d and MITC6e shell finite elements when *shear, membrane and bending* are treated. The dotted line shows the optimal convergence rate which is 4 for quadratic elements.

$\varepsilon = 10^{-2}$	$h = 0.25$	$h = 0.125$	$h = 0.0625$	<i>Ref sol</i>
<i>Total</i>	5.142788610e-10	5.357354700e-10	5.388140333e-10	5.391575296e-10
<i>Bending</i>	1.492309850e-11	2.087114520e-11	2.224962392e-11	2.249852075e-11
<i>Membrane</i>	4.921780555e-10	5.132309149e-10	5.161115410e-10	5.164252432e-10
<i>Shear</i>	7.275289688e-12	1.740791104e-12	5.613528621e-13	3.423416674e-13
$\varepsilon = 10^{-3}$	$h = 0.25$	$h = 0.125$	$h = 0.0625$	<i>Ref sol</i>
<i>Total</i>	5.798999686e-09	5.979973327e-09	5.998990268e-09	6.000953295e-09
<i>Bending</i>	3.960984668e-11	6.504691165e-11	6.885305365e-11	6.943181816e-11
<i>Membrane</i>	5.711132143e-09	5.908571215e-09	5.929187323e-09	5.931329548e-09
<i>Shear</i>	4.827724646e-11	6.380359656e-12	9.759075375e-13	2.180394092e-13
$\varepsilon = 10^{-4}$	$h = 0.25$	$h = 0.125$	$h = 0.0625$	<i>Ref sol</i>
<i>Total</i>	5.932764045e-08	6.163015845e-08	6.187506312e-08	6.189668695e-08
<i>Bending</i>	5.598401321e-11	1.780642739e-10	2.126460423e-10	2.159824075e-10
<i>Membrane</i>	5.860035750e-08	6.137437570e-08	6.165431470e-08	6.167980084e-08
<i>Shear</i>	6.713019067e-10	7.772461336e-11	8.109503700e-12	9.109533331e-13

Table 6.18: Energy values associated with the clamped hyperboloid shell problem and P_2 displacement-based shell finite elements for different values of ε and h , also the P_2 solution taken as reference.

$\varepsilon = 10^{-2}$		$h = 0.25$	$h = 0.125$	$h = 0.0625$
<i>Total</i>	<i>Reduced</i>	5.313287519e-10	5.386378663e-10	5.391849079e-10
	<i>Unreduced</i>	7.007754801e-10	5.548806408e-10	5.404578460e-10
<i>Bending</i>	<i>Reduced</i>	1.965029737e-11	2.238886036e-11	2.253228463e-11
	<i>Unreduced</i>	1.959089190e-11	2.236655348e-11	2.252485986e-11
<i>Membrane</i>	<i>Reduced</i>	5.093664728e-10	5.158833701e-10	5.164003365e-10
	<i>Unreduced</i>	5.071992002e-10	5.144402410e-10	5.159583348e-10
<i>Shear</i>	<i>Reduced</i>	2.409716708e-12	4.718519667e-13	3.602628182e-13
	<i>Unreduced</i>	1.740828072e-10	1.818008997e-11	2.082645828e-12
$\varepsilon = 10^{-3}$		$h = 0.25$	$h = 0.125$	$h = 0.0625$
<i>Total</i>	<i>Reduced</i>	5.889992135e-09	5.985962841e-09	5.996186056e-09
	<i>Unreduced</i>	3.677530128e-08	2.900105511e-08	6.615963449e-09
<i>Bending</i>	<i>Reduced</i>	5.676952148e-11	7.515581082e-11	7.001320503e-11
	<i>Unreduced</i>	5.661184016e-11	7.508850030e-11	7.000004735e-11
<i>Membrane</i>	<i>Reduced</i>	5.813742852e-09	5.907618412e-09	5.925717456e-09
	<i>Unreduced</i>	6.138765320e-09	5.941810419e-09	5.923120974e-09
<i>Shear</i>	<i>Reduced</i>	1.950328883e-11	3.214517077e-12	4.813636638e-13
	<i>Unreduced</i>	3.057994119e-08	2.298417772e-08	6.228683340e-10
$\varepsilon = 10^{-4}$		$h = 0.25$	$h = 0.125$	$h = 0.0625$
<i>Total</i>	<i>Reduced</i>	6.130087928e-08	6.246118510e-08	6.215948686e-08
	<i>Unreduced</i>	7.521054441e-07	7.100414393e-06	1.080359911e-05
<i>Bending</i>	<i>Reduced</i>	1.365126933e-10	2.493470739e-10	3.563850125e-10
	<i>Unreduced</i>	1.361435830e-10	2.491561467e-10	3.562614573e-10
<i>Membrane</i>	<i>Reduced</i>	6.071939806e-08	6.200696112e-08	6.175048866e-08
	<i>Unreduced</i>	6.874524323e-08	6.801839592e-08	6.301064521e-08
<i>Shear</i>	<i>Reduced</i>	4.449735743e-10	2.048833840e-10	5.261960309e-11
	<i>Unreduced</i>	6.832240605e-07	7.032146834e-06	1.074023219e-05

Table 6.19: *Reduced* and *unreduced* energy values associated with the clamped hyperboloid shell problem and MITC6a triangular shell finite element for different values of ε and h (*shear*, *membrane* and *bending* are treated).

$\varepsilon = 10^{-2}$		$h = 0.25$	$h = 0.125$	$h = 0.0625$
<i>Total</i>	<i>Reduced</i>	5.300067304e-10	5.378704772e-10	5.389855209e-10
	<i>Unreduced</i>	6.606321299e-10	5.484867162e-10	5.397504020e-10
<i>Bending</i>	<i>Reduced</i>	2.039750140e-11	2.228559616e-11	2.246700640e-11
	<i>Unreduced</i>	2.034852556e-11	2.226573654e-11	2.245927713e-11
<i>Membrane</i>	<i>Reduced</i>	5.082452161e-10	5.152541542e-10	5.162429217e-10
	<i>Unreduced</i>	5.058832374e-10	5.137996267e-10	5.158002587e-10
<i>Shear</i>	<i>Reduced</i>	1.463421845e-12	4.374731760e-13	3.837043308e-13
	<i>Unreduced</i>	1.344997449e-10	1.252814996e-11	1.598996137e-12
$\varepsilon = 10^{-3}$		$h = 0.25$	$h = 0.125$	$h = 0.0625$
<i>Total</i>	<i>Reduced</i>	5.872206428e-09	5.981257132e-09	5.995808754e-09
	<i>Unreduced</i>	2.495189948e-08	1.734164012e-08	6.377015230e-09
<i>Bending</i>	<i>Reduced</i>	5.526472585e-11	7.220441782e-11	6.986628942e-11
	<i>Unreduced</i>	5.512016068e-11	7.214721278e-11	6.985357055e-11
<i>Membrane</i>	<i>Reduced</i>	5.798632243e-09	5.905691325e-09	5.925531007e-09
	<i>Unreduced</i>	5.976322592e-09	5.918686110e-09	5.922507205e-09
<i>Shear</i>	<i>Reduced</i>	1.833325871e-11	3.387569667e-12	4.375608545e-13
	<i>Unreduced</i>	1.892047660e-08	1.135083061e-08	3.846804939e-10
$\varepsilon = 10^{-4}$		$h = 0.25$	$h = 0.125$	$h = 0.0625$
<i>Total</i>	<i>Reduced</i>	6.096124450e-08	6.222232968e-08	6.207990990e-08
	<i>Unreduced</i>	5.663338450e-07	4.073318463e-06	6.127947537e-06
<i>Bending</i>	<i>Reduced</i>	1.376952087e-10	2.536621886e-10	3.203815442e-10
	<i>Unreduced</i>	1.373255185e-10	2.535031104e-10	3.202916923e-10
<i>Membrane</i>	<i>Reduced</i>	6.049369013e-08	6.181915231e-08	6.173135634e-08
	<i>Unreduced</i>	6.559096267e-08	6.483358186e-08	6.247153863e-08
<i>Shear</i>	<i>Reduced</i>	3.298645347e-10	1.495222477e-10	2.817926371e-11
	<i>Unreduced</i>	5.006055605e-07	4.008231380e-06	6.065155707e-06

Table 6.20: *Reduced* and *unreduced* energy values associated with the clamped hyperboloid shell problem and MITC6b triangular shell finite element for different values of ε and h (*shear*, *membrane* and *bending* are treated).

$\varepsilon = 10^{-2}$		$h = 0.25$	$h = 0.125$	$h = 0.0625$
<i>Total</i>	<i>Reduced</i>	5.543233527e-10	5.551732172e-10	5.512822620e-10
	<i>Unreduced</i>	4.380163241e-09	2.520871070e-09	1.380131154e-09
<i>Membrane</i>	<i>Reduced</i>	5.543233527e-10	5.352271314e-10	5.289942292e-10
	<i>Unreduced</i>	5.354261027e-10	5.340771110e-10	5.285735115e-10
$\varepsilon = 10^{-3}$		$h = 0.25$	$h = 0.125$	$h = 0.0625$
<i>Total</i>	<i>Reduced</i>	6.370302955e-09	6.163527488e-09	6.072132014e-09
	<i>Unreduced</i>	9.238363524e-06	4.525721991e-07	1.126101929e-07
<i>Membrane</i>	<i>Reduced</i>	6.171539348e-09	6.068983790e-09	6.005542700e-09
	<i>Unreduced</i>	1.035201649e-08	6.589318313e-09	6.032902347e-09
$\varepsilon = 10^{-4}$		$h = 0.25$	$h = 0.125$	$h = 0.0625$
<i>Total</i>	<i>Reduced</i>	1.089034524e-07	7.299160988e-08	6.428919804e-08
	<i>Unreduced</i>	6.402328687e-02	1.607050344e-02	2.441099322e-04
<i>Membrane</i>	<i>Reduced</i>	9.608733005e-08	6.690623290e-08	6.338484821e-08
	<i>Unreduced</i>	4.453952378e-06	2.883852257e-07	8.254440020e-08

Table 6.21: *Reduced* and *unreduced* energy values associated with the clamped hyperboloid shell problem and MITC7 triangular shell finite element for different values of ε and h (*shear*, *membrane* and *bending* are treated).

$\varepsilon = 10^{-2}$		$h = 0.25$	$h = 0.125$	$h = 0.0625$
<i>Total</i>	<i>Reduced</i>	5.392788984e-10	5.409126028e-10	5.397710848e-10
	<i>Unreduced</i>	7.377550785e-10	5.605050620e-10	5.416830839e-10
<i>Bending</i>	<i>Reduced</i>	2.052126093e-11	2.262749556e-11	2.258417747e-11
	<i>Unreduced</i>	2.061068392e-11	2.266219386e-11	2.259544689e-11
<i>Membrane</i>	<i>Reduced</i>	5.160109701e-10	5.178252183e-10	5.169093071e-10
	<i>Unreduced</i>	5.232696900e-10	5.187849304e-10	5.170633457e-10
<i>Shear</i>	<i>Reduced</i>	2.848052830e-12	5.675682778e-13	3.858928678e-13
	<i>Unreduced</i>	1.939791423e-10	1.916678881e-11	2.132899249e-12
$\varepsilon = 10^{-3}$		$h = 0.25$	$h = 0.125$	$h = 0.0625$
<i>Total</i>	<i>Reduced</i>	6.023579457e-09	6.045360058e-09	6.007056409e-09
	<i>Unreduced</i>	2.737846364e-08	5.284418151e-08	8.233348552e-09
<i>Bending</i>	<i>Reduced</i>	5.708201599e-11	8.360589748e-11	7.221569099e-11
	<i>Unreduced</i>	5.723909733e-11	8.366547837e-11	7.223126429e-11
<i>Membrane</i>	<i>Reduced</i>	5.937616348e-09	5.954240074e-09	5.933591417e-09
	<i>Unreduced</i>	6.346637160e-09	6.090502327e-09	5.945139651e-09
<i>Shear</i>	<i>Reduced</i>	2.890491805e-11	7.541347668e-12	1.275962188e-12
	<i>Unreduced</i>	2.097461160e-08	4.667003925e-08	2.216004782e-09
$\varepsilon = 10^{-4}$		$h = 0.25$	$h = 0.125$	$h = 0.0625$
<i>Total</i>	<i>Reduced</i>	6.273091257e-08	6.326557759e-08	6.276592278e-08
	<i>Unreduced</i>	4.288613185e-07	4.158470079e-06	1.661454130e-05
<i>Bending</i>	<i>Reduced</i>	1.737786939e-10	2.443466008e-10	4.132127499e-10
	<i>Unreduced</i>	1.741405072e-10	2.445002224e-10	4.132662958e-10
<i>Membrane</i>	<i>Reduced</i>	6.219644274e-08	6.286736751e-08	6.226217939e-08
	<i>Unreduced</i>	6.944466674e-08	6.869918871e-08	6.486179518e-08
<i>Shear</i>	<i>Reduced</i>	3.606928920e-10	1.538702281e-10	9.053451173e-11
	<i>Unreduced</i>	3.592425115e-07	4.089526393e-06	1.654926622e-05

Table 6.22: *Reduced* and *unreduced* energy values associated with the clamped hyperboloid shell problem and MITC6c triangular shell finite element for different values of ε and h (*shear*, *membrane* and *bending* are treated).

$\varepsilon = 10^{-2}$		$h = 0.25$	$h = 0.125$	$h = 0.0625$
<i>Total</i>	<i>Reduced</i>	5.309244730e-10	5.398009867e-10	5.396207865e-10
	<i>Unreduced</i>	7.162044057e-10	5.571313826e-10	5.413185926e-10
<i>Bending</i>	<i>Reduced</i>	1.870349963e-11	2.224199107e-11	2.255327545e-11
	<i>Unreduced</i>	1.872754998e-11	2.224565698e-11	2.255352698e-11
<i>Membrane</i>	<i>Reduced</i>	5.090371979e-10	5.171842887e-10	5.168156036e-10
	<i>Unreduced</i>	5.065772270e-10	5.168377211e-10	5.167912088e-10
<i>Shear</i>	<i>Reduced</i>	3.274261727e-12	4.808514232e-13	3.600355149e-13
	<i>Unreduced</i>	1.909913150e-10	1.815426204e-11	2.081988403e-12
$\varepsilon = 10^{-3}$		$h = 0.25$	$h = 0.125$	$h = 0.0625$
<i>Total</i>	<i>Reduced</i>	5.888590197e-09	5.990373124e-09	6.000854414e-09
	<i>Unreduced</i>	8.669555070e-09	7.100721356e-09	6.033443774e-09
<i>Bending</i>	<i>Reduced</i>	3.694478196e-11	6.369300955e-11	6.916384480e-11
	<i>Unreduced</i>	3.696266840e-11	6.369475315e-11	6.916415282e-11
<i>Membrane</i>	<i>Reduced</i>	5.842780824e-09	5.925064915e-09	5.931465112e-09
	<i>Unreduced</i>	5.904534257e-09	5.927586820e-09	5.931481082e-09
<i>Shear</i>	<i>Reduced</i>	8.885070100e-12	1.640298127e-12	2.514551729e-13
	<i>Unreduced</i>	2.728078805e-09	1.109464965e-09	3.282454128e-11
$\varepsilon = 10^{-4}$		$h = 0.25$	$h = 0.125$	$h = 0.0625$
<i>Total</i>	<i>Reduced</i>	6.120322595e-08	6.180520873e-08	6.189084933e-08
	<i>Unreduced</i>	1.077287022e-07	8.799264824e-08	7.584927068e-08
<i>Bending</i>	<i>Reduced</i>	6.666511222e-11	1.733465786e-10	2.127798374e-10
	<i>Unreduced</i>	6.673175362e-11	1.733490008e-10	2.127799703e-10
<i>Membrane</i>	<i>Reduced</i>	6.105390401e-08	6.162701318e-08	6.167763558e-08
	<i>Unreduced</i>	6.308624620e-08	6.178646546e-08	6.168741628e-08
<i>Shear</i>	<i>Reduced</i>	8.266061109e-11	4.855548034e-12	4.409726679e-13
	<i>Unreduced</i>	4.457572776e-08	2.603284031e-08	1.394908158e-08

Table 6.23: *Reduced* and *unreduced* energy values associated with the clamped hyperboloid shell problem and MITC6d triangular shell finite element for different values of ε and h (*shear*, *membrane* and *bending* are treated).

$\varepsilon = 10^{-2}$		$h = 0.25$	$h = 0.125$	$h = 0.0625$
<i>Total</i>	<i>Reduced</i>	5.288268422e-10	5.401541794e-10	5.398661044e-10
	<i>Unreduced</i>	7.654536926e-10	5.603578131e-10	5.420328830e-10
<i>Bending</i>	<i>Reduced</i>	2.040090043e-11	2.263671696e-11	2.259671146e-11
	<i>Unreduced</i>	2.055384245e-11	2.271065142e-11	2.262115655e-11
<i>Membrane</i>	<i>Reduced</i>	5.031822984e-10	5.169143993e-10	5.169237823e-10
	<i>Unreduced</i>	5.051997421e-10	5.176318884e-10	5.172784894e-10
<i>Shear</i>	<i>Reduced</i>	5.335364953e-12	7.098560703e-13	4.539865045e-13
	<i>Unreduced</i>	2.397964188e-10	2.012468627e-11	2.242325067e-12
$\varepsilon = 10^{-3}$		$h = 0.25$	$h = 0.125$	$h = 0.0625$
<i>Total</i>	<i>Reduced</i>	6.167802487e-09	6.170269490e-09	6.017197303e-09
	<i>Unreduced</i>	6.246571079e-08	2.137510112e-07	1.619362065e-08
<i>Bending</i>	<i>Reduced</i>	1.057513863e-10	1.429289431e-10	8.213395298e-11
	<i>Unreduced</i>	1.060951047e-10	1.431091580e-10	8.217778421e-11
<i>Membrane</i>	<i>Reduced</i>	5.924711971e-09	5.977001057e-09	5.929553286e-09
	<i>Unreduced</i>	7.464510449e-09	6.640499316e-09	5.972252335e-09
<i>Shear</i>	<i>Reduced</i>	1.373539647e-10	5.035863085e-11	5.536464170e-12
	<i>Unreduced</i>	5.489513144e-08	2.069674345e-07	1.013921927e-08
$\varepsilon = 10^{-4}$		$h = 0.25$	$h = 0.125$	$h = 0.0625$
<i>Total</i>	<i>Reduced</i>	6.587143839e-08	6.717419673e-08	6.537303192e-08
	<i>Unreduced</i>	8.106772653e-07	1.042199870e-05	5.597688047e-05
<i>Bending</i>	<i>Reduced</i>	2.274829965e-10	3.589936552e-10	9.010217003e-10
	<i>Unreduced</i>	2.283269442e-10	3.593963665e-10	9.011796855e-10
<i>Membrane</i>	<i>Reduced</i>	6.412517671e-08	6.598905526e-08	6.398327205e-08
	<i>Unreduced</i>	8.715187472e-08	8.792369581e-08	7.486543158e-08
<i>Shear</i>	<i>Reduced</i>	1.518775428e-09	8.261498910e-10	4.887242139e-10
	<i>Unreduced</i>	7.232970626e-07	1.033371562e-05	5.590111384e-05

Table 6.24: *Reduced* and *unreduced* energy values associated with the clamped hyperboloid shell problem and MITC6e triangular shell finite element for different values of ε and h (*shear*, *membrane* and *bending* are treated).

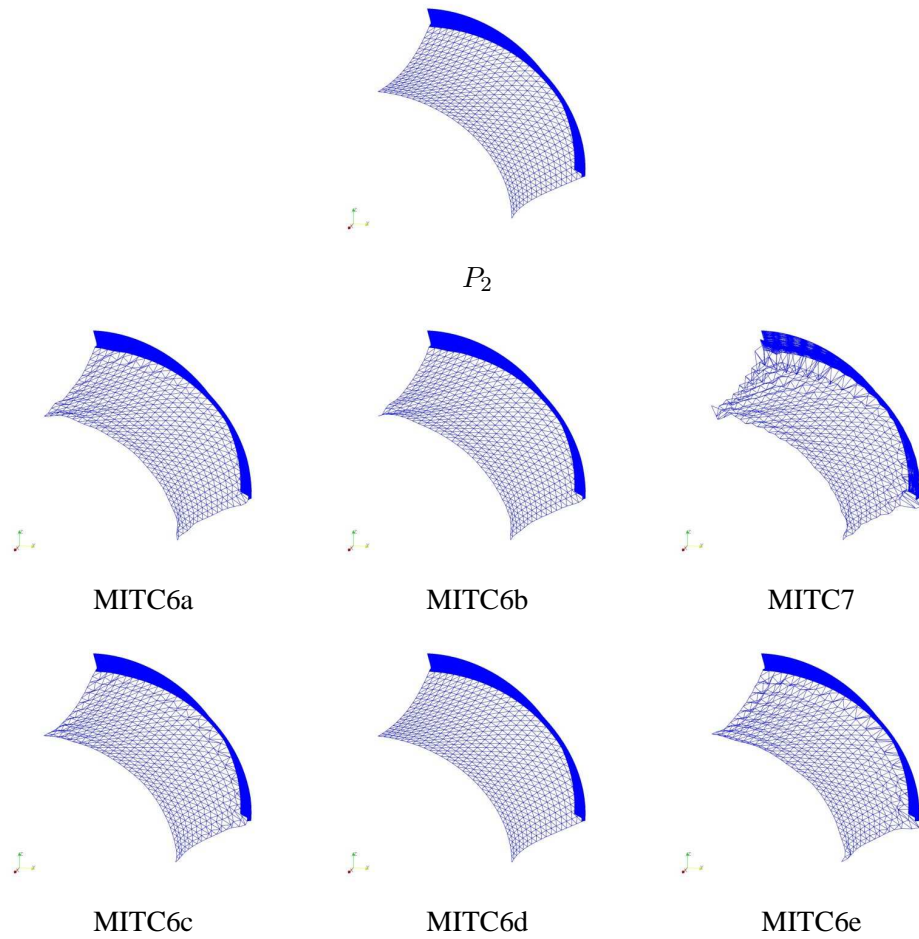


Figure 6.78: Midsurface deformed meshes associated with the clamped hyperboloid shell problem (5841 nodes, 2816 elements, $L = 1$, $\varepsilon = 10^{-4}$, boundary layer of width $6\sqrt{\varepsilon}L$, $scale = 10^6$).

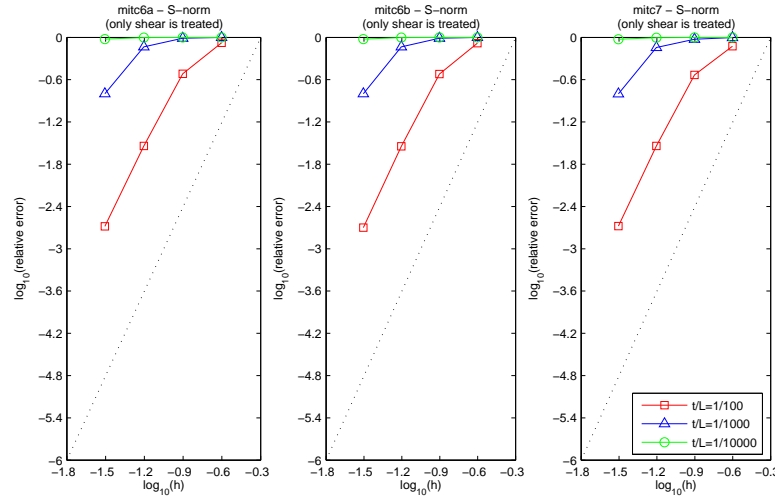


Figure 6.79: S-norm convergence curves associated with the free hyperboloid shell problem: MITC6a, MITC6b and MITC7 shell finite elements when *only shear* is treated. The dotted line shows the optimal convergence rate which is 4 for quadratic elements.

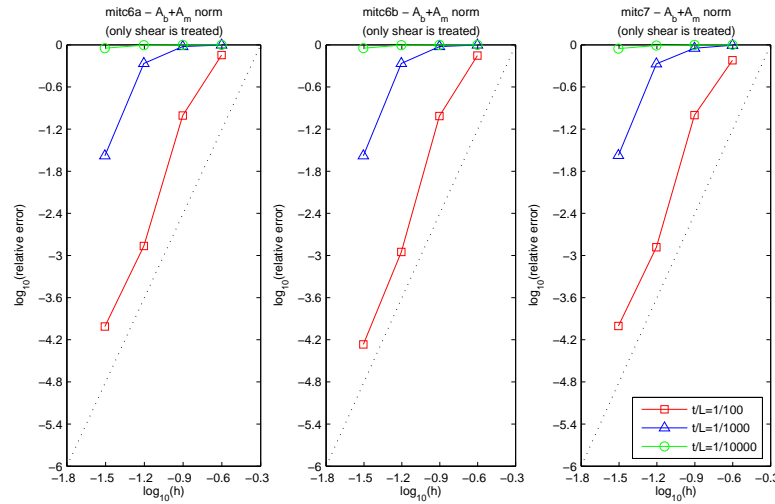


Figure 6.80: $A_b + A_m$ -norm convergence curves associated with the free hyperboloid shell problem: MITC6a, MITC6b and MITC7 shell finite elements when *only shear* is treated. The dotted line shows the optimal convergence rate which is 4 for quadratic elements.

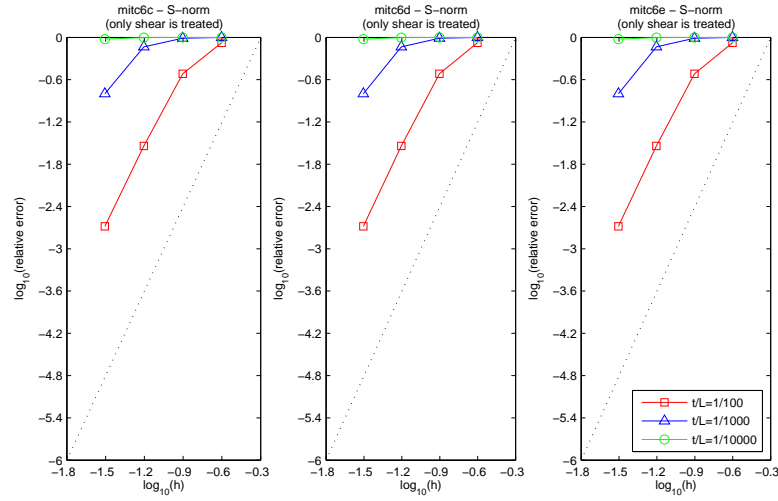


Figure 6.81: S-norm convergence curves associated with the free hyperboloid shell problem: MITC6c, MITC6d and MITC6e shell finite elements when *only shear* is treated. The dotted line shows the optimal convergence rate which is 4 for quadratic elements.

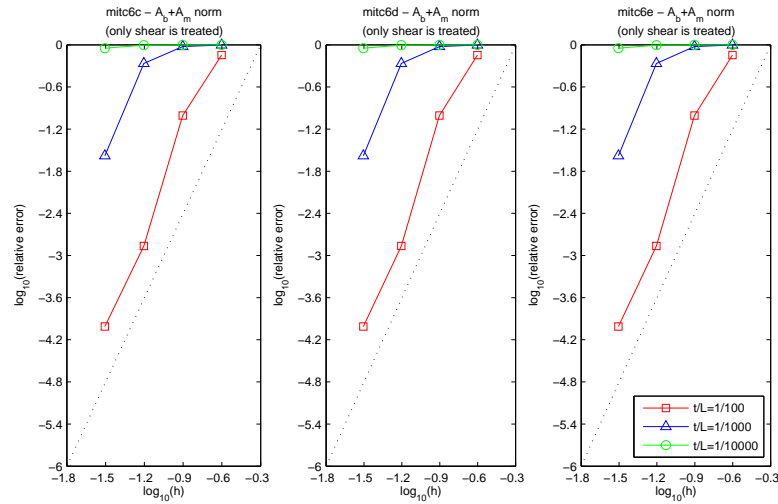


Figure 6.82: $A_b + A_m$ -norm convergence curves associated with the free hyperboloid shell problem: MITC6c, MITC6d and MITC6e shell finite elements when *only shear* is treated. The dotted line shows the optimal convergence rate which is 4 for quadratic elements.

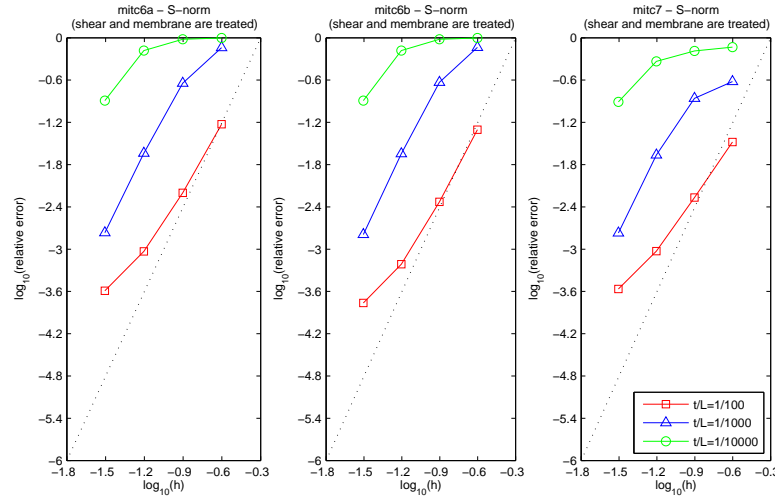


Figure 6.83: S-norm convergence curves associated with the free hyperboloid shell problem: MITC6a, MITC6b and MITC7 shell finite elements when *shear and membrane* are treated. The dotted line shows the optimal convergence rate which is 4 for quadratic elements.

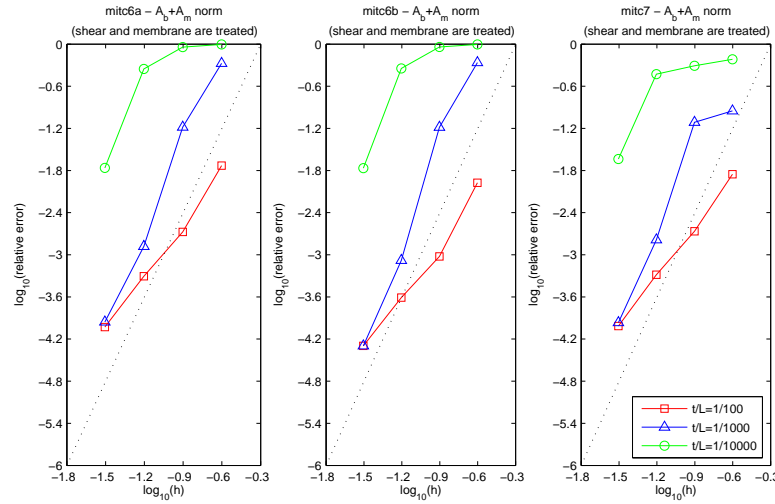


Figure 6.84: $A_b + A_m$ -norm convergence curves associated with the free hyperboloid shell problem: MITC6a, MITC6b and MITC7 shell finite elements when *shear and membrane* are treated. The dotted line shows the optimal convergence rate which is 4 for quadratic elements.

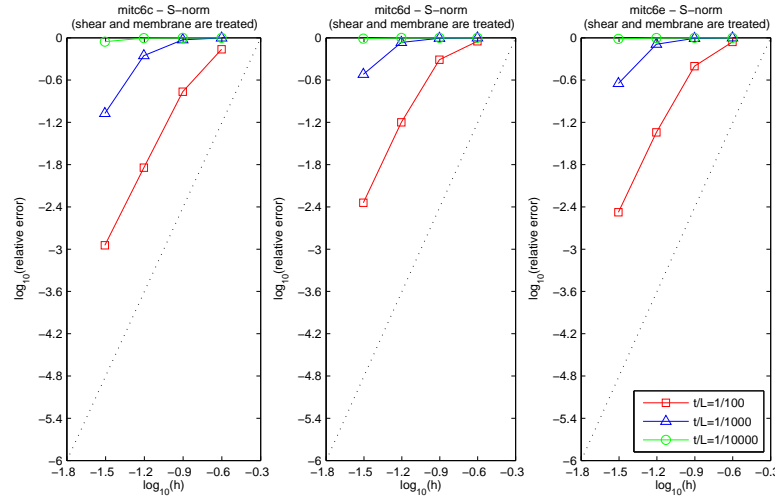


Figure 6.85: S-norm convergence curves associated with the free hyperboloid shell problem: MITC6c, MITC6d and MITC6e shell finite elements when *shear and membrane* are treated. The dotted line shows the optimal convergence rate which is 4 for quadratic elements.

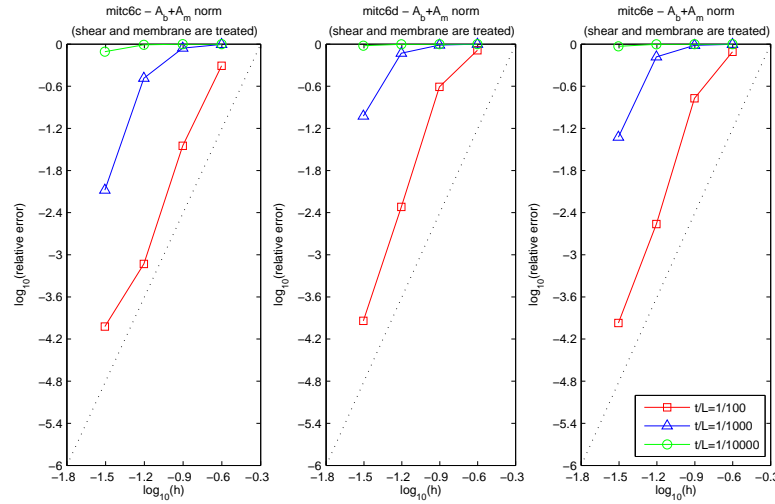


Figure 6.86: $A_b + A_m$ -norm convergence curves associated with the free hyperboloid shell problem: MITC6c, MITC6d and MITC6e shell finite elements when *shear and membrane* are treated. The dotted line shows the optimal convergence rate which is 4 for quadratic elements.

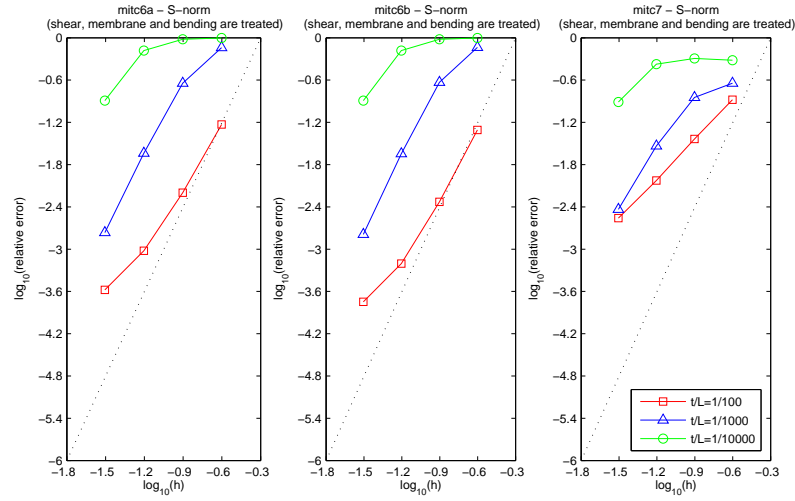


Figure 6.87: S-norm convergence curves associated with the free hyperboloid shell problem: MITC6a, MITC6b and MITC7 shell finite elements when *shear*, *membrane* and *bending* are treated. The dotted line shows the optimal convergence rate which is 4 for quadratic elements.

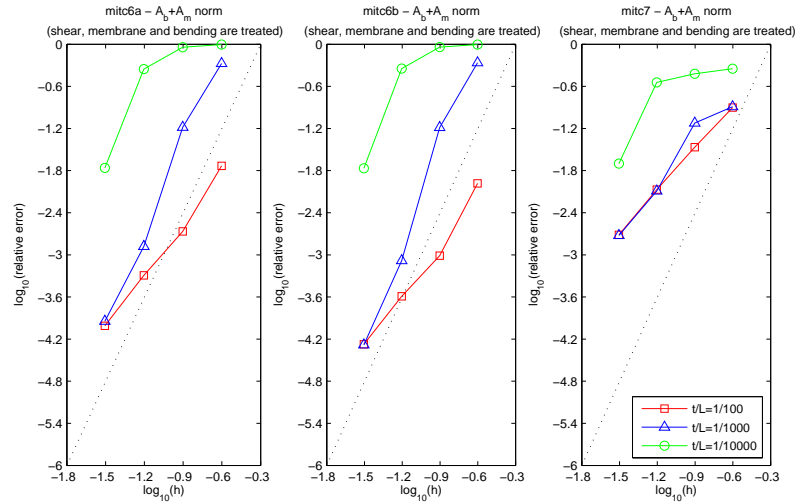


Figure 6.88: $A_b + A_m$ -norm convergence curves associated with the free hyperboloid shell problem: MITC6a, MITC6b and MITC7 shell finite elements when *shear*, *membrane* and *bending* are treated. The dotted line shows the optimal convergence rate which is 4 for quadratic elements.

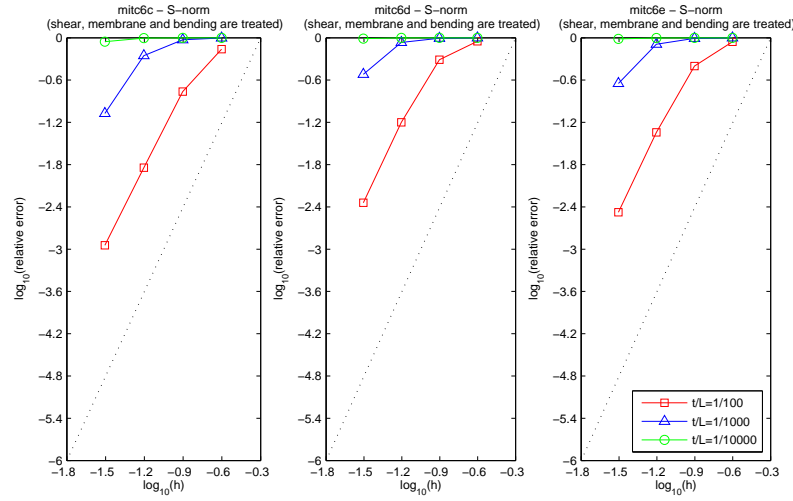


Figure 6.89: S-norm convergence curves associated with the free hyperboloid shell problem: MITC6c, MITC6d and MITC6e shell finite elements when *shear, membrane and bending* are treated. The dotted line shows the optimal convergence rate which is 4 for quadratic elements.

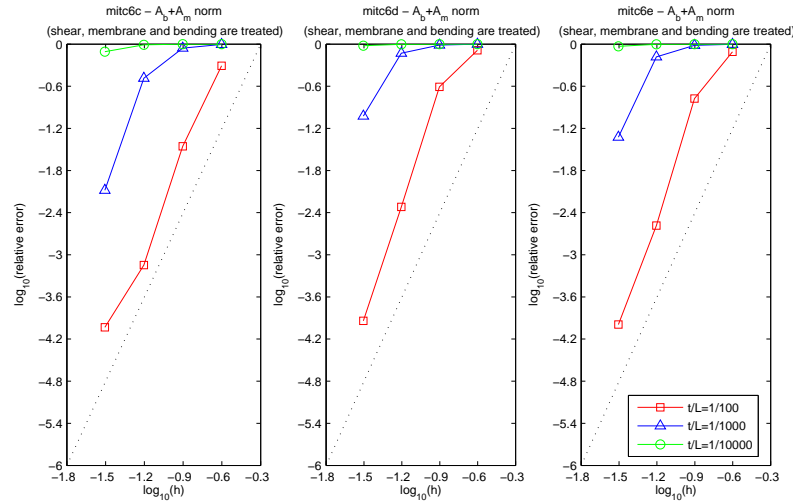


Figure 6.90: $A_b + A_m$ -norm convergence curves associated with the free hyperboloid shell problem: MITC6c, MITC6d and MITC6e shell finite elements when *shear, membrane and bending* are treated. The dotted line shows the optimal convergence rate which is 4 for quadratic elements.

	$\varepsilon = 10^{-2}$	$\varepsilon = 10^{-3}$	$\varepsilon = 10^{-4}$
<i>Total</i>	4.528066703e-07	4.485741919e-04	4.485263003e-01
<i>Bending</i>	4.488325137e-07	4.485084929e-04	4.485054904e-01
<i>Membrane</i>	3.754967847e-09	4.428402894e-08	1.709512468e-05
<i>Shear</i>	2.696770818e-10	2.193531077e-08	2.487364942e-06

Table 6.25: Reference energy values associated with the free hyperboloid shell problem and MITC4 shell finite element.

$\varepsilon = 10^{-2}$	$h = 0.25$	$h = 0.125$	$h = 0.0625$	$h = 0.03125$
<i>Total</i>	5.041368696e-08	2.838633034e-07	4.343977146e-07	4.514674840e-07
<i>Bending</i>	5.554399749e-09	1.798461887e-07	4.141238375e-07	4.462540795e-07
<i>Membrane</i>	3.538477724e-08	7.997949645e-08	1.571825241e-08	4.580828835e-09
<i>Shear</i>	9.474863529e-09	2.405707706e-08	4.601758706e-09	6.826899058e-10

$\varepsilon = 10^{-3}$	$h = 0.25$	$h = 0.125$	$h = 0.0625$	$h = 0.03125$
<i>Total</i>	5.557447831e-07	7.742024689e-06	9.491258118e-05	3.593800428e-04
<i>Bending</i>	7.747227039e-10	1.428799755e-07	2.089907449e-05	2.894161421e-04
<i>Membrane</i>	4.351797799e-07	5.818982762e-06	5.622530354e-05	5.279341227e-05
<i>Shear</i>	1.197901594e-07	1.780162607e-06	1.778823760e-05	1.717078598e-05

$\varepsilon = 10^{-4}$	$h = 0.25$	$h = 0.125$	$h = 0.0625$	$h = 0.03125$
<i>Total</i>	5.525914806e-06	7.829493077e-05	1.207182107e-03	1.826469393e-02
<i>Bending</i>	3.078688208e-10	1.756776195e-08	3.467108559e-06	7.793331986e-04
<i>Membrane</i>	4.324631669e-06	5.984056865e-05	9.116878110e-04	1.316901283e-02
<i>Shear</i>	1.200975229e-06	1.843679433e-05	2.920271521e-04	4.316501600e-03

Table 6.26: Energy values associated with the free hyperboloid shell problem and P_2 displacement-based shell finite elements for different values of ε and h .

$\varepsilon = 10^{-2}$		$h = 0.25$	$h = 0.125$	$h = 0.0625$	$h = 0.03125$
<i>Total</i>	<i>Reduced</i>	4.507763251e-07	4.576542204e-07	4.544685735e-07	4.532869623e-07
	<i>Unreduced</i>	7.098810434e-06	9.771226430e-07	4.906444032e-07	4.559755309e-07
<i>Bending</i>	<i>Reduced</i>	4.278707281e-07	4.518125878e-07	4.503382880e-07	4.492816258e-07
	<i>Unreduced</i>	4.290997168e-07	4.522301827e-07	4.504502435e-07	4.493101585e-07
<i>Membrane</i>	<i>Reduced</i>	1.869310669e-08	5.156781734e-09	3.856491262e-09	3.766078606e-09
	<i>Unreduced</i>	3.118158822e-06	2.211752491e-07	1.828124632e-08	4.851231031e-09
<i>Shear</i>	<i>Reduced</i>	4.238786903e-09	7.321264128e-10	3.241237733e-10	2.897391645e-10
	<i>Unreduced</i>	3.551610345e-06	3.037802536e-07	2.196784094e-08	1.865816286e-09
$\varepsilon = 10^{-3}$		$h = 0.25$	$h = 0.125$	$h = 0.0625$	$h = 0.03125$
<i>Total</i>	<i>Reduced</i>	1.298083660e-04	3.535985897e-04	4.402083822e-04	4.483736225e-04
	<i>Unreduced</i>	9.092691167e-02	5.114527062e-02	3.714923459e-03	6.663153887e-04
<i>Bending</i>	<i>Reduced</i>	4.491884541e-05	2.824813369e-04	4.305359890e-04	4.476482690e-04
	<i>Unreduced</i>	4.507688335e-05	2.827431535e-04	4.306361735e-04	4.476760131e-04
<i>Membrane</i>	<i>Reduced</i>	7.479283612e-05	6.949730878e-05	9.531201529e-06	6.932525197e-07
	<i>Unreduced</i>	2.710619732e-02	1.335844630e-02	1.329610636e-03	8.711361772e-05
<i>Shear</i>	<i>Reduced</i>	1.009477480e-05	1.618167028e-06	1.414575032e-07	3.254261910e-08
	<i>Unreduced</i>	6.377565022e-02	3.750409022e-02	1.954681311e-03	1.315275027e-04
$\varepsilon = 10^{-4}$		$h = 0.25$	$h = 0.125$	$h = 0.0625$	$h = 0.03125$
<i>Total</i>	<i>Reduced</i>	2.527052347e-03	2.157195323e-02	1.558996769e-01	3.919614231e-01
	<i>Unreduced</i>	6.032257988e+00	9.897730700e+01	4.596506045e+02	2.885299073e+01
<i>Bending</i>	<i>Reduced</i>	2.683296159e-04	1.902089219e-03	6.135421993e-02	3.428359895e-01
	<i>Unreduced</i>	2.678821792e-04	1.905124773e-03	6.138121352e-02	3.428587314e-01
<i>Membrane</i>	<i>Reduced</i>	1.876132048e-03	1.752703546e-02	9.137099726e-02	4.904019850e-02
	<i>Unreduced</i>	1.001343344e+00	4.901571753e+00	1.670904165e+01	6.693980256e+00
<i>Shear</i>	<i>Reduced</i>	3.825808980e-04	2.142784345e-03	3.175328241e-03	1.023052207e-04
	<i>Unreduced</i>	5.030646760e+00	9.407383016e+01	4.428801842e+02	2.181616352e+01

Table 6.27: *Reduced* and *unreduced* energy values associated with the free hyperboloid shell problem and MITC6a triangular shell finite element for different values of ε and h (*shear*, *membrane* and *bending* are treated).

$\varepsilon = 10^{-2}$		$h = 0.25$	$h = 0.125$	$h = 0.0625$	$h = 0.03125$
<i>Total</i>	<i>Reduced</i>	4.510862853e-07	4.567878427e-07	4.541650570e-07	4.532018008e-07
	<i>Unreduced</i>	6.759649626e-06	9.300669565e-07	4.862515472e-07	4.555338033e-07
<i>Bending</i>	<i>Reduced</i>	4.289764926e-07	4.511606495e-07	4.500554220e-07	4.492043778e-07
	<i>Unreduced</i>	4.302490741e-07	4.515803748e-07	4.501656026e-07	4.492326537e-07
<i>Membrane</i>	<i>Reduced</i>	1.857149474e-08	5.137164061e-09	3.855473358e-09	3.765892306e-09
	<i>Unreduced</i>	3.118564417e-06	2.206807576e-07	1.827140630e-08	4.850910610e-09
<i>Shear</i>	<i>Reduced</i>	3.564265032e-09	5.381579668e-10	3.045395296e-10	2.820044708e-10
	<i>Unreduced</i>	3.210869159e-06	2.578700668e-07	1.786960195e-08	1.501905347e-09
$\varepsilon = 10^{-3}$		$h = 0.25$	$h = 0.125$	$h = 0.0625$	$h = 0.03125$
<i>Total</i>	<i>Reduced</i>	1.267513483e-04	3.487145149e-04	4.399501029e-04	4.483035105e-04
	<i>Unreduced</i>	8.599286175e-02	3.857763606e-02	3.336096190e-03	6.442041389e-04
<i>Bending</i>	<i>Reduced</i>	4.528624119e-05	2.742489502e-04	4.301914398e-04	4.475822094e-04
	<i>Unreduced</i>	4.545511450e-05	2.744766059e-04	4.302910941e-04	4.476095846e-04
<i>Membrane</i>	<i>Reduced</i>	7.149185292e-05	7.120777368e-05	9.561200442e-06	6.929184315e-07
	<i>Unreduced</i>	2.510203667e-02	1.300962930e-02	1.329209068e-03	8.709990558e-05
<i>Shear</i>	<i>Reduced</i>	9.972510766e-06	3.256348326e-06	1.977423537e-07	2.879368648e-08
	<i>Unreduced</i>	6.084538877e-02	2.529353904e-02	1.576600558e-03	1.094962426e-04
$\varepsilon = 10^{-4}$		$h = 0.25$	$h = 0.125$	$h = 0.0625$	$h = 0.03125$
<i>Total</i>	<i>Reduced</i>	2.366792159e-03	2.152852082e-02	1.526263339e-01	3.916669975e-01
	<i>Unreduced</i>	6.328629734e+00	1.572377359e+02	3.613354324e+02	2.087866537e+01
<i>Bending</i>	<i>Reduced</i>	8.965553516e-05	2.308406187e-03	5.958474049e-02	3.422492608e-01
	<i>Unreduced</i>	8.972266494e-05	2.311447567e-03	5.959802447e-02	3.422684846e-01
<i>Membrane</i>	<i>Reduced</i>	2.012937715e-03	1.744338209e-02	9.121314387e-02	4.928596659e-02
	<i>Unreduced</i>	8.961564394e-01	4.768710081e+00	1.596817394e+01	6.688701933e+00
<i>Shear</i>	<i>Reduced</i>	2.641979786e-04	1.776724670e-03	1.829782877e-03	1.445827591e-04
	<i>Unreduced</i>	5.432383583e+00	1.524667146e+02	3.453076607e+02	1.384770110e+01

Table 6.28: *Reduced* and *unreduced* energy values associated with the free hyperboloid shell problem and MITC6b triangular shell finite element for different values of ε and h (*shear*, *membrane* and *bending* are treated).

$\varepsilon = 10^{-2}$		$h = 0.25$	$h = 0.125$	$h = 0.0625$	$h = 0.03125$
<i>Total</i>	<i>Reduced</i>	5.079831691e-07	4.706252866e-07	4.578573522e-07	4.542986688e-07
	<i>Unreduced</i>	7.490944976e-05	6.578542381e-06	8.978778228e-07	4.916679164e-07
<i>Membrane</i>	<i>Reduced</i>	1.463024395e-08	5.423547789e-09	3.879001720e-09	3.770454514e-09
	<i>Unreduced</i>	3.927043345e-06	2.398962244e-07	1.862521540e-08	4.861598801e-09
$\varepsilon = 10^{-3}$		$h = 0.25$	$h = 0.125$	$h = 0.0625$	$h = 0.03125$
<i>Total</i>	<i>Reduced</i>	4.055525903e-04	4.046680507e-04	4.436380812e-04	4.491892420e-04
	<i>Unreduced</i>	3.129095377e+00	4.625295452e-01	3.644120703e-02	2.979502421e-03
<i>Membrane</i>	<i>Reduced</i>	4.512924054e-05	2.880801986e-05	9.319879329e-06	7.003202455e-07
	<i>Unreduced</i>	2.431129847e-01	1.634288708e-02	1.349797744e-03	8.760476496e-05
$\varepsilon = 10^{-4}$		$h = 0.25$	$h = 0.125$	$h = 0.0625$	$h = 0.03125$
<i>Total</i>	<i>Reduced</i>	2.066126257e-01	2.101054131e-01	2.604978269e-01	3.953468205e-01
	<i>Unreduced</i>	4.651542331e+05	9.761254378e+04	1.314038328e+04	2.925943724e+02
<i>Membrane</i>	<i>Reduced</i>	1.318741831e-02	5.535678975e-02	5.340151558e-02	4.490680270e-02
	<i>Unreduced</i>	6.635562802e+03	4.637497431e+02	4.348229526e+01	6.740428640e+00

Table 6.29: *Reduced* and *unreduced* energy values associated with the free hyperboloid shell problem and MITC7 triangular shell finite element for different values of ε and h (*shear*, *membrane* and *bending* are treated).

$\varepsilon = 10^{-2}$		$h = 0.25$	$h = 0.125$	$h = 0.0625$	$h = 0.03125$
<i>Total</i>	<i>Reduced</i>	1.516392326e-07	3.812639266e-07	4.476672376e-07	4.527051724e-07
	<i>Unreduced</i>	2.031569440e-06	7.594971658e-07	4.769800677e-07	4.548310612e-07
<i>Bending</i>	<i>Reduced</i>	5.834430519e-08	3.170752280e-07	4.376093583e-07	4.483070443e-07
	<i>Unreduced</i>	5.879848860e-08	3.179806883e-07	4.379349820e-07	4.483921438e-07
<i>Membrane</i>	<i>Reduced</i>	8.562894130e-08	6.299285620e-08	9.775772808e-09	4.157838995e-09
	<i>Unreduced</i>	2.630250906e-07	1.493618145e-07	1.776467553e-08	4.714239662e-09
<i>Shear</i>	<i>Reduced</i>	7.645783034e-09	1.217234008e-09	3.298956664e-10	2.906034187e-10
	<i>Unreduced</i>	1.710037387e-06	2.928281482e-07	2.156538078e-08	1.836156371e-09
$\varepsilon = 10^{-3}$		$h = 0.25$	$h = 0.125$	$h = 0.0625$	$h = 0.03125$
<i>Total</i>	<i>Reduced</i>	2.942584374e-06	3.038706716e-05	2.000550351e-04	4.114430129e-04
	<i>Unreduced</i>	4.182698169e-04	5.066021431e-03	2.397929224e-03	5.839665174e-04
<i>Bending</i>	<i>Reduced</i>	8.315682893e-08	4.481481675e-06	9.700897379e-05	3.776581926e-04
	<i>Unreduced</i>	8.348202474e-08	4.485012957e-06	9.707424630e-05	3.777277805e-04
<i>Membrane</i>	<i>Reduced</i>	2.567334175e-06	2.476478084e-05	1.023533941e-04	3.373692753e-05
	<i>Unreduced</i>	8.061025509e-06	7.755383561e-05	2.605511592e-04	7.579077136e-05
<i>Shear</i>	<i>Reduced</i>	2.920586596e-07	1.140292137e-06	6.923120644e-07	4.820727482e-08
	<i>Unreduced</i>	4.101253318e-04	4.983985818e-03	2.040350859e-03	1.304997559e-04
$\varepsilon = 10^{-4}$		$h = 0.25$	$h = 0.125$	$h = 0.0625$	$h = 0.03125$
<i>Total</i>	<i>Reduced</i>	3.216808742e-05	4.097831862e-04	4.981098904e-03	5.366986380e-02
	<i>Unreduced</i>	1.128749054e-02	6.828889834e-01	1.617550938e+01	1.289020657e+01
<i>Bending</i>	<i>Reduced</i>	3.848268164e-07	7.548375376e-06	4.230834141e-04	8.766248566e-03
	<i>Unreduced</i>	3.857911336e-07	7.554411110e-06	4.230508707e-04	8.767131297e-03
<i>Membrane</i>	<i>Reduced</i>	2.909457034e-05	3.791162403e-04	4.447029234e-03	4.469663345e-02
	<i>Unreduced</i>	9.551682359e-05	1.102619184e-03	1.354298408e-02	1.246896636e-01
<i>Shear</i>	<i>Reduced</i>	2.688681024e-06	2.311811066e-05	1.109651708e-04	2.062536080e-04
	<i>Unreduced</i>	1.119158793e-02	6.817788097e-01	1.616154335e+01	1.275675193e+01

Table 6.30: *Reduced* and *unreduced* energy values associated with the free hyperboloid shell problem and MITC6c triangular shell finite element for different values of ε and h (*shear*, *membrane* and *bending* are treated).

$\varepsilon = 10^{-2}$		$h = 0.25$	$h = 0.125$	$h = 0.0625$	$h = 0.03125$
<i>Total</i>	<i>Reduced</i>	5.520410074e-08	2.385715055e-07	4.253984368e-07	4.510978882e-07
	<i>Unreduced</i>	1.224534035e-06	4.593331814e-07	4.316901261e-07	4.515654195e-07
<i>Bending</i>	<i>Reduced</i>	1.475554484e-08	1.282830959e-07	3.953565550e-07	4.451914898e-07
	<i>Unreduced</i>	1.479257690e-08	1.282768769e-07	3.953558400e-07	4.451914605e-07
<i>Membrane</i>	<i>Reduced</i>	3.479225432e-08	1.071692697e-07	2.964775064e-08	5.666539795e-09
	<i>Unreduced</i>	2.755146601e-08	5.350178779e-08	1.524275277e-08	4.582046007e-09
<i>Shear</i>	<i>Reduced</i>	5.642169357e-09	3.126241496e-09	4.372291210e-10	2.898160690e-10
	<i>Unreduced</i>	1.182178681e-06	2.775525962e-07	2.113343609e-08	1.841804437e-09
$\varepsilon = 10^{-3}$		$h = 0.25$	$h = 0.125$	$h = 0.0625$	$h = 0.03125$
<i>Total</i>	<i>Reduced</i>	9.908478453e-07	8.406058721e-06	6.396301678e-05	3.142471050e-04
	<i>Unreduced</i>	1.448186137e-04	3.557106997e-03	1.612351265e-03	3.878749599e-04
<i>Bending</i>	<i>Reduced</i>	2.346666116e-08	1.817554259e-06	1.151825792e-05	2.220093554e-04
	<i>Unreduced</i>	2.358136175e-08	1.819037588e-06	1.151824416e-05	2.220092554e-04
<i>Membrane</i>	<i>Reduced</i>	8.597107866e-07	5.980833242e-06	5.164862826e-05	9.206184332e-05
	<i>Unreduced</i>	9.819797519e-07	4.305516931e-06	2.390277935e-05	4.021723850e-05
<i>Shear</i>	<i>Reduced</i>	1.076605228e-07	6.073066736e-07	7.958628524e-07	1.760783426e-07
	<i>Unreduced</i>	1.438130458e-04	3.550982198e-03	1.576929960e-03	1.256485546e-04
$\varepsilon = 10^{-4}$		$h = 0.25$	$h = 0.125$	$h = 0.0625$	$h = 0.03125$
<i>Total</i>	<i>Reduced</i>	1.065995492e-05	1.343940863e-04	1.338776055e-03	1.138368409e-02
	<i>Unreduced</i>	2.418437193e-03	2.743491197e-01	1.183984177e+01	6.659031844e+00
<i>Bending</i>	<i>Reduced</i>	1.512602606e-07	2.478705001e-06	2.662831746e-04	7.374313474e-04
	<i>Unreduced</i>	1.520085008e-07	2.482118105e-06	2.663452411e-04	7.374430632e-04
<i>Membrane</i>	<i>Reduced</i>	9.393748809e-06	1.224101491e-04	1.016226831e-03	1.053922595e-02
	<i>Unreduced</i>	1.415872460e-05	1.375235854e-04	7.284088224e-04	4.719234438e-03
<i>Shear</i>	<i>Reduced</i>	1.114939010e-06	9.505025714e-06	5.625550100e-05	1.069965864e-04
	<i>Unreduced</i>	2.404126454e-03	2.742091137e-01	1.183884700e+01	6.653575193e+00

Table 6.31: *Reduced* and *unreduced* energy values associated with the free hyperboloid shell problem and MITC6d triangular shell finite element for different values of ε and h (*shear*, *membrane* and *bending* are treated).

$\varepsilon = 10^{-2}$		$h = 0.25$	$h = 0.125$	$h = 0.0625$	$h = 0.03125$
<i>Total</i>	<i>Reduced</i>	6.404007270e-08	2.750748998e-07	4.341705047e-07	4.518579166e-07
	<i>Unreduced</i>	1.131631386e-06	5.417292748e-07	4.539470863e-07	4.534078983e-07
<i>Bending</i>	<i>Reduced</i>	1.489621569e-08	1.649907834e-07	4.112915080e-07	4.465334697e-07
	<i>Unreduced</i>	1.504744600e-08	1.660305195e-07	4.119581863e-07	4.467188207e-07
<i>Membrane</i>	<i>Reduced</i>	4.156861111e-08	1.067374541e-07	2.248390724e-08	5.079658219e-09
	<i>Unreduced</i>	5.598404649e-08	1.069148882e-07	2.122921775e-08	5.040689675e-09
<i>Shear</i>	<i>Reduced</i>	7.582496104e-09	3.362300466e-09	4.407455628e-10	2.949654598e-10
	<i>Unreduced</i>	1.060676697e-06	2.695082394e-07	2.128370500e-08	1.829740368e-09
$\varepsilon = 10^{-3}$		$h = 0.25$	$h = 0.125$	$h = 0.0625$	$h = 0.03125$
<i>Total</i>	<i>Reduced</i>	1.162056894e-06	9.682103722e-06	8.613892220e-05	3.516333345e-04
	<i>Unreduced</i>	1.761873491e-04	2.927819819e-03	1.290862784e-03	4.716196422e-04
<i>Bending</i>	<i>Reduced</i>	3.056322399e-08	1.629822863e-06	1.760761477e-05	2.754883935e-04
	<i>Unreduced</i>	3.076819980e-08	1.633019906e-06	1.763831696e-05	2.756017867e-04
<i>Membrane</i>	<i>Reduced</i>	9.911791839e-07	7.519710282e-06	6.740404341e-05	7.585578906e-05
	<i>Unreduced</i>	1.677216319e-06	8.448644910e-06	6.655894873e-05	7.289727193e-05
<i>Shear</i>	<i>Reduced</i>	1.403084353e-07	5.325166450e-07	1.127436305e-06	2.893136020e-07
	<i>Unreduced</i>	1.744793387e-04	2.917738384e-03	1.206684166e-03	1.232021531e-04
$\varepsilon = 10^{-4}$		$h = 0.25$	$h = 0.125$	$h = 0.0625$	$h = 0.03125$
<i>Total</i>	<i>Reduced</i>	1.235283286e-05	1.450847374e-04	1.565949574e-03	1.628784884e-02
	<i>Unreduced</i>	2.010789498e-03	2.427711410e-01	1.024579743e+01	4.931101028e+00
<i>Bending</i>	<i>Reduced</i>	1.619146938e-07	2.099326643e-06	2.438280456e-04	8.961699889e-04
	<i>Unreduced</i>	1.620708829e-07	2.102962289e-06	2.439358315e-04	8.965844956e-04
<i>Membrane</i>	<i>Reduced</i>	1.067591072e-05	1.360384947e-04	1.279939400e-03	1.526416222e-02
	<i>Unreduced</i>	1.963624975e-05	1.743420608e-04	1.374297529e-03	1.500560254e-02
<i>Shear</i>	<i>Reduced</i>	1.515004171e-06	6.946792742e-06	4.217522890e-05	1.274539359e-04
	<i>Unreduced</i>	1.990991172e-03	2.425946956e-01	1.024417919e+01	4.915198968e+00

Table 6.32: *Reduced* and *unreduced* energy values associated with the free hyperboloid shell problem and MITC6e triangular shell finite element for different values of ε and h (*shear*, *membrane* and *bending* are treated).

6.4 Concluding remarks on the assessment results

In our analysis, we considered six isotropic triangular shell finite elements, performed numerical tests corresponding to well posed bending and membrane dominated shell problems for three different shell geometries and displayed convergence curves using appropriated norms. The different tying schemes were chosen based on the membrane locking test we have designed (see Section 5.2). The MITC6a shell finite element was firstly introduced by Lee and Bathe in [47], but we have performed a deeper analysis since the boundary layers were properly treated, suitable norms were used to analyse the convergence of displacements and a complete study of the reduced and unreduced energies (total and decomposed membrane, shear and bending) has been done for each benchmark. The original MITC7 plate finite element ([9]) was also incorporated to our shell analysis.

It is well understood that numerical locking occurs due to the constraint of shear and membrane vanishing strains for bending dominated situations, and the bending tensor is not supposed to be treated and it could be a source of consistency error (see Section 4.3). But the results presented here show that solutions obtained by re-interpolation of shear and membrane tensors only do not really differ from solutions obtained including bending treatment, except in the case of the MITC7 triangular shell finite element.

The analysis we have done confirms once more that uniformly optimal triangular shell finite elements are difficult to attain. As is known, membrane locking constitutes the main obstacle when developing effective general shell finite elements (see Section 5.1). Even if our particular choices of tying positions were motivated by a numerical test aimed at detecting such obstacle, we observed that spurious membrane energy modes may be introduced by the MITC approach and consistency may be lost for membrane dominated situations.

None of the finite elements we considered constitute a uniformly optimal candidate for engineering practice because either strong numerical locking occurs whereas consistent results are obtained for membrane-dominated shell problems; or parasitic membrane energy modes arise. We focus our conclusions on the cylindrical and hyperboloid shell problems we analyzed:

- When both ends are clamped, both situations correspond to *membrane-dominated shell problems* and displacement-based P_2 shell finite elements provide good numerical solutions. Effective MITC shell finite elements are meant to remain consistent, but we observed that once the membrane tensor is treated, convergence curves related to strains and displacements get worse for both cylindrical and hyperbic shell problems in a similar way. On the one hand, strain fields are slightly deteriorated as seen by means of the *s-norm*. But on the other hand, the original A_m norm –with membrane and shear terms– provide convergence curves that worsen for small thickness (in the case of the MITC6d shell finite element) or relative errors that are not admissible at all for the other MITC shell finite elements we analyzed. Moreover,

even if shear terms are discarded from the A_m norm, we observe that the convergence curves associated with the A_m norm without shear terms still deteriorate as thickness decreases and displacements *per se* do not show optimal nor uniform convergence for small ε values except for the MITC6d shell finite element which shows a nearly optimal and uniform behavior. In fact, *spurious membrane energy norms* seem to be present for all choices of tying positions, and they *reveal through the unreduced shear energy* which differs by several orders of magnitude from the reduced shear energy, whereas they are slightly reflected in the reduced and unreduced membrane energies, which differ in a weaker way.

- A *bending-dominated behavior* is observed when both ends are free for the cylindrical and hyperboloid shell problems, and all the elements we tested show more or less numerical locking for coarse meshes and small thickness, mainly for the free hyperboloid shell problem. The MITC6c, MITC6d and MITC6e shell finite elements strongly lock for both cylindrical and hyperboloid shell problems. On the other hand, the MITC6a and MITC6b –also the MITC7– elements provide quite good strain fields –as seen through the *s-norm*– and displacements and rotations –by means of the $A_b + A_m$ norm– for the free cylindrical shell problem. In spite of that, they show *some locking* for the free hyperboloid shell problem as *s-norm* and $A_b + A_m$ norm convergence curves deteriorate as thickness decreases, mainly for coarse meshes. In fact, we see that for the free hyperboloid shell problem reduced shear and particularly reduced membrane energies are too large as compared to reduced bending or total energy for coarse meshes and small relative thickness values, although numerical solutions are quickly improved as the mesh is refined. We also observe that the main source of *locking* is the membrane since *strong numerical locking* gives an *amplification by several orders of magnitude on the unreduced shear energies as compared to the reduced ones and closer reduced and unreduced membrane energies*, whereas *weak numerical locking* (for small relative thickness and coarse meshes) can be characterized by *huge unreduced membrane and shear energies as respectively compared to reduced membrane and shear energies*.

However, one of the best candidates we have investigated is the MITC6a shell finite element for which spurious membrane modes seem to appear in a membrane-dominated framework, but only slightly locks for coarse meshes in bending-dominated situations. The MITC6b shell finite element also behaves quite well and it only differs from the MITC6a shell finite element in the transverse shear strains interpolation.

When analyzing the tables related to the MITC6a energy values, we observe that this element captures the right asymptotic behavior of the structure for bending and membrane dominated shell problems as the mesh is refined and relative thickness decreases. In spite of that, spurious membrane energy modes seem to arise,

which can be assessed by means of the total and partial unreduced strain energies in comparison with the reduced ones. Such modes seem to be reflected in the unreduced shear energy as compared to the reduced shear energy, which constitutes a hint to improve the MITC6a shell finite element by a kind of *shear stabilization* method. Nevertheless, such “parasitic modes filtering” tool must be formulated in such a way to preserve the MITC’s performance in bending-dominated situations.

Chapter 7

Improving the MITC6a shell finite element

Lourenço Beirão da Veiga, Dominique Chapelle, Iria París

Abstract

The presence of spurious modes in the MITC6a solution of some membrane dominated problems is the cause of unsatisfactory error curves in the A_m norm. Moreover, the amplitude of these parasitic modes may dominate that of the underlying "correct" solution, giving erroneous displacement graphs. Considering that membrane shell problems are, by far, the most frequently encountered in engineering practice, such phenomena are a serious hindrance for the applicability of the MITC6a element. The objective of this section is therefore to develop some possible cures to these difficulties and not hinder the MITC performance in bending dominated –or otherwise penalized– shell problems.

We present a specific shell problem which we call the *trace shell problem*, specifically designed to make those parasitic membrane modes arise for the particular geometry in consideration. We have seen that the membrane spurious modes that appear for this particular membrane dominated shell problem mainly arise as oscillations of large amplitude near the free boundaries that also propagate inside the domain.

The cures that we have developed are typically based on the results obtained for this particular *trace shell problem*. The observations we have done indicate that the nature of the spurious part of the solution is mainly reflected in the shear energy. Moreover, it is well known that in general bending dominated situations the main source of locking is the membrane energy, and not the shear energy. The

combination of these two arguments suggests to stabilize/modify only the shear part of the MITC6a bilinear form, in order to reach our aforementioned goal.

Another viable choice is to adopt a richer interpolation space for the transverse shear strains, so we propose a new element, named the MITC6rs, which is similar to the MITC6a element, except in the transverse shear strain space and tying procedure.

In order to make an assessment for the new MITC6rs and the proposed stabilized formulations for the MITC6a and MITC6rs shell elements, we have thoroughly analyzed the trace shell problem, and two membrane dominated hyperboloid shell problems and a bending dominated shell problem for the same complex geometry.

7.1 MITC membrane spurious modes

As we have noticed in Section 6, the MITC shell finite elements may be sensitive to the presence of membrane spurious modes that would be more or less present depending on the geometry, boundary conditions and loading. The question now is to know how those modes –that are related to the reduced membrane strains– might deteriorate the numerical solution of a given problem and to identify them in more details.

As it is well known, in the bilinear form associated with a general shell problem in linear elasticity we can distinguish a bending part denoted by A_b and another part related to membrane and shear that is originally denoted by A_m . But in this section we will distinguish in the original A_m bilinear form between the pure membrane part denoted by A_m from now on, and the shear part denoted by A_s . When the MITC approach holds, both bilinear forms will be respectively denoted by A_m^h and A_s^h , where the h symbol refers to the reduction of the related strain components.

The membrane spurious modes are said to be those midsurface displacements \vec{u}_0 that have zero reduced membrane energy, namely:

$$A_m^h(\vec{u}_0, \vec{u}_0) = 0 \quad (7.1)$$

Such modes will be called *real membrane spurious modes* from now on. We can also consider the set of midsurface displacements that give $A_m^h(\vec{u}_0, \vec{u}_0)$ not exactly zero but:

$$A_m(\vec{u}_0, \vec{u}_0) \gg A_m^h(\vec{u}_0, \vec{u}_0) \quad (7.2)$$

in some way, where A_m denotes the unreduced pure membrane bilinear form. Such modes will be named *pseudo membrane spurious modes*. Obviously, the real membrane spurious modes also verify property (7.2).

Furthermore, the modes that verify (7.1) will also give:

$$A_m^h(\vec{u}_0, \vec{v}) = 0 \quad (7.3)$$

for all \vec{v} midsurface displacement that could hold, property that can be expressed in a matrix form as:

$$\begin{bmatrix} v^T & 0 \end{bmatrix} \begin{bmatrix} K_{vv}^{m,h} & 0 \\ 0 & 0 \end{bmatrix} \begin{bmatrix} u_0 \\ 0 \end{bmatrix} = 0 \quad (7.4)$$

where $[u_0]$ –and $[v]$ by extension– denotes the vector of nodal midsurface displacements related to \vec{u}_0 –or \vec{v} – and $[K_{vv}^{m,h}]$ denotes the reduced membrane global matrix coefficients related to the nodal midsurface displacements interaction. As it is known, the rotation fields do not affect the pure membrane bilinear form.

Hence, the most natural way to calculate the real membrane spurious modes is to determine the eigenvectors $[u_0]$ related to those *zero* eigenvalues τ^h that verify:

$$[K_{vv}^{m,h}] [u_0] = \tau^h [M_{vv}] [u_0] \quad (7.5)$$

where $[M_{vv}]$ denotes the mass global matrix coefficients related to the nodal midsurface displacements.

Standard displacement-based shell finite elements are characterized by giving a subspace of discretized inextensional displacements exactly reduced to $\{0\}$ when considering a membrane dominated shell problem, as the shell theory states (recall Section 2). As a consequence, we can consider as zero those τ^h eigenvalues that verify:

$$\tau^h / \tau_{min} < tol \quad (7.6)$$

for tol a given tolerance and τ_{min} the smallest eigenvalue of the displacement based pure membrane matrix that can be denoted by $[K_{vv}^m]^1$. The pseudo membrane spurious modes are supposed to verify condition (7.2).

Finally, given an exact or pseudo inextensional midsurface displacement \vec{u}_0 , the associated rotation field $\underline{\theta}_0$ is defined as that one that minimizes the functional:

$$A_{sb}^h(\vec{u}_0, \underline{\eta}; \vec{u}_0, \underline{\eta}) = \frac{1}{2} \left\{ A_s^h(\vec{u}_0, \underline{\eta}; \vec{u}_0, \underline{\eta}) + \varepsilon^2 A_b(\vec{u}_0, \underline{\eta}; \vec{u}_0, \underline{\eta}) \right\} \quad (7.7)$$

which is a bilinear form in $\underline{\eta}$. As a consequence, $\underline{\theta}_0$ must verify:

$$A_{sb}^h(\vec{u}_0, \underline{\theta}_0; \vec{0}, \underline{\eta}) = 0 \quad \forall \underline{\eta} \quad (7.8)$$

which can be expressed in matrix form as:

$$\begin{bmatrix} 0 & \eta^T \end{bmatrix} \begin{bmatrix} K_{vv}^{sb,h} & (K_{\eta v}^{sb,h})^T \\ K_{\eta v}^{sb,h} & K_{\eta\eta}^{sb,h} \end{bmatrix} \begin{bmatrix} u_0 \\ \theta_0 \end{bmatrix} = 0 \quad \forall [\eta] \quad (7.9)$$

where $[\theta_0]$ –and respectively $[\eta]$ – denotes the vector of nodal rotation fields related to $\underline{\theta}_0$ –or $\underline{\eta}$ – and $[K^{sb,h}]$ the global matrix associated with the bilinear form A_{sb}^h

¹We know that $[K_{vv}^m]$ is symmetric and positive definite, so its eigenvalues are strictly positive.

and the index v and η refer to the nodal midsurface displacements and rotations. We directly obtain that:

$$\begin{bmatrix} K_{\eta\eta}^{sb,h} \end{bmatrix} [\theta_0] = - \begin{bmatrix} K_{\eta v}^{sb,h} \end{bmatrix} [u_0] \quad (7.10)$$

given that (7.9) holds for all possible $[\eta]$.

Given a nodal displacement and rotation solution provided by an MITC shell finite element

$$[U_h^\varepsilon] = \begin{bmatrix} u_h^\varepsilon \\ \theta_h^\varepsilon \end{bmatrix} \quad (7.11)$$

we can easily quantify the *real* or *pseudo* membrane spurious modes participation. As it is well known, the bilinear form $A_m + A_s$ defines a norm in the space \mathcal{V}_m which typically denotes the set of all continuous displacements with bounded membrane/shear energy. Hence we can consider the associated matrix as $[K^m + K^s]$ and define the participation of a mode:

$$[U_0] = \begin{bmatrix} u_0 \\ \theta_0 \end{bmatrix}$$

as the projection of $[U_h^\varepsilon]$ along such mode direction:

$$Proj(U_h^\varepsilon, U_0) = \frac{|< U_h^\varepsilon, U_0 >|}{< U_0, U_0 >^{1/2} < U_h^\varepsilon, U_h^\varepsilon >^{1/2}} \quad (7.12)$$

for the scalar product defined by $A_m + A_s$, namely:

$$< U_h^\varepsilon, U_0 > = \begin{bmatrix} u_0^T & \theta_0^T \end{bmatrix} [K^m + K^s] \begin{bmatrix} u_h^\varepsilon \\ \theta_h^\varepsilon \end{bmatrix} \quad (7.13)$$

$$< U_0, U_0 > = \begin{bmatrix} u_0^T & \theta_0^T \end{bmatrix} [K^m + K^s] \begin{bmatrix} u_0 \\ \theta_0 \end{bmatrix} \quad (7.14)$$

$$< U_h^\varepsilon, U_h^\varepsilon > = \begin{bmatrix} u_h^{\varepsilon T} & \theta_h^{\varepsilon T} \end{bmatrix} [K^m + K^s] \begin{bmatrix} u_h^\varepsilon \\ \theta_h^\varepsilon \end{bmatrix} \quad (7.15)$$

7.2 The trace benchmark

This shell problem has been specifically designed to make the membrane spurious modes arise for the particular geometry described below. We want to see how the expected *correct* solution may be deteriorated by them.

We consider a shell of uniform thickness t given by the midsurface represented in Figure 7.1 and denoted by \mathcal{S} , which can be exactly obtained from the triangular 2D-domain ω of vertices $(-1, 0)$, $(1, 0)$ and $(0, 1/2)$ in curvilinear coordinates (ξ^1, ξ^2) by the following mapping:

$$\vec{\phi}(\xi^1, \xi^2) = \begin{pmatrix} L\xi^1 \\ L\xi^2 \\ L\frac{(\xi^1)^2 - (\xi^2)^2}{2} \end{pmatrix} \quad (7.16)$$

where L denotes the characteristic length of the structure, and for our particular analysis we have taken $L = 1$. The shell is clamped along the boundary defined by $\xi^2 = 0$.

As usual, we define $\varepsilon = t/L$. A boundary layer of width $3\sqrt{\varepsilon}L$ was numerically obtained, and we considered the sequence of meshes constructed as follows: inside of the boundary layer area we considered $2N + 1$ along the boundary by $N + 1$ vertices from $(-1, 0)$ to $(-1 + 3\sqrt{\varepsilon}, 3\sqrt{\varepsilon})$ and from $(1, 0)$ to $(1 - 3\sqrt{\varepsilon}, 3\sqrt{\varepsilon})$; the rest of the domain was meshed by $2N + 1$ vertices along the boundary by $N + 1$ vertices from $(-1 + 3\sqrt{\varepsilon}, 3\sqrt{\varepsilon})$ and $(1 - 3\sqrt{\varepsilon}, 3\sqrt{\varepsilon})$ to $(0, 1/2)$, see Fig. 7.1.

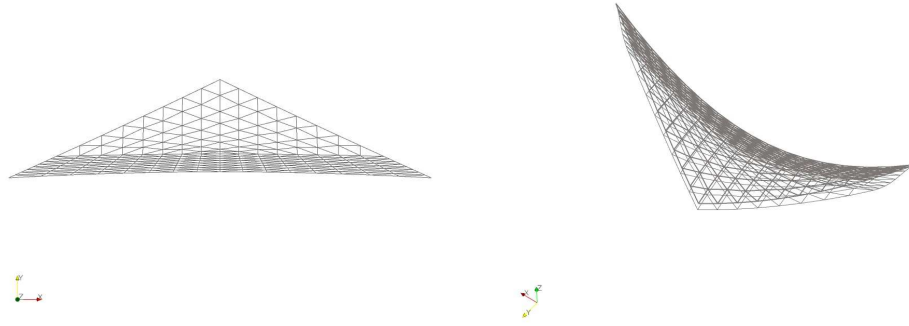


Figure 7.1: Trace shell problem: undeformed midsurface mesh containing 96 elements and 217 nodes for $\varepsilon = 10^{-3}$ on the left, and deformed midsurface graph compared to the undeformed one on the right, $scale = 1 \times 10^7$ ($E = 2.0 \times 10^{11}$, $\nu = 1/3$, boundary layer of width $3\sqrt{\varepsilon}L$, 1000 active DOF).

We define an admissible membrane loading:

$$F(\vec{v}) = \int_S tr(\underline{\underline{\gamma}}(\vec{v})) dS \quad (7.17)$$

that gives $F \in \mathcal{V}'_m$.

The resulting problem clearly falls into a membrane-dominated framework and we consider like a reference the standard P_2 displacement-based shell finite elements for a mesh of 6144 elements with a boundary layer treatment properly performed as described above.

7.2.1 MITC6a membrane spurious modes

We focus our analysis on the MITC6a shell finite element for a coarse mesh of 96 elements and 217 nodes and we consider $\varepsilon = 10^{-4}$ in order to capture the asymptotic behavior of the structure.

For this particular geometry, mesh, relative thickness and boundary conditions, the smallest modulus A_m eigenvalue is:

$$\tau_{min} = 2.186942906 \times 10^{10}$$

We have observed that there exactly exist 16 real membrane spurious modes related to A_m^h that roughly verify:

$$\tau_i^h / \tau_{min} \sim 10^{-10} \quad (7.18)$$

and give:

$$A_m^h(\vec{u}_0^i, \vec{u}_0^i) / A_m(\vec{u}_0^i, \vec{u}_0^i) < 10^{-12} \quad (7.19)$$

for $i = 1, \dots, 16$ (refer to Tables 7.1-7.2). On the other hand, the smallest modulus A_m^h eigenvalues that follow are of the same order of magnitude than τ_{min} roughly speaking, whereas they give:

$$A_m^h(\vec{u}_0, \vec{u}_0) / A_m(\vec{u}_0, \vec{u}_0) \sim 10^{-2} \quad (7.20)$$

Some of them are displayed in Table 7.3.

We observe that most of the real and pseudo membrane spurious modes that appear have a reduced shear energy that is higher than the reduced bending energy and dominant in the total reduced energy. Furthermore, whereas the unreduced bending energy remains close to the reduced bending energy, the unreduced shear energy is amplified by several orders of magnitude as compared to the reduced shear energy and it is highly dominant in the unreduced total energy as compared to the unreduced membrane energy. In addition, there only exists one real membrane spurious mode that has reduced bending energy of the same order of magnitude than the reduced shear energy –even if it is slightly lower– and also in this case the other observations hold.

Compared with the real spurious modes, the pseudo membrane spurious modes behave in a similar way, although the unreduced shear energy explosion is not so strong now, but it remains dominant in the unreduced total energy. There are some pseudo membrane spurious modes that give reduced bending energy of the same order of magnitude and even higher than reduced shear energy. It is important to notice that the pseudo spurious modes seem to be “physically admissible” modes as the corresponding eigenvalues are of the same order of magnitude as the smallest A_m eigenvalue.

Tables 7.1-7.3 summarizes the reduced and unreduced total and partial (membrane, shear and bending) energy values associated with the real membrane spurious modes we referred above and some other pseudo membrane spurious modes, and the related eigenvalue τ^h is also displayed in each case. It is important to notice that negative and complex A_m^h eigenvalues and energies in Tables 7.1-7.2 are of no particular concern as the largest modulus eigenvalue related to $[K_{vv}^{m,h}]$ is²:

$$\tau_{max}^h = 2.479605093 \times 10^{17}$$

²The largest modulus eigenvalue related to $[K_{vv}^m]$ is $\tau_{max} = 2.479687375 \times 10^{17}$.

and

$$|\tau_i^h|/\tau_{max}^h < eps \quad i = 1, \dots, 16 \quad (7.21)$$

where eps denotes the precision of floating point numbers used in our computations³. In such case, the modulus or absolute value are respectively considered in (7.18) and (7.19).

7.2.2 P_2 and MITC6a solutions

As expected, P_2 displacement-based shell finite elements provide good numerical solutions (see Fig. 7.4), and uniform quadratic convergence is fairly well achieved for strains (seen through the s -norm) and displacements and rotations (by means of the A_m norm). The subspace of discretized inextensional displacements is exactly reduced to $\{0\}$.

Total and partial energy values associated with the P_2 reference and target solutions are summarized in Table 7.5. It confirms that the asymptotic behavior of the structure is membrane-dominated: shear and bending energies vanish as the thickness decreases, whereas the membrane energy becomes dominant and it can be scaled by a factor of ε . Given a thickness value, total and partial energy values converge as the mesh is refined.

Error convergence curves associated with the MITC6a shell finite element are displayed in Fig. 7.5. We observe that this element provides good strains and quadratic convergence –slightly sensitive to thickness– is achieved as seen by means of the s -norm, whereas midsurface displacements and rotations are not well predicted for small relative thickness and coarse meshes as seen through the A_m norm. Even if shear terms are discarded from the A_m norm, displacements *per se* remain inadequate for $\varepsilon = 10^{-4}$ and coarse meshes.

Table 7.6 summarizes the reduced and unreduced energy values for decreasing thickness and more or less refined meshes for the MITC6a shell finite element. The membrane-dominated nature of the problem seems to be well captured by the MITC6a shell finite element given that reduced shear and bending energies vanish as thickness decreases, whereas the reduced membrane energy becomes dominant, close to P_2 reference values for all thickness values and it can be scaled by a factor of ε . In fact, the discrete space of inextensional displacements $\mathcal{V}_{0,h}$ is exactly reduced to zero as the smallest modulus eigenvalues associated with $K^{m,h} + K^{s,h}$ for each ε and h are not negligible in comparison with those associated with $K^m + K^s$ as Table 7.4 shows. Notice also that the smallest modulus eigenvalue corresponding to the reduced membrane matrix differs of several orders of magnitude as compared to the smallest displacement-based one for each h and ε considered.

On the other hand, the reduced and unreduced energy values summarized in Table 7.6 verify that⁴:

$$A_s(U_h^\varepsilon, U_h^\varepsilon) \gg A_s^h(U_h^\varepsilon, U_h^\varepsilon), \quad A_m(U_h^\varepsilon, U_h^\varepsilon) \sim A_m^h(U_h^\varepsilon, U_h^\varepsilon). \quad (7.22)$$

³ $eps \simeq 2.220446049 \times 10^{-16}$

⁴ U_h^ε denotes the MITC solution.

$\tau_1^h = -2.141070404\text{e-}01$	<i>Reduced</i>	<i>Unreduced</i>
<i>Total</i>	+6.369963661e+14	+7.309360659e+16
<i>Bending</i>	+2.236523016e+13	+2.233355422e+13
<i>Membrane</i>	-2.405047928e-01	+1.169107522e+14
<i>Shear</i>	+6.146310822e+14	+7.295436209e+16
$\tau_2^h = +3.152754788\text{e-}01$		
<i>Total</i>	+2.103289034e+13	+3.907549419e+15
<i>Bending</i>	+1.109652099e+12	+1.106864045e+12
<i>Membrane</i>	+1.164137855e-01	+1.592684030e+13
<i>Shear</i>	+1.992323633e+13	+3.890515672e+15
$\tau_3^h = -3.531140194\text{e-}01 \ -5.993849236\text{e-}01 \ i$		
<i>Total</i>	+9.768266690e+14	+1.100421839e+17
<i>Bending</i>	+4.440334063e+13	+4.438748272e+13
<i>Membrane</i>	-4.644082134e-01	+1.106932442e+14
<i>Shear</i>	+9.324232642e+14	+1.098871020e+17
$\tau_4^h = -3.531140194\text{e-}01 \ +5.993849236\text{e-}01 \ i$		
<i>Total</i>	+9.768266690e+14	+1.100421839e+17
<i>Bending</i>	+4.440334063e+13	+4.438748272e+13
<i>Membrane</i>	-4.644082134e-01	+1.106932442e+14
<i>Shear</i>	+9.324232642e+14	+1.098871020e+17
$\tau_5^h = -6.881664483\text{e-}01$		
<i>Total</i>	+4.497169297e+14	+1.003966603e+17
<i>Bending</i>	+1.592724211e+13	+1.589298712e+13
<i>Membrane</i>	-4.412494300e-01	+1.254483442e+14
<i>Shear</i>	+4.337896124e+14	+1.002553194e+17
$\tau_6^h = +1.147225780\text{e+}00$		
<i>Total</i>	+2.039318585e+15	+2.208636918e+17
<i>Bending</i>	+7.498820741e+13	+7.488826473e+13
<i>Membrane</i>	+2.806189443e-01	+2.656679494e+14
<i>Shear</i>	+1.964330214e+15	+2.205231346e+17
$\tau_7^h = +1.182723110\text{e+}00$		
<i>Total</i>	+1.330442164e+12	+3.333393001e+14
<i>Bending</i>	+6.156190218e+11	+6.141748400e+11
<i>Membrane</i>	+5.750380541e-01	+6.819119286e+12
<i>Shear</i>	+7.148228626e+11	+3.259059867e+14
$\tau_8^h = -2.768167247\text{e+}00$		
<i>Total</i>	+4.157084014e+14	+9.078722110e+16
<i>Bending</i>	+1.368419262e+13	+1.365590359e+13
<i>Membrane</i>	-1.882695528e+00	+1.100693416e+14
<i>Shear</i>	+4.020241417e+14	+9.066349621e+16

Table 7.1: *Reduced* and *unreduced* energy values associated with real MITC6a membrane spurious modes for the trace benchmark ($\varepsilon = 10^{-4}$, 96 elements and 217 nodes, boundary layer of width $3\sqrt{\varepsilon}L$).

$\tau_9^h = +3.124928814\text{e}+00$	<i>Reduced</i>	<i>Unreduced</i>
<i>Total</i>	+3.951503203e+15	+3.555156801e+17
<i>Bending</i>	+7.390525783e+13	+7.380655497e+13
<i>Membrane</i>	+1.300789593e+00	+3.544467772e+14
<i>Shear</i>	+3.877597700e+15	+3.550874246e+17
$\tau_{10}^h = +6.035838534\text{e}+00 -7.455315727\text{e}+00 \text{ i}$		
<i>Total</i>	+3.851369749e+15	+3.391027269e+17
<i>Bending</i>	+5.338774600e+13	+5.335581247e+13
<i>Membrane</i>	+3.198183576e+00	+2.568658114e+14
<i>Shear</i>	+3.797981776e+15	+3.387925025e+17
$\tau_{11}^h = +6.035838534\text{e}+00 +7.455315727\text{e}+00 \text{ i}$		
<i>Total</i>	+3.851369749e+15	+3.391027269e+17
<i>Bending</i>	+5.338774600e+13	+5.335581247e+13
<i>Membrane</i>	+3.198183576e+00	+2.568658114e+14
<i>Shear</i>	+3.797981776e+15	+3.387925025e+17
$\tau_{12}^h = -7.237805134\text{e}+00 -5.129190596\text{e}+00 \text{ i}$		
<i>Total</i>	+1.036783157e+15	+2.046703728e+17
<i>Bending</i>	+4.164491073e+13	+4.158171238e+13
<i>Membrane</i>	-3.668404229e+00	+1.749874212e+14
<i>Shear</i>	+9.951380928e+14	+2.044538036e+17
$\tau_{13}^h = -7.237805134\text{e}+00 +5.129190596\text{e}+00 \text{ i}$		
<i>Total</i>	+1.036783157e+15	+2.046703728e+17
<i>Bending</i>	+4.164491073e+13	+4.158171238e+13
<i>Membrane</i>	-3.668404229e+00	+1.749874212e+14
<i>Shear</i>	+9.951380928e+14	+2.044538036e+17
$\tau_{14}^h = +5.938763425\text{e}+00$		
<i>Total</i>	+9.393094236e+14	+9.942232580e+16
<i>Bending</i>	+3.827602342e+13	+3.823079864e+13
<i>Membrane</i>	+2.925863624e+00	+1.564870270e+14
<i>Shear</i>	+9.010333297e+14	+9.922760750e+16
$\tau_{15}^h = -1.197590040\text{e}+01$		
<i>Total</i>	+3.047065140e+15	+5.023267081e+17
<i>Bending</i>	+9.294230437e+13	+9.283362242e+13
<i>Membrane</i>	-5.383374318e+00	+2.722491167e+14
<i>Shear</i>	+2.954122444e+15	+5.019616250e+17
$\tau_{16}^h = +5.921453413\text{e}+00$		
<i>Total</i>	+2.090018166e+15	+2.949245704e+17
<i>Bending</i>	+6.563939692e+13	+6.555938644e+13
<i>Membrane</i>	+2.239656069e+00	+2.053265998e+14
<i>Shear</i>	+2.024378537e+15	+2.946536841e+17

Table 7.2: *Reduced* and *unreduced* energy values associated with real MITC6a membrane spurious modes for the trace benchmark ($\varepsilon = 10^{-4}$, 96 elements and 217 nodes, boundary layer of width $3\sqrt{\varepsilon}L$).

$\tau_{17}^h = +1.703368333e+10$	<i>Reduced</i>	<i>Unreduced</i>
<i>Total</i>	+1.456036093e+12	+2.707344967e+14
<i>Bending</i>	+1.645397489e+11	+1.643335423e+11
<i>Membrane</i>	+8.516841664e+09	+6.901894984e+11
<i>Shear</i>	+1.282979383e+12	+2.698799741e+14
$\tau_{18}^h = +2.078488522e+10$		
<i>Total</i>	+6.843439828e+12	+4.661184707e+14
<i>Bending</i>	+8.237882497e+10	+8.236712335e+10
<i>Membrane</i>	+1.039244261e+10	+4.014387601e+11
<i>Shear</i>	+6.750668264e+12	+4.656346636e+14
$\tau_{19}^h = +2.437612651e+10$		
<i>Total</i>	+2.307899115e+13	+4.835360771e+14
<i>Bending</i>	+2.760859883e+11	+2.761663978e+11
<i>Membrane</i>	+1.218806325e+10	+1.412650494e+12
<i>Shear</i>	+2.279071689e+13	+4.818472258e+14
$\tau_{20}^h = +3.536831385e+10$		
<i>Total</i>	+1.015451349e+13	+6.348709020e+14
<i>Bending</i>	+2.500778850e+11	+2.499777398e+11
<i>Membrane</i>	+1.768415693e+10	+6.971994650e+11
<i>Shear</i>	+9.886751114e+12	+6.339237175e+14
$\tau_{21}^h = +5.953031659e+10$		
<i>Total</i>	+1.491993368e+13	+8.026236872e+14
<i>Bending</i>	+3.544265399e+11	+3.543102400e+11
<i>Membrane</i>	+2.976515829e+10	+1.025313824e+12
<i>Shear</i>	+1.453574184e+13	+8.012440691e+14
$\tau_{22}^h = +1.190260989e+11$		
<i>Total</i>	+7.124614240e+12	+2.241566999e+14
<i>Bending</i>	+8.754462295e+10	+8.751639298e+10
<i>Membrane</i>	+5.951304942e+10	+6.260582772e+11
<i>Shear</i>	+6.977556638e+12	+2.234431257e+14
$\tau_{23}^h = +1.485547410e+11$		
<i>Total</i>	+1.916736541e+12	+2.076424565e+14
<i>Bending</i>	+1.101907274e+11	+1.102008939e+11
<i>Membrane</i>	+7.427737051e+10	+1.674531636e+12
<i>Shear</i>	+1.732268718e+12	+2.058577218e+14
$\tau_{24}^h = +1.635624588e+11$		
<i>Total</i>	+2.976129753e+12	+1.315956326e+15
<i>Bending</i>	+2.126207584e+12	+2.126321667e+12
<i>Membrane</i>	+8.178122942e+10	+3.082832693e+11
<i>Shear</i>	+7.681646397e+11	+1.313521743e+15

Table 7.3: *Reduced* and *unreduced* energy values associated with some MITC6a pseudo spurious modes for the trace benchmark ($\varepsilon = 10^{-4}$, 96 elements and 217 nodes, boundary layer of width $3\sqrt{\varepsilon}L$).

when $\varepsilon \ll 1$. Moreover, we observe that for $\varepsilon = 10^{-4}$ the MITC6a reduced bending energy is one order of magnitude higher as compared to the P_2 displacement-based solution for each h .

The deformed meshes associated with the P_2 displacement-based and MITC6a shell finite elements are displayed in Fig. 7.2 for the smallest relative thickness and coarsest mesh considered in our analysis ($\varepsilon = 10^{-4}$, $h = 0.25$: 96 elements and 217 nodes), and the nodal rotation field magnitude is plotted in Fig. 7.3 for both elements. We see that rotations are not well predicted by the MITC6a shell finite element in comparison with the references rotations provided by the P_2 displacement-based element. In fact, oscillations of large amplitude are observed near the free boundaries for the MITC6a deformed midsurface graph, a phenomena that is not correct as compared to the reference P_2 deformed midsurface plot.

In order to verify whether the membrane spurious modes are the cause of such oscillations, we have calculated the participation—in the sense of equation (7.12)—of the real and pseudo membrane parasitic modes displayed in Tables 7.1-7.3 into the MITC6a numerical solution and the results that we have obtained are summarized in Table 7.7. We can conclude that the pseudo modes mainly participate into the MITC6a solution as the real spurious modes have a lower (but not negligible) participation. Nevertheless, we can concentrate on the real and pseudo spurious modes displayed in Table 7.7 that have a participation of order 10^{-1} and seem to mainly deteriorate the MITC6a solution. The corresponding graphs are shown in Fig. 7.6-7.9 and a comparison can be made with the MITC6a deformed mesh displayed in Fig. 7.2: it seems likely that these spurious modes are the cause of large oscillations along the free boundaries that also propagate inside the domain.

In fact, the energy values and deformed midsurface plot of our MITC6a numerical solution leads us to conclude that *real* and *pseudo membrane spurious*

h	$A_m + A_s$	$A_m^h + A_s^h$	A_m	A_m^h
$\varepsilon = 0.01$				
0.25	2.764546995e+10	4.659820098e+09	9.704030289e+09	1.959160654e-04
0.125	1.573801818e+10	1.312277489e+09	3.658599382e+09	5.207111618e-04
0.0625	7.450201210e+09	4.089887722e+08	1.318817107e+09	5.680058475e-04
$\varepsilon = 0.001$				
0.25	3.365232665e+10	5.467717851e+09	1.957402479e+10	1.095612969e-03
0.125	2.210870487e+10	2.891364922e+09	9.107203410e+09	9.438917279e-03
0.0625	1.293118673e+10	1.095856903e+09	3.744603360e+09	3.006741839e-02
$\varepsilon = 0.0001$				
0.25	3.563259339e+10	2.810873623e+09	2.186942906e+10	-2.141076553e-01
0.125	2.371914818e+10	1.700497178e+09	1.102323682e+10	1.372091651e-01
0.0625	1.456200485e+10	1.440142003e+09	4.637100664e+09	5.399704373e-01

Table 7.4: Trace shell problem: smallest modulus eigenvalues associated with $A_m + A_s$ and A_m for the P_2 shell finite element, $A_m^h + A_s^h$ and A_m^h for the MITC6a.

modes clearly arise and deteriorate the expected behavior. Not only the real spurious modes, but also the pseudo membrane parasitic modes highly arise for this benchmark shell problem. As we have seen, most of the real and pseudo spurious modes produce an explosion in the unreduced shear energy in comparison with the reduced shear energy, but for example the 7th real spurious mode in Table 7.7 has a reduced bending energy that is of the same order of magnitude as the reduced shear energy (refer to Table 7.1), and this last consideration also holds for the 24th mode displayed in Table 7.3. But it is always the unreduced shear energy that dominates in the unreduced total energy in all cases. These observations give an explanation to the large unreduced shear energy associated with the MITC6a solution and also the high reduced bending energy increased of an order of magnitude as compared to the P_2 reference value.

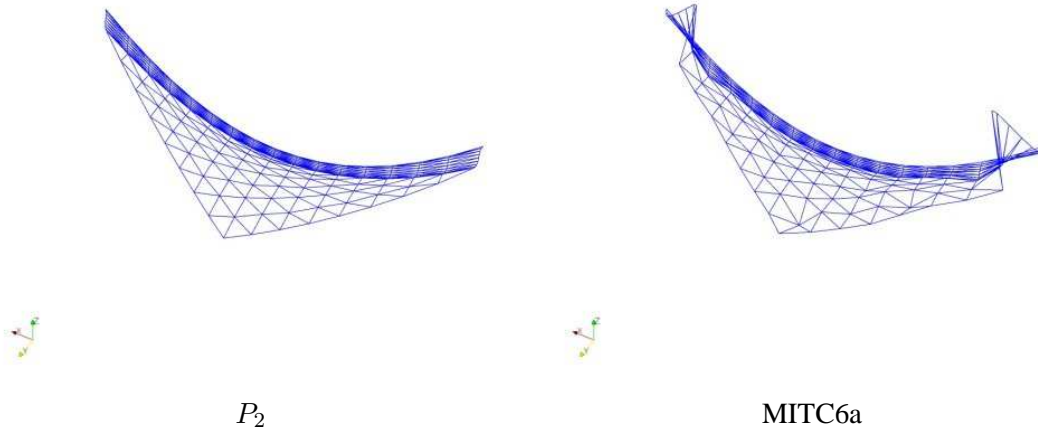


Figure 7.2: Deformed midsurface plots for the trace shell problem: P_2 (left) and MITC6a (right) shell finite elements for $\varepsilon = 10^{-4}$ and a mesh of 96 elements $-h = 0.25-$ and 217 nodes, boundary layer of width $3\sqrt{\varepsilon}L$ ($scale = 1 \times 10^6$).

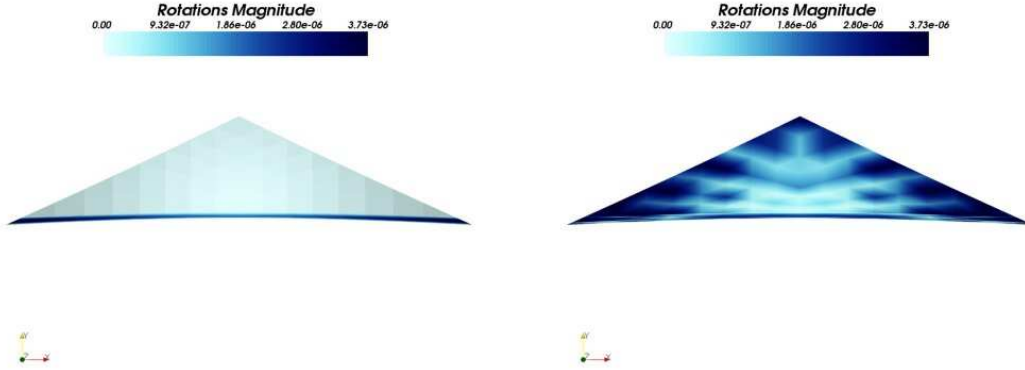


Figure 7.3: Magnitude of the rotation field for the trace shell problem: P_2 (left) and MITC6a (right) shell finite elements for $\varepsilon = 10^{-4}$ and a mesh of 96 elements $-h = 0.25-$ and 217 nodes, boundary layer of width $3\sqrt{\varepsilon}L$.

$\varepsilon = 10^{-2}$	$h = 0.25$	$h = 0.125$	$h = 0.0625$	<i>Ref sol</i>
<i>Total</i>	1.625614138e-10	1.636227424e-10	1.637919918e-10	1.638092595e-10
<i>Bending</i>	2.899686587e-12	3.443922227e-12	3.583705711e-12	3.602163776e-12
<i>Membrane</i>	1.592970032e-10	1.600679730e-10	1.601860052e-10	1.601980158e-10
<i>Shear</i>	4.323046650e-13	1.761754264e-13	8.726474189e-14	7.403760514e-14
$\varepsilon = 10^{-3}$	$h = 0.25$	$h = 0.125$	$h = 0.0625$	<i>Ref sol</i>
<i>Total</i>	1.745541193e-09	1.753056360e-09	1.754706364e-09	1.755258783e-09
<i>Bending</i>	1.318061523e-11	1.598817421e-11	1.617578273e-11	1.624272790e-11
<i>Membrane</i>	1.731816291e-09	1.736784713e-09	1.738305088e-09	1.738917129e-09
<i>Shear</i>	5.598601652e-13	3.001356466e-13	2.422948594e-13	1.156832852e-13
$\varepsilon = 10^{-4}$	$h = 0.25$	$h = 0.125$	$h = 0.0625$	<i>Ref sol</i>
<i>Total</i>	1.791391461e-08	1.801289895e-08	1.802635849e-08	1.802860067e-08
<i>Bending</i>	2.889606850e-11	5.421977711e-11	5.999243985e-11	5.937903190e-11
<i>Membrane</i>	1.788109973e-08	1.795776910e-08	1.796613404e-08	1.796901784e-08
<i>Shear</i>	3.922139514e-12	9.142441537e-13	2.363593308e-13	2.082007634e-13

Table 7.5: Energy values associated with the trace shell problem and P_2 displacement-based shell finite elements for different values of ε and h .

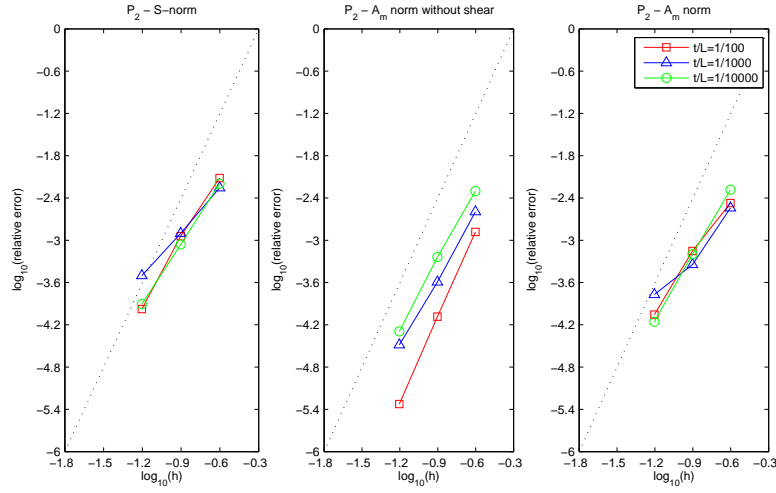


Figure 7.4: Convergence curves associated with the s-norm and A_m norm (shear terms discarded and not) for the trace shell problem and P_2 displacement-based shell finite elements. The dotted line shows the optimal convergence rate which is 4.

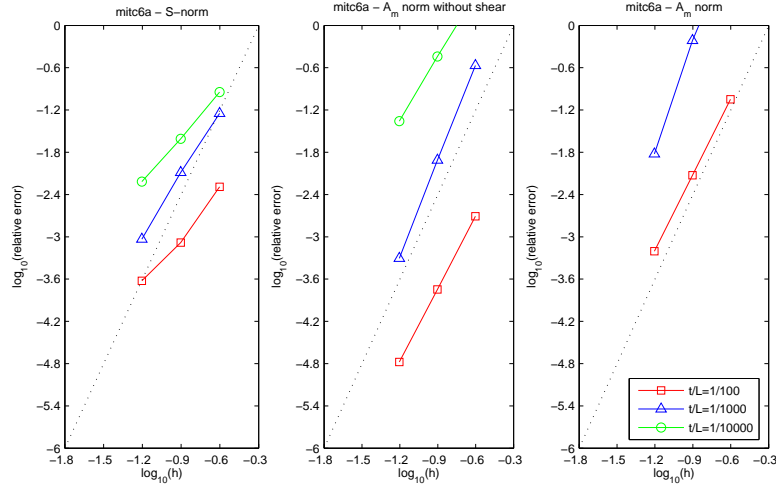


Figure 7.5: Convergence curves associated with the s-norm and membrane energy norm (with shear terms discarded and not) for the trace shell problem and MITC6a shell finite element. The dotted line shows the optimal convergence rate which is 4.

$\varepsilon = 10^{-2}$		$h = 0.25$	$h = 0.125$	$h = 0.0625$
<i>Total</i>	<i>Reduced</i>	1.635943071e-10	1.637427893e-10	1.638004556e-10
	<i>Unreduced</i>	1.782743337e-10	1.649619303e-10	1.639188685e-10
<i>Bending</i>	<i>Reduced</i>	3.707275380e-12	3.602355501e-12	3.606538670e-12
	<i>Unreduced</i>	3.704225021e-12	3.601609453e-12	3.606281368e-12
<i>Membrane</i>	<i>Reduced</i>	1.597151945e-10	1.600937939e-10	1.601762770e-10
	<i>Unreduced</i>	1.594303696e-10	1.598377553e-10	1.601017737e-10
<i>Shear</i>	<i>Reduced</i>	2.239399956e-13	1.079039190e-13	8.162652771e-14
	<i>Unreduced</i>	1.519089629e-11	1.583109201e-12	2.745765666e-13
$\varepsilon = 10^{-3}$		$h = 0.25$	$h = 0.125$	$h = 0.0625$
<i>Total</i>	<i>Reduced</i>	1.824418394e-09	1.761419957e-09	1.754729267e-09
	<i>Unreduced</i>	2.199030724e-08	2.843743147e-09	1.781053800e-09
<i>Bending</i>	<i>Reduced</i>	5.165339248e-11	2.140567412e-11	1.698796935e-11
	<i>Unreduced</i>	5.147666241e-11	2.140560730e-11	1.698723834e-11
<i>Membrane</i>	<i>Reduced</i>	1.766887584e-09	1.739098512e-09	1.737541751e-09
	<i>Unreduced</i>	2.352581643e-09	1.772663452e-09	1.738327613e-09
<i>Shear</i>	<i>Reduced</i>	5.879353460e-12	9.253863961e-13	2.143617913e-13
	<i>Unreduced</i>	1.958620655e-08	1.049680093e-09	2.575325829e-11
$\varepsilon = 10^{-4}$		$h = 0.25$	$h = 0.125$	$h = 0.0625$
<i>Total</i>	<i>Reduced</i>	1.981605327e-08	1.837589483e-08	1.811792133e-08
	<i>Unreduced</i>	4.812321121e-06	2.282277524e-06	7.336077997e-07
<i>Bending</i>	<i>Reduced</i>	6.515344241e-10	1.417090352e-10	1.001703188e-10
	<i>Unreduced</i>	6.505662494e-10	1.416300378e-10	1.001495601e-10
<i>Membrane</i>	<i>Reduced</i>	1.895572441e-08	1.820591533e-08	1.801124243e-08
	<i>Unreduced</i>	7.029725398e-08	2.519826050e-08	1.894450248e-08
<i>Shear</i>	<i>Reduced</i>	2.087915606e-10	2.827106350e-11	6.510695501e-12
	<i>Unreduced</i>	4.741373215e-06	2.256937611e-06	7.145631429e-07

Table 7.6: *Reduced* and *unreduced* energy values associated with the trace shell problem and MITC6a triangular shell finite element for different values of ε and h .

REAL SPURIOUS MODES

	τ^h eigenvalue	Participation
1)	-2.141070404e-01	0.1669696407
2)	+3.152754788e-01	0.3506535620
3)	-3.531140194e-01-5.993849236e-01i	0.2297446986
4)	-3.531140194e-01+5.993849236e-01i	0.2297446986
5)	-6.881664483e-01	0.3829011395
6)	+1.147225780e+00	0.1296906259
7)	+1.182723110e+00	0.2785644970
8)	-2.768167247e+00	0.3858308681
9)	+3.124928814e+00	0.0337226638
10)	+6.035838534e+00-7.455315727e+00i	0.0071562451
11)	+6.035838534e+00+7.455315727e+00i	0.0071562451
12)	-7.237805134e+00-5.129190596e+00i	0.0574613830
13)	-7.237805134e+00+5.129190596e+00i	0.0574613830
14)	+5.938763425e+00	0.0940793458
15)	-1.197590040e+01	0.3269648857
16)	+5.921453413e+00	0.2730570527

PSEUDO SPURIOUS MODES

	τ^h eigenvalue	Participation
17)	+1.703368333e+10	0.6719271944
18)	+2.078488522e+10	0.7475016955
19)	+2.437612651e+10	0.5517409451
20)	+3.536831385e+10	0.6667402212
21)	+5.953031659e+10	0.6606746105
22)	+1.190260989e+11	0.6277095171
23)	+1.485547410e+11	0.5752632565
24)	+1.635624588e+11	0.0765127192

Table 7.7: MITC6a *real* and *pseudo membrane spurious modes* participation into MITC6a solution for the trace shell problem ($\varepsilon = 10^{-4}$, mesh containing 96 elements and 217 nodes, boundary layer of width $3\sqrt{\varepsilon}L$).

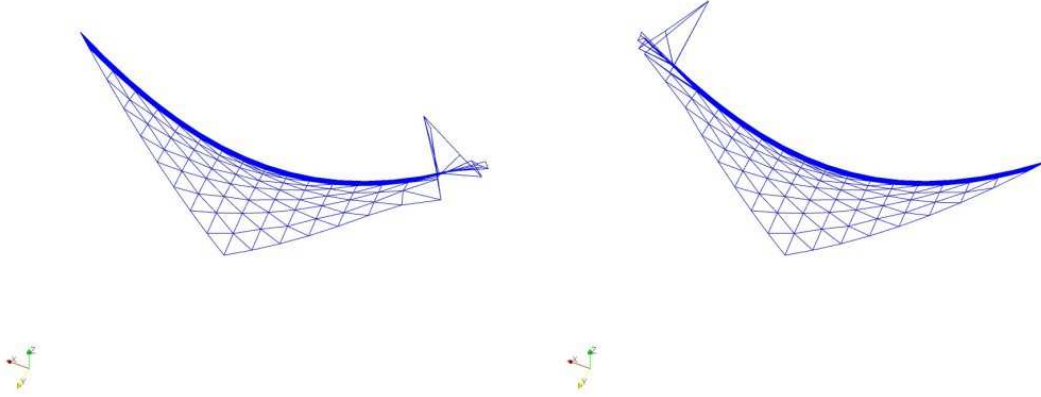


Figure 7.6: Graphs of the MITC6a real spurious modes corresponding to the zero eigenvalues τ_2^h —figure on the left— and τ_8^h —figure on the right— for $\varepsilon = 10^{-4}$ and a coarse mesh of 96 elements and 217 nodes, boundary layer of width $3\sqrt{\varepsilon}L$ ($scale = 1 \times 10^{-4}$).

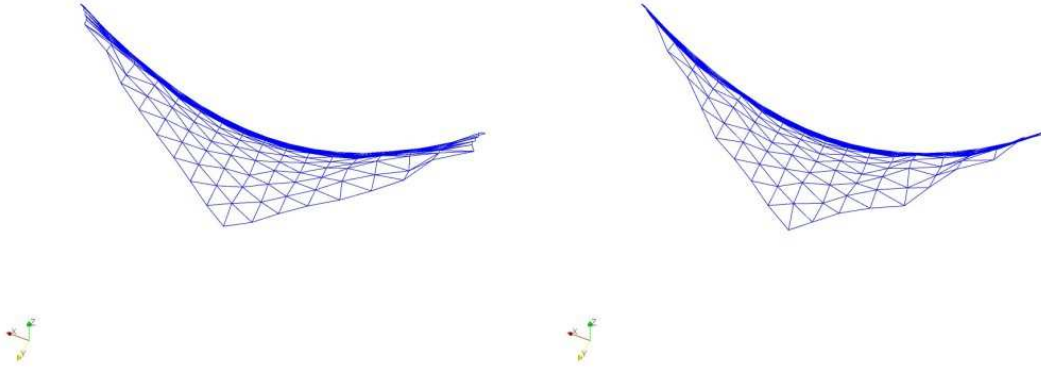


Figure 7.7: Graphs of the MITC6a pseudo spurious modes corresponding to the eigenvalues τ_{17}^h —figure on the left— and τ_{18}^h —figure on the right— for $\varepsilon = 10^{-4}$ and a coarse mesh of 96 elements and 217 nodes, boundary layer of width $3\sqrt{\varepsilon}L$ ($scale = 1 \times 10^{-4}$).

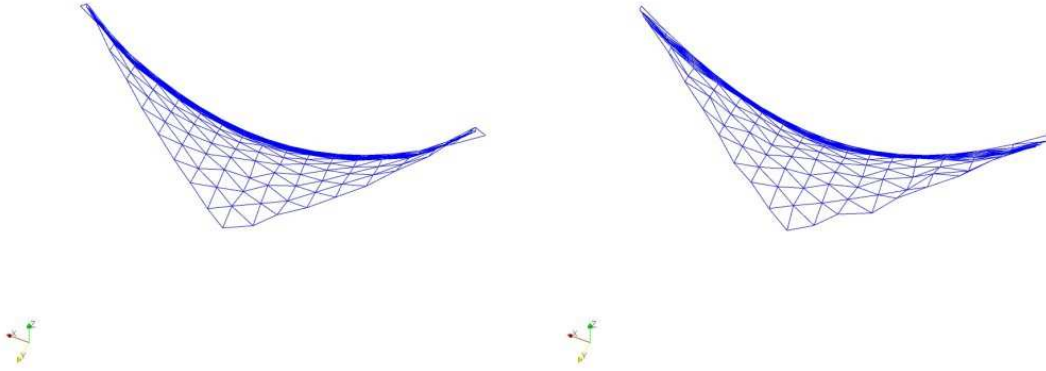


Figure 7.8: Graphs of the MITC6a pseudo spurious modes corresponding to the eigenvalues τ_{19}^h —figure on the left— and τ_{20}^h —figure on the right— for $\varepsilon = 10^{-4}$ and a coarse mesh of 96 elements and 217 nodes, boundary layer of width $3\sqrt{\varepsilon}L$ ($scale = 1 \times 10^{-4}$).

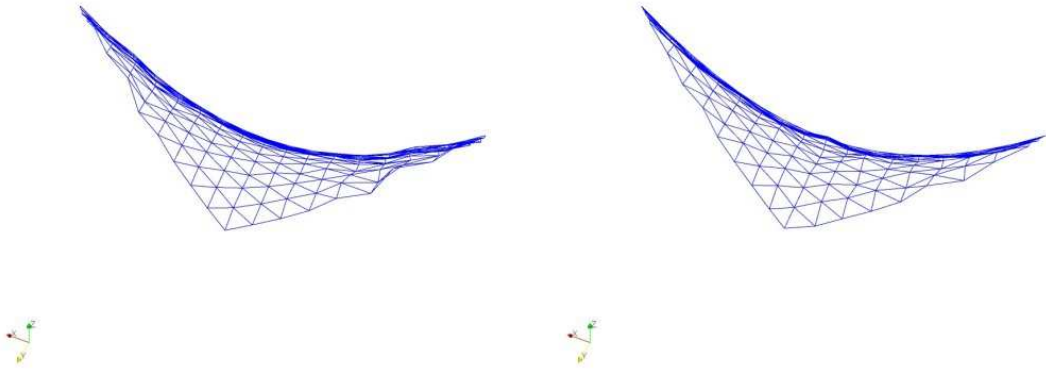


Figure 7.9: Graphs of the MITC6a pseudo spurious modes corresponding to the eigenvalues τ_{21}^h —figure on the left— and τ_{22}^h —figure on the right— for $\varepsilon = 10^{-4}$ and a coarse mesh of 96 elements and 217 nodes, boundary layer of width $3\sqrt{\varepsilon}L$ ($scale = 1 \times 10^{-4}$).

7.3 Improving the MITC6a element

As discussed in the previous section, the presence of spurious modes in the MITC6a solution of some membrane dominated problems is the cause of unsatisfactory error curves in the membrane norm. Moreover, the amplitude of these parasitic modes may dominate that of the underlying "correct" solution, giving erroneous displacement graphs. Considering that membrane shell problems are, by far, the most encountered in engineering practice, such phenomena are a serious hindrance for the applicability of the MITC6a element. The objective of this section is therefore to develop some possible cures to these difficulties.

In the "perfect MITC shell element" the discrete space of inextensional deformations

$$\mathcal{V}_{0,h} = \left\{ V \in \mathcal{V}_h : A_m^h(V, V) + A_s^h(V, V) = 0 \right\} \quad (7.23)$$

should be sufficiently rich in bending dominated cases and null in membrane dominated cases. The presence of spurious membrane modes is directly related to the failure of the second condition. Therefore the parasitic membrane modes can be characterized qualitatively as the discrete generalized displacements such that

$$A_m(V, V) + A_s(V, V) \gg A_m^h(V, V) + A_s^h(V, V), \quad V \in \mathcal{V}_h \quad (7.24)$$

in membrane dominated configurations. As already observed, spurious modes arise in the trace shell problem, as it appears when comparing the right and left hand sides of (7.24) in Table 7.6.

The main difficulty in the attempt of curing this phenomenon, is that the same characterization (7.24) is essentially shared by all the discrete inextensional modes in bending dominated problems. In other words, in bending dominated situations, almost all elements in $\mathcal{V}_{0,h}$ are expected to behave as in equation (7.24); this is exactly what distinguishes the "non-locking" MITC6a element from a "fully locking" classical $P2$ Galerkin method. As a consequence, any cure for membrane spurious modes which uses (7.24) as a starting basis will be at a strong risk of spoiling the method's performance in bending dominated situations. On the other hand, condition (7.24) is essentially the only general characterization at our disposal. The aim of this section therefore becomes to develop a cure for the MITC6a element in membrane dominated problems, which does not strongly hinder the method in bending dominated cases.

7.3.1 Weighted shear stabilization

In the energy Table 7.6 for the MITC6a element, a particular phenomena can be immediately noticed. For the solution U_h^ε , particularly when $\varepsilon \ll 1$, it happens that

$$A_s(U_h^\varepsilon, U_h^\varepsilon) \gg A_s^h(U_h^\varepsilon, U_h^\varepsilon), \quad A_m(U_h^\varepsilon, U_h^\varepsilon) \sim A_m^h(U_h^\varepsilon, U_h^\varepsilon). \quad (7.25)$$

In other words, there is an amplification of several orders of magnitude when comparing the reduced and unreduced shear energies, while the amplification is limited in the membrane energy. Furthermore, whenever the relative thickness is sufficiently small, the unreduced shear energy $A_s(U_h^\varepsilon, U_h^\varepsilon)$ is dominant over the total energy. This phenomenon is in complete contrast with the benchmark results in Table 7.5, where it is shown that the shear part of the energy in the "correct" solution should be negligible.

These observations, which hold for all the membrane shell problems considered, seem to indicate that the nature of the spurious part of the solution is mainly reflected in the shear energy. Moreover, it is well known that in typical bending dominated situations the main source of locking is the membrane energy, and not the shear energy. The combination of these two arguments suggests to stabilize/modify only the shear part of the MITC6a energy, in order to reach our aforementioned goal.

The most natural modification is to propose a MITC6a scheme in which the parasitic modes are handled by adding an unreduced weighted shear part to the discrete method. In other words, we modify the original bilinear form of the problem as follows

$$\begin{aligned} \mathcal{A}_{s1}^h(U_h, V) = & \varepsilon^3 A_b(U_h, V) + \varepsilon A_m^h(U_h, V) + \varepsilon(1 - C(\frac{h}{L})^\gamma) A_s^h(U_h, V) \\ & + C\varepsilon(\frac{h}{L})^\gamma A_s(U_h, V), \quad \forall U_h, V \in \mathcal{V}_h, \end{aligned} \quad (7.26)$$

where C, γ are fixed positive scalars, and h represents the characteristic mesh size to be better addressed later. Note that we include no dependence of C on ε in order to have a method which, in principle, provides an improved stability also in the $\varepsilon \rightarrow 0$ membrane limit problem.

In order to guide our choice for γ , we need to introduce some observations. First of all, note that the coercivity of \mathcal{A}_{s1}^h on the MITC6a spurious modes is mainly given by the $\varepsilon^3 A_b(U_h, V) + C(\frac{h}{L})^\gamma \varepsilon A_s(U_h, V)$ part. Secondly, any standard shell finite element method is expected to give satisfactory results in the range $h/L \sim \varepsilon$, where L is the characteristic length of the structure; such a condition is satisfied by the MITC6a element, of course. Finally, note that the bending bilinear form features an ε^2 scaling factor when compared to the membrane and shear forms. As a consequence, the above observations suggest the choice $\gamma = 2$, because it represents the lowest γ (i.e. the strongest correction) which guarantees an energetically balanced modification in the $h/L \sim \varepsilon$ range.

Furthermore, we can justify this choice by looking in more depth into the energy tables of the previous section. Let U_h^ε be the solution of the MITC6a method for a given membrane dominated problem. Then, it is reasonable to require that our correction factor $C(\frac{h}{L})^\gamma$ in (7.26) satisfies

$$C(\frac{h}{L})^\gamma A_s(U_h^\varepsilon, U_h^\varepsilon) \sim E^h(U_h^\varepsilon), \quad (7.27)$$

where $E^h(U_h^\varepsilon)$ represents the total reduced energy of the solution. Indeed, a significantly weaker left hand side in (7.27) would imply a negligible modification for the solution, while a significantly stronger left hand side would imply an over-constraining stabilization. With this in mind and looking at the Table 7.6, we can observe that, with the choice $\gamma = 2$, condition (7.27) is in general satisfied, indeed. Moreover, this study suggests that the constant C should be of order of magnitude 1. In the sequel, we will test the two cases $C = 1$ and $C = 1/5$.

Finally, in order to allow for strongly refined meshes, the scaling factor $C(\frac{h}{L})^\gamma$ appearing in (7.26) must be made local. Therefore, the final MITC6a *stabilized formulation* we here propose uses the following bilinear form:

$$\begin{aligned} \mathcal{A}_{s1}^h(U_h, V) = & \varepsilon^3 A_b(U_h, V) + \varepsilon A_m^h(U_h, V) + \varepsilon \sum_{T \in \mathcal{T}_h} \left[\left(1 - C \frac{h_T^2}{L^2}\right) A_{s,T}^h(U_h, V) \right. \\ & \left. + C \frac{h_T^2}{L^2} A_{s,T}(U_h, V) \right], \quad \forall U_h, V \in \mathcal{V}_h, \end{aligned} \quad (7.28)$$

where T represents the general triangle of the mesh \mathcal{T}_h , h_T the diameter of T , and $A_{s,T}$, $A_{s,T}^h$ the local bilinear forms integrated over the element.

7.3.2 Free boundary shear stabilization

As shown in Table 5.5, the multiplicity of the MITC6a zero eigenvalue in the considered problem behaves as h^{-1} ; in other words, the dimension of the kernel in the membrane form is directly proportional to the number of elements along the boundary, not the total number of elements. Moreover, the displacement plot in Fig. 7.2 shows that the spurious membrane modes arise mainly as oscillations of large amplitude near the free boundaries. These two observations suggest that the main parasitic membrane modes may be generated along the free boundaries of the shell and then propagated inside the domain. The larger amount of degrees of freedom due to the free boundaries, combined with the reduced integration, seem to be responsible for this membrane "parasitic" kernel. Note that, again, this same qualitative property is shared by the inextensional modes in bending dominated problems; therefore the same already mentioned considerations hold.

Nevertheless, this observation, combined with those of the previous section, suggests to add a free boundary shear stabilization term in the MITC6a element. In other words, we propose the following modified bilinear form

$$\begin{aligned} \mathcal{A}_{s2}^h(U_h, V) = & \varepsilon^3 A_b(U_h, V) + \varepsilon A_m^h(U_h, V) + \varepsilon \sum_{T \in \mathcal{T}_h^i} A_{s,T}^h(U_h, V) \\ & + \varepsilon \sum_{T \in \mathcal{T}_h^b} A_{s,T}(U_h, V), \quad \forall U_h, V \in \mathcal{V}_h, \end{aligned} \quad (7.29)$$

where \mathcal{T}_h^b represents the set of the triangles in \mathcal{T}_h which have at least one node on the free boundary, and $\mathcal{T}_h^i \subset \mathcal{T}_h$ the remaining elements.

Note that, in the absence of free boundaries, the above method does not differ from the original MITC6a element. On the other hand, in such cases the parasitic modes are in general weaker and the MITC6a element gives fairly better results. This can be seen for example from the error graphs for the clamped hyperboloid shown in Section 6.3.3.

Another key observation is the following. In shell analysis it is often adequate to adopt meshes which are refined near the boundaries, in order to cope with the presence of boundary layers in the solution. In such cases, the free boundary band of elements \mathcal{T}_h^b may have an area which is extremely small with respect to the total area of the domain. Nevertheless, the presence of a layer in the solution near the free boundary implies a higher concentration of energy. As a consequence, ad hoc mesh boundary refinements may not weaken significantly the shear stabilization effect in (7.29).

7.3.3 A richer shear interpolation: the MITC6rs

Due to the considerations developed at the start of Section 7.3, another viable choice is to adopt a richer interpolation space for the transverse shear strains. As we have seen in Section 6.2, the MITC6 family uses essentially the second order rotated Raviart Thomas space for the transverse shear strains in the reference element. Such space has dimension 8, and the related tying points are shown in Figure 6.2.

In analogy with the techniques adopted in plate elements, we now introduce the following richer space for the transverse shear strains on the reference element \hat{T} :

$$\hat{S}_h = \left\{ \rho \in [P_2(\hat{T})]^2 : \rho|_{\hat{e}} \cdot \tau_{\hat{e}} \in P_1(\hat{e}) \forall \hat{e} \text{ edge} \in \partial \hat{T} \right\}, \quad (7.30)$$

where $\tau_{\hat{e}}$ represents the anticlockwise tangent unit vector to edge \hat{e} . The space \hat{S}_h has dimension 9 and contains the second order rotated Raviart Thomas space. Therefore, as starting degrees of freedom for the \hat{S}_h space, we select the same isotropic tying points as in the MITC6a transverse shear interpolation. As a ninth and last degree of freedom, in order to keep the vertex numbering isotropy discussed in Section 4.3, we make the following construction.

Let \hat{e}_i , $i = 1, 2, 3$, denote the three edges of the reference element \hat{T} , and \hat{m}_i the respective midpoints. Moreover, let $\hat{\eta}_i = \hat{\psi}_i / \|\hat{\psi}_i\|$, where $\hat{\psi}_i$ is the vector connecting each midpoint m_i with the opposite vertex. Then, following the usual notation, the last degree of freedom R_9 for the \hat{S}_h space is given by

$$R_9(e_{rz}, e_{sz}) = \sum_{i=1}^3 e_{\hat{\eta}_i z}(m_i). \quad (7.31)$$

The value of the transverse shear component $e_{\hat{\eta}_i z}$ can be clearly obtained from e_{rz}, e_{sz} . It is easy to check that the evaluation rule (7.31) is isotropic with respect to vertex permutations by construction. Moreover, together with the MITC6a

shear tying points in figure 6.2, (7.31) constitutes a set of linearly independent and unisolvent degrees of freedom for \hat{S}_h .

Finally note that, although the adopted degrees of freedom are different, the space \hat{S}_h was already introduced as part of the triangular BDFM pair in [25] and applied for plate elements in [24].

We therefore propose a new element, named as MITC6rs, which is similar to the MITC6a element, except for the transverse shear strain space and tying procedure, which is the one introduced above.

7.4 The trace benchmark: improvements

As discussed in Section 7.2.2, P_2 displacement-based shell finite elements provide good numerical solutions for this particular benchmark (see Fig. 7.4), and uniform quadratic convergence is fairly well achieved for strains (seen through the s -norm) and displacements and rotations (by means of the A_m norm). Total and partial energy values associated with the P_2 reference and target solutions are summarized in Table 7.5.

The MITC6rs error convergence curves are displayed in Fig. 7.10. We observe that they are quite similar to the MITC6a ones (refer to Fig. 7.5): this element provides reasonably good strains and quadratic convergence –slightly sensitive to thickness– is achieved as seen by means of the s -norm, whereas midsurface displacements and rotations are not well predicted for small relative thickness and coarse meshes as seen through the A_m norm. Even if shear terms are discarded from the A_m norm, displacements *per se* remain inadequate for $\varepsilon = 10^{-4}$ and coarse meshes. Furthermore, reduced and unreduced energy values summarized in Table 7.8 still verify that⁵:

$$A_s(U_h^\varepsilon, U_h^\varepsilon) \gg A_s^h(U_h^\varepsilon, U_h^\varepsilon), \quad A_m(U_h^\varepsilon, U_h^\varepsilon) \sim A_m^h(U_h^\varepsilon, U_h^\varepsilon). \quad (7.32)$$

when $\varepsilon \ll 1$, although the difference between reduced and unreduced shear energies is lower as compared to the MITC6a values summarized in Table 7.6. In other words, *parasitic membrane modes are present* as for the MITC6a shell finite element and they arise for small relative thickness values. The membrane-dominated nature of the problem is well detected by the MITC6rs shell finite element given that the reduced shear and bending energies vanish as thickness decreases, whereas the reduced membrane energy becomes dominant, close to P_2 reference values for all thickness and it can be scaled by a factor of ε . The participation of the membrane parasitic modes is summarized in Table 7.18, and we observe that it is substantially smaller as compared to the original MITC6a solution (see Table 7.7), except for the 7th real spurious modes which participates a little more.

The shear stabilized convergence curves in Fig. 7.11-7.16 together with the energy tables in Tables 7.9-7.14 show that the presence of spurious membrane modes considerably weakens owing to the shear stabilizations methods. The *free boundary shear stabilizations* provide strains that are rather well predicted by means of the s -norm. The A_m norm convergence curves with shear terms discarded or not do not really differ from the original MITC6a and MITC6rs shell finite elements, although the free boundary shear stabilized MITC6rs element provides rather better rotations than the free boundary shear stabilized MITC6a for the smallest relative thickness considered in our analysis. But the difference between reduced and unreduced shear energies is remarkably smaller for both stabilizations as compared to the respective original elements. This observation, with the participations of parasitic modes displayed in Tables 7.15 and 7.19 that substantially get lower, show that parasitic membrane modes are considerably filtered out.

⁵ U_h^ε denotes the MITC solution.

The *weighted shear stabilizations* provide strains that remain well predicted as seen through the *s-norm* when considering $C = 1$ and $C = 1/5$ for the weighted shear stabilized MITC6a and MITC6rs shell finite elements. In addition, the mid-surface displacement and rotations give admissible errors for all relative thickness values by means of the A_m norm with shear terms discarded or not. Reduced and unreduced shear energies differ of less orders of magnitude than the original MITC6a and MITC6rs formulations and in a similar way as the free boundary shear stabilization. Nevertheless, the A_m norm convergence curves associated with $C = 1/5$ slightly rise for $\varepsilon = 10^{-4}$ in comparison with those ones corresponding to $C = 1$, although the reduced and unreduced energy values do not really differ. This fact is well understood given that a constant C of order of magnitude smaller than one gives a weaker improvement by weighted shear stabilization as it was commented in Section 7.3.1. We can also conclude that parasitic membrane modes are considerably filtered out as their participation considerably gets lower as Tables 7.16, 7.17, 7.20 and 7.21 show.

Midsurface deformed graphs are shown in Fig. 7.17-7.18 for the MITC6a, MITC6rs and the shear stabilizations we have applied to the original MITC6a and MITC6rs shell finite elements ($\varepsilon = 10^{-4}$, mesh of 96 elements and 217 nodes). We observe that the MITC6rs deformed midsurface plot in Fig 7.18 substantially differs from the P_2 reference one in Fig. 7.2 –that corresponds to the expected behavior given the membrane-dominated nature of this problem– and spurious membrane modes notably reveal as large oscillations near the free boundaries like for the MITC6a element. Free boundary and weighted shear stabilized formulations seem to correct this phenomena for both elements as oscillations considerably fall off for small relative thickness values.

The rotations magnitude plots are also displayed in Fig. 7.19-7.20 for the original MITC6a and MITC6rs shell finite elements and the shear stabilizations we have considered. In comparison with the P_2 rotations magnitude reference graph in Fig. 7.3, we observe that the rotation field is considerably improved when considering the free boundary of weighted shear stabilizations for the original MITC6a and MITC6rs shell finite elements. The original MITC6rs rotations magnitude graph also shows that a richer shear interpolation than the original MITC6a one provides quite better rotations.

We conclude that the free boundary and weighted shear stabilizations considerably improve the numerical results for this particular membrane-dominated shell problem, but also the richer transverse shear interpolation introduced with the MITC6rs shell finite element seems to constitute an effective cure for rotations. In fact, Tables 7.15-7.21 show that real and pseudo membrane spurious modes participation decreases as compared to Table 7.7 due to the richer shear interpolation and stabilizations described in the previous section. However, some shear stabilization is required in order to obtain reasonably accurate rotations as seen through the A_m norm with shear terms.

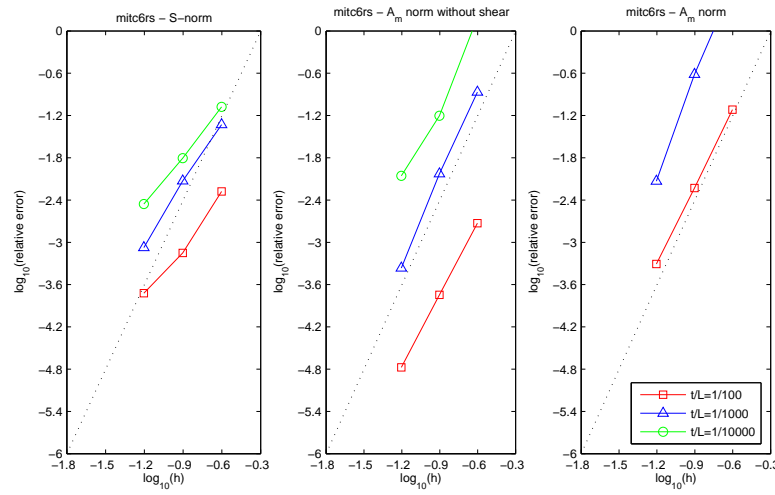


Figure 7.10: Convergence curves associated with the s-norm and membrane energy norm (with shear terms discarded and not) for the trace shell problem and MITC6rs shell finite element. The dotted line shows the optimal convergence rate which is 4.

$\varepsilon = 10^{-2}$		$h = 0.25$	$h = 0.125$	$h = 0.0625$
<i>Total</i>	<i>Reduced</i>	1.635021913e-10	1.637224979e-10	1.637974889e-10
	<i>Unreduced</i>	1.759090233e-10	1.646421809e-10	1.638814606e-10
<i>Bending</i>	<i>Reduced</i>	3.605343637e-12	3.593692015e-12	3.599844862e-12
	<i>Unreduced</i>	3.603556552e-12	3.593051380e-12	3.599588860e-12
<i>Membrane</i>	<i>Reduced</i>	1.596289533e-10	1.600772954e-10	1.601744394e-10
	<i>Unreduced</i>	1.592965003e-10	1.598165208e-10	1.600995429e-10
<i>Shear</i>	<i>Reduced</i>	3.201983301e-13	1.130063444e-13	8.726056607e-14
	<i>Unreduced</i>	1.306058430e-11	1.293395198e-12	2.461619510e-13
$\varepsilon = 10^{-3}$		$h = 0.25$	$h = 0.125$	$h = 0.0625$
<i>Total</i>	<i>Reduced</i>	1.806837990e-09	1.760097200e-09	1.754561635e-09
	<i>Unreduced</i>	9.397820333e-09	2.195723443e-09	1.767374391e-09
<i>Bending</i>	<i>Reduced</i>	3.896378716e-11	2.036254111e-11	1.694937361e-11
	<i>Unreduced</i>	3.882263995e-11	2.036223092e-11	1.694858410e-11
<i>Membrane</i>	<i>Reduced</i>	1.757257106e-09	1.738617918e-09	1.737472152e-09
	<i>Unreduced</i>	2.082000941e-09	1.765208066e-09	1.737992052e-09
<i>Shear</i>	<i>Reduced</i>	1.062044548e-11	1.126388515e-12	1.549427645e-13
	<i>Unreduced</i>	7.276975673e-09	4.101599673e-10	1.244811425e-11
$\varepsilon = 10^{-4}$		$h = 0.25$	$h = 0.125$	$h = 0.0625$
<i>Total</i>	<i>Reduced</i>	1.921282020e-08	1.821352077e-08	1.807090861e-08
	<i>Unreduced</i>	4.901370133e-07	2.125814265e-07	5.629620793e-08
<i>Bending</i>	<i>Reduced</i>	4.475502469e-10	9.282106969e-11	7.068307128e-11
	<i>Unreduced</i>	4.465348622e-10	9.277544576e-11	7.068378890e-11
<i>Membrane</i>	<i>Reduced</i>	1.857114808e-08	1.808832656e-08	1.798830389e-08
	<i>Unreduced</i>	4.846876695e-08	1.948931378e-08	1.821864072e-08
<i>Shear</i>	<i>Reduced</i>	1.941227076e-10	3.237558797e-11	1.192442963e-11
	<i>Unreduced</i>	4.412216709e-07	1.929993335e-07	3.800688467e-08

Table 7.8: *Reduced* and *unreduced* energy values associated with the trace shell problem and MITC6rs triangular shell finite element for different values of ε and h .

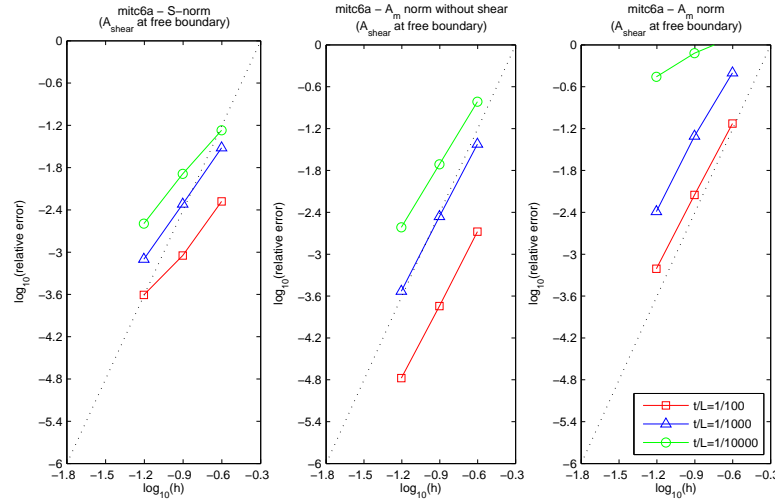


Figure 7.11: Convergence curves associated with the s-norm and membrane energy norm (with shear terms discarded and not) for the trace shell problem and MITC6a shell finite element with free boundary shear stabilization. The dotted line shows the optimal convergence rate which is 4.

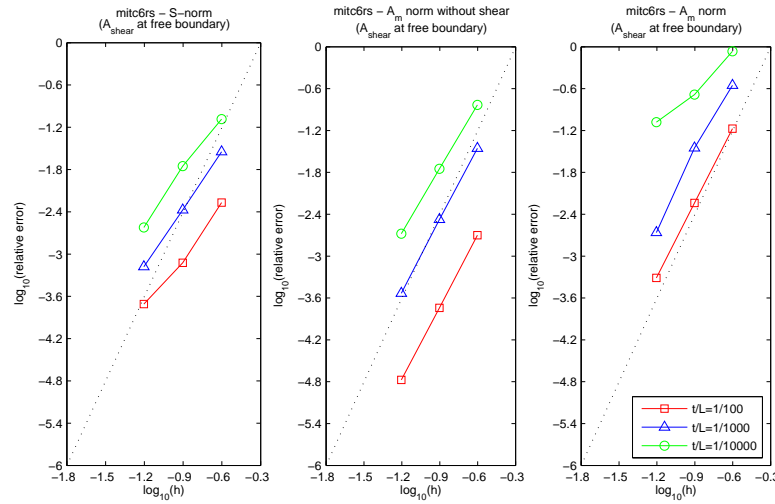


Figure 7.12: Convergence curves associated with the s-norm and membrane energy norm (with shear terms discarded and not) for the trace shell problem and MITC6rs shell finite element with free boundary shear stabilization. The dotted line shows the optimal convergence rate which is 4.

$\varepsilon = 10^{-2}$		$h = 0.25$	$h = 0.125$	$h = 0.0625$
<i>Total</i>	<i>Reduced</i>	1.633601762e-10	1.637271530e-10	1.637999818e-10
	<i>Unreduced</i>	1.753101184e-10	1.648620450e-10	1.639164780e-10
<i>Bending</i>	<i>Reduced</i>	3.507697527e-12	3.586081628e-12	3.605571867e-12
	<i>Unreduced</i>	3.506752398e-12	3.585423214e-12	3.605312598e-12
<i>Membrane</i>	<i>Reduced</i>	1.596377823e-10	1.600850624e-10	1.601759297e-10
	<i>Unreduced</i>	1.592321258e-10	1.598271608e-10	1.601013494e-10
<i>Shear</i>	<i>Reduced</i>	2.660252752e-13	1.167359681e-13	8.214512198e-14
	<i>Unreduced</i>	1.262207118e-11	1.510024264e-12	2.735711800e-13
$\varepsilon = 10^{-3}$		$h = 0.25$	$h = 0.125$	$h = 0.0625$
<i>Total</i>	<i>Reduced</i>	1.775496822e-09	1.755893334e-09	1.754360386e-09
	<i>Unreduced</i>	2.503933994e-09	1.844615291e-09	1.761053942e-09
<i>Bending</i>	<i>Reduced</i>	1.607923274e-11	1.706749935e-11	1.655071067e-11
	<i>Unreduced</i>	1.607301230e-11	1.706561165e-11	1.654977278e-11
<i>Membrane</i>	<i>Reduced</i>	1.756066633e-09	1.737761468e-09	1.737583328e-09
	<i>Unreduced</i>	1.850351775e-09	1.746519593e-09	1.737503943e-09
<i>Shear</i>	<i>Reduced</i>	3.351700217e-12	1.070904036e-12	2.405530697e-13
	<i>Unreduced</i>	6.375043577e-10	8.103504845e-11	7.014172409e-12
$\varepsilon = 10^{-4}$		$h = 0.25$	$h = 0.125$	$h = 0.0625$
<i>Total</i>	<i>Reduced</i>	1.841123017e-08	1.812787703e-08	1.804614312e-08
	<i>Unreduced</i>	4.216392037e-08	3.194534781e-08	2.433079003e-08
<i>Bending</i>	<i>Reduced</i>	5.897865424e-11	5.879548184e-11	6.229033835e-11
	<i>Unreduced</i>	5.897024090e-11	5.879329986e-11	6.229088711e-11
<i>Membrane</i>	<i>Reduced</i>	1.831864338e-08	1.806349475e-08	1.798223651e-08
	<i>Unreduced</i>	2.156380937e-08	1.853967095e-08	1.805242727e-08
<i>Shear</i>	<i>Reduced</i>	3.361060392e-11	5.589285066e-12	1.618385606e-12
	<i>Unreduced</i>	2.054113924e-08	5.879329986e-11	6.216073249e-09

Table 7.9: *Reduced* and *unreduced* energy values associated with the trace shell problem and MITC6a triangular shell finite element with free boundary shear stabilization, for different values of ε and h .

$\varepsilon = 10^{-2}$		$h = 0.25$	$h = 0.125$	$h = 0.0625$
<i>Total</i>	<i>Reduced</i>	1.632990475e-10	1.637103237e-10	1.637963640e-10
	<i>Unreduced</i>	1.739718516e-10	1.645985384e-10	1.638780725e-10
<i>Bending</i>	<i>Reduced</i>	3.432129302e-12	3.581773148e-12	3.599428016e-12
	<i>Unreduced</i>	3.431338553e-12	3.581147424e-12	3.599168065e-12
<i>Membrane</i>	<i>Reduced</i>	1.595644294e-10	1.600693466e-10	1.601733313e-10
	<i>Unreduced</i>	1.591373389e-10	1.598076488e-10	1.600983567e-10
<i>Shear</i>	<i>Reduced</i>	3.539336012e-13	1.201186084e-13	8.731053996e-14
	<i>Unreduced</i>	1.145440539e-11	1.270509104e-12	2.443447934e-13
$\varepsilon = 10^{-3}$		$h = 0.25$	$h = 0.125$	$h = 0.0625$
<i>Total</i>	<i>Reduced</i>	1.772737261e-09	1.755537275e-09	1.754278097e-09
	<i>Unreduced</i>	2.291818473e-09	1.820046926e-09	1.757552159e-09
<i>Bending</i>	<i>Reduced</i>	1.477012763e-11	1.692704358e-11	1.657541417e-11
	<i>Unreduced</i>	1.476416714e-11	1.692606074e-11	1.657472451e-11
<i>Membrane</i>	<i>Reduced</i>	1.753346956e-09	1.737561686e-09	1.737511089e-09
	<i>Unreduced</i>	1.840956284e-09	1.745705448e-09	1.737396199e-09
<i>Shear</i>	<i>Reduced</i>	4.621727138e-12	1.055427679e-12	2.058814018e-13
	<i>Unreduced</i>	4.360940640e-10	5.742074634e-11	3.595253342e-12
$\varepsilon = 10^{-4}$		$h = 0.25$	$h = 0.125$	$h = 0.0625$
<i>Total</i>	<i>Reduced</i>	1.838777548e-08	1.811962961e-08	1.804390612e-08
	<i>Unreduced</i>	3.448101108e-08	2.196073917e-08	1.955875020e-08
<i>Bending</i>	<i>Reduced</i>	5.106969392e-11	5.575985623e-11	6.157074211e-11
	<i>Unreduced</i>	5.106160082e-11	5.575836081e-11	6.157123050e-11
<i>Membrane</i>	<i>Reduced</i>	1.829005629e-08	1.805548167e-08	1.798021231e-08
	<i>Unreduced</i>	2.140838520e-08	1.849700454e-08	1.804201110e-08
<i>Shear</i>	<i>Reduced</i>	4.665206204e-11	8.390700593e-12	2.125335873e-12
	<i>Unreduced</i>	1.302156214e-08	3.407976375e-09	1.455169450e-09

Table 7.10: *Reduced* and *unreduced* energy values associated with the trace shell problem and MITC6rs triangular shell finite element with free boundary shear stabilization, for different values of ε and h .

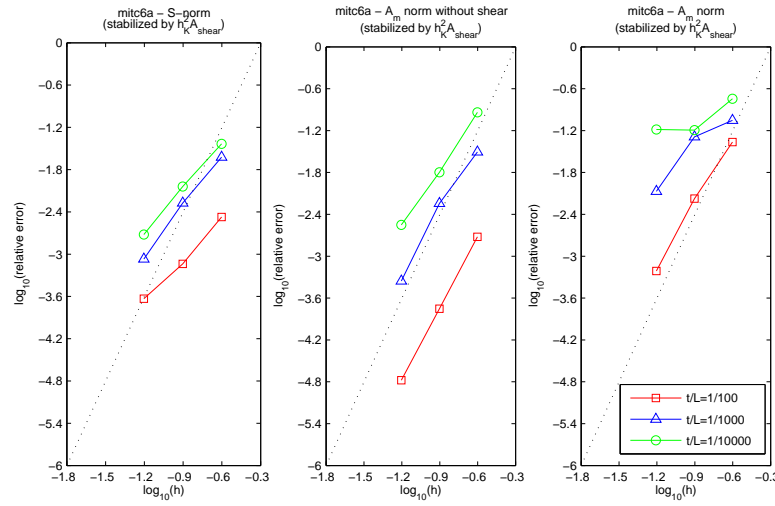


Figure 7.13: Convergence curves associated with the s-norm and membrane energy norm (with shear terms discarded and not) for the trace shell problem and MITC6a shell finite element with weighted shear stabilization ($C = 1$). The dotted line shows the optimal convergence rate which is 4.

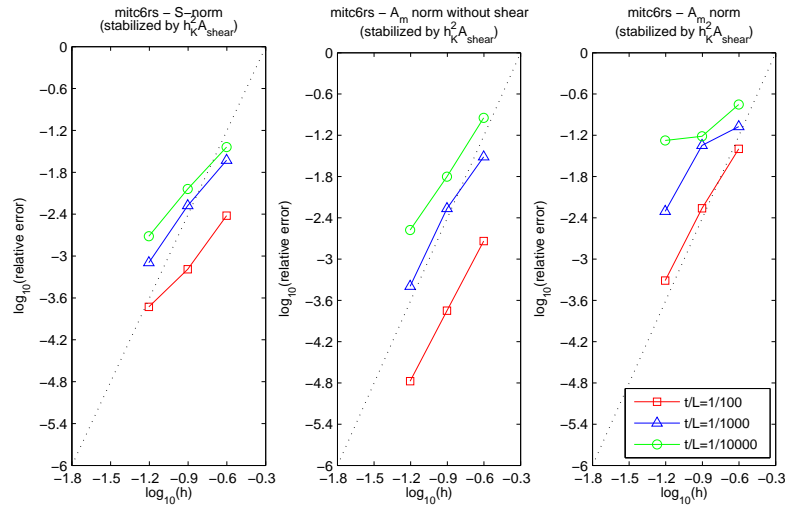


Figure 7.14: Convergence curves associated with the s-norm and membrane energy norm (with shear terms discarded and not) for the trace shell problem and MITC6rs shell finite element with weighted shear stabilization ($C = 1$). The dotted line shows the optimal convergence rate which is 4.

$\varepsilon = 10^{-2}$		$h = 0.25$	$h = 0.125$	$h = 0.0625$
<i>Total</i>	<i>Reduced</i>	1.629299058e-10	1.637189067e-10	1.637996071e-10
	<i>Unreduced</i>	1.692679217e-10	1.647744280e-10	1.639149712e-10
<i>Bending</i>	<i>Reduced</i>	3.116121162e-12	3.580205450e-12	3.605905640e-12
	<i>Unreduced</i>	3.114446847e-12	3.579475663e-12	3.605648683e-12
<i>Membrane</i>	<i>Reduced</i>	1.592728233e-10	1.600778667e-10	1.601757314e-10
	<i>Unreduced</i>	1.587984064e-10	1.598200215e-10	1.601012104e-10
<i>Shear</i>	<i>Reduced</i>	5.948236080e-13	1.221506890e-13	8.194516721e-14
	<i>Unreduced</i>	7.407723674e-12	1.435581070e-12	2.718794874e-13
$\varepsilon = 10^{-3}$		$h = 0.25$	$h = 0.125$	$h = 0.0625$
<i>Total</i>	<i>Reduced</i>	1.766920711e-09	1.757806616e-09	1.754643434e-09
	<i>Unreduced</i>	1.943389707e-09	1.853641822e-09	1.769469978e-09
<i>Bending</i>	<i>Reduced</i>	1.319190922e-11	1.802311495e-11	1.689474962e-11
	<i>Unreduced</i>	1.318470496e-11	1.802288637e-11	1.689411609e-11
<i>Membrane</i>	<i>Reduced</i>	1.744020215e-09	1.737656946e-09	1.737515076e-09
	<i>Unreduced</i>	1.826785181e-09	1.754548218e-09	1.738120093e-09
<i>Shear</i>	<i>Reduced</i>	9.712921257e-12	2.136479733e-12	2.484189680e-13
	<i>Unreduced</i>	1.034173851e-10	8.107848727e-11	1.447011015e-11
$\varepsilon = 10^{-4}$		$h = 0.25$	$h = 0.125$	$h = 0.0625$
<i>Total</i>	<i>Reduced</i>	1.831948476e-08	1.810968939e-08	1.804958523e-08
	<i>Unreduced</i>	2.193549291e-08	1.937358557e-08	1.925334674e-08
<i>Bending</i>	<i>Reduced</i>	3.665373242e-11	5.493334938e-11	6.238788547e-11
	<i>Unreduced</i>	3.664858706e-11	5.492919591e-11	6.238674848e-11
<i>Membrane</i>	<i>Reduced</i>	1.816312265e-08	1.803136928e-08	1.797934449e-08
	<i>Unreduced</i>	2.071651215e-08	1.844578294e-08	1.806664993e-08
<i>Shear</i>	<i>Reduced</i>	1.197113067e-10	2.338995569e-11	7.855884487e-12
	<i>Unreduced</i>	1.182331776e-09	8.728741248e-10	1.124312321e-09

Table 7.11: *Reduced* and *unreduced* energy values associated with the trace shell problem and MITC6a triangular shell finite element with weighted shear stabilization ($C = 1$), for different values of ε and h .

$\varepsilon = 10^{-2}$		$h = 0.25$	$h = 0.125$	$h = 0.0625$
<i>Total</i>	<i>Reduced</i>	1.629004939e-10	1.637031302e-10	1.637967966e-10
	<i>Unreduced</i>	1.686877751e-10	1.645277880e-10	1.638789514e-10
<i>Bending</i>	<i>Reduced</i>	3.079385004e-12	3.574981499e-12	3.599421984e-12
	<i>Unreduced</i>	3.077996651e-12	3.574353206e-12	3.599421984e-12
<i>Membrane</i>	<i>Reduced</i>	1.592322263e-10	1.600643807e-10	1.601739863e-10
	<i>Unreduced</i>	1.587526909e-10	1.598030754e-10	1.600990904e-10
<i>Shear</i>	<i>Reduced</i>	6.427193532e-13	1.252812923e-13	8.743158755e-14
	<i>Unreduced</i>	6.909857719e-12	1.211218171e-12	2.445303448e-13
$\varepsilon = 10^{-3}$		$h = 0.25$	$h = 0.125$	$h = 0.0625$
<i>Total</i>	<i>Reduced</i>	1.766357495e-09	1.757495558e-09	1.754516294e-09
	<i>Unreduced</i>	1.935205909e-09	1.841895520e-09	1.763032118e-09
<i>Bending</i>	<i>Reduced</i>	1.322074614e-11	1.798234286e-11	1.688706316e-11
	<i>Unreduced</i>	1.321384641e-11	1.798234286e-11	1.688634089e-11
<i>Membrane</i>	<i>Reduced</i>	1.743832001e-09	1.737518769e-09	1.737460645e-09
	<i>Unreduced</i>	1.824510313e-09	1.753509944e-09	1.737888650e-09
<i>Shear</i>	<i>Reduced</i>	9.309031691e-12	2.004395283e-12	1.834167800e-13
	<i>Unreduced</i>	9.747928480e-11	7.041215514e-11	8.271505738e-12
$\varepsilon = 10^{-4}$		$h = 0.25$	$h = 0.125$	$h = 0.0625$
<i>Total</i>	<i>Reduced</i>	1.831388743e-08	1.810874832e-08	1.804851188e-08
	<i>Unreduced</i>	2.186308524e-08	1.931584803e-08	1.903130899e-08
<i>Bending</i>	<i>Reduced</i>	3.547862285e-11	5.484359878e-11	6.232919503e-11
	<i>Unreduced</i>	3.547402033e-11	5.484011362e-11	6.232826458e-11
<i>Membrane</i>	<i>Reduced</i>	1.815602432e-08	1.803075522e-08	1.797876401e-08
	<i>Unreduced</i>	2.066027283e-08	1.844129384e-08	1.806169596e-08
<i>Shear</i>	<i>Reduced</i>	1.223873364e-10	2.315267906e-11	7.421720118e-12
	<i>Unreduced</i>	1.167337988e-09	8.197147589e-10	9.072870509e-10

Table 7.12: *Reduced* and *unreduced* energy values associated with the trace shell problem and MITC6rs triangular shell finite element with weighted shear stabilization ($C = 1$), for different values of ε and h .

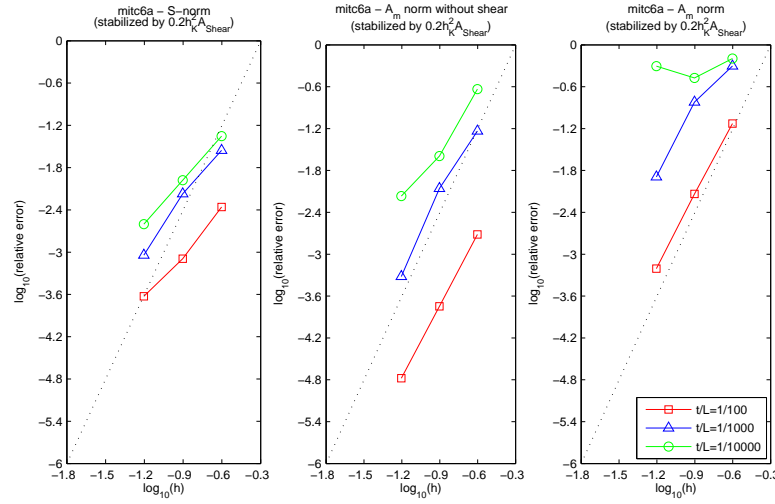


Figure 7.15: Convergence curves associated with the s-norm and membrane energy norm (with shear terms discarded and not) for the trace shell problem and MITC6a shell finite element with weighted shear stabilization ($C = 1/5$). The dotted line shows the optimal convergence rate which is 4.

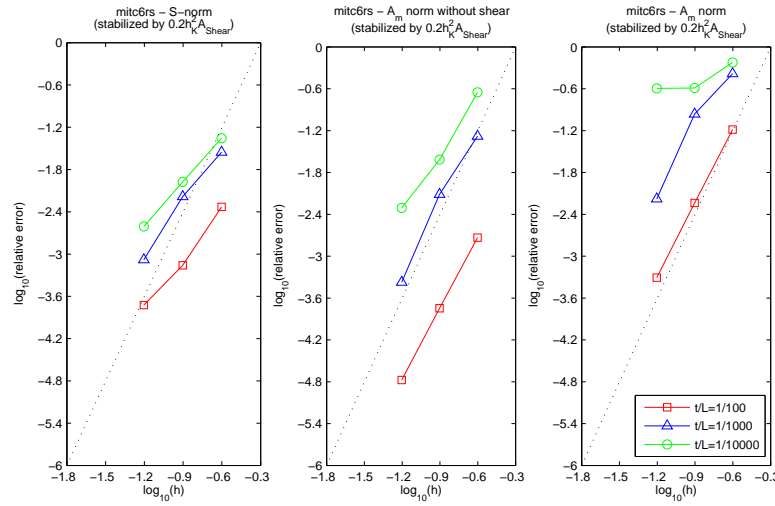


Figure 7.16: Convergence curves associated with the s-norm and membrane energy norm (with shear terms discarded and not) for the trace shell problem and MITC6rs shell finite element with weighted shear stabilization ($C = 1/5$). The dotted line shows the optimal convergence rate which is 4.

$\varepsilon = 10^{-2}$		$h = 0.25$	$h = 0.125$	$h = 0.0625$
<i>Total</i>	<i>Reduced</i>	1.634167127e-10	1.637378142e-10	1.638002851e-10
	<i>Unreduced</i>	1.754131028e-10	1.649215515e-10	1.639180827e-10
<i>Bending</i>	<i>Reduced</i>	3.517115582e-12	3.597612866e-12	3.606410919e-12
	<i>Unreduced</i>	3.514638597e-12	3.596869988e-12	3.606153684e-12
<i>Membrane</i>	<i>Reduced</i>	1.595991940e-10	1.600904828e-10	1.601761674e-10
	<i>Unreduced</i>	1.592542817e-10	1.598340535e-10	1.601016606e-10
<i>Shear</i>	<i>Reduced</i>	3.529579247e-13	1.109940079e-13	8.169106775e-14
	<i>Unreduced</i>	1.269572240e-11	1.551194036e-12	2.740324803e-13

$\varepsilon = 10^{-3}$		$h = 0.25$	$h = 0.125$	$h = 0.0625$
<i>Total</i>	<i>Reduced</i>	1.783609216e-09	1.759839543e-09	1.754707951e-09
	<i>Unreduced</i>	2.711204074e-09	2.035639438e-09	1.777157301e-09
<i>Bending</i>	<i>Reduced</i>	1.864982304e-11	1.960731251e-11	1.696158280e-11
	<i>Unreduced</i>	1.861054901e-11	1.960870928e-11	1.696088603e-11
<i>Membrane</i>	<i>Reduced</i>	1.749986677e-09	1.738575148e-09	1.737535367e-09
	<i>Unreduced</i>	1.903483341e-09	1.763520093e-09	1.738273032e-09
<i>Shear</i>	<i>Reduced</i>	1.497713278e-11	1.666991343e-12	2.258158857e-13
	<i>Unreduced</i>	7.891049331e-10	2.525178758e-10	2.193770128e-11

$\varepsilon = 10^{-4}$		$h = 0.25$	$h = 0.125$	$h = 0.0625$
<i>Total</i>	<i>Reduced</i>	1.850529435e-08	1.814719913e-08	1.806434766e-08
	<i>Unreduced</i>	3.061264600e-08	2.436271577e-08	2.700908478e-08
<i>Bending</i>	<i>Reduced</i>	5.931713173e-11	6.467456319e-11	6.602949826e-11
	<i>Unreduced</i>	5.928995048e-11	6.465476227e-11	6.602911630e-11
<i>Membrane</i>	<i>Reduced</i>	1.829126268e-08	1.805219375e-08	1.798613096e-08
	<i>Unreduced</i>	2.318493891e-08	1.869064257e-08	1.816939314e-08
<i>Shear</i>	<i>Reduced</i>	1.547176342e-10	3.033399740e-11	1.219019422e-11
	<i>Unreduced</i>	7.368413694e-09	5.607418501e-09	8.773664388e-09

Table 7.13: *Reduced* and *unreduced* energy values associated with the trace shell problem and MITC6a triangular shell finite element with weighted shear stabilization ($C = 1/5$), for different values of ε and h .

$\varepsilon = 10^{-2}$		$h = 0.25$	$h = 0.125$	$h = 0.0625$
<i>Total</i>	<i>Reduced</i>	1.633461959e-10	1.637185169e-10	1.637973500e-10
	<i>Unreduced</i>	1.737587826e-10	1.646182887e-10	1.638809565e-10
<i>Bending</i>	<i>Reduced</i>	3.441283922e-12	3.589765136e-12	3.599759822e-12
	<i>Unreduced</i>	3.439657665e-12	3.589127113e-12	3.599504002e-12
<i>Membrane</i>	<i>Reduced</i>	1.595275002e-10	1.600746445e-10	1.601743486e-10
	<i>Unreduced</i>	1.591513162e-10	1.598137585e-10	1.600994522e-10
<i>Shear</i>	<i>Reduced</i>	4.300951878e-13	1.156071206e-13	8.729507131e-14
	<i>Unreduced</i>	1.121969747e-11	1.276204360e-12	2.458340418e-13
$\varepsilon = 10^{-3}$		$h = 0.25$	$h = 0.125$	$h = 0.0625$
<i>Total</i>	<i>Reduced</i>	1.781209171e-09	1.759156666e-09	1.754551044e-09
	<i>Unreduced</i>	2.554480208e-09	1.959260659e-09	1.766072792e-09
<i>Bending</i>	<i>Reduced</i>	1.820090796e-11	1.935530921e-11	1.693376878e-11
	<i>Unreduced</i>	1.816273700e-11	1.935502922e-11	1.693299749e-11
<i>Membrane</i>	<i>Reduced</i>	1.749028311e-09	1.738277287e-09	1.737469574e-09
	<i>Unreduced</i>	1.889267527e-09	1.760432020e-09	1.737966622e-09
<i>Shear</i>	<i>Reduced</i>	1.398424033e-11	1.533977308e-12	1.625356590e-13
	<i>Unreduced</i>	6.470448984e-10	1.794810569e-10	1.118753776e-11
$\varepsilon = 10^{-4}$		$h = 0.25$	$h = 0.125$	$h = 0.0625$
<i>Total</i>	<i>Reduced</i>	1.849133484e-08	1.814105205e-08	1.805832592e-08
	<i>Unreduced</i>	2.987135963e-08	2.294292507e-08	2.267392932e-08
<i>Bending</i>	<i>Reduced</i>	5.745279518e-11	6.401862307e-11	6.484440624e-11
	<i>Unreduced</i>	5.743020548e-11	6.400156748e-11	6.484363155e-11
<i>Membrane</i>	<i>Reduced</i>	1.828386907e-08	1.804955668e-08	1.798338090e-08
	<i>Unreduced</i>	2.300676253e-08	1.865496005e-08	1.812282959e-08
<i>Shear</i>	<i>Reduced</i>	1.500159485e-10	2.747993082e-11	1.010365014e-11
	<i>Unreduced</i>	6.807163537e-09	4.223963582e-09	4.486258166e-09

Table 7.14: *Reduced* and *unreduced* energy values associated with the trace shell problem and MITC6rs triangular shell finite element with weighted shear stabilization ($C = 1/5$), for different values of ε and h .

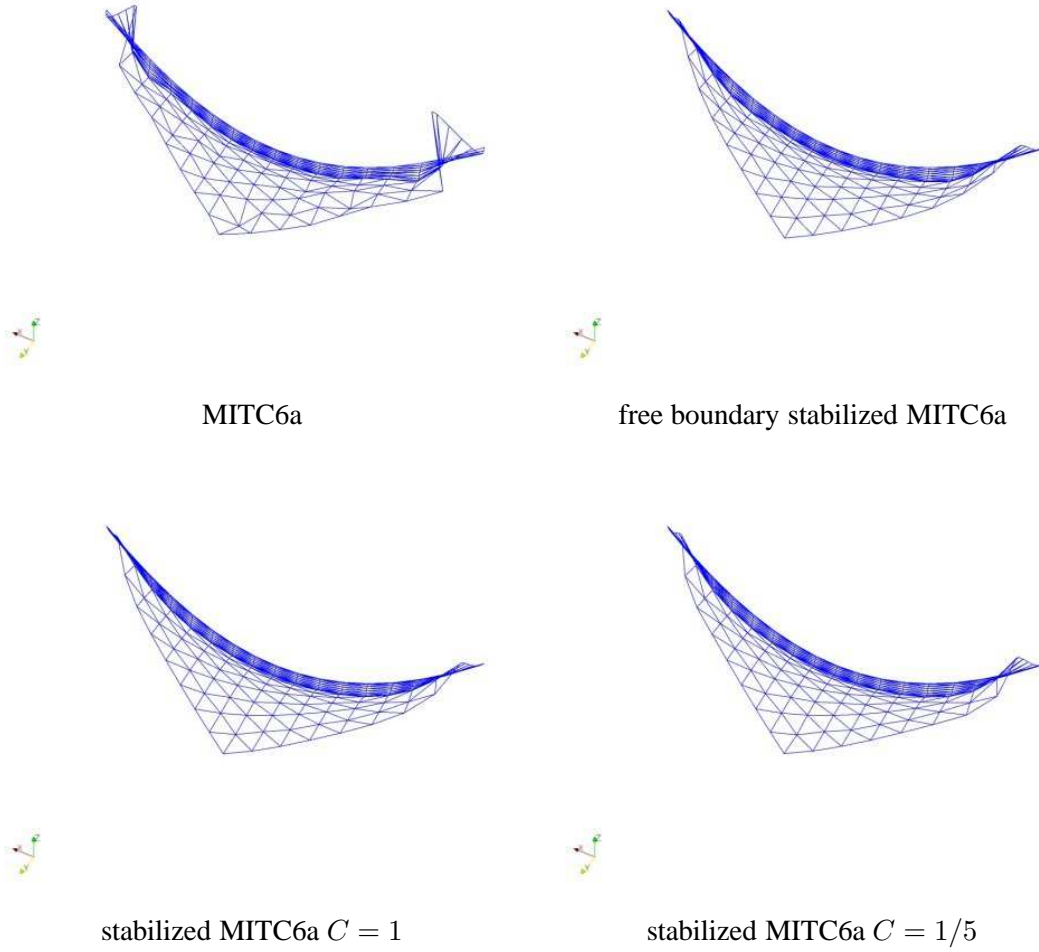


Figure 7.17: Deformed midsurfaces for the trace shell problem: MITC6a (top left), MITC6a with free boundary shear stabilization (top right), MITC6a with weighted shear stabilization for $C = 1$ (bottom left), and MITC6a with weighted shear stabilization for $C = 1/5$ (bottom right) ($\varepsilon = 10^{-4}$, 217 nodes, 96 elements, $scale = 1 \times 10^6$).

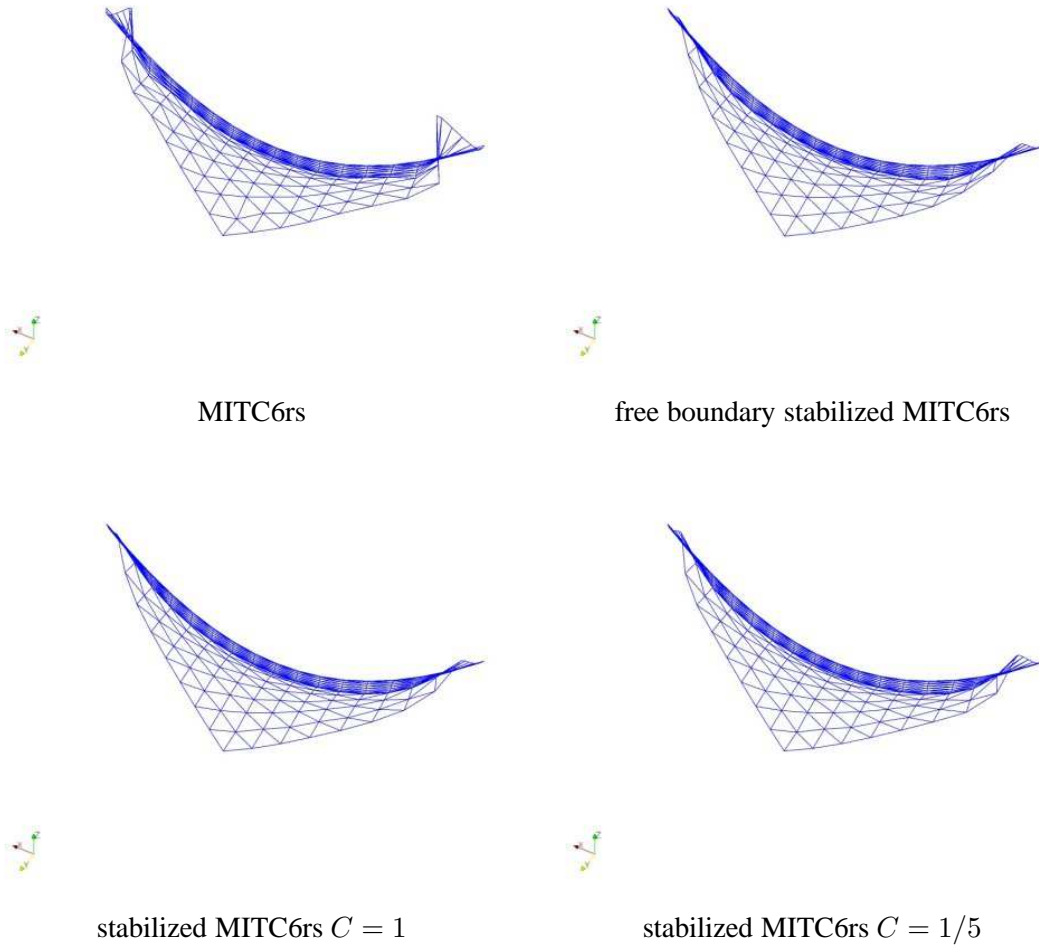


Figure 7.18: Deformed midsurfaces for the trace shell problem: MITC6rs (top left), MITC6rs with free boundary shear stabilization (top right), MITC6rs with weighted shear stabilization for $C = 1$ (bottom left), and MITC6rs with weighted shear stabilization for $C = 1/5$ (bottom right) ($\varepsilon = 10^{-4}$, 217 nodes, 96 elements, $scale = 1 \times 10^6$).

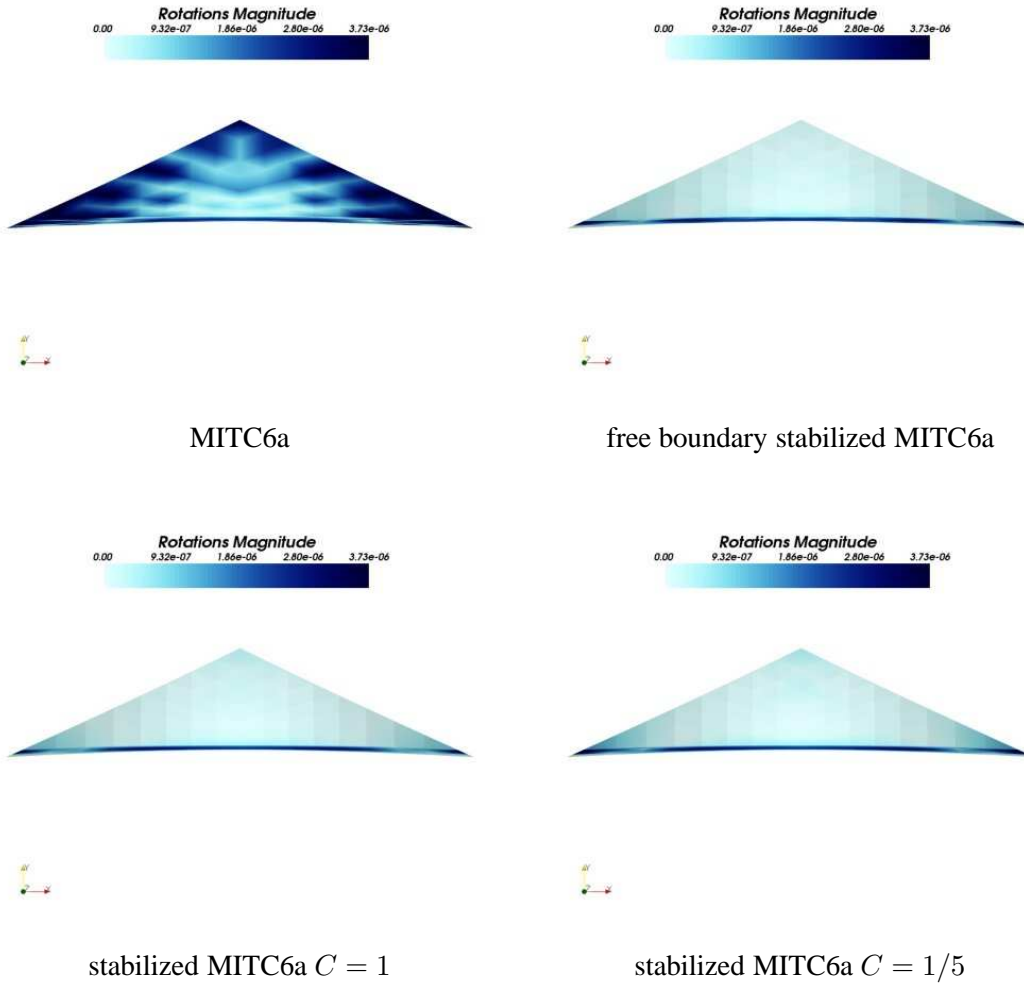


Figure 7.19: Magnitude of the rotation field for the trace shell problem: MITC6a (top left), MITC6a with free boundary shear stabilization (top right), MITC6a with weighted shear stabilization for $C = 1$ (bottom left), and MITC6a with weighted shear stabilization for $C = 1/5$ (bottom right) ($\varepsilon = 10^{-4}$, 217 nodes, 96 elements).

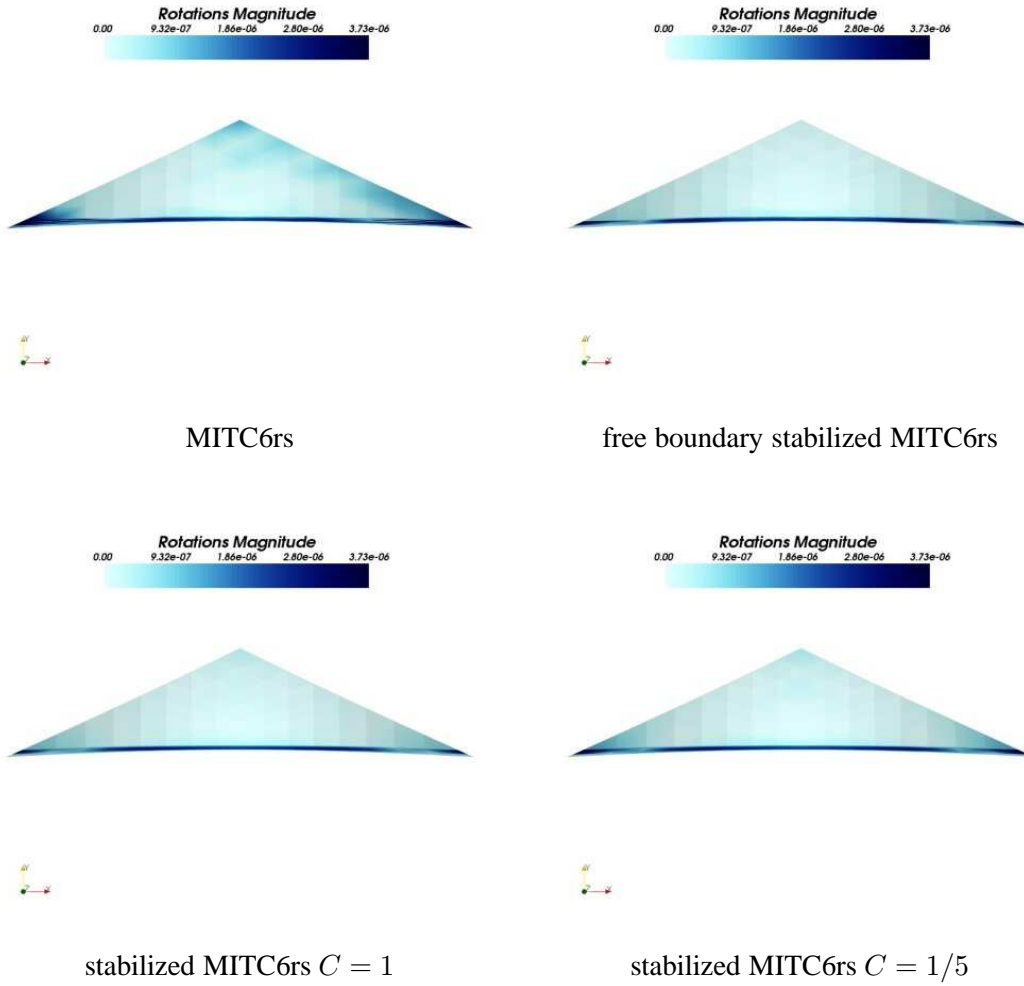


Figure 7.20: Magnitude of the rotation field for the trace shell problem: MITC6rs (top left), MITC6rs with free boundary shear stabilization (top right), MITC6rs with weighted shear stabilization for $C = 1$ (bottom left), and MITC6rs with weighted shear stabilization for $C = 1/5$ (bottom right) ($\varepsilon = 10^{-4}$, 217 nodes, 96 elements).

REAL SPURIOUS MODES

	τ^h eigenvalue	Participation
1)	-2.14107040e-01	0.0100762488
2)	+3.152754788e-01	0.0186516959
3)	-3.531140194e-01-5.993849236e-01i	0.0011439610
4)	-3.531140194e-01+5.993849236e-01i	0.0011439610
5)	-6.881664483e-01	0.0114256791
6)	+1.147225780e+00	0.0144702340
7)	+1.182723110e+00	0.0067126782
8)	-2.768167247e+00	0.0115901655
9)	+3.124928814e+00	0.0160628511
10)	+6.035838534e+00-7.455315727e+00i	0.0118469294
11)	+6.035838534e+00+7.455315727e+00i	0.0118469294
12)	-7.237805134e+00-5.129190596e+00i	0.0063471413
13)	-7.237805134e+00+5.129190596e+00i	0.0063471413
14)	+5.938763425e+00	0.0135249447
15)	-1.197590040e+01	0.0021889740
16)	+5.921453413e+00	0.0039670052

PSEUDO SPURIOUS MODES

	τ^h eigenvalue	Participation
17)	+1.703368333e+10	0.0210386511
18)	+2.078488522e+10	0.0020808088
19)	+2.437612651e+10	0.0144341897
20)	+3.536831385e+10	0.0129858719
21)	+5.953031659e+10	0.0070800150
22)	+1.190260989e+11	0.0716058204
23)	+1.485547410e+11	0.0995854150
24)	+1.635624588e+11	0.0340277875

Table 7.15: MITC6a *real* and *pseudo membrane spurious modes* participation into the free boundary shear stabilized MITC6a solution for the trace shell problem ($\varepsilon = 10^{-4}$, mesh containing 96 elements and 217 nodes, boundary layer of width $3\sqrt{\varepsilon}L$).

REAL SPURIOUS MODES

	τ^h eigenvalue	Participation
1)	-2.14107040e-01	0.0018856245
2)	+3.152754788e-01	0.0469217366
3)	-3.531140194e-01-5.993849236e-01i	0.0024072807
4)	-3.531140194e-01+5.993849236e-01i	0.0024072807
5)	-6.881664483e-01	0.0200893518
6)	+1.147225780e+00	0.0009845880
7)	+1.182723110e+00	0.0540947859
8)	-2.768167247e+00	0.0241734566
9)	+3.124928814e+00	0.0083884493
10)	+6.035838534e+00-7.455315727e+00i	0.0094377041
11)	+6.035838534e+00+7.455315727e+00i	0.0094377041
12)	-7.237805134e+00-5.129190596e+00i	0.0215077282
13)	-7.237805134e+00+5.129190596e+00i	0.0215077282
14)	+5.938763425e+00	0.0012382464
15)	-1.197590040e+01	0.0211585790
16)	+5.921453413e+00	0.0121518772

PSEUDO SPURIOUS MODES

	τ^h eigenvalue	Participation
17)	+1.703368333e+10	0.0406437651
18)	+2.078488522e+10	0.0084436813
19)	+2.437612651e+10	0.0283641086
20)	+3.536831385e+10	0.0063956480
21)	+5.953031659e+10	0.0112092602
22)	+1.190260989e+11	0.0009938034
23)	+1.485547410e+11	0.0028556174
24)	+1.635624588e+11	0.0020128537

Table 7.16: MITC6a *real* and *pseudo membrane spurious modes* participation into the weighted shear stabilized MITC6a solution with $C = 1$ for the trace shell problem ($\varepsilon = 10^{-4}$, mesh containing 96 elements and 217 nodes, boundary layer of width $3\sqrt{\varepsilon}L$).

REAL SPURIOUS MODES

	τ^h eigenvalue	Participation
1)	-2.14107040e-01	0.0198333277
2)	+3.152754788e-01	0.1174154818
3)	-3.531140194e-01-5.993849236e-01i	0.0506682253
4)	-3.531140194e-01+5.993849236e-01i	0.0506682253
5)	-6.881664483e-01	0.0552305720
6)	+1.147225780e+00	0.0086569534
7)	+1.182723110e+00	0.1364522493
8)	-2.768167247e+00	0.0642318896
9)	+3.124928814e+00	0.0270996155
10)	+6.035838534e+00-7.455315727e+00i	0.0432876912
11)	+6.035838534e+00+7.455315727e+00i	0.0432876912
12)	-7.237805134e+00-5.129190596e+00i	0.0690953710
13)	-7.237805134e+00+5.129190596e+00i	0.0690953710
14)	+5.938763425e+00	0.0007591425
15)	-1.197590040e+01	0.0673195570
16)	+5.921453413e+00	0.0513530038

PSEUDO SPURIOUS MODES

	τ^h eigenvalue	Participation
17)	+1.703368333e+10	0.0752867279
18)	+2.078488522e+10	0.0018284529
19)	+2.437612651e+10	0.1144907012
20)	+3.536831385e+10	0.0258661196
21)	+5.953031659e+10	0.0130367414
22)	+1.190260989e+11	0.0218687985
23)	+1.485547410e+11	0.0263420157
24)	+1.635624588e+11	0.0037170449

Table 7.17: MITC6a *real* and *pseudo membrane spurious modes* participation into the weighted shear stabilized MITC6a solution with $C = 1/5$ for the trace shell problem ($\varepsilon = 10^{-4}$, mesh containing 96 elements and 217 nodes, boundary layer of width $3\sqrt{\varepsilon}L$).

REAL SPURIOUS MODES

	τ^h eigenvalue	Participation
1)	-2.141070404e-01	0.1152055247
2)	+3.152754788e-01	0.2942484951
3)	-3.531140194e-01-5.993849236e-01i	0.1371102874
4)	-3.531140194e-01+5.993849236e-01i	0.1371102874
5)	-6.881664483e-01	0.2246301563
6)	+1.147225780e+00	0.0938559384
7)	+1.182723110e+00	0.3542600575
8)	-2.768167247e+00	0.0737395853
9)	+3.124928814e+00	0.0113420338
10)	+6.035838534e+00-7.455315727e+00i	0.2005191446
11)	+6.035838534e+00+7.455315727e+00i	0.2005191446
12)	-7.237805134e+00-5.129190596e+00i	0.0190786001
13)	-7.237805134e+00+5.129190596e+00i	0.0190786001
14)	+5.938763425e+00	0.0045257473
15)	-1.197590040e+01	0.0316200151
16)	+5.921453413e+00	0.2340152543

PSEUDO SPURIOUS MODES

	τ^h eigenvalue	Participation
17)	+1.703368333e+10	0.1892062729
18)	+2.078488522e+10	0.0275578135
19)	+2.437612651e+10	0.2127773292
20)	+3.536831385e+10	0.1387751144
21)	+5.953031659e+10	0.0415364779
22)	+1.190260989e+11	0.0037407075
23)	+1.485547410e+11	0.1535663819
24)	+1.635624588e+11	0.0035377157

Table 7.18: MITC6rs *real* and *pseudo membrane spurious modes* participation into the MITC6rs solution for the trace shell problem ($\varepsilon = 10^{-4}$, mesh containing 96 elements and 217 nodes, boundary layer of width $3\sqrt{\varepsilon}L$).

REAL SPURIOUS MODES

	τ^h eigenvalue	Participation
1)	-2.14107040e-01	0.0056993159
2)	+3.152754788e-01	0.0197078451
3)	-3.531140194e-01-5.993849236e-01i	0.0043863300
4)	-3.531140194e-01+5.993849236e-01i	0.0043863300
5)	-6.881664483e-01	0.0156491296
6)	+1.147225780e+00	0.0080998604
7)	+1.182723110e+00	0.0279091121
8)	-2.768167247e+00	0.0190860237
9)	+3.124928814e+00	0.0135824918
10)	+6.035838534e+00-7.455315727e+00i	0.0144872145
11)	+6.035838534e+00+7.455315727e+00i	0.0144872145
12)	-7.237805134e+00-5.129190596e+00i	0.0022125400
13)	-7.237805134e+00+5.129190596e+00i	0.0022125400
14)	+5.938763425e+00	0.0061004189
15)	-1.197590040e+01	0.0274855091
16)	+5.921453413e+00	0.0030226202

PSEUDO SPURIOUS MODES

	τ^h eigenvalue	Participation
17)	+1.703368333e+10	0.0435566048
18)	+2.078488522e+10	0.0019519675
19)	+2.437612651e+10	0.0117787631
20)	+3.536831385e+10	0.0193261848
21)	+5.953031659e+10	0.0020708717
22)	+1.190260989e+11	0.0303314954
23)	+1.485547410e+11	0.0929330521
24)	+1.635624588e+11	0.0249323392

Table 7.19: MITC6rs *real* and *pseudo membrane spurious modes* participation into the free boundary shear stabilized MITC6rs solution for the trace shell problem ($\varepsilon = 10^{-4}$, mesh containing 96 elements and 217 nodes, boundary layer of width $3\sqrt{\varepsilon}L$).

REAL SPURIOUS MODES

	τ^h eigenvalue	Participation
1)	-2.14107040e-01	0.0005850832
2)	+3.152754788e-01	0.0444835861
3)	-3.531140194e-01-5.993849236e-01i	0.0128988579
4)	-3.531140194e-01+5.993849236e-01i	0.0128988579
5)	-6.881664483e-01	0.0180459190
6)	+1.147225780e+00	0.0022547108
7)	+1.182723110e+00	0.0523230102
8)	-2.768167247e+00	0.0226928996
9)	+3.124928814e+00	0.0102122566
10)	+6.035838534e+00-7.455315727e+00i	0.0085545048
11)	+6.035838534e+00+7.455315727e+00i	0.0085545048
12)	-7.237805134e+00-5.129190596e+00i	0.0061861223
13)	-7.237805134e+00+5.129190596e+00i	0.0061861223
14)	+5.938763425e+00	0.0002412823
15)	-1.197590040e+01	0.0178782381
16)	+5.921453413e+00	0.0096203802

PSEUDO SPURIOUS MODES

	τ^h eigenvalue	Participation
17)	+1.703368333e+10	0.0386454662
18)	+2.078488522e+10	0.0061637568
19)	+2.437612651e+10	0.0281852564
20)	+3.536831385e+10	0.0031558180
21)	+5.953031659e+10	0.0120545490
22)	+1.190260989e+11	0.0016813810
23)	+1.485547410e+11	0.0016744875
24)	+1.635624588e+11	0.0021352172

Table 7.20: MITC6rs *real* and *pseudo membrane spurious modes* participation into the weighted shear stabilized MITC6rs solution with $C' = 1$ for the trace shell problem ($\varepsilon = 10^{-4}$, mesh containing 96 elements and 217 nodes, boundary layer of width $3\sqrt{\varepsilon}L$).

REAL SPURIOUS MODES

	τ^h eigenvalue	Participation
1)	-2.141070404e-01	0.0134353048
2)	+3.152754788e-01	0.1165466038
3)	-3.531140194e-01-5.993849236e-01i	0.0570103346
4)	-3.531140194e-01+5.993849236e-01i	0.0570103346
5)	-6.881664483e-01	0.0547644989
6)	+1.147225780e+00	0.0040072424
7)	+1.182723110e+00	0.1338886875
8)	-2.768167247e+00	0.0573312541
9)	+3.124928814e+00	0.0321339421
10)	+6.035838534e+00-7.455315727e+00i	0.0014150355
11)	+6.035838534e+00+7.455315727e+00i	0.0014150355
12)	-7.237805134e+00-5.129190596e+00i	0.0607839217
13)	-7.237805134e+00+5.129190596e+00i	0.0607839217
14)	+5.938763425e+00	0.0054727514
15)	-1.197590040e+01	0.0574719658
16)	+5.921453413e+00	0.0476706566

PSEUDO SPURIOUS MODES

	τ^h eigenvalue	Participation
17)	+1.703368333e+10	0.0728885353
18)	+2.078488522e+10	0.0072809827
19)	+2.437612651e+10	0.1118405661
20)	+3.536831385e+10	0.0448880478
21)	+5.953031659e+10	0.0145888971
22)	+1.190260989e+11	0.0189728146
23)	+1.485547410e+11	0.0140987181
24)	+1.635624588e+11	0.0058648327

Table 7.21: MITC6rs *real* and *pseudo membrane spurious modes* participation into the weighted shear stabilized MITC6rs solution with $C = 1/5$ for the trace shell problem ($\varepsilon = 10^{-4}$, mesh containing 96 elements and 217 nodes, boundary layer of width $3\sqrt{\varepsilon}L$).

7.5 Axisymmetric hyperboloid

We consider the axisymmetric hyperboloid of uniform thickness t and length $2L$ introduced in Section 6.3.3 and displayed in Fig. 7.21. This particular geometry was carefully chosen given that two non-zero principal curvatures of opposite signs exist, no corner singularities are present –which means that no special grading other than boundary layers capturing is necessary– and the two fundamental asymptotic behaviors with well-posed limit problems can be reached by changing the boundary conditions. The loading imposed is the smoothly varying periodic pressure normal to the midsurface given by:

$$p(\varphi) = p_0 \cos(2\varphi) \quad (7.33)$$

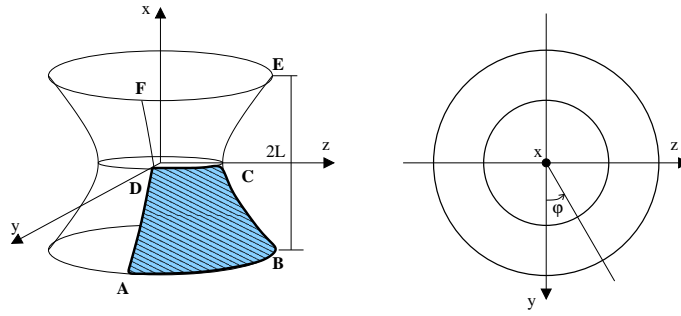


Figure 7.21: Axisymmetric hyperboloid shell problem loaded by smoothly varying periodic pressure normal to the surface ($L = 1.0$, $E = 2.0 \times 10^{11}$, $\nu = 1/3$ and $p_0 = 1.0$).

Two different asymptotic behaviors are observed depending on boundary conditions: a *membrane dominated* behavior is asymptotically obtained when the hyperboloid is fully clamped or clamped at the bottom and free at the top; on the other hand, when both ends are free the asymptotic behavior corresponds to a *bending-dominated* framework.

When boundary conditions are the same at the top and the bottom, the analysis can be restricted to the $ABCD$ domain shown in Fig. 7.21, which represents one eighth of the whole structure, the following symmetry conditions being imposed:

$$u_x = \alpha_2 = 0 \quad \text{along } CD \quad (7.34)$$

$$u_y = \alpha_1 = 0 \quad \text{along } BC \quad (7.35)$$

$$u_z = \alpha_1 = 0 \quad \text{along } AD \quad (7.36)$$

For the *clamped case* we must also set:

$$u_x = u_y = u_z = \alpha_1 = \alpha_2 = 0 \quad \text{along } AB \quad (7.37)$$

When the hyperboloid is half-clamped –namely clamped at the bottom and free at the top– only one fourth of the structure must be considered –the $ABEF$ area in Fig. 6.56– and symmetry and clamped conditions are set as follows:

$$u_y = \alpha_1 = 0 \quad \text{along } BE \quad (7.38)$$

$$u_z = \alpha_1 = 0 \quad \text{along } AF \quad (7.39)$$

$$u_x = u_y = u_z = \alpha_1 = \alpha_2 = 0 \quad \text{along } AB \quad (7.40)$$

Boundary layers must be appropriately meshed in order to obtain accurate results. In all cases –free, fully and bottom clamped– it is known that boundary layers are present, and their width is of order $\sqrt{\varepsilon}L$.

For the clamped cases, the boundary layer was numerically identified to be of width $6\sqrt{\varepsilon}L$. The sequence of meshes was constructed as follows:

- $N + 1$ (axial direction) by $2N + 1$ (circumferential direction) vertices outside of the boundary layer area for the fully clamped shell problem, and $2N + 1$ (axial direction) by $2N + 1$ (circumferential direction) vertices outside of the boundary layer area for the bottom clamped shell problem;
- $N_{BL}(\varepsilon) + 1$ (axial) by $2N + 1$ (circumferential) vertices into the boundary layer area, where $N_{BL}(\varepsilon) \sim N\varepsilon^{-1/4}$ (refer to Table 6.17 and Fig. 6.57).

Naturally, the P_2 displacement-based shell finite element is taken as reference for the error computations. We refer the reader to Appendix E for more details on boundary layer treatment.

When both ends are free, the boundary layer was estimated to be of width $0.5\sqrt{\varepsilon}L$ (see [31]) and the meshing strategy used is described as follows: $2N + 1$ (axial direction) by $2N + 1$ (circumferential direction) vertices for the area outside of the boundary layers and $N + 1$ (axial) by $2N + 1$ (circumferential) vertices for the boundary layer area (taking $N = 2, 4, 8, 16$). The reference meshes were constructed by the same strategy using the MITC4⁶ shell finite element –which does not seem to suffer from locking in this case– for $N = 32$.

7.5.1 Fully clamped hyperboloid shell problem

Displacements and strains are well predicted by P_2 displacement-based shell finite elements, respectively seen by means of the A_m norm –shear terms being discarded or not– and the s -norm (refer to Fig. 7.23). Uniform and optimal convergence rate is achieved.

Total and partial energy values associated with the reference and P_2 target solutions are displayed in Table 7.25. It confirms that the asymptotic behavior of the structure is membrane-dominated: shear and bending energies vanish as thickness decreases, whereas the membrane energy becomes dominant and it can be scaled by a factor of ε . Given a thickness value, energy values converge as the mesh is

⁶Described in Appendix A.

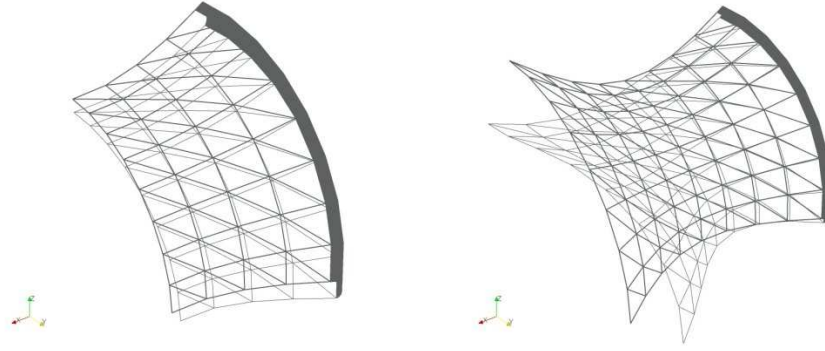


Figure 7.22: Undeformed (thickest plots) and expected deformed midsurface graphs for the fully clamped (figure on the left, $scale = 1 \times 10^6$) and the bottom clamped (figure on the right, $scale = 5 \times 10^5$) hyperboloid shell problems ($\varepsilon = 10^{-4}$, $N = 4$, $N_{BL} = 40$, boundary layer of width $6\sqrt{\varepsilon}L$).

refined. Such behavior is expected because the P_2 general shell finite element gives the subspace of inextensional discretized displacements exactly reduced to $\{0\}$ for this particular shell problem.

Real spurious membrane modes do not exist in this framework. In fact, the smallest modulus eigenvalues associated with the reduced membrane A_m^h are slightly smaller than those ones associated with A_m , the unreduced membrane bilinear form⁷ (refer to Table 7.22). In spite of that, the original A_m norm convergence curves associated with the MITC6a and MITC6rs elements (when shear terms are not discarded) are not good for small relative thickness values due to not admissible relative errors (see Fig. 7.24-7.25). By contrast, midsurface displacements *per se* remain well predicted as seen by the A_m norm without shear terms, which means that the original A_m norm large errors come from rotations. The A_m norm without shear convergence curves associated with the MITC6a shell finite element rise when $\varepsilon \ll 1$, whereas the MITC6rs shell finite element shows a better convergence, rather uniform and optimal. On the other hand, strains are rather well predicted by both shell elements as seen by means of the s -norm, and it is the MITC6rs shell finite element which provides better strains for small relative thickness.

Reduced and unreduced energy values are summarized in Tables 7.26-7.27 for the MITC6a and MITC6rs elements and different values of ε and h . We observe that reduced and unreduced shear energies differ by several orders of magnitude mainly for the MITC6a element, whereas such difference is much smaller for reduced and unreduced membrane energies, fact that explains the large errors that

⁷Notice that it is the mesh that depends on ε owing to boundary layers treatment, and consequently the results in Table 7.22 slightly differ as the relative thickness decreases.

h	A_m	A_m^h
$\varepsilon = 0.01$		
0.25	1.501843449e+10	7.603591185e+09
0.125	7.435627053e+09	1.881780473e+09
0.0625	3.207930744e+09	4.628609131e+08
$\varepsilon = 0.001$		
0.25	1.547988729e+10	2.326506388e+09
0.125	6.069407831e+09	3.331110819e+08
0.0625	2.379839869e+09	5.442823403e+07
$\varepsilon = 0.0001$		
0.25	1.862274000e+10	2.475035546e+09
0.125	6.368699128e+09	3.860446362e+08
0.0625	2.400708469e+09	8.302716681e+07

Table 7.22: Fully clamped hyperboloid shell problem: smallest modulus eigenvalues associated with A_m for the P_2 shell finite element, A_m^h for the MITC6a and MITC6rs.

appear when shear terms are not discarded from the A_m norm. The unreduced shear energy is commonly larger than the unreduced membrane energy, or at least of the same order of magnitude.

However, reduced shear and bending energies vanish as thickness decreases, whereas the reduced membrane energy becomes dominant and it can be scaled by a factor of ε for both shell finite elements. Namely, these elements behave as expected from the energy point of view and the asymptotic nature of the problem is well detected by them. In fact, the subspace of discretized inextensional displacements $\mathcal{V}_{0,h}$ is reduced to $\{0\}$ for all h and ε (see Table 7.22).

The weighted shear stabilizations with $C = 1$ and $C = 1/5$ applied to the MITC6a and MITC6rs shell finite elements provide numerical results highly improved as the converge curves displayed in Fig. 7.26-7.29 show: strains, midsurface displacements and rotations achieve uniform and almost optimal convergence rate, respectively seen by means of the s -norm and A_m norm (with shear terms discarded and not), but the A_m norm (with shear terms) convergence curves for $C = 1/5$ slightly rise as thickness decreases. On the other hand, reduced and unreduced shear energies get closer, although the difference is not negligible but considerably lower as compared to the original MITC6a and MITC6rs shell finite elements. We also notice that the results obtained for $C = 1$ do not really differ from those obtained when considering $C = 1/5$.

The midsurface deformed graphs and the rotations magnitude plots are displayed in Fig. 7.31-7.32 for the MITC6a, MITC6rs and the respective weighted shear stabilizations when considering $\varepsilon = 10^{-4}$ and the coarsest mesh of our analysis properly meshed (176 elements and 405 nodes). Fig. 7.30 shows the expected graphs associated with the P_2 shell finite element –given the membrane dominated

nature of this problem— for the same relative thickness and mesh.

We observe that the MITC6a deformed midsurface graph and rotations plot substantially differ from the P_2 reference ones, whereas the difference for the MITC6rs is substantially weaker. In fact, some oscillations appear in the original MITC6a deformed midsurface, but the MITC6a weighted shear stabilized elements seem to correct this phenomena as oscillations considerably decay and rotations are better predicted. The original MITC6rs shell finite element provides better rotations than the original MITC6a element, and oscillations on the deformed midsurface slightly appear, but when applying the weighted shear stabilizations, midsurface displacements and rotations get much better.

So, the richer transverse shear interpolation related to the MITC6rs shell finite element and the weighted shear stabilizations for $C = 1$ and $C = 1/5$ constitute an effective cure for midsurface displacements and mainly for rotations in this particular framework.

7.5.2 Bottom clamped hyperboloid shell problem

In the analysis of the *trace shell problem* (Section 7.2), we observed that real parasitic membrane modes mainly manifest as large oscillations near the free boundaries. The point now is to see what happens in a membrane dominated framework for the axisymmetric hyperboloid and applied load described above when free boundaries exist. Even if the hyperboloid is clamped at the bottom and free at the top, the pressure distribution in (7.33) leads to a well posed membrane-dominated shell problem.

As is well known, the subspace of inextensional discretized displacements associated with the P_2 shell finite element is exactly reduced to zero. In fact, standard P_2 displacement-based shell finite elements provide good numerical solutions and uniform quadratic convergence is achieved for strains as seen through the s -norm, and midsurface displacements and rotations by means of the A_m norm (refer to Fig. 7.33).

Total and partial energy values associated with the P_2 reference and target solutions are displayed in Table 7.32. As expected, shear and bending energies vanish as thickness decreases, whereas the membrane energy becomes dominant and it can be scaled by a factor of ε . Given a thickness value, total and partial energy values converge as the mesh is refined.

Strains are rather well predicted by the original MITC6a shell finite element as seen by means of the s -norm, although the convergence curves slightly rise as thickness decreases (refer to Fig. 7.34). On the other hand, the MITC6rs shell finite element provides better strains as the s -norm convergence curves in Fig. 7.35 seem less sensitive to thickness. The A_m norm with shear terms convergence curves in Fig. 7.34-7.35 show that both elements have difficulties to provide good rotations as relative errors are inadequate for small relative thickness and coarse meshes. Even when shear terms are discarded from the A_m norm, the MITC6a shell finite element provides not admissible midsurface displacements for small relative thickness and

coarse meshes, whereas optimal and almost uniform convergence is achieved by the MITC6rs shell finite element (see Fig. 7.35).

Tables 7.33-7.34 summarize the reduced and unreduced energy values for different meshes as thickness decreases for the MITC6a and MITC6rs shell finite elements. The membrane-dominated nature of the problem seems to be well captured by them: reduced shear and bending energies vanish as thickness decreases, whereas the reduced membrane energy becomes dominant, close to P_2 reference values for all thickness and it can be scaled by a factor of ε . But we also observe that the unreduced membrane energy is larger than the reduced membrane energy when $\varepsilon \ll 1$, mainly for the MITC6a shell finite element (the difference is lower for the MITC6rs shell finite element). Moreover, the unreduced shear energy is larger than the unreduced membrane energy, or at least of the same order of magnitude.

On the other hand, whereas the reduced and unreduced bending energy values remain quite close for both elements, we observe that such values are higher than the P_2 ones in particular for the MITC6a shell finite element, small thickness and coarse meshes. Furthermore, the unreduced shear energy values fairly differ by several orders of magnitude as compared to the reduced ones, but such difference is smaller for the MITC6rs shell finite element.

Such behavior is quite similar to that observed when considering the *trace shell problem*. In fact, there exist eigenvalues related to the MITC6a and MITC6rs reduced membrane A_m^h that are smaller of several orders of magnitude than the smallest modulus eigenvalue corresponding to the unreduced bilinear form A_m for each ε and h in consideration (see Table 7.23). Furthermore, given a relative thickness, the difference is remarkably increased as the mesh is refined. Hence, *parasitic membrane modes* are present and may deteriorate the underlying “correct” solution when considering the original MITC6a and MITC6rs shell finite elements.

From the shear stabilized convergence curves in Fig. 7.36-7.37 and the associated reduced and unreduced energy values summarized in Tables 7.35-7.36 we clearly see that the *free boundary shear stabilized* MITC6a and MITC6rs shell finite elements achieve better convergence for strains than the original elements as seen by means of the *s-norm*, although the MITC6a in particular remains slightly sensitive to decreasing thickness. On the other hand, displacements *per se* are fairly improved by the MITC6a stabilized element as seen through the A_m norm without shear terms, whereas the MITC6rs shell finite element still provides midsurface displacements close to the reference ones. In spite of that, rotations remain not admissible for both elements as large errors are obtained by means of the original A_m norm with shear terms, although the free boundary shear stabilized MITC6rs element behaves a little better than the original one. The *parasitic membrane modes* seem to be filtered out as the reduced and unreduced membrane energy values are remarkably closer as compared to the original elements, mainly for the MITC6a shell finite element. But the reduced and unreduced shear energies still differ by several orders of magnitude, although the difference is considerably smaller now, and the reduced and unreduced bending energies remain close but slightly higher

h	A_m	A_m^h
$\varepsilon = 0.01$		
0.25	2.913928354e+09	2.184404158e+08
0.125	1.157739440e+09	2.441488007e+07
0.0625	4.550016362e+08	6.819074668e+05
$\varepsilon = 0.001$		
0.25	2.719848743e+09	9.303474420e+05
0.125	1.100898251e+09	5.203905932e+02
0.0625	4.030518720e+08	2.001784484e-04
$\varepsilon = 0.0001$		
0.25	2.705415816e+09	1.529344010e+05
0.125	1.137771854e+09	5.886683913e+00
0.0625	4.214806504e+08	2.587579443e-04

Table 7.23: Bottom clamped hyperboloid shell problem: smallest modulus eigenvalues associated with A_m for the P_2 shell finite element, A_m^h for the MITC6a and MITC6rs.

than the P_2 expected values for small relative thickness.

The *weighted shear stabilizations* with $C = 1$ and $C = 1/5$ substantially improve the MITC6a and MITC6rs behavior: optimal and uniform convergence is achieved for strains and midsurface displacements respectively seen by means of the s -norm and A_m norm when shear terms are discarded, whereas uniform and optimal convergence curves are obtained for the A_m norm with shear terms when considering $C = 1$, although the A_m norm convergence (for displacements and rotations) slightly deteriorates as thickness decreases⁸ for $C = 1/5$. Furthermore, a nearly optimal energy profile is obtained for the MITC6a and MITC6rs shear stabilized elements with $C = 1$ as the reduced and unreduced shear energies slightly differ in this case (not even of one order of magnitude) and reduced and unreduced membrane energies are quite close. The reduced bending energy values are lower and close to the unreduced and P_2 values as compared to the respective original MITC6a and MITC6rs shell finite elements. Namely, membrane parasitic modes are considerably filtered out when considering $C = 1$. For $C = 1/5$ these observations also hold, but the difference between the reduced and unreduced shear energies is smaller as compared to the original elements, but a little larger as compared to $C = 1$.

The midsurface deformed graphs are shown in Fig. 7.43-7.44 for the MITC6a, MITC6rs and the free boundary and weighted shear stabilizations we have applied when considering $\varepsilon = 10^{-4}$ and a mesh of 192 elements and 441 nodes. The corresponding rotations magnitude plots are displayed in Fig. 7.45-7.46. Fig. 7.42

⁸This fact is well understood given that a constant of order of magnitude smaller than one gives a weaker improvement by weighted shear stabilization as it was discussed in Section 7.3.1

shows the deformed midsurface graph and rotations magnitude plot associated with the P_2 shell finite element for the same relative thickness and mesh.

We observe that the original MITC6a deformed midsurface plot in Fig. 7.43 substantially differs from the reference one displayed in Fig. 7.42 and spurious membrane modes notably manifest as large oscillations near the free boundaries; the MITC6rs deformed midsurface plot in Fig. 7.44 also suffers from these parasitic oscillations, but in a softer manner owing to the richer transverse shear strains reduction. Accordingly, the MITC6a shell finite element provides worse rotations than the MITC6rs element.

The *free boundary shear stabilization* seems to correct this phenomenon for both elements as oscillations considerably decay, but rotations still remain inadequate, principally for the MITC6a free boundary stabilized element.

On the other hand, we see that the MITC6a and MITC6rs *weighted shear stabilizations* with $C = 1$ and $C = 1/5$ constitute an effective cure for midsurface displacements and rotations, as the associated graphs suitably look like the P_2 reference ones for the mesh and thickness in consideration.

7.5.3 Free hyperboloid shell problem

The free boundary and weighted shear stabilizations have been developed in order to filter out those membrane parasitic modes that may deteriorate the “correct” underlying solution provided by a MITC6 shell finite element. We have seen in the previous sections that such techniques may constitute useful cures in membrane dominated situations, but it is also important to keep the performance of the MITC tool in bending dominated frameworks. In order to see if the original MITC6a and MITC6rs are not strongly hindered by these shear stabilizations, we have analyzed the bending dominated shell problem obtained when considering the axisymmetric hyperboloid in Fig. 6.56 loaded by the normal pressure described in (7.33) with no boundary conditions.

The MITC4 quadrilateral shell finite element is taken as reference for a mesh properly refined depending on the thickness. The corresponding reduced total and partial energies are summarized in Table 7.41. We see that the reduced bending energy is dominant as compared to the reduced shear and membrane energies which vanish as thickness decreases, whereas the reduced bending energy can be scaled by a factor of ε^3 . Namely, the MITC4 shell finite element captures well the bending nature of the problem.

As expected, P_2 displacement based shell finite elements behave much too stiffly: strains and midsurface displacements and rotations are not well predicted as respectively seen by means of the *s-norm* and $A_b + A_m$ norm, the associated curves deteriorate as ε decreases, and no convergence is obtained for small relative thickness (see Fig. 7.47). Furthermore, Table 7.42 shows that shear and membrane energies remain large and dominant for small thickness as compared to the bending energy, which is several orders of magnitude smaller than the reference values. We also notice that the membrane energy is higher than the shear energy for all ε and

h .

The MITC6a and MITC6rs shell finite elements also show some locking for small thickness values and coarse meshes in a similar way, but the convergence is quickly improved for both elements as the mesh is refined for strains and mid-surface displacements and rotations, respectively seen by means of the s -norm and $A_b + A_m$ norm. The MITC6a shell finite element behaves a little better than the MITC6rs.

For these elements, the reduced membrane and shear energies are too large for small thickness and coarse meshes, but get lower as the mesh is refined. Reduced and unreduced bending energies remain close for all ε and h , and the reduced bending energy converges in h towards the reference MITC4 value for a fixed ε . Furthermore, the reduced and corresponding unreduced shear energy values differ by several orders of magnitude for all ε and h , and the same observation holds for the reduced and unreduced membrane energies although the difference is smaller. We also notice that the reduced membrane energy is dominant as compared to the reduced shear energy, whereas the unreduced shear energy is larger than the unreduced membrane energy for small ε and both elements.

The *free boundary shear stabilized* MITC6a and MITC6rs shell finite elements provide numerical results that do not differ very much from those related to the original formulations: the same observations about the s -norm and $A_b + A_m$ norm convergence curves hold (see Fig. 7.50-7.51), and also the considerations related to the reduced and unreduced energies which are displayed in Tables 7.45-7.46.

Notice that when boundary layers are treated⁹ the area of the band of elements that have at least one node on the free boundary is extremely small as compared to the total area of the domain, although it is well known that a significant amount of energy is concentrated in this band.

In order to see if the mesh boundary refinements might weaken the shear stabilization effect, we have considered a set of uniform meshes that consist on $2N + 1$ (axial direction) by $2N + 1$ (circumferential direction) vertices for $N = 2, 4, 8, 16$, and the same analysis has been undertaken for the original MITC6a shell finite element. We observe that strains, midsurface displacements and rotations – respectively seen by means of the s -norm and $A_b + A_m$ norm – are predicted in a similar way as compared to the results obtained with boundary layers treatment for the MITC6a shell finite element (see Fig 7.56), but Table 7.51 shows that the unreduced shear energy is considerably higher for small thickness and coarse meshes when no boundary treatment is done, whereas the reduced bending energy is lower and the reduced membrane and shear energies remain of the same order as when treating the boundary layers, which also holds for the unreduced membrane energies.

On the other hand, the free boundary shear stabilized MITC6a when no boundary layer treatment is done gives s -norm and $A_b + A_m$ norm convergence curves that tend to rise for all ε and h as compared to those ones obtained for the same

⁹Estimated to be of width $0.5\sqrt{\varepsilon}L$

stabilized element when a refinement of width $0.5\sqrt{\varepsilon}L$ is considered near the free boundary (see Fig. 7.57). We also notice that the reduced shear and membrane energy values are substantially smaller for the free boundary shear stabilized MITC6a with no layer treatment for small thickness and coarse meshes as compared to the values obtained when it is done, whereas the unreduced shear energies are considerably lower; the unreduced membrane values are smaller, but remain of the same order (refer to Table 7.52). However, when $\varepsilon \ll 1$ and the mesh is sufficiently refined, it is the shear stabilized MITC6a element with boundary layer treatment that gives smaller reduced shear and membrane energies, and also a reduced bending energy closer to the reference values. So boundary layers properly treated seem to help the element to behave better for refined meshes and small thickness, even when a free boundary shear stabilization is done.

The *weighted shear stabilizations* with $C = 1$ and $C = 1/5$ lock substantially more than the original MITC6a and MITC6rs shell elements for small thickness and coarse meshes, but a nice convergence rate is quickly achieved when the mesh is refined “enough” (refer to Fig. 7.52, 7.53, 7.54 and 7.55). Obviously, such *weak locking* is stronger for $C = 1$ than $C = 1/5$ because the unreduced shear *participation* is considerably higher in the first case. The *s-norm* and $A_b + A_m$ norm convergence curves slightly rise for the stabilized elements and all relative thickness, mainly for coarse meshes. The reduced and unreduced shear and membrane energies are respectively closer for small thickness and coarse meshes as compared to the original MITC6a and MITC6rs values. When it occurs, the reduced shear is of the same order but larger than the reduced membrane, whereas the bending energy is lower than them of several orders of magnitude, which indicates that *more shear locking* occurs (see Tables 7.47, 7.48, 7.49 and 7.50).

It is interesting to notice that the smallest modulus eigenvalue associated with the reduced MITC6a membrane A_m^h differs by several orders of magnitude as compared to the smallest modulus one of A_m for each ε and h as Table 7.24 shows. In spite of that, the subspace $\mathcal{V}_{0,h}$ is not rich enough to completely avoid numerical locking as the difference between the respective smallest modulus eigenvalues associated with $A_m^h + A_s^h$ on the one hand and $A_m + A_s$ on the other hand only differ, roughly speaking, by three orders of magnitude. As it is well known, the goal is to obtain $\mathcal{V}_{0,h}$ not reduced to zero and rich enough in a bending dominated framework in order to avoid numerical locking. The modes associated with the zero A_m^h eigenvalue are good candidates to be an element of this subspace, but in our particular case we observe that $\mathcal{V}_{0,h}$ is indeed “reduced to $\{0\}$ ”.

Consequently, we can conclude that the free boundary and weighted shear stabilizations do not hinder so much the performance of the original MITC6a and MITC6rs shell finite elements in this bending dominated framework. Those elements suffer from *weak locking* for small relative thickness and coarse meshes, and the same behavior is obtained with the stabilized formulations, although the constant $C = 1/5$ is preferable because it adds less *shear locking* than $C = 1$.

h	$A_m + A_s$	$A_m^h + A_s^h$	A_m	A_m^h
$\varepsilon = 0.01$				
0.25	2.950156152e+08	5.840252366e+05	4.726215123e+07	6.578039861e-04
0.125	1.989024032e+07	5.762144855e+04	3.099451635e+06	1.623524725e-03
0.0625	1.279066949e+06	4.879874192e+03	1.974149671e+05	-5.271233620e-04
$\varepsilon = 0.001$				
0.25	3.017827364e+08	5.483461521e+05	4.745632697e+07	-2.995407179e-03
0.125	2.040497523e+07	4.586850175e+04	3.115231185e+06	-4.114088372e-03
0.0625	1.313347276e+06	4.405014270e+03	1.983814546e+05	-2.467836061e-02
$\varepsilon = 0.0001$				
0.25	3.041666715e+08	4.862295158e+05	4.754165145e+07	4.221575371e-03
0.125	2.057084393e+07	4.351175965e+04	3.125939839e+06	2.579683322e-02
0.0625	1.325609613e+06	4.060781174e+03	1.989844652e+05	-3.243334286e-02

Table 7.24: Free hyperboloid shell problem: smallest modulus eigenvalues associated with $A_m + A_s$ and A_m for the P_2 shell finite element, $A_m^h + A_s^h$ and A_m^h for the MITC6a.

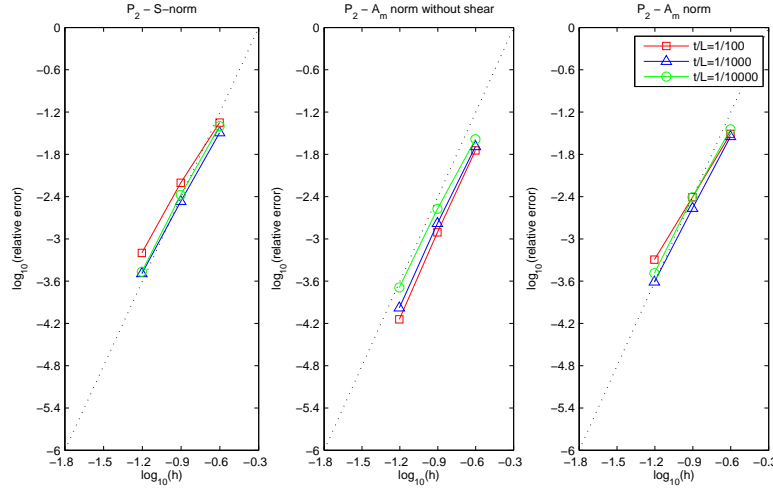


Figure 7.23: Convergence curves associated with the s-norm and membrane energy norm (with shear terms discarded and not) for the clamped hyperboloid shell problem and P_2 displacement-based shell finite elements. The dotted line shows the optimal convergence rate which is 4.

$\varepsilon = 10^{-2}$	$h = 0.25$	$h = 0.125$	$h = 0.0625$	Ref sol
Total	5.142788610e-10	5.357354700e-10	5.388140333e-10	5.391575296e-10
Bending	1.492309850e-11	2.087114520e-11	2.224962392e-11	2.249852075e-11
Membrane	4.921780555e-10	5.132309149e-10	5.161115410e-10	5.164252432e-10
Shear	7.275289688e-12	1.740791104e-12	5.613528621e-13	3.423416674e-13
$\varepsilon = 10^{-3}$	$h = 0.25$	$h = 0.125$	$h = 0.0625$	Ref sol
Total	5.798999686e-09	5.979973327e-09	5.998990268e-09	6.000953295e-09
Bending	3.960984668e-11	6.504691165e-11	6.885305365e-11	6.943181816e-11
Membrane	5.711132143e-09	5.908571215e-09	5.929187323e-09	5.931329548e-09
Shear	4.827724646e-11	6.380359656e-12	9.759075375e-13	2.180394092e-13
$\varepsilon = 10^{-4}$	$h = 0.25$	$h = 0.125$	$h = 0.0625$	Ref sol
Total	5.932764045e-08	6.163015845e-08	6.187506312e-08	6.189668695e-08
Bending	5.598401321e-11	1.780642739e-10	2.126460423e-10	2.159824075e-10
Membrane	5.860035750e-08	6.137437570e-08	6.165431470e-08	6.167980084e-08
Shear	6.713019067e-10	7.772461336e-11	8.109503700e-12	9.109533331e-13

Table 7.25: Energy values associated with the clamped hyperboloid shell problem and P_2 displacement-based shell finite elements for different values of ε and h , also the P_2 solution taken as reference.

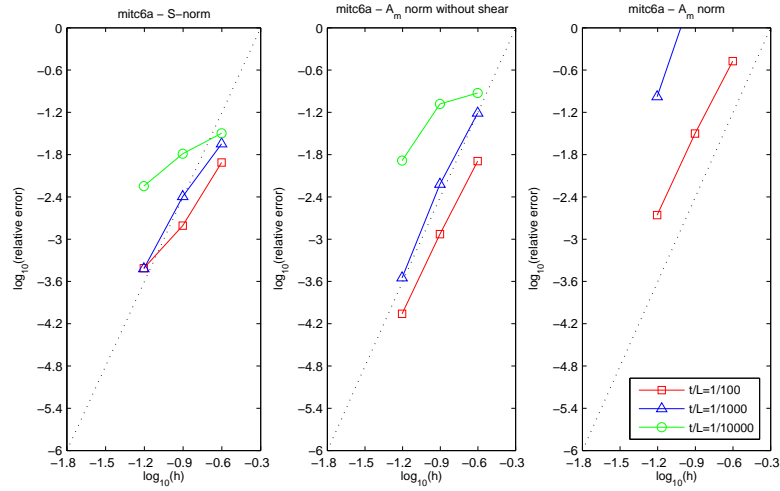


Figure 7.24: Convergence curves associated with the s-norm and membrane energy norm (with shear terms discarded and not) for the clamped hyperboloid shell problem and MITC6a shell finite element. The dotted line shows the optimal convergence rate which is 4.

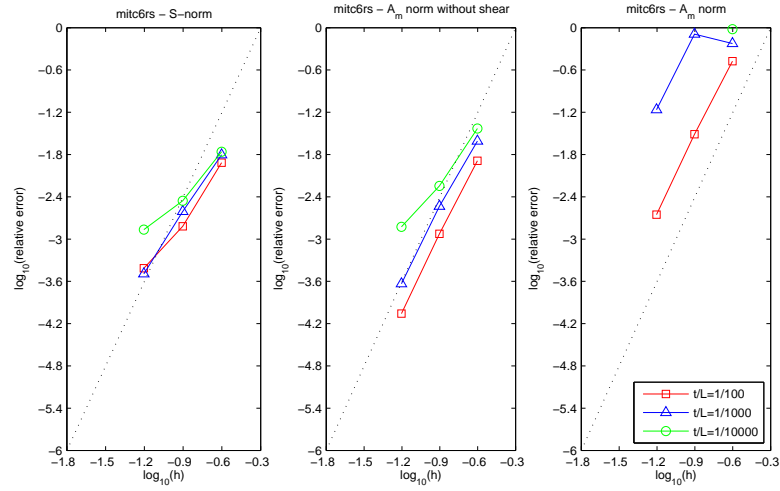


Figure 7.25: Convergence curves associated with the s-norm and membrane energy norm (with shear terms discarded and not) for the clamped hyperboloid shell problem and MITC6rs shell finite element. The dotted line shows the optimal convergence rate which is 4.

$\varepsilon = 10^{-2}$		$h = 0.25$	$h = 0.125$	$h = 0.0625$
<i>Total</i>	<i>Reduced</i>	5.313287519e-10	5.386378663e-10	5.391849079e-10
	<i>Unreduced</i>	7.007754801e-10	5.548806408e-10	5.404578460e-10
<i>Bending</i>	<i>Reduced</i>	1.965029737e-11	2.238886036e-11	2.253228463e-11
	<i>Unreduced</i>	1.959089190e-11	2.236655348e-11	2.252485986e-11
<i>Membrane</i>	<i>Reduced</i>	5.093664728e-10	5.158833701e-10	5.164003365e-10
	<i>Unreduced</i>	5.071992002e-10	5.144402410e-10	5.159583348e-10
<i>Shear</i>	<i>Reduced</i>	2.409716708e-12	4.718519667e-13	3.602628182e-13
	<i>Unreduced</i>	1.740828072e-10	1.818008997e-11	2.082645828e-12
$\varepsilon = 10^{-3}$		$h = 0.25$	$h = 0.125$	$h = 0.0625$
<i>Total</i>	<i>Reduced</i>	5.889992135e-09	5.985962841e-09	5.996186056e-09
	<i>Unreduced</i>	3.677530128e-08	2.900105511e-08	6.615963449e-09
<i>Bending</i>	<i>Reduced</i>	5.676952148e-11	7.515581082e-11	7.001320503e-11
	<i>Unreduced</i>	5.661184016e-11	7.508850030e-11	7.000004735e-11
<i>Membrane</i>	<i>Reduced</i>	5.813742852e-09	5.907618412e-09	5.925717456e-09
	<i>Unreduced</i>	6.138765320e-09	5.941810419e-09	5.923120974e-09
<i>Shear</i>	<i>Reduced</i>	1.950328883e-11	3.214517077e-12	4.813636638e-13
	<i>Unreduced</i>	3.057994119e-08	2.298417772e-08	6.228683340e-10
$\varepsilon = 10^{-4}$		$h = 0.25$	$h = 0.125$	$h = 0.0625$
<i>Total</i>	<i>Reduced</i>	6.130087928e-08	6.246118510e-08	6.215948686e-08
	<i>Unreduced</i>	7.521054441e-07	7.100414393e-06	1.080359911e-05
<i>Bending</i>	<i>Reduced</i>	1.365126933e-10	2.493470739e-10	3.563850125e-10
	<i>Unreduced</i>	1.361435830e-10	2.491561467e-10	3.562614573e-10
<i>Membrane</i>	<i>Reduced</i>	6.071939806e-08	6.200696112e-08	6.175048866e-08
	<i>Unreduced</i>	6.874524323e-08	6.801839592e-08	6.301064521e-08
<i>Shear</i>	<i>Reduced</i>	4.449735743e-10	2.048833840e-10	5.261960309e-11
	<i>Unreduced</i>	6.832240605e-07	7.032146834e-06	1.074023219e-05

Table 7.26: *Reduced* and *unreduced* energy values associated with the clamped hyperboloid shell problem and MITC6a triangular shell finite element for different values of ε and h .

$\varepsilon = 10^{-2}$		$h = 0.25$	$h = 0.125$	$h = 0.0625$
<i>Total</i>	<i>Reduced</i>	5.315439905e-10	5.386986956e-10	5.392168037e-10
	<i>Unreduced</i>	7.002049363e-10	5.545877886e-10	5.405290427e-10
<i>Bending</i>	<i>Reduced</i>	1.975717888e-11	2.240211531e-11	2.251239861e-11
	<i>Unreduced</i>	1.969032770e-11	2.237992746e-11	2.250537124e-11
<i>Membrane</i>	<i>Reduced</i>	5.092717966e-10	5.159215770e-10	5.164235983e-10
	<i>Unreduced</i>	5.073109299e-10	5.144804654e-10	5.159817912e-10
<i>Shear</i>	<i>Reduced</i>	2.612501595e-12	4.813149610e-13	3.888007622e-13
	<i>Unreduced</i>	1.733016891e-10	1.783382535e-11	2.149897867e-12
$\varepsilon = 10^{-3}$		$h = 0.25$	$h = 0.125$	$h = 0.0625$
<i>Total</i>	<i>Reduced</i>	5.849991733e-09	5.977019052e-09	5.995895393e-09
	<i>Unreduced</i>	9.291875860e-09	1.076116625e-08	6.399122041e-09
<i>Bending</i>	<i>Reduced</i>	5.285070082e-11	6.782451755e-11	6.978231645e-11
	<i>Unreduced</i>	5.269567647e-11	6.777144495e-11	6.976904045e-11
<i>Membrane</i>	<i>Reduced</i>	5.783239535e-09	5.905273308e-09	5.925683190e-09
	<i>Unreduced</i>	5.830064865e-09	5.904324225e-09	5.922165638e-09
<i>Shear</i>	<i>Reduced</i>	1.392295752e-11	3.945598165e-12	4.558151375e-13
	<i>Unreduced</i>	3.409137454e-09	4.789095978e-09	4.072133803e-10
$\varepsilon = 10^{-4}$		$h = 0.25$	$h = 0.125$	$h = 0.0625$
<i>Total</i>	<i>Reduced</i>	6.038117731e-08	6.167447192e-08	6.189537304e-08
	<i>Unreduced</i>	1.193505507e-07	1.733362774e-07	4.171260540e-07
<i>Bending</i>	<i>Reduced</i>	1.434524471e-10	2.059270544e-10	2.186709368e-10
	<i>Unreduced</i>	1.429976826e-10	2.057821046e-10	2.186310531e-10
<i>Membrane</i>	<i>Reduced</i>	6.005530177e-08	6.141442254e-08	6.164498058e-08
	<i>Unreduced</i>	6.161636811e-08	6.163372793e-08	6.176998574e-08
<i>Shear</i>	<i>Reduced</i>	1.824230667e-10	5.412849446e-11	3.172771006e-11
	<i>Unreduced</i>	5.759118922e-08	1.114967741e-07	3.551374442e-07

Table 7.27: *Reduced* and *unreduced* energy values associated with the clamped hyperboloid shell problem and MITC6rs triangular shell finite element for different values of ε and h .

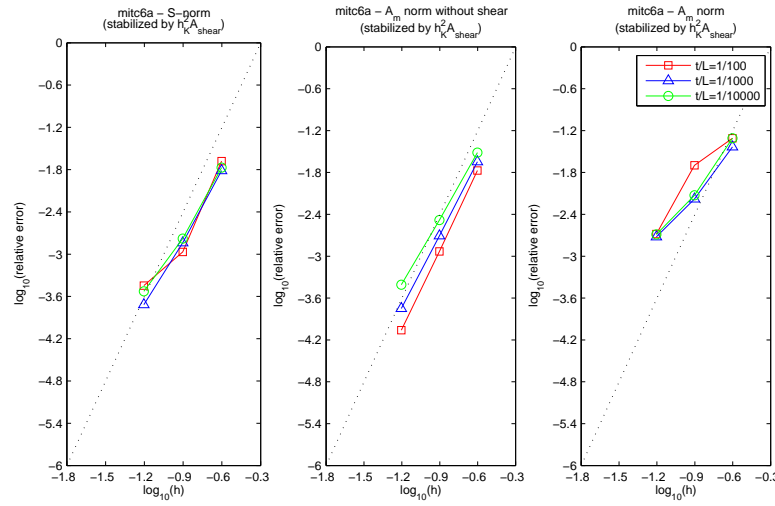


Figure 7.26: Convergence curves associated with the s-norm and membrane energy norm (with shear terms discarded and not) for the clamped hyperboloid shell problem and MITC6a shell finite element with weighted shear stabilization ($C = 1$). The dotted line shows the optimal convergence rate which is 4.

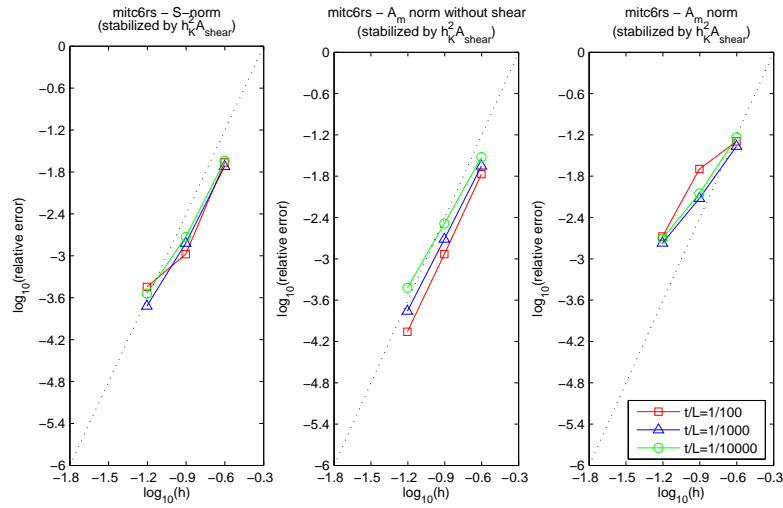


Figure 7.27: Convergence curves associated with the s-norm and membrane energy norm (with shear terms discarded and not) for the clamped hyperboloid shell problem and MITC6rs shell finite element with weighted shear stabilization ($C = 1$). The dotted line shows the optimal convergence rate which is 4.

$\varepsilon = 10^{-2}$		$h = 0.25$	$h = 0.125$	$h = 0.0625$
<i>Total</i>	<i>Reduced</i>	5.168239385e-10	5.375542884e-10	5.391522249e-10
	<i>Unreduced</i>	5.263904561e-10	5.465368791e-10	5.403180580e-10
<i>Bending</i>	<i>Reduced</i>	1.496493816e-11	2.154060308e-11	2.250889798e-11
	<i>Unreduced</i>	1.492955305e-11	2.152184231e-11	2.250164345e-11
<i>Membrane</i>	<i>Reduced</i>	4.956648326e-10	5.149321285e-10	5.163731304e-10
	<i>Unreduced</i>	4.933539203e-10	5.134754064e-10	5.159309588e-10
<i>Shear</i>	<i>Reduced</i>	6.290920261e-12	1.187579617e-12	3.780645564e-13
	<i>Unreduced</i>	1.820590544e-11	1.164621279e-11	1.993470096e-12
$\varepsilon = 10^{-3}$		$h = 0.25$	$h = 0.125$	$h = 0.0625$
<i>Total</i>	<i>Reduced</i>	5.791677005e-09	5.968278744e-09	5.995100657e-09
	<i>Unreduced</i>	5.838166606e-09	5.977935316e-09	6.000719025e-09
<i>Bending</i>	<i>Reduced</i>	4.516200015e-11	6.563169101e-11	6.918963387e-11
	<i>Unreduced</i>	4.504353291e-11	6.558773480e-11	6.917720295e-11
<i>Membrane</i>	<i>Reduced</i>	5.713322428e-09	5.899309760e-09	5.925369373e-09
	<i>Unreduced</i>	5.706098446e-09	5.883617041e-09	5.920447650e-09
<i>Shear</i>	<i>Reduced</i>	3.321355287e-11	3.362702848e-12	5.676427540e-13
	<i>Unreduced</i>	8.704592418e-11	2.875605804e-11	1.112019237e-11
$\varepsilon = 10^{-4}$		$h = 0.25$	$h = 0.125$	$h = 0.0625$
<i>Total</i>	<i>Reduced</i>	5.948285997e-08	6.154368659e-08	6.183119675e-08
	<i>Unreduced</i>	6.066551646e-08	6.168816117e-08	6.189430453e-08
<i>Bending</i>	<i>Reduced</i>	8.660047916e-11	1.969591078e-10	2.149181433e-10
	<i>Unreduced</i>	8.636941548e-11	1.968285516e-10	2.148823298e-10
<i>Membrane</i>	<i>Reduced</i>	5.889634335e-08	6.131606087e-08	6.161166507e-08
	<i>Unreduced</i>	5.931555321e-08	6.122893119e-08	6.157554706e-08
<i>Shear</i>	<i>Reduced</i>	4.999203072e-10	3.067335980e-11	4.620850298e-12
	<i>Unreduced</i>	1.263597742e-09	2.624081225e-10	1.038823443e-10

Table 7.28: *Reduced* and *unreduced* energy values associated with the clamped hyperboloid shell problem and MITC6a triangular shell finite element with weighted shear stabilization ($C = 1$), for different values of ε and h .

$\varepsilon = 10^{-2}$		$h = 0.25$	$h = 0.125$	$h = 0.0625$
<i>Total</i>	<i>Reduced</i>	5.164035011e-10	5.376183922e-10	5.391833132e-10
	<i>Unreduced</i>	5.264480034e-10	5.466926349e-10	5.403908682e-10
<i>Bending</i>	<i>Reduced</i>	1.465127119e-11	2.154804515e-11	2.249007142e-11
	<i>Unreduced</i>	1.461431425e-11	2.152888107e-11	2.248318122e-11
<i>Membrane</i>	<i>Reduced</i>	4.948759910e-10	5.149683146e-10	5.163957260e-10
	<i>Unreduced</i>	4.926749924e-10	5.135163536e-10	5.159538131e-10
<i>Shear</i>	<i>Reduced</i>	6.972756289e-12	1.208051510e-12	4.053965466e-13
	<i>Unreduced</i>	1.925746304e-11	1.175403338e-11	2.061905786e-12
$\varepsilon = 10^{-3}$		$h = 0.25$	$h = 0.125$	$h = 0.0625$
<i>Total</i>	<i>Reduced</i>	5.765554633e-09	5.967823800e-09	5.995123695e-09
	<i>Unreduced</i>	5.823385882e-09	5.982444658e-09	5.999558832e-09
<i>Bending</i>	<i>Reduced</i>	4.355506698e-11	6.524684711e-11	6.921586827e-11
	<i>Unreduced</i>	4.343758919e-11	6.520086840e-11	6.920307609e-11
<i>Membrane</i>	<i>Reduced</i>	5.663402178e-09	5.898192388e-09	5.925394835e-09
	<i>Unreduced</i>	5.654128422e-09	5.882399731e-09	5.920404154e-09
<i>Shear</i>	<i>Reduced</i>	5.861709430e-11	4.409842877e-12	5.389796054e-13
	<i>Unreduced</i>	1.258402516e-10	3.486949101e-11	9.977622905e-12
$\varepsilon = 10^{-4}$		$h = 0.25$	$h = 0.125$	$h = 0.0625$
<i>Total</i>	<i>Reduced</i>	5.905484176e-08	6.152316625e-08	6.183059552e-08
	<i>Unreduced</i>	6.032365730e-08	6.173474368e-08	6.188710863e-08
<i>Bending</i>	<i>Reduced</i>	8.277063673e-11	1.951962753e-10	2.145178155e-10
	<i>Unreduced</i>	8.254522111e-11	1.950625667e-10	2.144809380e-10
<i>Membrane</i>	<i>Reduced</i>	5.807575858e-08	6.127853009e-08	6.161128308e-08
	<i>Unreduced</i>	5.840887185e-08	6.118578654e-08	6.157274103e-08
<i>Shear</i>	<i>Reduced</i>	8.963131765e-10	4.944614421e-11	4.801903178e-12
	<i>Unreduced</i>	1.832242917e-09	3.539011185e-10	9.989386256e-11

Table 7.29: *Reduced* and *unreduced* energy values associated with the clamped hyperboloid shell problem and MITC6rs triangular shell finite element with weighted shear stabilization ($C = 1$), for different values of ε and h .

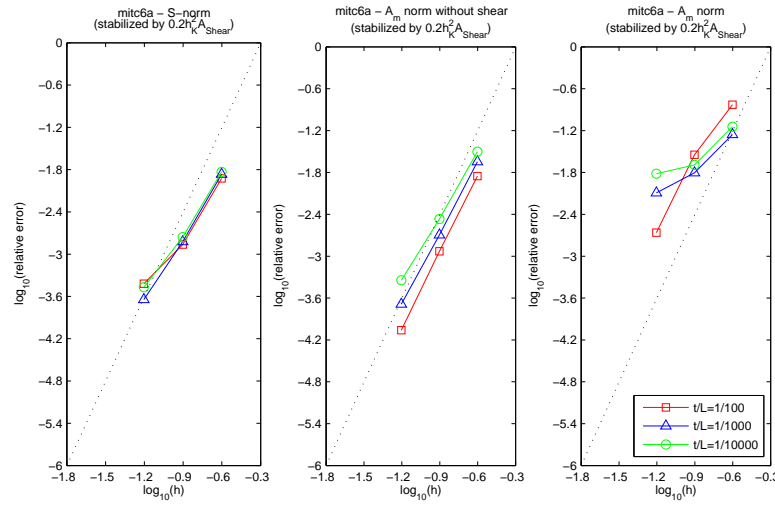


Figure 7.28: Convergence curves associated with the s-norm and membrane energy norm (with shear terms discarded and not) for the clamped hyperboloid shell problem and MITC6a shell finite element with weighted shear stabilization ($C = 1/5$). The dotted line shows the optimal convergence rate which is 4.

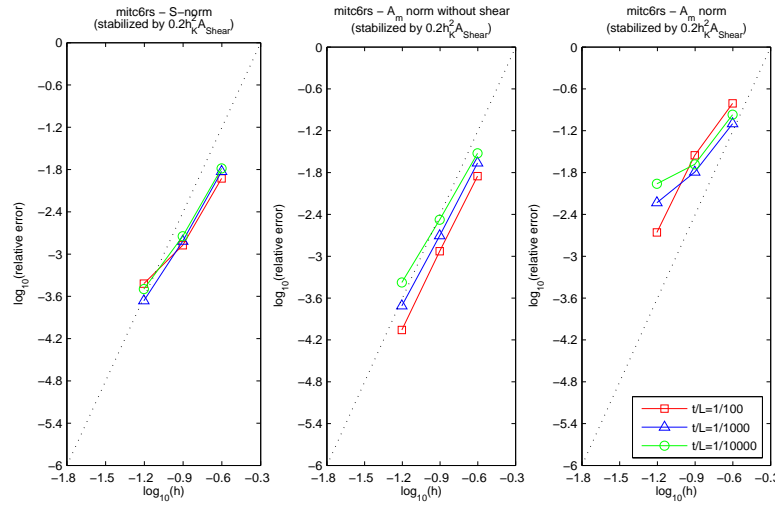


Figure 7.29: Convergence curves associated with the s-norm and membrane energy norm (with shear terms discarded and not) for the clamped hyperboloid shell problem and MITC6rs shell finite element with weighted shear stabilization ($C = 1/5$). The dotted line shows the optimal convergence rate which is 4.

$\varepsilon = 10^{-2}$		$h = 0.25$	$h = 0.125$	$h = 0.0625$
<i>Total</i>	<i>Reduced</i>	5.247735968e-10	5.383795873e-10	5.391782543e-10
	<i>Unreduced</i>	5.901627215e-10	5.526684474e-10	5.404290330e-10
<i>Bending</i>	<i>Reduced</i>	1.593686527e-11	2.215548715e-11	2.252744328e-11
	<i>Unreduced</i>	1.589115644e-11	2.213406530e-11	2.252005331e-11
<i>Membrane</i>	<i>Reduced</i>	5.032778026e-10	5.156578459e-10	5.163948020e-10
	<i>Unreduced</i>	5.010284230e-10	5.142111552e-10	5.159527648e-10
<i>Shear</i>	<i>Reduced</i>	5.656580835e-12	6.724559898e-13	3.639636374e-13
	<i>Unreduced</i>	7.334130401e-11	1.642956520e-11	2.064213457e-12
$\varepsilon = 10^{-3}$		$h = 0.25$	$h = 0.125$	$h = 0.0625$
<i>Total</i>	<i>Reduced</i>	5.819653007e-09	5.970976248e-09	5.995444987e-09
	<i>Unreduced</i>	6.004789845e-09	6.036559855e-09	6.038298553e-09
<i>Bending</i>	<i>Reduced</i>	4.691621088e-11	6.597171070e-11	6.932241839e-11
	<i>Unreduced</i>	4.679247752e-11	6.592652898e-11	6.930980889e-11
<i>Membrane</i>	<i>Reduced</i>	5.756262742e-09	5.901764613e-09	5.925521710e-09
	<i>Unreduced</i>	5.758367121e-09	5.888098573e-09	5.921208058e-09
<i>Shear</i>	<i>Reduced</i>	1.649610162e-11	3.265474120e-12	6.268761564e-13
	<i>Unreduced</i>	1.996523283e-10	8.256031843e-11	4.780670150e-11
$\varepsilon = 10^{-4}$		$h = 0.25$	$h = 0.125$	$h = 0.0625$
<i>Total</i>	<i>Reduced</i>	5.990492140e-08	6.157680781e-08	6.183728630e-08
	<i>Unreduced</i>	6.304302784e-08	6.255086511e-08	6.272117648e-08
<i>Bending</i>	<i>Reduced</i>	9.464515178e-11	2.009385646e-10	2.152916293e-10
	<i>Unreduced</i>	9.439290137e-11	2.008053460e-10	2.152557031e-10
<i>Membrane</i>	<i>Reduced</i>	5.958494732e-08	6.134539244e-08	6.161385090e-08
	<i>Unreduced</i>	6.023698746e-08	6.129892161e-08	6.159128862e-08
<i>Shear</i>	<i>Reduced</i>	2.253334732e-10	3.048362295e-11	8.151092479e-12
	<i>Unreduced</i>	2.711651736e-09	1.051144917e-09	9.146393674e-10

Table 7.30: *Reduced* and *unreduced* energy values associated with the clamped hyperboloid shell problem and MITC6a triangular shell finite element with weighted shear stabilization ($C = 1/5$), for different values of ε and h .

$\varepsilon = 10^{-2}$		$h = 0.25$	$h = 0.125$	$h = 0.0625$
<i>Total</i>	<i>Reduced</i>	5.247773217e-10	5.384439601e-10	5.392099933e-10
	<i>Unreduced</i>	5.937807648e-10	5.525522690e-10	5.405006755e-10
<i>Bending</i>	<i>Reduced</i>	1.580150704e-11	2.217052725e-11	2.250778420e-11
	<i>Unreduced</i>	1.575224085e-11	2.214909739e-11	2.250078488e-11
<i>Membrane</i>	<i>Reduced</i>	5.028871047e-10	5.156975217e-10	5.164179343e-10
	<i>Unreduced</i>	5.008094712e-10	5.142537465e-10	5.159761056e-10
<i>Shear</i>	<i>Reduced</i>	6.186025576e-12	6.821707304e-13	3.922462068e-13
	<i>Unreduced</i>	7.731721029e-11	1.625590225e-11	2.131805516e-12
$\varepsilon = 10^{-3}$		$h = 0.25$	$h = 0.125$	$h = 0.0625$
<i>Total</i>	<i>Reduced</i>	5.806414436e-09	5.970887912e-09	5.995392276e-09
	<i>Unreduced</i>	6.123703134e-09	6.038791061e-09	6.024918601e-09
<i>Bending</i>	<i>Reduced</i>	4.611988899e-11	6.589542644e-11	6.933317343e-11
	<i>Unreduced</i>	4.599217669e-11	6.584720235e-11	6.932022450e-11
<i>Membrane</i>	<i>Reduced</i>	5.728041442e-09	5.901435266e-09	5.925539501e-09
	<i>Unreduced</i>	5.728103576e-09	5.886996730e-09	5.920964382e-09
<i>Shear</i>	<i>Reduced</i>	3.227373126e-11	3.582641212e-12	5.456158617e-13
	<i>Unreduced</i>	3.496286750e-10	8.597262928e-11	3.466002399e-11
$\varepsilon = 10^{-4}$		$h = 0.25$	$h = 0.125$	$h = 0.0625$
<i>Total</i>	<i>Reduced</i>	5.967511048e-08	6.155983805e-08	6.183525489e-08
	<i>Unreduced</i>	6.471066301e-08	6.254432354e-08	6.245004915e-08
<i>Bending</i>	<i>Reduced</i>	9.539536625e-11	1.995346959e-10	2.150000827e-10
	<i>Unreduced</i>	9.512007700e-11	1.993962750e-10	2.149628870e-10
<i>Membrane</i>	<i>Reduced</i>	5.913112851e-08	6.132701330e-08	6.161345740e-08
	<i>Unreduced</i>	5.966350618e-08	6.125946610e-08	6.158404252e-08
<i>Shear</i>	<i>Reduced</i>	4.485867069e-10	3.329640126e-11	6.804699100e-12
	<i>Unreduced</i>	4.952040360e-09	1.085467842e-09	6.510509477e-10

Table 7.31: *Reduced* and *unreduced* energy values associated with the clamped hyperboloid shell problem and MITC6rs triangular shell finite element with weighted shear stabilization ($C = 1/5$), for different values of ε and h .

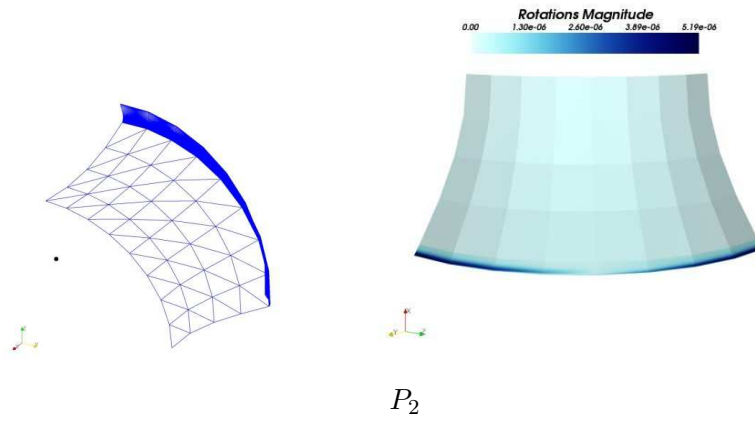


Figure 7.30: Deformed midsurface graph and rotations magnitude plot for the clamped hyperboloid shell problem and P_2 displacement-based shell finite elements ($\varepsilon = 10^{-4}$, 405 nodes, 176 elements, $scale = 1 \times 10^6$ for deformed midsurface).

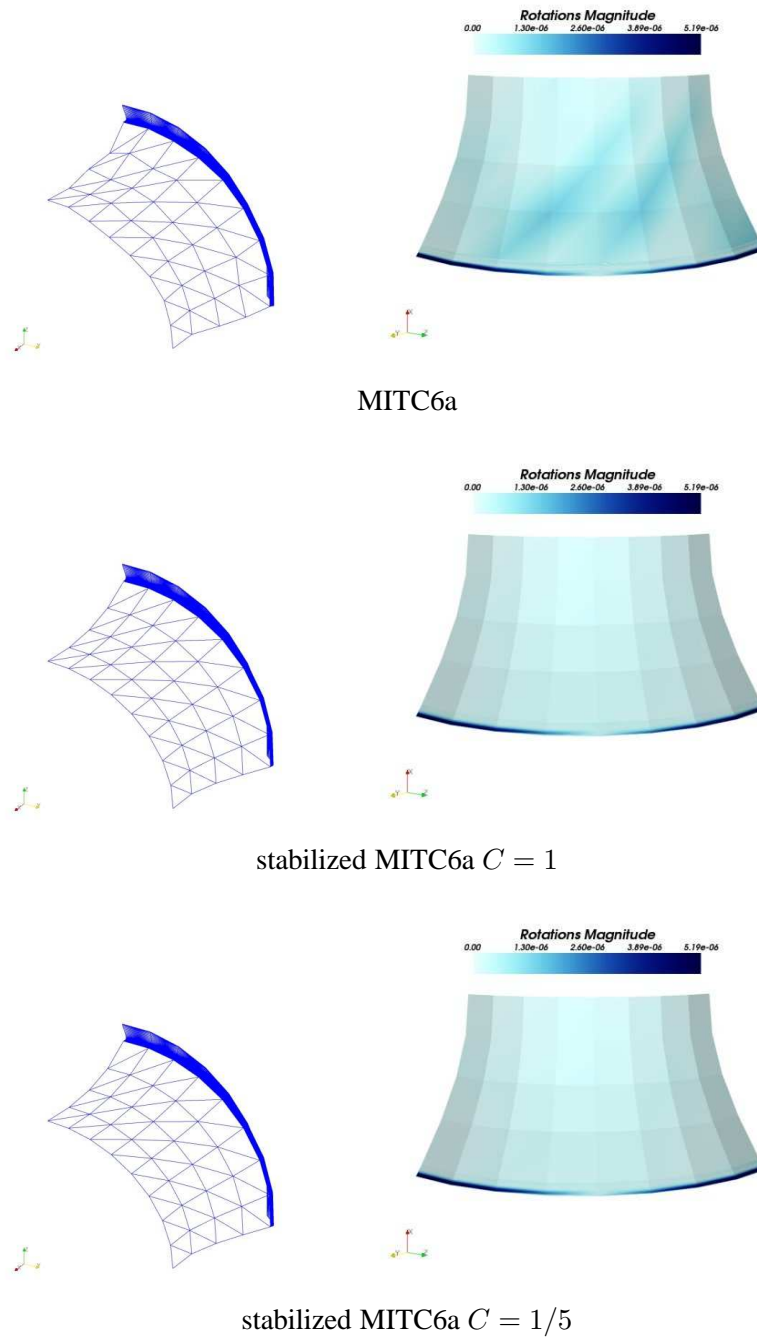


Figure 7.31: Deformed midsurface graphs and rotations magnitude plots for the clamped hyperboloid shell problem: MITC6a (top), MITC6a with weighted shear stabilization for $C = 1$ (center), MITC6a with weighted shear stabilization for $C = 1/5$ (bottom) ($\varepsilon = 10^{-4}$, 405 nodes, 176 elements, $scale = 1 \times 10^6$ for deformed midsurface).

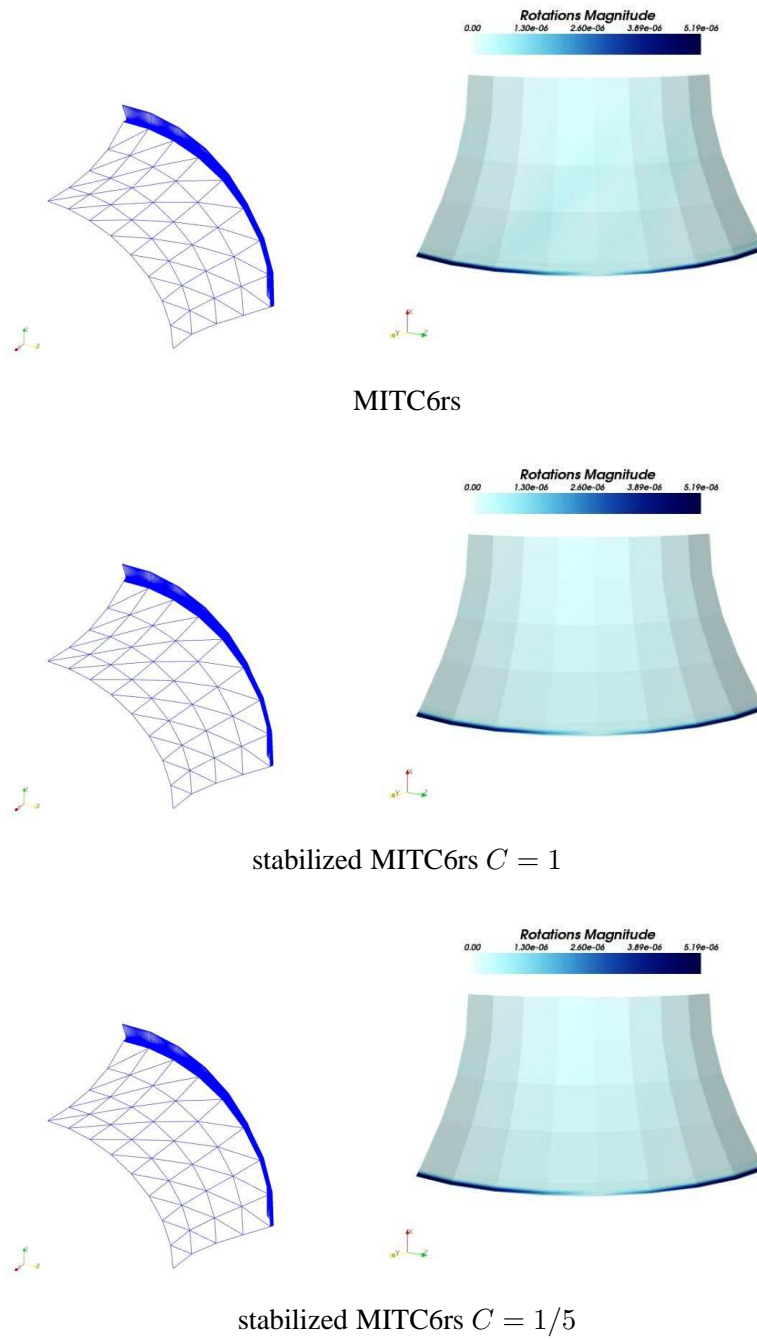


Figure 7.32: Deformed midsurface graphs and rotations magnitude plots for the clamped hyperboloid shell problem: MITC6rs (top), MITC6rs with weighted shear stabilization for $C = 1$ (center), MITC6rs with weighted shear stabilization for $C = 1/5$ (bottom) ($\varepsilon = 10^{-4}$, 405 nodes, 176 elements, $scale = 1 \times 10^6$ for deformed midsurface).

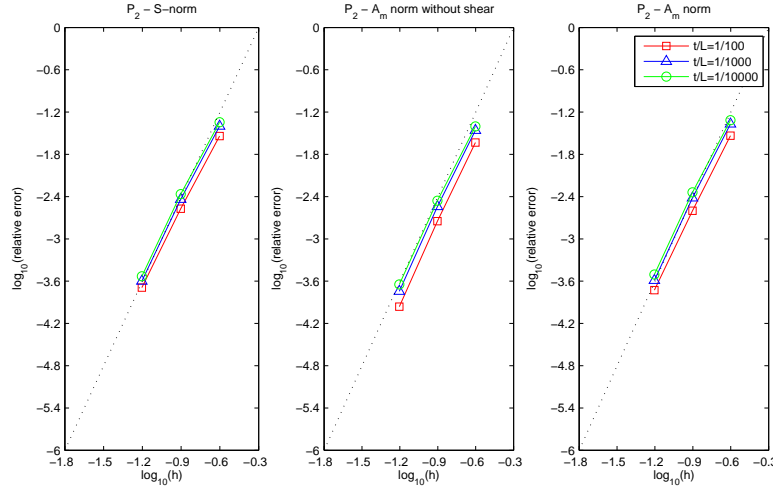


Figure 7.33: Convergence curves associated with the s-norm and membrane energy norm (with shear terms discarded and not) for the free-clamped hyperboloid shell problem and P_2 displacement-based shell finite elements. The dotted line shows the optimal convergence rate which is 4.

$\varepsilon = 10^{-2}$	$h = 0.25$	$h = 0.125$	$h = 0.0625$	Ref sol
Total	3.432581369e-09	3.526736281e-09	3.535572077e-09	3.536297838e-09
Bending	1.532336602e-11	1.930057252e-11	2.027888086e-11	2.043816844e-11
Membrane	3.396305470e-09	3.504506365e-09	3.514647734e-09	3.515478830e-09
Shear	2.083946821e-11	2.813637475e-12	5.274445844e-13	2.622203978e-13

$\varepsilon = 10^{-3}$	$h = 0.25$	$h = 0.125$	$h = 0.0625$	Ref sol
Total	3.444030088e-08	3.575076478e-08	3.587213250e-08	3.588113275e-08
Bending	3.328582654e-11	5.671401071e-11	6.038094143e-11	6.093438534e-11
Membrane	3.411652660e-08	3.566045844e-08	3.580871439e-08	3.581986778e-08
Shear	2.904866876e-10	3.359525375e-11	3.041201984e-12	3.347353008e-13

$\varepsilon = 10^{-4}$	$h = 0.25$	$h = 0.125$	$h = 0.0625$	Ref sol
Total	3.441294391e-07	3.589906089e-07	3.604323097e-07	3.605376126e-07
Bending	4.933795630e-11	1.690891453e-10	2.033075827e-10	2.066532971e-10
Membrane	3.407837934e-07	3.584216277e-07	3.601954238e-07	3.603284227e-07
Shear	3.296308441e-09	3.998959148e-10	3.358313844e-11	2.541734383e-12

Table 7.32: Energy values associated with the free-clamped hyperboloid shell problem and P_2 displacement-based shell finite elements for different values of ε and h , also the P_2 solution taken as reference.

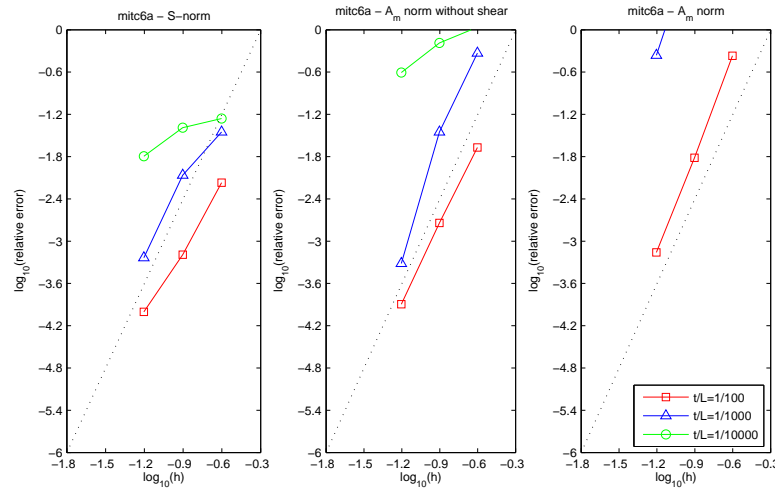


Figure 7.34: Convergence curves associated with the s-norm and membrane energy norm (with shear terms discarded and not) for the bottom clamped hyperboloid shell problem and MITC6a shell finite element. The dotted line shows the optimal convergence rate which is 4.

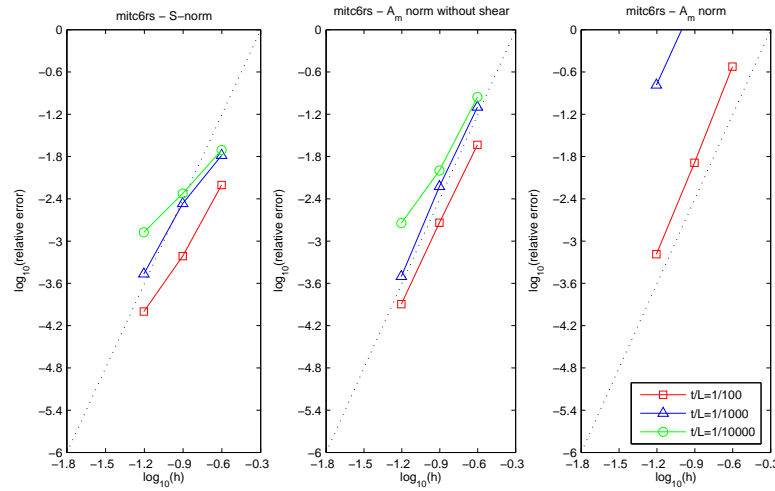


Figure 7.35: Convergence curves associated with the s-norm and membrane energy norm (with shear terms discarded and not) for the bottom clamped hyperboloid shell problem and MITC6rs shell finite element. The dotted line shows the optimal convergence rate which is 4.

$\varepsilon = 10^{-2}$		$h = 0.25$	$h = 0.125$	$h = 0.0625$
<i>Total</i>	<i>Reduced</i>	3.535661878e-09	3.535459981e-09	3.536153525e-09
	<i>Unreduced</i>	5.051643076e-09	3.588694370e-09	3.538529441e-09
<i>Bending</i>	<i>Reduced</i>	2.622884968e-11	2.099504125e-11	2.050927957e-11
	<i>Unreduced</i>	2.607118656e-11	2.097685653e-11	2.050445140e-11
<i>Membrane</i>	<i>Reduced</i>	3.506533554e-09	3.513802954e-09	3.515222744e-09
	<i>Unreduced</i>	3.586757669e-09	3.518408951e-09	3.515138643e-09
<i>Shear</i>	<i>Reduced</i>	2.807019533e-12	5.517481869e-13	3.037154758e-13
	<i>Unreduced</i>	1.438720854e-09	4.919896017e-11	2.768556178e-12
$\varepsilon = 10^{-3}$		$h = 0.25$	$h = 0.125$	$h = 0.0625$
<i>Total</i>	<i>Reduced</i>	3.697304624e-08	3.619973008e-08	3.590692449e-08
	<i>Unreduced</i>	1.952533768e-06	6.855350688e-07	5.154387751e-08
<i>Bending</i>	<i>Reduced</i>	2.219631997e-10	2.313164979e-10	7.495535779e-11
	<i>Unreduced</i>	2.187059195e-10	2.282176193e-10	7.481268196e-11
<i>Membrane</i>	<i>Reduced</i>	3.655735121e-08	3.595190545e-08	3.582960784e-08
	<i>Unreduced</i>	5.525750449e-08	3.774415839e-08	3.588778612e-08
<i>Shear</i>	<i>Reduced</i>	1.937434759e-10	1.651013750e-11	2.367256291e-12
	<i>Unreduced</i>	1.897057333e-06	6.475625805e-07	1.558128305e-08
$\varepsilon = 10^{-4}$		$h = 0.25$	$h = 0.125$	$h = 0.0625$
<i>Total</i>	<i>Reduced</i>	3.784430934e-07	3.752363345e-07	3.664103178e-07
	<i>Unreduced</i>	5.175204935e-05	2.872040555e-04	2.795797382e-04
<i>Bending</i>	<i>Reduced</i>	2.335683427e-10	9.951140737e-10	2.906821136e-09
	<i>Unreduced</i>	2.319515081e-10	9.839776216e-10	2.878559920e-09
<i>Membrane</i>	<i>Reduced</i>	3.737290579e-07	3.716562050e-07	3.632271809e-07
	<i>Unreduced</i>	7.985921757e-07	6.264350787e-07	4.611308987e-07
<i>Shear</i>	<i>Reduced</i>	4.480464867e-09	2.584961609e-09	2.762246423e-10
	<i>Unreduced</i>	5.095322516e-05	2.865766360e-04	2.791157281e-04

Table 7.33: *Reduced* and *unreduced* energy values associated with the bottom clamped hyperboloid shell problem and MITC6a triangular shell finite element for different values of ε and h .

$\varepsilon = 10^{-2}$		$h = 0.25$	$h = 0.125$	$h = 0.0625$
<i>Total</i>	<i>Reduced</i>	3.532965159e-09	3.535328518e-09	3.536165996e-09
	<i>Unreduced</i>	4.585644084e-09	3.580186874e-09	3.538401634e-09
<i>Bending</i>	<i>Reduced</i>	2.427483043e-11	2.091365239e-11	2.050037973e-11
	<i>Unreduced</i>	2.417340335e-11	2.089753848e-11	2.049618354e-11
<i>Membrane</i>	<i>Reduced</i>	3.504587445e-09	3.513714593e-09	3.515217250e-09
	<i>Unreduced</i>	3.586257365e-09	3.518098954e-09	3.515132211e-09
<i>Shear</i>	<i>Reduced</i>	4.005402816e-12	5.898828203e-13	3.307892981e-13
	<i>Unreduced</i>	9.751305755e-10	4.108117706e-11	2.655708124e-12
$\varepsilon = 10^{-3}$		$h = 0.25$	$h = 0.125$	$h = 0.0625$
<i>Total</i>	<i>Reduced</i>	3.633582710e-08	3.601380625e-08	3.589852397e-08
	<i>Unreduced</i>	1.850106039e-07	1.254488014e-07	4.179279887e-08
<i>Bending</i>	<i>Reduced</i>	5.549303479e-11	8.030342817e-11	6.667688060e-11
	<i>Unreduced</i>	5.521407994e-11	8.017124519e-11	6.665535082e-11
<i>Membrane</i>	<i>Reduced</i>	3.612890437e-08	3.588527390e-08	3.582915895e-08
	<i>Unreduced</i>	3.966992929e-08	3.630124174e-08	3.586487288e-08
<i>Shear</i>	<i>Reduced</i>	1.514182635e-10	4.822423171e-11	2.692218543e-12
	<i>Unreduced</i>	1.452854471e-07	8.906739193e-08	5.861275625e-09
$\varepsilon = 10^{-4}$		$h = 0.25$	$h = 0.125$	$h = 0.0625$
<i>Total</i>	<i>Reduced</i>	3.665253856e-07	3.624834467e-07	3.611117978e-07
	<i>Unreduced</i>	2.145409587e-06	2.270934455e-06	2.729705574e-06
<i>Bending</i>	<i>Reduced</i>	1.349360489e-10	2.023296110e-10	2.293423167e-10
	<i>Unreduced</i>	1.345015609e-10	2.021730595e-10	2.292873380e-10
<i>Membrane</i>	<i>Reduced</i>	3.645760146e-07	3.613985262e-07	3.606060138e-07
	<i>Unreduced</i>	4.134510283e-07	3.679134028e-07	3.621225958e-07
<i>Shear</i>	<i>Reduced</i>	1.814431812e-09	8.825926684e-10	2.764399449e-10
	<i>Unreduced</i>	1.731824057e-06	1.902818884e-06	2.367353695e-06

Table 7.34: *Reduced* and *unreduced* energy values associated with the bottom clamped hyperboloid shell problem and MITC6rs triangular shell finite element for different values of ε and h .

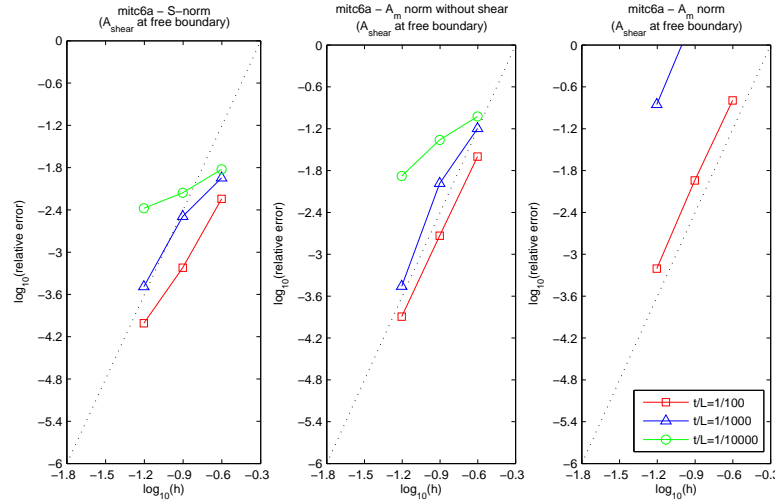


Figure 7.36: Convergence curves associated with the s-norm and membrane energy norm (with shear terms discarded and not) for the bottom clamped hyperboloid shell problem and MITC6a shell finite element with free boundary shear stabilization. The dotted line shows the optimal convergence rate which is 4.

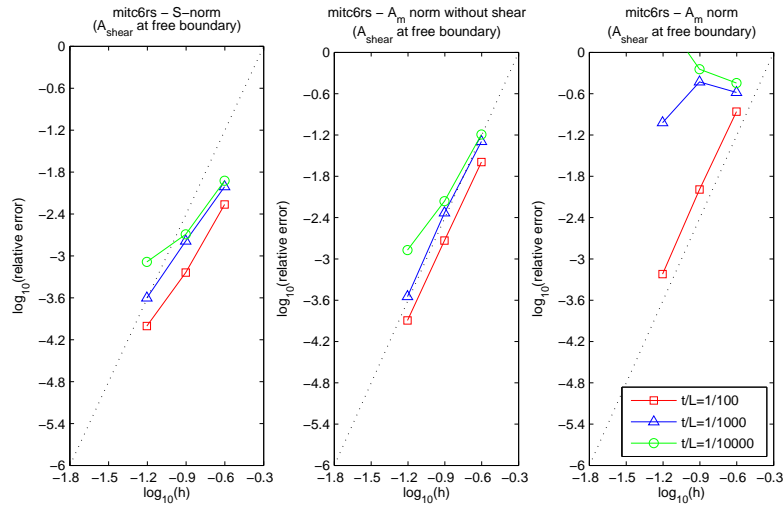


Figure 7.37: Convergence curves associated with the s-norm and membrane energy norm (with shear terms discarded and not) for the bottom clamped hyperboloid shell problem and MITC6rs shell finite element with free boundary shear stabilization. The dotted line shows the optimal convergence rate which is 4.

$\varepsilon = 10^{-2}$		$h = 0.25$	$h = 0.125$	$h = 0.0625$
<i>Total</i>	<i>Reduced</i>	3.525026899e-09	3.535074001e-09	3.536116832e-09
	<i>Unreduced</i>	4.076485735e-09	3.574310747e-09	3.538205928e-09
<i>Bending</i>	<i>Reduced</i>	2.107128508e-11	2.084127369e-11	2.050779443e-11
	<i>Unreduced</i>	2.101976294e-11	2.082596208e-11	2.050303501e-11
<i>Membrane</i>	<i>Reduced</i>	3.499831136e-09	3.513529338e-09	3.515170765e-09
	<i>Unreduced</i>	3.575140270e-09	3.517753635e-09	3.515071015e-09
<i>Shear</i>	<i>Reduced</i>	3.958709450e-12	5.633590120e-13	3.060298946e-13
	<i>Unreduced</i>	4.802283752e-10	3.562344330e-11	2.514835966e-12
$\varepsilon = 10^{-3}$		$h = 0.25$	$h = 0.125$	$h = 0.0625$
<i>Total</i>	<i>Reduced</i>	3.600676490e-08	3.599657088e-08	3.589760443e-08
	<i>Unreduced</i>	7.457472584e-08	1.358465277e-07	4.095032853e-08
<i>Bending</i>	<i>Reduced</i>	5.295962026e-11	9.320707059e-11	6.656244325e-11
	<i>Unreduced</i>	5.282612294e-11	9.312593700e-11	6.654811215e-11
<i>Membrane</i>	<i>Reduced</i>	3.587289186e-08	3.589061423e-08	3.582912242e-08
	<i>Unreduced</i>	3.828921687e-08	3.641738267e-08	3.586418543e-08
<i>Shear</i>	<i>Reduced</i>	8.090417670e-11	1.275544641e-11	1.923533941e-12
	<i>Unreduced</i>	3.623268006e-08	9.933600252e-08	5.019600783e-09
$\varepsilon = 10^{-4}$		$h = 0.25$	$h = 0.125$	$h = 0.0625$
<i>Total</i>	<i>Reduced</i>	3.632311195e-07	3.631420654e-07	3.621371899e-07
	<i>Unreduced</i>	1.273436275e-06	9.225457987e-06	3.972224662e-05
<i>Bending</i>	<i>Reduced</i>	1.616560686e-10	2.512279775e-10	6.867891180e-10
	<i>Unreduced</i>	1.611837289e-10	2.510414224e-10	6.866102407e-10
<i>Membrane</i>	<i>Reduced</i>	3.619255032e-07	3.625757940e-07	3.613337461e-07
	<i>Unreduced</i>	3.997212032e-07	3.812978194e-07	3.683102245e-07
<i>Shear</i>	<i>Reduced</i>	1.143960356e-09	3.150474177e-10	1.166530338e-10
	<i>Unreduced</i>	8.735538872e-07	8.843909109e-06	3.935324970e-05

Table 7.35: *Reduced* and *unreduced* energy values associated with the bottom clamped hyperboloid shell problem and the MITC6a triangular shell finite element with free boundary shear stabilization, for different values of ε and h .

$\varepsilon = 10^{-2}$		$h = 0.25$	$h = 0.125$	$h = 0.0625$
<i>Total</i>	<i>Reduced</i>	3.523919109e-09	3.535015174e-09	3.536135637e-09
	<i>Unreduced</i>	3.993409704e-09	3.569664082e-09	3.538164505e-09
<i>Bending</i>	<i>Reduced</i>	2.044776548e-11	2.078211082e-11	2.049753151e-11
	<i>Unreduced</i>	2.039551882e-11	2.076662787e-11	2.049326642e-11
<i>Membrane</i>	<i>Reduced</i>	3.499328705e-09	3.513503850e-09	3.515173693e-09
	<i>Unreduced</i>	3.573489969e-09	3.517572536e-09	3.515076569e-09
<i>Shear</i>	<i>Reduced</i>	3.968494389e-12	5.879820527e-13	3.321438396e-13
	<i>Unreduced</i>	3.994279202e-10	3.121639960e-11	2.477629537e-12
$\varepsilon = 10^{-3}$		$h = 0.25$	$h = 0.125$	$h = 0.0625$
<i>Total</i>	<i>Reduced</i>	3.592867263e-08	3.594294631e-08	3.589507760e-08
	<i>Unreduced</i>	4.531561321e-08	4.936402749e-08	3.933037623e-08
<i>Bending</i>	<i>Reduced</i>	4.531119410e-11	6.320032988e-11	6.464942244e-11
	<i>Unreduced</i>	4.518586092e-11	6.314745890e-11	6.463497807e-11
<i>Membrane</i>	<i>Reduced</i>	3.582536282e-08	3.586815718e-08	3.582892277e-08
	<i>Unreduced</i>	3.764223555e-08	3.610327061e-08	3.585678445e-08
<i>Shear</i>	<i>Reduced</i>	5.798717824e-11	1.158552206e-11	1.507568242e-12
	<i>Unreduced</i>	7.628193609e-09	1.319761396e-08	3.408961817e-09
$\varepsilon = 10^{-4}$		$h = 0.25$	$h = 0.125$	$h = 0.0625$
<i>Total</i>	<i>Reduced</i>	3.617607959e-07	3.614184583e-07	3.609238121e-07
	<i>Unreduced</i>	4.928844939e-07	5.676546962e-07	1.589162966e-06
<i>Bending</i>	<i>Reduced</i>	1.333123501e-10	1.984461267e-10	2.201220883e-10
	<i>Unreduced</i>	1.329000412e-10	1.983071242e-10	2.200774025e-10
<i>Membrane</i>	<i>Reduced</i>	3.608425724e-07	3.610590090e-07	3.606014105e-07
	<i>Unreduced</i>	3.849422941e-07	3.644879083e-07	3.615746487e-07
<i>Shear</i>	<i>Reduced</i>	7.849081238e-10	1.610064772e-10	1.022785698e-10
	<i>Unreduced</i>	1.078093022e-07	2.029684854e-07	1.227368244e-06

Table 7.36: *Reduced* and *unreduced* energy values associated with the bottom clamped hyperboloid shell problem and the MITC6rs triangular shell finite element with free boundary shear stabilization, for different values of ε and h .

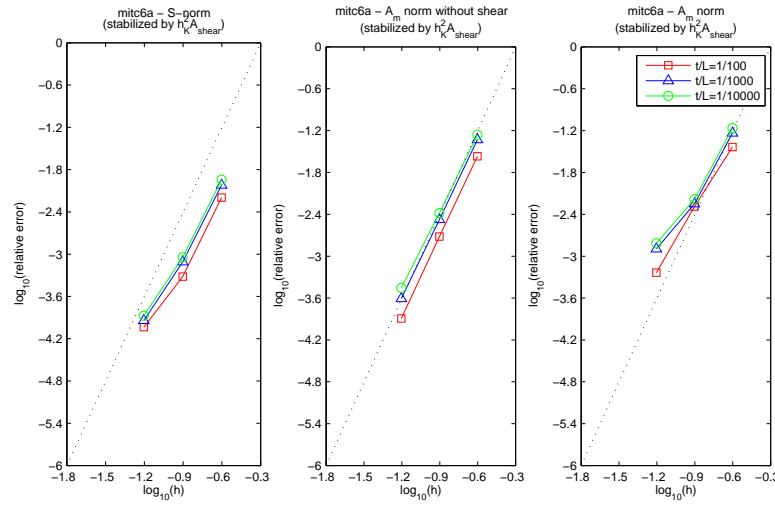


Figure 7.38: Convergence curves associated with the s-norm and membrane energy norm (with shear terms discarded and not) for the bottom clamped hyperboloid shell problem and MITC6a shell finite element with weighted shear stabilization ($C = 1$). The dotted line shows the optimal convergence rate which is 4.

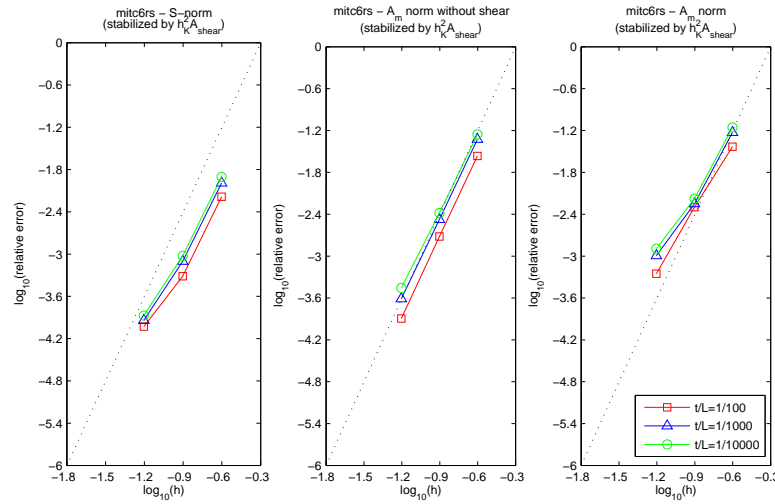


Figure 7.39: Convergence curves associated with the s-norm and membrane energy norm (with shear terms discarded and not) for the bottom clamped hyperboloid shell problem and MITC6rs shell finite element with weighted shear stabilization ($C = 1$). The dotted line shows the optimal convergence rate which is 4.

$\varepsilon = 10^{-2}$		$h = 0.25$	$h = 0.125$	$h = 0.0625$
<i>Total</i>	<i>Reduced</i>	3.503174356e-09	3.533733286e-09	3.536101248e-09
	<i>Unreduced</i>	3.598450028e-09	3.549104347e-09	3.538015273e-09
<i>Bending</i>	<i>Reduced</i>	1.631676689e-11	2.003497555e-11	2.048565377e-11
	<i>Unreduced</i>	1.631105916e-11	2.002409945e-11	2.048101862e-11
<i>Membrane</i>	<i>Reduced</i>	3.474165087e-09	3.512196411e-09	3.515157974e-09
	<i>Unreduced</i>	3.546989381e-09	3.516216016e-09	3.515066391e-09
<i>Shear</i>	<i>Reduced</i>	1.249619207e-11	1.369377414e-12	3.344717701e-13
	<i>Unreduced</i>	3.505286604e-11	1.275432059e-11	2.350280700e-12
$\varepsilon = 10^{-3}$		$h = 0.25$	$h = 0.125$	$h = 0.0625$
<i>Total</i>	<i>Reduced</i>	3.572218898e-08	3.590320155e-08	3.589071124e-08
	<i>Unreduced</i>	3.753473726e-08	3.611956202e-08	3.594565392e-08
<i>Bending</i>	<i>Reduced</i>	3.949931674e-11	5.785619360e-11	6.098577224e-11
	<i>Unreduced</i>	3.940272475e-11	5.781839088e-11	6.097497729e-11
<i>Membrane</i>	<i>Reduced</i>	3.549681651e-08	3.583421269e-08	3.582789961e-08
	<i>Unreduced</i>	3.708120201e-08	3.597876309e-08	3.584693602e-08
<i>Shear</i>	<i>Reduced</i>	1.858609169e-10	1.113421738e-11	1.829976854e-12
	<i>Unreduced</i>	4.141356434e-10	8.298520867e-11	3.774778662e-11
$\varepsilon = 10^{-4}$		$h = 0.25$	$h = 0.125$	$h = 0.0625$
<i>Total</i>	<i>Reduced</i>	3.589944237e-07	3.609148041e-07	3.606755359e-07
	<i>Unreduced</i>	3.809311441e-07	3.635676362e-07	3.613585056e-07
<i>Bending</i>	<i>Reduced</i>	8.181208659e-11	1.887467787e-10	2.056789771e-10
	<i>Unreduced</i>	8.159476152e-11	1.886217863e-10	2.056447390e-10
<i>Membrane</i>	<i>Reduced</i>	3.565606425e-07	3.606031171e-07	3.604499753e-07
	<i>Unreduced</i>	3.758934755e-07	3.624953972e-07	3.607252740e-07
<i>Shear</i>	<i>Reduced</i>	2.351969818e-09	1.229445032e-10	1.988664286e-11
	<i>Unreduced</i>	4.956076004e-09	8.836218399e-10	4.275919139e-10

Table 7.37: *Reduced* and *unreduced* energy values associated with the bottom clamped hyperboloid shell problem and MITC6a triangular shell finite element with weighted shear stabilization ($C = 1$), for different values of ε and h .

$\varepsilon = 10^{-2}$		$h = 0.25$	$h = 0.125$	$h = 0.0625$
<i>Total</i>	<i>Reduced</i>	3.502771065e-09	3.533749689e-09	3.536116309e-09
	<i>Unreduced</i>	3.598558842e-09	3.548787381e-09	3.537967670e-09
<i>Bending</i>	<i>Reduced</i>	1.615550930e-11	2.005562965e-11	2.047834959e-11
	<i>Unreduced</i>	1.614962717e-11	2.004490769e-11	2.047426583e-11
<i>Membrane</i>	<i>Reduced</i>	3.473434663e-09	3.512195744e-09	3.515157269e-09
	<i>Unreduced</i>	3.546786810e-09	3.516182573e-09	3.515065787e-09
<i>Shear</i>	<i>Reduced</i>	1.298430460e-11	1.365850304e-12	3.576793973e-13
	<i>Unreduced</i>	3.552577612e-11	1.245015815e-11	2.310210418e-12
$\varepsilon = 10^{-3}$		$h = 0.25$	$h = 0.125$	$h = 0.0625$
<i>Total</i>	<i>Reduced</i>	3.570147420e-08	3.590233099e-08	3.589052873e-08
	<i>Unreduced</i>	3.752238785e-08	3.611754046e-08	3.593604196e-08
<i>Bending</i>	<i>Reduced</i>	3.806328616e-11	5.750130283e-11	6.100450677e-11
	<i>Unreduced</i>	3.796790540e-11	5.746182986e-11	6.099344686e-11
<i>Membrane</i>	<i>Reduced</i>	3.546115562e-08	3.583320228e-08	3.582790322e-08
	<i>Unreduced</i>	3.705387097e-08	3.597683648e-08	3.584643998e-08
<i>Shear</i>	<i>Reduced</i>	2.022420084e-10	1.162883739e-11	1.625083376e-12
	<i>Unreduced</i>	4.305513813e-10	8.324674063e-11	2.861337584e-11
$\varepsilon = 10^{-4}$		$h = 0.25$	$h = 0.125$	$h = 0.0625$
<i>Total</i>	<i>Reduced</i>	3.586134626e-07	3.608908959e-07	3.606730886e-07
	<i>Unreduced</i>	3.806143523e-07	3.635431793e-07	3.612625236e-07
<i>Bending</i>	<i>Reduced</i>	7.807265236e-11	1.869048750e-10	2.053224045e-10
	<i>Unreduced</i>	7.786135911e-11	1.867770781e-10	2.052871836e-10
<i>Membrane</i>	<i>Reduced</i>	3.558887287e-07	3.605675908e-07	3.604494791e-07
	<i>Unreduced</i>	3.752374058e-07	3.624477535e-07	3.607183940e-07
<i>Shear</i>	<i>Reduced</i>	2.646658986e-09	1.364041160e-10	1.829220645e-11
	<i>Unreduced</i>	5.299086337e-09	9.086532516e-10	3.388474827e-10

Table 7.38: *Reduced* and *unreduced* energy values associated with the bottom clamped hyperboloid shell problem and MITC6rs triangular shell finite element with weighted shear stabilization ($C = 1$), for different values of ε and h .

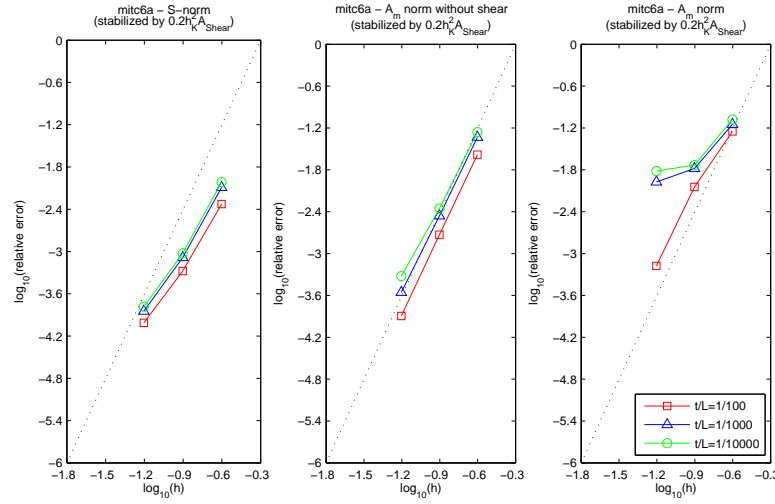


Figure 7.40: Convergence curves associated with the s-norm and membrane energy norm (with shear terms discarded and not) for the bottom clamped hyperboloid shell problem and MITC6a shell finite element with weighted shear stabilization ($C = 1/5$). The dotted line shows the optimal convergence rate which is 4.

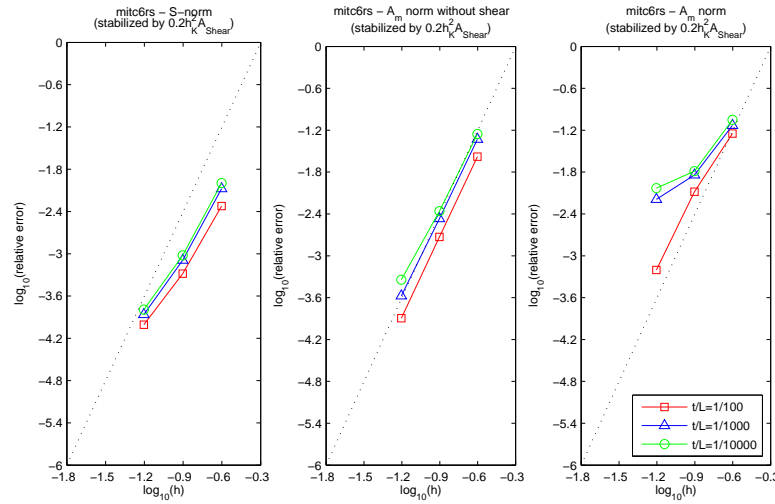


Figure 7.41: Convergence curves associated with the s-norm and membrane energy norm (with shear terms discarded and not) for the bottom clamped hyperboloid shell problem and MITC6rs shell finite element with weighted shear stabilization ($C = 1/5$). The dotted line shows the optimal convergence rate which is 4.

$\varepsilon = 10^{-2}$		$h = 0.25$	$h = 0.125$	$h = 0.0625$
<i>Total</i>	<i>Reduced</i>	3.516543645e-09	3.534855701e-09	3.536142248e-09
	<i>Unreduced</i>	3.691508820e-09	3.565188875e-09	3.538402252e-09
<i>Bending</i>	<i>Reduced</i>	1.689202676e-11	2.053521145e-11	2.050356229e-11
	<i>Unreduced</i>	1.687115449e-11	2.052070460e-11	2.049877582e-11
<i>Membrane</i>	<i>Reduced</i>	3.490995451e-09	3.513269547e-09	3.515208668e-09
	<i>Unreduced</i>	3.565678726e-09	3.517576788e-09	3.515122762e-09
<i>Shear</i>	<i>Reduced</i>	8.536788336e-12	9.366234016e-13	3.111715624e-13
	<i>Unreduced</i>	1.088648271e-10	2.698193824e-11	2.662976920e-12
$\varepsilon = 10^{-3}$		$h = 0.25$	$h = 0.125$	$h = 0.0625$
<i>Total</i>	<i>Reduced</i>	3.589052482e-08	3.591661951e-08	3.589317122e-08
	<i>Unreduced</i>	3.833905558e-08	3.653914032e-08	3.628617249e-08
<i>Bending</i>	<i>Reduced</i>	4.114076004e-11	5.840887508e-11	6.150419025e-11
	<i>Unreduced</i>	4.103812534e-11	5.836957513e-11	6.149172297e-11
<i>Membrane</i>	<i>Reduced</i>	3.576029310e-08	3.584359633e-08	3.582840062e-08
	<i>Unreduced</i>	3.740584829e-08	3.600904077e-08	3.585285162e-08
<i>Shear</i>	<i>Reduced</i>	8.908995802e-11	1.461880313e-11	3.271480915e-12
	<i>Unreduced</i>	8.921729869e-10	4.717353347e-10	3.718344126e-10
$\varepsilon = 10^{-4}$		$h = 0.25$	$h = 0.125$	$h = 0.0625$
<i>Total</i>	<i>Reduced</i>	3.611361935e-07	3.610710242e-07	3.607097486e-07
	<i>Unreduced</i>	3.908674289e-07	3.682036381e-07	3.663647370e-07
<i>Bending</i>	<i>Reduced</i>	8.931299439e-11	1.928639310e-10	2.062276080e-10
	<i>Unreduced</i>	8.907573358e-11	1.927362519e-10	2.061931304e-10
<i>Membrane</i>	<i>Reduced</i>	3.599371631e-07	3.607211664e-07	3.604597182e-07
	<i>Unreduced</i>	3.802278033e-07	3.629048467e-07	3.608374663e-07
<i>Shear</i>	<i>Reduced</i>	1.109719673e-09	1.569985352e-10	4.380804002e-11
	<i>Unreduced</i>	1.055055236e-08	5.106059840e-09	5.321082721e-09

Table 7.39: *Reduced* and *unreduced* energy values associated with the bottom clamped hyperboloid shell problem and MITC6a triangular shell finite element with weighted shear stabilization ($C = 1/5$), for different values of ε and h .

$\varepsilon = 10^{-2}$		$h = 0.25$	$h = 0.125$	$h = 0.0625$
<i>Total</i>	<i>Reduced</i>	3.516232805e-09	3.534804660e-09	3.536155402e-09
	<i>Unreduced</i>	3.691522621e-09	3.562450216e-09	3.538297116e-09
<i>Bending</i>	<i>Reduced</i>	1.685665883e-11	2.053663566e-11	2.049515693e-11
	<i>Unreduced</i>	1.683573359e-11	2.052307760e-11	2.049098458e-11
<i>Membrane</i>	<i>Reduced</i>	3.490440001e-09	3.513233644e-09	3.515204409e-09
	<i>Unreduced</i>	3.565665233e-09	3.517406299e-09	3.515117811e-09
<i>Shear</i>	<i>Reduced</i>	8.816384256e-12	9.200045691e-13	3.371797613e-13
	<i>Unreduced</i>	1.089283674e-10	2.441164971e-11	2.570821085e-12
$\varepsilon = 10^{-3}$		$h = 0.25$	$h = 0.125$	$h = 0.0625$
<i>Total</i>	<i>Reduced</i>	3.587442736e-08	3.591444641e-08	3.589217154e-08
	<i>Unreduced</i>	3.840286229e-08	3.645669356e-08	3.613381999e-08
<i>Bending</i>	<i>Reduced</i>	3.988770905e-11	5.829345525e-11	6.139372750e-11
	<i>Unreduced</i>	3.978437302e-11	5.825172449e-11	6.138181754e-11
<i>Membrane</i>	<i>Reduced</i>	3.573330581e-08	3.584301380e-08	3.582836205e-08
	<i>Unreduced</i>	3.738480118e-08	3.600187965e-08	3.585040077e-08
<i>Shear</i>	<i>Reduced</i>	1.012315542e-10	1.314334948e-11	2.420567745e-12
	<i>Unreduced</i>	9.782799242e-10	3.965673549e-10	2.220424409e-10
$\varepsilon = 10^{-4}$		$h = 0.25$	$h = 0.125$	$h = 0.0625$
<i>Total</i>	<i>Reduced</i>	3.608507020e-07	3.610321194e-07	3.606964724e-07
	<i>Unreduced</i>	3.920566343e-07	3.673269892e-07	3.642070761e-07
<i>Bending</i>	<i>Reduced</i>	8.840663349e-11	1.908849533e-10	2.059088477e-10
	<i>Unreduced</i>	8.815602009e-11	1.907530508e-10	2.058732966e-10
<i>Membrane</i>	<i>Reduced</i>	3.594585440e-07	3.606994785e-07	3.604584652e-07
	<i>Unreduced</i>	3.797820482e-07	3.628000928e-07	3.608015221e-07
<i>Shear</i>	<i>Reduced</i>	1.303749521e-09	1.417602205e-10	3.210348005e-11
	<i>Unreduced</i>	1.218643212e-08	4.336148041e-09	3.199685855e-09

Table 7.40: *Reduced* and *unreduced* energy values associated with the bottom clamped hyperboloid shell problem and MITC6rs triangular shell finite element with weighted shear stabilization ($C = 1/5$), for different values of ε and h .

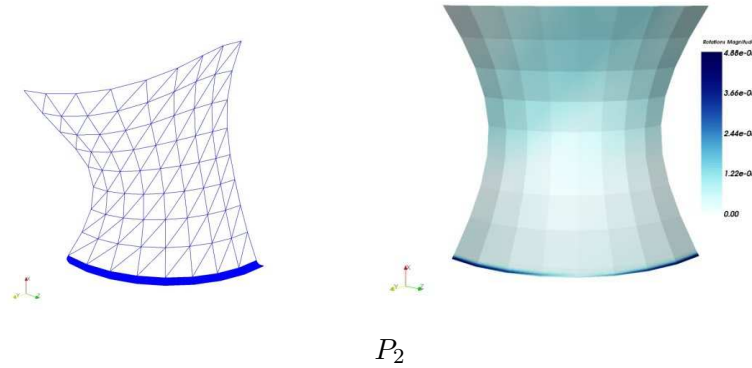


Figure 7.42: Deformed midsurface graph and rotations magnitude plot for the bottom clamped hyperboloid shell problem and P_2 displacement-based shell finite elements ($\varepsilon = 10^{-4}$, 441 nodes, 192 elements, $scale = 5 \times 10^5$ for deformed midsurface).

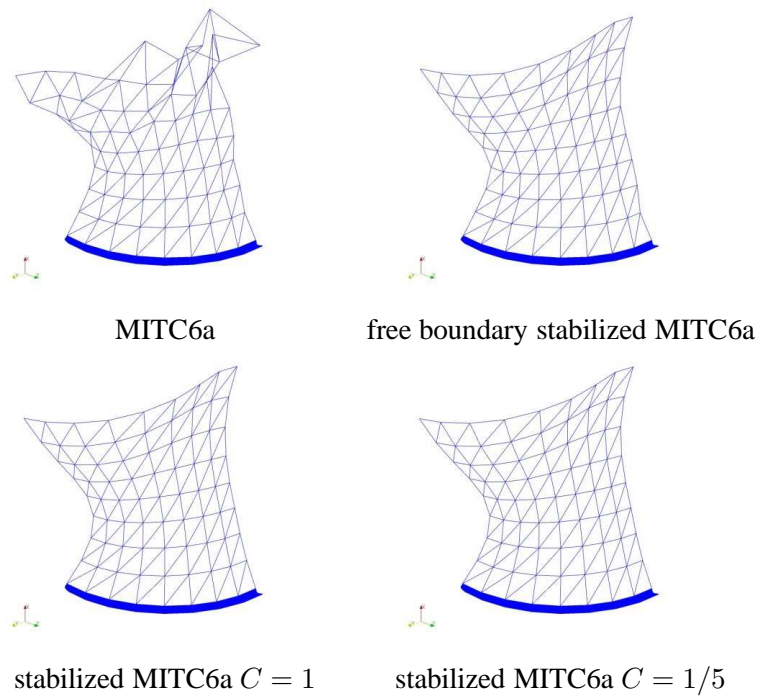


Figure 7.43: Deformed midsurface graphs for the bottom clamped hyperboloid shell problem: MITC6a (top left), MITC6a with free boundary shear stabilization (top right), MITC6a with weighted shear stabilization for $C = 1$ (bottom left), MITC6a with weighted shear stabilization for $C = 1/5$ (bottom right) ($\varepsilon = 10^{-4}$, 441 nodes, 192 elements, $scale = 5 \times 10^5$).

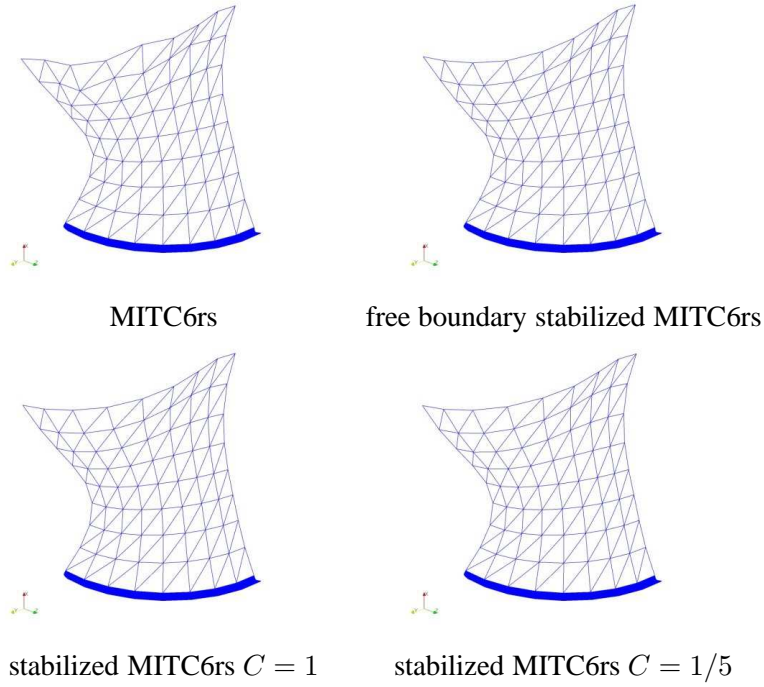


Figure 7.44: Deformed midsurface graphs for the bottom clamped hyperboloid shell problem: MITC6rs (top left), MITC6rs with free boundary shear stabilization (top right), MITC6rs with weighted shear stabilization for $C = 1$ (bottom left), MITC6rs with weighted shear stabilization for $C = 1/5$ (bottom right) ($\varepsilon = 10^{-4}$, 441 nodes, 192 elements, $scale = 5 \times 10^5$).

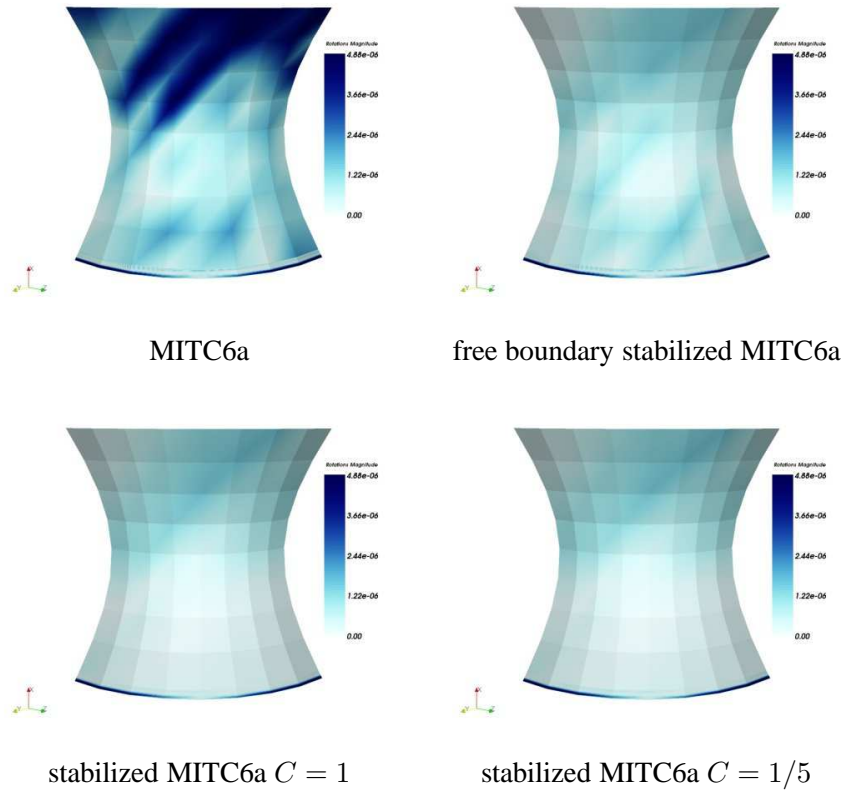


Figure 7.45: Rotations magnitude plots for the bottom clamped hyperboloid shell problem: MITC6a (top left), MITC6a with free boundary shear stabilization (top right), MITC6a with weighted shear stabilization for $C = 1$ (bottom left), MITC6a with weighted shear stabilization for $C = 1/5$ (bottom right) ($\epsilon = 10^{-4}$, 441 nodes, 192 elements).

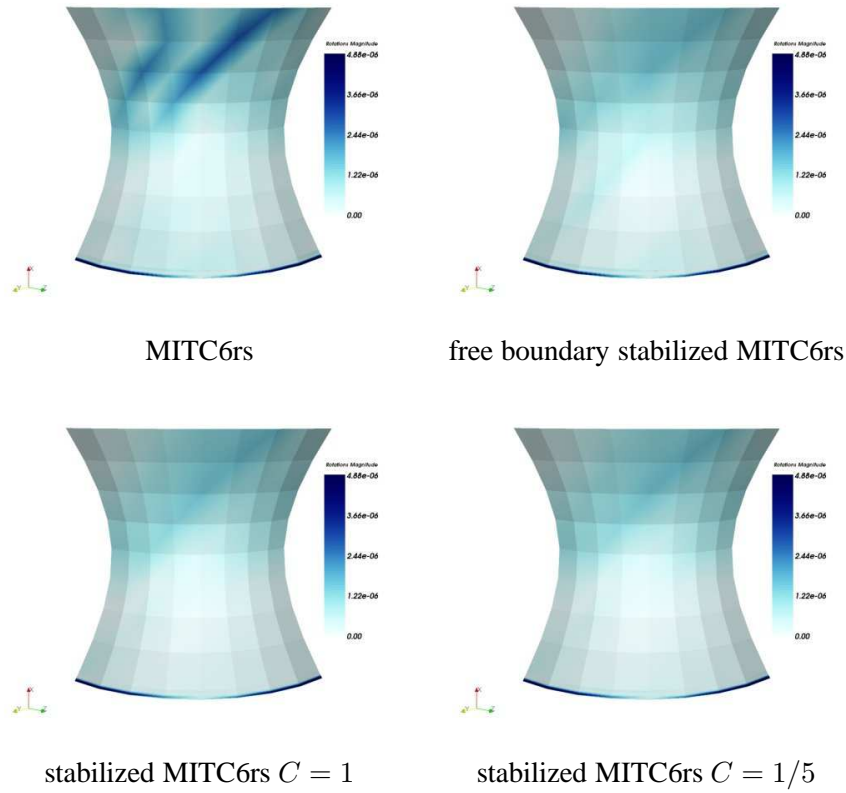


Figure 7.46: Rotations magnitude plots for the bottom clamped hyperboloid shell problem: MITC6rs (top left), MITC6rs with free boundary shear stabilization (top right), MITC6rs with weighted shear stabilization for $C = 1$ (bottom left), MITC6rs with weighted shear stabilization for $C = 1/5$ (bottom right) ($\varepsilon = 10^{-4}$, 441 nodes, 192 elements).

	$\varepsilon = 10^{-2}$	$\varepsilon = 10^{-3}$	$\varepsilon = 10^{-4}$
<i>Total</i>	4.528066703e-07	4.485741919e-04	4.485263003e-01
<i>Bending</i>	4.488325137e-07	4.485084929e-04	4.485054904e-01
<i>Membrane</i>	3.754967847e-09	4.428402894e-08	1.709512468e-05
<i>Shear</i>	2.696770818e-10	2.193531077e-08	2.487364942e-06

Table 7.41: Reference energy values associated with the free hyperboloid shell problem and MITC4 shell finite element.

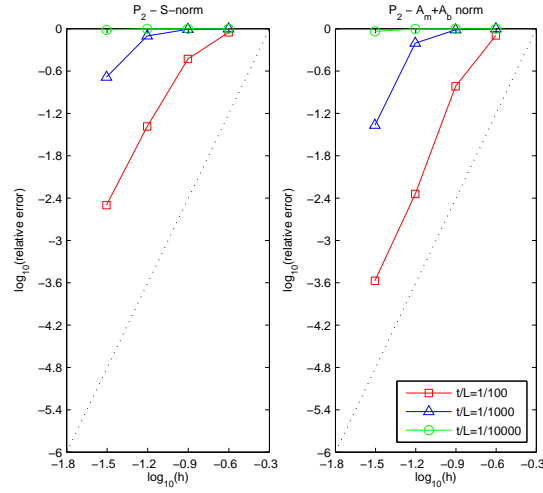


Figure 7.47: S-norm and $A_b + A_m$ -norm convergence curves associated with the free hyperboloid shell problem and P_2 displacement-based shell finite elements. The dotted line shows the optimal convergence rate which is 4.

$\varepsilon = 10^{-2}$	$h = 0.25$	$h = 0.125$	$h = 0.0625$	$h = 0.03125$
<i>Total</i>	5.041368696e-08	2.838633034e-07	4.343977146e-07	4.514674840e-07
<i>Bending</i>	5.554399749e-09	1.798461887e-07	4.141238375e-07	4.462540795e-07
<i>Membrane</i>	3.538477724e-08	7.997949645e-08	1.571825241e-08	4.580828835e-09
<i>Shear</i>	9.474863529e-09	2.405707706e-08	4.601758706e-09	6.826899058e-10
$\varepsilon = 10^{-3}$	$h = 0.25$	$h = 0.125$	$h = 0.0625$	$h = 0.03125$
<i>Total</i>	5.557447831e-07	7.742024689e-06	9.491258118e-05	3.593800428e-04
<i>Bending</i>	7.747227039e-10	1.428799755e-07	2.089907449e-05	2.894161421e-04
<i>Membrane</i>	4.351797799e-07	5.818982762e-06	5.622530354e-05	5.279341227e-05
<i>Shear</i>	1.197901594e-07	1.780162607e-06	1.778823760e-05	1.717078598e-05
$\varepsilon = 10^{-4}$	$h = 0.25$	$h = 0.125$	$h = 0.0625$	$h = 0.03125$
<i>Total</i>	5.525914806e-06	7.829493077e-05	1.207182107e-03	1.826469393e-02
<i>Bending</i>	3.078688208e-10	1.756776195e-08	3.467108559e-06	7.793331986e-04
<i>Membrane</i>	4.324631669e-06	5.984056865e-05	9.116878110e-04	1.316901283e-02
<i>Shear</i>	1.200975229e-06	1.843679433e-05	2.920271521e-04	4.316501600e-03

Table 7.42: Energy values associated with the free hyperboloid shell problem and P_2 displacement-based shell finite elements for different values of ε and h .

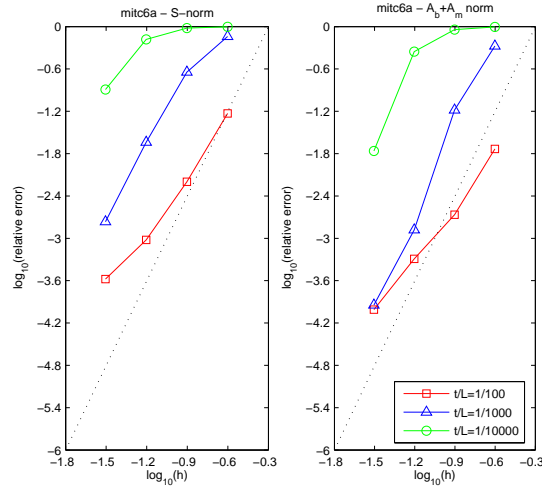


Figure 7.48: Convergence curves associated with the s-norm and $A_b + A_m$ norm for the free hyperboloid shell problem and MITC6a shell finite element. The dotted line shows the optimal convergence rate which is 4.

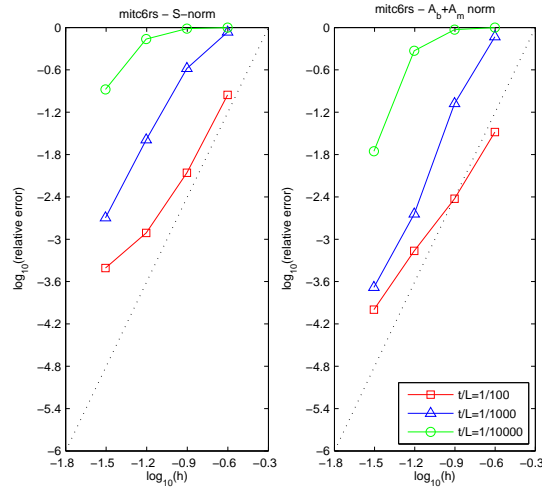


Figure 7.49: Convergence curves associated with the s-norm and $A_b + A_m$ norm for the free hyperboloid shell problem and MITC6rs shell finite element. The dotted line shows the optimal convergence rate which is 4.

$\varepsilon = 10^{-2}$		$h = 0.25$	$h = 0.125$	$h = 0.0625$	$h = 0.03125$
<i>Total</i>	<i>Reduced</i>	4.507763251e-07	4.576542204e-07	4.544685735e-07	4.532869623e-07
	<i>Unreduced</i>	7.098810434e-06	9.771226430e-07	4.906444032e-07	4.559755309e-07
<i>Bending</i>	<i>Reduced</i>	4.278707281e-07	4.518125878e-07	4.503382880e-07	4.492816258e-07
	<i>Unreduced</i>	4.290997168e-07	4.522301827e-07	4.504502435e-07	4.493101585e-07
<i>Membrane</i>	<i>Reduced</i>	1.869310669e-08	5.156781734e-09	3.856491262e-09	3.766078606e-09
	<i>Unreduced</i>	3.118158822e-06	2.211752491e-07	1.828124632e-08	4.851231031e-09
<i>Shear</i>	<i>Reduced</i>	4.238786903e-09	7.321264128e-10	3.241237733e-10	2.897391645e-10
	<i>Unreduced</i>	3.551610345e-06	3.037802536e-07	2.196784094e-08	1.865816286e-09
$\varepsilon = 10^{-3}$		$h = 0.25$	$h = 0.125$	$h = 0.0625$	$h = 0.03125$
<i>Total</i>	<i>Reduced</i>	1.298083660e-04	3.535985897e-04	4.402083822e-04	4.483736225e-04
	<i>Unreduced</i>	9.092691167e-02	5.114527062e-02	3.714923459e-03	6.663153887e-04
<i>Bending</i>	<i>Reduced</i>	4.491884541e-05	2.824813369e-04	4.305359890e-04	4.476482690e-04
	<i>Unreduced</i>	4.507688335e-05	2.827431535e-04	4.306361735e-04	4.476760131e-04
<i>Membrane</i>	<i>Reduced</i>	7.479283612e-05	6.949730878e-05	9.531201529e-06	6.932525197e-07
	<i>Unreduced</i>	2.710619732e-02	1.335844630e-02	1.329610636e-03	8.711361772e-05
<i>Shear</i>	<i>Reduced</i>	1.009477480e-05	1.618167028e-06	1.414575032e-07	3.254261910e-08
	<i>Unreduced</i>	6.377565022e-02	3.750409022e-02	1.954681311e-03	1.315275027e-04
$\varepsilon = 10^{-4}$		$h = 0.25$	$h = 0.125$	$h = 0.0625$	$h = 0.03125$
<i>Total</i>	<i>Reduced</i>	2.527052347e-03	2.157195323e-02	1.558996769e-01	3.919614231e-01
	<i>Unreduced</i>	6.032257988e+00	9.897730700e+01	4.596506045e+02	2.885299073e+01
<i>Bending</i>	<i>Reduced</i>	2.683296159e-04	1.902089219e-03	6.135421993e-02	3.428359895e-01
	<i>Unreduced</i>	2.678821792e-04	1.905124773e-03	6.138121352e-02	3.428587314e-01
<i>Membrane</i>	<i>Reduced</i>	1.876132048e-03	1.752703546e-02	9.137099726e-02	4.904019850e-02
	<i>Unreduced</i>	1.001343344e+00	4.901571753e+00	1.670904165e+01	6.693980256e+00
<i>Shear</i>	<i>Reduced</i>	3.825808980e-04	2.142784345e-03	3.175328241e-03	1.023052207e-04
	<i>Unreduced</i>	5.030646760e+00	9.407383016e+01	4.428801842e+02	2.181616352e+01

Table 7.43: *Reduced* and *unreduced* energy values associated with the free hyperboloid shell problem and MITC6a shell finite element for different values of ε and h .

$\varepsilon = 10^{-2}$		$h = 0.25$	$h = 0.125$	$h = 0.0625$	$h = 0.03125$
<i>Total</i>	<i>Reduced</i>	4.272420434e-07	4.557977272e-07	4.541273112e-07	4.532226697e-07
	<i>Unreduced</i>	6.775556542e-06	9.147493280e-07	4.848169882e-07	4.555943291e-07
<i>Bending</i>	<i>Reduced</i>	3.878355599e-07	4.495613596e-07	4.499528275e-07	4.492115458e-07
	<i>Unreduced</i>	3.890192290e-07	4.499314277e-07	4.500479208e-07	4.492362165e-07
<i>Membrane</i>	<i>Reduced</i>	1.901239125e-08	5.165552506e-09	3.854762007e-09	3.765748125e-09
	<i>Unreduced</i>	2.858117857e-06	2.228387582e-07	1.831352867e-08	4.851169089e-09
<i>Shear</i>	<i>Reduced</i>	2.036352754e-08	1.114499119e-09	3.697050635e-10	2.958056247e-10
	<i>Unreduced</i>	3.528420715e-06	2.420420557e-07	1.651042811e-08	1.558592613e-09
$\varepsilon = 10^{-3}$		$h = 0.25$	$h = 0.125$	$h = 0.0625$	$h = 0.03125$
<i>Total</i>	<i>Reduced</i>	6.543108150e-05	3.368398912e-04	4.388790974e-04	4.481817354e-04
	<i>Unreduced</i>	1.982298505e-02	4.304550893e-02	3.254622633e-03	6.241554130e-04
<i>Bending</i>	<i>Reduced</i>	1.031944262e-05	2.577716508e-04	4.286560165e-04	4.474014664e-04
	<i>Unreduced</i>	1.035171876e-05	2.580324053e-04	4.287564369e-04	4.474263099e-04
<i>Membrane</i>	<i>Reduced</i>	3.444383771e-05	6.974093320e-05	9.578521300e-06	6.921940167e-07
	<i>Unreduced</i>	6.831618607e-03	1.221903921e-02	1.328038009e-03	8.713790471e-05
<i>Shear</i>	<i>Reduced</i>	2.066549081e-05	9.320684530e-06	6.445710205e-07	8.837745068e-08
	<i>Unreduced</i>	1.298101425e-02	3.056844432e-02	1.497832767e-03	8.959281591e-05
$\varepsilon = 10^{-4}$		$h = 0.25$	$h = 0.125$	$h = 0.0625$	$h = 0.03125$
<i>Total</i>	<i>Reduced</i>	7.956733411e-04	1.517906207e-02	1.435194755e-01	3.909237946e-01
	<i>Unreduced</i>	3.014892443e-01	1.461720161e+01	1.358585026e+02	2.246284346e+01
<i>Bending</i>	<i>Reduced</i>	2.593644437e-06	5.794142609e-04	4.796640593e-02	3.410474554e-01
	<i>Unreduced</i>	2.595978518e-06	5.799809874e-04	4.798158684e-02	3.410703026e-01
<i>Membrane</i>	<i>Reduced</i>	4.961523582e-04	1.276910078e-02	9.065401326e-02	4.937630293e-02
	<i>Unreduced</i>	1.011261190e-01	2.505661452e+00	1.422629255e+01	6.668771938e+00
<i>Shear</i>	<i>Reduced</i>	2.969266444e-04	1.830516166e-03	4.899496033e-03	4.838137437e-04
	<i>Unreduced</i>	2.003605293e-01	1.211096019e+01	1.215842290e+02	1.545300636e+01

Table 7.44: *Reduced* and *unreduced* energy values associated with the free hyperboloid shell problem and MITC6rs shell finite element for different values of ε and h .

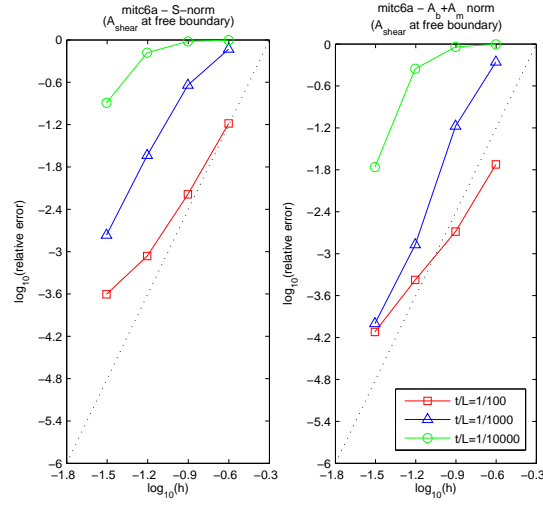


Figure 7.50: Convergence curves associated with the s-norm and $A_b + A_m$ norm for the free hyperboloid shell problem and MITC6a shell finite element with free boundary shear stabilization. The dotted line shows the optimal convergence rate which is 4.

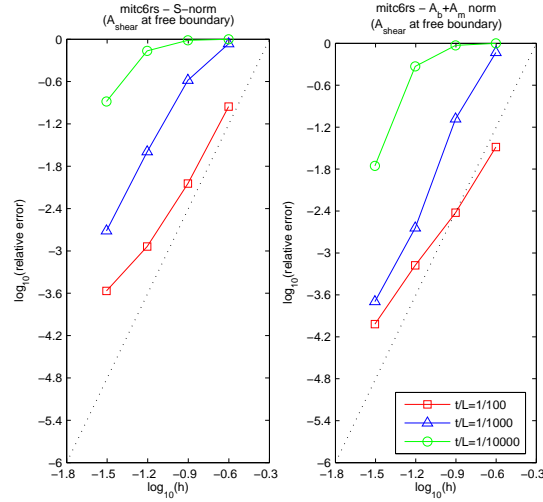


Figure 7.51: Convergence curves associated with the s-norm and $A_b + A_m$ norm for the trace shell problem and MITC6rs shell finite element with free boundary shear stabilization. The dotted line shows the optimal convergence rate which is 4.

$\varepsilon = 10^{-2}$		$h = 0.25$	$h = 0.125$	$h = 0.0625$	$h = 0.03125$
<i>Total</i>	<i>Reduced</i>	4.477346947e-07	4.575877991e-07	4.545060901e-07	4.532938428e-07
	<i>Unreduced</i>	6.964373386e-06	9.750847860e-07	4.905921651e-07	4.559640113e-07
<i>Bending</i>	<i>Reduced</i>	4.218290003e-07	4.515733856e-07	4.503709001e-07	4.492922774e-07
	<i>Unreduced</i>	4.230696479e-07	4.519921755e-07	4.504828674e-07	4.493208153e-07
<i>Membrane</i>	<i>Reduced</i>	1.939644718e-08	5.165402827e-09	3.856111871e-09	3.766013238e-09
	<i>Unreduced</i>	3.075883997e-06	2.211345121e-07	1.828327857e-08	4.851199912e-09
<i>Shear</i>	<i>Reduced</i>	6.482967808e-09	8.674923017e-10	3.149000131e-10	2.787589816e-10
	<i>Unreduced</i>	3.465473471e-06	3.020210406e-07	2.188094052e-08	1.843672465e-09
$\varepsilon = 10^{-3}$		$h = 0.25$	$h = 0.125$	$h = 0.0625$	$h = 0.03125$
<i>Total</i>	<i>Reduced</i>	1.227701916e-04	3.528511935e-04	4.401712008e-04	4.483798056e-04
	<i>Unreduced</i>	7.775505196e-02	5.087622953e-02	3.712321032e-03	6.662192488e-04
<i>Bending</i>	<i>Reduced</i>	3.993137843e-05	2.815141052e-04	4.304668402e-04	4.476491292e-04
	<i>Unreduced</i>	4.007497022e-05	2.817766769e-04	4.305671717e-04	4.476768755e-04
<i>Membrane</i>	<i>Reduced</i>	7.291964604e-05	6.953925598e-05	9.532887944e-06	6.932955254e-07
	<i>Unreduced</i>	2.431050600e-02	1.330096834e-02	1.329390497e-03	8.711597824e-05
<i>Shear</i>	<i>Reduced</i>	9.916315066e-06	1.790395249e-06	1.671826237e-07	3.546467780e-08
	<i>Unreduced</i>	5.340448141e-02	3.729349351e-02	1.952367994e-03	1.314279666e-04
$\varepsilon = 10^{-4}$		$h = 0.25$	$h = 0.125$	$h = 0.0625$	$h = 0.03125$
<i>Total</i>	<i>Reduced</i>	2.325272501e-03	2.140655675e-02	1.558424571e-01	3.919991329e-01
	<i>Unreduced</i>	4.856505796e+00	9.581771977e+01	4.588195590e+02	2.885328317e+01
<i>Bending</i>	<i>Reduced</i>	1.030848369e-04	1.883302926e-03	6.130619457e-02	3.428677894e-01
	<i>Unreduced</i>	1.031885100e-04	1.886366046e-03	6.133322956e-02	3.428905574e-01
<i>Membrane</i>	<i>Reduced</i>	1.809495669e-03	1.738751154e-02	9.136286580e-02	4.903424880e-02
	<i>Unreduced</i>	8.501385399e-01	4.836526789e+00	1.669636996e+01	6.694452683e+00
<i>Shear</i>	<i>Reduced</i>	4.126892865e-04	2.135720890e-03	3.174167713e-03	1.085973697e-04
	<i>Unreduced</i>	4.006264073e+00	9.097930668e+01	4.420618581e+02	2.181596305e+01

Table 7.45: *Reduced* and *unreduced* energy values associated with the free hyperboloid shell problem and MITC6a shell finite element with free boundary shear stabilization, for different values of ε and h .

$\varepsilon = 10^{-2}$		$h = 0.25$	$h = 0.125$	$h = 0.0625$	$h = 0.03125$
<i>Total</i>	<i>Reduced</i>	4.269728007e-07	4.556914021e-07	4.541273281e-07	4.532242699e-07
	<i>Unreduced</i>	6.720298351e-06	9.123425349e-07	4.846975101e-07	4.555431539e-07
<i>Bending</i>	<i>Reduced</i>	3.869687832e-07	4.493231457e-07	4.499407690e-07	4.492005727e-07
	<i>Unreduced</i>	3.881518939e-07	4.496937938e-07	4.500358380e-07	4.492252350e-07
<i>Membrane</i>	<i>Reduced</i>	1.939025835e-08	5.173790660e-09	3.854937169e-09	3.765761557e-09
	<i>Unreduced</i>	2.849700129e-06	2.227602906e-07	1.831361620e-08	4.851184688e-09
<i>Shear</i>	<i>Reduced</i>	2.054692986e-08	1.210266252e-09	3.671546045e-10	3.010938500e-10
	<i>Unreduced</i>	3.482449535e-06	2.399513205e-07	1.640294083e-08	1.518384597e-09
$\varepsilon = 10^{-3}$		$h = 0.25$	$h = 0.125$	$h = 0.0625$	$h = 0.03125$
<i>Total</i>	<i>Reduced</i>	6.536800850e-05	3.372550947e-04	4.388872276e-04	4.481913758e-04
	<i>Unreduced</i>	1.982496098e-02	4.314595864e-02	3.253179034e-03	6.240486044e-04
<i>Bending</i>	<i>Reduced</i>	1.005775774e-05	2.581564234e-04	4.286594191e-04	4.474031961e-04
	<i>Unreduced</i>	1.008884197e-05	2.584174549e-04	4.287598474e-04	4.474280402e-04
<i>Membrane</i>	<i>Reduced</i>	3.463324881e-05	6.989186504e-05	9.579967589e-06	6.922051843e-07
	<i>Unreduced</i>	6.834901808e-03	1.225106187e-02	1.328121308e-03	8.714220045e-05
<i>Shear</i>	<i>Reduced</i>	2.067499077e-05	9.195667455e-06	6.433856649e-07	9.399470218e-08
	<i>Unreduced</i>	1.297996973e-02	3.063648623e-02	1.496302364e-03	8.948011276e-05
$\varepsilon = 10^{-4}$		$h = 0.25$	$h = 0.125$	$h = 0.0625$	$h = 0.03125$
<i>Total</i>	<i>Reduced</i>	7.949808982e-04	1.518219156e-02	1.435857879e-01	3.909561334e-01
	<i>Unreduced</i>	3.003922886e-01	1.462928821e+01	1.360499494e+02	2.246392306e+01
<i>Bending</i>	<i>Reduced</i>	2.394180461e-06	5.741776535e-04	4.796940091e-02	3.410717390e-01
	<i>Unreduced</i>	2.397220486e-06	5.747412220e-04	4.798457586e-02	3.410945903e-01
<i>Membrane</i>	<i>Reduced</i>	4.957538317e-04	1.277520896e-02	9.072870462e-02	4.938045865e-02
	<i>Unreduced</i>	1.008189604e-01	2.507071455e+00	1.424206043e+01	6.669406428e+00
<i>Shear</i>	<i>Reduced</i>	2.968324230e-04	1.832773460e-03	4.889809350e-03	4.781525802e-04
	<i>Unreduced</i>	1.995709309e-01	1.212164202e+01	1.217599036e+02	1.545341720e+01

Table 7.46: *Reduced* and *unreduced* energy values associated with the free hyperboloid shell problem and MITC6rs shell finite element with free boundary shear stabilization, for different values of ε and h .

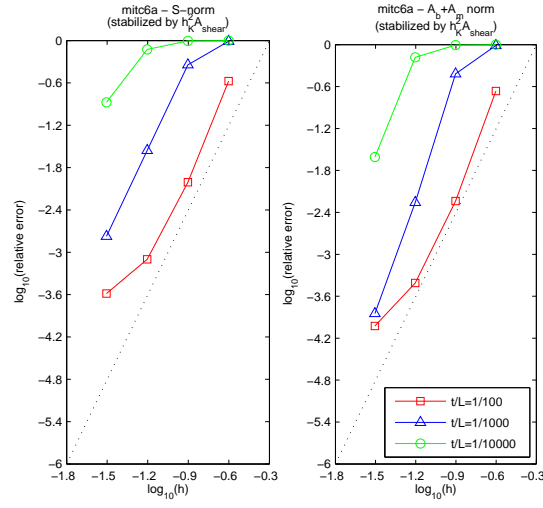


Figure 7.52: Convergence curves associated with the s-norm and $A_b + A_m$ norm for the free hyperboloid shell problem and MITC6a shell finite element with weighted shear stabilization ($C = 1$). The dotted line shows the optimal convergence rate which is 4.

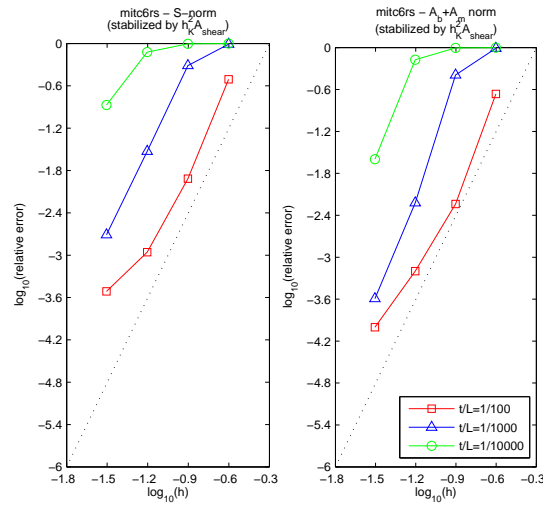


Figure 7.53: Convergence curves associated with the s-norm and $A_b + A_m$ norm for the free hyperboloid shell problem and MITC6rs shell finite element with weighted shear stabilization ($C = 1$). The dotted line shows the optimal convergence rate which is 4.

$\varepsilon = 10^{-2}$		$h = 0.25$	$h = 0.125$	$h = 0.0625$	$h = 0.03125$
<i>Total</i>	<i>Reduced</i>	2.617075960e-07	4.456436129e-07	4.539661706e-07	4.532369235e-07
	<i>Unreduced</i>	1.543340357e-06	7.605373836e-07	4.866381678e-07	4.558562669e-07
<i>Bending</i>	<i>Reduced</i>	1.538499529e-07	4.315915183e-07	4.493760420e-07	4.491828526e-07
	<i>Unreduced</i>	1.543043914e-07	4.319389121e-07	4.494840690e-07	4.492112978e-07
<i>Membrane</i>	<i>Reduced</i>	1.947900700e-08	5.258345101e-09	3.856061214e-09	3.765933014e-09
	<i>Unreduced</i>	1.078471755e-06	2.132433560e-07	1.826196270e-08	4.850884145e-09
<i>Shear</i>	<i>Reduced</i>	8.750031502e-08	8.168543949e-09	6.090445922e-10	2.949335181e-10
	<i>Unreduced</i>	3.106550056e-07	1.154213101e-07	1.894700656e-08	1.845748454e-09
$\varepsilon = 10^{-3}$		$h = 0.25$	$h = 0.125$	$h = 0.0625$	$h = 0.03125$
<i>Total</i>	<i>Reduced</i>	6.222257326e-06	1.741097189e-04	4.287683284e-04	4.479335823e-04
	<i>Unreduced</i>	8.050331328e-05	4.270335153e-03	2.139118937e-03	6.055529224e-04
<i>Bending</i>	<i>Reduced</i>	9.735732664e-08	6.946071275e-05	4.103743646e-04	4.468658187e-04
	<i>Unreduced</i>	9.761382851e-08	6.951647052e-05	4.104545472e-04	4.468904420e-04
<i>Membrane</i>	<i>Reduced</i>	1.134921331e-06	2.834584571e-05	9.605762268e-06	6.947885557e-07
	<i>Unreduced</i>	6.263292822e-05	3.164527208e-03	1.263886900e-03	8.702127447e-05
<i>Shear</i>	<i>Reduced</i>	4.989453660e-06	7.619681235e-05	8.627131079e-06	3.292293427e-07
	<i>Unreduced</i>	1.777282485e-05	1.036299429e-03	4.647826750e-04	7.164290542e-05
$\varepsilon = 10^{-4}$		$h = 0.25$	$h = 0.125$	$h = 0.0625$	$h = 0.03125$
<i>Total</i>	<i>Reduced</i>	6.198217125e-05	2.857619745e-03	8.441896366e-02	3.795546743e-01
	<i>Unreduced</i>	8.050540942e-04	1.133362643e-01	6.328838392e+00	8.726433347e+00
<i>Bending</i>	<i>Reduced</i>	1.836280677e-08	2.226501950e-05	1.619627805e-02	3.215254504e-01
	<i>Unreduced</i>	1.836373218e-08	2.227808434e-05	1.619956111e-02	3.215410561e-01
<i>Membrane</i>	<i>Reduced</i>	1.152290842e-05	7.932526733e-04	3.868123324e-02	4.786111755e-02
	<i>Unreduced</i>	6.261951328e-04	8.531104756e-02	4.723587374e+00	6.244441604e+00
<i>Shear</i>	<i>Reduced</i>	5.044084743e-05	2.042073113e-03	2.953575203e-02	1.013976265e-02
	<i>Unreduced</i>	1.788406030e-04	2.800294126e-02	1.589051455e+00	2.160475047e+00

Table 7.47: *Reduced* and *unreduced* energy values associated with the free hyperboloid shell problem and MITC6a shell finite element with weighted shear stabilization ($C = 1$), for different values of ε and h .

$\varepsilon = 10^{-2}$		$h = 0.25$	$h = 0.125$	$h = 0.0625$	$h = 0.03125$
<i>Total</i>	<i>Reduced</i>	2.503041479e-07	4.446947735e-07	4.536949344e-07	4.531737634e-07
	<i>Unreduced</i>	1.430948643e-06	7.572149749e-07	4.824466653e-07	4.554853484e-07
<i>Bending</i>	<i>Reduced</i>	1.409619802e-07	4.301621238e-07	4.491192842e-07	4.491153678e-07
	<i>Unreduced</i>	1.413836728e-07	4.305022280e-07	4.492134277e-07	4.491400114e-07
<i>Membrane</i>	<i>Reduced</i>	1.927642993e-08	5.269928585e-09	3.854500627e-09	3.765610050e-09
	<i>Unreduced</i>	1.000934422e-06	2.134908598e-07	1.829028290e-08	4.850826317e-09
<i>Shear</i>	<i>Reduced</i>	8.925747743e-08	8.638452716e-09	5.961046382e-10	2.995476659e-10
	<i>Unreduced</i>	2.887079573e-07	1.132873834e-07	1.499779720e-08	1.546149012e-09
$\varepsilon = 10^{-3}$		$h = 0.25$	$h = 0.125$	$h = 0.0625$	$h = 0.03125$
<i>Total</i>	<i>Reduced</i>	5.695310974e-06	1.658401872e-04	4.278244937e-04	4.478265801e-04
	<i>Unreduced</i>	6.836129958e-05	3.912349537e-03	2.140165558e-03	5.933099161e-04
<i>Bending</i>	<i>Reduced</i>	8.064092524e-08	6.308044538e-05	4.087052837e-04	4.467599771e-04
	<i>Unreduced</i>	8.086239774e-08	6.313153547e-05	4.087873845e-04	4.467836734e-04
<i>Membrane</i>	<i>Reduced</i>	1.026105567e-06	2.657686853e-05	9.607863584e-06	6.935367740e-07
	<i>Unreduced</i>	5.325610483e-05	2.891063170e-03	1.259387388e-03	8.702318281e-05
<i>Shear</i>	<i>Reduced</i>	4.588117487e-06	7.608575681e-05	9.350780530e-06	3.294299914e-07
	<i>Unreduced</i>	1.502437499e-05	9.581615617e-04	4.719958945e-04	5.950468312e-05
$\varepsilon = 10^{-4}$		$h = 0.25$	$h = 0.125$	$h = 0.0625$	$h = 0.03125$
<i>Total</i>	<i>Reduced</i>	5.690405121e-05	2.662240584e-03	8.190584076e-02	3.787828209e-01
	<i>Unreduced</i>	6.872105586e-04	9.918532699e-02	6.012112390e+00	8.736427482e+00
<i>Bending</i>	<i>Reduced</i>	1.655018065e-08	1.791721621e-05	1.533152948e-02	3.202511701e-01
	<i>Unreduced</i>	1.655573734e-08	1.793046442e-05	1.533467153e-02	3.202671894e-01
<i>Membrane</i>	<i>Reduced</i>	1.042897128e-05	7.135713054e-04	3.663800338e-02	4.771178662e-02
	<i>Unreduced</i>	5.352037939e-04	7.446177350e-02	4.458245975e+00	6.219546971e+00
<i>Shear</i>	<i>Reduced</i>	4.645848312e-05	1.930726300e-03	2.993142314e-02	1.076868193e-02
	<i>Unreduced</i>	1.519902129e-04	2.470562505e-02	1.538532369e+00	2.196644003e+00

Table 7.48: *Reduced* and *unreduced* energy values associated with the free hyperboloid shell problem and MITC6rs shell finite element with weighted shear stabilization ($C = 1$), for different values of ε and h .

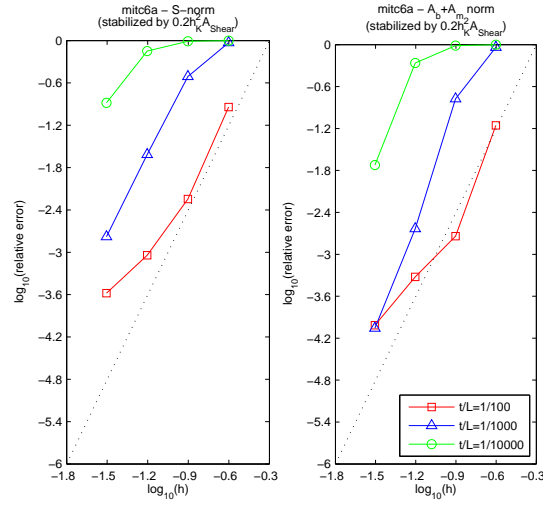


Figure 7.54: Convergence curves associated with the s-norm and $A_b + A_m$ norm for the free hyperboloid shell problem and MITC6a shell finite element with weighted shear stabilization ($C = 1/5$). The dotted line shows the optimal convergence rate which is 4.

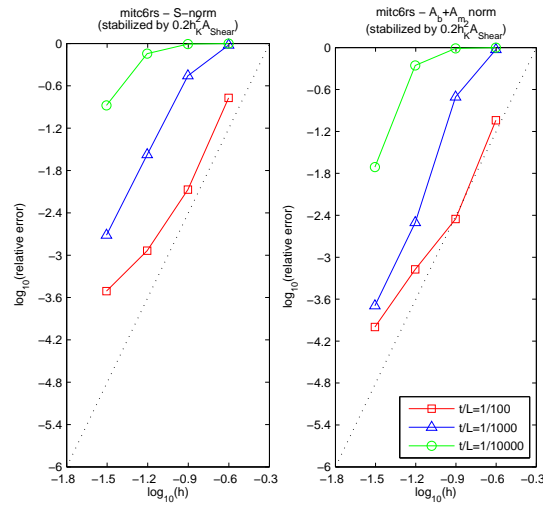


Figure 7.55: Convergence curves associated with the s-norm and $A_b + A_m$ norm for the free hyperboloid shell problem and MITC6rs shell finite element with weighted shear stabilization ($C = 1/5$). The dotted line shows the optimal convergence rate which is 4.

$\varepsilon = 10^{-2}$		$h = 0.25$	$h = 0.125$	$h = 0.0625$	$h = 0.03125$
<i>Total</i>	<i>Reduced</i>	3.674793797e-07	4.541893126e-07	4.543640212e-07	4.532769475e-07
	<i>Unreduced</i>	3.336862582e-06	8.812805284e-07	4.897480936e-07	4.559516195e-07
<i>Bending</i>	<i>Reduced</i>	2.939076115e-07	4.455424982e-07	4.501347350e-07	4.492618520e-07
	<i>Unreduced</i>	2.947723015e-07	4.459310302e-07	4.502458109e-07	4.492903671e-07
<i>Membrane</i>	<i>Reduced</i>	2.029986341e-08	5.179924211e-09	3.856393533e-09	3.766049696e-09
	<i>Unreduced</i>	2.122811288e-06	2.193379901e-07	1.827737791e-08	4.851161756e-09
<i>Shear</i>	<i>Reduced</i>	5.294455994e-08	3.374373487e-09	3.880835591e-10	2.907883049e-10
	<i>Unreduced</i>	9.193937366e-07	2.160757583e-07	2.127982090e-08	1.861763057e-09
$\varepsilon = 10^{-3}$		$h = 0.25$	$h = 0.125$	$h = 0.0625$	$h = 0.03125$
<i>Total</i>	<i>Reduced</i>	2.700488114e-04	2.700488114e-04	4.364975169e-04	4.482635823e-04
	<i>Unreduced</i>	1.087913838e-02	1.087913838e-02	2.465185292e-03	6.455077729e-04
<i>Bending</i>	<i>Reduced</i>	8.771434770e-07	1.644278506e-04	4.240862895e-04	4.474383075e-04
	<i>Unreduced</i>	8.795035894e-07	1.645572574e-04	4.241714654e-04	4.474650314e-04
<i>Membrane</i>	<i>Reduced</i>	5.529600967e-06	6.064873068e-05	9.729182224e-06	6.936848238e-07
	<i>Unreduced</i>	5.753441758e-04	7.725615186e-03	1.312510133e-03	8.709516622e-05
<i>Shear</i>	<i>Reduced</i>	1.247760012e-05	4.492134977e-05	2.648951083e-06	1.230778115e-07
	<i>Unreduced</i>	2.168232134e-04	2.988979814e-03	7.285085187e-04	1.109493003e-04
$\varepsilon = 10^{-4}$		$h = 0.25$	$h = 0.125$	$h = 0.0625$	$h = 0.03125$
<i>Total</i>	<i>Reduced</i>	1.943076397e-04	6.760774985e-03	1.177428393e-01	3.879878085e-01
	<i>Unreduced</i>	8.458487586e-03	6.610661723e-01	1.295613065e+01	9.507414204e+00
<i>Bending</i>	<i>Reduced</i>	1.835533486e-07	1.151878176e-04	3.109391072e-02	3.357267082e-01
	<i>Unreduced</i>	1.834683906e-07	1.152644560e-04	3.110004041e-02	3.357428730e-01
<i>Membrane</i>	<i>Reduced</i>	5.982511865e-05	3.952808231e-03	7.324710056e-02	4.980045018e-02
	<i>Unreduced</i>	6.132986565e-03	4.802622801e-01	9.398674359e+00	6.563550910e+00
<i>Shear</i>	<i>Reduced</i>	1.342988608e-04	2.692747132e-03	1.339907110e-02	2.467725070e-03
	<i>Unreduced</i>	2.325317594e-03	1.806886409e-01	3.526357226e+00	2.608123597e+00

Table 7.49: *Reduced* and *unreduced* energy values associated with the free hyperboloid shell problem and MITC6a shell finite element with weighted shear stabilization ($C = 1/5$), for different values of ε and h .

$\varepsilon = 10^{-2}$		$h = 0.25$	$h = 0.125$	$h = 0.0625$	$h = 0.03125$
<i>Total</i>	<i>Reduced</i>	3.458889502e-07	4.528053131e-07	4.540386790e-07	4.532128839e-07
	<i>Unreduced</i>	3.038833025e-06	8.540926340e-07	4.843084193e-07	4.555725029e-07
<i>Bending</i>	<i>Reduced</i>	2.604771362e-07	4.439468055e-07	4.497802529e-07	4.491922987e-07
	<i>Unreduced</i>	2.612789765e-07	4.443078639e-07	4.498751450e-07	4.492169640e-07
<i>Membrane</i>	<i>Reduced</i>	2.010840769e-08	5.189965591e-09	3.854701338e-09	3.765720718e-09
	<i>Unreduced</i>	1.903709240e-06	2.203970102e-07	1.830877743e-08	4.851100466e-09
<i>Shear</i>	<i>Reduced</i>	6.499752814e-08	3.573949784e-09	4.186460172e-10	2.965592037e-10
	<i>Unreduced</i>	8.739224396e-07	1.894515418e-07	1.617937741e-08	1.556085293e-09
$\varepsilon = 10^{-3}$		$h = 0.25$	$h = 0.125$	$h = 0.0625$	$h = 0.03125$
<i>Total</i>	<i>Reduced</i>	1.482755682e-05	2.550228678e-04	4.355831914e-04	4.480992095e-04
	<i>Unreduced</i>	5.030632690e-04	9.955765362e-03	2.419144422e-03	6.146141969e-04
<i>Bending</i>	<i>Reduced</i>	5.361146997e-07	1.469085833e-04	4.227059968e-04	4.472444668e-04
	<i>Unreduced</i>	5.376530098e-07	1.470320355e-04	4.227958363e-04	4.472689960e-04
<i>Membrane</i>	<i>Reduced</i>	3.802150990e-06	5.594963377e-05	9.741993002e-06	6.924793832e-07
	<i>Unreduced</i>	3.590715460e-04	6.939471574e-03	1.309203122e-03	8.711204840e-05
<i>Shear</i>	<i>Reduced</i>	1.048861401e-05	5.211758330e-05	3.102000531e-06	1.539155795e-07
	<i>Unreduced</i>	1.434542504e-04	2.869272244e-03	6.871501858e-04	8.023484513e-05
$\varepsilon = 10^{-4}$		$h = 0.25$	$h = 0.125$	$h = 0.0625$	$h = 0.03125$
<i>Total</i>	<i>Reduced</i>	1.525962314e-04	5.997125051e-03	1.145705157e-01	3.872844855e-01
	<i>Unreduced</i>	5.358500787e-03	5.340727144e-01	1.246664869e+01	9.462812052e+00
<i>Bending</i>	<i>Reduced</i>	1.401465547e-07	8.575417506e-05	2.963950988e-02	3.346428283e-01
	<i>Unreduced</i>	1.401732944e-07	8.582440609e-05	2.964572062e-02	3.346601016e-01
<i>Membrane</i>	<i>Reduced</i>	4.077482478e-05	3.214859861e-03	6.981235880e-02	4.968192235e-02
	<i>Unreduced</i>	3.823491537e-03	3.802771869e-01	8.923651120e+00	6.541895278e+00
<i>Shear</i>	<i>Reduced</i>	1.116811707e-04	2.696482440e-03	1.511667616e-02	2.961882592e-03
	<i>Unreduced</i>	1.534869095e-03	1.537097124e-01	3.513351322e+00	2.586247026e+00

Table 7.50: *Reduced* and *unreduced* energy values associated with the free hyperboloid shell problem and MITC6rs shell finite element with weighted shear stabilization ($C = 1/5$), for different values of ε and h .

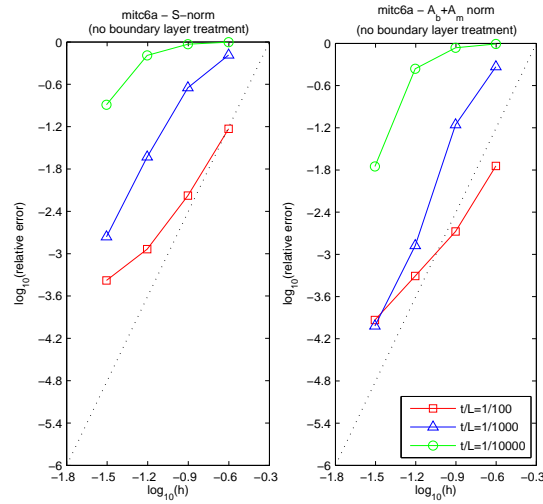


Figure 7.56: Convergence curves associated with the s-norm and $A_b + A_m$ norm for the free hyperboloid shell problem and MITC6a shell finite element, with no boundary layer treatment. The dotted line shows the optimal convergence rate which is 4.

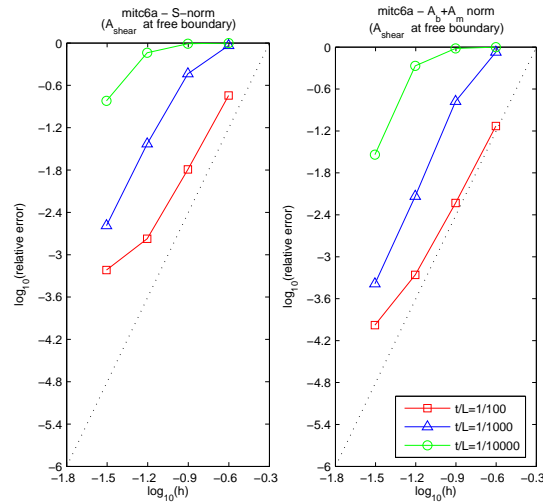


Figure 7.57: Convergence curves associated with the s-norm and $A_b + A_m$ norm for the trace shell problem and MITC6a shell finite element with free boundary shear stabilization and no boundary layer treatment. The dotted line shows the optimal convergence rate which is 4.

$\varepsilon = 10^{-2}$		$h = 0.25$	$h = 0.125$	$h = 0.0625$	$h = 0.03125$
<i>Total</i>	<i>Reduced</i>	4.507233380e-07	4.573636497e-07	4.542297250e-07	4.530863733e-07
	<i>Unreduced</i>	7.566373074e-06	1.008506642e-06	4.924788127e-07	4.558934836e-07
<i>Bending</i>	<i>Reduced</i>	4.277860283e-07	4.515729532e-07	4.502130801e-07	4.491267001e-07
	<i>Unreduced</i>	4.290354074e-07	4.519956747e-07	4.503255222e-07	4.491549465e-07
<i>Membrane</i>	<i>Reduced</i>	1.991229907e-08	5.301644490e-09	3.869239089e-09	3.769829904e-09
	<i>Unreduced</i>	3.229688983e-06	2.298307251e-07	1.881854547e-08	4.882390475e-09
<i>Shear</i>	<i>Reduced</i>	3.050804309e-09	5.363500457e-10	1.977071373e-10	2.402935822e-10
	<i>Unreduced</i>	3.907701794e-06	3.267421093e-07	2.338946594e-08	1.907750673e-09
$\varepsilon = 10^{-3}$		$h = 0.25$	$h = 0.125$	$h = 0.0625$	$h = 0.03125$
<i>Total</i>	<i>Reduced</i>	1.625527648e-04	3.542093800e-04	4.399435278e-04	4.483329616e-04
	<i>Unreduced</i>	2.213331861e-01	5.761405752e-02	3.787082143e-03	6.700306366e-04
<i>Bending</i>	<i>Reduced</i>	8.166357389e-05	2.859230172e-04	4.300404225e-04	4.476071873e-04
	<i>Unreduced</i>	8.196436906e-05	2.861738012e-04	4.301418498e-04	4.476350181e-04
<i>Membrane</i>	<i>Reduced</i>	7.057751185e-05	6.668469937e-05	9.794706658e-06	7.125797186e-07
	<i>Unreduced</i>	4.197162623e-02	1.352934486e-02	1.345882261e-03	8.829757076e-05
<i>Shear</i>	<i>Reduced</i>	1.030592070e-05	1.599509029e-06	1.086717771e-07	1.368905197e-08
	<i>Unreduced</i>	1.792796358e-01	4.379855064e-02	2.011062702e-03	1.340996811e-04
$\varepsilon = 10^{-4}$		$h = 0.25$	$h = 0.125$	$h = 0.0625$	$h = 0.03125$
<i>Total</i>	<i>Reduced</i>	3.795086703e-03	3.336341783e-02	1.615416760e-01	3.916439848e-01
	<i>Unreduced</i>	2.101648248e+01	7.288439425e+02	7.805958067e+02	3.085277625e+01
<i>Bending</i>	<i>Reduced</i>	6.249320038e-05	6.685707443e-03	7.047872658e-02	3.424147377e-01
	<i>Unreduced</i>	6.273443807e-05	6.692161711e-03	7.049826760e-02	3.424368908e-01
<i>Membrane</i>	<i>Reduced</i>	3.204400254e-03	2.227019226e-02	8.786015733e-02	4.911452411e-02
	<i>Unreduced</i>	2.264870437e+00	1.160360454e+01	1.775391842e+01	6.707542217e+00
<i>Shear</i>	<i>Reduced</i>	5.281877927e-04	4.407258082e-03	3.202484078e-03	1.144199903e-04
	<i>Unreduced</i>	1.875154934e+01	7.172336462e+02	7.627713904e+02	2.380279822e+01

Table 7.51: *Reduced* and *unreduced* energy values associated with the free hyperboloid shell problem and MITC6a shell finite element with no boundary layer treatment, for different values of ε and h .

$\varepsilon = 10^{-2}$		$h = 0.25$	$h = 0.125$	$h = 0.0625$	$h = 0.03125$
<i>Total</i>	<i>Reduced</i>	3.906678996e-07	4.517187583e-07	4.538314463e-07	4.530498728e-07
	<i>Unreduced</i>	5.909376812e-06	9.791006141e-07	4.912392593e-07	4.557747340e-07
<i>Bending</i>	<i>Reduced</i>	3.375224014e-07	4.422016934e-07	4.493941135e-07	4.489797582e-07
	<i>Unreduced</i>	3.385367142e-07	4.426155258e-07	4.495061954e-07	4.490076196e-07
<i>Membrane</i>	<i>Reduced</i>	3.494950442e-08	5.707114866e-09	3.880255991e-09	3.770903449e-09
	<i>Unreduced</i>	2.366145607e-06	2.244462965e-07	1.880419273e-08	4.883337388e-09
<i>Shear</i>	<i>Reduced</i>	1.779738770e-08	3.590829000e-09	4.688154146e-10	2.789262502e-10
	<i>Unreduced</i>	3.204789408e-06	3.121007746e-07	2.298354838e-08	1.935379969e-09
$\varepsilon = 10^{-3}$		$h = 0.25$	$h = 0.125$	$h = 0.0625$	$h = 0.03125$
<i>Total</i>	<i>Reduced</i>	3.703815892e-05	2.863902958e-04	4.323866289e-04	4.476472572e-04
	<i>Unreduced</i>	7.153594506e-03	3.849456976e-02	3.768046354e-03	6.669176113e-04
<i>Bending</i>	<i>Reduced</i>	3.645565783e-06	1.946299695e-04	4.178393432e-04	4.463886639e-04
	<i>Unreduced</i>	3.656332715e-06	1.948008195e-04	4.179330964e-04	4.464163840e-04
<i>Membrane</i>	<i>Reduced</i>	2.748871019e-05	8.225624625e-05	1.190840606e-05	7.290022839e-07
	<i>Unreduced</i>	2.245334923e-03	8.783409413e-03	1.298715845e-03	8.804267001e-05
<i>Shear</i>	<i>Reduced</i>	5.899032523e-06	9.387508146e-06	2.507780378e-06	4.578378626e-07
	<i>Unreduced</i>	4.904605264e-03	2.951637551e-02	2.051402390e-03	1.324601793e-04
$\varepsilon = 10^{-4}$		$h = 0.25$	$h = 0.125$	$h = 0.0625$	$h = 0.03125$
<i>Total</i>	<i>Reduced</i>	4.107995755e-04	9.842821768e-03	1.231315974e-01	3.800249874e-01
	<i>Unreduced</i>	9.076374984e-02	9.626838158e+00	2.047326283e+02	3.019371918e+01
<i>Bending</i>	<i>Reduced</i>	4.562553585e-07	2.708335446e-04	3.906618079e-02	3.242544071e-01
	<i>Unreduced</i>	4.576055603e-07	2.710998353e-04	3.907802530e-02	3.242736184e-01
<i>Membrane</i>	<i>Reduced</i>	3.386462745e-04	8.830963551e-03	8.066875899e-02	5.323334766e-02
	<i>Unreduced</i>	2.789327516e-02	1.119271354e+00	1.081929908e+01	6.283499738e+00
<i>Shear</i>	<i>Reduced</i>	7.169643746e-05	7.408704492e-04	3.385548762e-03	2.484766222e-03
	<i>Unreduced</i>	6.287001734e-02	8.507295730e+00	1.938742520e+02	2.358594630e+01

Table 7.52: *Reduced* and *unreduced* energy values associated with the free hyperboloid shell problem and MITC6a shell finite element with free boundary shear stabilization and no boundary layer treatment, for different values of ε and h .

7.6 Concluding remarks

The existence of spurious membrane modes in the MITC6a solution on some membrane dominated shell problems leads us to unsatisfactory error curves, erroneous displacement graphs and bad rotations. Namely, it substantially deteriorates the performance of this element in membrane dominated situations.

On the other hand, the MITC6a shell finite element displays some locking only for small thickness and coarse meshes in general bending-dominated cases, and it is one of the best MITC6 candidates that we have found until now. So, it is interesting to develop some *spurious modes filtering procedures* that do not deteriorate its performance in bending dominated situations.

As we have seen in Section 7.1, the existence of spurious membrane modes can be numerically evidenced for a particular shell problem. We observed that not only the real membrane spurious modes, but also a kind of *pseudo parasitic modes* may have a high participation into the “correct” solution that fairly deteriorates the expected behavior.

The *trace shell problem* presented in this work has been especially designed to make those parasitic membrane modes arise for the particular geometry in consideration. We have seen that the membrane spurious modes that appear for this particular membrane dominated shell problem mainly arise as oscillations of large amplitude near the free boundaries that also propagate inside the domain. As a consequence, there is a difference of several orders of magnitude when comparing the reduced and unreduced shear energies of the MITC6a solution as rotations are really badly predicted, but the amplification is weaker in the unreduced membrane energy as compared to the reduced one. In fact, those real and pseudo modes are characterized by a quite high unreduced shear energy amount.

The cures that we have developed are typically based on the results obtained for this particular *trace shell problem*. The observations we have done indicate that the nature of the spurious part of the solution is mainly reflected in the shear energy. Moreover, it is well known that in general bending dominated situations the main source of locking is the membrane energy, and not the shear energy. The combination of these two arguments suggested to stabilize/modify only the shear part of the MITC6a and MITC6rs bilinear forms, in order to reach our aforementioned goal. Such considerations led us to firstly formulate the weighted shear stabilization method described in Section 7.3.1.

As we have noticed, the real and pseudo membrane spurious modes seem to mainly arise as oscillations near the free boundary. The larger number of degrees of freedom along the free boundaries, combined with the reduced integration, may explain this membrane “parasitic” kernel¹⁰ that seems to be increased in h^{-1} for the *trace shell problem*, and we proposed the free boundary shear stabilization formulated in Section 7.3.2 owing to this observation.

¹⁰Note that this same qualitative property is shared by the inextensional modes in bending dominated shell problems.

Another strategy is to adopt a richer interpolation space for the transverse shear strains. The MITC6a shell finite element uses essentially the second order rotated Raviart Thomas space for the transverse shear strains in the reference element and such space has dimension 8. We therefore proposed a new element, named the MITC6rs, which is similar to the MITC6a element, except on the transverse shear strain space and tying procedure, which is the richer one introduced in Section 7.3.3.

In order to perform an assessment for the new MITC6rs and the proposed stabilized formulations for the MITC6a and MITC6rs shell elements, we have analyzed the trace shell problem again, but also two membrane dominated hyperboloid shell problems and a bending dominated one for the same complex geometry. We globally observe that the richer shear transverse strains and shear stabilizations (free boundary and weighted) constitute effective cures to rotations and midsurface displacements in membrane dominated situations. The numerical results are substantially improved as seen by means of the s -norm, A_m norm and deformed graphs as compared to the original MITC6a element. The free boundary shear stabilization works quite well when free boundaries exist as parasitic membrane modes are considerably filtered out. As regards the weighted shear stabilizations we propose, we observe that it is $C = 1$ that provides better results in membrane dominated situations as compared to $C = 1/5$, whereas it is $C = 1/5$ that works better in the bending dominated problem we considered. This fact is well understood given that a smaller constant C gives a weaker improvement by the weighted shear stabilization in membrane dominated shell problems as it was commented in Section 7.3.1, but adds *less shear locking* in bending dominated cases. A compromise must be found, and we propose the weighted shear stabilization for $C = 1/5$ as a good candidate for engineering practice.

In shell analysis it is often adequate to adopt meshes which are refined near the boundaries in order to cope with the presence of boundary layers in the solution. In such cases, the free boundary band of elements may have an area which is extremely small with respect to the total area of the domain. Nevertheless, the presence of a layer in the solution near the free boundary implies a higher concentration of energy. In our analysis we have seen that boundary layers properly treated help the element convergence for refined meshes and small thickness, even when a free boundary shear stabilization is used.

Finally, we conclude that the MITC6rs and the stabilized formulations presented in this work constitute an effective cure for the MITC6a shell finite element in membrane dominated shell problems, whereas the MITC performance is not severely hindered for the bending dominated shell problem that we have analyzed. Namely, *some locking* still occurs for small relative thickness and coarse meshes, but the stabilized results do not differ very much from the original MITC6a ones and are substantially improved as the mesh is refined. Furthermore, the membrane spurious modes are substantially filtered out for membrane dominated shell problems and almost optimal and uniform convergence is achieved.

Chapter 8

The ‘Scordelis-Lo Roof’: a mixed behavior

Dominique Chapelle, Iria París

Abstract

We consider in this section a shell problem for which pure bending is inhibited, but the condition “ $G \in \mathcal{V}'_m$ ” does not hold. Namely, the asymptotic behavior corresponds to an *ill-posed* membrane problem as the membrane deformation energy by itself is unable to appropriately control some specific displacement fields that are excited by the loading. Strong singularities appear near the free boundaries of the structure when the thickness gets small and most of the energy is concentrated in the generated layers (see [43], [60] and the references therein). We can focus our analysis on a sequence of scaled variational problems parametrized by ε , which can be formulated in the boundary layer domain and are known to have a well-defined limit solution when ε tends to 0. This scaled layer problem takes the form of a penalized formulation for $\varepsilon \rightarrow 0$, which typically induces *numerical locking* for standard shell finite elements.

The aim of this section is to assess the performance of the MITC6a and MITC6rs shell finite elements, and the associated free boundary and weighted shear stabilizations presented in Section 7.3. Although these stabilizations have been specifically designed to filter out those parasitic membrane modes that may substantially deteriorate the correct solution in membrane dominated situations, the objective is to preserve the MITC performance in bending dominated –or otherwise penalized– shell problems, which is why we consider this particular benchmark.

8.1 The ‘Scordelis-Lo Roof’ shell problem

We consider an elastic shell of cylindrical midsurface \mathcal{S} displayed in Fig. 8.1 with relative thickness

$$\varepsilon = \frac{t}{L} \quad (8.1)$$

where t and L respectively denote the thickness and a characteristic length of the structure. For the sake of simplicity, the thickness is taken as constant over all the domain but we allow it to vary in order to analyze the asymptotic behavior.

The 2D-chart that represents the midsurface can be defined as:

$$\vec{\phi}(\xi^1, \xi^2) = \begin{pmatrix} R - \xi^1 \\ R \sin\left(\frac{2\pi}{9} - \frac{\xi^2}{R}\right) \\ R \cos\left(\frac{2\pi}{9} - \frac{\xi^2}{R}\right) \end{pmatrix}, \quad (\xi^1, \xi^2) \in \omega \quad (8.2)$$

for $\omega = [0, R] \times [0, l]$ and $l = \frac{2\pi}{9}R$ the circumferential length of the computational domain. Accordingly, the parameter ξ^1 defines the surface along the axial direction, whereas ξ^2 represents the circumferential coordinate. The transverse coordinate through the thickness is denoted by ξ^3 , as usual, and we classically denote Young’s modulus by E and Poisson’s ratio by ν .

The kinematic boundary conditions displayed in Fig. 8.1 ensure that the subspace of inextensional displacements is exactly reduced to zero, since displacements prescribed on the cross-section AD make the entire corresponding band inhibited.

The shell is loaded by a vertical distributed surface force \vec{g} scaled by ε that is different from zero along the free axial boundary, namely

$$F(\vec{v}) = \int_{\omega} \varepsilon \vec{g} \cdot \vec{v} dS \quad (8.3)$$

A vertical distributed surface force of magnitude 0.625 (in consistent units) is used for $\varepsilon = 10^{-2}$, and for other relative thickness the corresponding scalings follow. As we can see in [31], such a surface force constitutes a non-admissible membrane loading and strong singularities appear near the free boundaries when the thickness becomes small. In fact, the energy concentrates in a boundary layer of width proportional to $\varepsilon^{1/4}$ along the free edge.

The displacement solution will be denoted by ${}^1\vec{U}^\varepsilon = ({}^1\vec{u}^\varepsilon, {}^1\vec{\theta}^\varepsilon)$ and we have:

$$\begin{aligned} {}^1\vec{u}^\varepsilon &= {}^1u_\lambda^\varepsilon \vec{a}^\lambda + {}^1u_3^\varepsilon \vec{a}_3 \\ {}^1\vec{\theta}^\varepsilon &= {}^1\theta_\lambda^\varepsilon \vec{a}^\lambda \end{aligned} \quad (8.4)$$

The scaled energy

$$\varepsilon^{\frac{3}{4}} \int_{\mathcal{S}} \vec{g} \cdot {}^1\vec{u}^\varepsilon dS \quad (8.5)$$

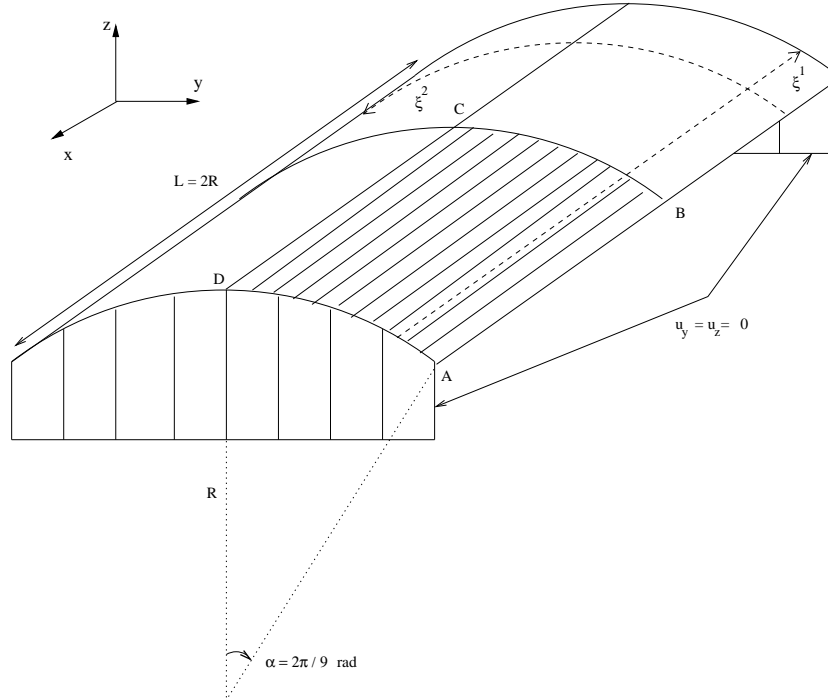


Figure 8.1: Scordelis-Lo Roof shell problem ($R = L = 300$, $\nu = 0$, $E = 3 \times 10^6$).

converges to a finite non-zero value as the scaling corresponding to

$$\rho = \frac{7}{4} \quad (8.6)$$

is known to provide an admissible asymptotic behavior (see [46]), but a direct convergence of the displacements is not obtained and they must be properly scaled, as we explain below.

Owing to symmetry conditions, only one fourth of the domain –the ABCD area represented in Fig 8.1– needs to be numerically analyzed and the following conditions must be imposed:

$$u_y = u_z = 0 \quad \text{along} \quad AD \quad (8.7)$$

$$u_y = \theta_2 = 0 \quad \text{along} \quad CD \quad (8.8)$$

$$u_x = \theta_1 = 0 \quad \text{along} \quad BC \quad (8.9)$$

The MITC4 shell finite element is taken as the reference for our numerical assessments.

The characteristic length of the layer at the free boundary can be expressed in a general form as

$$d_{BL} = C\varepsilon^{\frac{1}{4}}R \quad (8.10)$$

where C denotes a constant to be determined. In view of Fig. 8.3, 8.4 and 8.5 –that show the normalized displacements along AB , BC and AD obtained for a uniform mesh of 72×72 MITC4 elements– the width of the layer can be identified by the circumferential distance corresponding to the angle d measured from the free edge AB to the first peak of the normalized deflection for each ε . Such computed values are summarized in Table 8.1 and we observe that $C = 2.35$ provides an adequate characteristic length by formula (8.10).

Accordingly, uniform meshes consisting on $2N + 1$ (axial direction) by $2N + 1$ (circumferential direction) vertices are used for $\varepsilon = 10^{-2}$ ($N = 2, 4, 8$ for current meshes and $N = 36$ for the reference one), whereas for $\varepsilon = 10^{-3}$ and $\varepsilon = 10^{-4}$ anisotropic meshes with triangles elongated in the axial direction are obtained as follows:

- $N_{BL}(\varepsilon) + 1$ (axial direction) by $2N + 1$ (circumferential direction) vertices inside of the boundary layer area,
- $N + 1$ (axial direction) by $2N + 1$ (circumferential direction) vertices outside of the boundary layer area,

where

$$N_{BL}(\varepsilon) \sim N\varepsilon^{-1/4} \quad (8.11)$$

with $N = 2, 4, 8$ for target meshes, and $N = 36$ for the reference ones (refer to Table 8.2 and Fig. 8.2).

ε	<i>Computed</i> d	<i>Circumferential distance</i> $d\pi R/180$	<i>Distance by formula</i> $d_{BL} = 2.35\varepsilon^{\frac{1}{4}}R$
10^{-2}	40.0000	209.4395	222.9406
10^{-3}	23.3333	122.1729	125.3687
10^{-4}	13.3333	69.8130	70.5000

Table 8.1: Characteristic circumferential length of the layer: angular distance d measured from the free edge to the first peak of the normalized deflection for the Scordelis-Lo Roof shell problem.

8.2 The layer problem

We introduce the scaled circumferential coordinate

$$\tilde{\xi}^2 = \varepsilon^{-\frac{1}{4}}\xi^2 \quad (8.12)$$

	N	$N_{BL}(10^{-3})$	$N_{BL}(10^{-4})$	h
<i>Target</i>	2	12	20	0.25
	4	24	40	0.125
	8	48	80	0.0625
<i>Reference</i>	36	216	360	

Table 8.2: ε -dependant sequence of reference and target meshes for the Scordelis-Lo Roof shell problem.

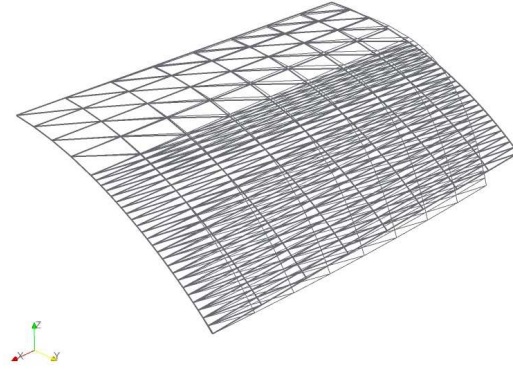


Figure 8.2: Undeformed (thickest plot) and expected deformed midsurface graphs for the Scordelis-Lo Roof shell problem ($N = 4$, $\varepsilon = 10^{-3}$, $scale = 1$).

designed to *zoom into* the boundary layer area. The scaled displacement components

$$\begin{aligned}\tilde{u}_1^\varepsilon &= \varepsilon^{\frac{1}{2}} u_1^\varepsilon \\ \tilde{u}_2^\varepsilon &= \varepsilon^{\frac{3}{4}} u_2^\varepsilon \\ \tilde{u}_3^\varepsilon &= \varepsilon^1 u_3^\varepsilon\end{aligned}\tag{8.13}$$

and rotation components

$$\begin{aligned}\tilde{\theta}_1^\varepsilon &= \varepsilon^1 \theta_1^\varepsilon \\ \tilde{\theta}_2^\varepsilon &= \varepsilon^{\frac{5}{4}} \theta_2^\varepsilon\end{aligned}\tag{8.14}$$

satisfy a sequence of variational problems parametrized by ε in the scaled domains

$$\tilde{\mathcal{B}}_\varepsilon = [0, L] \times [0, l\varepsilon^{-1/4}]\tag{8.15}$$

as we describe below.

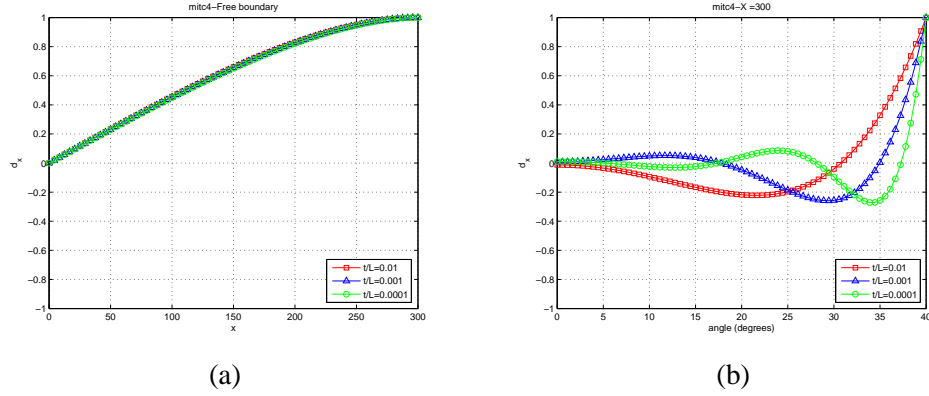


Figure 8.3: Normalized displacement in x-direction for the Scordelis-Lo Roof shell problem: (a) along the free boundary AB , (b) along AD .

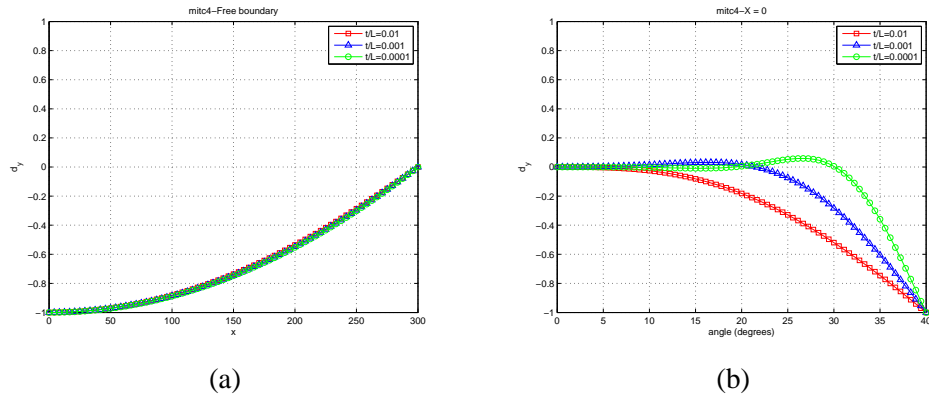


Figure 8.4: Normalized displacement in y-direction for the Scordelis-Lo Roof shell problem: (a) along the free boundary AB , (b) along BC .

Defining $\psi = \frac{2\pi}{9} - \frac{\xi^2}{R}$, the vertical displacement ${}^1u_z^\varepsilon$ can be expressed as

$${}^1u_z^\varepsilon = \cos \psi {}^1u_3^\varepsilon + \sin \psi {}^1u_2^\varepsilon \quad (8.16)$$

If we define the scaled vertical displacement

$$\tilde{u}_z^\varepsilon = \varepsilon {}^1u_z^\varepsilon \quad (8.17)$$

we have that

$$\tilde{u}_z^\varepsilon = \cos \psi \tilde{u}_3^\varepsilon + \varepsilon^{\frac{1}{4}} \sin \psi \tilde{u}_2^\varepsilon \quad (8.18)$$

and hence the well-defined limit behavior of \tilde{u}_z^ε is governed by that of \tilde{u}_3^ε .

We start by introducing the variational formulation obtained when assuming vanishing normal stresses through the thickness, namely the “basic shell model”

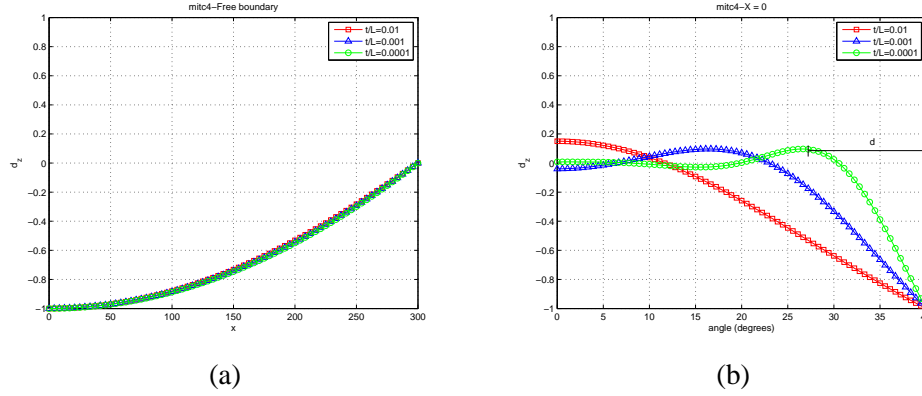


Figure 8.5: Normalized deflection for the Scordelis-Lo Roof shell problem: (a) along the free boundary AB , (b) along BC .

presented in [31], which reads

$$\int_{\Omega} \left[C^{\alpha\beta\lambda\mu} e_{\alpha\beta}({}^1\vec{U}^\varepsilon) e_{\lambda\mu}(\vec{V}) + D^{\alpha\lambda} e_{\alpha 3}({}^1\vec{U}^\varepsilon) e_{\lambda 3}(\vec{V}) \right] dV = F(\vec{V}) \quad (8.19)$$

where Ω represents the 3D domain of the shell, $C^{\alpha\beta\lambda\mu}$ and $D^{\alpha\lambda}$ denote the constitutive tensor components and $\vec{V} = (\vec{v}, \underline{\eta})$ an arbitrary test function satisfying the Reissner-Mindlin kinematical assumption and the appropriate boundary conditions (recall Section 1.2). The infinitesimal volume denoted by dV is given by

$$dV = \sqrt{g} d\xi^1 d\xi^2 d\xi^3 \quad (8.20)$$

where g denotes the Jacobian corresponding to (ξ^1, ξ^2, ξ^3) , and the covariant strain components can be developed to obtain

$$\begin{aligned} e_{\alpha\beta} &= \gamma_{\alpha\beta}(\vec{v}) + \xi^3 \chi_{\alpha\beta}(\vec{v}, \underline{\eta}) - (\xi^3)^2 \kappa_{\alpha\beta}(\underline{\eta}) \\ e_{\alpha 3} &= \zeta_{\alpha}(\vec{v}, \underline{\eta}) \end{aligned} \quad (8.21)$$

where the tensors $\underline{\gamma}$, $\underline{\chi}$ and $\underline{\zeta}$ are respectively the membrane, bending and shear strain tensors defined by

$$\begin{aligned} \gamma_{\alpha\beta}(\vec{v}) &= \frac{1}{2}(v_{\alpha|\beta} + v_{\beta|\alpha}) - b_{\alpha\beta} v_3 \\ \chi_{\alpha\beta}(\vec{v}, \underline{\eta}) &= \frac{1}{2}(\eta_{\alpha|\beta} + \eta_{\beta|\alpha} - b_{\beta}^{\lambda} v_{\lambda|\alpha} - b_{\alpha}^{\lambda} v_{\lambda|\beta}) + c_{\alpha\beta} v_3 \\ \zeta_{\alpha}(\vec{v}, \underline{\eta}) &= \frac{1}{2}(\eta_{\alpha} + v_{3,\alpha} + b_{\alpha}^{\lambda} v_{\lambda}) \end{aligned} \quad (8.22)$$

and

$$\kappa_{\alpha\beta}(\underline{\eta}) = \frac{1}{2} \left(b_{\beta}^{\lambda} \eta_{\lambda|\alpha} + b_{\alpha}^{\lambda} \eta_{\lambda|\beta} \right) \quad (8.23)$$

These tensors can be expressed in terms of the scaled coordinate $\tilde{\xi}^2$ and the displacements and rotations scaled like in (8.13)-(8.14), which gives:

- $\underline{\underline{\gamma}}(\vec{v})$:

$$\begin{aligned}\gamma_{11}(\vec{v}) &= \varepsilon^{-\frac{1}{2}} \frac{\partial \tilde{v}_1}{\partial \xi^1} \\ \gamma_{22}(\vec{v}) &= \varepsilon^{-1} \left(\frac{\partial \tilde{v}_2}{\partial \xi^2} - b_{22} \tilde{v}_3 \right) \\ \gamma_{12}(\vec{v}) &= \frac{1}{2} \varepsilon^{-\frac{3}{4}} \left(\frac{\partial \tilde{v}_1}{\partial \xi^2} + \frac{\partial \tilde{v}_2}{\partial \xi^1} \right)\end{aligned}\tag{8.24}$$

- $\underline{\underline{\chi}}(\vec{v}, \underline{\eta})$:

$$\begin{aligned}\chi_{11}(\vec{v}, \underline{\eta}) &= \varepsilon^{-1} \frac{\partial \tilde{\eta}_1}{\partial \xi^1} \\ \chi_{22}(\vec{v}, \underline{\eta}) &= \varepsilon^{-\frac{6}{4}} \frac{\partial \tilde{\eta}_2}{\partial \xi^2} + \varepsilon^{-1} \left(-b_2^2 \frac{\partial \tilde{\eta}_2}{\partial \xi^2} + c_{22} \tilde{v}_3 \right) \\ \chi_{12}(\vec{v}, \underline{\eta}) &= \frac{1}{2} \varepsilon^{-\frac{5}{4}} \left(\frac{\partial \tilde{\eta}_1}{\partial \xi^2} + \frac{\partial \tilde{\eta}_2}{\partial \xi^1} \right)\end{aligned}\tag{8.25}$$

- $\underline{\underline{\kappa}}(\underline{\eta})$:

$$\begin{aligned}\kappa_{11}(\underline{\eta}) &= 0 \\ \kappa_{22}(\underline{\eta}) &= \varepsilon^{-\frac{6}{4}} b_2^2 \frac{\partial \tilde{\eta}_2}{\partial \xi^2} \\ \kappa_{12}(\underline{\eta}) &= \frac{1}{2} \varepsilon^{-\frac{5}{4}} b_2^2 \frac{\partial \tilde{\eta}_2}{\partial \xi^1}\end{aligned}\tag{8.26}$$

- $\underline{\underline{\zeta}}(\vec{v}, \underline{\eta})$:

$$\begin{aligned}\zeta_1(\vec{v}, \underline{\eta}) &= \frac{1}{2} \varepsilon^{-1} \left(\tilde{\eta}_1 + \frac{\partial \tilde{v}_3}{\partial \xi^1} \right) \\ \zeta_2(\vec{v}, \underline{\eta}) &= \frac{1}{2} \left[\varepsilon^{-\frac{5}{4}} \left(\tilde{\eta}_2 + \frac{\partial \tilde{v}_3}{\partial \xi^2} \right) + b_2^2 \varepsilon^{-\frac{3}{4}} \tilde{v}_2 \right]\end{aligned}\tag{8.27}$$

The infinitesimal area corresponding to the differentials $(d\xi^1, d\xi^2)$ of the coordinates can be expressed as

$$dS = \sqrt{a} d\xi^1 d\xi^2\tag{8.28}$$

and the g quantity appearing in the volume measure (8.20) is given by

$$g = a \left(1 - 2H\xi^3 + K(\xi^3)^2 \right)^2\tag{8.29}$$

where H and K respectively denote the mean and Gaussian curvatures of the mid-surface (refer to [31]). Hence, it follows that

$$\sqrt{g} = \sqrt{a} \left(1 + \mathcal{O}(\xi^3) \right)\tag{8.30}$$

In the same manner, we can use the Taylor expansions of $C^{\alpha\beta\lambda\mu}$ and $D^{\alpha\lambda}$ around $\xi^3 = 0$ that give

$$C^{\alpha\beta\lambda\mu} = {}^0C^{\alpha\beta\lambda\mu} + \mathcal{O}(\xi^3) \quad (8.31)$$

$$D^{\alpha\lambda} = {}^0D^{\alpha\lambda} + \mathcal{O}(\xi^3) \quad (8.32)$$

where ${}^0C^{\alpha\beta\lambda\mu}$ and ${}^0D^{\alpha\lambda}$ denote the constitutive tensor components for $\xi^3 = 0$, namely:

$$\begin{aligned} {}^0C^{\alpha\beta\lambda\mu} &= \frac{E}{2(1+\nu)}(a^{\alpha\lambda}a^{\beta\mu} + a^{\alpha\mu}a^{\beta\lambda} + \frac{2\nu}{1-\nu}a^{\alpha\beta}a^{\lambda\mu}) \\ {}^0D^{\alpha\lambda} &= \frac{2E}{1+\nu}a^{\alpha\lambda} \end{aligned} \quad (8.33)$$

We point out that the terms in $\mathcal{O}(\xi^3)$ will have no asymptotic impact in the scaled variational formulation of the layer problem given that they provide terms with positive powers of ε when performing the integration through the thickness that can be neglected, as we explain below. Furthermore, the same considerations hold for those terms that involve the components of $\underline{\kappa}$.

From the definition of the $2D$ -chart in (8.2) we can easily calculate

$$\vec{a}_1(\xi^1, \xi^2) = \begin{pmatrix} -1 \\ 0 \\ 0 \end{pmatrix}, \quad \vec{a}_2(\xi^1, \xi^2) = \begin{pmatrix} 0 \\ -\cos\left(\frac{2\pi}{9} - \frac{\xi^2}{R}\right) \\ \sin\left(\frac{2\pi}{9} - \frac{\xi^2}{R}\right) \end{pmatrix} \quad (8.34)$$

and

$$\vec{a}_3(\xi^1, \xi^2) = \begin{pmatrix} 0 \\ \sin\left(\frac{2\pi}{9} - \frac{\xi^2}{R}\right) \\ \cos\left(\frac{2\pi}{9} - \frac{\xi^2}{R}\right) \end{pmatrix} \quad (8.35)$$

Hence, we have

$$a = a_{11}a_{22} - (a_{12})^2 = 1 \quad (8.36)$$

and

$$b_{11} = b_{12} = 0, \quad b_{22} = \frac{1}{R} \quad (8.37)$$

$$b_1^1 = b_1^2 = 0, \quad b_2^2 = -\frac{1}{R} \quad (8.38)$$

Using the simplifications

- \sqrt{a} for \sqrt{g} in the volume measure dV ;
- $\gamma_{\alpha\beta} + \xi^3\chi_{\alpha\beta}$ for $e_{\alpha\beta}$;
- ${}^0C^{\alpha\beta\lambda\mu}$ and ${}^0D^{\alpha\lambda}$ for $C^{\alpha\beta\lambda\mu}$ and $D^{\alpha\lambda}$,

and performing the integration with respect to ξ^3 , the variational problem that follows from (8.19) reads:

$$\begin{aligned}
 & t \int_{\omega} {}^0 C^{\alpha\beta\lambda\mu} \gamma_{\alpha\beta}({}^1 \underline{\vec{u}}^\varepsilon) \gamma_{\lambda\mu}(\vec{v}) dS + \\
 & \frac{t^3}{12} \int_{\omega} {}^0 C^{\alpha\beta\lambda\mu} \chi_{\alpha\beta}({}^1 \underline{\vec{u}}^\varepsilon, {}^1 \underline{\theta}^\varepsilon) \chi_{\lambda\mu}(\vec{v}, \underline{\eta}) dS + \\
 & t \int_{\omega} {}^0 D^{\alpha\lambda} \zeta_{\alpha}({}^1 \underline{\vec{u}}^\varepsilon, {}^1 \underline{\theta}^\varepsilon) \zeta_{\lambda}(\vec{v}, \underline{\eta}) dS = F(\vec{v}) \quad \forall (\vec{v}, \underline{\eta})
 \end{aligned} \tag{8.39}$$

with

$$F(\vec{v}) = \int_{\omega} \varepsilon g_z v_z dS \tag{8.40}$$

for our particular framework. We substitute the expressions (8.24), (8.25), (8.27) and (8.40) in (8.39) to obtain:

$$\begin{aligned}
 & \varepsilon L \int_{\tilde{B}_\varepsilon} \left\{ {}^0 C^{1111} \varepsilon^{-1} \frac{\partial \tilde{u}_1^\varepsilon}{\partial \xi^1} \frac{\partial \tilde{v}_1}{\partial \xi^1} + {}^0 C^{2222} \varepsilon^{-2} \left(\frac{\partial \tilde{u}_2^\varepsilon}{\xi_2} - b_{22} \tilde{u}_3^\varepsilon \right) \left(\frac{\partial \tilde{v}_2}{\xi_2} - b_{22} \tilde{v}_3 \right) + \right. \\
 & {}^0 C^{1122} \varepsilon^{-\frac{3}{2}} \frac{\partial \tilde{u}_1^\varepsilon}{\partial \xi^1} \left(\frac{\partial \tilde{v}_2}{\xi_2} - b_{22} \tilde{v}_3 \right) + {}^0 C^{2211} \varepsilon^{-\frac{3}{2}} \left(\frac{\partial \tilde{u}_2^\varepsilon}{\xi_2} - b_{22} \tilde{u}_3^\varepsilon \right) \frac{\partial \tilde{v}_1}{\partial \xi^1} + \\
 & {}^0 C^{1211} \varepsilon^{-\frac{5}{4}} \left(\frac{\partial \tilde{u}_1^\varepsilon}{\partial \xi^2} + \frac{\partial \tilde{u}_2^\varepsilon}{\partial \xi^1} \right) \frac{\partial \tilde{v}_1}{\partial \xi^1} + {}^0 C^{1112} \varepsilon^{-\frac{5}{4}} \frac{\partial \tilde{u}_1^\varepsilon}{\partial \xi^1} \left(\frac{\partial \tilde{v}_1}{\partial \xi^2} + \frac{\partial \tilde{v}_2}{\partial \xi^1} \right) + \\
 & {}^0 C^{1222} \varepsilon^{-\frac{7}{4}} \left(\frac{\partial \tilde{u}_1^\varepsilon}{\partial \xi^2} + \frac{\partial \tilde{u}_2^\varepsilon}{\partial \xi^1} \right) \left(\frac{\partial \tilde{v}_2}{\xi_2} - b_{22} \tilde{v}_3 \right) + \\
 & {}^0 C^{2212} \varepsilon^{-\frac{7}{4}} \left(\frac{\partial \tilde{u}_2^\varepsilon}{\xi_2} - b_{22} \tilde{u}_3^\varepsilon \right) \left(\frac{\partial \tilde{v}_1}{\partial \xi^2} + \frac{\partial \tilde{v}_2}{\partial \xi^1} \right) + \\
 & \left. {}^0 C^{1212} \varepsilon^{-\frac{6}{4}} \left(\frac{\partial \tilde{u}_1^\varepsilon}{\partial \xi^2} + \frac{\partial \tilde{u}_2^\varepsilon}{\partial \xi^1} \right) \left(\frac{\partial \tilde{v}_1}{\partial \xi^2} + \frac{\partial \tilde{v}_2}{\partial \xi^1} \right) \right\} d\xi^1 d\xi^2 + \\
 & \varepsilon^3 \frac{L^3}{12} \int_{\tilde{B}_\varepsilon} \left\{ {}^0 C^{1111} \varepsilon^{-2} \frac{\partial \tilde{\theta}_1^\varepsilon}{\partial \xi^1} \frac{\partial \tilde{\eta}_1}{\partial \xi^1} + \right. \\
 & {}^0 C^{2222} \left[\varepsilon^{-3} \frac{\partial \tilde{\theta}_2^\varepsilon}{\partial \xi^2} \frac{\partial \tilde{\eta}_2}{\partial \xi^2} + \varepsilon^{-2} \left(-b_2^2 \frac{\partial \tilde{u}_2^\varepsilon}{\partial \xi_2} + c_{22} \tilde{u}_3^\varepsilon \right) \left(-b_2^2 \frac{\partial \tilde{v}_2}{\partial \xi_2} + c_{22} \tilde{v}_3 \right) + \right. \\
 & \left. \varepsilon^{-\frac{10}{4}} \frac{\partial \tilde{\theta}_2^\varepsilon}{\partial \xi^2} \left(-b_2^2 \frac{\partial \tilde{v}_2}{\partial \xi_2} + c_{22} \tilde{v}_3 \right) + \varepsilon^{-\frac{10}{4}} \left(-b_2^2 \frac{\partial \tilde{u}_2^\varepsilon}{\partial \xi_2} + c_{22} \tilde{u}_3^\varepsilon \right) \frac{\partial \tilde{\eta}_2}{\partial \xi^2} \right] + \\
 & {}^0 C^{1122} \varepsilon^{-1} \frac{\partial \tilde{\theta}_1^\varepsilon}{\partial \xi^1} \left[\varepsilon^{-\frac{6}{4}} \frac{\partial \tilde{\eta}_2}{\partial \xi^2} + \varepsilon^{-1} \left(-b_2^2 \frac{\partial \tilde{v}_2}{\partial \xi_2} + c_{22} \tilde{v}_3 \right) \right] + \\
 & \left. {}^0 C^{2211} \varepsilon^{-1} \left[\varepsilon^{-\frac{6}{4}} \frac{\partial \tilde{\theta}_2^\varepsilon}{\partial \xi^2} + \varepsilon^{-1} \left(-b_2^2 \frac{\partial \tilde{u}_2^\varepsilon}{\partial \xi_2} + c_{22} \tilde{u}_3^\varepsilon \right) \right] \frac{\partial \tilde{\eta}_1}{\partial \xi^1} + \right.
 \end{aligned}$$

$$\begin{aligned}
 & {}^0C^{1211}\varepsilon^{-\frac{9}{4}}\left(\frac{\partial\tilde{\theta}_1^\varepsilon}{\partial\xi^2}+\frac{\partial\tilde{\theta}_5^\varepsilon}{\partial\xi^1}\right)\frac{\partial\tilde{\eta}_1}{\partial\xi^1}+{}^0C^{1112}\varepsilon^{-\frac{9}{4}}\frac{\partial\tilde{\theta}_1^\varepsilon}{\partial\xi^1}\left(\frac{\partial\tilde{\eta}_1}{\partial\xi^2}+\frac{\partial\tilde{\eta}_2}{\partial\xi^1}\right)+ \\
 & {}^0C^{1222}\varepsilon^{-\frac{5}{4}}\left(\frac{\partial\tilde{\theta}_1^\varepsilon}{\partial\xi^2}+\frac{\partial\tilde{\theta}_5^\varepsilon}{\partial\xi^1}\right)\left[\varepsilon^{-\frac{6}{4}}\frac{\partial\tilde{\eta}_2}{\partial\xi^2}+\varepsilon^{-1}\left(-b_2^2\frac{\partial\tilde{v}_2}{\partial\xi^2}+c_{22}\tilde{v}_3\right)\right]+ \\
 & {}^0C^{2212}\varepsilon^{-\frac{5}{4}}\left[\varepsilon^{-\frac{6}{4}}\frac{\partial\tilde{\theta}_5^\varepsilon}{\partial\xi^2}+\varepsilon^{-1}\left(-b_2^2\frac{\partial\tilde{u}_2^\varepsilon}{\partial\xi^2}+c_{22}\tilde{u}_3^\varepsilon\right)\right]\left(\frac{\partial\tilde{\eta}_1}{\partial\xi^2}+\frac{\partial\tilde{\eta}_2}{\partial\xi^1}\right)+ \\
 & {}^0C^{1212}\varepsilon^{-\frac{10}{4}}\left(\frac{\partial\tilde{\theta}_1^\varepsilon}{\partial\xi^2}+\frac{\partial\tilde{\theta}_5^\varepsilon}{\partial\xi^1}\right)\left(\frac{\partial\tilde{\eta}_1}{\partial\xi^2}+\frac{\partial\tilde{\eta}_2}{\partial\xi^1}\right)\Big\}d\xi^1d\tilde{\xi}^2 \quad + \\
 & \varepsilon L\int_{\tilde{B}_\varepsilon}\left\{\frac{{}^0D^{11}}{4}\varepsilon^{-2}\left(\tilde{\theta}_1^\varepsilon+\frac{\partial\tilde{u}_3^\varepsilon}{\partial\xi^1}\right)\left(\tilde{\eta}_1+\frac{\partial\tilde{v}_3}{\partial\xi^1}\right)+\right. \\
 & \frac{{}^0D^{22}}{4}\left[\varepsilon^{-\frac{10}{4}}\left(\tilde{\theta}_2^\varepsilon+\frac{\partial\tilde{u}_2^\varepsilon}{\partial\xi^2}\right)\left(\tilde{\eta}_2+\frac{\partial\tilde{v}_3}{\partial\xi^2}\right)+\varepsilon^{-\frac{6}{4}}(b_2^2)^2\tilde{u}_2^\varepsilon\tilde{v}_2+\right. \\
 & \left.\left.\varepsilon^{-\frac{8}{4}}\left(\tilde{\theta}_2^\varepsilon+\frac{\partial\tilde{u}_3^\varepsilon}{\partial\xi^2}\right)b_2^2\tilde{v}_2+\varepsilon^{-\frac{8}{4}}b_2^2\tilde{u}_2^\varepsilon\left(\tilde{\eta}_2+\frac{\partial\tilde{v}_3}{\partial\xi^2}\right)\right]+\right. \\
 & \frac{{}^0D^{12}}{4}\varepsilon^{-1}\left(\tilde{\theta}_1^\varepsilon+\frac{\partial\tilde{u}_3^\varepsilon}{\partial\xi^1}\right)\left[\varepsilon^{-\frac{5}{4}}\left(\tilde{\eta}_2+\frac{\partial\tilde{v}_3}{\partial\xi^2}\right)+b_2^2\varepsilon^{-\frac{3}{4}}\tilde{v}_2\right]+ \\
 & \left.\frac{{}^0D^{21}}{4}\varepsilon^{-1}\left[\varepsilon^{-\frac{5}{4}}\left(\tilde{\theta}_2^\varepsilon+\frac{\partial\tilde{u}_3^\varepsilon}{\partial\xi^2}\right)+b_2^2\varepsilon^{-\frac{3}{4}}\tilde{u}_2^\varepsilon\right]\left(\tilde{\eta}_1+\frac{\partial\tilde{v}_3}{\partial\xi^1}\right)\right\}d\xi^1d\tilde{\xi}^2 \quad = \\
 & \int_{\tilde{B}_\varepsilon}\varepsilon g_z\left(\varepsilon^{-1}\cos\psi\tilde{v}_3+\varepsilon^{-\frac{3}{4}}\sin\psi\tilde{v}_2\right)d\xi^1d\tilde{\xi}^2
 \end{aligned} \tag{8.41}$$

Note that although the integrals are performed over the domain \tilde{B}_ε that grows asymptotically when ε tends to zero, due to the asymptotic decay of the layers, a truncation of the domain “sufficiently far” from the boundary (with corresponding homogeneous boundary conditions) would provide a good approximation of the problem (see [60]). Then, since we are interested in the *asymptotic behavior* of the solution, we neglect all the terms associated with positive powers of ε —namely, the regular/singular perturbation terms— and the formulation reduces to

$$\begin{aligned}
 & L \int_{\tilde{B}_\varepsilon} {}^0C^{1111} \frac{\partial \tilde{u}_1^\varepsilon}{\partial \xi^1} \frac{\partial \tilde{v}_1}{\partial \xi^1} d\xi^1 d\tilde{\xi}^2 + \frac{L^3}{12} \int_{\tilde{B}_\varepsilon} {}^0C^{2222} \frac{\partial \tilde{\theta}_2^\varepsilon}{\partial \xi^2} \frac{\partial \tilde{\eta}_2}{\partial \xi^2} d\xi^1 d\tilde{\xi}^2 + \\
 & L\varepsilon^{-\frac{1}{4}} \int_{\tilde{B}_\varepsilon} \left\{ {}^0C^{1211} \left(\frac{\partial \tilde{u}_1^\varepsilon}{\partial \xi^2} + \frac{\partial \tilde{u}_2^\varepsilon}{\partial \xi^1} \right) \frac{\partial \tilde{v}_1}{\partial \xi^1} + {}^0C^{1112} \frac{\partial \tilde{u}_1^\varepsilon}{\partial \xi^1} \left(\frac{\partial \tilde{v}_1}{\partial \xi^2} + \frac{\partial \tilde{v}_2}{\partial \xi^1} \right) \right\} d\xi^1 d\tilde{\xi}^2 + \\
 & L\varepsilon^{-\frac{2}{4}} \int_{\tilde{B}_\varepsilon} \left\{ {}^0C^{1122} \frac{\partial \tilde{u}_1^\varepsilon}{\partial \xi^1} \left(\frac{\partial \tilde{v}_2}{\partial \xi_2} - b_{22} \tilde{v}_3 \right) + {}^0C^{2211} \left(\frac{\partial \tilde{u}_2^\varepsilon}{\partial \xi_2} - b_{22} \tilde{u}_3^\varepsilon \right) \frac{\partial \tilde{v}_1}{\partial \xi^1} + \right. \\
 & \quad \left. {}^0C^{1212} \left(\frac{\partial \tilde{u}_1^\varepsilon}{\partial \xi^2} + \frac{\partial \tilde{u}_2^\varepsilon}{\partial \xi^1} \right) \left(\frac{\partial \tilde{v}_1}{\partial \xi^2} + \frac{\partial \tilde{v}_2}{\partial \xi^1} \right) + \frac{{}^0D^{22}}{4} (b_2^2)^2 \tilde{u}_2^\varepsilon \tilde{v}_2 \right\} d\xi^1 d\tilde{\xi}^2 + \\
 & L\varepsilon^{-\frac{3}{4}} \int_{\tilde{B}_\varepsilon} \left\{ {}^0C^{1222} \left(\frac{\partial \tilde{u}_1^\varepsilon}{\partial \xi^2} + \frac{\partial \tilde{u}_2^\varepsilon}{\partial \xi^1} \right) \left(\frac{\partial \tilde{v}_2}{\partial \xi_2} - b_{22} \tilde{v}_3 \right) + \right. \\
 & \quad \left. {}^0C^{2212} \left(\frac{\partial \tilde{u}_2^\varepsilon}{\partial \xi_2} - b_{22} \tilde{u}_3^\varepsilon \right) \left(\frac{\partial \tilde{v}_1}{\partial \xi^2} + \frac{\partial \tilde{v}_2}{\partial \xi^1} \right) + \right. \\
 & \quad \left. \frac{{}^0D^{12}}{4} \left(\tilde{\theta}_1^\varepsilon + \frac{\partial \tilde{u}_3^\varepsilon}{\partial \xi^1} \right) b_2^2 \tilde{v}_2 + \frac{{}^0D^{21}}{4} b_2^2 \tilde{u}_2^\varepsilon \left(\tilde{\eta}_1 + \frac{\partial \tilde{v}_3}{\partial \xi^1} \right) \right\} d\xi^1 d\tilde{\xi}^2 + \\
 & L\varepsilon^{-1} \int_{\tilde{B}_\varepsilon} \left\{ {}^0C^{2222} \left(\frac{\partial \tilde{u}_2^\varepsilon}{\partial \xi_2} - b_{22} \tilde{u}_3^\varepsilon \right) \left(\frac{\partial \tilde{v}_2}{\partial \xi_2} - b_{22} \tilde{v}_3 \right) + \right. \\
 & \quad \frac{{}^0D^{11}}{4} \left(\tilde{\theta}_1^\varepsilon + \frac{\partial \tilde{u}_3^\varepsilon}{\partial \xi^1} \right) \left(\tilde{\eta}_1 + \frac{\partial \tilde{v}_3}{\partial \xi^1} \right) + \\
 & \quad \left. \frac{{}^0D^{22}}{4} \left[\left(\tilde{\theta}_2^\varepsilon + \frac{\partial \tilde{u}_3^\varepsilon}{\partial \xi^2} \right) b_2^2 \tilde{v}_2 + b_2^2 \tilde{u}_2^\varepsilon \left(\tilde{\eta}_2 + \frac{\partial \tilde{v}_3}{\partial \xi^2} \right) \right] \right\} d\xi^1 d\tilde{\xi}^2 + \\
 & L\varepsilon^{-\frac{5}{4}} \int_{\tilde{B}_\varepsilon} \left\{ \frac{{}^0D^{12}}{4} \left(\tilde{\theta}_1^\varepsilon + \frac{\partial \tilde{u}_3^\varepsilon}{\partial \xi^1} \right) \left(\tilde{\eta}_2 + \frac{\partial \tilde{v}_3}{\partial \xi^2} \right) + \right. \\
 & \quad \left. \frac{{}^0D^{21}}{4} \left(\tilde{\theta}_2^\varepsilon + \frac{\partial \tilde{u}_3^\varepsilon}{\partial \xi^2} \right) \left(\tilde{\eta}_1 + \frac{\partial \tilde{v}_3}{\partial \xi^1} \right) \right\} d\xi^1 d\tilde{\xi}^2 + \\
 & L\varepsilon^{-\frac{6}{4}} \int_{\tilde{B}_\varepsilon} \frac{{}^0D^{22}}{4} \left(\tilde{\theta}_2^\varepsilon + \frac{\partial \tilde{u}_3^\varepsilon}{\partial \xi^2} \right) \left(\tilde{\eta}_2 + \frac{\partial \tilde{v}_3}{\partial \xi^2} \right) d\xi^1 d\tilde{\xi}^2 = \\
 & \int_{\tilde{B}_\varepsilon} g_z \tilde{v}_3 \cos \psi d\xi^1 d\tilde{\xi}^2
 \end{aligned} \tag{8.42}$$

We observe that the terms appearing in this formulation are all the membrane strain components, a term related to the circumferential bending strain, both transverse shear strains and the midsurface displacement along the circumferential direction. It is important to notice that this layer problem is a penalized formulation when ε vanishes, which typically implies numerical locking for classical finite element approximations, although this “local locking” substantially differs from the classical membrane and shear locking for non-inhibited shells.

The constraints that are penalized in the layer are summarized in Table 8.3 and correspond to the vanishing of the terms in (8.42) with negative powers of ε . No-

tice that for non-inhibited shells the membrane and shear strain components are all penalized in the same manner with quadratic negative powers of ε , whereas for this particular framework different negative powers of ε appear, the axial in-plane membrane strain component is not penalized at all, and the most severe penalization corresponds to

$$\tilde{\eta}_2 + \frac{\partial \tilde{v}_3}{\partial \tilde{\xi}^2}$$

which is directly related to $\zeta_2(\vec{v}, \underline{\eta})$. Another important observation is that the mid-surface displacement along the circumferential direction is also penalized, which does not happen in bending-dominated situations.

Penalized term	\tilde{v}_2	$\tilde{\gamma}_{12}(\vec{v})$	$\tilde{\gamma}_{22}(\vec{v})$	$\tilde{\zeta}_1(\vec{v}, \underline{\eta})$	$\tilde{\eta}_2 + \frac{\partial \tilde{v}_3}{\partial \tilde{\xi}^2}$
Coefficient	$\varepsilon^{-1/2}$	$\varepsilon^{-1/2}$	ε^{-1}	ε^{-1}	$\varepsilon^{-3/2}$

Table 8.3: Layer problem: penalized terms when $\varepsilon \rightarrow 0$ and associated negative powers of ε .

8.3 Norms for the Scordelis-Lo Roof shell problem

As is well known, the *s-norm* is useful to analyze the convergence of strains, but it does not provide complete information regarding the displacements convergence. Wrong conclusions may be drawn when only considering this norm for numerical assessments as in particular it does not detect the presence of *membrane spurious modes* that may highly deteriorate the correct solution of a membrane dominated shell problem.

In order to properly assess the convergence of displacements, a suitable norm must be considered. One possible choice is the norm deduced from the asymptotic formulation of the shell problem in consideration, taking into account the vanishing terms scaled up to order one for penalized formulations.

Hence, the convergence behavior of the Scordelis-Lo Roof shell problem will be assessed using two different error measures:

- the *s-norm* for strains as usual;
- a particular norm –named *SL-norm* from now on– for displacements, which is obtained by firstly considering $\varepsilon = 1$ in (8.42) and then substituting the scaled domain and displacement and rotation components by the original ones.

It is easy to verify that:

$$\frac{\partial \tilde{\eta}_2}{\partial \tilde{\xi}^2} = \varepsilon^{\frac{3}{2}} \frac{\partial \eta_2}{\partial \xi^2} \quad (8.43)$$

$$\frac{1}{2} \left(\tilde{\eta}_2 + \frac{\partial \tilde{v}_3}{\partial \tilde{\xi}^2} \right) = \varepsilon^{\frac{5}{4}} \frac{1}{2} \left(\eta_2 + \frac{\partial v_3}{\partial \xi^2} \right) \quad (8.44)$$

and a proper norm could be defined as follows:

$$\begin{aligned} \|(\vec{v}, \underline{\eta})\|_{SL1}^2 = & L\varepsilon \int_{\mathcal{B}_\varepsilon} C^{1111} \gamma_{11}(\vec{v}) \gamma_{11}(\vec{v}) d\xi^1 d\xi^2 + \\ & \frac{L^3}{12} \varepsilon^3 \int_{\mathcal{B}_\varepsilon} C^{2222} \frac{\partial \eta_2}{\partial \xi^2} \frac{\partial \eta_2}{\partial \xi^2} d\xi^1 d\xi^2 + \\ & L\varepsilon^{\frac{5}{4}} \int_{\mathcal{B}_\varepsilon} \{ C^{1211} \gamma_{12}(\vec{v}) \gamma_{11}(\vec{v}) + C^{1112} \gamma_{11}(\vec{v}) \gamma_{12}(\vec{v}) \} d\xi^1 d\xi^2 + \\ & L\varepsilon^{\frac{3}{2}} \int_{\mathcal{B}_\varepsilon} \{ C^{1122} \gamma_{11}(\vec{v}) \gamma_{22}(\vec{v}) + C^{2211} \gamma_{22}(\vec{v}) \gamma_{11}(\vec{v}) + \\ & \quad C^{1212} \gamma_{12}(\vec{v}) \gamma_{12}(\vec{v}) + \frac{D^{22}}{4} (b_2^2)^2 v_2 v_2 \} d\xi^1 d\xi^2 + \\ & L\varepsilon^{\frac{7}{4}} \int_{\mathcal{B}_\varepsilon} \{ C^{1222} \gamma_{12}(\vec{v}) \gamma_{22}(\vec{v}) + C^{2212} \gamma_{22}(\vec{v}) \gamma_{12}(\vec{v}) + \\ & \quad \frac{D^{12}}{4} \zeta_1(\vec{v}, \underline{\eta}) b_2^2 v_2 + \frac{D^{21}}{4} b_2^2 v_2 \zeta_1(\vec{v}, \underline{\eta}) \} d\xi^1 d\xi^2 + \\ & L\varepsilon^2 \int_{\mathcal{B}_\varepsilon} \{ C^{2222} \gamma_{22}(\vec{v}) \gamma_{22}(\vec{v}) + \frac{D^{11}}{4} \zeta_1(\vec{v}, \underline{\eta}) \zeta_1(\vec{v}, \underline{\eta}) + \\ & \quad \frac{D^{22}}{2} \zeta_2(\vec{v}, \underline{\eta}) b_2^2 v_2 \} d\xi^1 d\xi^2 + \\ & L\varepsilon^{\frac{9}{4}} \int_{\mathcal{B}_\varepsilon} \left\{ \frac{D^{12}}{4} \zeta_1(\vec{v}, \underline{\eta}) \left(\eta_2 + \frac{\partial v_3}{\partial \xi^2} \right) + \right. \\ & \quad \left. \frac{D^{21}}{4} \left(\eta_2 + \frac{\partial v_3}{\partial \xi^2} \right) \zeta_1(\vec{v}, \underline{\eta}) \right\} d\xi^1 d\xi^2 + \\ & L\varepsilon^{\frac{5}{2}} \int_{\mathcal{B}_\varepsilon} \frac{D^{22}}{4} \left(\eta_2 + \frac{\partial v_3}{\partial \xi^2} \right) \left(\eta_2 + \frac{\partial v_3}{\partial \xi^2} \right) d\xi^1 d\xi^2 \end{aligned} \quad (8.45)$$

where \mathcal{B}_ε denotes the non-zoomed boundary layer area. An equivalent norm is:

$$\begin{aligned} \|(\vec{v}, \underline{\eta})\|_{SL}^2 = & L\varepsilon \|\gamma_{11}(\vec{v})\|_{L^2(\mathcal{B}_\varepsilon)}^2 + L\varepsilon^{\frac{3}{2}} \|\gamma_{12}(\vec{v})\|_{L^2(\mathcal{B}_\varepsilon)}^2 + \\ & L\varepsilon^2 \|\gamma_{22}(\vec{v})\|_{L^2(\mathcal{B}_\varepsilon)}^2 + L\varepsilon^2 \|\zeta_1(\vec{v}, \underline{\eta})\|_{L^2(\mathcal{B}_\varepsilon)}^2 + \\ & L\varepsilon^{\frac{5}{2}} \|\zeta_2(\vec{v}, \underline{\eta})\|_{L^2(\mathcal{B}_\varepsilon)}^2 + \frac{L^3}{12} \varepsilon^3 \left\| \frac{\partial \eta_2}{\partial \xi^2} \right\|_{L^2(\mathcal{B}_\varepsilon)}^2 + \\ & L\varepsilon^{\frac{3}{2}} \|v_2\|_{L^2(\mathcal{B}_\varepsilon)}^2 \end{aligned} \quad (8.46)$$

which is easier to implement, and will be used for the displacements assessment in our analysis.

8.4 Numerical computations and conclusions

The Scordelis-Lo Roof shell problem is frequently used for the evaluation of shell finite elements procedures. As we can see in [31], the membrane deformation energy does not control some specific displacements fields excited by the vertical force presented in this work, and strong singularities will appear near the free boundaries for small thickness where most of the energy is concentrated in the boundary layer developed along free edges. Although the subspace of inextensional displacements is known to be exactly reduced to zero, the asymptotic state does not correspond to membrane energy only and it can be classified as a mixed –or ill-posed membrane– shell problem.

As discussed in Section 8.2, the scaling $\rho = 7/4$ provides an admissible asymptotic behavior, and a convergence for displacements can only be obtained by properly scaling each displacement and rotation component. The reduced membrane and bending energies remain of the same order of magnitude and the reduced shear energy becomes negligible as the thickness decreases, as usual. Furthermore, the identity proven in [5] states that the asymptotic proportion of bending energy with respect to the total strain energy for this particular shell problem is

$$R_b = \frac{3}{8} = 0.3750 \quad (8.47)$$

We now consider this test problem in order to assess the performance of the MITC6a and MITC6rs shell elements, and the corresponding free boundary and weighted shear stabilized formulations. The convergence of the scaled strain energy will be verified by using a proper factor. In our analysis we consider the energy obtained for the loading proportional to ε , and we know that multiplying this energy by the factor

$$\left(\frac{\varepsilon}{0.01}\right)^{\rho-2} = \left(\frac{\varepsilon}{0.01}\right)^{-\frac{1}{4}} \quad (8.48)$$

a stable value must be obtained for the scaled energy as $\varepsilon \rightarrow 0$.

Tables 8.4 and 8.5 respectively show the reference scaled energy values and proportion of bending energy for the MITC4 meshes taken as reference for each ε . We observe that the proportion of bending energy with respect to the total strain energy gets close to $\frac{3}{8}$ as ε decreases, and the scaled total strain energies converge to a fixed value, while the bending and membrane energy remain of the same order of magnitude and the proportion of scaled shear energy gets smaller with ε .

As expected, the P_2 displacement-based shell finite element locks for small relative thickness and coarse meshes due to the penalized nature of the boundary layer problem in (8.42) as $\varepsilon \rightarrow 0$. The convergence curves shown in Fig. 8.6 considerably rise as ε decreases. Accordingly, the scaled shear energy is quite high for small thickness and coarse meshes, and the total strain energy substantially differs from the reference values, whereas the difference between the proportion of

bending energy (with respect to the total energy) and the expected value is quite large (see Tables 8.6 and 8.7).

The MITC6a and MITC6rs shell finite elements provide quite good strains and displacements, respectively seen by means of the *s-norm* and *SL-norm* (refer to Fig. 8.7 and 8.11). The expected convergence rate is achieved for displacements, but not for strains. The corresponding scaled reduced total strain energy values are close to the reference ones for each ε and h as Tables 8.8 and 8.16 show, whereas the proportion of bending energy is close to the expected value in each case.

On the one hand, we observe that the free boundary shear stabilization does not much reduce the MITC performance, although the convergence curves seem to slightly rise for all relative thickness and coarse meshes (see Fig. 8.8 and 8.12). The scaled energies displayed in Table 8.10 and 8.18 show that the reduced shear energy increases as compared to the original elements, mainly for the MITC6rs element with free boundary shear stabilization, whereas the bending energy proportion with respect to the total strain energy does not differ very much for both stabilized MITC6a and MITC6rs shell elements as compared to the values associated with the original elements for each ε and h . On the other hand, the weighted shear stabilization term does not much hinder the convergence behavior of the MITC6a and MITC6rs shell finite elements, except for the smallest value of the thickness together with coarse meshes (refer to Fig. 8.9-8.10 and Fig. 8.13-8.14), and the results are substantially improved as the mesh is refined. This fact is well understood due to the *penalized* asymptotic nature of the problem, similar to a non-inhibited situation. Remember that the shear stabilizations have been specifically designed to filter out those parasitic membrane modes that may considerably deteriorate the *correct solution* in membrane dominated situations, but it is important to have in mind that the risk is to hinder the MITC performance in non-inhibited –or equivalently penalized– situations. As expected, $C = 1/5$ provides better results given that less shear locking is added. In view of the tables of scaled energies and bending proportions for the weighted shear stabilized elements (see Table 8.12-8.15 and Table 8.20-8.23), it appears that *locking* only occurs for the smallest relative thickness together with coarse meshes as the difference between the scaled reduced strain energy and the reference values is large, the shear energy is increased and the ratio of bending energy considerably decreases.

Notice that wrong conclusions may be obtained from the *s-norm* convergence curves: the optimal convergence rate is not achieved and, furthermore, the convergence curves tend to rise for the smallest relative thickness considered in all cases. But the *SL-norm* convergence curves show that the MITC6a, MITC6rs and the corresponding shear stabilized elements provide good numerical results as the expected quadratic convergence rate is achieved for displacements. The weighted shear stabilizations hinder a little the good performance of the MITC approach *only* for the smallest value of the thickness together with coarse meshes, although the numerical results are substantially improved as the mesh is refined. As expected, the constant $C = 1/5$ is preferable for the weighted shear stabilization because less *shear locking* is added than when considering $C = 1$.

	$\varepsilon = 10^{-2}$	$\varepsilon = 10^{-3}$	$\varepsilon = 10^{-4}$
<i>Total</i>	1.450676071e+04	1.492773323e+04	1.476092313e+04
<i>Bending</i>	7.575508385e+03	5.957620118e+03	5.414474223e+03
<i>Membrane</i>	6.907057733e+03	8.969269603e+03	9.346437481e+03
<i>Shear</i>	2.531827829e+01	8.706618600e-01	1.831702758e-02

Table 8.4: Table of reference scaled reduced energies for the Scordelis-Lo Roof shell problem and the MITC4 shell finite element.

R_b	
$\varepsilon = 10^{-2}$	0.5222
$\varepsilon = 10^{-3}$	0.3991
$\varepsilon = 10^{-4}$	0.3668

Table 8.5: Proportion of bending energy with respect to the total strain energy (R_b) for the Scordelis-Lo Roof shell problem and the reference MITC4 shell finite element.

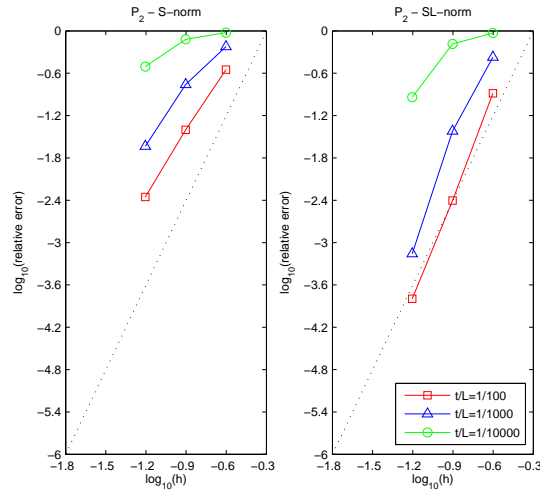


Figure 8.6: Convergence curves associated with the s-norm and SL-norm for the Scordelis-Lo Roof shell problem and P_2 displacement-based shell finite element. The dotted line shows the optimal convergence rate which is 4.

$\varepsilon = 10^{-2}$	$h = 0.25$	$h = 0.125$	$h = 0.0625$
<i>Total</i>	1.038461730e+04	1.394305767e+04	1.445656422e+04
<i>Bending</i>	2.940432251e+03	6.839152336e+03	7.519726267e+03
<i>Membrane</i>	7.148754930e+03	6.956479426e+03	6.902666032e+03
<i>Shear</i>	2.960322948e+02	1.484649097e+02	3.528986937e+01

$\varepsilon = 10^{-3}$	$h = 0.25$	$h = 0.125$	$h = 0.0625$
<i>Total</i>	6.088799369e+03	1.244833892e+04	1.463960492e+04
<i>Bending</i>	5.836014592e+02	3.600841449e+03	5.647045109e+03
<i>Membrane</i>	3.303976160e+03	7.489633487e+03	8.782684731e+03
<i>Shear</i>	2.201229889e+03	1.357884567e+03	2.099019409e+02

$\varepsilon = 10^{-4}$	$h = 0.25$	$h = 0.125$	$h = 0.0625$
<i>Total</i>	8.138930456e+02	3.615905648e+03	1.031512088e+04
<i>Bending</i>	4.343927161e+01	2.001136697e+02	2.158170378e+03
<i>Membrane</i>	3.141591005e+02	1.644598468e+03	5.949507665e+03
<i>Shear</i>	4.562946909e+02	1.771193675e+03	2.207439067e+03

Table 8.6: Table of energies for the Scordelis-Lo Roof shell problem and the P_2 displacement-based shell finite element.

	$h = 0.25$	$h = 0.125$	$h = 0.0625$
$\varepsilon = 10^{-2}$	0.2832	0.4905	0.5202
$\varepsilon = 10^{-3}$	0.0958	0.2893	0.3857
$\varepsilon = 10^{-4}$	0.0534	0.0553	0.2092

Table 8.7: Proportion of bending energy with respect to the total strain energy (R_b) for the Scordelis-Lo Roof shell problem and the P_2 displacement-based shell finite element.

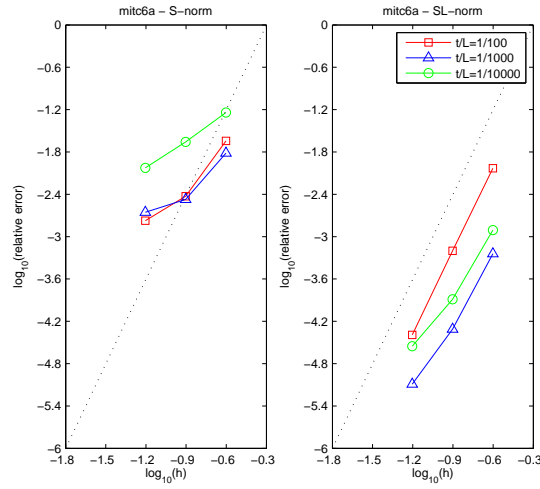


Figure 8.7: Convergence curves associated with the s-norm and SL-norm for the Scordelis Lo Roof shell problem and MITC6a shell finite element. The dotted line shows the optimal convergence rate which is 4.

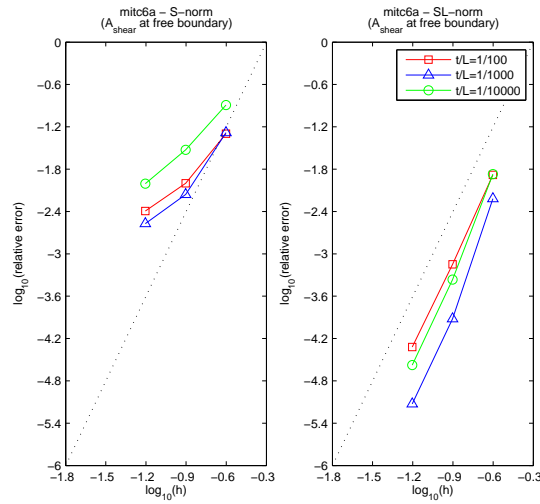


Figure 8.8: Convergence curves associated with the s-norm and SL-norm for the Scordelis Lo Roof shell problem and MITC6a shell finite element with free boundary shear stabilization. The dotted line shows the optimal convergence rate which is 4.

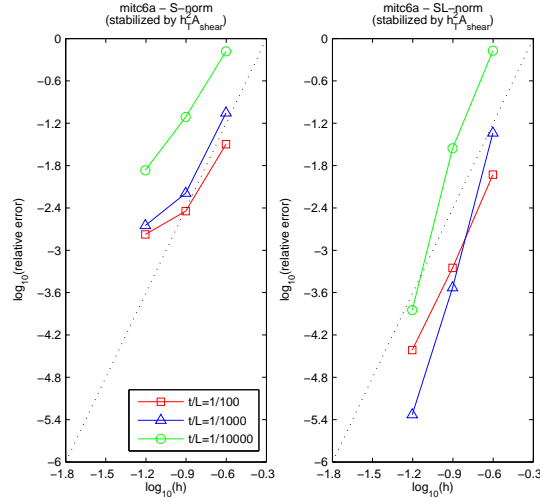


Figure 8.9: Convergence curves associated with the s-norm and SL-norm for the Scordelis Lo Roof shell problem and MITC6a shell finite element with weighted shear stabilization ($C = 1$). The dotted line shows the optimal convergence rate which is 4.

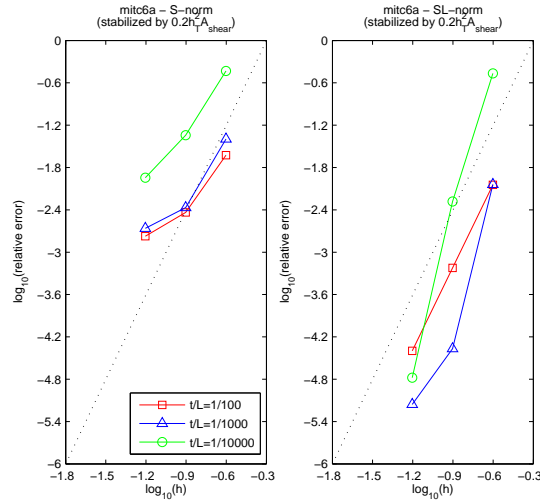


Figure 8.10: Convergence curves associated with the s-norm and SL-norm for the Scordelis Lo Roof shell problem and MITC6a shell finite element with weighted shear stabilization ($C = 1/5$). The dotted line shows the optimal convergence rate which is 4.

$\varepsilon = 10^{-2}$	$h = 0.25$	$h = 0.125$	$h = 0.0625$
<i>Total</i>	1.464652471e+04	1.459390281e+04	1.453017880e+04
<i>Bending</i>	7.529354470e+03	7.641027286e+03	7.601031529e+03
<i>Membrane</i>	7.102224523e+03	6.941736530e+03	6.911702773e+03
<i>Shear</i>	1.593611632e+01	1.225722833e+01	1.856917670e+01
$\varepsilon = 10^{-3}$	$h = 0.25$	$h = 0.125$	$h = 0.0625$
<i>Total</i>	1.490760249e+04	1.498125417e+04	1.496593605e+04
<i>Bending</i>	5.873575321e+03	5.976380328e+03	5.979760631e+03
<i>Membrane</i>	9.030044180e+03	9.004098669e+03	8.985701249e+03
<i>Shear</i>	3.959619774e+00	7.978433872e-01	5.016229504e-01
$\varepsilon = 10^{-4}$	$h = 0.25$	$h = 0.125$	$h = 0.0625$
<i>Total</i>	1.434848939e+04	1.465850357e+04	1.483971396e+04
<i>Bending</i>	5.994982272e+03	5.450318004e+03	5.466482262e+03
<i>Membrane</i>	8.351077240e+03	9.207436113e+03	9.372942143e+03
<i>Shear</i>	2.427912778e+00	7.410428901e-01	2.916725257e-01

Table 8.8: Table of scaled reduced energies for the Scordelis-Lo Roof shell problem and the MITC6a shell finite element.

	$h = 0.25$	$h = 0.125$	$h = 0.0625$
$\varepsilon = 10^{-2}$	0.5141	0.5236	0.5231
$\varepsilon = 10^{-3}$	0.3940	0.3989	0.3996
$\varepsilon = 10^{-4}$	0.4178	0.3718	0.3684

Table 8.9: Proportion of bending energy with respect to the total strain energy (R_b) for the Scordelis-Lo Roof shell problem and the MITC6a shell finite element.

$\varepsilon = 10^{-2}$	$h = 0.25$	$h = 0.125$	$h = 0.0625$
<i>Total</i>	1.422177568e+04	1.450169237e+04	1.449575372e+04
<i>Bending</i>	7.065606542e+03	7.500149577e+03	7.544314928e+03
<i>Membrane</i>	6.907855393e+03	6.902301230e+03	6.897095289e+03
<i>Shear</i>	1.181774455e+02	3.088165753e+01	2.040188714e+01
$\varepsilon = 10^{-3}$	$h = 0.25$	$h = 0.125$	$h = 0.0625$
<i>Total</i>	1.434860682e+04	1.492740046e+04	1.495889576e+04
<i>Bending</i>	5.440020845e+03	5.909657027e+03	5.969800498e+03
<i>Membrane</i>	8.680347878e+03	8.970783535e+03	8.981316344e+03
<i>Shear</i>	2.094683512e+02	3.609135587e+01	2.292867466e+00
$\varepsilon = 10^{-4}$	$h = 0.25$	$h = 0.125$	$h = 0.0625$
<i>Total</i>	1.326342628e+04	1.454073904e+04	1.483267971e+04
<i>Bending</i>	5.381100739e+03	5.327103842e+03	5.458490310e+03
<i>Membrane</i>	7.597534462e+03	9.125408165e+03	9.367956920e+03
<i>Shear</i>	2.812508370e+02	8.586405381e+01	5.001533704e+00

Table 8.10: Table of scaled reduced energies for the Scordelis-Lo Roof shell problem and the MITC6a shell finite element with free boundary shear stabilization.

	$h = 0.25$	$h = 0.125$	$h = 0.0625$
$\varepsilon = 10^{-2}$	0.4968	0.5172	0.5204
$\varepsilon = 10^{-3}$	0.3791	0.3959	0.3991
$\varepsilon = 10^{-4}$	0.4057	0.3664	0.3680

Table 8.11: Proportion of bending energy with respect to the total strain energy (R_b) for the Scordelis-Lo Roof shell problem and the MITC6a shell finite element with free boundary shear stabilization.

$\varepsilon = 10^{-2}$	$h = 0.25$	$h = 0.125$	$h = 0.0625$
<i>Total</i>	1.415517253e+04	1.456493680e+04	1.452767682e+04
<i>Bending</i>	7.001710823e+03	7.602037096e+03	7.597329827e+03
<i>Membrane</i>	6.860028867e+03	6.926951850e+03	6.910460712e+03
<i>Shear</i>	2.643090923e+02	2.880736172e+01	1.894601915e+01
$\varepsilon = 10^{-3}$	$h = 0.25$	$h = 0.125$	$h = 0.0625$
<i>Total</i>	1.223885201e+04	1.481151866e+04	1.495640511e+04
<i>Bending</i>	3.568186289e+03	5.838852260e+03	5.971998508e+03
<i>Membrane</i>	7.154089189e+03	8.872245159e+03	8.977565359e+03
<i>Shear</i>	1.511528614e+03	9.832197508e+01	6.324096246e+00
$\varepsilon = 10^{-4}$	$h = 0.25$	$h = 0.125$	$h = 0.0625$
<i>Total</i>	3.425758791e+03	1.258869611e+04	1.463889664e+04
<i>Bending</i>	1.908540468e+02	3.917903147e+03	5.399668504e+03
<i>Membrane</i>	1.537044139e+03	7.461483099e+03	9.123282754e+03
<i>Shear</i>	1.697805412e+03	1.208798432e+03	1.157553282e+02

Table 8.12: Table of scaled reduced energies for the Scordelis-Lo Roof shell problem and the MITC6a shell finite element with weighted shear stabilization ($C = 1$).

	$h = 0.25$	$h = 0.125$	$h = 0.0625$
$\varepsilon = 10^{-2}$	0.4946	0.5219	0.5230
$\varepsilon = 10^{-3}$	0.2915	0.3942	0.3993
$\varepsilon = 10^{-4}$	0.0557	0.3112	0.3689

Table 8.13: Proportion of bending energy with respect to the total strain energy (R_b) for the Scordelis-Lo Roof shell problem and the MITC6a shell finite element with weighted shear stabilization ($C = 1$).

$\varepsilon = 10^{-2}$	$h = 0.25$	$h = 0.125$	$h = 0.0625$
<i>Total</i>	1.446696302e+04	1.458748016e+04	1.452967725e+04
<i>Bending</i>	7.318692046e+03	7.631906528e+03	7.600288683e+03
<i>Membrane</i>	7.010521253e+03	6.938439348e+03	6.911453728e+03
<i>Shear</i>	1.324313745e+02	1.659469658e+01	1.864636594e+01

$\varepsilon = 10^{-3}$	$h = 0.25$	$h = 0.125$	$h = 0.0625$
<i>Total</i>	1.383327597e+04	1.491287355e+04	1.496323080e+04
<i>Bending</i>	4.967716729e+03	5.926842510e+03	5.977042048e+03
<i>Membrane</i>	8.242071602e+03	8.947334478e+03	8.983347303e+03
<i>Shear</i>	6.220906420e+02	3.829124201e+01	2.759923966e+00

$\varepsilon = 10^{-4}$	$h = 0.25$	$h = 0.125$	$h = 0.0625$
<i>Total</i>	6.897762648e+03	1.382082693e+04	1.475295301e+04
<i>Bending</i>	8.372992691e+02	5.047188863e+03	5.438782233e+03
<i>Membrane</i>	3.487039800e+03	8.319853774e+03	9.276979689e+03
<i>Shear</i>	2.573344410e+03	4.536534642e+02	3.715123654e+01

Table 8.14: Table of scaled reduced energies for the Scordelis-Lo Roof shell problem and the MITC6a shell finite element with weighted shear stabilization ($C = 1/5$).

	$h = 0.25$	$h = 0.125$	$h = 0.0625$
$\varepsilon = 10^{-2}$	0.5059	0.5232	0.5231
$\varepsilon = 10^{-3}$	0.3591	0.3974	0.3994
$\varepsilon = 10^{-4}$	0.1214	0.3652	0.3687

Table 8.15: Proportion of bending energy with respect to the total strain energy (R_b) for the Scordelis-Lo Roof shell problem and the MITC6a shell finite element with weighted shear stabilization ($C = 1/5$).

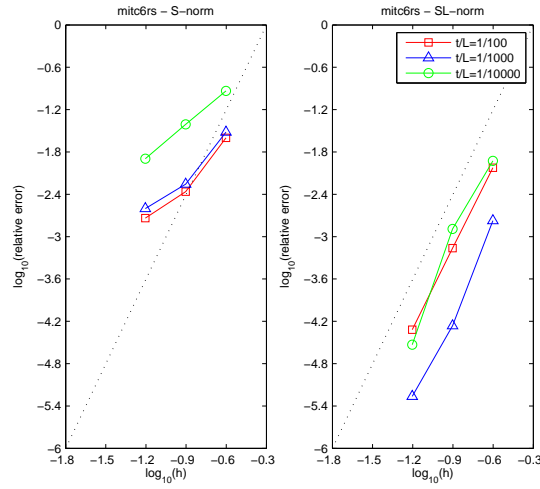


Figure 8.11: Convergence curves associated with the s-norm and SL-norm for the Scordelis Lo Roof shell problem and MITC6rs shell finite element. The dotted line shows the optimal convergence rate which is 4.

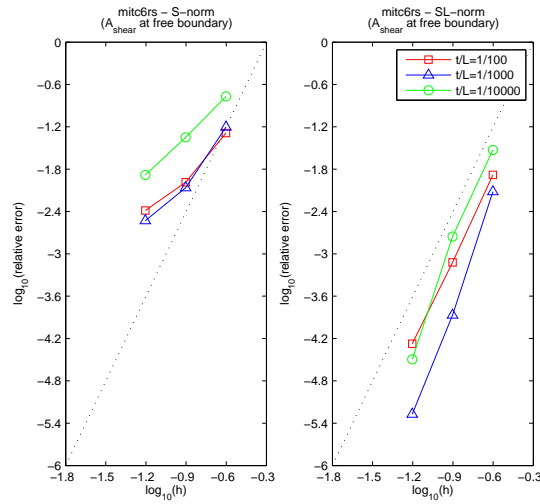


Figure 8.12: Convergence curves associated with the s-norm and SL-norm for the Scordelis Lo Roof shell problem and MITC6rs shell finite element with free boundary shear stabilization. The dotted line shows the optimal convergence rate which is 4.

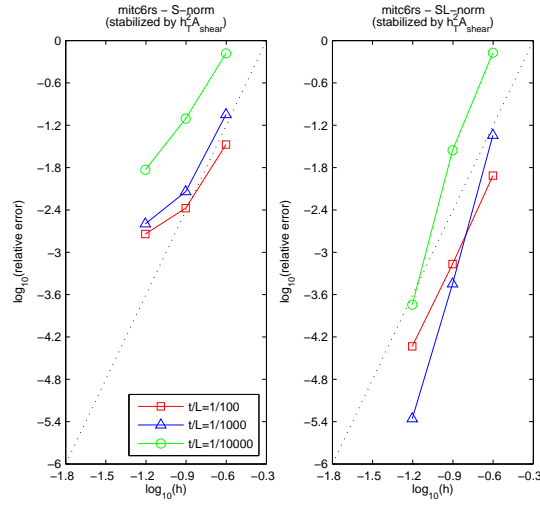


Figure 8.13: Convergence curves associated with the s-norm and SL-norm for the Scordelis Lo Roof shell problem and MITC6rs shell finite element with weighted shear stabilization ($C = 1$). The dotted line shows the optimal convergence rate which is 4.

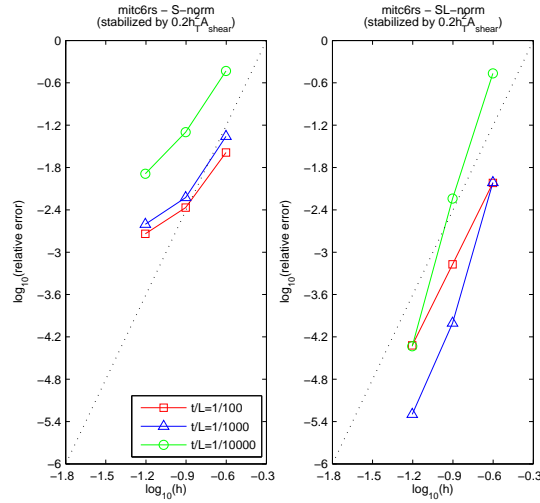


Figure 8.14: Convergence curves associated with the s-norm and SL-norm for the Scordelis Lo Roof shell problem and MITC6rs shell finite element with weighted shear stabilization ($C = 1/5$). The dotted line shows the optimal convergence rate which is 4.

$\varepsilon = 10^{-2}$	$h = 0.25$	$h = 0.125$	$h = 0.0625$
<i>Total</i>	1.460573228e+04	1.459023300e+04	1.453744991e+04
<i>Bending</i>	7.495194570e+03	7.632280342e+03	7.597811975e+03
<i>Membrane</i>	7.073030936e+03	6.938679182e+03	6.914554727e+03
<i>Shear</i>	3.848946674e+01	2.038566530e+01	2.620362236e+01
$\varepsilon = 10^{-3}$	$h = 0.25$	$h = 0.125$	$h = 0.0625$
<i>Total</i>	1.461308776e+04	1.493141931e+04	1.495901626e+04
<i>Bending</i>	5.724328523e+03	5.948046266e+03	5.975343798e+03
<i>Membrane</i>	8.792594909e+03	8.963545603e+03	8.979630187e+03
<i>Shear</i>	9.618516388e+01	1.985375347e+01	4.069951733e+00
$\varepsilon = 10^{-4}$	$h = 0.25$	$h = 0.125$	$h = 0.0625$
<i>Total</i>	1.336287412e+04	1.436378104e+04	1.476940361e+04
<i>Bending</i>	5.203330065e+03	5.407518897e+03	5.439987913e+03
<i>Membrane</i>	7.895300671e+03	8.891429132e+03	9.313969453e+03
<i>Shear</i>	2.642406292e+02	6.483568008e+01	1.544307974e+01

Table 8.16: Table of scaled reduced energies for the Scordelis-Lo Roof shell problem and the MITC6rs shell finite element.

	$h = 0.25$	$h = 0.125$	$h = 0.0625$
$\varepsilon = 10^{-2}$	0.5132	0.5231	0.5226
$\varepsilon = 10^{-3}$	0.3917	0.3984	0.3994
$\varepsilon = 10^{-4}$	0.3894	0.3765	0.3683

Table 8.17: Proportion of bending energy with respect to the total strain energy (R_b) for the Scordelis-Lo Roof shell problem and the MITC6rs shell finite element.

$\varepsilon = 10^{-2}$	$h = 0.25$	$h = 0.125$	$h = 0.0625$
<i>Total</i>	1.419726277e+04	1.449636979e+04	1.449499902e+04
<i>Bending</i>	7.040636418e+03	7.496267877e+03	7.543295548e+03
<i>Membrane</i>	6.887836793e+03	6.898795550e+03	6.896572181e+03
<i>Shear</i>	1.378414800e+02	3.291516694e+01	2.119320703e+01
$\varepsilon = 10^{-3}$	$h = 0.25$	$h = 0.125$	$h = 0.0625$
<i>Total</i>	1.412663212e+04	1.488462859e+04	1.495192572e+04
<i>Bending</i>	5.330942133e+03	5.890101003e+03	5.965994790e+03
<i>Membrane</i>	8.493419448e+03	8.934716610e+03	8.975211010e+03
<i>Shear</i>	2.837913311e+02	4.897562500e+01	5.237284481e+00
$\varepsilon = 10^{-4}$	$h = 0.25$	$h = 0.125$	$h = 0.0625$
<i>Total</i>	1.254851031e+04	1.427654515e+04	1.476393769e+04
<i>Bending</i>	4.734316804e+03	5.312410205e+03	5.433712047e+03
<i>Membrane</i>	7.334619024e+03	8.831516959e+03	9.310105808e+03
<i>Shear</i>	4.764530930e+02	1.303247953e+02	1.889327084e+01

Table 8.18: Table of scaled reduced energies for the Scordelis-Lo Roof shell problem and the MITC6rs shell finite element with free boundary shear stabilization.

	$h = 0.25$	$h = 0.125$	$h = 0.0625$
$\varepsilon = 10^{-2}$	0.4959	0.5171	0.5204
$\varepsilon = 10^{-3}$	0.3774	0.3957	0.3990
$\varepsilon = 10^{-4}$	0.3773	0.3721	0.3680

Table 8.19: Proportion of bending energy with respect to the total strain energy (R_b) for the Scordelis-Lo Roof shell problem and the MITC6rs shell finite element with free boundary shear stabilization.

$\varepsilon = 10^{-2}$	$h = 0.25$	$h = 0.125$	$h = 0.0625$
<i>Total</i>	1.413595572e+04	1.456247611e+04	1.453488614e+04
<i>Bending</i>	6.984447718e+03	7.595559070e+03	7.594150484e+03
<i>Membrane</i>	6.849468722e+03	6.924853256e+03	6.913294405e+03
<i>Shear</i>	2.730081686e+02	3.491571550e+01	2.649273617e+01
$\varepsilon = 10^{-3}$	$h = 0.25$	$h = 0.125$	$h = 0.0625$
<i>Total</i>	1.225059193e+04	1.480433430e+04	1.495278122e+04
<i>Bending</i>	3.580487844e+03	5.836855787e+03	5.970782523e+03
<i>Membrane</i>	7.164897327e+03	8.867039563e+03	8.974415817e+03
<i>Shear</i>	1.500139135e+03	9.834195844e+01	7.066133557e+00
$\varepsilon = 10^{-4}$	$h = 0.25$	$h = 0.125$	$h = 0.0625$
<i>Total</i>	3.425699760e+03	1.258968674e+04	1.462615750e+04
<i>Bending</i>	1.894935310e+02	3.921191775e+03	5.398823127e+03
<i>Membrane</i>	1.538919836e+03	7.467167434e+03	9.109847056e+03
<i>Shear</i>	1.697231295e+03	1.200811767e+03	1.172954141e+02

Table 8.20: Table of scaled reduced energies for the Scordelis-Lo Roof shell problem and the MITC6rs shell finite element with weighted shear stabilization ($C = 1$).

	$h = 0.25$	$h = 0.125$	$h = 0.0625$
$\varepsilon = 10^{-2}$	0.4941	0.5216	0.5225
$\varepsilon = 10^{-3}$	0.2923	0.3943	0.3993
$\varepsilon = 10^{-4}$	0.0553	0.3115	0.3691

Table 8.21: Proportion of bending energy with respect to the total strain energy (R_b) for the Scordelis-Lo Roof shell problem and the MITC6rs shell finite element with weighted shear stabilization ($C = 1$).

$\varepsilon = 10^{-2}$	$h = 0.25$	$h = 0.125$	$h = 0.0625$
<i>Total</i>	1.444423333e+04	1.458412172e+04	1.453693600e+04
<i>Bending</i>	7.308354978e+03	7.623784353e+03	7.597077314e+03
<i>Membrane</i>	6.994343104e+03	6.935632082e+03	6.914302074e+03
<i>Shear</i>	1.362262686e+02	2.415933802e+01	2.626307458e+01
$\varepsilon = 10^{-3}$	$h = 0.25$	$h = 0.125$	$h = 0.0625$
<i>Total</i>	1.380503923e+04	1.489314485e+04	1.495740881e+04
<i>Bending</i>	4.960170893e+03	5.918904062e+03	5.974026493e+03
<i>Membrane</i>	8.223342927e+03	8.932428612e+03	8.978244421e+03
<i>Shear</i>	6.201330687e+02	4.140816958e+01	5.056667694e+00
$\varepsilon = 10^{-4}$	$h = 0.25$	$h = 0.125$	$h = 0.0625$
<i>Total</i>	6.894852101e+03	1.378482018e+04	1.473193479e+04
<i>Bending</i>	8.338832462e+02	5.053845010e+03	5.427539327e+03
<i>Membrane</i>	3.482899880e+03	8.290221437e+03	9.258983981e+03
<i>Shear</i>	2.577989945e+03	4.406226156e+02	4.537091076e+01

Table 8.22: Table of scaled reduced energies for the Scordelis-Lo Roof shell problem and the MITC6rs shell finite element with weighted shear stabilization ($C = 1/5$).

	$h = 0.25$	$h = 0.125$	$h = 0.0625$
$\varepsilon = 10^{-2}$	0.5060	0.5227	0.5226
$\varepsilon = 10^{-3}$	0.3593	0.3974	0.3994
$\varepsilon = 10^{-4}$	0.1209	0.3666	0.3684

Table 8.23: Proportion of bending energy with respect to the total strain energy (R_b) for the Scordelis-Lo Roof shell problem and the MITC6rs shell finite element with weighted shear stabilization ($C = 1/5$).

APPENDIX

Appendix A

The MITC4 element

The MITC4 element has been used as reference for bending dominated shell problems. It is a 4-node shell element whose geometry and discretized space of displacements are respectively given by:

$$\begin{aligned}\vec{x}(r, s, z) &= \sum_{i=1}^4 \lambda_i(r, s) \left(\vec{x}^{(i)} + z \frac{t^{(i)}}{2} \vec{a}_3^{(i)} \right) \\ \vec{U}(r, s, z) &= \sum_{i=1}^4 \lambda_i(r, s) \left(\vec{u}^{(i)} + z \frac{t^{(i)}}{2} \left(\alpha_1^{(i)} \vec{V}_1^{(i)} + \alpha_2^{(i)} \vec{V}_2^{(i)} \right) \right)\end{aligned}\tag{A.1}$$

where λ_i denote the associated $2d$ Lagrange shape functions, i.e. we have

$$\mathcal{V}_h = \mathcal{U}_h \times \mathcal{B}_h \tag{A.2}$$

with

$$\begin{aligned}\mathcal{U}_h &= \left\{ \vec{v} \in [H^1(\Omega)]^3, \quad \vec{v}|_K \in [\mathcal{Q}_1(K)]^3 \quad \forall K \in \mathcal{M}_h \right\} \\ \mathcal{B}_h &= \left\{ \underline{\eta} \in [H^1(\Omega)]^2, \quad \underline{\eta}|_K \in [\mathcal{Q}_1(K)]^2 \quad \forall K \in \mathcal{M}_h \right\}\end{aligned}\tag{A.3}$$

where \mathcal{M}_h denotes the collection of elements that constitute the mesh. Only the transverse shear strains are treated by the MITC procedure, as Fig.A.1 shows.

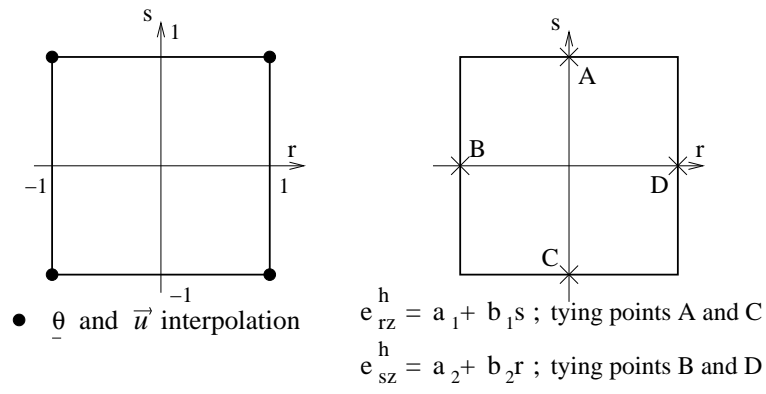


Figure A.1: MITC4 element

Appendix B

MITC7 static condensation

In the case of the MITC7 shell finite element, the θ -interpolation involves one additional internal node: the barycenter inside each element. Nevertheless, we can manage to numerically work with nodes on edges and “*treat*” the degrees of freedom associated with this internal node in an implicit manner. Any strategy of this kind is commonly known as *static condensation*.

Let \mathbf{U} denote the nodal displacement/rotation vector. Given an element e , the associated elemental stiffness matrix can be descomposed as:

$$\begin{pmatrix} \mathbf{K}_{bb}^e & (\mathbf{K}_{ib}^e)^T \\ \mathbf{K}_{ib}^e & \mathbf{K}_{ii}^e \end{pmatrix} \quad (\text{B.1})$$

where the symbol b refers to the nodes on the edges of the element and i refers to the internal one.

At the assembly level, each internal node only gets contributions of nodes in the same element. So, the matrix formulation associated with a general finite element discretization reads:

$$\begin{pmatrix} \ddots & \vdots & \vdots & \ddots \\ \cdots & (\cdots + \mathbf{K}_{bb}^e + \cdots) & (\mathbf{K}_{ib}^e)^T & \cdots \\ 0 & \mathbf{K}_{ib}^e & \mathbf{K}_{ii}^e & 0 \\ \ddots & \vdots & \vdots & \ddots \end{pmatrix} \begin{pmatrix} \vdots \\ \mathbf{U}_b \\ \mathbf{U}_i \\ \vdots \end{pmatrix} = \begin{pmatrix} \vdots \\ F_b \\ F_i \\ \vdots \end{pmatrix} \quad (\text{B.2})$$

where $\cdots + \mathbf{K}_{bb}^e + \cdots$ refers to the rest of elemental contributions for nodes on edges. It follows that:

$$\begin{cases} \cdots + (\cdots + \mathbf{K}_{bb}^e + \cdots) \mathbf{U}_b + (\mathbf{K}_{ib}^e)^T \mathbf{U}_i + \cdots = F_b \\ \mathbf{K}_{ib}^e \mathbf{U}_b + \mathbf{K}_{ii}^e \mathbf{U}_i = F_i \end{cases} \quad (\text{B.3})$$

The second equation in (B.3) gives:

$$\mathbf{U}_i = (\mathbf{K}_{ii}^e)^{-1} (\mathbf{F}_i - \mathbf{K}_{ib}^e \mathbf{U}_b) \quad (\text{B.4})$$

and then using (B.4) in the first equation of (B.3) we obtain:

$$\cdots + \left[(\cdots + \mathbf{K}_{bb}^e + \cdots) - (\mathbf{K}_{ib}^e)^T (\mathbf{K}_{ii}^e)^{-1} \mathbf{K}_{ib}^e \right] \mathbf{U}_b + \cdots = \mathbf{F}_b - (\mathbf{K}_{ib}^e)^T (\mathbf{K}_{ii}^e)^{-1} \mathbf{F}_i \quad (\text{B.5})$$

which can be implemented at the elemental level for each finite element. We point out that \mathbf{K}_{ii}^e is a matrix of size 2×2 in our particular case –only two degrees of freedom are considered for the barycenter inside each element– and its inverse is not numerically expensive to calculate.

So, the dimension of system (B.2) can be reduced and only nodes on edges need to be considered. An equivalent formulation reads:

$$\begin{pmatrix} \ddots & & \vdots & & \ddots \\ & \cdots & \left[(\cdots + \mathbf{K}_{bb}^e + \cdots) - (\mathbf{K}_{ib}^e)^T (\mathbf{K}_{ii}^e)^{-1} \mathbf{K}_{ib}^e \right] & \cdots & \\ & & \vdots & & \ddots \end{pmatrix} \begin{pmatrix} \vdots \\ \mathbf{U}_b \\ \vdots \end{pmatrix} = \begin{pmatrix} \vdots \\ F_b - (\mathbf{K}_{ib}^e)^T (\mathbf{K}_{ii}^e)^{-1} F_i \\ \vdots \end{pmatrix} \quad (\text{B.6})$$

Appendix C

Projection into shell meshes

We consider a shell problem for ε fixed. Let $\vec{U}_{ref} \equiv (\vec{u}_{ref}, \underline{\theta}_{ref})$ denote the reference solution for a reference mesh, and $\vec{U}_h \equiv (\vec{u}_h, \underline{\theta}_h)$ be the current finite element solution associated with the same problem when considering a triangular mesh of the same shell structure that will be referred as target solution in the sequel. From now on, we assume that nodes are located on the exact midsurface for all meshes.

The aim is to calculate the target displacement and rotation fields for points pertaining to the reference domain—that may correspond to nodes or Gauss points—from target displacements and rotations. So, it is necessary to firstly locate the reference points in consideration in the target mesh.

Let O denote the origin of the global Cartesian coordinate system and M be a generic point in the reference domain of local coordinates $(r_{ref}, s_{ref}, z_{ref})$ inside a reference element, thus we have

$$O\vec{M} = \sum_{i=1}^m \beta_i(r_{ref}, s_{ref}) \left(\vec{x}^{(i)} + z_{ref} \frac{t(i)}{2} \vec{a}_3^{(i)} \right) \quad (C.1)$$

where the set $\{\beta_i\}_{i=1}^m$ refers to the $2d$ shape functions associated with the reference m -node isoparametric procedure, $\{\vec{x}^{(i)}\}_{i=1}^m$ denote the nodal position vectors in global Cartesian coordinates for the reference element in consideration, and $\vec{a}_3^{(i)}$ the normal vector at node i .

We denote by P_M the approximate projection of M into the reference midsurface (see Fig. C.1), which is commonly given by

$$O\vec{P}_M = \sum_{i=1}^m \beta_i(r_{ref}, s_{ref}) \vec{x}^{(i)} \quad (C.2)$$

The approximate normal vector at P_M is

$$\vec{a}_3(r, s) = \sum_{i=1}^m \beta_i(r_{ref}, s_{ref}) \vec{a}_3^{(i)} \quad (C.3)$$

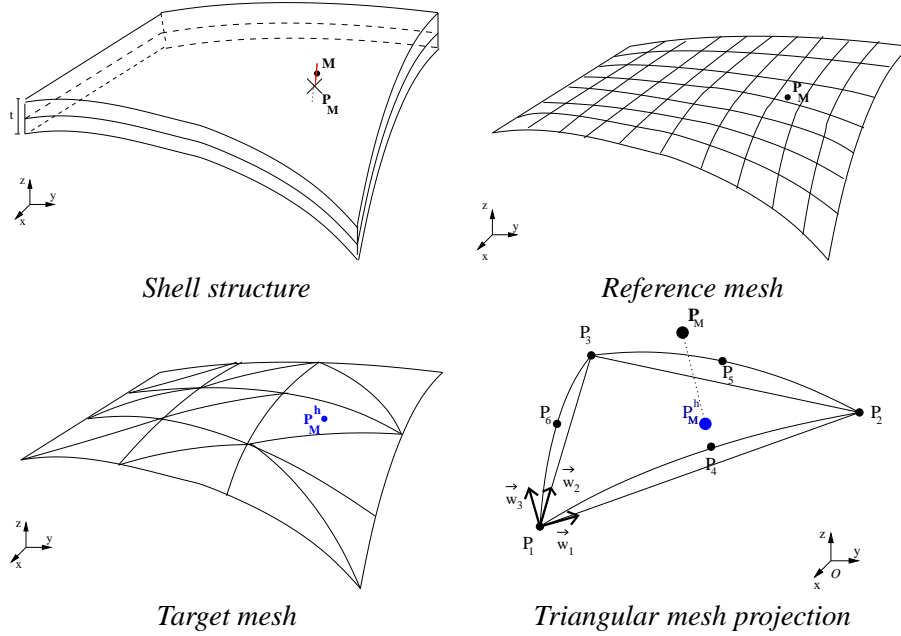


Figure C.1: Projection into a triangular mesh.

The target finite element where P_M is located can be easily calculated by the procedure described below:

1. Let us consider a curvilinear target element of nodes P_i and associated Cartesian coordinates (X_i, Y_i, Z_i) for $i = 1, \dots, k$ as shown in Fig. C.1. We consider the vertices P_1, P_2, P_3 (see Fig. C.2) and we define the vectors

$$\vec{w}_1 = \frac{P_1 \vec{P}_2}{\|P_1 \vec{P}_2\|_2}, \quad \vec{w}_2 = \frac{P_1 \vec{P}_3}{\|P_1 \vec{P}_3\|_2} \quad (\text{C.4})$$

and the normal vector

$$\vec{w}_3 = \frac{\vec{w}_1 \times \vec{w}_2}{\|\vec{w}_1 \times \vec{w}_2\|_2} \quad (\text{C.5})$$

2. We define P_M^h as the projection of P_M into the triangle or vertices P_1, P_2, P_3 , namely

$$O \vec{P}_M^h = O \vec{P}_M - (O \vec{P}_M \cdot \vec{w}_3) \vec{w}_3 \quad (\text{C.6})$$

Its global Cartesian coordinates are denoted by (X, Y, Z) .

3. We set:

$$\delta = \left[\begin{pmatrix} X_1 - X_3 \\ Y_1 - Y_3 \\ Z_1 - Z_3 \end{pmatrix} \times \begin{pmatrix} X_2 - X_3 \\ Y_2 - Y_3 \\ Z_2 - Z_3 \end{pmatrix} \right] \cdot \vec{w}_3 = (P_3 \vec{P}_1 \times P_3 \vec{P}_2) \cdot \vec{w}_3 \quad (\text{C.7})$$

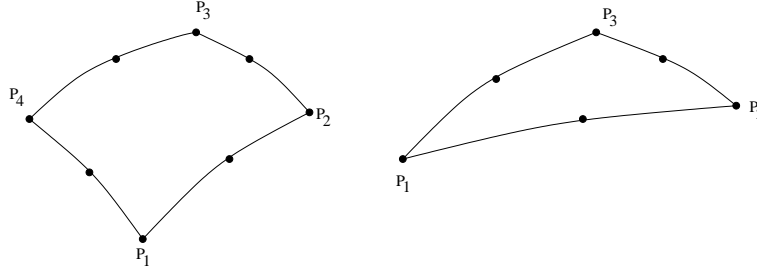


Figure C.2: Geometric orientation conventions for vertex numbering.

Then, the barycentric coordinates $(\lambda_b^1, \lambda_b^2, \lambda_b^3)$ corresponding to P_M^h are:

$$\begin{aligned}\lambda_b^1 &= \frac{1}{\delta} \left(P_2 \vec{P}_M \times P_3 \vec{P}_2 \right) \cdot \vec{w}_3 = \frac{1}{\delta} \left[\begin{pmatrix} X - X_2 \\ Y - Y_2 \\ Z - Z_2 \end{pmatrix} \times \begin{pmatrix} X_2 - X_3 \\ Y_2 - Y_3 \\ Z_2 - Z_3 \end{pmatrix} \right] \cdot \vec{w}_3 \\ \lambda_b^2 &= \frac{1}{\delta} \left(P_3 \vec{P}_M \times P_1 \vec{P}_3 \right) \cdot \vec{w}_3 = \frac{1}{\delta} \left[\begin{pmatrix} X - X_3 \\ Y - Y_3 \\ Z - Z_3 \end{pmatrix} \times \begin{pmatrix} X_3 - X_1 \\ Y_3 - Y_1 \\ Z_3 - Z_1 \end{pmatrix} \right] \cdot \vec{w}_3 \\ \lambda_b^3 &= \frac{1}{\delta} \left(P_1 \vec{P}_M \times P_2 \vec{P}_1 \right) \cdot \vec{w}_3 = \frac{1}{\delta} \left[\begin{pmatrix} X - X_1 \\ Y - Y_1 \\ Z - Z_1 \end{pmatrix} \times \begin{pmatrix} X_1 - X_2 \\ Y_1 - Y_2 \\ Z_1 - Z_2 \end{pmatrix} \right] \cdot \vec{w}_3\end{aligned}\tag{C.8}$$

4. If $\lambda_b^i \geq 0$ for $i = 1, 2, 3$, it means that P_M^h lies inside the triangle of vertex $\{P_1, P_2, P_3\}$ and then we will assume that P_M is located in the corresponding target finite element.

Otherwise,

- when dealing with triangular shell finite elements, the same procedure is accomplished for another element;
- when considering quadrangular elements, we define P_M^h as the projection of P_M into the triangle or vertices P_1, P_3, P_4 (instead of P_1, P_2, P_3 , see Fig. C.2), being the related Cartesian coordinates denoted by (X, Y, Z) , and a similar strategy is accomplished to calculate the related δ and λ_b^i for $i = 1, 2, 3$. If the corresponding barycentric coordinates are not admissible, another element is considered and the same procedure described above is accomplished again.

Once the corresponding target finite element is found, the associated local coordinates (r_h, s_h) can be obtained by solving

$$\min_{(r,s)} \left\{ O\vec{P}_M - \sum_{i=1}^k \lambda_i(r, s) \vec{x}_h^{(i)} \right\}^2 \quad (\text{C.9})$$

where the set $\{\lambda_i\}_{i=1}^k$ represents the $2d$ shape functions associated with the k -node isoparametric procedure, $\vec{x}_h^{(i)}$ denotes the position of the target node i in the global Cartesian coordinate system and

$$(\vec{X} - \vec{Y})^2 = (\vec{X} - \vec{Y}) \cdot (\vec{X} - \vec{Y}) \quad (\text{C.10})$$

refers to the standard Euclidian dot product between two vectors in global Cartesian coordinates. Namely, the local coordinates (r_h, s_h) are obtained by minimization of the Euclidian distance measure given by (C.9). It is important to notice that the differential system derived from the minimization of equation (C.9) is not necessary linear, so it is solved using a Newton procedure.

Once (C.9) is solved we set

$$z_h = z_{ref} \quad (\text{C.11})$$

and following a standard isoparametric approach, we could define the target displacement for M as:

$$\vec{U}_h^M = \sum_i^k \lambda_i(r_h, s_h) \left(\vec{u}_h^{(i)} + z_h \frac{t^{(i)}}{2} \vec{\theta}_h^{(i)} \right) \quad (\text{C.12})$$

where $\vec{u}_h^{(i)}$ and $\vec{\theta}_h^{(i)}$ respectively denote the target midsurface displacement and rotation field associated with the target node i . But even if for all target nodes the orthogonality property

$$\vec{\theta}_h^{(i)} \cdot \vec{a}_{3h}^{(i)} = 0 \quad (\text{C.13})$$

holds, the vector

$$\vec{\theta}_h^M = \sum_i^k \lambda_i(r_h, s_h) \vec{\theta}_h^{(i)} \quad (\text{C.14})$$

does not provide a rotation field verifying the Reissner-Mindlin assumption, since in general we do not have

$$\vec{\theta}_h^M \cdot \vec{a}_3 = 0 \quad (\text{C.15})$$

for \vec{a}_3 the normal vector at the reference point M in consideration.

In consequence, we define the target midsurface displacement and tangential rotation fields related to M as:

$$\begin{aligned} \vec{u}_h^M &= \sum_i^k \lambda_i(r_h, s_h) \vec{u}_h^{(i)} \\ \vec{\theta}_h^M &= \pi \left(\sum_i^k \lambda_i(r_h, s_h) \vec{\theta}_h^{(i)} \right) \end{aligned} \quad (\text{C.16})$$

where π denotes the projection onto the tangential plane in the reference framework, namely

$$\pi(\vec{\psi}) = \vec{\psi} - (\vec{\psi} \cdot \vec{a}_3)\vec{a}_3 \quad (\text{C.17})$$

for any vector field $\vec{\psi}$ defined on the midsurface.

Appendix D

The s-norm

Let $\vec{U}_{ref}^\varepsilon \equiv (\vec{u}_{ref}^\varepsilon, \underline{\theta}_{ref}^\varepsilon)$ denote the reference solution of a shell problem for ε set, and $\vec{U}_h^\varepsilon \equiv (\vec{u}_h^\varepsilon, \underline{\theta}_h^\varepsilon)$ be a current finite element solution associated with the same relative thickness, that will be referred as target solution in the sequel.

The *s-norm* is obtained by comparing the approximate and reference strains by means of the governing discretized energy in the reference domain. For general shell element procedures and in the case of an isotropic material, it is numerically defined as:

$$\|\vec{U}_{ref}^\varepsilon - \vec{U}_h^\varepsilon\|_s^2 = \int_{\Omega_{ref}} \Delta\epsilon^T \Delta\sigma dV \quad (D.1)$$

where $\Delta\epsilon$ and $\Delta\sigma$ respectively denote the difference between the discretized strain¹ and stress component-vectors in the global Cartesian coordinate system, namely

$$\Delta\epsilon = \epsilon_{ref}(\vec{x}) - \epsilon_h(\vec{x}_h) \quad (D.2)$$

$$\Delta\sigma = \sigma_{ref}(\vec{x}) - \sigma_h(\vec{x}_h) = C_{ref}(\vec{x})\epsilon_{ref}(\vec{x}) - C_h(\vec{x}_h)\epsilon_h(\vec{x}_h) \quad (D.3)$$

with

$$\epsilon = [\epsilon_{xx}, \epsilon_{yy}, \epsilon_{zz}, 2\epsilon_{xy}, 2\epsilon_{yz}, 2\epsilon_{zx}]^T \quad (D.4)$$

$$\sigma = [\sigma_{xx}, \sigma_{yy}, \sigma_{zz}, \sigma_{xy}, \sigma_{yz}, \sigma_{zx}]^T \quad (D.5)$$

and where C_{ref} denotes the material stress-strain matrix associated with the reference discretized geometry and C_h denotes the target one. The position vectors \vec{x} and \vec{x}_h respectively correspond to the reference and discretized domains, and the relationship between them is given by the projection procedure described in Appendix C.

So, a suitable Gauss numerical integration is used to numerically calculate (D.1), and we introduce n_e integration points of local coordinates

$$(r_p, s_p, z_p), \quad p = 1, \dots, n_e \quad (D.6)$$

¹Taking into account the MITC procedure when it holds.

inside each reference element K . The associated position vectors are easily obtained by means of the approximate reference chart, and the projection strategy described in Appendix C is applied in order to obtain the associated target covariant-covariant strain components by means of the approximate displacement \vec{U}_h^ε .

In order to calculate the stress-strain matrices associated with the reference (C_{ref}) and target (C_h) geometries, we introduce in each case the shell-aligned coordinate system $(\tilde{r}, \tilde{s}, z)$ of tangent vectors

$$\vec{e}_{\tilde{r}} = \frac{\vec{g}_s \times \vec{g}_z}{\|\vec{g}_s \times \vec{g}_z\|_2}, \quad \vec{e}_{\tilde{s}} = \frac{\vec{g}_z \times \vec{e}_{\tilde{r}}}{\|\vec{g}_z \times \vec{e}_{\tilde{r}}\|_2}, \quad \vec{e}_z = \frac{\vec{g}_z}{\|\vec{g}_z\|_2} \quad (\text{D.7})$$

where $\{\vec{g}_r, \vec{g}_s, \vec{g}_z\}$ are related to the reference or target geometry in consideration. The strain-stress law for this particular coordinate system reads

$$C_{al} = \frac{E}{1 - \nu^2} \begin{pmatrix} 1 & \nu & 0 & 0 & 0 & 0 \\ \nu & 1 & 0 & 0 & 0 & 0 \\ 0 & 0 & 0 & 0 & 0 & 0 \\ 0 & 0 & 0 & \frac{1-\nu}{2} & 0 & 0 \\ 0 & 0 & 0 & 0 & k\frac{1-\nu}{2} & 0 \\ 0 & 0 & 0 & 0 & 0 & k\frac{1-\nu}{2} \end{pmatrix} \quad (\text{D.8})$$

where k typically denotes an optional shear correction factor².

Let us denote by ϵ_{rsz} the reference or target covariant-covariant strain component-vector in the respective (r, s, z) local coordinate system, namely

$$\epsilon_{rsz} = [e_{rr}, e_{ss}, e_{zz}, 2e_{rs}, 2e_{sz}, 2e_{zr}]^T \quad (\text{D.9})$$

where the strain component e_{zz} can be obtained from the planar stress assumption $\sigma^{33} = 0$ that gives

$$e_{zz} = -\frac{\nu}{1 + \nu} \frac{t^2}{4} g^{\alpha\beta} e_{\alpha\beta} \quad (\text{D.10})$$

or as a consequence of the Reissner-Mindlin kinematical assumption

$$e_{zz} = 0 \quad (\text{D.11})$$

However, the transverse strain component has no special impact in the formulation described in this section as (D.10) is recovered once the in-plane strains e_{rr} , e_{ss} and e_{rs} are known.

The global Cartesian strain component-vector ϵ is directly calculated as

$$\epsilon = [Q] \epsilon_{rsz} \quad (\text{D.12})$$

²For our analysis we set $k = 1$.

with

$$Q = \begin{pmatrix} l_1 l_1 & m_1 m_1 & n_1 n_1 & l_1 m_1 & m_1 n_1 & n_1 l_1 \\ l_2 l_2 & m_2 m_2 & n_2 n_2 & l_2 m_2 & m_2 n_2 & n_2 l_2 \\ l_3 l_3 & m_3 m_3 & n_3 n_3 & l_3 m_3 & m_3 n_3 & n_3 l_3 \\ 2l_1 l_2 & 2m_1 m_2 & 2n_1 n_2 & l_1 m_2 + l_2 m_1 & m_1 n_2 + m_2 n_1 & n_1 l_2 + n_2 l_1 \\ 2l_2 l_3 & 2m_2 m_3 & 2n_2 n_3 & l_2 m_3 + l_3 m_2 & m_2 n_3 + m_3 n_2 & n_2 l_3 + n_3 l_2 \\ 2l_3 l_1 & 2m_3 m_1 & 2n_3 n_1 & l_3 m_1 + l_1 m_3 & m_3 n_1 + m_1 n_3 & n_3 l_1 + n_1 l_3 \end{pmatrix} \quad (\text{D.13})$$

for

$$\begin{aligned} l_1 &= \vec{g}^r \cdot \vec{i} & m_1 &= \vec{g}^s \cdot \vec{i} & n_1 &= \vec{g}^z \cdot \vec{i} \\ l_2 &= \vec{g}^r \cdot \vec{j} & m_2 &= \vec{g}^s \cdot \vec{j} & n_2 &= \vec{g}^z \cdot \vec{j} \\ l_3 &= \vec{g}^r \cdot \vec{k} & m_3 &= \vec{g}^s \cdot \vec{k} & n_3 &= \vec{g}^z \cdot \vec{k} \end{aligned} \quad (\text{D.14})$$

and $\{\vec{i}, \vec{j}, \vec{k}\}$ the classical Cartesian basis, namely

$$\vec{i} = \begin{pmatrix} 1 \\ 0 \\ 0 \end{pmatrix}, \quad \vec{j} = \begin{pmatrix} 0 \\ 1 \\ 0 \end{pmatrix}, \quad \vec{k} = \begin{pmatrix} 0 \\ 0 \\ 1 \end{pmatrix} \quad (\text{D.15})$$

Then, the reference and target stress Cartesian component-vector can be obtained as

$$\sigma = [\tilde{Q}]^T [C_{al}] [\tilde{Q}] \epsilon \quad (\text{D.16})$$

where \tilde{Q} denotes the matrix that transforms the strain component-vector from the global Cartesian system into the respective shell-aligned basis defined in (D.7), which is formulated from (D.13) by suitably setting

$$\begin{aligned} l_1 &= \vec{i} \cdot \vec{e}_{\tilde{r}} & m_1 &= \vec{j} \cdot \vec{e}_{\tilde{r}} & n_1 &= \vec{k} \cdot \vec{e}_{\tilde{r}} \\ l_2 &= \vec{i} \cdot \vec{e}_{\tilde{s}} & m_2 &= \vec{j} \cdot \vec{e}_{\tilde{s}} & n_2 &= \vec{k} \cdot \vec{e}_{\tilde{s}} \\ l_3 &= \vec{i} \cdot \vec{e}_{\tilde{z}} & m_3 &= \vec{j} \cdot \vec{e}_{\tilde{z}} & n_3 &= \vec{k} \cdot \vec{e}_{\tilde{z}} \end{aligned} \quad (\text{D.17})$$

Appendix E

Analysis of boundary layers

In general, when solving a shell problem, the deformation field of the shell may be split into a piecewise smooth component plus other layers that substantially decay from particular lines or points, which may correspond to the boundaries, lines or points where the load is irregular and certain characteristic lines for parabolic or hyperbolic midsurfaces. In the case of the shell problems that we have analyzed in our work, uniform smooth loads are considered and the layers are more particularly related to the boundaries.

The boundary layer area must be properly meshed in order to obtain accurate results. If a mesh spacing of width h is used to capture the smooth components of the solution, then a local refinement of mesh spacing at least of order

$$h_{BL} \sim \frac{d}{L}h \quad (\text{E.1})$$

is often required to capture with the same relative accuracy a boundary layer component of length scale d . Nevertheless, when locking occurs it is even more complicated to achieve the desired accuracy, and an overrefinement may be needed.

Many studies have been undertaken to identify the layer lengths for certain shell problems (see [54] and references therein), and the problem of scale resolution is usually treated numerically. The scale

$$\varepsilon^{\frac{1}{2}}L \quad (\text{E.2})$$

is known from many analytical studies, but not as well known are the longer scales $\varepsilon^{\frac{1}{4}}L$ and $\varepsilon^{\frac{1}{3}}L$ which may appear in parabolic and hyperbolic shells (see [54] and references therein). The characteristic length expressed as

$$d = C\varepsilon^\alpha L \quad (\text{E.3})$$

can be numerically determined using a suitable reference solution for a sufficiently refined mesh: each displacement component can be displayed along the boundary lines and in cross-sections originating from boundaries.

- *Clamped cylindrical benchmark:*

In view of Fig. E.1, E.2, E.3 and E.4 –that respectively show the non-zero normalized displacement and rotation components along AB , BC and CD obtained using a mesh of 48×48 P_2 displacement-based shell finite elements–, the length of the layer can be determined by the distance d displayed in Fig. E.4-(h) which corresponds to the distance measured from the clamped top to the first peak of the rotation along V_2 for each ε , which is known to be of order $\sim \varepsilon^{-\frac{1}{2}}$ (refer to [54]).

We observe that when setting

$$d = C\sqrt{\varepsilon}L \quad (\text{E.4})$$

the constant $C = 5$ provides an adequate characteristic length as Table E.1 shows.

ε	<i>Computed</i> d	<i>Distance by formula</i> $d = 5\sqrt{\varepsilon}L$
10^{-2}	0.3	0.5
10^{-3}	0.1	0.16
10^{-4}	0.05	0.05

Table E.1: Layer length for the clamped cylindrical shell problem: distance d computed from the clamped edge to the first peak of the normalized rotation along V_2 .

A suitable local refinement is needed in order to capture the solution with the same accuracy everywhere. Assume that N shell finite elements are considered outside of the boundary layer area using a mesh spacing h , namely

$$h = \frac{L - d}{N} \quad (\text{E.5})$$

Hence, a suitable local refinement with mesh spacing

$$h_{BL} = \frac{d}{N_{BL}} \quad (\text{E.6})$$

inside of the boundary layer area must be determined.

Given the interpolation operator \mathcal{I}_k associated with a reference k -node shell approach, the aim is to obtain

$$\|(\vec{u}, \underline{\theta}) - \mathcal{I}_k(\vec{u}, \underline{\theta})\|_0 \leq Ch^k \quad (\text{E.7})$$

for $(\vec{u}, \underline{\theta})$ smooth enough, where $\|\cdot\|_0$ typically denotes the L^2 -norm over the shell domain and C a general constant. In particular, over the boundary layer area we have that for the variable of largest amplitude, namely the rotation,

$$\|\underline{\theta} - \mathcal{I}_k(\underline{\theta})\|_{0,BL} \leq Ch_{BL}^k |\underline{\theta}|_{k,BL} \quad (\text{E.8})$$

and from [54] it follows that

$$\|\underline{\theta} - \mathcal{I}_k(\underline{\theta})\|_{0,BL} \leq C \left(\frac{\varepsilon^{1/2}}{N_{BL}} \right)^k \frac{\varepsilon^{-1/2}}{(\varepsilon^{1/2})^k} = C \frac{\varepsilon^{-1/2}}{N_{BL}^k} \quad (\text{E.9})$$

Consequently, when using P_2 displacement-based shell finite elements it is necessary to take

$$N_{BL} \sim \varepsilon^{-\frac{1}{4}} N \quad (\text{E.10})$$

in order to obtain $\mathcal{O}(h^2)$ accuracy everywhere for this particular benchmark.

- *Clamped hyperboloid shell problem:*

The non-zero normalized displacement and rotation fields along AD , BC and CD are displayed in Fig. E.5, E.6, E.7 and E.8 when using a mesh of 48×48 P_2 displacement-based shell finite elements. For this particular shell problem no analytical irregularity of the solution as $\varepsilon \rightarrow 0$ has been proven so far, but from [55] we know that a layer exists like for the clamped cylindrical shell problem since both structures are loaded by the same normal periodic distributed force for identical boundary conditions, and layers are known to be influenced by the geometric nature of the midsurface only when setting boundary conditions along characteristic lines, which does not correspond to this specific case.

In fact, Fig. E.5-(b), E.6-(d), E.7-(f) and Fig. E.8 show that a layer exists close to the clamped boundary and the rotation component along V_2 explodes in a similar manner as for the clamped cylindrical shell problem as ε decreases (compare Fig. E.4 and Fig. E.8). The length of the layer can be numerically determined by the distance d displayed in Fig. E.7-(f) or equivalently E.6-(d): it corresponds to the distance measured from the clamped bottom to the first peak of the normalized deflection for each ε .

If we consider

$$d = C\sqrt{\varepsilon}L \quad (\text{E.11})$$

we observe that setting $C = 6$, an adequate characteristic length is obtained for each ε by formula (E.11), as Table E.2 shows.

Assume that N finite elements are considered to capture the smooth part of the solution outside of the boundary layer area, being the corresponding mesh spacing

$$h = \frac{L - d}{N} \quad (\text{E.12})$$

ε	<i>Computed</i> d	<i>Distance by formula</i> $d = 6\sqrt{\varepsilon}L$
10^{-2}	0.25	0.6
10^{-3}	0.15	0.19
10^{-4}	0.06	0.06

Table E.2: Layer length for the clamped hyperboloid shell problem: distance d computed from the clamped edge to the first peak of the normalized deflection.

A local refinement with mesh spacing $h_{BL} = d/N_{BL}$ inside of the boundary layer by setting

$$N_{BL} \sim N \quad (\text{E.13})$$

would provide poor accuracy of the numerical solution as the rotation along V_2 grows in a stronger manner than the displacement in z -direction and in a similar way as the cylindrical shell problem. Hence, a larger number of elements is required. By the same analysis done in (E.9) we have that it is suitable to set

$$N_{BL} \sim \varepsilon^{-\frac{1}{4}} N \quad (\text{E.14})$$

which substantially improves the numerical results.

- *Free hyperboloid shell problem:*

A boundary layer of length

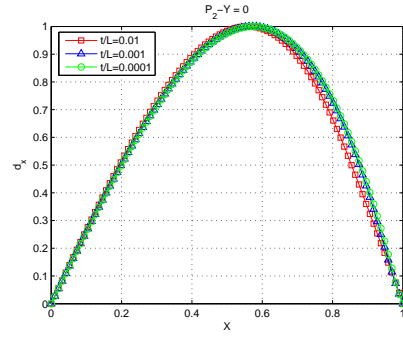
$$d = 0.5\sqrt{\varepsilon}L \quad (\text{E.15})$$

is properly meshed by setting

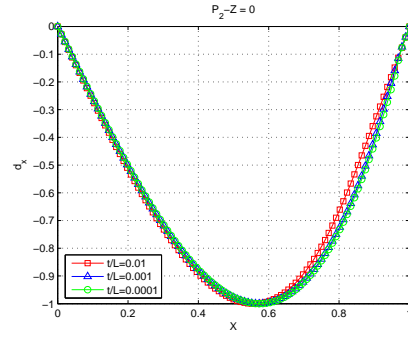
$$N_{BL} = N \quad (\text{E.16})$$

(see [31] and references therein).

The non-zero normalized displacement and rotation fields along AD , BC , CD and the bottom free boundary are displayed in Fig. E.9, E.10, E.11, E.12 and E.13 when considering a mesh of 96×96 MITC4 shell finite elements for this particular benchmark.



(a)



(b)

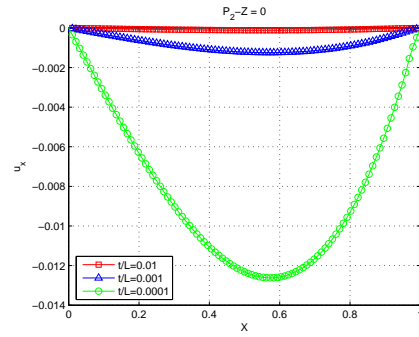
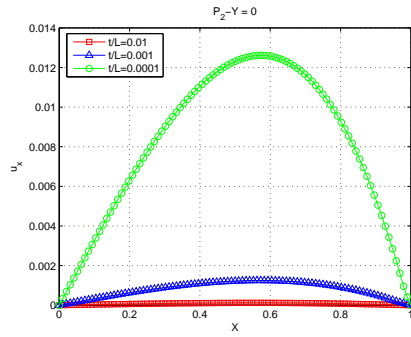


Figure E.1: Normalized (top) and non-normalized (bottom) displacement in x -direction for the clamped cylindrical shell problem: (a) along CD , (b) along AB .

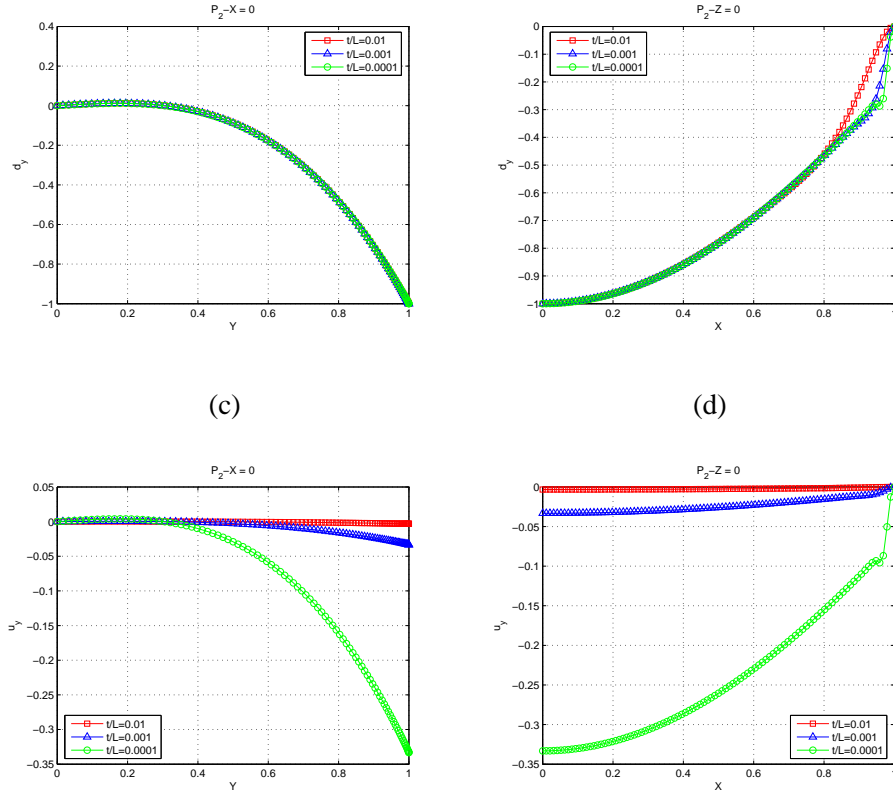
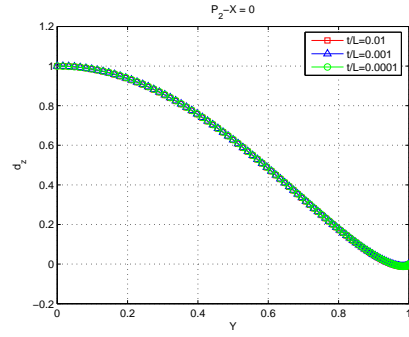
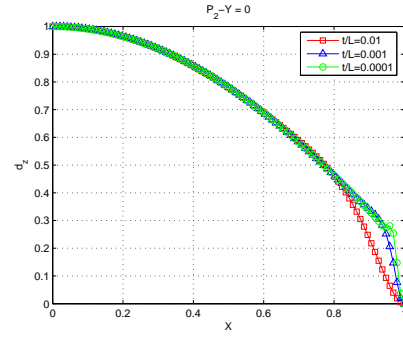


Figure E.2: Normalized (top) and non-normalized (bottom) displacement in y -direction for the clamped cylindrical shell problem: (c) along BC , (d) along AB .



(e)



(f)

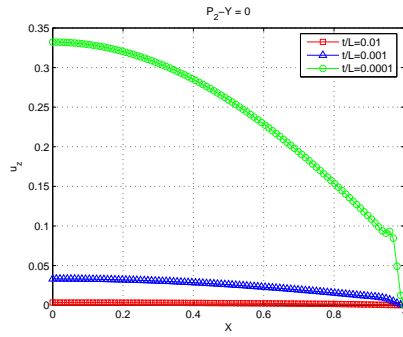
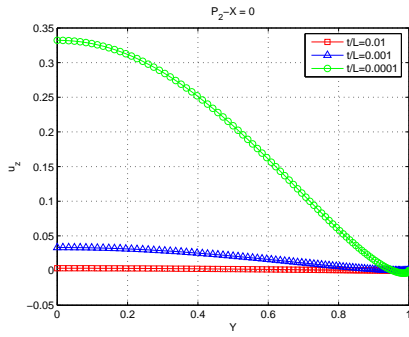
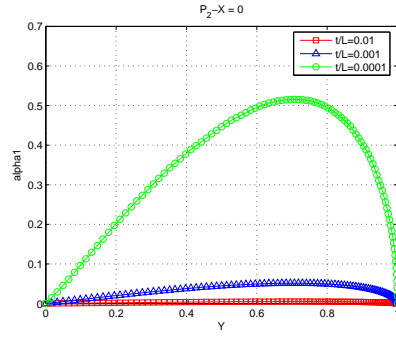
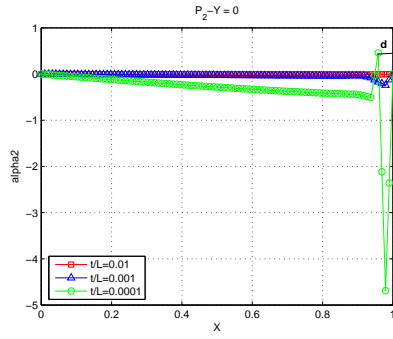


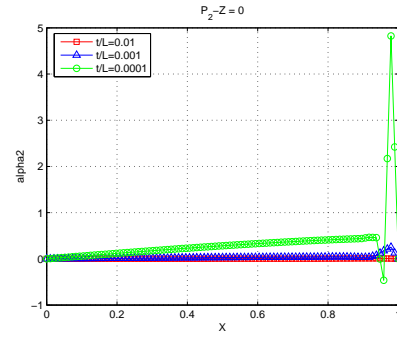
Figure E.3: Normalized (top) and non-normalized (bottom) displacement in z -direction for the clamped cylindrical shell problem: (e) along BC , (f) along CD .



(g)



(h)



(i)

Figure E.4: Rotation components for the clamped cylindrical shell problem: (g) along V_1 and BC , (h) along V_2 and CD , (i) along V_2 and AB .

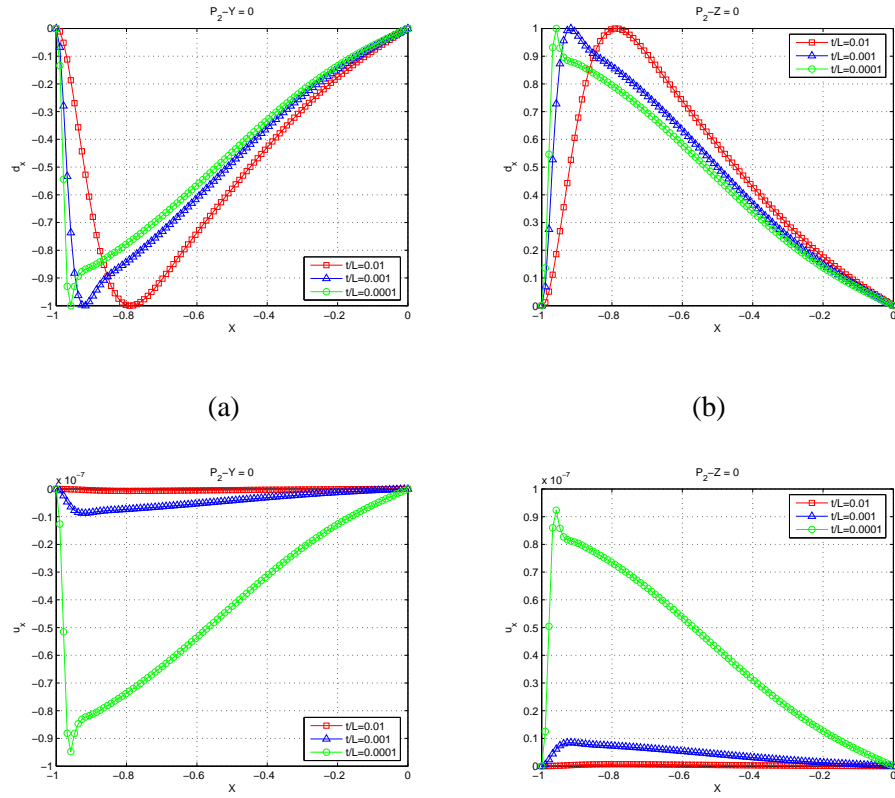
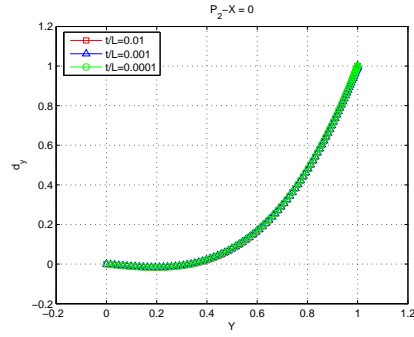
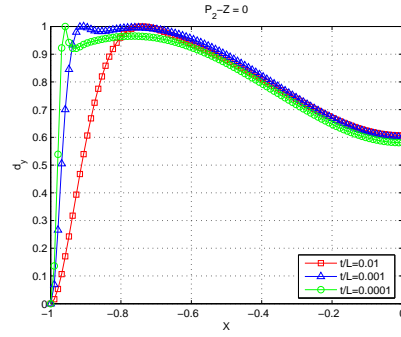


Figure E.5: Normalized (top) and non-normalized (bottom) displacement in x -direction for the clamped hyperboloid shell problem: (a) along BC , (b) along AD .



(c)



(d)

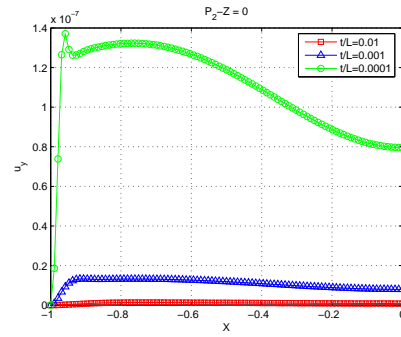
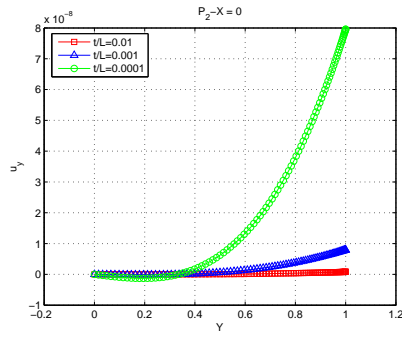
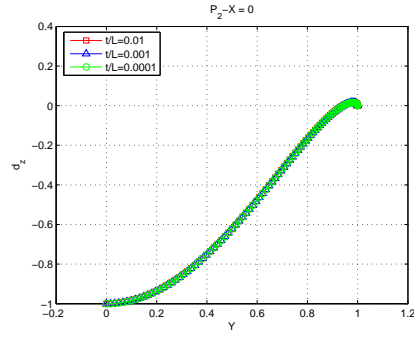
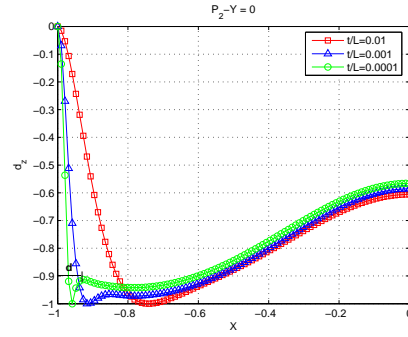


Figure E.6: Normalized (top) and non-normalized (bottom) displacement in y -direction for the clamped hyperboloid shell problem: (c) along CD , (d) along AD .



(e)



(f)

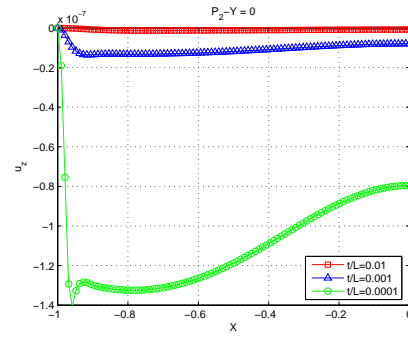
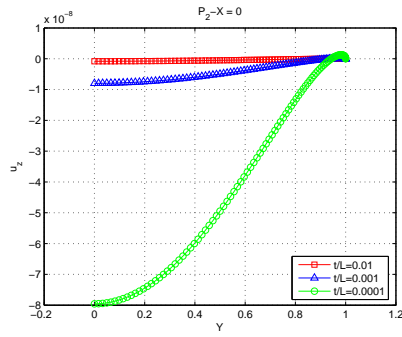
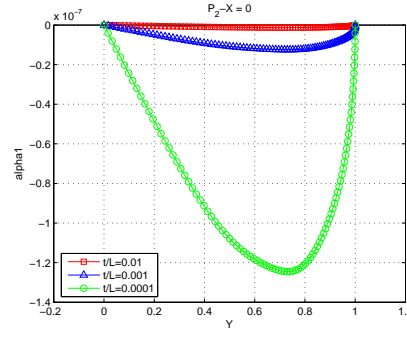
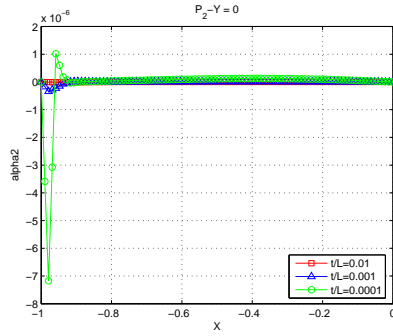


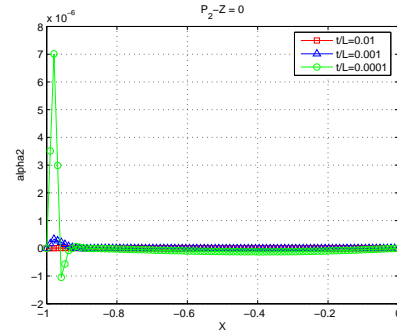
Figure E.7: Normalized (top) and non-normalized (bottom) displacement in z -direction for the clamped hyperboloid shell problem: (e) along CD , (f) along BC .



(g)

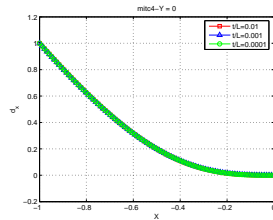


(h)

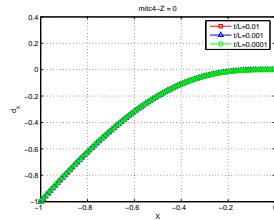


(i)

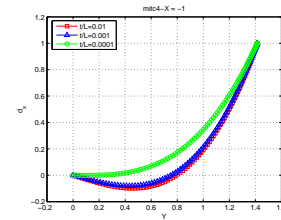
Figure E.8: Rotation components for the clamped hyperboloid shell problem: (g) along V_1 and CD , (h) along V_2 and BC , (i) along V_2 and AD .



(a)



(b)



(c)

Figure E.9: Normalized displacement in x -direction for the free hyperboloid shell problem: (a) along BC , (b) along AD , (c) along free boundary.

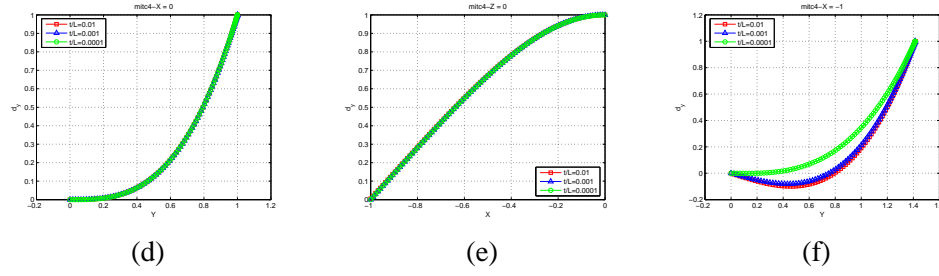


Figure E.10: Normalized displacement in y -direction for the free hyperboloid shell problem: (d) along CD , (e) along AD , (f) along free boundary.

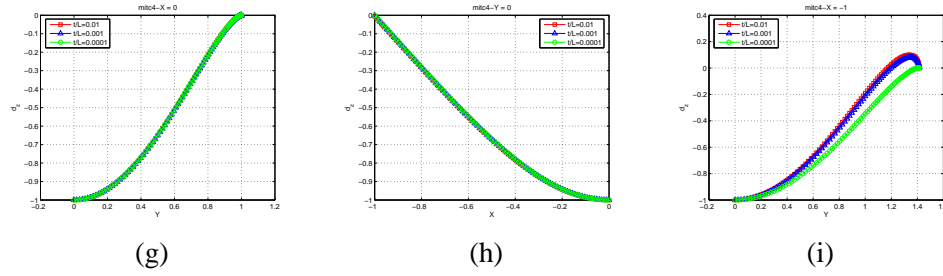


Figure E.11: Normalized displacement in z -direction for the free hyperboloid shell problem: (g) along CD , (h) along BC , (i) along free boundary.

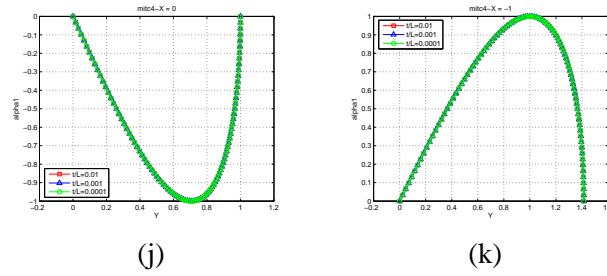


Figure E.12: Rotation along V_1 for the free hyperboloid shell problem: (j) along CD , (k) along free boundary.

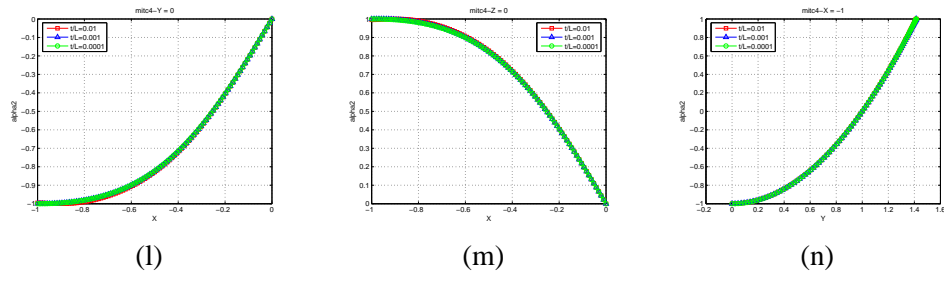


Figure E.13: Rotation along V_2 for the free hyperboloid shell problem: (l) along BC , (m) along AD , (n) along free boundary.

Appendix F

Other strategies

Lourenço Beirão da Veiga, Dominique Chapelle, Iria París

We continue on the research of a formulation that could effectively capture all the characteristic features of shell deformations simultaneously. As is well known, numerical difficulties are expected for low-order standard shell elements when approximating a bending dominated or otherwise pealized deformation state. The MITC approach is characterized as a reduced strain formulation where the strain components are modified. The aim is to avoid numerical locking as a reduced bilinear form $A_m^h(\cdot, \cdot)$ replaces the original one and

$$\left\{ V \in \mathcal{V}_h / A_m^h(V, V) = 0 \right\} \supset \mathcal{V}_0 \cap \mathcal{V}_h \quad (\text{F.1})$$

due to the reduction operators applied to $\underline{\underline{\gamma}}$ and $\underline{\underline{\zeta}}$, where \mathcal{V}_0 denotes the subspace of inextensional displacement fields. But the risk is to introduce membrane spurious modes that could deteriorate the underlying “correct” solution in membrane dominated situations as we have shown in Section 7.1.

Based on the works of Huve and Pitkaranta [39]-[40], the subspace \mathcal{V}_0 can be obtained by Fourier expansion for different geometries. In the same manner, a subspace of (nearly) inextensional discretized displacement fields has been numerically obtained when considering the reduction (shear) operators for the MITC4 shell finite element.

Let us assume that the domain Ω is meshed by 6-node triangular shell finite elements of characteristic mesh spacing h , and that a similar strategy could be undertaken, namely the subspace

$$\mathcal{V}_{0,h|_K} \quad (\text{F.2})$$

can be numerically approached for each finite element K in the mesh \mathcal{M}_h in such a manner that for each $V \in \mathcal{V}_0$ there exists $\tilde{V} \in \mathcal{V}_{0,h}$ such that¹

$$|||V - \tilde{V}||| \leq Ch^2 \quad (\text{F.3})$$

where $||| \cdot |||$ denotes the H^1 -norm or equivalently

$$||| \cdot |||^2 = A_b(\cdot, \cdot) + A_m(\cdot, \cdot) \quad (\text{F.4})$$

and the constant C depends on some norm of V . In particular we have that

$$A_m(\tilde{V}, \tilde{V})^{\frac{1}{2}} \leq Ch^2 \quad (\text{F.5})$$

Let us consider the two scaled variational formulations for the membrane (M) and bending (B) cases:

(M) Find $U \in \mathcal{V}_M$ such that

$$A_M(U, V) = \varepsilon^2 A_b(U, V) + A_m(U, V) = G(V) \quad \forall V \in \mathcal{V}_M \quad (\text{F.6})$$

(B) Find $U \in \mathcal{V}_B$ such that

$$A_B(U, V) = A_b(U, V) + \varepsilon^{-2} A_m(U, V) = G(V) \quad \forall V \in \mathcal{V}_B \quad (\text{F.7})$$

where \mathcal{V}_M and \mathcal{V}_B respectively denote the membrane and bending energy spaces. Hence, the asymptotic problem corresponding to (F.7) reads:

(B_0) Find $U_0 \in \mathcal{V}_0$ such that

$$A_b(U_0, V) = G(V) \quad \forall V \in \mathcal{V}_0 \quad (\text{F.8})$$

We introduce the standard FE-schemes solving (F.6) and (F.7), which respectively are

(M_h) Find $U_h \in \mathcal{V}_{M,h}$ such that

$$A_{M,h}(U_h, V) = \varepsilon^2 A_b(U_h, V) + A_m(U_h, V) = G(V) \quad \forall V \in \mathcal{V}_{M,h} \quad (\text{F.9})$$

(B_h) Find $U_h \in \mathcal{V}_{B,h}$ such that

$$A_{B,h}(U_h, V) = A_b(U_h, V) + \varepsilon^{-2} A_m(U_h, V) = G(V) \quad \forall V \in \mathcal{V}_{B,h} \quad (\text{F.10})$$

Passing to the limit $\varepsilon \rightarrow 0$ in (F.10), we obtain the discretized formulation of the asymptotic problem (F.8):

($B_{0,h}$) Find $U_{0h} \in \mathcal{V}_0 \cap \mathcal{V}_{B,h}$ such that

$$A_b(U_{0h}, V) = G(V) \quad \forall V \in \mathcal{V}_0 \cap \mathcal{V}_{B,h} \quad (\text{F.11})$$

Let us denote

$$\|\cdot\|_{M,h} = \sqrt{A_{M,h}(\cdot, \cdot)}, \quad \|\cdot\|_{B,h} = \sqrt{A_{B,h}(\cdot, \cdot)} \quad (\text{F.12})$$

¹ $W \in \mathcal{V}_{0,h}$ means that $W|_K \in \mathcal{V}_{0,h|_K} \quad \forall K \in \mathcal{M}_h$.

The discretization errors

$$e_M = \|U - U_h\|_{M,h}, \quad e_B = \|U - U_h\|_{B,h} \quad (\text{F.13})$$

originating from (F.9) and (F.10) can be split into two components to be bounded in both cases, namely the approximation errors

$$e_{a,M}(U) = \min_{V \in \mathcal{V}_{M,h}} \|U - V\|_{M,h} \quad (\text{F.14})$$

$$e_{a,B}(U) = \min_{V \in \mathcal{V}_{B,h}} \|U - V\|_{B,h} \quad (\text{F.15})$$

and the consistency errors

$$e_{c,M}(U) = \sup_{V \in \mathcal{V}_{M,h}} \frac{(A_M - A_{M,h})(U, V)}{\|V\|_{M,h}} \quad (\text{F.16})$$

$$e_{c,B}(U) = \sup_{V \in \mathcal{V}_{B,h}} \frac{(A_B - A_{B,h})(U, V)}{\|V\|_{B,h}} \quad (\text{F.17})$$

that give

$$e_M^2 = e_{a,M}^2 + e_{c,M}^2 \quad (\text{F.18})$$

$$e_B^2 = e_{a,B}^2 + e_{c,B}^2 \quad (\text{F.19})$$

New strategies different from the MITC approach have been considered during our research, but no satisfactory results have been obtained. The aim is to avoid the presence of membrane spurious modes when formulating efficient elements to approximate nearly inextensional (or bending-dominated) deformations.

Notice that in the bending dominated case, from (F.7) and (F.8) we have that

$$A_b(U - U_0, V) = 0 \quad \forall V \in \mathcal{V}_0 \quad (\text{F.20})$$

and then

$$U_0 = \Pi_{\mathcal{V}_0}^{A_b + \lambda(\varepsilon)A_m}(U) \quad (\text{F.21})$$

for any $\lambda(\varepsilon) = \varepsilon^{-\lambda}$ or 0.

In the same manner, from (F.10) and (F.11) we obtain that

$$A_b(U_h - U_{0h}, V) = 0 \quad \forall V \in \mathcal{V}_0 \cap \mathcal{V}_h \quad (\text{F.22})$$

and consequently

$$U_{0h} = \Pi_{\mathcal{V}_0 \cap \mathcal{V}_h}^{A_b + \lambda(\varepsilon)A_m}(U_h) \quad (\text{F.23})$$

Furthermore, if we define

$$U_0^\perp = \left(Id - \Pi_{\mathcal{V}_0}^{A_b + \lambda(\varepsilon)A_m} \right) U \quad (\text{F.24})$$

and

$$U_{0h}^\perp = \left(Id - \Pi_{\mathcal{V}_0 \cap \mathcal{V}_h}^{A_b + \lambda(\varepsilon)A_m} \right) U_h \quad (\text{F.25})$$

we respectively obtain

$$A_b(U_0^\perp, V) = 0 \quad \forall V \in \mathcal{V}_0 \implies A_B(U_0^\perp, V) = 0 \quad \forall V \in \mathcal{V}_0 \quad (\text{F.26})$$

and

$$A_b(U_{0h}^\perp, V) = 0 \quad \forall V \in \mathcal{V}_0 \cap \mathcal{V}_h \implies A_{B,h}(U_{0h}^\perp, V) = 0 \quad \forall V \in \mathcal{V}_0 \cap \mathcal{V}_h \quad (\text{F.27})$$

These considerations suggest to modify the discretized variational formulations by considering a projection into the discretized space of (nearly) inextensional displacements (F.2), where we have available information.

The difficulties we have encountered are described below.

F.1 Projection into $\mathcal{V}_{0,h}$

For $V \in \mathcal{V}$, let us define $\Pi_h V \in \mathcal{V}_{0,h}$ as

$$\begin{aligned} \langle V - \Pi_h V, W \rangle &= 0 & \forall W \in \mathcal{V}_{0,h} \\ \langle \Pi_h V, W \rangle &= 0 & \forall W \in [\mathcal{V}_{0,h}]^\perp \end{aligned} \quad (\text{F.28})$$

for

$$\langle \cdot, \cdot \rangle = A_b(\cdot, \cdot) + \varepsilon^{-2} A_m(\cdot, \cdot) \quad (\text{F.29})$$

and

$$\Pi_h^\perp V = V - \Pi_h V = (Id - \Pi_h) V \quad (\text{F.30})$$

Let us introduce the modified discretized formulation

Find $U_h \in \mathcal{V}_h$ such that

$$A_B^h(U_h, V) = G(V) \quad \forall V \in \mathcal{V}_h \quad (\text{F.31})$$

where A_B^h is a bilinear form that could provide adequate consistency and approximation errors:

- Setting

$$A_B^h(V, W) = A_b(V, W) + \varepsilon^{-2} A_m(\Pi_h^\perp V, \Pi_h^\perp W) \quad (\text{F.32})$$

it follows that

$$\begin{aligned} (A_B - A_B^h)(U, V) &= \varepsilon^{-2} A_m(U, V) - \varepsilon^{-2} A_m(\Pi_h^\perp U, \Pi_h^\perp V) \\ &= \varepsilon^{-2} A_m(\Pi_h^\perp U, \Pi_h V) + \varepsilon^{-2} A_m(\Pi_h U, \Pi_h^\perp V) + \\ &\quad \varepsilon^{-2} A_m(\Pi_h U, \Pi_h V), \quad \forall V \in \mathcal{V}_h \end{aligned} \quad (\text{F.33})$$

but we can say nothing about $\varepsilon^{-2} A_m(W, W)$ for $W \in [\mathcal{V}_{0,h}]^\perp$ and then the consistency error $e_{c,B}(U)$ is difficult to bound.

In fact, even the term $\varepsilon^{-2} A_m(\Pi_h U, \Pi_h V)$ induces difficulties because the coefficient ε^{-2} cannot be removed from the error estimate.

- Notice that given $V \in \mathcal{V}_h$, we have that

$$\begin{aligned} A_B(U, V) &= A_b(\Pi_h U, \Pi_h V) + \varepsilon^{-2} A_m(\Pi_h U, \Pi_h V) + \\ &\quad A_b(\Pi_h^\perp U, \Pi_h^\perp V) + \varepsilon^{-2} A_m(\Pi_h^\perp U, \Pi_h^\perp V) \end{aligned} \quad (\text{F.34})$$

Hence, setting

$$A_B^h(V, W) = A_b(\Pi_h V, \Pi_h W) + A_b(\Pi_h^\perp V, \Pi_h^\perp W) + \varepsilon^{-2} A_m(\Pi_h^\perp V, \Pi_h^\perp W) \quad (\text{F.35})$$

we obtain

$$A_B^h(U, V) = G(V) - \varepsilon^{-2} A_m(\Pi_h U, \Pi_h V) \quad \forall V \in \mathcal{V}_h \quad (\text{F.36})$$

and then

$$(A_B - A_B^h)(U, V) = \varepsilon^{-2} A_m(\Pi_h U, \Pi_h V) \quad (\text{F.37})$$

which does not represent a difficulty any more. But the approximation error $e_{a,B}(U)$ verifies

$$\min_{V \in \mathcal{V}_h} \|U - V\|_{B,h} \leq \min_{V \in \mathcal{V}_{0,h}} \|U - V\|_{B,h} \quad (\text{F.38})$$

and for $V \in \mathcal{V}_{0,h}$ we have

$$\begin{aligned} A_B^h(U - V, U - V) &= A_b(\Pi_h U, \Pi_h U) + A_b(\Pi_h^\perp U, \Pi_h^\perp U) + A_b(V, V) + \\ &\quad \varepsilon^{-2} A_m(\Pi_h^\perp U, \Pi_h^\perp U) - 2A_b(\Pi_h U, V) \end{aligned} \quad (\text{F.39})$$

but on the one hand we only know that

$$A_b(\Pi_h^\perp U, \Pi_h^\perp U) + \varepsilon^{-2} A_m(\Pi_h^\perp U, \Pi_h^\perp U) = A_b(\Pi_h^\perp U, U) + \varepsilon^{-2} A_m(\Pi_h^\perp U, U) \quad (\text{F.40})$$

and on the other hand no estimation is available for the bending energy of elements in $\mathcal{V}_{0,h}$.

F.2 Projection into $[\gamma(\mathcal{V}_{0,h})]^\perp$

For this section, let us denote by $\gamma(\cdot)$ the membrane and shear strains.

Another possible reduced formulation in the sense of the MITC approach could be

Find $U_h \in \mathcal{V}_h$ such that

$$A_B^h(U_h, V) = G(V) \quad \forall V \in \mathcal{V}_h \quad (\text{F.41})$$

with

$$A_B^h(V, W) = A_b(V, W) + \varepsilon^{-2} \langle \tilde{\gamma}(V), \tilde{\gamma}(W) \rangle \quad (\text{F.42})$$

where $\langle \cdot, \cdot \rangle$ denotes the L^2 dot product of surface (membrane and shear) tensors involving the corresponding strain-stress law coefficients, and $\tilde{\gamma}(V) \in [\gamma(\mathcal{V}_{0,h})]^\perp$ for $V \in \mathcal{V}$ is defined as

$$\begin{aligned} \langle \gamma(V) - \tilde{\gamma}(V), \bar{\gamma} \rangle &= 0 & \forall \bar{\gamma} \in [\gamma(\mathcal{V}_{0,h})]^\perp \\ \langle \tilde{\gamma}(V), \bar{\gamma} \rangle &= 0 & \forall \bar{\gamma} \in \gamma(\mathcal{V}_{0,h}) \end{aligned} \quad (\text{F.43})$$

Hence, the bending consistency error $e_{c,B}(U)$ can be bounded since

$$(A_B - A_B^h)(U, V) = \varepsilon^{-2} \sum_K \langle \gamma(U) - \tilde{\gamma}(U), \gamma(V) \rangle \quad \forall V \in \mathcal{V}_h \quad (\text{F.44})$$

and $\gamma(U) - \tilde{\gamma}(U) \in \gamma(\mathcal{V}_{0,h})$. But in general nothing can be said about the approximation error $e_{a,B}(U)$ since

$$A_{B,h}(U - V, U - V) = A_b(U - V, U - V) + \varepsilon^{-2} \langle \tilde{\gamma}(U) - \tilde{\gamma}(V), \tilde{\gamma}(U) - \tilde{\gamma}(V) \rangle \quad (\text{F.45})$$

and we could think about considering an orthogonal decomposition of the kind

$$\mathcal{V} = \mathcal{V}_{0,h} \oplus \mathcal{V}_{0,h}^\perp \quad (\text{F.46})$$

but nothing can be said in general about $\tilde{\gamma} \in \gamma(\mathcal{V}_{0,h}^\perp)$ in terms of L^2 -norm.

F.3 Enhanced shell finite elements

Another strategy could be to develop a mixed enhanced shell method based (see [3], [17], [42] and the references therein).

Let us consider the discretized variational formulation in a bending dominated framework that reads

Find $\vec{U}_h = (\vec{u}_h, \vec{\theta}_h) \in \mathcal{V}_h$ such that

$$\begin{aligned} \int_\omega \underline{\underline{\chi}}(\vec{u}_h, \vec{\theta}_h) : \underline{\underline{\chi}}(\vec{v}, \underline{\eta}) dS + \varepsilon^{-2} \int_\omega \underline{\underline{\gamma}}(\vec{u}_h) : \underline{\underline{\gamma}}(\vec{v}) dS + \\ \varepsilon^{-2} \int_\omega \underline{\underline{\zeta}}(\vec{u}_h, \vec{\theta}_h) \cdot \underline{\underline{\zeta}}(\vec{v}, \underline{\eta}) dS = G(\vec{v}), \quad \forall \vec{V} = (\vec{v}, \underline{\eta}) \in \mathcal{V}_h \end{aligned} \quad (\text{F.47})$$

where the stress-strain law is involved for “:” and “·”. The bilinear form in the left hand side is equivalent to

$$\begin{aligned} \int_\omega \underline{\underline{\chi}}(\vec{u}_h, \vec{\theta}_h) : \underline{\underline{\chi}}(\vec{v}, \underline{\eta}) dS + \int_\omega \underline{\underline{\gamma}}(\vec{u}_h) : \underline{\underline{\gamma}}(\vec{v}) dS + \int_\omega \underline{\underline{\zeta}}(\vec{u}_h, \vec{\theta}_h) \cdot \underline{\underline{\zeta}}(\vec{v}, \underline{\eta}) dS + \\ \tilde{\varepsilon}^{-2} \int_\omega \underline{\underline{\gamma}}(\vec{u}_h) : \underline{\underline{\gamma}}(\vec{v}) dS + \tilde{\varepsilon}^{-2} \int_\omega \underline{\underline{\zeta}}(\vec{u}_h, \vec{\theta}_h) \cdot \underline{\underline{\zeta}}(\vec{v}, \underline{\eta}) dS = G(\vec{v}) \end{aligned} \quad (\text{F.48})$$

by simply setting

$$\tilde{\varepsilon} = \frac{1}{\sqrt{\varepsilon^{-2} - 1}} \quad (\text{F.49})$$

which provides coercivity to the mixed formulations that could be derived from (F.48). In the sequel, we denote

$$A_b^E(\vec{w}, \vec{\eta}; \vec{w}, \vec{\tau}) = \int_{\omega} \underline{\underline{\chi}}(\vec{v}, \vec{\eta}) : \underline{\underline{\chi}}(\vec{w}, \vec{\tau}) dS + \int_{\omega} \underline{\underline{\gamma}}(\vec{v}) : \underline{\underline{\gamma}}(\vec{w}) dS + \int_{\omega} \underline{\underline{\zeta}}(\vec{v}, \vec{\eta}) \cdot \underline{\underline{\zeta}}(\vec{w}, \vec{\tau}) dS \quad (\text{F.50})$$

Let us introduce the enhanced strain space

$$\Gamma_h = \left\{ \left(\underline{\underline{\gamma}}(\vec{v}), \underline{\underline{\zeta}}(\vec{v}, \vec{\eta}) \right), (\vec{v}, \vec{\eta}) \in \mathcal{V}_{0,h} \right\} \quad (\text{F.51})$$

and the enhanced strain fomulation:

Find $(\vec{u}_h, \vec{\theta}_h) \in \mathcal{V}_h$ and $(\underline{\underline{m}}_h, \underline{\underline{s}}_h) \in \Gamma_h$ such that

$$\begin{aligned} A_b^E(\vec{u}_h, \vec{\theta}_h; \vec{v}, \vec{\eta}) + \tilde{\varepsilon}^{-2} \left[\int_{\omega} \left(\underline{\underline{\gamma}}(\vec{u}_h) + \underline{\underline{m}}_h \right) : \left(\underline{\underline{\gamma}}(\vec{v}) + \underline{\underline{m}} \right) dS + \right. \\ \left. \int_{\omega} \left(\underline{\underline{\zeta}}(\vec{u}_h, \vec{\theta}_h) + \underline{\underline{s}}_h \right) \cdot \left(\underline{\underline{\zeta}}(\vec{v}, \vec{\eta}) + \underline{\underline{s}} \right) dS \right] = G(\vec{v}) \end{aligned} \quad (\text{F.52})$$

$\forall \vec{V} = (\vec{v}, \vec{\eta}) \in \mathcal{V}_h$ and $\forall (\underline{\underline{m}}, \underline{\underline{s}}) \in \Gamma_h$.

It is easy to verify that there exist $(\vec{v}, \vec{\eta}) \in \mathcal{V}_h$ and $(\underline{\underline{m}}, \underline{\underline{s}}) \in \Gamma_h$ such that

$$\|(\vec{v}, \vec{\eta})\|_1 + \frac{1}{\tilde{\varepsilon}} \|(\underline{\underline{\gamma}}(\vec{v}) + \underline{\underline{m}}, \underline{\underline{\zeta}}(\vec{v}, \vec{\eta}) + \underline{\underline{s}})\|_0 \leq 1 \quad (\text{F.53})$$

and

$$\begin{aligned} & \|(\vec{u}_h, \vec{\theta}_h) - (\vec{u}_I, \vec{\theta}_I)\|_1 + \tilde{\varepsilon}^{-1} \|\underline{\underline{\gamma}}(\vec{u}_h - \vec{u}_I) + \underline{\underline{m}}_h - \underline{\underline{m}}_I\|_0 + \\ & \tilde{\varepsilon}^{-1} \|\underline{\underline{\zeta}}(\vec{u}_h - \vec{u}_I, \vec{\theta}_h - \vec{\theta}_I) + \underline{\underline{s}}_h - \underline{\underline{s}}_I\|_0 \leq \\ & A_b^E(\vec{u} - \vec{u}_I, \vec{v}) + \underbrace{\tilde{\varepsilon}^{-2} \int_{\omega} \left(\underline{\underline{\gamma}}(\vec{u}) - \underline{\underline{\gamma}}(\vec{u}_I) - \underline{\underline{m}}_I \right) : \left(\underline{\underline{\gamma}}(\vec{v}) + \underline{\underline{m}} \right) dS}_{(I)} + \\ & \underbrace{\tilde{\varepsilon}^{-2} \int_{\omega} \left(\underline{\underline{\zeta}}(\vec{u}, \vec{\theta}) - \underline{\underline{\zeta}}(\vec{u}_I, \vec{\theta}_I) - \underline{\underline{s}}_I \right) \cdot \left(\underline{\underline{\zeta}}(\vec{v}, \vec{\eta}) + \underline{\underline{s}} \right) dS}_{(II)} + \\ & \underbrace{\tilde{\varepsilon}^{-2} \int_{\omega} \underline{\underline{\gamma}}(\vec{u}) : \underline{\underline{m}} dS + \tilde{\varepsilon}^{-2} \int_{\omega} \underline{\underline{\zeta}}(\vec{u}, \vec{\theta}) \cdot \underline{\underline{s}} dS}_{(III)} \end{aligned} \quad (\text{F.54})$$

In particular, when estimating the error, it is necessary to bound the (consistency) term (III), and therefore we need an orthogonality property of Γ_h at least with respect to constants, which is not achieved in general, a consideration that suggests us to modify the original enhanced space and consider

$$\Gamma_h = \left\{ \left(\underline{\underline{\gamma}}(\vec{v}) - \overline{\underline{\underline{\gamma}}(\vec{v})}, \underline{\underline{\zeta}}(\vec{v}, \vec{\eta}) - \overline{\underline{\underline{\zeta}}(\vec{v}, \vec{\eta})} \right), (\vec{v}, \vec{\eta}) \in \mathcal{V}_{0,h} \right\} \quad (\text{F.55})$$

But then the terms (I) and (II) in (F.54) are expected to cause the failure of the method since the interpolation estimation fails.

Note that introducing the space

$$S_h = \left\{ (\underline{\underline{\gamma}}(\vec{v}) + \underline{\underline{\tilde{m}}}, \underline{\underline{\zeta}}(\vec{v}, \vec{\eta}) + \underline{\underline{\tilde{s}}}) : (\vec{v}, \vec{\eta}) \in \mathcal{V}_h, (\underline{\underline{\tilde{m}}}, \underline{\underline{\tilde{s}}}) \in \Gamma_h, \right. \\ \left. \int_{\omega} (\underline{\underline{\gamma}}(\vec{v}) + \underline{\underline{\tilde{m}}}) : \underline{\underline{\tilde{m}}} dS + \int_{\omega} (\underline{\underline{\zeta}}(\vec{v}, \vec{\eta}) + \underline{\underline{\tilde{s}}}) \cdot \underline{\underline{\tilde{s}}} dS = 0 \quad \forall (\underline{\underline{\tilde{m}}}, \underline{\underline{\tilde{s}}}) \in \Gamma_h \right\} \quad (\text{F.56})$$

for any Γ_h that could work, the mixed enhanced formulation (F.52) is equivalent to the shell formulation

Find $(\vec{u}_h, \vec{\theta}_h) \in \mathcal{V}_h$ such that

$$\int_{\omega} \underline{\underline{\chi}}(\vec{u}, \vec{\theta}) : \underline{\underline{\chi}}(\vec{v}, \vec{\eta}) dS + \int_{\omega} \underline{\underline{\gamma}}(\vec{u}) : \underline{\underline{\gamma}}(\vec{v}) dS + \int_{\omega} \underline{\underline{\zeta}}(\vec{u}, \vec{\theta}) \cdot \underline{\underline{\zeta}}(\vec{v}, \vec{\eta}) dS + \\ + \tilde{\varepsilon}^{-2} \left[\int_{\omega} \Pi_{S_h} \left(\underline{\underline{\gamma}}(\vec{u}) \right) : \underline{\underline{\gamma}}(\vec{v}) dS + \int_{\omega} \Pi_{S_h} \left(\underline{\underline{\zeta}}(\vec{u}, \vec{\theta}) \right) \cdot \underline{\underline{\zeta}}(\vec{v}, \vec{\eta}) dS \right] = G(\vec{v}) \quad (\text{F.57})$$

$\forall (\vec{v}, \vec{\eta}) \in \mathcal{V}_h$, where Π_{S_h} denotes a kind of L^2 projection into the space S_h . But this kind of variational form leads us to the observations done in the previous sections.

Bibliography

- [1] S. Ahmad, B.M. Irons, and O.C. Zienkiewicz. Analysis of thick and thin shell structures by curved finite elements. *Internat. J. Numer. Methods Engrg.*, 2:419–451, 1970.
- [2] F. Armero. On the locking and stability of finite elements in finite deformation plane strain problems. *Computers and Structures*, 75:261–290, 2000.
- [3] Auricchio F., Beirão da Veiga, L., Lovadina, C., and Reali, A. An analysis of some mixed-enhanced finite element for plane linear elasticity. *Comput. Methods Appl. Mech. Engrg.*, 194:2947–2968, 2005.
- [4] I. Babuška. The finite element method with Lagrangian multipliers. *Numer. Math.*, 20:179–192, 1973.
- [5] C. Baiocchi and C. Lovadina. A shell classification by interpolation. *Math. Models Methods Appl. Sci.*, 12(10):1359–1380, 2002.
- [6] K.J. Bathe. *Finite Element Procedures*. Prentice Hall, Englewood Cliffs, 1996.
- [7] K.J. Bathe and F. Brezzi. On the convergence of a four-node plate bending element based on Mindlin-Reissner plate theory and a mixed interpolation. In J.R. Whiteman, editor, *The Mathematics of Finite Elements and Applications V*, pages 491–503, New York, 1985. Academic Press.
- [8] K.J. Bathe and F. Brezzi. A simplified analysis of two plate bending elements—the MITC4 and MITC9 elements. In *Proceedings, Numerical Methods in Engineering: Theory and Applications*, 1987.
- [9] K.J. Bathe, F. Brezzi, and S.W. Cho. The MITC7 and MITC9 plate bending elements. *Comput. & Structures*, 32(3/4):797–814, 1989.
- [10] K.J. Bathe, M. Bucalem, and F. Brezzi. Displacement and stress convergence for our MITC plate bending elements. *Eng. Comput.*, 7:291–302, 1990.
- [11] K.J. Bathe, D. Chapelle, and P.S. Lee. A shell problem ‘highly sensitive’ to thickness changes. *Internat. J. Numer. Methods Engrg.*, 57:1039–1052, 2003.

- [12] K.J. Bathe and E.N. Dvorkin. A four-node plate bending element based on Mindlin/Reissner plate theory and a mixed interpolation. *Internat. J. Numer. Methods Engrg.*, 21:367–383, 1985.
- [13] K.J. Bathe and E.N. Dvorkin. A formulation of general shell elements—the use of mixed interpolation of tensorial components. *Internat. J. Numer. Methods Engrg.*, 22:697–722, 1986.
- [14] K.J. Bathe, A. Iosilevich, and D. Chapelle. An evaluation of the MITC shell elements. *Comput. & Structures*, 75(1):1–30, 2000.
- [15] K.J. Bathe, A. Iosilevich, and D. Chapelle. An inf-sup test for shell finite elements. *Comput. & Structures*, 75(5):439–456, 2000.
- [16] J.L. Batoz and G. Dhatt. *Modélisation des Structures par Eléments Finis*. Hermes, 1990.
- [17] J.C. Simo B.D. Reddy. Stability and convergence of a class of enhanced strain methods. *Siam. J. Numer. Anal.*, 6:1705–1728, 1995.
- [18] M. Bernadou. *Finite Element Methods for Thin Shell Problems*. John Wiley & Sons, New York, 1996.
- [19] A. Blouza, F. Brezzi, and C. Lovadina. Sur la classification des coques linéairement élastiques. *C. R. Acad. Sci. Paris, Série I*, 328:831–836, 1999.
- [20] J.H. Bramble and T. Sun. A locking-free finite element method for Naghdi shells. *J. Comput. Appl. Math.*, 89:119–133, 1997.
- [21] F. Brezzi. On the existence, uniqueness and approximation of saddle-point problems arising from lagrangian multipliers. *R.A.I.R.O., Anal. Numér.*, 8:129–151, 1974.
- [22] F. Brezzi, K.J. Bathe, and M. Fortin. Mixed-interpolated elements for Reissner-Mindlin plates. *Internat. J. Numer. Methods Engrg.*, 28:1787–1801, 1989.
- [23] F. Brezzi and M. Fortin. *Mixed and Hybrid Finite Element Methods*. Springer-Verlag, New York, 1991.
- [24] F. Brezzi, M. Fortin, and R. Stenberg. Error analysis of mixed-interpolated elements for Reissner-Mindlin plates. *Math. Models Methods Appl. Sci.*, 1(2):125–151, 1991.
- [25] Franco Brezzi, Jim Douglas, Jr., Michel Fortin, and L. Donatella Marini. Efficient rectangular mixed finite elements in two and three space variables. *RAIRO Modél. Math. Anal. Numér.*, 21(4):581–604, 1987.

- [26] M. Bucalem and K.J. Bathe. Higher-order MITC general shell elements. *Internat. J. Numer. Methods Engrg.*, 36:3729–3754, 1993.
- [27] F. Auricchio C. Lovadina. On the enhanced strain technique for elasticity problems. *Computers and Structures*, 81:777–787, 2003.
- [28] C.R. Calladine. *Theory of Shell Structures*. Cambridge University Press, Cambridge, 1983.
- [29] D Chapelle. On the numerical locking phenomena arising in the approximation of thin shell problems. Laboratoire Central des Ponts et Chaussées, 1996.
- [30] D. Chapelle and K.J. Bathe. The mathematical shell model underlying general shell elements. *Internat. J. Numer. Methods Engrg.*, 48(2):289–313, 2000.
- [31] D. Chapelle and K.J. Bathe. *The Finite Element Analysis of Shells – Fundamentals*. Springer-Verlag, 2003.
- [32] D. Chapelle, A. Ferent, and K.J. Bathe. 3d-shell finite elements and their underlying model. *Math. Models Methods Appl. Sci.*, 14(1):105–142, 2004.
- [33] D. Chapelle and R. Stenberg. Stabilized finite element formulations for shells in a bending dominated state. *SIAM J. Numer. Anal.*, 36(1):32–73, 1998.
- [34] C. Chinosi and C. Lovadina. Numerical analysis of some mixed finite element methods for Reissner-Mindlin plates. *Comput. Mech.*, 16:36–44, 1995.
- [35] P.G. Ciarlet. *The Finite Element Method for Elliptic Problems*. North-Holland, Amsterdam, 1978.
- [36] P.G. Ciarlet. *Mathematical Elasticity - Volume III: Theory of Shells*. North-Holland, Amsterdam, 2000.
- [37] E.N. Dvorkin and K.J. Bathe. A continuum mechanics based four-node shell element for general non-linear analysis. *Eng. Comput.*, 1:77–88, 1984.
- [38] W. Flügge. *Stresses in Shells*. Springer-Verlag, New York, Heidelberg, 2nd edition, 1973.
- [39] V. Havu and J. Pitkäranta. Analysis of a bilinear finite element for shallow shells. I: Approximation of inextensional deformations. *Math. Comp.*, 71:923–943, 2002.
- [40] V. Havu and J. Pitkäranta. Analysis of a bilinear finite element for shallow shells: II: Consistency error. *Math. Comp.*, 72(244):1635–1653, 2003.
- [41] T.J.R. Hughes. *The Finite Element Method*. Prentice-Hall, 1987.

- [42] M.S. Rifai J.C. Simo. A class of mixed assumed strain methods and the method of incompatible modes. *Internat. J. Numer. Methods Engrg.*, 29:1595–1638, 1990.
- [43] P. Karamian, J. Sanchez-Hubert, and E. Sanchez-Palencia. A model problem for boundary layers of thin elastic shells. *M2AN Math. Model. Numer. Anal.*, 34:1–30, 2000.
- [44] W.T. Koiter. On the nonlinear theory of thin elastic shells. *Proc. Kon. Ned. Akad. Wetensch.*, B69:1–54, 1965.
- [45] Phill-Seung Lee. *On Triangular Finite Elements for General Shell Structures*. PhD thesis, Massachusetts Institute of Technology, 2004.
- [46] P.S. Lee and K.J. Bathe. On the asymptotic behavior of shell structures and the evaluation in finite element solutions. *Computers and Structures*, 80:235–255, 2002.
- [47] P.S. Lee and K.J. Bathe. Development of MITC isotropic triangular shell finite elements. *Computers & Structures*, 82:945–962, 2004.
- [48] J.L. Lions and E. Sanchez-Palencia. Problèmes sensitifs et coques élastiques minces. In J. Céa, D. Chenais, G. Geymonat, and J.L. Lions, editors, *Partial Differential Equations and Functional Analysis - In Memory of Pierre Grisvard*, pages 207–220, Boston, 1996. Birkhäuser.
- [49] R.D. Mindlin. Influence of rotary inertia and shear on flexural motion of isotropic elastic plates. *J. Appl. Mech.*, 18:31–38, 1951.
- [50] P.M. Naghdi. Foundations of elastic shell theory. In *Progress in Solid Mechanics*, volume 4, pages 1–90. North-Holland, Amsterdam, 1963.
- [51] V.V. Novozhilov. *Thin Shell Theory*. Wolters-Noordhoff Publishing, Groningen, 2nd edition, 1970.
- [52] Jyrki Piila and Juhani Pitkäranta. Characterization of the membrane theory of a clamped shell. The parabolic case. *Math. Models Methods Appl. Sci.*, 3(3):417–442, 1993.
- [53] J. Pitkäranta. The problem of membrane locking in finite element analysis of cylindrical shells. *Numer. Math.*, 61:523–542, 1992.
- [54] J. Pitkäranta, Y. Leino, O. Ovaskainen, and J. Piila. Shell deformation states and the finite element method: a benchmark study of cylindrical shells. *Comput. Methods Appl. Mech. Engrg.*, 128:81–121, 1995.
- [55] J. Pitkäranta, A.M. Matache, and C. Schwab. Fourier mode analysis of layers in shallow shell deformations. *Comput. Methods Appl. Mech. Engrg.*, 190:2943–2975, 2001.

- [56] E. Reissner. The effect of transverse shear deformation on the bending of elastic plates. *J. Appl. Mech.*, 67:A69–A77, 1945.
- [57] E. Reissner. Stress strain relations in the theory of thin elastic shells. *J. Math. Phys.*, 31:109–119, 1952.
- [58] J. E. Roberts and J.M. Thomas. Mixed and hybrid methods. In *Handbook of numerical analysis, Vol. II*, Handb. Numer. Anal., II, pages 523–639. North-Holland, 1991.
- [59] J. Sanchez-Hubert and E. Sanchez-Palencia. *Coques Elastiques Minces - Propriétés Asymptotiques*. Masson, Paris, 1997.
- [60] J. Sanchez-Hubert and E. Sanchez-Palencia. Anisotropic finite element estimates and local locking for shells: parabolic case. *C. R. Acad. Sci. Paris, Série IIB*, 329:153–159, 2001.
- [61] E. Sanchez-Palencia. Statique et dynamique des coques minces. II. Cas de flexion pure inhibée - Approximation membranaire. *C. R. Acad. Sci. Paris, Série I*, 309:531–537, 1989.
- [62] E. Sanchez-Palencia. Statique et dynamique des coques minces. II. Cas de flexion pure inhibée. Approximation membranaire. *C. R. Acad. Sci. Paris Sér. I Math.*, 309(7):531–537, 1989.
- [63] S. Timoshenko and S. Woinowsky-Krieger. *Theory of Plates and Shells*. McGraw-Hill, New York, 1959.
- [64] R. Valid. *The Nonlinear Theory of Shells through Variational Principles*. John Wiley & Sons, Chichester, 1995.
- [65] W. Wunderlich. On a consistent shell theory in mixed tensor formulation. In *Proc. 3rd IUTAM Symposium on Shell Theory: Theory of Shells*, Amsterdam, 1980. North Holland.